PETROLOGY, GEOCHEMISTRY AND TECTONIC IMPLICATIONS OF IGNEOUS ROCKS IN THE NAN SUTURE, THAILAND
and
AN EMPIRICAL STUDY OF THE EFFECTS OF Ca/Na, Al/Si and H_2O ON PLAGIOCLASE - MELT EQUILIBRIA AT 5 - 10 KB PRESSURE

by

Yuenyong Panjasawatwong

B.S. (Chiang Mai University), M.Sc. (University of Durham)

Submitted in fulfilment of the requirements
for the degree of

Doctor of Philosophy

University of Tasmania
Hobart

January, 1991

STATEMENT

This thesis contains the results of research done in the Geology Department, University of Tasmania from May, 1987 to January, 1991. It contains no material which has been accepted for the award of any other degree or diploma in any University and, to the best of my knowledge and belief, contains no copy or paraphrase of material previously published or written by another person, except where due reference is made.

Yuenyong Panjasawatwong

Yuenyong Panjasawatwong
University of Tasmania
January, 1991

THESIS CONTENTS

LIST OF FIGURES

LIST OF TABLES

ACKNOWLEDGEMENTS

First I would like to thank my supervisors Dr. Tony Crawford and Professor David Green for their patient guidance, support, enthusiasm, interest, encouragement and stimulation throughout all stages of this thesis, and critical reading and comments on Part I (Dr. A.J. Crawford) and Part II (Professor D.H. Green and Dr. A.J. Crawford). I am also indebted to Dr. Clive Burrett for the opportunity to carry out research at the University of Tasmania.

I am grateful to the Australian International Development Assistance Bureau (AIDAB) for financial support and various arrangements during my stay in Australia. Nan Mine Co., Ltd., and CIG Co., Ltd. are also thanked for providing accommodation, transportation and field assistants during fieldwork in Thailand.

Thanks are extended to many people who have assisted me during this study, particularly:

-Wieslaw Jablonski for his instructions in operation of electron microprobe and scanning electron microscope;

-Keith Harris for detailed instructions in the use of the piston cylinder apparatus, manufacturing most of the components used in high-pressure assemblages and critical reading and comments on Part II;

-Phillip Robinson for his assistance in the analytical work in Part I;

-Simon Stevens for his help in making thin-sections and polished thin-sections, and polishing probe mounts;

-Peter Cornish and Andrew Gillion for their help in the workshop;

-Dr. Michael Worthing for critical reading and comments on parts of Part I;

-Dr. Steve Eggins for his helpful discussions on Part I, and critical reading and comments on Part II;

-to various scientists for their fruitful discussions, including Drs. Rick Varne, Clive Burrett, Ron Berry, Wayne Taylor, Trevor Falloon, Russell Sweeney, Christian Ballhaus, Joe Stolz , Mark Barsdell, Ian Buick and Yoshiyuki Tatsumi;

-to Professor S. Hada and Dr. Shin-ichi Yoshikura (Kochi University) who provided useful information on Part I;

-to Mungkorn Haraluk and Winai Yaowanoiyothin (Chiang Mai University) who assisted many times during fieldwork for Part I;

-to the graduate students of this department for their hospitality, companionship, support and encouragement; Massimo Gasparon, Geoff Nichols, Michael Seitz, Ruth Lanyon, Baharuddin, Udi Hortono, Salman Palgunady, Thanis Wongwanich, Ai Yang, Pol Choadumrong, Sjafra Dwipa, Khin Zaw, Djojomihardjo Soetijos, Memet

Rahmat Hermanto, Michael Roach, Garry Davidson, David Huston, Vanessa Guthrie, Greg Yaxley, Sampan Singharajwarapan, Ingvar Sigurdsson, Nick Odling, John Adam, Margaret Wallace and Malcolm Wallace;
-to all members of the Geology Department not already mentioned for their help and for providing a happy working environment.

I would like to express my gratitude to Dr. Russell Sweeney for providing accomodation during the last month of my stay in Hobart.

Finally, I wish to give special thanks to my parents and family for their support and encouragement.

ABSTRACT

Part I: Igneous Rocks in the Nan Suture

The Nan mafic-ultramafic belt is widely believed to represent a continental suture between the Shan-Thai (to the west) and Indochina (east) cratons. Geological mapping of selected areas has shown for the first time that this belt is an extensive melange, made up of variably sized blocks (up to a few km across) of igneous, metamorphic and sedimentary rocks in a serpentinite matrix. Igneous rocks as blocks within the Nan Suture melange consist of lavas, dolerites, microgabbros and cumulate gabbroic and ultramafic rocks. Lavas, microgabbros and dolerites may be chemically separated into three main compositional groups that reflect their tectonic settings of eruption, namely intraplate ocean-island basalts (Group A), backarc basin basalts and andesites (Group B) and island-arc basalts and andesites (Group C). Cumulates include gabbros/amphibolites and associated ultramafics and chromitites. A brief assessment of mineral equilibria in blueschists blocks is also presented.

Group A lavas are intraplate basalts that include tholeiites (Subgroup A-1), and transitional tholeiites and alkalic basalts (Subgroup A-2). Subgroup A-1 tholeiites are chemically analogous to tholeiites from the Hawaiian and Tasmantid intraplate seamount chains. Subgroup A-2 basalts show markedly greater LREE enrichment relative to HREE and are comparable with transitional tholeiitic and alkalic basalts such as those erupted in the postshield stages of Haleakala and Mauna Kea in the Hawaiian chain.

Group B includes basalts and andesites that have been chemically subdivided into four compositionally distinct subgroups that all show geochemical features transitional from arc basalts to backarc basin basalts. They are thus assigned to an eruption setting associated with the incipient rifting of an oceanic arc and development of an immature backarc basin.

Group C basalts and andesites are subdivided into 2 subgroups. Subgroup C-1 includes basalts and andesites with compositional characteristics most similar to many oceanic island-arc low-K to medium-K basalts and andesites. Subgroup C-2 samples are compositionally transitional between island arc tholeiitic and calc-alkalic basalts and andesites, and are typical of calc-alkalic lavas formed in an island arc or active continental margin.

Cumulate gabbros are compositionally most similar to the Subgroup C-1 arc suite, but field relationships rule against direct affinities with the Group C arc suite.

The gabbros probably represent basement rocks of an earlier arc sequence subsequently invaded by Subgroup C-1 arc magmas following reorganisation of plate boundaries related to arc-continent collision (see later). Ultramafic rocks associated with the gabbros show the crystallisation sequence olivine+chromite+orthopyroxene - clinopyroxene - plagioclase. This, together with spinel compositions, supports affinities with the low-Ti ophiolitic association, and implies generation in a supra-subduction zone setting. Chromitites contain highly refractory chromites comparable to those in high Ca-boninites, and were also probably generated in a supra-subduction environment.

Occasional blocks of blueschist are probably derived from tuffaceous sediments associated with the intraplate Group A magma suite. They probably formed at about 7 kb in temperatures range 390 - 450°C, i.e. geothermal gradients 15-18°C/km.

Based on these new data regarding the tectonic settings of eruption of igneous rocks in the Nan suture melange, and other available geological and age constraints, a plate-tectonic scenario for the Shan Thai - Indochina continental collision is proposed. In the Late Carboniferous, the Shan-Thai and Indochina cratons were separated by a major ocean basin, and an island arc probably formed above an east-dipping subduction zone at the leading edge of the Indochina craton. Ocean-island basalts (Group A samples) in seamount volcanoes on the subducting ocean crust were transported into the subduction zone and partly scraped off on to the forearc slope of this arc.

Arc rifting possibly occurred in Early Permian time, giving rise to a backarc basin floored in its earliest phase of opening by Group B tholeiites. The thinned leading margin of the Shan-Thai craton eventually arrived at the subduction zone fronting this arc - backarc basin system that had developed at the leading edge of the Indochina craton, resulting in arc-continent collision, occurring probably initially in the Middle Permian. As the result of collision, backarc spreading terminated and a reversal of subduction polarity may have taken place. Arc magma Subgroup C-1 was produced above this new subduction zone and intruded the older arc represented by the foliated mafic-ultramafic plutonic rocks. This subduction episode eventually dragged the Shan-Thai craton into collision with the Middle to Late Permian foldbelt formed during arc-continent collision involving the Indochina craton. This continent-continent collision, culminating in the Late Triassic, produced the Nan Suture. The original geometry of this suture has been largely modified by movements of transcurrent faults that formed widespread pull-apart basins in the Late Triassic, and

the Cainozoic. The Nan Suture itself has probably acted as a locus of transcurrent fault motion since the final collision.

Part II: Plagioclase-Melt Equilibria

The presence of highly calcic plagioclase (>An80) in arc lavas and cumulates and some mid-ocean ridge basalts is well known, but there is presently no adequate model explaining such occurrences. An experimental study has been carried to test the effects of bulk composition, pressure, temperature and water pressure on the composition of liquidus or near-liquidus plagioclase formed in a variety of starting compositions. Experiments were carried out on synthetic starting mixes covering the calcic basalt to andesite range.

Probably the strongest single control of the composition of crystallising plagioclase is the Ca# (molecular Ca/(Ca+Na)) of the bulk composition. The K_DCa# values for plagioclase crystallising from any bulk composition from anhydrous experiments at 5 kb are always significantly higher than those from anhydrous experiments at 10 kb, but lower than those for hydrous experiments at 5 or 10 kb, or anhydrous experiments at 1 atmosphere. The effect of water on the composition of plagioclase is most marked for bulk compositions with Ca# ranging from 60 to 80, in which plagioclase is up to 10 mol% An more calcic than plagioclase crystallising from the same bulk composition under anhydrous conditions at similar pressure.

These results form the basis of a discussion of the various models for the existence of highly calcic plagioclase in many arc lavas and cumulates, and provide a more thorough assessment of the petrogenetic significance of highly calcic plagioclases in mid-ocean ridge basalts.

PART I

PETROLOGY, GEOCHEMISTRY AND TECTONIC IMPLICATIONS OF IGNEOUS ROCKS IN THE NAN SUTURE, THAILAND

CHAPTER 1

INTRODUCTION

1.1 Summary of Previous Studies

Thailand is generally believed to be constituted by the two main continental cratons of Southeast Asia, the Shan-Thai craton in the west and the Indochina craton to the east, that are separated by the Nan-Uttaradit Ophiolitic Suture Zone. This suture (herein the Nan Suture) extends intermittently in NE-SW direction for over 150 km (Fig. 1.1), and represents the zone formed by collision of the two cratons (Gatinsky *et al.*, 1978; Thanasuthipitak, 1978; Asanachinda, 1978; Chantaramee, 1978; Beckinsale *et al.*, 1979; Bunopas and Vella, 1978, 1983; Bunopas, 1981; Burton, 1984; Sengor, 1984; Hahn, 1985; Hahn *et al.*, 1986; Barr and MacDonald, 1987; Hayashi, 1989; Cooper *et al.*, 1989; Barr *et al.*, 1990). The Nan Suture trends northward into Laos, and may correlate with the Changning-Shuangjiang suture zone in southern China (Barr and MacDonald, 1987; C. Bolin and Z. Ruyuan, pers. comm., 1989). The southern continuation of the Nan Suture may be the mafic-ultramafic belts in southeastern Thailand, and the Bentong Raub ophiolite line in Malaysia (Gatinsky *et al.* 1978; Hutchison, 1983; Bunopas, 1981; Bunopas and Vella, 1983; Burton, 1984; Barr and MacDonald, 1987).

Plate tectonic models accounting for the continent-continent collision in northern Thailand have been proposed by a number of workers. There is general agreement that a palaeo-ocean, represented by the Nan Suture, lay between the Shan-Thai and Indochina cratons in Late Palaeozoic time. However, geometry and timing of collision remain controversial.

These models involve convergence between the two cratons by subduction of intervening oceanic crust. Westward subduction beneath the Shan-Thai was proposed by Bunopas and Vella (1978), Chantaramee (1978), Asanachinda (1978), Barr and MacDonald (1987), Hayashi (1989) and Barr *et al.* (1990), whereas eastward subduction beneath the Indochina was proposed by Beckinsale *et al.* (1979). An intermediate model with a pair of subduction zones, one dipping west and the other dipping east, was suggested by Gatinsky *et al.* (1978), Thanasuthipitak (1978), Bunopas (1981), Bunopas and Vella (1983), and Cooper *et al.* (1989). Timing of collision includes pre-Late Permian (Helmcke and Kraikhong, 1982; Helmcke and Lindenberg, 1983; Helmcke, 1985, 1986; Hahn, 1985), Middle to Late Permian (Burton, 1984; Barr and MacDonald,1987); Permo-Triassic (Thanasuthipitak ,1978;

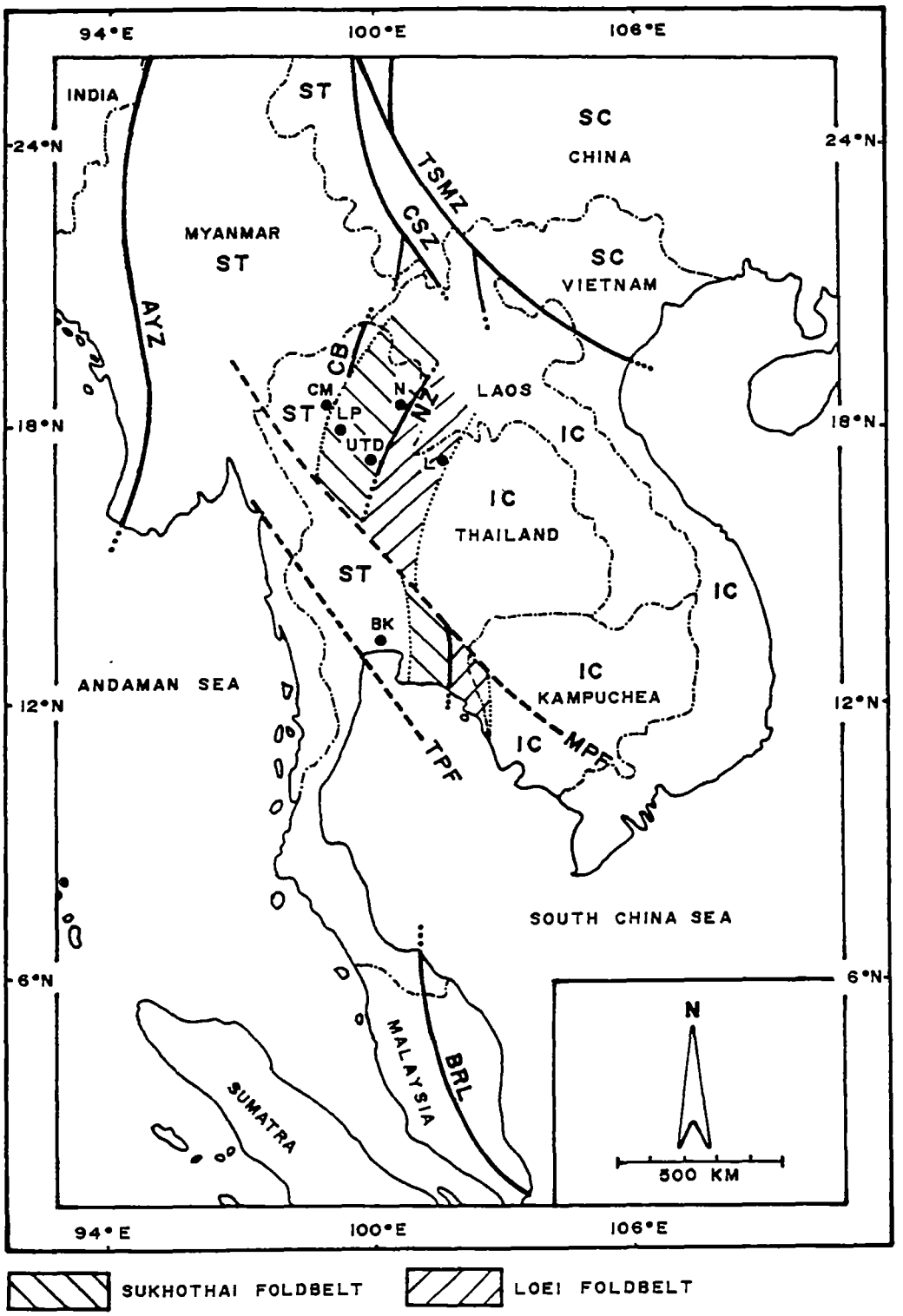

Figure 1.1. Generalised map showing tectonic framework of Southeast Asia as described in the text (modified from Bunopas, 1981, and Barr and MacDonald, 1987). SC = South China Craton; ST = Shan-Thai Craton; IC = Indochina Craton; NZ = Nan Suture Zone; CB = Chiang Mai Mafic-Ultramafic Belt; TSMZ = Tengiaohe-Song Ma Suture Zone; CSZ = Changning-Shuangjiang Suture Zone; BRL = Bentong Raub Line; AYZ = Arakan Yoma Suture Zone; MPF = Mae Ping Fault; TPF = Three Pagodas Fault; CM = Chiang Mai; LP = Lampang; N = Nan; UTD = Uttaradit; L = Loei; BK = Bangkok.

Cooper *et al.*, 1989; Barr *et al.*, 1990), Triassic (Chantaramee, 1978; Beckinsale *et al.*, 1979) and Late Triassic (Asanachinda, 1978; Bunopas and Vella, 1978, 1983; Bunopas, 1981; Sengor, 1984; Hutchison, 1989).

Helmcke and Lindenberg (1983) also questioned whether, in fact, the Nan Suture mafic-ultramafic rocks are a true (albeit dismembered) ophiolite, and thus the tectonic setting of formation of the mafic-ultramafic rocks along the Nan Suture, i.e. do they represent remnants of Palaeotethys, a marginal sea lying east of Gondwanaland, or a marginal sea which lay off Palaeoeurasia ?

The widely different opinions reflect both the complicated tectonic evolution and inadequate data. Belts of poorly-studied volcanic and flyschoid rocks broadly parallel to the Nan Suture in the Sukhothai and Loei Foldbelts (Fig. 1.1), Late Triassic extensional collapse of the overthickened crust (Cooper *et al.*, 1989) and Late Triassic to Cainozoic transcurrent movements (Cooper *et al.*, 1989; Sattayarak *et al.*, 1989; Polachan and Sattayarak, 1989) enhance this complexity.

Petrochemical studies of the mafic-ultramafic rocks occurring along the Nan Suture were carried out by Bunopas (1981), MacDonald and Barr (1984) and Barr and MacDonald (1987). Platinum-group-element (PGE) analyses were also performed by Orberger *et al.* (1989). The data of Bunopas (1981) are less significant because they include only whole-rock major element analyses. MacDonald and Barr (1984) analysed whole-rock major and trace elements on a limited number of samples (5 basaltic rocks, 3 gabbros, 3 epidote amphibolites and 1 garnet amphibolite) collected from the ophiolite along the Nan River. They concluded that the mafic rocks have calc-alkalic affinities rather than affinities with tholeiitic mid-ocean ridge basalts (herein MORB), and suggested that if the Nan Suture represents a geosuture, collision involved no significant overthrusting of the oceanic crust onto the Shan-Thai craton. Subsequently, Barr and MacDonald (1987) analysed a number of samples from the Doi Phuk Sung area (8 gabbroic samples) and from the Uttaradit area (2 basaltic and 5 gabbroic samples) and reinterpreted the mafic rocks in the Doi Phuk Sung, Nan River and Uttaradit regions of the Nan Suture as having formed by spreading processes above a subduction zone (i.e. in a back-arc basin). From this deduction, and the occurrence of blueschist in the Doi Phuk Sung area (Barr *et al.*, 1985), they argued that the Nan Suture represents the main suture zone between the Shan-Thai and Indochina cratons. Furthermore, on the basis of K-Ar age on actinolite from a greenschist (Phasom Group) from the Uttaradit area, they concluded that the minimum age of metamorphism (presumably collision-related) is 269±12 Ma (late Middle Permian-early Late Permian), although this conclusion is debatable.

1.2 Purpose of Study

In constructing the plate-tectonic evolution of any foldbelt, reliable data from many different branches of geology are needed. As outlined in Section 1.1, the plate-tectonic history of the collision of the Shan-Thai and Indochina cratons remain controversial. Detailed petrochemical study of the mafic-ultramafic rocks occurring within the Nan Suture Zone should provide important clues towards clarifying certain aspects and problems of the evolution of this region. So far, only very limited useful geochemical data are available (see above). Therefore, a geochemical study of the Nan Suture mafic-ultramafic rocks has been undertaken.

The main aim of this project was to study the occurrence, petrology and geochemistry of the meta-igneous rocks along the Nan Suture in order to determine tectonic settings of eruption of rock suites represented, and thereby clarify the sequence and timing of collisional events involved in production of this complex tectonic zone.

A planned complementary study of the regional structural-metamorphic history of this suture zone was unavoidably delayed several years and has only recently commenced (S. Singharajwarapan: Ph.D. programme, Univ. of Tasmania).

1.3 Field Relations

Field investigation and sampling was done in five key areas, namely the Mae Charim, the Doi Phuk Sung, the Nan River, the Sirikit Reservoir, and the Uttaradit areas (Fig. 1.2).

1.3.1 Mae Charim Area

In the Mae Charim area, due to guerilla and military activity, field work could only be done in a few very limited areas. Mafic-ultramafic rocks cropping out in this area comprise lava, tuff, volcanic breccia, isotropic gabbro, layered gabbro, amphibolite, garnet amphibolite, pyroxenite, chromitite, silicified serpentinite and serpentinised peridotite. Abundant float rocks collected from the Wa River (approximately 8 km south of Mae Charim) reveal that dolerite and microgabbro are also present. A float sample of quartz-garnet-white mica schist has been collected from the Tuang River (about 6.5 km east of Mae Charim). Contact relationships between these rocks could not be clearly ascertained due to the scarcity of outcrops and logistic problems. Where exposure is good, lavas are interbedded with marble, pillow breccia and strongly foliated tuff (greenschist); all dip around 25° W and are bounded by serpentinite containing small blocks (less than 20 cm across) of serpentinised

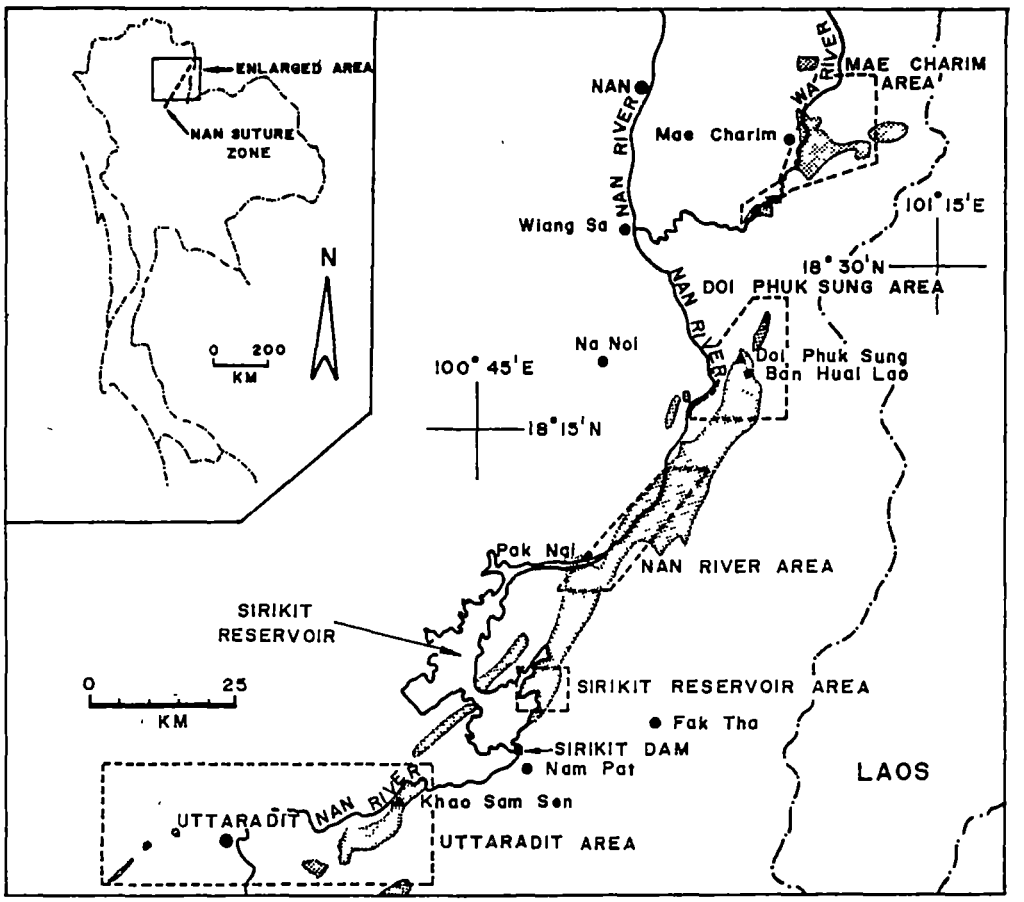

Figure 1.2. Simplified map showing distribution patterns of mafic-ultramafic rocks along the Nan Suture (compiled and modified from Thanasuthipitak,1978; Imjai *et al.*, 1986; Kleebai *et al.*, 1986; Plang *et al.*, 1986; Chaturongkawanich and Leewongcharoen, 1987; Lumjuan and Sinpoonanunt, 1987; Sukvattananunt and Assavapatchara, 1987; and Wannapeera and Kosuwan, 1987). Location of the Nan Suture is shown in the inset, and the investigated areas are bordered by dashed lines.

peridotite. Lavas were also found as rounded blocks with diameter less than 1 m across enclosed in foliated serpentinite. Mafic lavas exposed at the southwest tip of the area are amygdaloidal and fault juxtaposed against the Upper Triassic-Lower Jurassic molasse sequence (pre-Khorat correlates ?) (Hess and Koch, 1975; Sukvattananunt and Assavapatchara, 1987). This mafic-ultramafic body trends northeasterly into Laos.

Sedimentary sequences are not uncommon in the study region, but detailed investigation of these was not carried out. Consequently, discussion of the stratigraphic sequences in this area is based on the work of Wannapeera and Kosuwan (1987), who classified the sediments into Middle Permian, undifferentiated (Middle Permian-Triassic ?) and Mesozoic (Jurassic-Cretaceous) sequences. The Permian sequence is made up of greyish sandstone and shale in the lower parts but higher in the sequence is grey massive to thickly bedded limestone with Middle Permian fusulinids and algae. The undifferentiated sequence includes greyish and greenish micaceous sandstone with local limestone intercalations. These rocks in some domains are severely deformed greenschists and marbles. The Mesozoic sequence comprises reddish brown to purplish brown sandstone, and conglomerate with clasts of limestone, mafic volcanics, quartz, chert, shale and sandstone.

Field investigation in the present study has revealed that parts of the undifferentiated deformed sequence are tuffaceous sediment or tuff with marble intercalations, and are likely to be portions of the (broadly) ophiolitic volcanic sequence, since they are very similar in lithology and appearance to foliated tuffs which occur interbedded with lava, volcanic breccia and marble in the ophiolitic suite. Further evidence supporting this idea is that these highly schistose tuffs with intercalated marble appear to be enclosed in foliated serpentinite near the Wa River (about 4 km east of Mae Charim). An additional sedimentary sequence, of unknown age, present in this area is greenish grey sandstone interbedded with highly deformed conglomerate containing clasts of mafic volcanics.

1.3.2 Doi Phuk Sung Area

Reconnaissance mapping in the Doi Phuk Sung area was conducted by Barr *et al.* (1985), and later, detailed field mapping at a scale of 1:15,000 in this vicinity was done by students in the Department of Geological Sciences, Chiang Mai University under the author's supervision. The rocks in the Doi Phuk Sung area can be broadly subdivided structurally into two units, melange and non-melange. The rock sequences in the melange unit are chaotic in appearance, consisting of blocks of gabbro, dolerite/microgabbro, mafic lava, serpentinised peridotite, pyroxenite, silicified

serpentinite, chromitite, magnesite, plagiogranite, amphibolite, blueschist, actinolite schist, epidosite, pyroclastic rocks and various sedimentary rocks in a foliated serpentinite matrix. Relationships between blocks are not fully understood due to poor exposure. These blocks range in size from mesoscopic scale to almost 2 km across. The melange is therefore classified as serpentinite melange according to Cowan (1985). This melange zone trends approximately NE-SW.

The eastern margin of the melange unit is faulted against a Lower Jurassic-Lower Cretaceous molasse sequence (Khorat Group ?) (Hess and Koch, 1975; Sukvattananunt and Assavapatchara, 1987) that is made up of red conglomerate, red to green sandstone and green tuff. This sequence dips 50°-60° NW, and importantly, conglomerates contain gabbroic clasts.

The western edge of the melange unit is also faulted against a sedimentary sequence (dips 30°-60° SW), made up of greywacke, greyish black siltstone and shale, tuff, chert, limestone and chert laminite (made up of thin laminae of shale and chert), believed to be of Permo-Triassic age (Sukvattananunt and Assavapatchara, 1987). This sedimentary sequence and parts of the melange unit are overlain by the Lower Jurassic-Lower Cretaceous molasse sequence (Khorat Group ?), as indicated by an airborne magnetics survey (P. Kuttigul, pers. comm., 1987). Bedding planes, transposed layering, and fold axial planes in the western non-melange unit all dip westwards.

In the melange zone, gabbro/amphibolite and serpentinised peridotites are the dominant igneous lithology. Gabbros vary texturally, showing weak to pronounced foliation, and some are best defined as massive amphibolite (Ishizuka, 1987). Garnet amphibolite sporadically occurs between the gabbros/amphibolites, however, their relationships are unknown due to concealed contacts. Well-defined layers of pyroxenite approximately 1-2 cm thick occur locally in the gabbro/amphibolite and trend parallel to foliation. In addition to the massive amphibolite, banded layered amphibolite composed of plagioclase-rich and amphibole-rich bands is present in the melange zone. The gabbro/massive amphibolite has been invaded by dolerite/microgabbro and pegmatoid gabbro, whereas the banded amphibolite contains only pegmatoid gabbroic veins, which strike parallel to its foliation. The attitudes of foliation in these mafic rocks in different blocks are not consistent, as might be expected.

Blueschist blocks have been identified just south of Doi Phuk Sung. Some fine-grained blueschists are interlayered with quartzite, and typically show two sets of

lineations. Pyroclastic rocks include pillow breccia and tuff. Tuffs in the area northwest of Ban Huai Lao are cross-cut by plagiogranite dykes.

Metabasic lavas which are occasionally present occur either as isolated blocks or as lensoid masses in strongly deformed sedimentary strata. Outcrops of dolerites north of Doi Phuk Sung are faulted against Upper Triassic-Lower Jurassic molasse (Hess and Koch, 1975; Sukvattananunt and Assavapatchara, 1987). Dolerites in this region vary texturally from fine-grained aphyric to coarse-grained porphyritic rocks. At a road-cut approximately 8 km north-northeast of Ban Huai Lao, the coarse-grained to fine-grained dolerites occur together and show complicated relationships, suggestive of sheeted dykes.

Sedimentary rocks in the melange unit include varying proportions of chert, chert laminite, shale, sandstone, conglomerate and limestone. The sedimentary blocks show many deformation structures, including folds, cleavage, transposed layering, boudinage and mullion structures, and zones of cataclasis. In one sedimentary block in the southern portion of the Doi Phuk Sung area, slumped blocks of white, red and green chert, are enclosed in a green feldspathic greywacke (Fig. 1.3). The red chert contains radiolarias indicative of upper Middle Permian to lower Upper Permian (S. Hada, pers. comm., 1986) and provide a maximum age for the melange. The nature of the contact between one sedimentary block consisting of shale and sandstone, and serpentinite matrix is shown in Figure 1.4. Dolerite/microgabbro dykes intruding a sedimentary block made up of black shale interbedded with greywacke have been observed in the southern part of the Doi Phuk Sung area (Fig. 1.5).

The attitudes of foliation in the serpentinite matrix vary greatly. This might in part be due to cleavage wrapping around large blocks, as seen in some outcrops (Fig. 1.6). However, the majority of foliation trends are NE-SW, parallel to the strike of the mafic-ultramafic belt.

1.3.3 Nan River Area

According to MacDonald and Barr (1984), and Barr and MacDonald (1987), the mafic-ultramafic body along the Nan River is composed predominantly of gabbro, amphibolite (with sporadic plagiogranite dykes), and basaltic flows, tuffs and dykes with minor amounts of serpentinite, peridotite, hornblendite and pyroxenite, which crop out along the core of a major northeasterly-trending anticline. The mafic volcanics are interpreted to be underlain by gabbro and amphibolite but no contact between these units was observed. Barr and MacDonald (1987) indicated that ultramafic rocks occur in only two areas on the eastern margin of the mafic-ultramafic belt, possibly as fault-

(a)

(b)

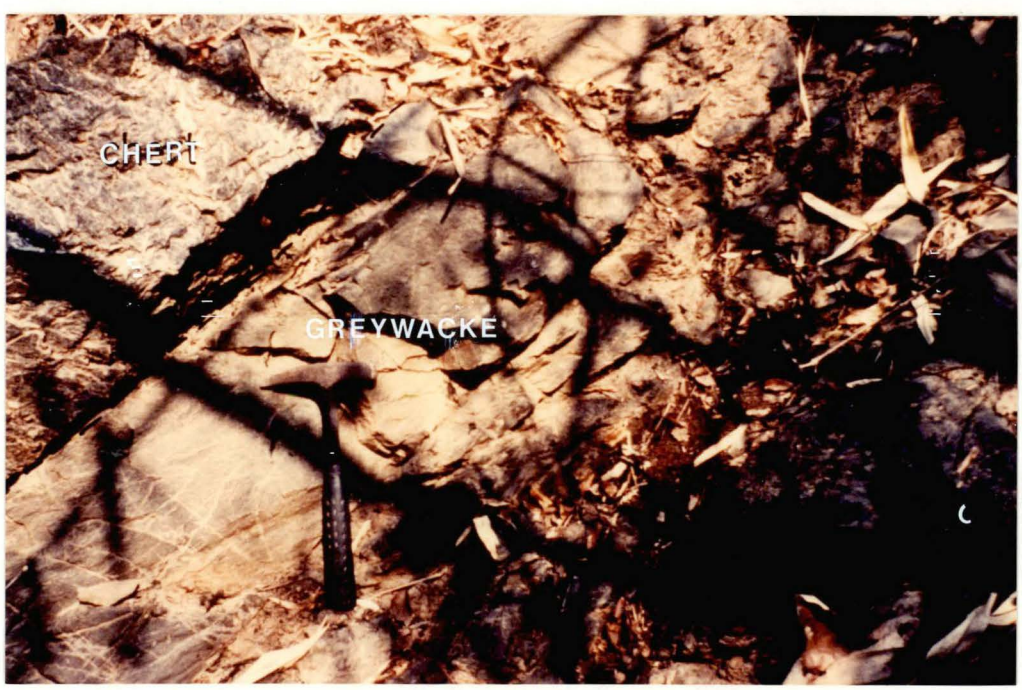

Figure 1.3. Slumped upper Middle to lower Upper Permian radiolarian chert blocks in green feldspathic greywacke approximately 7 km southwest of Ban Huai Lao (Doi Phuk Sung Area) showing (a) an irregular-shaped chert block and (b) the bedding plane of chert nearly perpendicular to the contact.

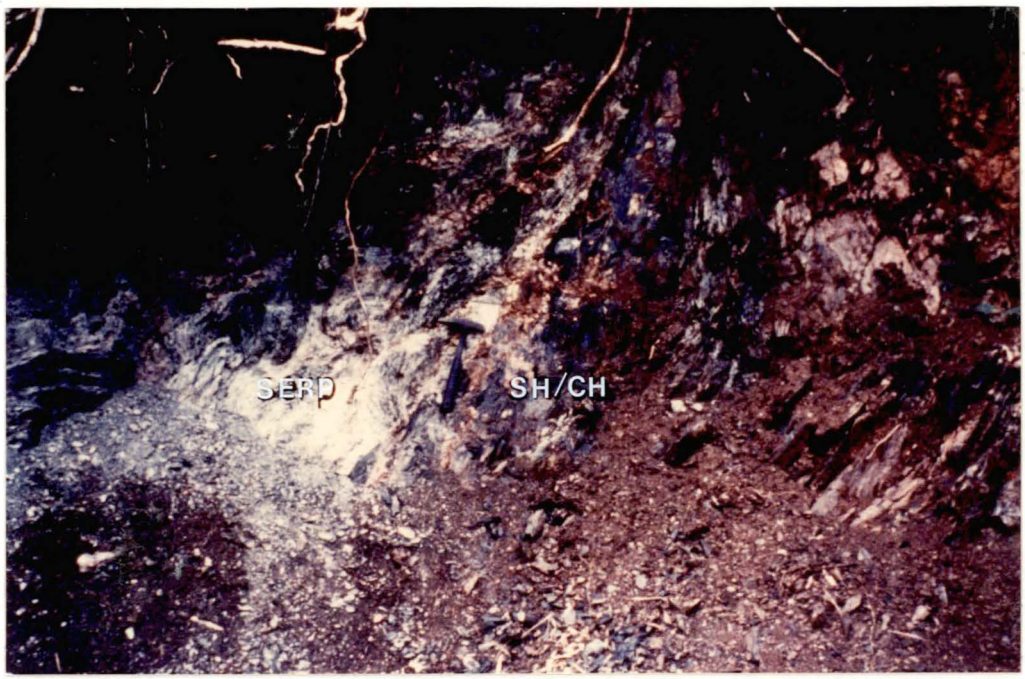

Figure 1.4. The nature of contact between serpentinite (SERP) and a sedimentary block made up of chert laminite (SH/CH) (see definition in the text) about 7 km southwest of Ban Huai Lao (Doi Phuk Sung area).

Figure 1.5. Dolerite (darker colour) intruding black shale (lighter colour) in the creek about 4 km SSW of Ban Huai Lao (Doi Phuk Sung area). The contact between the two contrasting rock types is shown by pens.

Figure 1.6. Different-sized serpentinised peridotite blocks in serpentinite matrix in Huai Nam Khang approximately 2 km SW of Ban Huai Lao (Doi Phuk Sung area).

bounded lenses. Field observations made in the present study in the Nan River area suggest that ultramafic rocks, in fact, are present at many localities, mainly as blocks enclosed in foliated serpentinite. Outcrops of mafic lavas are scarce but mafic lavas occurring as float in many localities, probably have been eroded from the serpentinite melange. Outcrops of mafic lavas at some localities in Huai Luang (approximately 7 km northeast of Pak Nai) have intercalated pillow breccia, and clearly occur as blocks (up to 10 m across) embedded in serpentinite matrix. It is probable that detailed field mapping along the Nan River will show similar relationships (i.e. blocks in melange) to those mapped in the Doi Phuk Sung area. The dominant mafic-ultramafic rock in this area is layered gabbro/banded amphibolite (Fig. 1.7) and serpentinised ultramafic rock.

1.3.4 Sirikit Reservoir Area

The rocks in this area are made up of manganiferous schists, serpentinite, silicified serpentinite, serpentinised peridotite, pyroxenite, layered gabbro/amphibolite and mafic lavas. Field relations among these diverse rock types could not be ascertained due to the scarcity of rock exposures; only outcrops of cumulus gabbro/ amphibolite with foliation trending N 45° E were observed.

1.3.5 Uttaradit Area

Detailed field mapping in the Uttaradit area was done by students in the Department of Geological Sciences, Chiang Mai University, and a map has been compiled by Thanasuthipitak (1978). The fault-bounded mafic-ultramafic rock sections in this region (up to 20 km long) includes discrete blocks of mafic lava, tuff and agglomerate, chert, gabbro, amphibolite, peridotite, pyroxenite and dolerite, similar in lithology to those in the Doi Phuk Sung arca. The best outcrops of these rocks are located around Khao Sam Sen, but outcrops of lava and tuff are widely scattered and poorly exposed throughout the area. As evident from Khao Sam Sen, the distribution of lithologies including chert blocks up to 30 m across, again, indicates a melange. Gabbro/massive amphibolite and banded amphibolite are cross-cut by dolerite/ microgabbro and tonalite.

1.4 Constraints on Timing of Magmatism and Continental Collision

It is clear that the Nan Suture is a very complex melange zone containing abundant mafic-ultramafic blocks, as might be expected in a continental collision zone. Timing of magmatism and collision can be deduced from the following facts:

(a)

(b)

Figure 1.7. Cumulus gabbro/banded amphibolite in Huai Pang Noi approximately 21 km NE of Pak Nai (Nan River area) showing (a) transposed compositional banding (the darker and the lighter layers are rich in amphibole and plagioclase, respectively) and (b) a pegmatoid gabbro vein which has the same foliation trend as its country rock.

1. The presence of upper Middle Permian-lower Upper Permian radiolarians in slumped cherts in a greywacke block, and the existence of gabbroic clasts in a Lower Jurassic to Lower Cretaceous conglomerate (Doi Phuk Sung area) constrain the emplacement of the mafic-ultramafic rocks sometime between late Middle Permian and Early Cretaceous.

2. On the basis of surface and subsurface (seismic and rocks penetrated into petroleum exploration wells) data from northeastern Thailand (poorly understood Loei Foldbelt and Indochina craton, east of the Nan Suture), highly deformed Permian strata (carbonates and clastics) are overlain by extensive Middle to Upper Triassic clastics (molasse) from less than 300 m to over 3,000 m thick. Seismic profiles show that these Triassic strata were deposited in half-graben basins believed to be produced during post-collisional extension (Cooper *et al.*, 1989; Sattayarak *et al.*, 1989). This indicates that the continental collision took place in Permo-Triassic time.

3. In the Wang Chin and Sop Prap areas (parts of poorly understood Sukhothai Foldbelt, west of the Nan Suture), the Triassic Lampang Group is notably less intensely folded relative to adjacent Palaeozoic sequences (Silurian to Early Carboniferous, Permo-Carboniferous and Middle to Late Permian)(Wolfart, 1987). Also mentioned by Bristow (1990), major compressional tectonic activity probably occurred in the Middle to Late Permian. For example, in the region located east of the southern unexposed continuation of the Nan Suture (in the Loei Foldbelt), Upper Carboniferous (?) to Middle Permian pelagics (mainly chert, shale and limestone) and a middle Middle Permian (greywacke-shale) succession are unconformably overlain by upper Middle Permian molasse (sandstone and shale with limestone intercalations in the upper parts)(Helmcke and Kraikhong, 1982; Helmcke and Lindenberg, 1983; Helmcke, 1985, 1986). This indicates that the first stages of collision of arc/continental margin components of the Shan-Thai and Indochina cratons may have occurred in late Middle to early Late Permian.

4. The existence of Permo-Carboniferous fossils in calcareous matrix of a volcanic breccia (between Doi Phuk Sung and Nan River areas) (Hahn,1985) implies that the volcanic fragments and their matrix are synchronous or that the volcanic rock is older than Permo-Carboniferous (Hahn *et al.*,1986). The intercalation of limestone, tuff, volcanic breccia and mafic lava in the Mae Charim area seems to support the former interpretation, i.e. the lava is Permo-Carboniferous in age.

5. The K-Ar age obtained from actinolite (0.34 % K) from a greenschist from the Pha Som Group (Uttaradit area), which is spatially related to the mafic-ultramafic belt, is 269 ± 12 Ma (late Middle Permian - early Late Permian)(Barr and MacDonald, 1987).

The Pha Som Group is interpreted as a dominantly sedimentary sequence deposited on the inner slope of an active trench in Siluro-Devonian time (Bunopas, 1981), and this date may accurately record metamorphism accompanying (one stage of) ophiolite emplacement.

6. The recognition of Middle Triassic radiolarian chert blocks in serpentinite matrix in southeastern Thailand and radiolarian chert clasts of the same age in a Lower Jurassic to Lower Cretaceous conglomerate which unconformably overlies serpentinite in the Nan Suture indicates that subduction was still active in the Middle Triassic (S. Hada, pers. comm., 1990).

Collisions leading to final continent-continent suturing appear to have started from Middle Permian time. Eventual suturing of the two cratons (continental collision), probably in Late Triassic, would likely have been preceded by collision of at least one arc with a passive continental margin. More detailed and well-constrained Ar-Ar dating needs to be performed to accurately date the emplacement of the ophiolite.

1.5 Summary

Preliminary mapping and sampling indicates that the Nan Suture is a complex belt comprising mainly serpentinite melange with blocks up to 2 km across. Diverse igneous-dominated lithologies make up the majority of the blocks, and blueschists are recorded. Available evidence based largely on regional geological information and a single K-Ar date suggest that the Nan Suture probably formed by Middle Permian to Late Triassic collision between the Shan-Thai and Indochina cratons. The aim of this study is to thoroughly document the petrology and geochemistry of the igneous rocks in the Nan Suture to determine their tectonic settings of eruption and further constrain models for the geological evolution of this complex and poorly-known region.

CHAPTER 2

SAMPLE SELECTION, ANALYSIS AND COMPOSITIONAL GROUPINGS

2.1 Textural and Mineralogical Classifications

The meta-igneous rocks discussed in this study are texturally and mineralogically grouped into lavas, dolerites, microgabbros, gabbros/amphibolites and ultramafic rocks. The lavas are defined as very fine-grained rocks with or without glass whereas the dolerites show doleritic textures and microgabbros, fine grainsizes but are devoid of interstitial glass.

The gabbros in this account are fine- to coarse-grained basic rocks and may show prominent cumulus texture. Fine-grained gabbros are differentiated from the microgabbros in having cumulus textures. These gabbros have suffered variable degrees of deformation and metamorphism as evidenced by their weak to pronounced foliation, and some are best defined as massive and banded amphibolites (Ishizuka, 1987). A mineralogical and textural continuum exists between the amphibolites and the gabbros; therefore, they are grouped and discussed together.

The ultramafic rocks are separated following the modal classification scheme recommended by the IUGS Subcomission, i.e. in having mafic minerals greater than 90% (Streckeisen, 1976). These include websterite, clinopyroxenite, olivine clinopyroxenite, wehrlite, harzburgite, dunite and chromitite.

In addition to the meta-igneous rocks, the studied samples include blueschist.

2.2 Chemical Groupings

2.2.1 Methods

Whole-rock analyses were performed on lavas, dolerites and microgabbros to gain compositional data which could provide information about their tectonic setting of formation. These samples were carefully selected to avoid, in general, rocks showing

(1) extensive development of mesoscopic domains of secondary minerals such as epidote, albite, chlorite or amphibole
(2) a well-developed foliation or mineral layering
(3) abundant amygdale minerals

(4) quartz, epidote or calcite veining or patches totalling more than approximately 5 modal%.

Occasional samples had somewhat more than 5 modal% calcite and showed pronounced foliation but were included in this study in the absence of better-preserved rocks from that particular area. In addition, several layered gabbros and amphibolites were also analysed for major and trace elements. Accordingly, seventy-eight least altered samples were analysed for major elements (Si, Al, Fe, Mg, Ca, Na, K, Ti, P, Mn and ignition loss) and a range of trace elements (Nb, Zr, Y, Sr, Rb, Ni, Cr, V, Ba and Sc); thirty three of these were analysed for rare-earth elements (herein REE: La, Ce, Pr, Nd, Sm, Eu, Gd, Dy, Er and Yb).

The selected samples were prepared for analysis by firstly splitting into pea-sized fragments using a hydraulic splitter, and discarding chips with weathered surfaces. The fragments were then crushed with a steel jaw crusher and cleaned with an airhose; 30-50 g aliquots of the crushed fragments showing no signs of oxidation surfaces, vein and amygdale minerals or steel smeared from the jaw crusher were ground for a few minutes in a tungsten-carbide Tema swing mill.

Analytical work was carried out in the Geology Department, University of Tasmania. All analyses, except for ignition loss, were obtained using an automated Philips PW1410 X-ray fluorescence (XRF) spectrometer. Major elements were measured from fusion discs prepared with 1.5 g lithium borate flux, 0.02 g lithium nitrate and 0.28 g sample powder. Trace elements were determined on pressed powder pills backed by boric acid. Mass absorption coefficients calculated from major-element compositions were used for the determinations of trace elements. The analytical methods for major- and trace-elements are outlined in Norrish and Hutton (1969) and Norrish and Chappel (1967). All major-element analyses were recalculated to 100% total on a volatile-free basis to minimise dilution effects of metamorphic hydration and for comparative purpose. However, measured ignition losses are reported for each sample analysed.

REE analyses for each sample analysed were done via a combined ion exchange - XRF technique described by Robinson *et al.* (1986). Samples are decomposed using a sodium peroxide sinter, followed by a two-stage ion-exchange procedure using hydrochloric and nitric acids; REE are adsorbed on ion-exchange papers for XRF analysis. The precision for La, Ce, Pr, Nd, Sm, Gd and Dy is 1-4% whereas that for Eu, Er and Yb is more variable (4-13% for Eu, 2-7% for Er, and 2-5% for Yb) because of their relatively low abundances. The accuracy of this method is considered to be better than for instrumental neutron activation analysis (INAA).

Ignition loss was gravimetrically determined by heating approximately 1 g of sample at 1,000 °C for 12 hours.

2.2.2 Alteration

All the rocks studied in this project are low- to medium-grade metamorphic rocks, and therefore their present compositions are unlikely to be primary. However, it has been well documented that carefully selected samples of greenstones can be informative with regards to their primary affinities if due care is taken with the selection of elements and element ratios used in the diagnosis.

Major elements are useful when cautiously interpreted, although the frequent occurrence in greenstone terrains of veins and localisations of calcite, quartz, albite, sericite and to a lesser extent epidote, indicate significant addition/subtraction of Si, Ca and the alkalis during element redistribution in the greenstone pile. However, it is generally agreed that total iron and MgO are little removed from primary values, and may be used as an indicator of fractionation in any greenstone suite in terms of either total iron as FeO (herein FeO*)/MgO (Miyashiro, 1973, 1975a, 1975b, 1975c; Beccaluva *et al.*, 1979; Grenne and Roberts, 1980; Crawford and Keays, 1987; Hawkins and Evans, 1983) or FeO*/(FeO*+MgO)(Serri, 1981; Ivanov *et al.*, 1987; Brouxel and Lapierre, 1988).

Following the early work of Cann (1970), numerous studies have shown that especially the high field strength elements (herein HFSE) Ti, Zr, Y, Nb and P, and also the transitional elements Ni, Cr, V and Sc remain relatively immobile during the alteration and low-grade metamorphism of basaltic and more evolved lavas and intrusives (Pearce and Cann, 1973; Pearce *et al.*, 1975; Coish, 1977; Floyd and Winchester, 1975; Winchester and Floyd, 1977; Shervais, 1982; Holm, 1985). In addition, although occasional reports have appeared of REE-, especially light REE (herein LREE), mobility during hydrothermal alteration and low-grade metamorphism (Frey *et al.*, 1974, Humphris *et al.*, 1978; Floyd, 1977; Hellman and Anderson, 1979; Whitford *et al.*, 1988), the overwhelming consensus of opinion is that the REE patterns of carefully selected greenstones are probably little removed from their primary patterns. Limited LREE mobility or parallel dilution/enrichment (upward and downward) trends of REE patterns are certainly unlikely to lead to a different petrogenetic interpretation than that gleaned from primary patterns (see Whitford *et al.*, 1988), had they been available. Therefore, in attempting to determine the geochemical affinities and tectonic significance of the meta-igneous suites occurring

within the Nan Suture, concentration has focussed on the relatively immobile elements, namely the HFSE, REE and transition elements Ni, Cr, V and Sc.

2.2.3 Magmatic Groups

The analysed samples show a wide compositional range, and therefore, chemical grouping is necessary. Rocks used for defining (magmatic) groups include only lavas, dolerites and microgabbros, to avoid ambiguities involved in comparing crystal cumulates (gabbros) with liquid or near-liquid compositions (lavas, dolerites and microgabbros). Consideration of the compositional data shows that three major magmatic groups, namely ocean-island basalts (Group A), backarc basin suites (Group B), and arc suites (Group C), are represented.

Rocks classified as Group A are differentiated from those of other groups by their higher Nb/Y, Ti/Y and Ni contents at similar levels of MgO, and lower Zr/Nb values. Group B samples show variable geochemical characteristics; all have similar Y, but lower TiO_2 and Nb contents relative to Group A samples. Rocks categorised as Group C are characterised by relatively low values of HFSE. These groups are discussed separately in the following Chapters.

2.3 Mineral Analysis

Extensive mineral analyses were carried out on a wide variety of relict igneous and metamorphic minerals, including clinopyroxene, orthopyroxene, olivine, spinel, garnet and amphiboles. However, only informative minerals are reported.

Analytical work was done by an energy dispersive analytical system attached to a JEOL JXA-50A scanning electron microprobe in the Central Science Laboratory at the University of Tasmania. The beam current used was 7×10^{-10} amperes at 15 kV. Spectra between 0 and 20 keV were counted for 60 seconds and data reduction was done on-line by a computer program TAS-SUEDS (Griffin, 1979).

2.4 Presentation Layout

In the Nan Suture, igneous rocks occur as blocks from pea- to 2 km-sizes, chaotically distributed through a foliated serpentinite matrix. No direct age relationship data between magmatic groups is available, and therefore, for the sake of convenience, the rocks in each compositional group are discussed separately in the following Chapters:

Chapter 3 - Ocean-island Basaltic Suites (Group A)
Chapter 4 - Backarc Basin Suites (Group B)
Chapter 5 - Arc Suites (Group C)
Chapter 6 - Petrology and Mineral Chemistry of Plutonic and Significant Metamorphic Rocks
Chapter 7 - Implications for Plate Tectonic Models

The discussion in each chapter will cover subdivision, field occurrence, petrography, mineral chemistry, and where data are available, whole-rock chemistry, P-T condition of formation and tectonic setting of formation.

CHAPTER 3

OCEAN-ISLAND BASALTIC SUITES (GROUP A)

3.1 General Chemical Characteristics

All Group A samples have basaltic compositions as indicated both by their major element compositions (Tables 3.1 and 3.2) and by their positions on the least mobile-element variation diagrams Zr/TiO_2-Nb/Y (Fig. 3.1). Although SiO_2 is generally regarded as somewhat mobile, their SiO_2 contents (46-52 wt%) also lie well within a range of world-wide unaltered basalts. In terms of relatively immobile elements, these basaltic rocks are characterised by moderately high to high concentrations of TiO_2 (1.4-4.4 wt%), Nb (7-41 ppm), Zr (78-313 ppm) and Y (18-50 ppm). These HFSE abundances partly overlap those of the other groups; however, when immobile-element ratios are taken into consideration, Group A rocks are clearly differentiated by their higher Nb/Y (>0.34) (Figs. 3.1 and 3.2) and Ti/Y (>420) (Fig. 3.2), and lower Zr/Nb (8-15) (Fig. 3.3). In addition, they have higher Ni contents (38-732 ppm) at similar values for MgO (Fig. 3.4).

The Group A basaltic rocks may be further chemically subdivided into tholeiites (Subgroup A-1), and transitional tholeiites and alkalic basalts (Subgroup A-2).

3.2 Ocean-island Tholeiitic Basalts (Subgroup A-1)

3.2.1 Occurrence and Petrography

The sixteen whole-rock analysed samples constituting Subgroup A-1 include lavas (14 samples) and dolerites (2 samples) collected from both outcrops and float in the Mae Charim, Doi Phuk Sung, Nan River and Uttaradit areas. In the Mae Charim and Nan River areas, they evidently occur as different-sized blocks up to 10 m across in serpentinite matrix. Rocks intercalated with the lavas of this subgroup in many blocks include volcanic breccia (Mae Charim and Nan River areas), tuff (Mae Charim area) and marble (Mae Charim area). In the Doi Phuk Sung area, field relations of the whole-rock analysed samples are uncertain, but an unanalysed lava sample, inferred to be Subgroup A-1 by spinel composition (see Section 3.2.2), occurs as lensoid masses in highly deformed metasedimentary rock (? tuff). Float of Subgroup A-1 lava in the Uttaradit area also occurs together with float of tuff and agglomerate. Sample locations of the analysed samples are given in Table I-1 (Appendix I).

TABLE 3.1. WHOLEROCK XRF ANALYSES AND SOME SELECTED RATIOS OF THE STUDIED OCEAN-ISLAND THOLEIITIC LAVAS AND DOLERITES (SUBGROUP A-1); MAJOR ELEMENTS ARE NORMALISED TO 100% ON THE BASIS OF LOSS ON IGNITION FREE

Sample no.	56.3	1.26	56.1	68	50.2	1.18	C[1]	1.7	1.30	1.31	1.17[1]	1.3	1.6	1.4	1.15	B
SiO2	51.48	49.71	52.11	48.88	51.77	47.32	51.02	49.03	46 42	47.64	50.47	48.75	50.13	49.21	51.45	51.13
TiO2	1.73	1.80	1.89	1.36	1.93	1.95	1.67	1.65	1.94	2.46	2.03	2.39	2.19	2.32	1.84	1.68
Al2O3	10.99	12.86	11.73	18.11	13.14	17.26	17.03	17.52	16.89	15.46	14.83	14.63	15.99	16.99	13.85	16.54
FeO*	11.23	11.77	10.94	8.40	10.67	10.08	10.74	8.94	10.31	11.75	11.65	12.02	10.02	11.02	11.04	11.88
MnO	0.16	0.18	0.17	0.14	0.21	0.17	0.15	0.17	0.16	0.16	0.18	0.18	0.15	0.16	0.16	0.17
MgO	12.64	11.51	10.18	7 05	8.30	7 82	8.22	6.83	7 28	7.42	7.30	7.00	5.78	6.27	6.16	6.37
CaO	7.99	9.33	8.50	11.91	8.82	12.07	6.43	11.87	13.10	11.43	8.95	11.65	11.09	9.14	11.14	6.86
Na2O	3.41	2.42	3.24	2.82	4.77	2.89	4.40	2.91	2.78	2.95	4.05	2.78	3.60	4.24	4 00	5.13
K2O	0.21	0.22	1 04	1.18	0.21	0.21	0.21	0.88	0.92	0.45	0.34	0.30	0.80	0.37	0.11	0.05
P2O5	0.17	0.20	0.20	0.16	0.19	0.23	0.14	0.20	0.21	0.27	0.21	0.30	0.25	0.29	0.25	0.19
LOI	3.27	3.33	2 42	2.99	2.70	4.02	4.10	3.30	3.41	3.39	3.55	3.38	2.28	3.20	2.57	3.56
FeO*/MgO	0.89	1.02	1.08	1.19	1.29	1.29	1.31	1.31	1.42	1.58	1.60	1.72	1.73	1.76	1.79	1.87
Nb	8	9	10	7	9	9	8	8	9	12	10	11	12	13	9	9
Zr	101	119	115	78	114	116	84	102	121	148	115	146	142	154	110	97
Y	22	22	23	18	26	23	23	21	24	29	23	30	26	27	25	24
Sr	64	46	78	1081	140	85	99	596	494	115	208	118	802	264	211	87
Rb	<2	4	20	15	3	4	5	14	19	8	2	3	15	5	1	<1
Ni	732	338	441	148	281	93	126	93	95	89	71	82	51	58	92	110
Cr	942	714	883	530	769	278	318	310	374	205	119	168	94	113	255	391
V	223	261	236	215	277	273	218	235	286	333	289	310	290	304	296	229
Ba	26	66	69	155	65	96	33	131	135	105	99	90	154	116	61	48
Sc	24	30	26	31	32	38	30	32	40	41	36	37	32	34	34	28
Ti/Zr	103	91	99	105	101	101	119	97	96	100	106	98	92	90	100	104
Zr/Nb	13	13	12	11	13	13	11	13	13	12	12	13	12	12	12	11
Zr/Y	4.6	5.4	5	4.3	4.4	5	3.7	4.9	5	5.1	5	4.9	5 5	5.7	4.4	4
Y/Nb	2.8	2.4	2.3	2.6	2.9	2.6	2.9	2 6	2.7	2.4	2.3	2.7	2 2	2.1	2.8	2.7

[1] = DOLERITE, FeO* = TOTAL IRON AS FeO, LOI = LOSS ON IGNITION.

TABLE 3.2. WHOLEROCK XRF ANALYSES AND SOME SELECTED RATIOS OF THE STUDIED OCEAN-ISLAND TRANSITIONAL THOLEIITIC AND ALKALIC BASALTS (SUBGROUP A-2); MAJOR ELEMENTS ARE NORMALISED TO 100% ON THE BASIS OF LOSS ON IGNITION FREE

Sample no.	27.7	27 1	27.3	28 8	28.2	36.1	27.4	28.6	27.6	28.4	36.3	1.25[1]
SiO2	50.10	49.75	48.80	48.60	48.66	50.04	49.18	47.46	49.43	51.36	51.47	48 25
TiO2	3.26	2.92	3.55	4.01	4.03	3.21	4.45	3.40	4.28	3.19	4.31	3 79
Al2O3	14.52	16.61	14.66	15.20	15.43	16.36	13.76	15.30	13.46	14.94	13.50	13.93
FeO*	12 53	10.70	11.95	12.82	12.50	10.89	13.48	13.91	13.81	11.83	11.95	15.05
MnO	0.14	0.16	0.15	0.16	0.15	0.13	0.21	0.19	0.19	0.13	0.13	0.19
MgO	8.64	6.77	7.24	7.34	7.12	5.55	6.54	6.41	6.30	5.39	5.26	5.40
CaO	7.35	9.07	9 06	6.33	6.69	9.05	7.76	9.19	7.49	7.71	7.87	8.78
Na2O	2.90	3 49	3.69	4.64	4.55	3.84	2.87	2.91	3.56	3.42	4.57	3.68
K2O	0 09	0.06	0.40	0.07	0.07	0.48	0.95	0.75	0.61	1.60	0.46	0.34
P2O5	0.47	0.47	0.51	0.81	0.78	0.45	0.81	0.49	0.86	0 44	0.47	0.59
LOI	4.96	4.20	3.71	4.04	3.97	3.58	3.61	4 05	3.15	3.08	2.27	2.88
FeO*/MgO	1.45	1.58	1.65	1.75	1.76	1.96	2.06	2.17	2.19	2.20	2.27	2.79
Nb	25	27	30	35	37	28	39	26	41	24	37	23
Zr	220	206	284	265	284	227	302	240	313	233	308	269
Y	30	31	37	38	40	32	48	35	50	35	40	46
Sr	184	138	281	120	136	203	267	182	270	394	101	138
Rb	2	2	6	3	2	10	14	25	10	61	9	3
Ni	257	149	79	88	92	82	57	123	39	104	40	38
Cr	265	189	147	81	87	160	28	206	10	170	22	8
V	195	180	266	273	279	211	320	238	310	215	294	375
Ba	45	42	92	70	72	156	152	138	334	193	147	212
Sc	17	19	24	20	20	20	24	24	24	17	27	29
Ti/Zr	89	85	75	91	85	85	88	85	82	82	84	118
Zr/Nb	9	8	9	8	8	8	8	9	8	10	8	15
Zr/Y	7.3	6.6	7.7	7	7.1	7.1	6.3	6.9	6.3	6.7	7.7	6.6
Y/Nb	1.2	1 1	1.2	1.1	1.1	1.1	1.2	1.3	1 2	1.5	1.1	2.3

[1] = LAVA, FeO* = TOTAL IRON AS FeO, LOI = LOSS ON IGNITION.

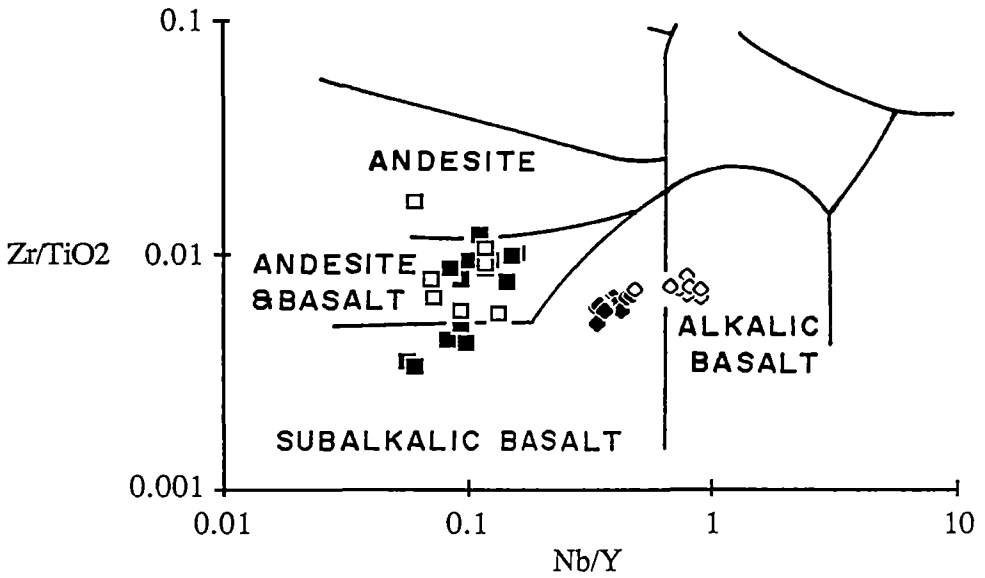

Figure 3.1. Plot of Zr/TiO_2 against Nb/Y for the analysed lavas, dolerites and micro-gabbros, excluding analyses with Nb content less than 2 ppm (close to the detection limit determined by XRF). Field boundaries for different magma types are taken from Winchester and Floyd (1977). Symbols are as follows: diamond, Group A (solid, Subgroup A-1; open, Subgroup A-2), solid square, Group B; and open square, Group C.

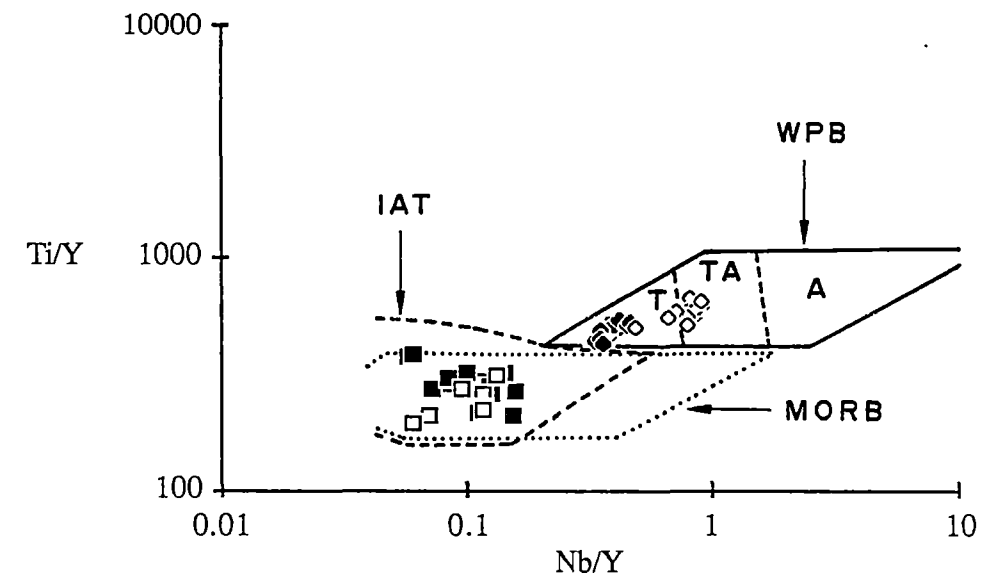

Figure 3.2. Distribution of data points for Groups A, B and C samples (symbols as in Fig. 3.1) on Ti/Y - Nb/Y tectonomagmatic discrimination diagram of Pearce (1982). Data with Nb content less than 2 ppm (close to the detection limit determined by XRF) are excluded. WPB=within-plate basalts (T=tholeiites, TA=transitional tholeiites, A=alkalic basalts), MORB=mid-ocean ridge basalts, VAB=volcanic arc basalts.

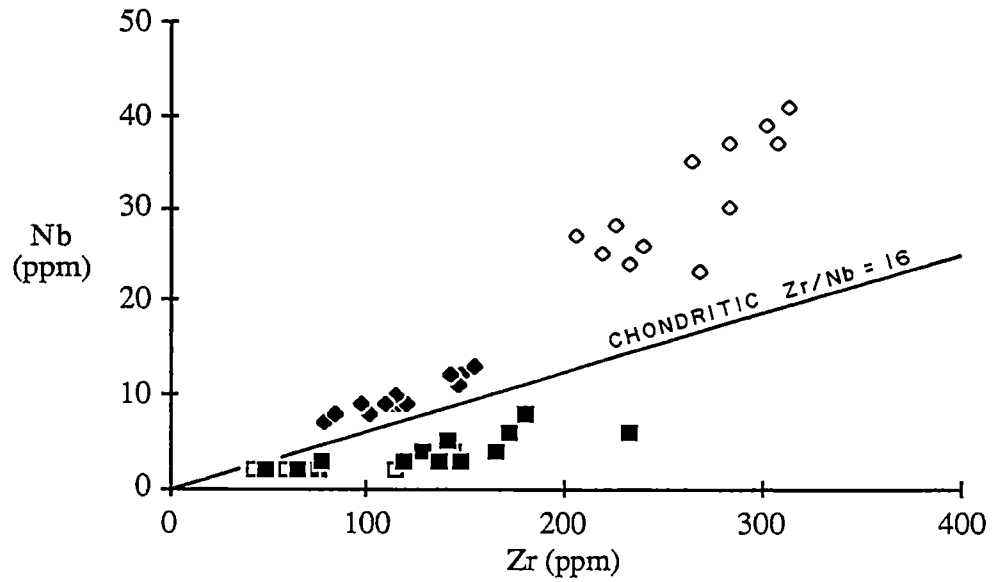

Figure 3.3. Variation of Nb relative to Zr for the analysed lavas, dolerites and micro-gabbros, except for samples for which their Nb concentrations are below 2 ppm (close to the detection limit determined by XRF)(symbols as in Fig. 3.1). Note that Group A rock samples are clearly separated from the others and that samples of Subgroups A-1 and A-2 are different in Zr/Nb (see text for discussion). The chondritic Zr/Nb value is taken from Nesbitt and Sun (1976).

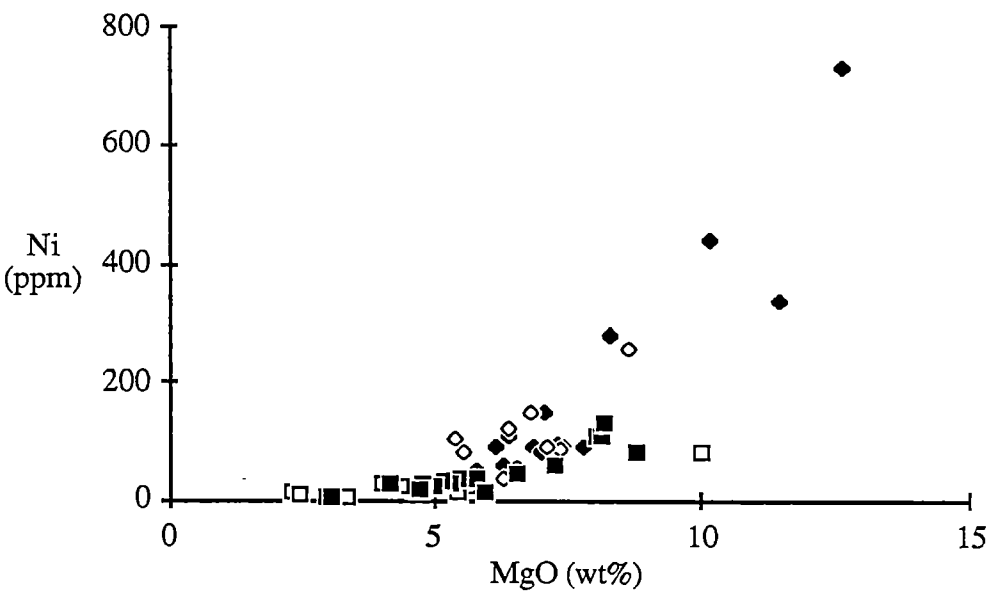

Figure 3.4. Ni against MgO variation diagram for all the analysed samples showing the slightly higher Ni concentration of Group A samples relative to Group B and C samples (symbols as in Fig. 3.1).

Petrography of lavas

The lavas of Subgroup A-1 show a variety of textures ranging from vitrophyric (Fig. 3.5) to porphyritic/microporphyritic (Fig. 3.6) with fine-grained groundmass (<1 mm across). They contain variable amounts and sizes of phenocryst/ microphenocryst minerals including the assemblages olivine, olivine + spinel, plagioclase + colourless clinopyroxene, and plagioclase + colourless clinopyroxene + chrome-spinel + Fe-Ti oxide minerals. Olivine, clinopyroxene and plagioclase phenocrysts and microphenocrysts are occasionally glomerocrystic; some of them exhibit disequilibrium phenomena as indicated by their rounded edges, embayment features and devitrified groundmass inclusions (Fig. 3.7). The glassy groundmass is composed largely of dark brown altered glass, and quenched plagioclase laths arranged in stellate and variolitic aggregates (Fig. 3.5), whereas the intergranular groundmass is made up largely of felted plagioclase laths, and intergranular colourless clinopyroxenes (Fig. 3.6). Vesicles infilled with quartz, chlorite, epidote, calcite and pumpellyite are occasionally present in a few samples. Veinlets with any of quartz, chlorite, epidote, bluish amphibole, stilpnomelane, zoisite, clinozoisite, pumpellyite, Fe sulphide and Fe-Ti oxide infillings are also present in many samples. The metamorphic assemblage is typical of very low- to low-grade metamorphic rocks of regional metamorphism. Petrographic features of individual samples are presented in Table II-1 (Appendix II).

Olivine occurs only as an euhedral to subhedral phenocryst/microphenocryst phase, and always totally pseudomorphed by serpentinite/chlorite minerals (Figs. 3.5 and 3.6) with sparse Fe-Ti oxides, Fe sulphides and pale actinolitic amphiboles. When they coexist with plagioclase and pyroxene microphenocrysts/phenocrysts, they are the least abundant microphenocryst/phenocryst phases. A few olivine microphenocrysts/ phenocrysts contain spinel inclusions (Fig. 3.6).

Pyroxene phenocrysts and microphenocrysts are euhedral to subhedral, and often show sector zoning. When altered, they are pale brown (?amphibole) and are partially replaced by chlorite along fractures, and tiny blue amphibole crystals have grown along some cracks.

Plagioclase, both as phenocryst and microphenocryst phases, usually exhibits subhedral to anhedral outlines and is always albitised. Its alteration products include chlorite, epidote, pumpellyite and indeterminate dark brown clayey minerals.

Chrome-spinels are subhedral to anhedral, and occur either as inclusions in olivines or as discrete small crystals outside olivine grains. Fe-Ti oxide

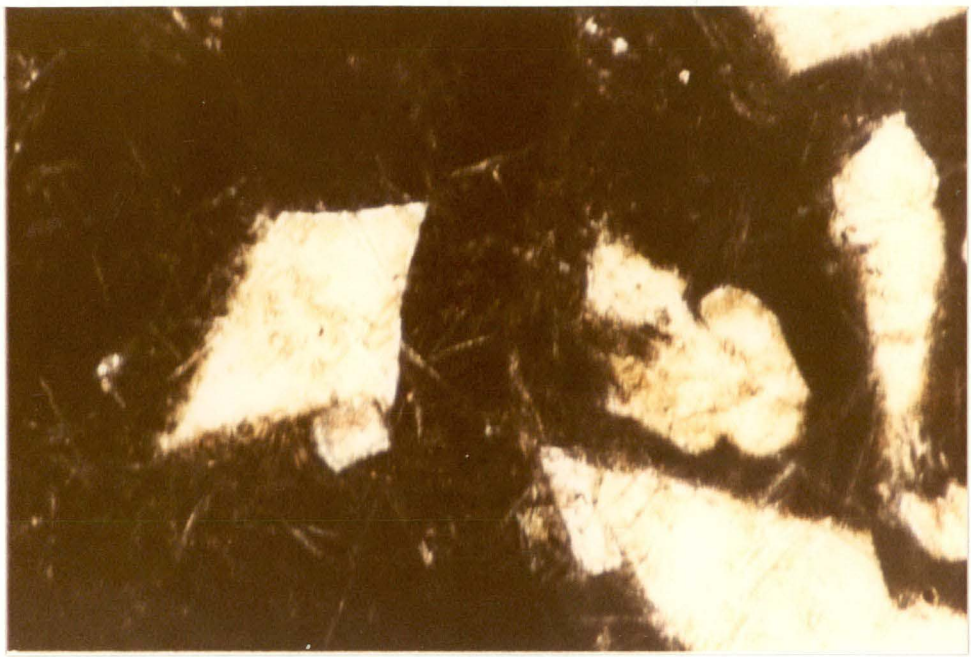

Figure 3.5. Photomicrograph of the studied ocean-island tholeiitic lava (Subgroup A-1)(sample 56.3) showing altered olivine microphenocrysts and glassy groundmass made up largely of dark brown glass, and stellate and variolitic aggregates of quenched plagioclase crystals. Ordinary light, X 65.

Figure.3.6. Photomicrograph of the studied ocean-island tholeiitic lava (Subgroup A-1)(sample 56.1) illustrating corroded olivine phenocrysts (pseudomorphed by chlorite/serpentine) with chromite inclusions (black spots). Microcrystalline groundmass is made up chiefly of albitised plagioclases and clinopyroxenes. Ordinary light, X 65.

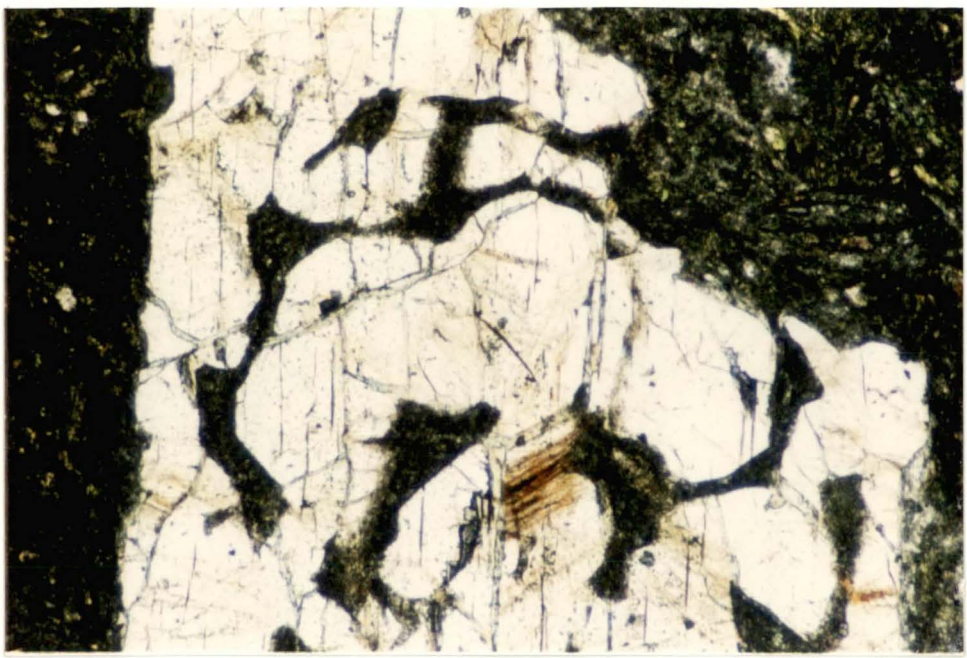

Figure 3.7. Photomicrograph of the studied ocean-island tholeiitic lava (Subgroup A-1)(sample 1.30) showing disequilibrium features of a clinopyroxene phenocryst. Ordinary light, X 65.

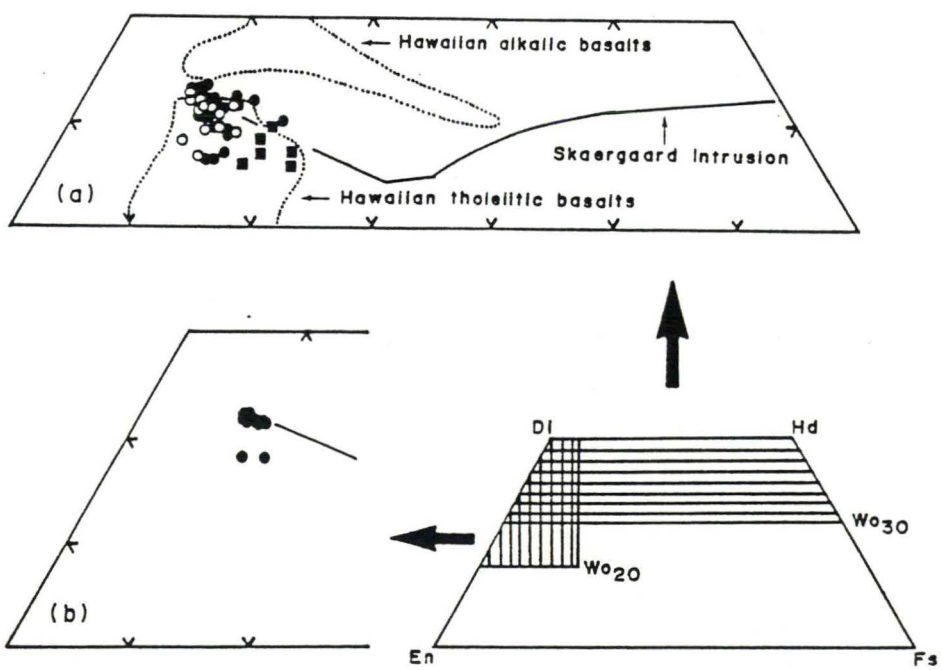

Figure 3.8. Compositions of (a) clinopyroxene phenocrysts and microphenocrysts in Subgroup A-1 lavas (solid circle, core; open circle, near rim and rim), and groundmass clinopyroxenes in a dolerite sample (solid square), and (b) a single clinopyroxene phenocryst in sample 68 of Subgroup A-1 in terms of quadrilateral components. Solid line represents the equilibrium crystallisation trend of the Skaergaard Intrusion (Brown, 1967). Compositional fields of Hawaiian tholeiitic and alkalic clinopyroxenes are taken from Basaltic Volcanism Study Project (1981). See discussion in the text.

microphenocrysts include numerous and evenly distributed ilmenite and magnetite crystals. Ilmenite often forms bladed crystals with small indentations, caused by shearing, along their long sides whereas magnetite is equigranular subhedral to anhedral. These Fe-Ti oxides are partially or totally pseudomorphed by leucoxene.

Petrography of dolerites

The two dolerites of Subgroup A-1 have similar mineralogies to the lavas but lack olivine. They are texturally different, partly due to different cooling histories, alteration and deformation styles. Petrographic features of individual samples are presented in Table II-1 (Appendix II).

These dolerites vary texturally from aphyric to sparsely porphyritic with dominant subhedral plagioclase phenocrysts and microphenocrysts, and subordinate anhedral colourless clinopyroxenes. Their major constituents comprise plagioclase laths and anhedral intergranular to subophitic colourless clinopyroxenes. Fe-Ti oxides, including ilmenite blades and skeletal magnetites, and Fe sulphides may be present as accessories.

Plagioclases are albitised, and also pseudomorphed by epidote, pumpellyite and chlorite whereas clinopyroxenes are partially replaced by chlorite and/or indeterminate brownish red mineral aggregates. Fe-Ti oxide minerals are completely transformed to leucoxene. Albite, quartz, epidote and calcite may occur sparsely along occasional microshears. The metamorphic minerals present are indicative of very low- to low-grade regional metamorphic conditions.

3.2.2 Mineral Chemistry

Clinopyroxenes

Clinopyroxene is the most abundant relict igneous mineral preserved in the lavas and dolerites of Subgroup A-1. Analyses of clinopyroxene phenocrysts and microphenocrysts in basaltic lavas, and clinopyroxenes in a dolerite sample are listed in Table 3.3.

The analysed clinopyroxenes are all augites ($Wo_{35.5\text{-}43.7}En_{41.5\text{-}51.5}Fs_{8.3\text{-}20.7}$) according to the nomenclature established by the Subcommittee on Pyroxenes, I.M.A. (1988), with $Mg/(Mg+Fe^{2+})$(herein Mg#) ranging from 0.68 to 0.86. In terms of quadrilateral components (Fig. 3.8a), they define a broad Fe-enrichment and Ca-

TABLE 3.3. ELECTRON MICROPROBE ANALYSES OF CLINOPYROXENE IN THE STUDIED OCEAN-ISLAND THOLEIITES (SUBGROUP A-1). FeO AND Fe_2O_3 ARE CALCULATED ASSUMING STOICHIOMETRY ON THE BASIS OF 4 CATIONS AND 6 OXYGENS. END-MEMBERS IN TERMS OF WOLLASTONITE, ENSTATITE AND FERROSILITE ARE CALCULATED ACCORDING TO THE METHOD RECOMMENDED BY THE SUBCOMMITTEE ON PYROXENES, IMA (1988).

Sample no.	1.3								1.6					
Analysis no.	1mpc	1mpnr	2mpc	3mpc	4mpc	5mpc	6mpc	7mpc	1mpc	2mpc	3mpc	4mpc	5mpc	6mpc
SiO2	52.62	50.52	52.76	51.71	52.07	52.34	51.66	50.81	52.96	52.56	52.74	51.82	53.02	52.88
TiO2	0.75	1.14	0.67	0.40	0.75	0.58	0.85	1.02	0.59	0.66	0.72	0.84	0.81	0.60
Al2O3	2.81	4 20	2.47	3.26	2.80	2.53	3.53	3.96	1.79	2.51	2.06	3.60	2.13	2.06
Cr2O3	0.51	0.30	0.51	0.29	0 63	0.61	0.52	0.70	-	0.33	0.32	0.24	-	0.27
Fe2O3	-	-	-	-	-	0.23	-	0.37	-	0.80	1.05	0.39	-	-
FeO	6.70	8 72	6.65	8 39	7.02	6.09	7.59	6.67	7.08	6.74	6.22	8.37	7.42	7.03
MgO	16.95	16.02	16 68	16 34	16.26	16.91	16 62	16.42	16 81	16.26	16.94	16.19	16.71	16.98
CaO	20 59	18.75	20.96	19.18	20.42	20.98	19.22	20.10	20.41	20.59	20.35	18.63	20.39	20.52
Na2O	-	-	-	-	-	-	-	-	-	0.29	0.26	0.35	-	-
Total	100.93	99.65	100.70	99 57	99.95	100.27	99 99	100.05	99.64	100.74	100 66	100.43	100 48	100.34
Si	1.915	1.874	1.926	1 914	1.917	1 917	1.900	1.871	1.952	1.922	1.926	1.902	1.940	1.937
ivAl	0.085	0.127	0.074	0 086	0 083	0.083	0 100	0.130	0 048	0.078	0.074	0.098	0.060	0.063
Total tetra.	2.000	2.000	2.000	2 000	2.000	2.000	2.000	2.000	2.000	2.000	2.000	2.000	2.000	2.000
viAl	0.036	0.057	0.032	0 057	0.039	0 027	0.053	0.042	0.030	0.030	0.015	0.058	0.032	0.026
Ti	0.021	0.032	0.018	0 011	0 021	0.016	0 024	0.028	0.016	0.018	0.020	0.023	0.022	0 017
Cr	0 015	0.009	0.015	0 009	0.018	0 018	0.015	0.021	-	0.010	0.009	0.007	-	0 008
Fe3+	-	-	-	-	-	0 006	-	0.010	-	0.022	0.029	0.011	-	-
Fe2+	0 204	0 270	0 203	0.260	0 216	0.187	0 233	0 205	0.218	0.206	0.190	0.257	0 227	0 215
Mg	0.919	0 885	0.907	0 902	0 892	0 923	0 911	0.901	0.923	0.886	0 922	0.886	0.911	0 927
Total octa	1.194	1.254	1.176	1.238	1.186	1.177	1 236	1.207	1.187	1.173	1.185	1.242	1 192	1.193
Ca	0 803	0.745	0.820	0.761	0.806	0 824	0.757	0.793	0.806	0.807	0 796	0.733	0.799	0 806
Na	-	-	-	-	-	-	-	-	-	0.021	0 019	0.025	-	-
Total cats	3 997	3.999	3.995	3.999	3.992	4 000	3.993	4 000	3.993	4 000	4 000	4.000	3 992	3 998
Mg/(Mg+Fe^{2+})	0.818	0.766	0.812	0.776	0.805	0 832	0.796	0 814	0.809	0 811	0 829	0.775	0.801	0 811
Wo	41.69	39.19	42.47	39.58	42.09	42.46	39 83	41.53	41.39	41.99	41.10	38.85	41.25	41.35
En	47.73	46.58	47 01	46.90	46.62	47.59	47.90	47.18	47.40	46.13	47.60	46.95	47.04	47.59
Fs	10.59	14 23	10.52	13.52	11.30	09.95	12 27	11 29	11.21	11.88	11.30	14.20	11.71	11 06

Sample no	1 6		1.15					1.18						
Analysis no	7mpc	8mpc	1mpc	2mpc	3mpc	4mpc	5mpc	1pc	1pnr	2mpc	2mpnr	3pc	3pnr	4pc
SiO2	52 82	52.22	49 12	49.70	48.98	50.38	52.72	51.35	53 02	52 47	52.13	52.38	52.80	53.22
TiO2	0.54	0 75	1.65	1.26	1.87	1.24	0.62	0.75	0 55	0.66	0.76	0.68	0.60	0.60
Al2O3	2.07	2.61	5.20	4.65	4.88	4.55	2 08	4.03	2.50	2.56	2.98	2.46	2 68	1.75
Cr2O3	0 45	0.34	0 44	-	-	0 86	0.26	0.67	0.54	0 51	0 63	0 30	0.56	-
Fe2O3	0.61	-	1.07	1.45	0.98	0.05	-	-	-	-	-	0 32	-	-
FeO	7.43	7.04	8.04	8.56	10 70	7.61	8 63	5.96	6.39	6.68	7.28	8.05	6 89	9.10
MgO	15.84	16 63	15.19	14.79	14.24	15.41	17 66	16.00	17 02	16 81	17.25	15.71	16.78	17 31
CaO	19 85	20.45	19 60	20 01	18 87	20.52	18.17	20.87	20.06	20.66	19.39	19 89	20.61	18.53
Na2O	0.55	-	-	-	-	-	-	-	-	-	-	0.37	-	-
Total	100 16	100 04	100.31	100.42	100.52	100 62	100.14	99.63	100.08	100 35	100.42	100.16	100.92	100.51
Si	1.945	1.920	1 819	1.843	1.826	1.854	1.936	1.891	1.931	1.921	1.907	1.932	1.923	1.951
ivAl	0 055	0.080	0.181	0.157	0.174	0.146	0 064	0.109	0.069	0 079	0.093	0.068	0 077	0 049
Total tetra.	2.000	2.000	2.000	2.000	2.000	2.000	2.000	2.000	2.000	2.000	2.000	2.000	2.000	2.000
viAl	0.035	0.033	0.046	0 046	0.041	0 051	0.026	0 066	0 039	0.032	0 036	0.039	0 038	0 026
Ti	0.015	0.021	0.046	0 035	0.053	0.034	0.017	0.021	0.015	0.018	0.021	0.019	0.016	0 017
Cr	0.013	0.010	0.013	-	-	0.025	0.008	0 019	0.016	0.015	0 018	0.009	0 016	-
Fe3+	0.017	-	0.030	0.041	0.028	0.001	-	-	-	-	-	0 009	-	-
Fe2+	0.229	0.217	0.249	0.266	0 334	0.234	0.265	0.184	0.195	0.205	0 223	0.248	0 210	0.279
Mg	0 869	0.911	0.838	0 817	0.791	0.845	0.967	0.878	0.924	0 917	0.940	0 864	0.911	0 946
Total octa.	1.178	1.192	1.222	1.205	1.246	1.191	1.283	1.168	1.188	1.187	1 238	1.187	1.191	1.267
Ca	0 783	0.806	0.778	0.795	0.754	0.809	0.715	0.824	0 804	0.811	0 760	0.786	0 804	0.728
Na	0.039	-	-	-	-	-	-	-	-	-	-	0 026	-	-
Total cats.	4.000	3.998	4.000	4.000	4.000	4.000	3 998	3.991	3.992	3.998	3.998	4.000	3.995	3.995
Mg/(Mg+Fe^{2+})	0.792	0 808	0.771	0.755	0.703	0.783	0.785	0 827	0 826	0 818	0.804	0.777	0.813	0.772
Wo	41.26	41 68	41.06	41.44	39.55	42.81	36 72	43.68	41.82	41.94	39.52	41.23	41.79	37.28
En	45.80	47.13	44 24	42.61	41.50	44.72	49 66	46.58	48.05	47.46	48 89	45.28	47.31	48 44
Fs	12.94	11.20	14.71	15 96	18 95	12.46	13 62	09 74	10.13	10 59	11 59	13 49	10.91	14 29

Sample no.	1.18				1 30						1.31			
Analysis no.	4pnr	1pc	1pnr	2pc	2pnr	3pc	4pc	4pnr	5pc	5pnr	1mpc	2mpc	3mpc	4pc
SiO2	52.79	53.12	51.89	52.75	52.84	52.42	52.66	52.86	52 30	52.77	52 08	52.57	53 88	52 42
TiO2	0.68	0.53	0.61	0 54	0.51	0 56	0.59	0 52	0 62	0.79	0.64	0 61	0.57	0 67
Al2O3	2.05	1.85	3 17	3.00	2.12	2.72	2.65	2.80	2.80	2.07	2.86	2.53	1.67	2.91
Cr2O3	-	0.33	0.85	1.09	0.73	0.77	0.30	0.81	0.67	-	0.39	0.58	-	0 81
Fe2O3	0.38	-	0.31	-	-	-	0.22	-	0.22	0.36	0.12	-	-	-
FeO	7.58	6 88	6.01	5.31	6.24	6 08	7 09	5.41	5.68	7.94	6 91	6.13	8.39	6.00
MgO	16.85	17.29	16 88	17.03	17.42	16.80	17.09	17 12	16.97	17.14	16.74	16.74	18.02	16.70
CaO	20 39	20.24	20 68	21.22	20.50	20.79	20 26	21.18	21 21	19.76	20.38	21.35	18 29	21.19
Na2O	-	-	-	-	-	-	-	-	-	-	-	-	-	-
Total	100.72	100.24	100 40	100.94	100 36	100 14	100 86	100.70	100 47	100.83	100.12	100 51	100 82	100 70
Si	1.932	1.945	1.898	1.913	1.931	1.920	1 919	1.921	1.910	1.929	1.913	1.922	1.959	1.911
ivAl	0.068	0 056	0.102	0.087	0.069	0.080	0 081	0.080	0.090	0.071	0.087	0.079	0.041	0.089
Total tetra.	2.000	2.000	2.000	2.000	2.000	2.000	2.000	2.000	2.000	2.000	2.000	2.000	2 000	2.000
viAl	0 020	0 024	0.035	0.041	0.022	0.037	0 033	0.040	0 030	0.018	0 037	0.031	0.030	0.036
Ti	0 019	0.015	0 017	0.015	0.014	0.016	0.016	0 014	0.017	0 022	0.018	0.017	0.016	0 018
Cr	-	0.010	0.024	0.031	0.021	0.022	0 009	0 023	0 019	-	0.011	0 017	-	0 024
Fe3+	0.010	-	0.009	-	-	-	0.006	-	0.006	0 010	0.003	-	-	-
Fe2+	0.232	0.211	0.184	0.161	0.191	0.186	0.216	0 164	0.174	0.243	0.212	0.187	0.255	0.183
Mg	0.919	0.943	0.921	0 920	0.948	0.917	0.928	0.927	0.924	0.934	0.916	0.912	0 976	0.907
Total octa	1.200	1.202	1.189	1.168	1.196	1.179	1.209	1.169	1.170	1.226	1.198	1.163	1.277	1.169
Ca	0.800	0.794	0.811	0 825	0.802	0.816	0.791	0 825	0.830	0.774	0 802	0.836	0.713	0.828
Na	-	-	-	-	-	-	-	-	-	-	-	-	-	-
Total cats	4 000	3.996	4.000	3.993	3.999	3.995	4.000	3 994	4.000	4 000	4.000	3.999	3.990	3 996
Mg/(Mg+Fe^{2+})	0.798	0.817	0.834	0 851	0 833	0.831	0.811	0.849	0 842	0.794	0 812	0.830	0.793	0 832
Wo	40 77	40.76	42.14	43.26	41.33	42.51	40.75	43.03	42.93	39.48	41.48	43.20	36.65	43.16
En	46 87	48.42	47.86	48.29	48.85	47.79	47.81	48.38	47.78	47.63	47 37	47.12	50.22	47.30
Fs	12.36	10 82	10 00	08.45	09.82	09 70	11.44	08.58	09.29	12 89	11.15	09.68	13.12	09.54

TABLE 3.3. CONTINUED

Sample no	1.31								68					
Analysis no.	4pnr	5mpc	5mpnr	1pc	1pnr	2pc	2pnr	3pc	4pc	5pc	6pc	7pr.	.....	.....
SiO2	51.31	53.38	53.63	53.29	52.77	52.49	53.52	52.70	53.04	53.10	53.76	53.69	53.01	52.93
TiO2	1.14	0.58	0.51	0.81	0.58	0.78	0.50	0.70	0.85	0.56	0.52	0.58	0.54	0.62
Al2O3	4.35	2.12	1.89	2.03	2.58	2.48	2.59	2.71	2.79	2.59	1.89	1.81	2.89	2.48
Cr2O3	0.33	0.56	0.38	-	0.57	0.29	0 72	0.60	0.39	0.44	0 31	0.49	0.99	0.62
Fe2O3	-	-	-	-	-	-	-	-	-	-	-	-	-	-
FeO	7 98	6.42	7.90	7.67	6.21	7.21	5.52	6.51	6 67	6.91	7.00	6 54	5.17	6.25
MgO	15.67	17 56	18.12	16.70	16.71	16.59	17 44	16.65	16.88	16.71	17.59	18.47	17.40	17.12
CaO	20.20	20.38	18.36	20.12	20.68	20.37	20.93	20.96	20.93	20.98	20.12	19.38	20.58	20.31
Na2O	-	-	-	-	-	-	-	-	-	-	-	-	-	-
Total	100.98	101.00	100.79	100.62	100.10	100.21	101 22	100.83	101.55	101.29	101.19	100.96	100.58	100.33
Si	1.876	1.936	1.949	1.947	1.932	1.926	1 932	1.920	1.918	1.927	1.948	1.943	1.923	1.932
ivAl	0.124	0 064	0.051	0.053	0.068	0.074	0.068	0.080	0.082	0.073	0.053	0 057	0.077	0 069
Total tetra.	2.000	2.000	2.000	2.000	2.000	2.000	2.000	2.000	2.000	2.000	2.000	2.000	2.000	2.000
viAl	0.064	0.027	0.030	0 034	0.043	0.034	0.042	0.036	0.037	0.038	0.028	0.020	0.046	0 038
Ti	0.031	0.016	0.014	0.022	0.016	0 022	0 014	0.019	0.023	0.015	0.014	0.016	0.015	0.017
Cr	0.009	0.016	0.011	-	0.017	0.009	0 021	0 017	0 011	0.013	0 009	0.014	0.028	0.018
Fe3+	-	-	-	-	-	-	-	-	-	-	-	-	-	-
Fe2+	0.244	0.195	0.240	0 234	0 190	0.221	0 167	0.198	0.202	0.210	0.212	0 198	0.157	0.191
Mg	0.854	0 949	0.981	0.910	0.912	0.908	0 938	0.904	0.910	0.904	0.950	0.996	0.941	0 931
Total octa.	1.203	1.203	1.276	1.200	1.177	1.193	1.181	1.176	1.183	1.180	1.213	1.244	1.187	1.195
Ca	0.791	0.792	0.715	0.788	0.811	0 801	0.809	0.818	0.811	0.816	0 781	0.751	0.800	0.794
Na	-	-	-	-	-	-	-	-	-	-	-	-	-	-
Total cats.	3.994	3.995	3.991	3.988	3 988	3.994	3.990	3.994	3.994	3.996	3.994	3.996	3.987	3.989
Mg/(Mg+Fe^{2+})	0.778	0 830	0 803	0.795	0 827	0 804	0 849	0.820	0.818	0 812	0 818	0 834	0.857	0 830
Wo	41.88	40.92	36.91	40.78	42.41	41.51	42.27	42.59	42.18	42.28	40.19	38 62	42.15	41.44
En	45.20	49.03	50.68	47.09	47.66	47.03	49 02	47.08	47.33	46 84	48.90	51.21	49.58	48.60
Fs	12.92	10 05	12.40	12.13	9 93	11.46	8.70	10.33	10 49	10 87	10 91	10 17	8 27	9.96

Sample no.	68													
Analysis no.	.. ...	... .	.....	.....	.....	.....	.....	.....	7pc.....	.....	.....	.....	.....	.....
SiO2	53.47	53.41	53.31	53.59	52.60	52.79	53.50	52.51	52.49	52.94	52.83	52.89	52.22	52.57
TiO2	0.66	0.51	0.35	0.46	0.68	0.69	0.42	0.59	0.58	0.44	0.53	0 53	0.70	0.55
Al2O3	2.33	2.20	2.54	2.30	2.22	2.61	2.21	2.66	2.56	2.47	2.34	2.38	2.65	2.32
Cr2O3	0 24	-	0.32	0.31	0.33	0.19	0.29	0.29	0.25	0 22	0.32	-	0.23	0.23
Fe2O3	-	-	-	-	-	-	-	-	-	-	-	-	0.05	-
FeO	5.67	5 79	- 7.65	5.41	5.65	6.33	5.77	6.40	6.50	5.98	5.77	5.68	6 08	5.79
MgO	17.53	17.67	17.47	17.41	17.21	17.20	17.41	16.91	17.02	16.99	17.32	17.13	17.13	17.20
CaO	21.20	20.96	18.78	21.06	20.84	20.26	20.72	20.36	20.63	20.44	20.50	20 60	20.66	20.68
Na2O	-.	-	-	-	-	-	-	-	-	-	-	-	-	-
Total	101.10	100.54	100 42	100 54	99.53	100.07	100.32	99.73	100.03	99.48	99.61	99 21	99.72	99.34
Si	1.934	1 941	1.943	1.945	1.933	1.930	1.947	1.929	1 925	1.944	1.938	1.945	1.919	1.935
ivAl	0.066	0.059	0.057	0 055	0.067	0.070	0.053	0.071	0.075	0.056	0.062	0 055	0.081	0 065
Total tetra.	2 000	2 000	2.000	2 000	2.000	2.000	2.000	2 000	2 000	2.000	2 000	2.000	2.000	2.000
viAl	0.033	0 035	0 052	0 043	0 029	0 043	0.042	0.044	0 036	0.051	0.039	0.048	0.034	0 036
Ti	0.018	0 014	0 010	0.013	0.019	0 019	0.012	0 016	0.016	0.012	0.015	0.015	0.019	0.015
Cr	0.007	-	0 009	0 009	0.010	0.006	0 009	0 009	0.007	0.006	0.009	-	0.007	0.007
Fe3+	-	-	-	-	-	-	-	-	-	-	-	-	0.001	-
Fe2+	0.172	0.176	0.233	0.164	0.174	0.193	0.176	0.197	0.199	0.184	0.177	0.175	0.187	0.178
Mg	0.945	0.957	0.949	0 942	0.943	0.938	0.944	0.926	0.930	0.930	0.947	0.939	0.938	0.944
Total octa.	1.174	1.182	1.254	1.170	1.174	1.198	1.182	1.192	1.189	1.183	1.187	1.177	1.186	1.180
Ca	0.821	0 816	0.734	0.819	0.821	0.794	0 808	0 801	0 811	0.804	0.806	0 812	0.814	0.816
Na	-	-	-	-	-	-	-	-	-	-	-	-	-	-
Total cats.	3 995	3.998	3.988	3.989	3.995	3.992	3.990	3.993	4.000	3.987	3.992	3 988	4.000	3.996
Mg/(Mg+Fe^{2+})	0.846	0.845	0.803	0.852	0.844	0 829	0 843	0.825	0.824	0.835	0 842	0.843	0.834	0.841
Wo	42.39	41.87	38.28	42.54	42.36	41.24	41.90	41.65	41.78	41.93	41.75	42.16	41.94	42.09
En	48.76	49.09	49.55	48.93	48.67	48.71	48 98	48.12	47.95	48.50	49 07	48.76	48.36	48.71
Fs	8 85	9 03	12 18	8 53	8 97	10 05	9.12	10.23	10 27	9.57	9 18	9 08	9.70	9 20

Sample no.	68			C[1]					
Analysis no.	.....		7pnr	1	2	3	4	5	6
SiO2	52.60	52.65	52.56	52.51	52.01	51.52	52.08	51.76	52.60
TiO2	0.51	0.62	0.53	0 74	0.73	0.46	0.77	0.82	0.73
Al2O3	2.34	2.24	2.43	1.97	2.14	2 84	2.09	2 45	2.05
Cr2O3	0.23	0.33	0.34	-	-	-	-	-	-
Fe2O3	-	-	-	-	-	1.61	0.40	0.43	-
FeO	5.63	5.59	5 41	10.67	10.27	10.00	12.41	12.69	10.88
MgO	17.06	17.30	17.24	15.21	15.68	16.55	15.11	15.31	16.04
CaO	20.90	20 60	20.76	19.53	18.96	17.58	18.45	17 69	18 34
Na2O	-	-	-	-	-	-	-	-	-
Total	99.27	99.33	99.27	100 63	99.79	100.56	101.31	101.15	100 64
Si	1.937	1.937	1.934	1.943	1.936	1.903	1.928	1.918	1.941
ivAl	0.063	0.063	0.066	0 057	0.064	0.097	0 072	0 082	0.059
Total tetra.	2 000	2.000	2.000	2.000	2.000	2.000	2 000	2.000	2.000
viAl	0.039	0.034	0.039	0.029	0.030	0.027	0.019	0.025	0.031
Ti	0 014	0 017	0 015	0.021	0 021	0 013	0 021	0.023	0.020
Cr	0 007	0.010	0.010	-	-	-	-	-	-
Fe3+	-	-	-	-	-	0.045	0 011	0.012	-
Fe2+	0.174	0.172	0.167	0 330	0 320	0.309	0.384	0.393	0 336
Mg	0.936	0.948	0.945	0 839	0 870	0.911	0 833	0.845	0.882
Total octa.	1.170	1.181	1.176	1.219	1.240	1.304	1.269	1.298	1.269
Ca	0 825	0.812	0.818	0 774	0.756	0.696	0.732	0.702	0.725
Na	-	-	-	-	-	-	-	-	-
Total cats.	3.994	3 993	3.994	3.993	3 997	4.000	4 000	4.000	3.994
Mg/(Mg+Fe^{2+})	0.844	0 846	0 850	0.717	0 731	0.747	0.684	0.682	0.714
Wo	42.63	42.02	42.39	39.84	38 86	35.49	37 32	35.95	37.32
En	48.40	49 08	48.97	43.17	44 72	46.48	42.52	43.29	45.40
Fs	8.97	8 90	8.63	16 99	16 42	18 04	20 16	20 75	17 28

P = PHENOCRYST, MP = MICROPHENOCRYST, C = CORE, NR = NEAR RIM, R = RIM.
[1] = DOLERITE, - = BELOW DETECTION LIMIT.

depletion trend close to the well-known tholeiitic solidus crystallisation trend of the Skaergaard Intrusion (Brown, 1967).

Clinopyroxene phenocrysts and microphenocrysts in the lavas are slightly compositionally zoned, with both normal and reverse zoning being detected. One least altered clinopyroxene phenocryst (2 mm across) has been systematically analysed, using an interval of 0.2 mm, along its long axis; data are plotted in the pyroxene quadrilateral in Figure. 3.8b. Plots of Al_2O_3, TiO_2, Cr_2O_3 and Mg# against distance from rim through core to near rim (Fig. 3.9) show that Cr_2O_3 and Mg# increase slightly from core to rim whereas Al_2O_3 and TiO_2 are relatively constant. This reverse zoning may possibly be explained by mixing of genetically related batches of hotter magma with slightly more evolved magma represented by the core region.

The subgroup A-1 clinopyroxenes have an average Ti content (0.019±0.007) and average Cr content (0.011±0.008) closest to clinopyroxenes in non-orogenic tholeiites (Fig. 3.10). Their compositional fields on the pyroxene quadrilateral (Fig. 3.8), TiO_2 (0.3-1.9 wt%), Al_2O_3 (1.7-5.2 wt%) and Na_2O (trace-0.6 wt%, average 0.02 wt%) contents closely resemble those of the Hawaiian tholeiitic clinopyroxenes, in particular those from Mauna Loa (Basaltic Volcanism Study Project, 1981) and Loihi (Hawkins and Melchior, 1983).

Chrome-spinels

Small chrome-spinel crystals are largely restricted in the lavas containing olivine as the sole phenocryst/microphenocryst phase. In the lavas which have dominant plagioclase and clinopyroxene phenocrysts and microphenocrysts, they occur only as inclusions in olivine phenocrysts and microphenocrysts. The compositions of chrome-spinels both in the whole-rock analysed samples and in an unanalysed (but inferred to be Subgroup A-1) sample which occurs as a lensoid mass in metasedimentary rock are presented in Table 3.4.

The analysed spinels are chromites and have relatively low Fe^{3+} contents (Fe_2O_3 = 5.9-13.0 wt%) suggestive of low fO_2 during crystallisation (Fisk and Bence, 1980; Dick and Bullen, 1984). Their compositions on Cr/(Cr+Al) (herein Cr#) and $Fe^{3+}/(Fe^{3+}+Al+Cr)$ (herein Fe^{3+}#) versus Mg# plots (Fig. 3.11) overlap the compositional fields of chromites from Hawaiian tholeiites. Their TiO_2 contents (1.1-3.3 wt%) are also comparable to those in the Hawaiian tholeiitic spinels (Evans and Wright, 1972; Clague *et al.*, 1980; Basaltic Volcanism Study Project, 1981; Hawkins and Melchior, 1983; Sen and Presnall, 1986).

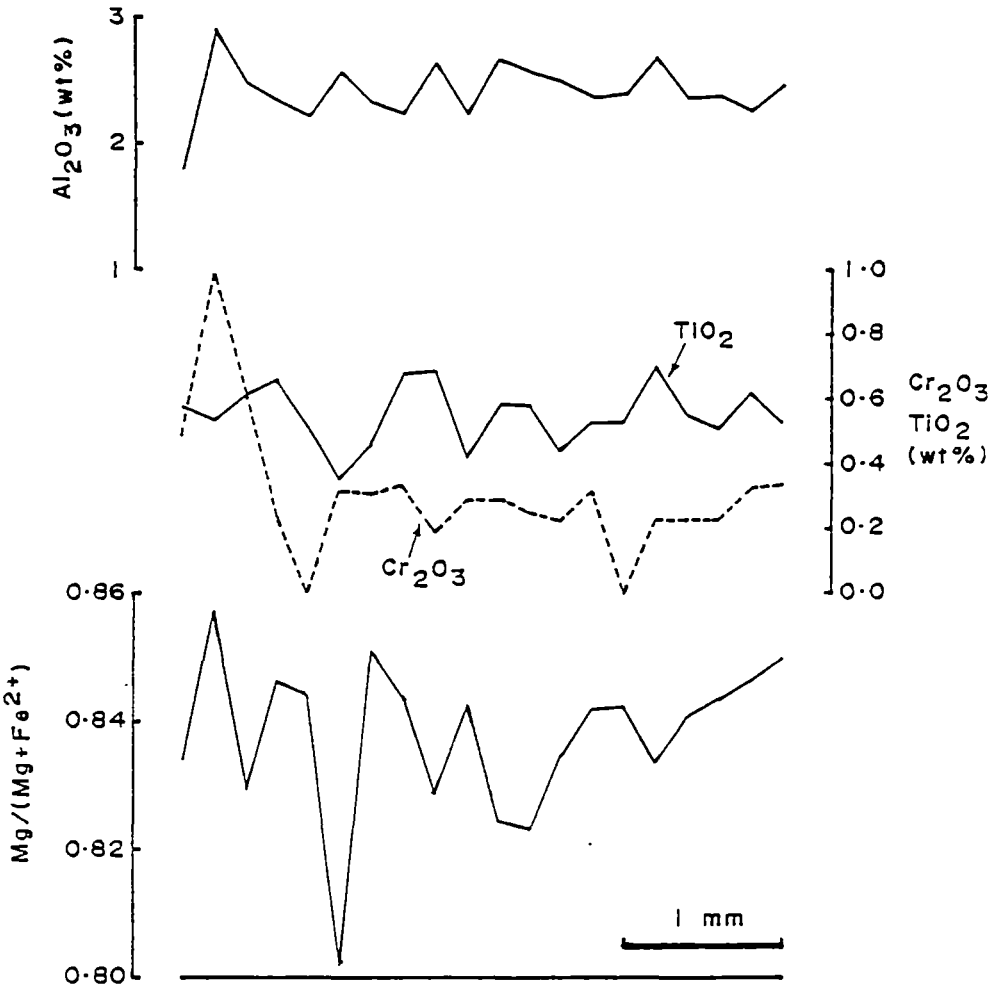

Figure 3.9. Rim-core-near rim traverse through a clinopyroxene phenocryst in sample 68 (Subgroup A-1) in terms of Al_2O_3, TiO_2, Cr_2O_3 and Mg#. Note that the points at the extreme end on the right-hand side are not true rim but are near-rim compositions.

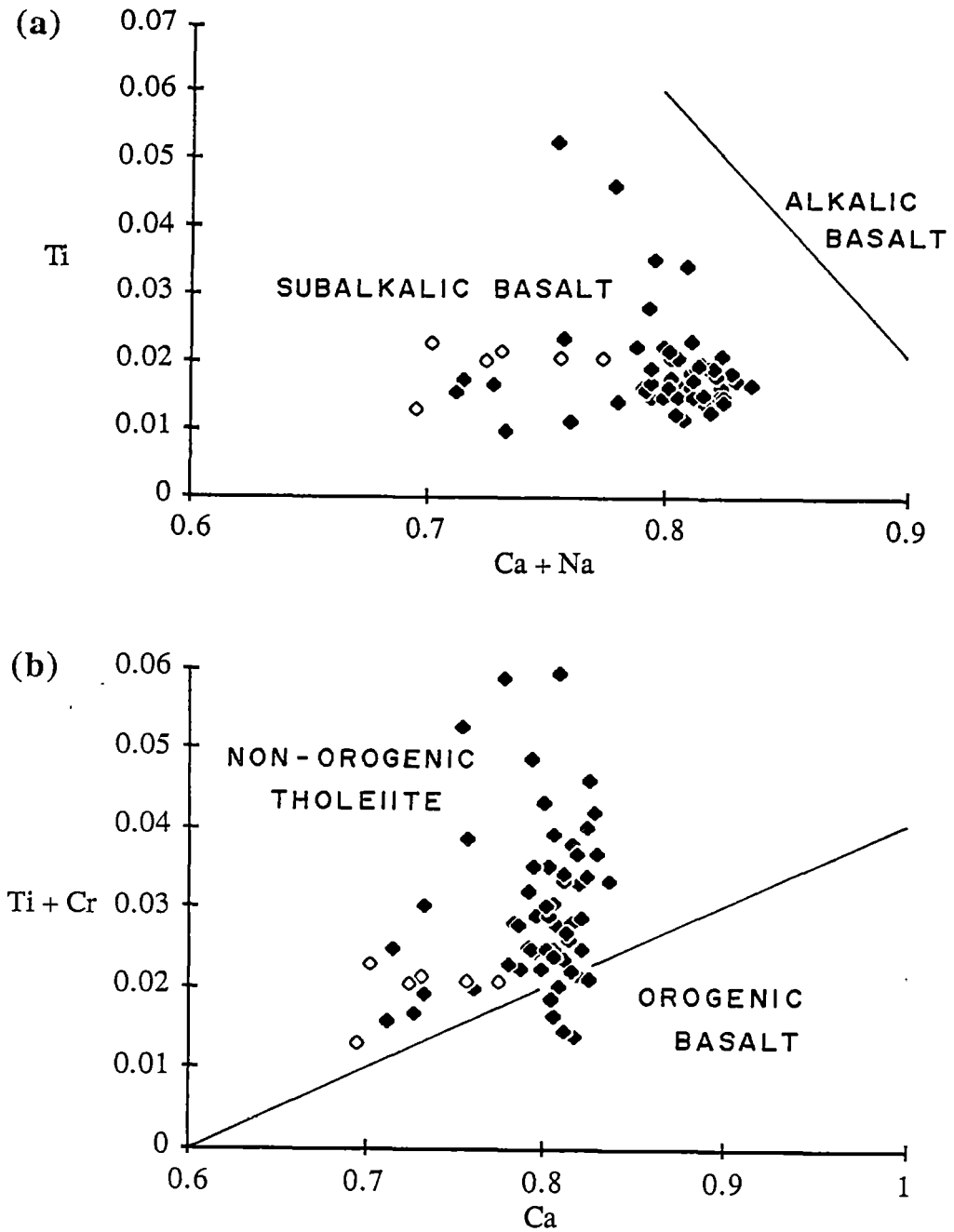

Figure 3.10. Plots of (a) Ti against Ca + Na, and (b) Ti + Cr against Ca (on the basis of 6 oxygens) for cores of clinopyroxene phenocrysts and microphenocrysts present in basaltic lavas (solid symbol) and groundmass clinopyroxenes in a dolerite sample (open symbol) of Subgroup A-1. Field boundaries are after Leterrier *et al.* (1982).

TABLE 3.4. ELECTRON MICROPROBE ANALYSES OF CHROME-SPINELS IN THE STUDIED OCEAN-ISLAND THOLEIITIC LAVAS (SUBGROUP A-1). FeO AND Fe_2O_3 ARE CALCULATED ASSUMING STOICHIOMETRY ON THE BASIS OF 3 CATIONS AND 4 OXYGENS.

Sample no.	A[1]							B			50 2	1.30	56 1
Analysis no.	1[2]	2[2]	3[2]	4[2]	5[2]	6[2]	7[2]	1	2	3	1	1[2]	1
TiO2	2.79	3.06	2 97	2.48	2.90	2.34	2.34	1.17	1.10	1 42	1.78	1.80	2.13
Al2O3	16.45	16.39	16.33	16.69	11.46	15.85	16.00	18.69	18.69	18.58	14 92	17 58	16.16
Cr2O3	42.47	42.76	42 40	43.29	45.48	44.44	44.47	41.02	41.26	39.45	45 50	37.17	44.42
Fe2O3	7.08	6.79	7.20	6.96	10.74	6.65	6.79	9.74	9.38	10.65	6.56	13.01	6.84
FeO	20.49	20.69	20 41	20.17	18.61	20.46	19.94	19.60	19 03	19.53	22.75	19.96	18.94
NiO	-	-	0.35	-	-	-	-	-	-	-	0.36	-	-
MgO	10.88	11.02	10 87	11.04	11.80	10.63	11.00	10.93	11.16	10 99	8.47	10.71	11.44
Total	100.16	100.71	100.53	100 63	100 99	100.37	100.54	101.15	100.62	100.62	100.34	100.23	99 93
Ti	0 067	0.073	0.071	0 059	0.070	0.056	0.056	0.028	0.026	0.034	0.044	0.043	0 051
Al	0 621	0.615	0.615	0.626	0 437	0.600	0.602	0.694	0.696	0.693	0.575	0.662	0.609
Cr	1.075	1.076	1.070	1.089	1.162	1.127	1.122	1.021	1.030	0.987	1.176	0.939	1 123
Fe3+	0.170	0.163	0.173	0 167	0.261	0 160	0.163	0 230	0 222	0.253	0 161	0.313	0.165
Fe2+	0.548	0.550	0.545	0 536	0.502	0.548	0.533	0.515	0.501	0.516	0 622	0.533	0.507
Ni	-	-	0.009	-	-	-	-	-	-	-	-	-	-
Mg	0.519	0.523	0 517	0.524	0 568	0 508	0 523	0.513	0 525	0.518	0 413	0.510	0 545
Total cats.	3.000	3.000	3 000	3 000	3.000	3 000	3.000	3.000	3.000	3.000	3.000	3 000	3.000
Cr/Cr+Al	0.634	0.636	0.635	0.635	0 727	0.653	0.651	0.595	0 597	0 587	0.672	0.586	0.648
$Fe^{3+}/(Fe^{3+}+Al+Cr)$	0 091	0.088	0.093	0.088	0.140	0.085	0.087	0.118	0 114	0.131	0.084	0.163	0.087
$Mg/(Mg+Fe^{2+})$	0 486	0 487	0 487	0 494	0 531	0 481	0 495	0 499	0.512	0 501	0 399	0 489	0 518

Sample no.	56.1								56 3					
Analysis no	2	3	4	5[2]	6[2]	7[2]	8	9[2]	1	2	3	4	5	6
TiO2	2 36	3 29	2.46	2.44	2 93	2 52	2 20	2 68	2.28	2.20	2.34	2.18	2 33	2 34
Al2O3	15.79	15.60	16.51	16.78	15 82	16.71	15 86	16.72	16.40	16.19	16.33	16 23	16.15	16.53
Cr2O3	45.43	43.22	42.95	43.25	43.00	43.09	44.91	43.03	44.64	44 83	44.32	44.53	44 47	44 10
Fe2O3	6.51	7.29	7.50	6.74	7.71	7 42	7.31	7 33	5 86	6.36	6.50	6.62	6.13	6.22
FeO	19.46	20.26	19.01	19.48	19 50	19 28	19.02	19 51	19 04	18.75	19.023	18.44	18.59	18.74
NiO	-	-	-	-	-	-	-	-	-	-	-	-	-	-
MgO	11 41	11.44	11.64	11 36	11.64	11 65	11 59	11 65	11 44	11 61	11 55	11.76	11 66	11 66
Total	100.96	101 10	100.07	100 05	100.60	100 67	100.89	100 92	99 66	99.945	100.06	99.76	99 33	99.59
Ti	0.095	0 079	0.059	0 059	0.070	0 060	0.052	0 064	0 055	0.053	0.056	0.052	0 056	0.056
Al	0.591	0.584	0 620	0.631	0 593	0 624	0.593	0.623	0 619	0 609	0.614	0.611	0.611	0.623
Cr	1.141	1.085	1.082	1.090	1 082	1.079	1.127	1.075	1.130	1.132	1.118	1.125	1.129	1.115
Fe3+	0.156	0.174	0.180	0.162	0 185	0.177	0.175	0.174	0 141	0 153	0.156	0.159	0.148	0.150
Fe2+	0.157	0.538	0.507	0 519	0.519	0 511	0 505	0 516	0.510	0.501	0.507	0 493	0.499	0.501
Ni	-	-	-	-	-	-	-	-	-	-	-	-	-	-
Mg	0 540	0.541	0 553	0 540	0 552	0 550	0 548	0 549	0 546	0 553	0 549	0 560	0.558	0 556
Total cats.	3.000	3.000	3 000	3 000	3.000	3.000	3.000	3.000	3 000	3.000	3.000	3.000	3 000	3 000
Cr/Cr+Al	0.659	0.650	0.630	0.634	0 646	0.634	0 655	0 633	0.646	0.650	0.645	0.648	0.649	0.641
$Fe^{3+}/(Fe^{3+}+Al+Cr)$	0.082	0.094	0.096	0.086	0.099	0.094	0.092	0.093	0.075	0.081	0.083	0.084	0.078	0.079
$Mg/(Mg+Fe^{2+})$	0 511	0.502	0 522	0.510	0 515	0.519	0.521	0 516	0.517	0 525	0 520	0 532	0 528	0 526

[1] = WHOLEROCK XRF ANALYSES HAVE NOT BEEN CARRIED OUT.
[2] = INCLUSION IN OLIVINE.
- = BELOW DETECTION LIMIT.

TABLE 3.5. REE ANALYSES AND SELECTED CHONDRITE-NORMALISED RATIOS FOR THE STUDIED OCEAN-ISLAND LAVAS AND DOLERITES (GROUP A)

	SUBGROUP A-1								SUBGROUP A-2			
Sample no.	56.3	1.26	50 2	C[1]	1.17[1]	1.4	1.15	B	27.7[1]	27 1[1]	28 6[1]	36 3[1]
La	6 6	9.24	7 4	5.71	7.68	16.9	9.64	5.88	21.9	23.7	20.4	25.6
Ce	17.6	23.3	20.9	14	20.2	42.7	23 4	14.9	49.7	50.4	55.0	59 2
Pr	2.7	3.21	3.2	1.98	2.86	6.08	3.13	2.14	7.05	6.33	6.94	7.69
Nd	12.9	14.9	15.8	9.55	13 6	28.3	15.5	11.1	31.1	28.1	30 5	35.7
Sm	3.86	3.26	4.55	2.6	3.73	6.46	4.16	3.51	6.76	5.93	6.77	8.12
Eu	1.54	0.98	1.57	0.96	1.13	2.27	1.52	1.33	2.29	2 11	2.41	2.71
Gd	4.91	3.86	5.48	3.38	4.25	7.5	4.99	4.55	7.65	6.67	7.69	8.6
Dy	4.49	4.18	4 99	4.37	4.7	7.73	4.64	4.7	6 5	6.66	7.61	7.73
Er	2.24	2.19	2.78	2.47	2.61	4.26	2.47	2.59	2.58	3.2	3.5	3.94
Yb	1.64	1.6	2.23	2.02	2.09	3.37	1.86	2.06	1.71	2.22	2.47	2.75
[La/Sm]cn	1.04	1.73	1	1.34	1.25	1.59	1.41	1.02	1.97	2.44	1.84	1.92
[Sm/Yb]cn	2.55	2 21	2 21	1.39	1.93	2.08	2.42	1.85	4.28	2 89	2.97	3.2

1 = DOLERITE.

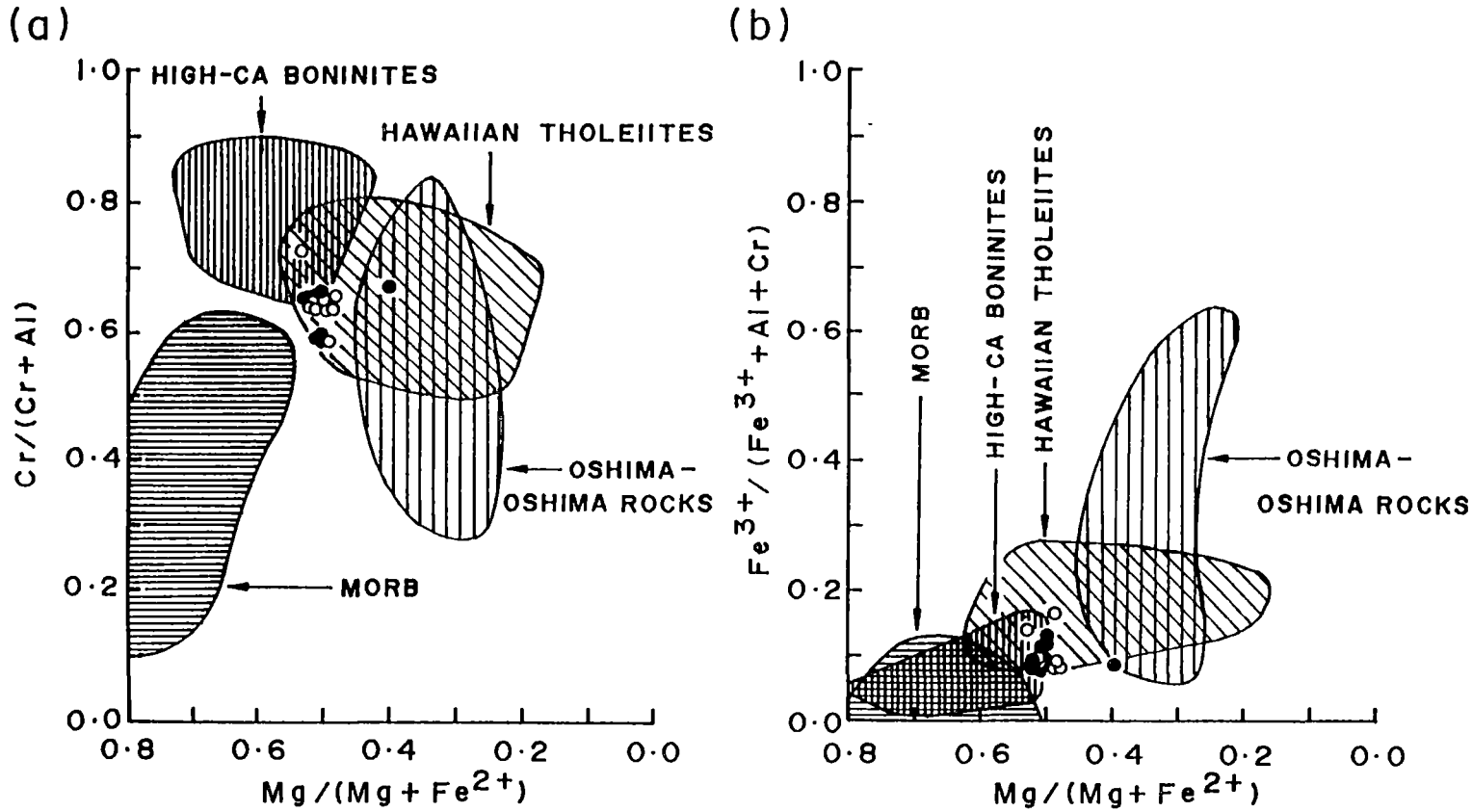

Figure 3.11. Relationships of (a) Cr/(Cr+Al) and (b) $Fe^{3+}/(Fe^{3+}+Al+Cr)$ with $Mg/(Mg+Fe^{2+})$ for chromites in Subgroup A-1 lavas (solid circles, inclusions in olivine phenocrysts and microphenocrysts; open circles, chromite microphenocrysts). Also shown are compositional fields for chromites in mid-ocean ridge basalts (Dick and Bullen, 1984), Hawaiian tholeiites (compiled from Evans and Wright, 1972; Clague *et al.*, 1980; Basaltic Volcanism Study Project, 1981; Hawkins and Melchior, 1983; and Sen and Presnall, 1986), Oshima-Oshima arc lavas and associated ultramafics (Yamamoto, 1984), and high-Ca boninites (compiled from Cameron, 1985; Duncan and Green, 1987; Falloon and Green, 1986; and Falloon *et al.*, 1989). Note that many data points of chromite inclusions are superimposed by those of chromite microphenocrysts.

In summary, based on compositions of relict clinopyroxene and chrome-spinel phenocrysts and microphenocrysts, the Subgroup A-1 rocks appear to have strong compositional affinities with intraplate ocean-island tholeiites, in particular those from Hawaii.

3.2.3 Whole-rock Chemistry

Major elements

The basaltic lavas and dolerites of Subgroup A-1 span the ranges in FeO*, TiO_2 and MgO from 8.4 to 12.0, 1.4 to 2.5, and 5.8 to 12.6 wt%, respectively. In spite of the variable MgO contents, their FeO*/MgO values are relatively limited, ranging from 0.9 to 1.9. These basaltic rocks show broad enrichment of FeO*, TiO_2 and V with increasing differentiation, expressed as FeO*/MgO (Fig. 3.12). Their Nb/Y values range from 0.3 to 0.5, indicating that they are essentially tholeiitic (Pearce and Cann, 1973; Floyd and Winchester, 1975, Pearce, 1982).

These tholeiitic rocks are broadly comparable to ocean-island tholeiites, MORB and backarc basin basalts (herein BABB) in terms of FeO*, TiO_2, MgO and FeO*/MgO values (Figs. 3.12 and 3.13). However, considering the more primitive samples, their FeO* are notably higher than typical MORB and BABB and are more reminiscent of ocean-island basalts.

Minor and trace elements

Figure 3.14 shows further least mobile minor- and trace-element variations in relation to FeO*/MgO. P_2O_5, Zr, Y and Nb form broadly positive trends similar to the previously discussed patterns for FeO*, TiO_2 and V, typical of incompatible element behaviour. The trends for Ni and Cr descend steeply relative to FeO*/MgO in the early stages of fractionation, recording rapid olivine and chrome-spinel crystallisation and removal. Sc displays a well-defined positive trend against FeO*/MgO in the earlier stages and a negative trend in the later stages of fractionation, the change in slope presumably recording the start of crystallisation of abundant clinopyroxenes.

From these data, it could be inferred that the liquid line of descent is probably controlled dominantly by chrome-spinel and olivine in the earlier stages of fractionation, and subsequently, by olivine and clinopyroxene. Although plagioclase phenocrysts are present in many samples, the role of plagioclase fractionation cannot

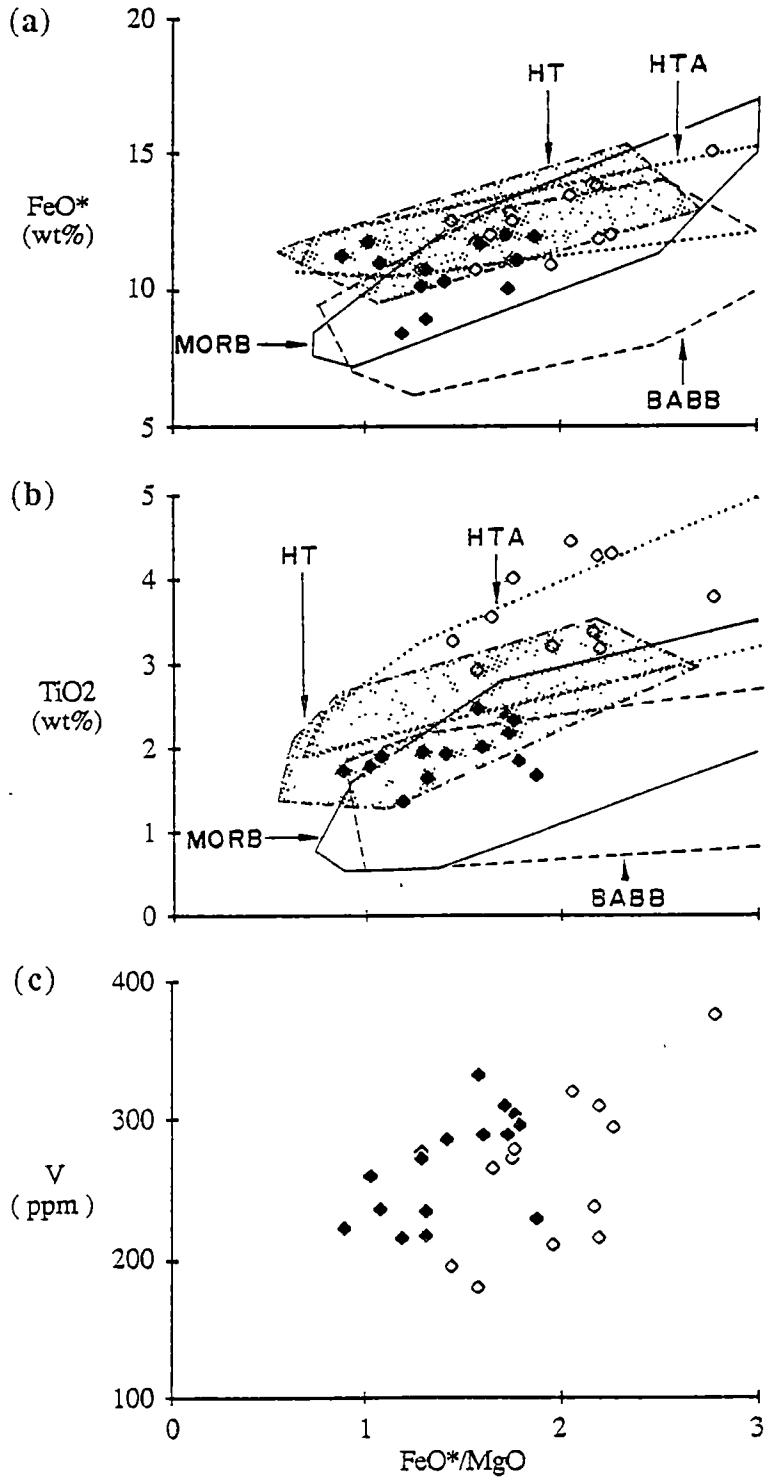

Figure 3.12. Variation diagrams of (a) FeO*, (b) TiO_2 and (c) V versus FeO*/MgO for the studied ocean-island lavas and dolerites (solid symbol, Subgroup A-1; open symbol, Subgroup A-2). Also shown are compositional fields for modern mid-ocean ridge basalts (MORB)(database from A.J. Crawford, pers. comm., 1990), backarc basin tholeiites (BABB)(data from Saunders and Tarney, 1979; Weaver *et al.*, 1979; Marsh *et al.*, 1980; Sinton and Fryer, 1987; Volpe *et al.*, 1988; Aggrey *et al.*, 1988; Ikeda and Yuasa, 1989; and Price *et al.*, 1990), Hawaiian tholeiites (HT)(data from Kilauea and Mauna Loa Volcanoes (Basaltic Volcanism Study Project, 1981), Waipio Valley transitional tholeiites and tholeiites, Kohala Volcano (Feigenson *et al.*, 1983) and Loihi tholeiites (Frey and Clague, 1983)), and transitional tholeiites and alkalic basalts (HTA)(data from Hamakua lavas, Mauna Kea Volcano (Frey *et al.*, 1990)).

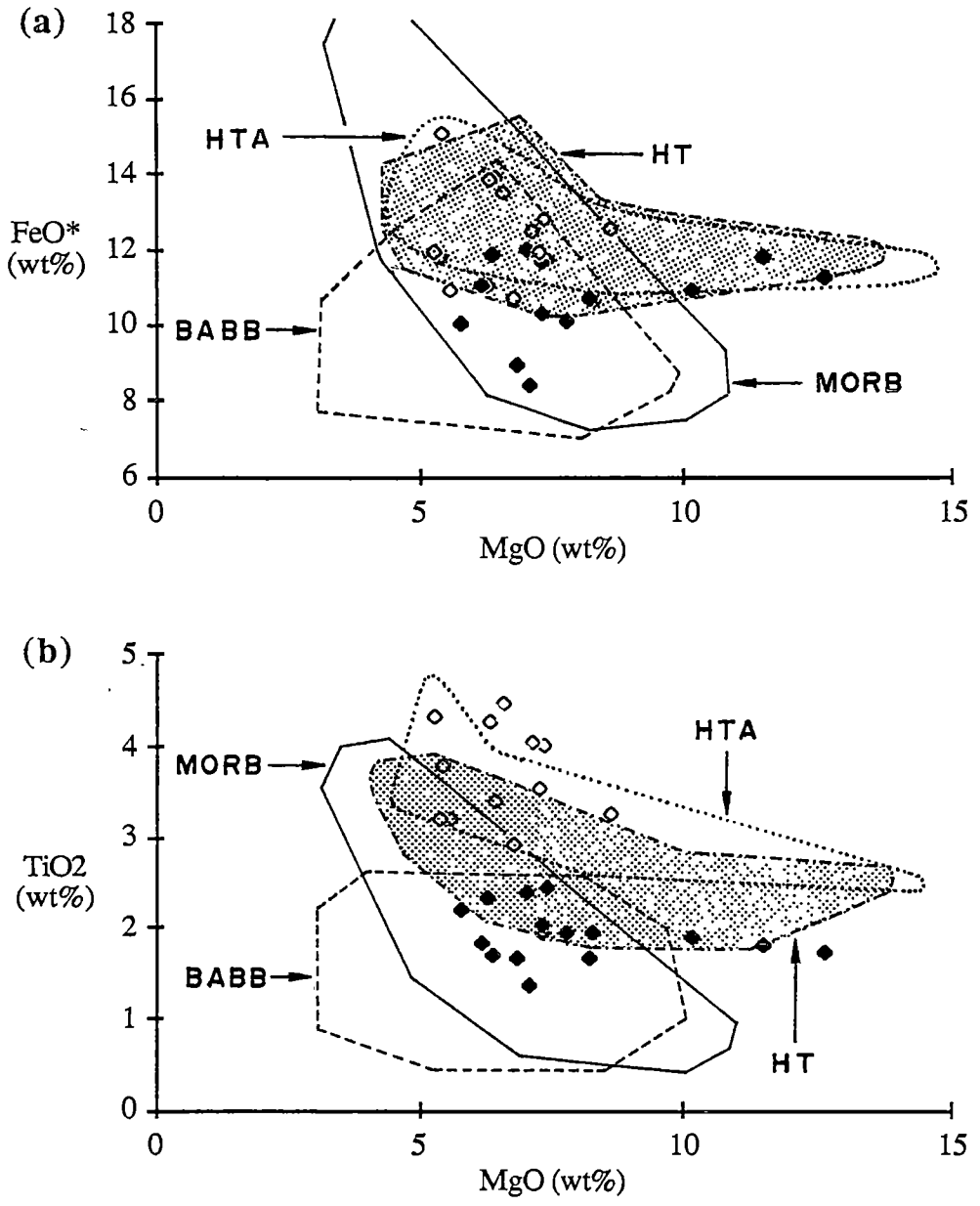

Figure 3.13. Diagrams showing the relationships between (a) FeO* and MgO, and (b) TiO_2 and MgO for the studied ocean-island lavas and dolerites (solid symbol, Subgroup A-1; open symbol, Subgroup A-2). Data sources for compositional fields of mid-ocean ridge basalts (MORB), backarc basin tholeiites (BABB), Hawaiian tholeiites (HT), and Hawaiian transitional tholeiites and alkalic basalts (HTA) are as in Figure 3.12.

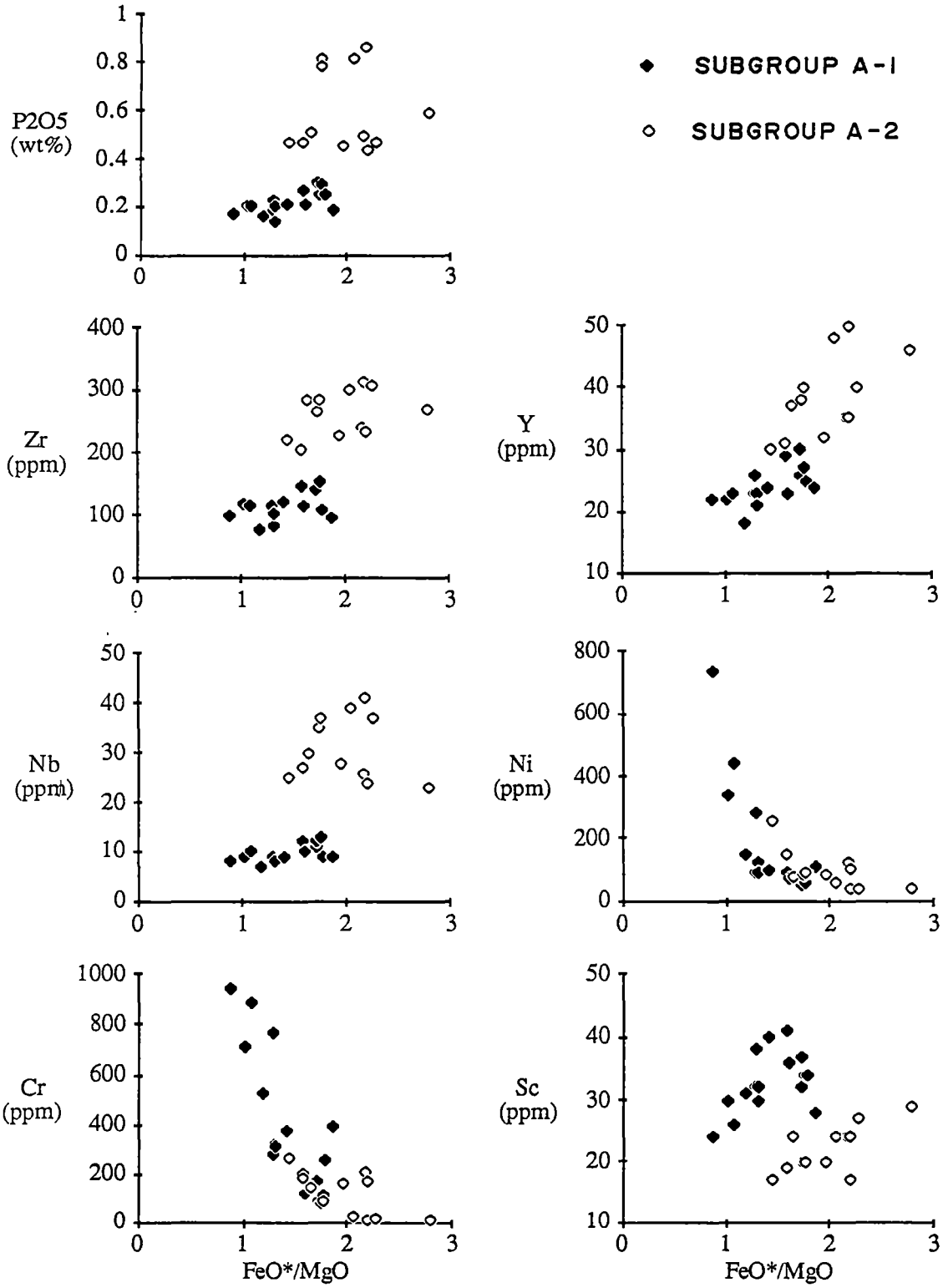

Figure 3.14. FeO*/MgO variation plots of P_2O_5, Zr, Y, Nb, Ni, Cr and Sc for the studied ocean-island lavas and dolerites (solid symbol, Subgroup A-1; open symbol, Subgroup A-2).

be geochemically assessed with confidence, since the prime constituents of plagioclase, both major and trace elements, are susceptible to alteration.

The relationships between incompatible-element pairs for Subgroup A-1 samples, such as Ti-Zr, Nb-Zr and Y-Zr (Fig. 3.15), and Ti-V (Fig. 3.16a), are linear but do not trace back to the origin. The values for Ti/Zr (90-119) and Zr/Nb (11-13) are only slightly less than the chondritic values, whereas Zr/Y (3.7-5.7) and Ti/V (37-48) are higher than the chondritic values. The Zr/Nb values seem to support the ocean-island affinities as those for N-MORB and E-MORB largely vary from 30 to 55 and 6 to 10, but those for ocean-island tholeiites are mostly in a range of 6 to 15 (Basaltic Volcanism Study Project, 1981).

It is clear from the compositional fields of Subgroup A-1 rocks in the discrimination diagrams in Figures 3.2, 3.16 and 3.17 that these rocks are almost certainly within-plate tholeiites. The similarity of Nb/Y, Ti/Zr, Zr/Nb, Zr/Y and Ti/V to these values for ocean-island tholeiites is striking and persuasive.

Rare-earth elements

REE analyses for 6 lavas and 2 dolerites of Subgroup A-1 are presented in Table 3.5, and their chondrite-normalised values are plotted in Figure 3.18. These tholeiites have relatively flat LREE patterns with chondrite-normalised La/Sm (herein (La/Sm)n) between 1.0 to 1.6, and exhibit heavy REE depletion (herein HREE) with chondrite-normalised Sm/Yb (herein (Sm/Yb)n) ranging from 1.4 to 2.6. Most show a slight convex upward LREE pattern; a few display a small negative Eu anomaly with a ratio of chondrite-normalised Eu and Eu extrapolated from chondrite-normalised Sm and Gd (herein Eu/Eu*) of approximately 0.9-1.1. Their La and Yb abundances vary from 18.1 to 53.6 and 7.7 to 16.2 times chondritic values.

These patterns are very similar to those of some ocean-island tholeiites, e.g. Kilauea and Mauna Loa Volcanoes, Hawaii (Basaltic Volcanism Study Project, 1981); Kohala Volcano, Hawaii (Feigenson *et al.*, 1983); Loihi Seamount, Hawaii (Frey and Clague, 1983); and Britannia and Derwent Hunter Seamounts, Tasman Sea (Eggins *et al.*, 1990)(Figs. 3.19 and 3.20).

Comparisons with modern suites

Many empirical diagrams for discriminating tectonic settings of eruption of lavas have appeared in the literature (e.g. Figs. 3.2, 3.16 and 3.17). Nevertheless, several recent studies, e.g. Holm (1982), Prestvik (1982), Duncan (1987) and Myers

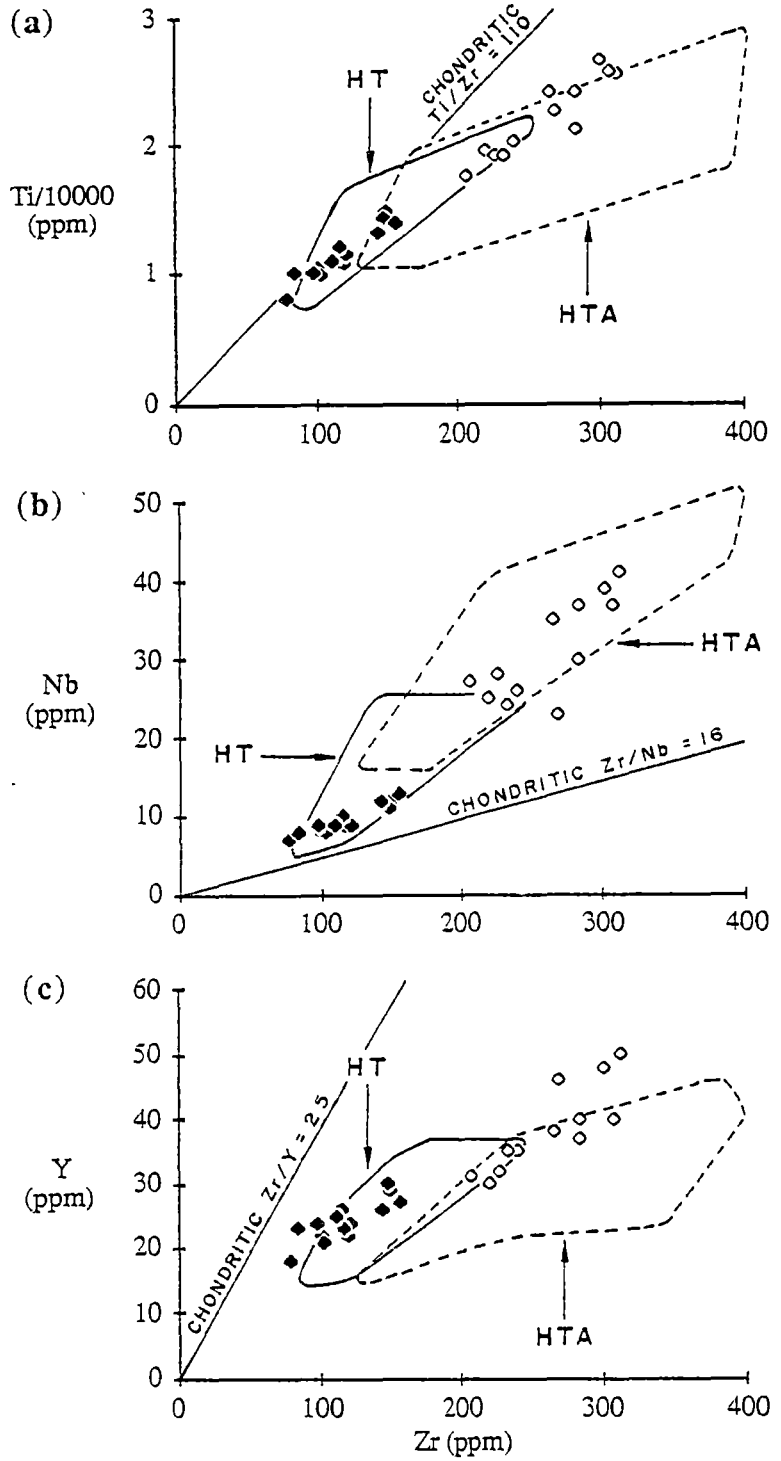

Figure 3.15. Binary plots of HFSE for the studied ocean-island basaltic lavas and dolerites (solid symbol, Subgroup A-1; open symbol, Subgroup A-2) showing the relations between (a) Ti and Zr, (b) Nb and Zr and (c) Y and Zr. Also shown are compositional fields for Hawaiian tholeiites (HT)(data from Kilauea and Mauna Loa Volcanoes (Basaltic Volcanism Study Project, 1981), and Loihi Seamount (Frey and Clague, 1983)), and transitional tholeiites and alkalic basalts (HTA)(data from Kula series, Haleakala Volcano, Maui (Chen and Frey, 1985), and Hamakua lavas, Mauna Kea Volcano (Frey *et al.*, 1990)). Data for the alkalic basalts of Kula series are excluded from (a) and (c) since no data are available. The chondritic values for Ti/Zr, Zr/Nb and Zr/Y are taken from Nesbitt and Sun (1976).

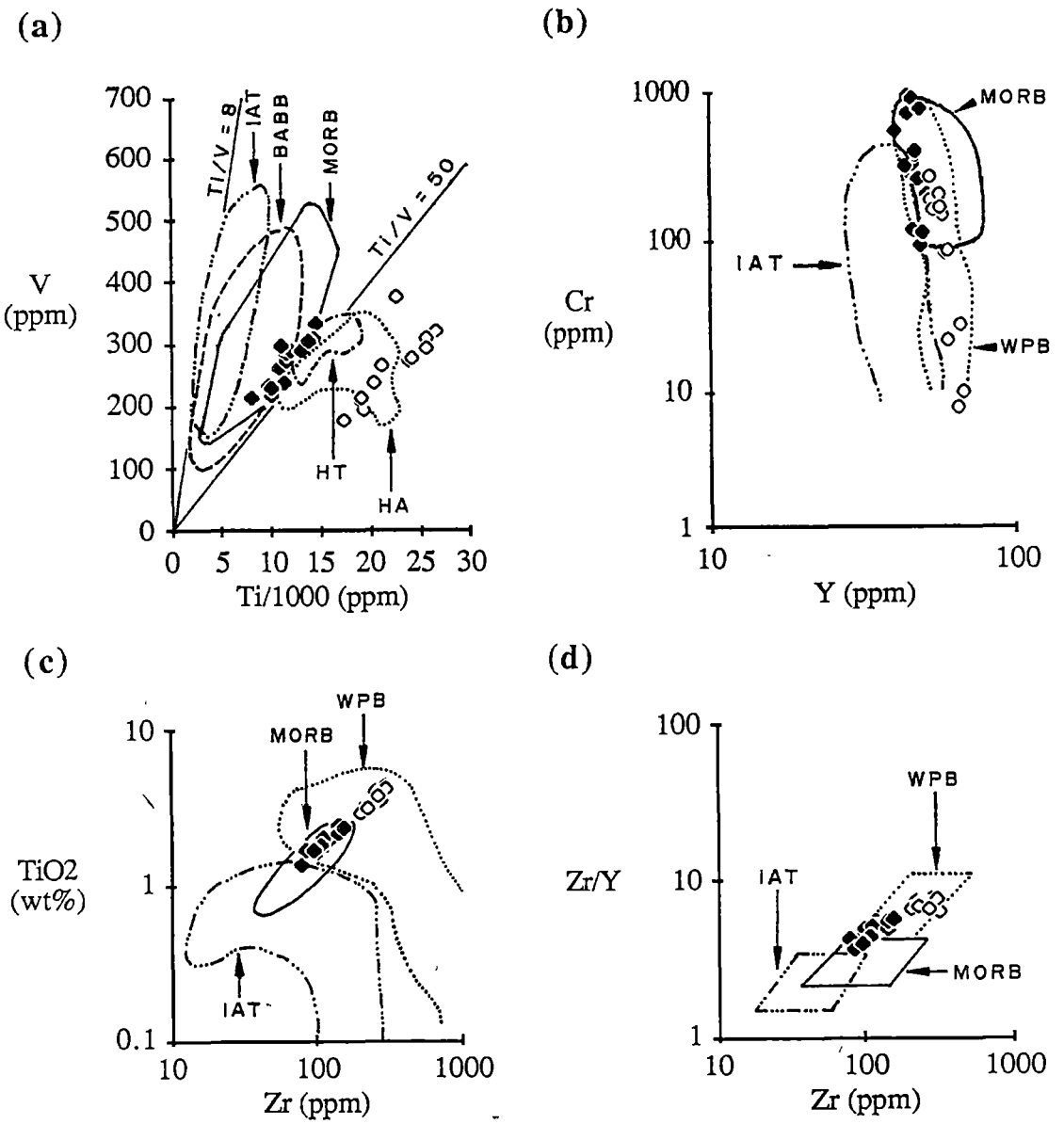

Figure 3.16. Plots of (a) V against Ti, (b) Cr against Y, (c) TiO_2 against Zr and (d) Zr/Y against Zr for the studied ocean-island basaltic lavas and dolerites (solid symbol, Subgroup A-1; open symbol, Subgroup A-2). Field boundaries of basalts from different tectonic settings in (a), (b) and (c), and (d) are after Shervais (1982), Pearce (1980), and Pearce and Norry (1979), respectively. HA = Hawaiian alkalic basalts, HT = Hawaiian tholeiites, MORB = mid-ocean ridge basalts, BABB = backarc basin basalts, IAT = island-arc tholeiites; WPB = within-plate basalts. A chondritic Ti/V ratio of 8 is taken from Nesbitt and Sun (1976).

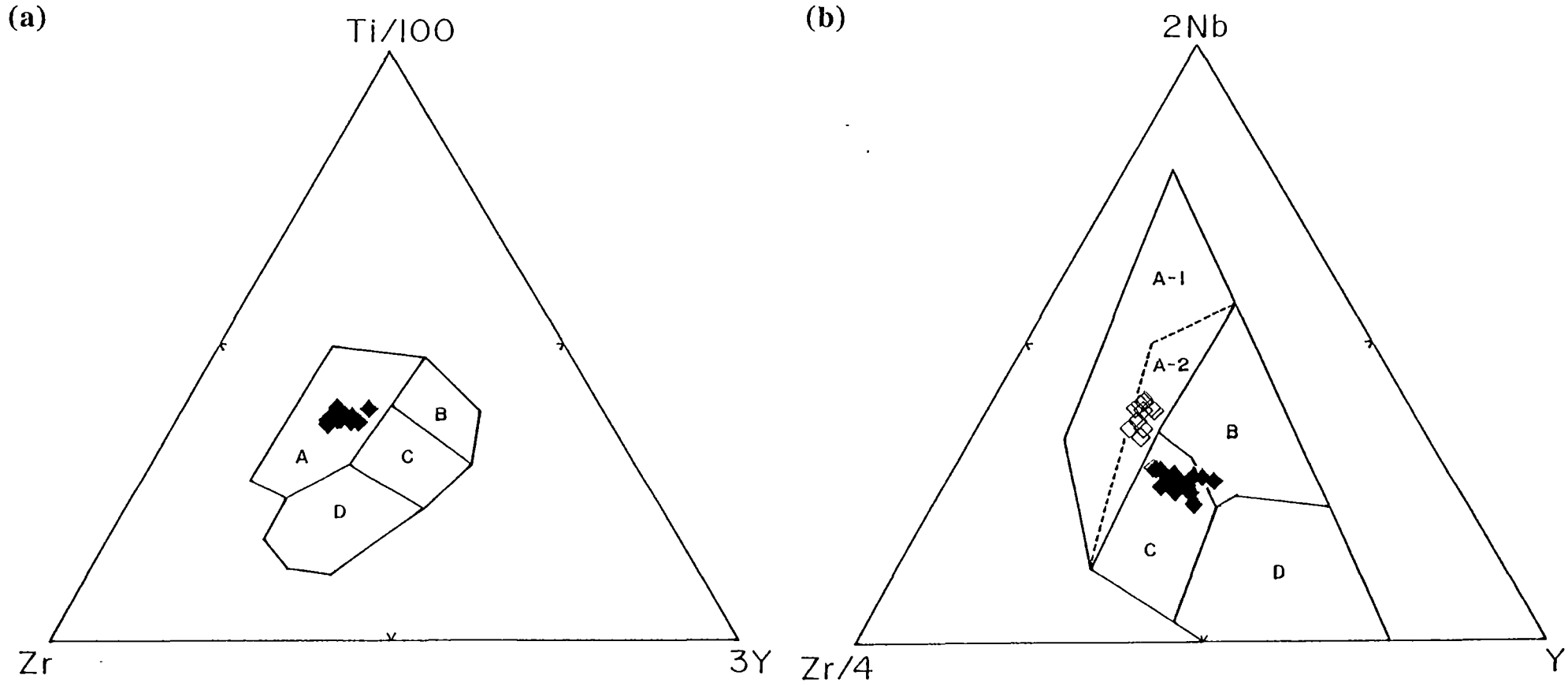

Figure 3.17. Plots of (a) Ti-Zr-Y showing fields of within-plate basalts (A), mid-ocean ridge basalts (C), island-arc tholeiites (B+C), and calc-alkalic basalts (C+D)(after Pearce and Cann, 1973), and (b) Nb-Zr-Y displaying fields of within-plate basalts (A-1 + A-2 = alkalic basalts, A-2 = transitional tholeiites, A-2 + C = tholeiites), mid-ocean ridge basalts (B = E-MORB, D = N-MORB), and volcanic arc basalts (C+D)(after Meschede, 1986). Samples plotted are the studied ocean-island tholeiites (Subgroup A-1)(solid symbol), and transitional tholeiites and alkalic basalts (Subgroup A-2)(open symbol). Data for the Subgroup A-2 samples are omitted in (a) since the compositional fields in this diagram did not include transitional tholeiites and alkalic basalts.

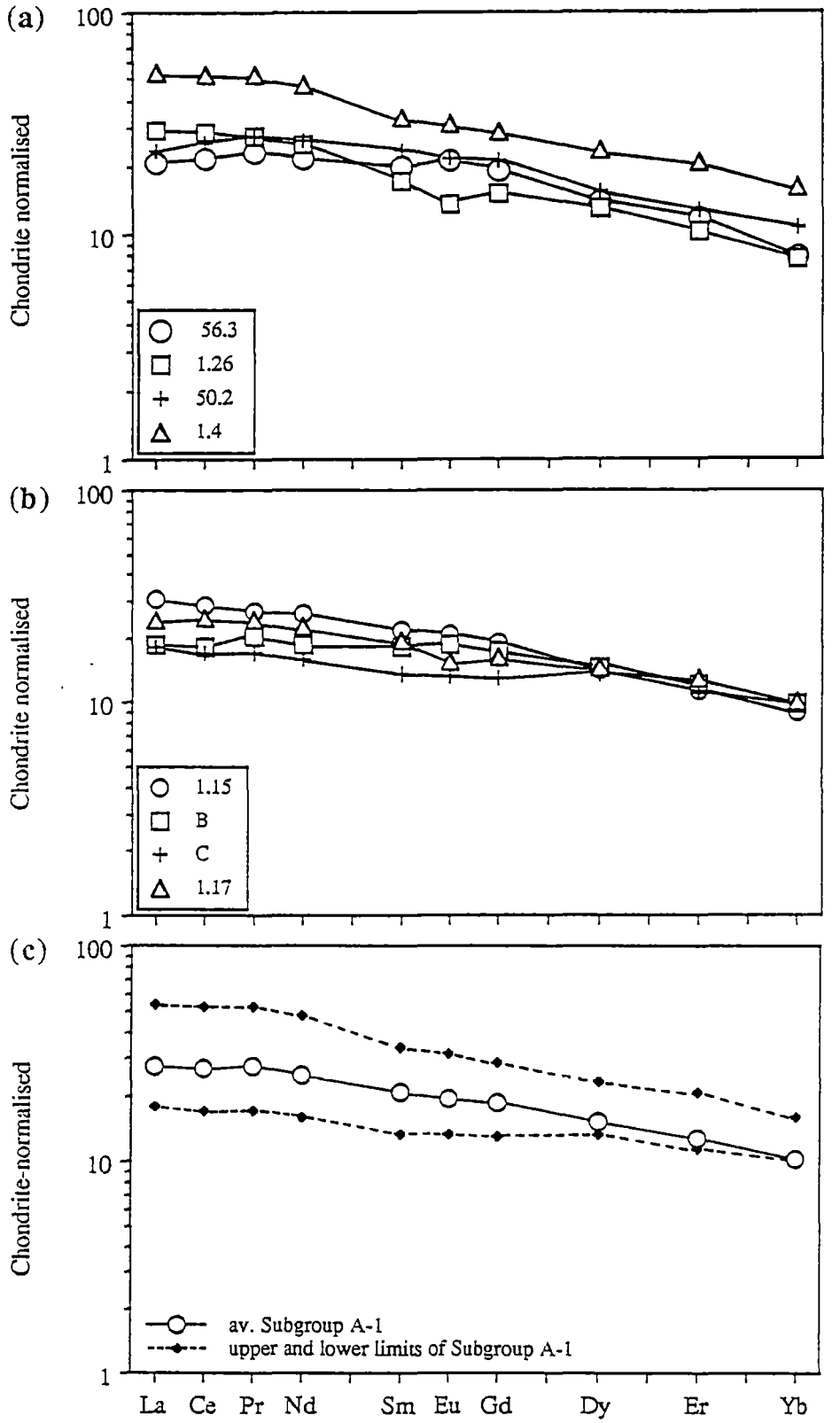

Figure 3.18. Chondrite-normalised REE patterns for the studied ocean-island tholeiitic lavas and dolerites (Subgroup A-1). REE patterns for individual samples are shown in (a) and (b), whereas their average and range are shown in (c). Normalising values in this and subsequent figures are those of Taylor and Gorton (1977).

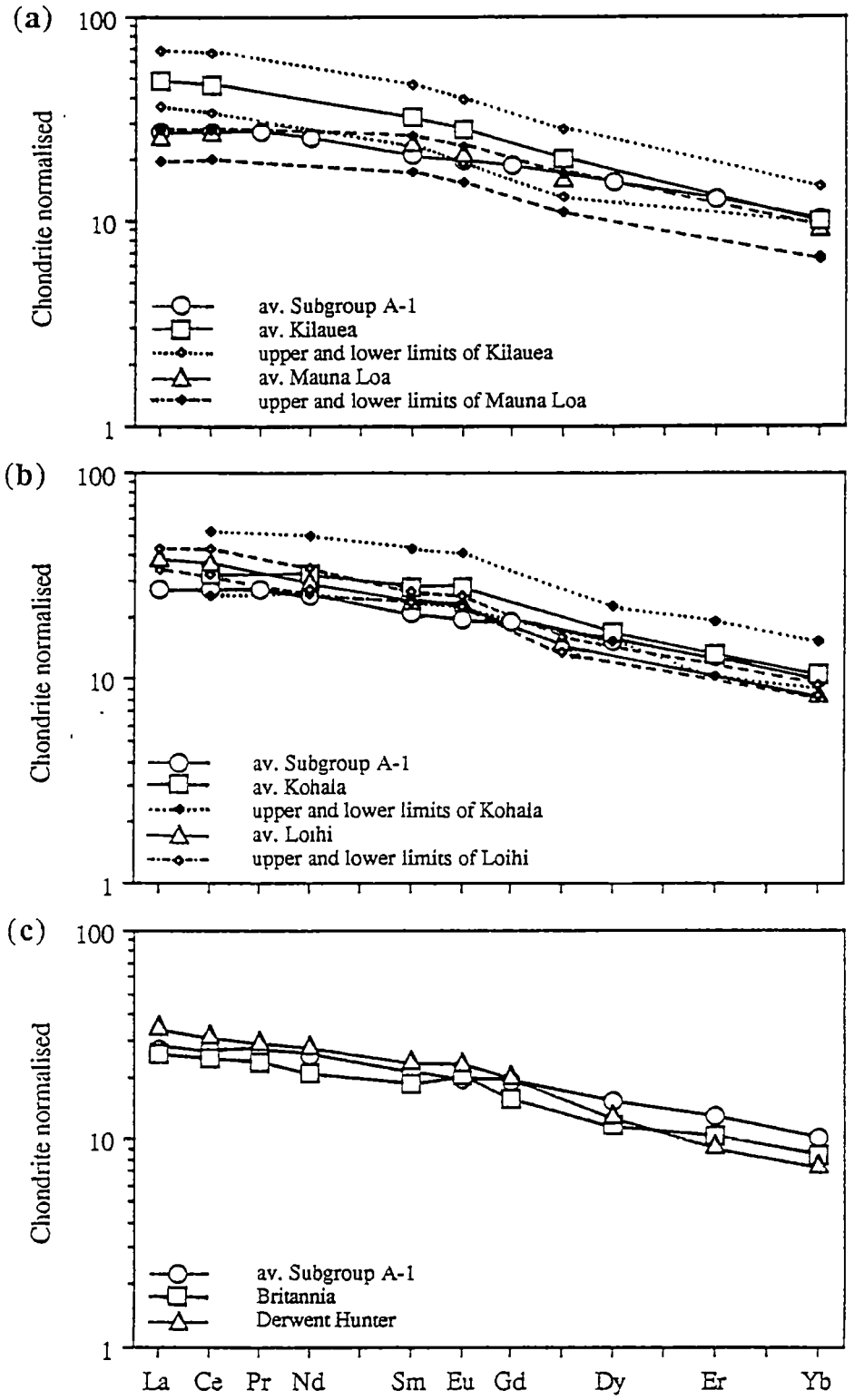

Figure 3.19. Chondrite-normalised REE pattern for the averaged studied ocean-island tholeiites (Subgroup A-1) compared with those for tholeiites of Kilauea and Mauna Loa Volcanoes, Hawaii (Basaltic Volcanism Study Project, 1981)(a), Waipio Valley transitional and tholeiitic basalts, Kohala Volcano, Hawaii (Feigenson *et al.*, 1983); and tholeiites from Loihi Seamount, Hawaii (Frey and Clague, 1983)(b); and tholeiites from Britannia and Derwent Hunter Seamounts, Tasmantids (Eggins *et al.*, 1990)(c).

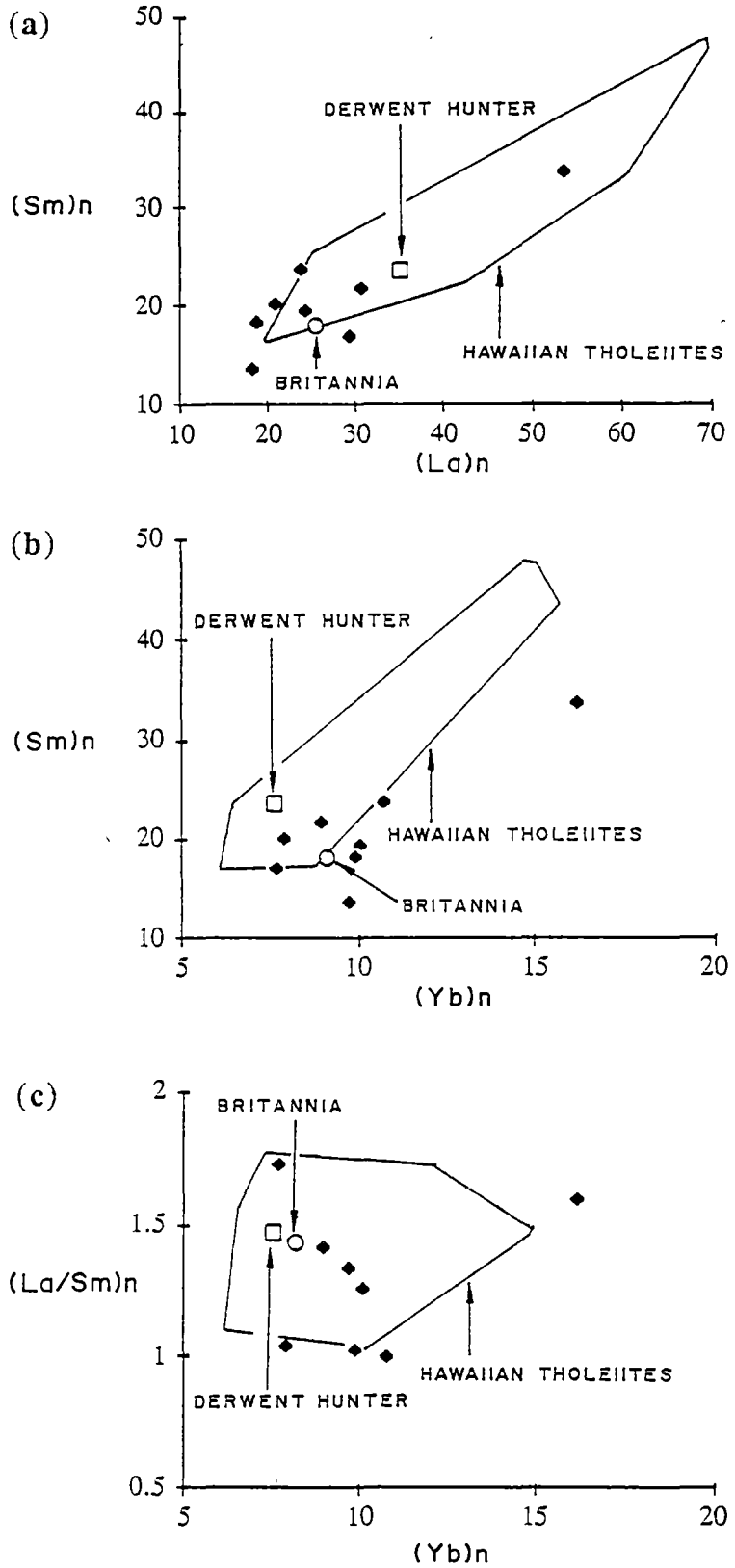

Figure 3.20. Comparative diagrams in terms of chondrite-normalised REE for the studied ocean-island tholeiitic lavas and dolerites (Subgroup A-1), and tholeiites from Hawaii and Tasmantids (data sources as in Fig. 3.19): (a) La vs Sm, (b) Sm vs Yb, and (c) La/Sm vs Yb.

and Breitkopf (1989), have demonstrated that these diagrams may often fail to unequivocally classify tectonic settings of formation of altered lavas. The mineral chemical, and major-, minor- and trace-element compositional data presented above all strongly support an assignment of the Subgroup A-1 lavas and dolerites as ocean-island tholeiites, and pronounced similarities with several Hawaiian tholeiitic suites are evident.

The most useful element variation diagram for the studied samples is a subset of the N-MORB - normalised multi-element plot of Pearce (1982, 1983) which covers a range of immobile elements from Yb to Nb. Since Hf contents have not been determined in this study, the values for Hf in both the studied samples and reference suites are estimated from Zr concentrations using Zr/Hf=39, as suggested by Wood *et al.* (1979). Figure 3.21 is such a diagram for the average abundances of Subgroup A-1 and the modern ocean-island tholeiitc suites. All the patterns shown are very similar. In conclusion, the basalts and dolerites constituing Subgroup A-1 form a coherent differentiation series of ocean-island tholeiites, with strong similarities to several Hawaiian and Tasmantid tholeiitic suites.

3.3 Ocean-Island Transitional Tholeiites and Alkalic Basalts (Subgroup A-2)

3.3.1 Occurrence and Petrography

The analysed samples of Subgroup A-2 include one basaltic lava and eleven dolerites that locally occur as float weathering from serpentinite melange, in the Mae Charim, Doi Phuk Sung and Nan River areas. Sample locations and petrography of individual analysed samples are given in Tables I-1 (Appendix I) and I-2 (Appendix II), respectively.

Petrography of lava sample

The Subgroup A-2 lava is a slightly porphyritic rock with subhedral plagioclase, and euhedral to subhedral pink clinopyroxene microphenocrysts; the latter occasionally show hour-glass zoning. It is quite altered and consequently, its primary groundmass constituents cannot be precisely determined.

All plagioclases have undergone albitisation and been replaced by pumpellyite, epidote and sericite with variable quartz and chlorite. Mixtures of green chlorite, actinolitic hornblende and leucoxene that are common interstitially, are likely to be alteration products of clinopyroxene, Fe-Ti oxides and/or glass. Chlorite, quartz, Fe-

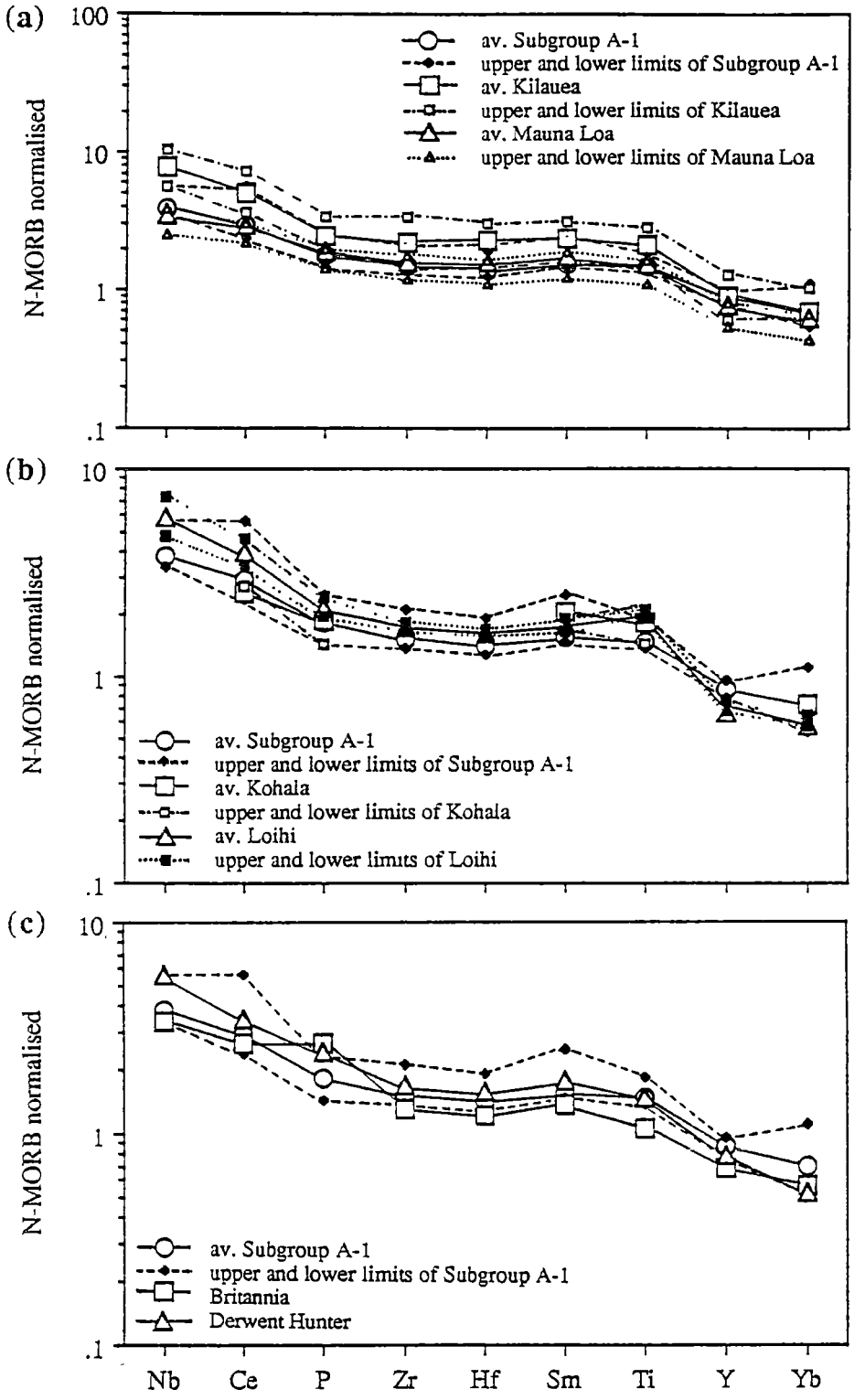

Figure 3.21. A subset of N-MORB normalised multi-element diagram of Pearce (1982, 1983) showing the patterns for averaged tholeiites of Subgroup A-1 compared with those from Kilauea and Mauna Loa Volcanoes, Hawaii (a), Kohala Volcano and Loihi Seamount (b), and Britannia and Derwent Hunter Seamounts, Tasmantids (c). Also shown in (a) and (b) are the lower and upper limits of the reference suites. Sources of data for the modern ocean-island tholeiites are the same as in Figure 3.19. In this and subsequent figures, N-MORB normalising values are those of Sun and McDonough (1989), and Hf content is estimated from Zr content using Zr/Hf=39, as suggested by Wood *et al.* (1979).

Ti oxides and Fe sulphides rarely occur. These secondary minerals are characteristic of very low- to low-grade regional metamorphism.

Petrography of dolerites

The dolerites of Subgroup A-2 are mineralogically similar, consisting predominantly of plagioclase laths and subhedral to anhedral pink clinopyroxene with minor magnetite and bladed ilmenite (Fig. 3.22). Euhedral apatite occurs as inclusions in plagioclase in a few samples. In spite of their similar mineralogies, they show variable textures from seriate to equigranular and subophitic.

Plagioclase is often albitised and partially or totally pseudomorphed by pumpellyite, epidote, sericite and chlorite. In some plagioclase sites, quartz, prehnite and bluish amphibole have developed. Clinopyroxenes are much more resistant to alteration relative to other igneous minerals, and are only slightly replaced by chlorite and bluish and greenish amphiboles. All Fe-Ti oxides are partially or wholly transformed to leucoxene, and many show exsolution textures. The metamorphic minerals in the Subgroup A-2 dolerites are typical of very low- to low-grade metamorphic rocks of regional metamorphism.

3.3.2 Mineral Chemistry

Pink clinopyroxene, a diagnostic mineral of Subgroup A-2 samples, is the only informative igneous phase present. Clinopyroxene analyses of dolerites are given in Table 3.6 and plotted in the conventional pyroxene quadrilateral in Figure 3.23. They range compositionally from augites to diopsides with $Wo_{36.4\text{-}46.7}En_{36.1\text{-}48.0}Fs_{13.9\text{-}22.1}$ (Subcommittee on Pyroxenes, I.M.A., 1988). Unlike in the Subgroup A-1 tholeiites, these clinopyroxenes do not define an Fe-enrichment trend. Rather they show a trend of strong Ca-depletion at fairly constant Mg# and fall largely between the solidus and subsolidus clinopyroxene trends of the Skaergaard Intrusion.

The Subgroup A-2 pyroxenes appear to be transitional between subalkalic and alkalic clinopyroxenes (Figs. 3.23 and 3.24a). On average, the Ti content of Subgroup A-2 pyroxenes (0.041±0.015) is significantly higher than that of the Subgroup A-1 pyroxenes and comparable to that of transitional tholeiitic and alkalic clinopyroxenes of Hamakua lavas, Mauna Kea Volcano, Hawaii (Frey *et al.*, 1990). It bears a positive relationship to Al^{iv} in the approximate ratio $Ti:Al^{iv}= 1:2.7$, indicating multiple coupled substitutions dominated by $(Ti^{4+}/2)$ - Al^{iv} (Fig. 3.24b).

TABLE 3.6. ELECTRON MICROPROBE ANALYSES OF PINK CLINOPYROXENES IN THE STUDIED OCEAN-ISLAND TRANSITIONAL THOLEIITES AND ALKALIC DOLERITES (SUBGROUP A-2). FeO AND Fe_2O_3 ARE CALCULATED ASSUMING STOICHIOMETRY ON THE BASIS OF 4 CATIONS AND 6 OXYGENS. END-MEMBERS IN TERMS OF WOLLASTONITE, ENSTATITE AND FERROSILITE ARE CALCULATED ACCORDING TO THE METHOD RECOMMENDED BY THE SUBCOMMITTEE ON PYROXENES, IMA (1988).

Sample no.	27.1						27.3					27.4				
Analysis no.	1	2	3	4	5	6	1	2	3	4	5	1	2	3	4	5
SiO2	50 01	50.33	50.34	49 65	51 67	51.50	49.81	51.26	51.35	50.03	51.17	48.81	51.11	52.58	50.63	50.10
TiO2	1 91	1.12	1.21	2.05	1 25	0.96	1.80	1.10	0.80	1.78	1.28	1.63	1.34	0.76	1.30	1.33
Al2O3	3.06	2.52	2.69	3.82	2.37	2.04	3.78	2.45	1.93	3.87	2.93	4.37	2.66	1.39	3.09	3.13
Cr2O3	-	-	-	0.22	-	-	-	-	-	-	-	-	-	-	-	-
Fe2O3	0.08	0 30	1.74	0.59	-	-	-	-	-	0.35	0 93	1.90	-	-	1.46	0 58
FeO	8.80	10 27	8.96	8.96	10.37	12.34	10.09	10.86	10.65	9.87	9.80	8.08	9.34	10.16	8.97	9.67
MnO	-	-	-	-	-	0 24	-	0.23	-	-	-	-	-	-	-	-
MgO	14.11	13.81	14 01	14.18	14.41	13 78	13.28	14.63	14 47	13.20	13.04	13.38	14.34	14.82	13.60	13.96
CaO	21.52	20.54	20.34	21.06	20.58	19.69	21.14	19.54	20.03	21.88	21.18	20.50	21 07	20.28	21.09	20.72
Na2O	-	-	0 28	-	-	-	-	-	-	-	0 47	0.35	-	-	0.32	-
Total	99.49	98.89	99.57	100.53	100.65	100.55	99.90	100.07	99.23	100.98	100.80	99.02	99.86	99.99	100.46	99.49
Si	1.878	1.907	1.892	1.847	1.919	1.929	1.869	1.916	1.935	1.861	1.904	1.842	1.909	1.959	1.887	1 885
ivAl	0.123	0.093	0.108	0.153	0.082	0.071	0.131	0 084	0.065	0.140	0 096	0.158	0.092	0.041	0.113	0.115
Total tetra.	2 000	2.000	2.000	2.000	2.000	2.000	2.000	2.000	2.000	2.000	2.000	2.000	2.000	2.000	2.000	2.000
viAl	0.013	0.020	0.011	0.015	0.022	0.019	0.036	0.024	0.021	0.030	0 032	0.037	0.026	0.020	0 023	0.024
Ti	0 054	0.032	0.034	0.057	0.035	0.027	0.051	0 031	0.023	0.050	0.036	0.046	0.038	0.021	0.036	0.038
Cr	-	-	-	0.007	-	-	-	-	-	-	-	-	-	-	-	-
Fe3+	0.002	0.009	0.049	0.017	-	-	-	-	-	0.010	0.026	0.054	-	-	0.041	0.016
Fe2+	0.276	0.325	0.282	0.279	0.322	0.387	0.317	0.340	0.336	0.307	0.305	0.255	0.292	0.317	0.280	0.304
Mn	-	-	-	-	-	0.008	-	0.007	-	-	0.000	-	-	-	-	-
Mg	0.789	0.780	0.785	0.786	0 797	0 769	0.743	0.815	0.812	0.732	0.723	0.753	0.798	0.823	0.755	0.783
Total octa.	1.134	1.166	1.161	1.160	1.176	1.209	1.147	1.217	1.191	1.128	1.122	1.145	1.153	1.180	1.135	1.165
Ca	0.866	0.834	0.819	0 840	0.819	0.790	0 850	0.783	0.809	0.872	0.844	0.829	0.843	0 809	0.842	0.835
Na	-	-	0 020	-	-	-	-	-	-	-	0.034	0.026	-	-	0.023	-
Total cats.	4.000	4.000	4.000	4.000	3.995	3.999	3 997	3.999	4.000	4 000	4.000	4.000	3.995	3.990	4.000	4.000
Mg/(Mg+Fe^{2+})	0.741	0.706	0.736	0.738	0 712	0.665	0.701	0.706	0.708	0.704	0.703	0.747	0.732	0.722	0.730	0.720
CaSiO3	44.77	42.81	42.33	43.70	42.25	40.45	44.52	40.25	41.34	45.41	44.47	43.85	43.62	41.53	43 90	43.07
MgSiO3	40.82	40.04	40.57	40.92	41.14	39.38	38.90	41.92	41.52	38.10	38 08	39.81	41.29	42.22	39.38	40.39
FeSiO3	14.41	17.15	17 10	15.38	16.61	20 17	16.59	17.83	17.15	16.49	17.45	16.34	15 09	16 24	16.72	16.54

Sample no	27.4	27 6					27.7						28 2			
Analysis no	6	1	2	3	4	5	1	2	3	4	5	6	1	2	3	4
SiO2	49 36	49.54	50.20	49 36	50.44	52.46	51.44	51.53	51.02	50.65	49.38	49.34	51.86	50.61	50 21	51 80
TiO2	1.84	1.81	1.48	1.79	1.16	0.77	1.52	1.19	0.97	1 56	1.64	1.88	0.72	0.68	1.49	1.03
Al2O3	4.31	3 59	3.47	4.02	3.24	1.61	2.65	2.78	2.42	2 89	4.22	4.16	1.57	3 09	2.89	2.14
Cr2O3	-	-	-	-	-	-	-	0.20	-	-	-	-	-	0.57	-	-
Fe2O3	1.46	0.57	1.47	1.15	0.01	-	-	-	-	-	1.80	1.85	-	0.75	1.04	1.28
FeO	8.18	10.68	8.99	9.71	11.36	10.84	11.05	11.34	11.58	10.78	9.29	9.65	11.32	7 94	10 92	10.03
MnO	-	-	-	-	0 23	0.26	-	0 23	0.23	-	-	-	-	-	-	0.25
MgO	13.19	13.37	13.52	13.71	13.36	14.37	14.89	14.01	13.83	13.90	13.54	13.80	15.15	16 98	14 93	14.42
CaO	21.55	20.58	21 03	20.67	20.25	20.17	19 34	19.85	19.56	20.19	19.76	19.38	18.78	17.89	18 61	20 07
Na2O	0 30	-	0 29	-	-	-	-	-	-	-	0 38	0 35	-	-	-	0.26
Total	100 19	100 14	100 45	100.41	100 05	100.48	100.89	101.13	99.61	99.97	100.01	100.41	99 40	98 51	100.09	101 28
Si	1 844	1.861	1 872	1.845	1.895	1.952	1.905	1.911	1 923	1.898	1.849	1.842	1.948	1.894	1.880	1.916
ivAl	0.156	0.139	0.128	0.155	0.105	0 048	0.095	0.089	0.077	0.102	0 151	0.158	0 052	0.106	0.120	0.084
Total tetra	2.000	2.000	2 000	2.000	2.000	2.000	2.000	2 000	2.000	2.000	2.000	2.000	2.000	2.000	2.000	2 000
viAl	0.034	0.020	0 025	0.022	0.039	0 023	0.021	0 032	0.030	0.026	0.035	0.025	0 018	0.030	0.007	0 009
Ti	0.052	0 051	0.041	0.050	0 033	0 022	0.042	0.033	0.028	0 044	0.046	0 053	0.020	0.019	0.042	0 029
Cr	-	-	-	-	-	-	-	0 006	-	-	-	-	-	0 017	-	-
Fe3+	0.041	0.016	0.041	0.032	-	-	-	-	-	-	0.051	0.052	-	0 021	0 029	0.036
Fe2+	0 256	0 336	0.280	0.304	0 357	0.338	0.342	0 352	0.365	0.338	0.291	0.301	0.355	0.249	0.342	0 310
Mn	-	-	-	-	0 007	0.008	-	0.007	0.007	-	-	-	-	-	-	0 008
Mg	0.734	0.748	0 751	0.764	0.748	0 797	0.822	0.774	0.777	0.776	0.756	0.768	0.848	0.947	0 833	0.795
Total octa.	1.116	1.171	1.139	1.172	1.185	1.187	1.227	1 204	1.207	1.184	1.179	1.200	1.242	1.283	1.253	1.186
Ca	0.862	0.829	0 840	0.828	0.816	0.804	0.767	0.789	0.790	0.811	0.793	0.775	0.756	0.717	0.747	0.795
Na	0 022	-	0.021	-	-	-	-	-	-	-	0.028	0.025	-	-	-	0 018
Total cats.	4.000	4 000	4.000	4.000	4.000	3.991	3.995	3.992	3.996	3.994	4.000	4 000	3.997	4.000	4.000	4 000
Mg/(Mg+Fe^{2+})	0.742	0.690	0 728	0.716	0 677	0.703	0.706	0.688	0.680	0.697	0.722	0.718	0.705	0.792	0.709	0 719
CaSiO3	45.55	42.97	43.92	42.94	42.29	41.30	39.73	41.04	40.74	42.12	41.93	40.87	38.56	37.09	38.27	40.92
MgSiO3	38.78	38 80	39 26	39 63	38 81	40.95	42.56	40 29	40.06	40.33	39.99	40.50	43.30	48.97	42.71	40.89
FeSiO3	15 66	18 23	16.81	17.43	18 90	17.75	17.71	18.67	19 21	17.55	18.08	18.63	18.14	13.94	19 02	18 19

TABLE 3 6 CONTINUED

Sample no.	28.2	28.4						28.6					28.8			
Analysis no.	5	1	2	3	4	5	6	1	2	3	4	5	1	2	3	4
SiO2	50.81	50.58	50.24	51.30	49 42	50.04	49.64	49.05	50.18	49 26	49.82	52.08	48.45	48.13	49.02	46.95
TiO2	1.32	1.27	1.45	0.97	2 08	1.50	1.80	1.82	1.34	1.72	1.59	0.63	2.45	2.38	1.85	3.59
Al2O3	2.54	3.10	3.14	1.73	4.19	3.61	4.16	3.97	3.10	4.23	3.34	1.45	4.65	4.45	4.14	5.58
Cr2O3	-	-	-	-	-	-	-	-	-	0.19	-	-	-	-	-	-
Fe2O3	0.20	-	-	-	1.78	1.67	0.25	0.17	1.31	1.16	-	-	0.78	0.86	0.44	-
FeO	11.64	12.36	11 83	12 84	11.18	9 26	10.92	11.51	9.67	9.27	9.98	12.36	9.77	9.21	9.70	9.68
MnO	0.36	-	-	0.22	-	-	-	-	-	-	-	-	-	-	-	-
MgO	15.01	13.41	13 01	14 39	11.73	13.48	13 05	13.78	14.16	14.37	13.91	15.20	12.77	12.71	12.89	12.22
CaO	18.11	19.21	20.39	18 11	18.92	20.75	20.91	18.90	19.50	19.05	20.45	17.61	21.55	21.73	21.54	21.50
Na2O	-	-	-	-	1.00	0.29	-	-	0.28	0.25	-	-	-	-	-	-
Total	99.99	99.93	100.06	99.56	100.30	100.60	100.73	99.20	99.54	99.50	99.09	99.33	100.42	99.47	99.58	99.53
Si	1.904	1.903	1.892	1.937	1.860	1.866	1.854	1.857	1.885	1.848	1.881	1.959	1.817	1.821	1.849	1.772
ivAl	0.096	0.097	0.108	0.063	0.141	0.134	0.146	0.143	0.115	0.152	0.119	0.041	0.183	0.179	0.151	0.228
Total tetra.	2.000	2.000	2 000	2.000	2.000	2.000	2.000	2.000	2.000	2.000	2.000	2.000	2.000	2.000	2.000	2.000
viAl	0.016	0 041	0 031	0.014	0.045	0.024	0.037	0.035	0.023	0.035	0.030	0.023	0.022	0.019	0.033	0.022
Ti	0.037	0.036	0.041	0.028	0.059	0.042	0.051	0.052	0.038	0.049	0.045	0.018	0.069	0.068	0.052	0.103
Cr	-	-	-	-	-	-	-	-	-	0.006	-	-	-	-	-	-
Fe3+	0 006	-	-	-	0.051	0.047	0.007	0.005	0 037	0.033	-	-	0.022	0.024	0.013	-
Fe2+	0.365	0 389	0.373	0.406	0.352	0.289	0.341	0.364	0.304	0.291	0.315	0.389	0.307	0.291	0.306	0.306
Mn	0.011	-	-	0.007	-	-	-	-	-	-	-	-	-	-	-	-
Mg	0 838	0 752	0.730	0 810	0.658	0.749	0.727	0.778	0.793	0.804	0.783	0.852	0.714	0.717	0.725	0 693
Total octa.	1.273	1.218	1.175	1.264	1.164	1.151	1.163	1.233	1 195	1 216	1.173	1.282	1.134	1.119	1.129	1.124
Ca	0 727	0.775	0 823	0.733	0.763	0.829	0 837	0.767	0.785	0.766	0.827	0.710	0 866	0.881	0 871	0 876
Na	-	-	-	-	0 073	0 021	-	-	0 021	0 018	-	-	-	-	-	-
Total cats.	4.000	3.992	3.997	3.997	4.000	4.000	4.000	4.000	4.000	4.000	4.000	3.991	4.000	4.000	4.000	4.000
Mg/(Mg+Fe^{2+})	0 697	0.659	0.662	0.663	0.651	0.722	0.680	0.681	0.723	0.734	0.713	0 687	0.700	0.711	0.703	0 694
CaSiO3	37.34	40.44	42.73	37.48	41.85	43.31	43.77	40.06	40.90	40.44	42.96	36.38	45.38	46.05	45.49	46.73
MgSiO3	43.05	39 26	37.92	41.42	36.09	39.14	38.01	40 64	41.33	42.46	40.67	43.69	37.40	37.46	37.87	36.95
FeSiO3	19.61	20.30	19.35	21 11	22.07	17.55	18 22	19 30	17 77	17.10	16.36	19.93	17 22	16.50	16 64	16.32

Sample no	28.8		36.1					36.3						
Analysis no.	5	6	1	2	3	4	5	6	1	2	3	4	5	6
SiO2	49.15	49.17	52.51	51 02	50 02	50.52	50.48	51.09	52.32	52.72	51 11	51 76	51.55	51 64
TiO2	2.11	2.07	0.90	1.13	1.89	1.75	1.64	1.25	0.95	0.76	1.12	1 06	1.43	1.45
Al2O3	4.45	4.52	1.85	2.42	3.73	3.48	3.49	2.73	1.85	1.64	2.59	2.42	2.89	2.86
Cr2O3	-	-	-	-	-	0 21	-	-	-	-	-	-	-	-
Fe2O3	1.97	-	-	-	-	0.19	1.57	0.68	-	-	-	-	-	0 52
FeO	8.25	10.01	9 59	10 84	9 93	9.16	7.90	9 60	10.13	10 76	9.75	11 82	8.98	8.53
MnO	-	-	-	-	-	-	0.21	-	-	-	-	-	-	-
MgO	12.99	13 00	15 23	13 83	14.35	14.49	14.59	14.24	15.43	15.32	14.42	14.96	15.35	14.92
CaO	21.91	21.20	20 07	20.26	19.83	21 08	20.65	20.32	19.34	19.11	20.79	18.63	20.58	20.92
Na2O	0 26	-	-	-	-	-	0 27	0 26	-	-	-	-	-	0.25
Total	101.09	99 97	100.15	99.50	99 75	100.88	100 80	100.17	100.02	100.31	99.78	100 65	100.78	101.09
Si	1.825	1.845	1.946	1 921	1.871	1.870	1.866	1.905	1.944	1.955	1.912	1.923	1.900	1.900
ivAl	0.175	0.155	0 054	0.080	0.129	0.130	0.134	0.095	0.056	0.045	0.088	0.078	0 100	0.101
Total tetra.	2.000	2.000	2.000	2.000	2.000	2.000	2.000	2.000	2.000	2.000	2.000	2.000	2.000	2.000
viAl	0 020	0.045	0.027	0.028	0.035	0.022	0 018	0 025	0.025	0 027	0.026	0 029	0.026	0.024
Ti	0.059	0.058	0 025	0 032	0 053	0.049	0.046	0 035	0 026	0 021	0.032	0.030	0.040	0.040
Cr	-	-	-	-	-	0.006	-	-	-	-	-	-	-	-
Fe3+	0.055	-	-	-	-	0.005	0.044	0.019	-	-	-	-	-	0.014
Fe2+	0.256	0 314	0.297	0.341	0.311	0.283	0 244	0.299	0.315	0.334	0 305	0 367	0 277	0 263
Mn	-	-	-	-	-	-	0.006	-	-	-	-	-	-	-
Mg	0.719	0.727	0.841	0.776	0.800	0.799	0 804	0.791	0.854	0.847	0.804	0 828	0.843	0.818
Total octa.	1.109	1.144	1.191	1.177	1.199	1.164	1.162	1.170	1.220	1 228	1.167	1 254	1.185	1.158
Ca	0.872	0.852	0.797	0.817	0 795	0.836	0.818	0.812	0.770	0.759	0.833	0.741	0.813	0 824
Na	0.019	-	-	-	-	-	0.020	0.019	-	-	-	-	-	-
Total cats.	4.000	3.997	3.988	3.994	3.994	4.000	4 000	4.000	3.989	3.988	4.000	3.995	3.998	4.000
Mg/(Mg+Fe^{2+})	0.737	0.694	0.739	0.694	0.720	0.738	0.767	0.725	0 731	0 717	0.725	0 693	0.753	0.757
CaSiO3	45.84	45.01	41.18	42 24	41.71	43.45	42.68	42.25	39.70	39 14	42.89	38 28	42.05	42.96
MgSiO3	37.79	38.40	43.47	40.12	42.00	41.54	41.95	41.18	44.06	43.65	41.40	42.77	43 62	42 61
FeSiO3	16.37	16.59	15.35	17.65	16 29	15.01	15 37	16 58	16 24	17.20	15.71	18.95	14.32	14.43

- = BELOW DETECTION LIMIT.

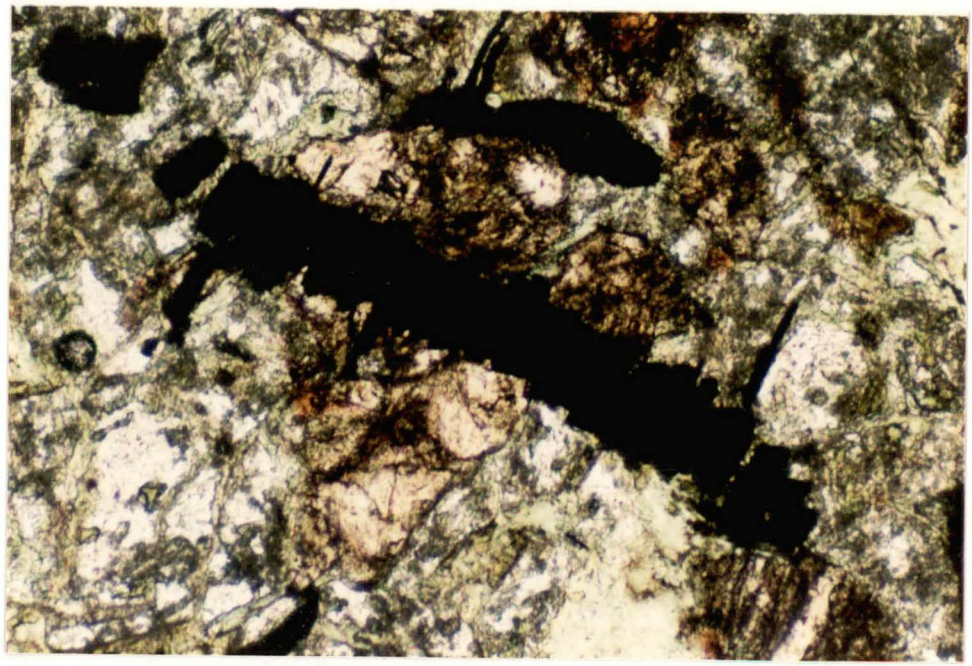

Figure 3.22. Photomicrograph of the studied ocean-island transitional tholeiitic and alkalic dolerite (Subgroup A-2)(sample 27.7) showing clinopyroxenes (pale pink) and a bladed ilmenite crystal with indentations and offsets in the crystal margin, caused by traverse shearing. Ordinary light, X 130.

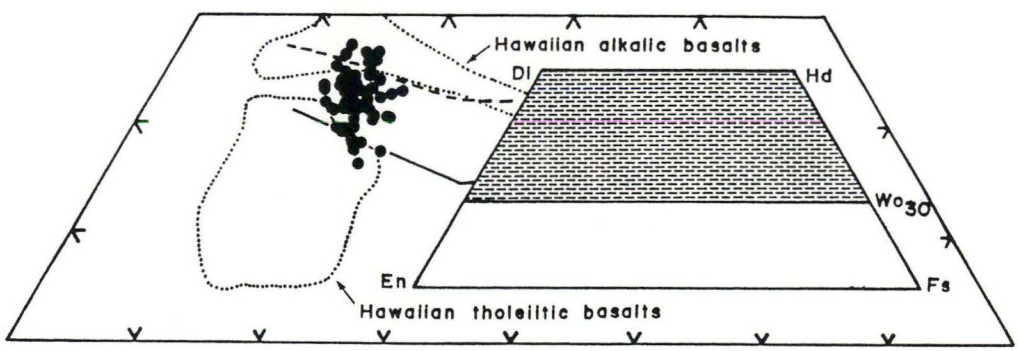

Figure 3.23. Compositions of pink clinopyroxenes in the studied ocean-island transitional tholeiitic and alkalic dolerites (Subgroup A-2). Also shown are the solidus (solid line) and subsolidus (dashed line) trends for Skaergaard clinopyroxenes (Brown, 1967; Nwe, 1976), and the compositional fields for Hawaiian tholeiitic and alkalic clinopyroxenes (Basaltic Volcanism Study Project, 1981).

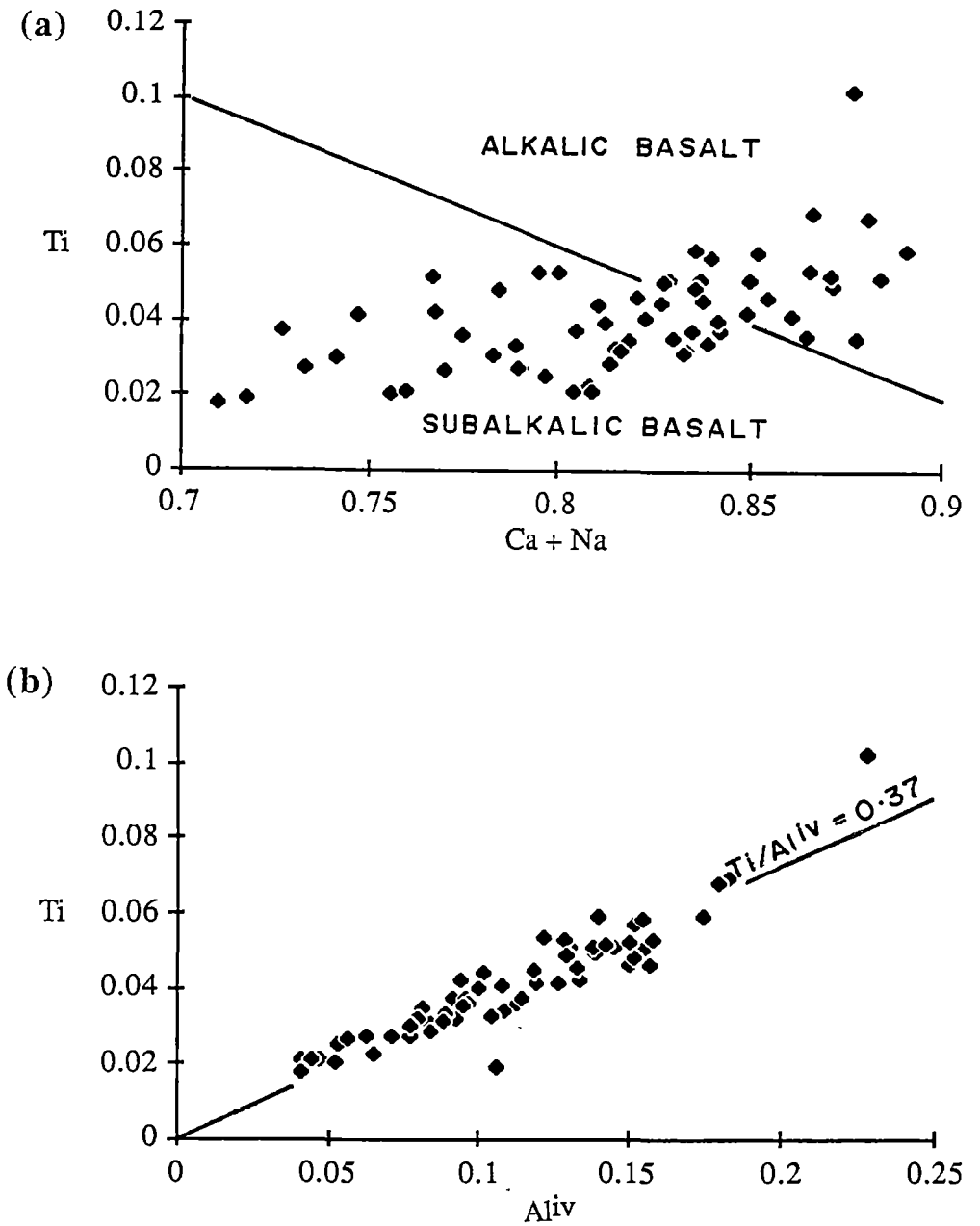

Figure 3.24. Plot of Ti against (a) Ca+Na and (b) Al^{iv} (on the basis of 6 oxygens) for clinopyroxenes in the studied ocean-island alkalic dolerites (Subgroup A-2). The clearly defined positive trend in (b) is caused by $(Ti^{4+}/2)$-Al^{iv} substitution. The compositional field boundary in (a) is taken from Leterrier *et al.* (1982).

3.3.3 Whole-rock Chemistry

Major elements

Almost all Subgroup A-2 basaltic rocks are quite evolved, being characterised by high FeO* (average 12.6±1.2 wt%), TiO_2 (average 3.7±0.5 wt%) and P_2O_5 (average 0.6±0.2 wt%), and relatively low MgO. Although they have FeO* contents comparable to evolved MORB and ocean-island basalts, their notably high TiO_2 contents (and Ti-rich clinopyroxenes), however, preclude the possibility of their being MORB (Figs. 3.12 and 3.13).

These basaltic rocks exhibit broad FeO*, TiO_2 and V enrichment trends relative to FeO*/MgO as do the Subgroup A-1 tholeiites, but they have higher FeO* and in particular, TiO_2, and lower V concentrations at similar FeO*/MgO values (Fig. 3.12). Their Nb/Y values are almost close to unity (Fig. 3.1), characteristic of transitional tholeiites to alkalic basalts (Pearce and Cann, 1973, Floyd and Winchester, 1975, Pearce, 1982). Their high TiO_2 and relatively low V abundances result in the high values for Ti/V (>50), consistent with those of alkalic basalts (Shervais, 1982)(Fig. 3.16a).

Minor and trace elements

FeO*/MgO variation diagrams for minor and trace elements (Fig. 3.14) show that the basaltic rocks of Subgroup A-2 are also significantly enriched in P_2O_5 and other HFSE (206-313 ppm Zr, 23-41 ppm Nb, and 30-50 ppm Y), but slightly depleted in Ni, Cr and Sc relative to the Subgroup A-1 tholeiites. Their Zr, Y and Sc concentrations are positively correlated with FeO*/MgO, whereas Ni and Cr contents diminish with increasing degrees of fractionation. The increase in Sc indicates that clinopyroxene has not fractionated to a significant degree. P_2O_5 and Nb appear to have poor correlation with FeO*/MgO although Nb and Zr display a broadly positive relationship (Fig. 3.15).

The compositional trends for the Subgroup A-2 transitional tholeiites and alkalic basalts on Ti-Zr, Nb-Zr, and Y-Zr plots (Fig. 3.15) appear to be the continuation of those for the Subgroup A-1 tholeiites to higher absolute values. However, ratios for these HFSE pairs are remarkably different, i.e. almost all have Ti/Zr and Zr/Nb values less than 87 and 10, respectively, but Zr/Y greater than 5.7, contrasting with the Subgroup A-1 tholeiites. These ratios are similar to those of the Hawaiian transitional tholeiites and alkalic basalts (Fig. 3.15). Their positions on

tectonomagmatic discrimination diagrams in Figures 3.2, 3.16a and 3.17 also support the within-plate transitional tholeiitic and alkalic affinities.

Rare-earth elements

REE abundances for four Subgroup A-2 dolerites are given in Table 3.5 and their chondrite-normalised values are plotted in Figure 3.25. Their REE patterns show markedly greater LREE enrichment relative to HREE than those of Subgroup A-1 tholeiites. They have HREE concentrations, expressed as Yb, ranging from 8 to 13 times chondritic values (similar to those of Subgroup A-1 tholeiites) and LREE concentrations, in terms of La, varying from 65 to 81 times chondritic values.

Comparisons with modern suites

An extensive search for the modern suites chemically comparable to the Subgroup A-2 basaltic rocks has been carried out. Despite the scarcity of data for modern analogues, the Subgroup A-2 transitional tholeiites and alkalic basalts are comparable with the alkalic Kula volcanic series, Haleakala Volcano, east Maui (Chen and Frey, 1985), and Hamakua transitional tholeiites and alkalic basalts, Mauna Kea Volcano, Hawaii (Frey *et al.*, 1990) that were erupted in the postshield stage of volcano construction. This is particularly true for REE abundances and REE patterns (Fig. 3.25b), FeO*, TiO_2, and MgO (Figs. 3.12 and 3.13), element ratios (Figs. 3.15 and 3.26), and N-MORB - normalised multi-element patterns (Fig. 3.27).

From the above chemical features, it can be inferred that the Subgroup A-2 samples are unequivocal ocean-island transitional tholeiitic and alkalic basalts which probably formed in alkalic capping stage atop large volcanoes composed dominantly of Subgroup A-1 ocean-island tholeiites.

3.4 Summary

The rock classified as Group A are all basalts, and differentiated from the other groups by their higher Nb/Y (>0.3), Ti/Y (>420) and Ni contents (38-732 ppm) at similar MgO values, and lower Zr/Nb values (8-15). On compositional grounds, these may be subdivided into ocean-island tholeiites (Subgroup A-1), and transitional tholeiites and alkalic basalts (Subgroup A-2).

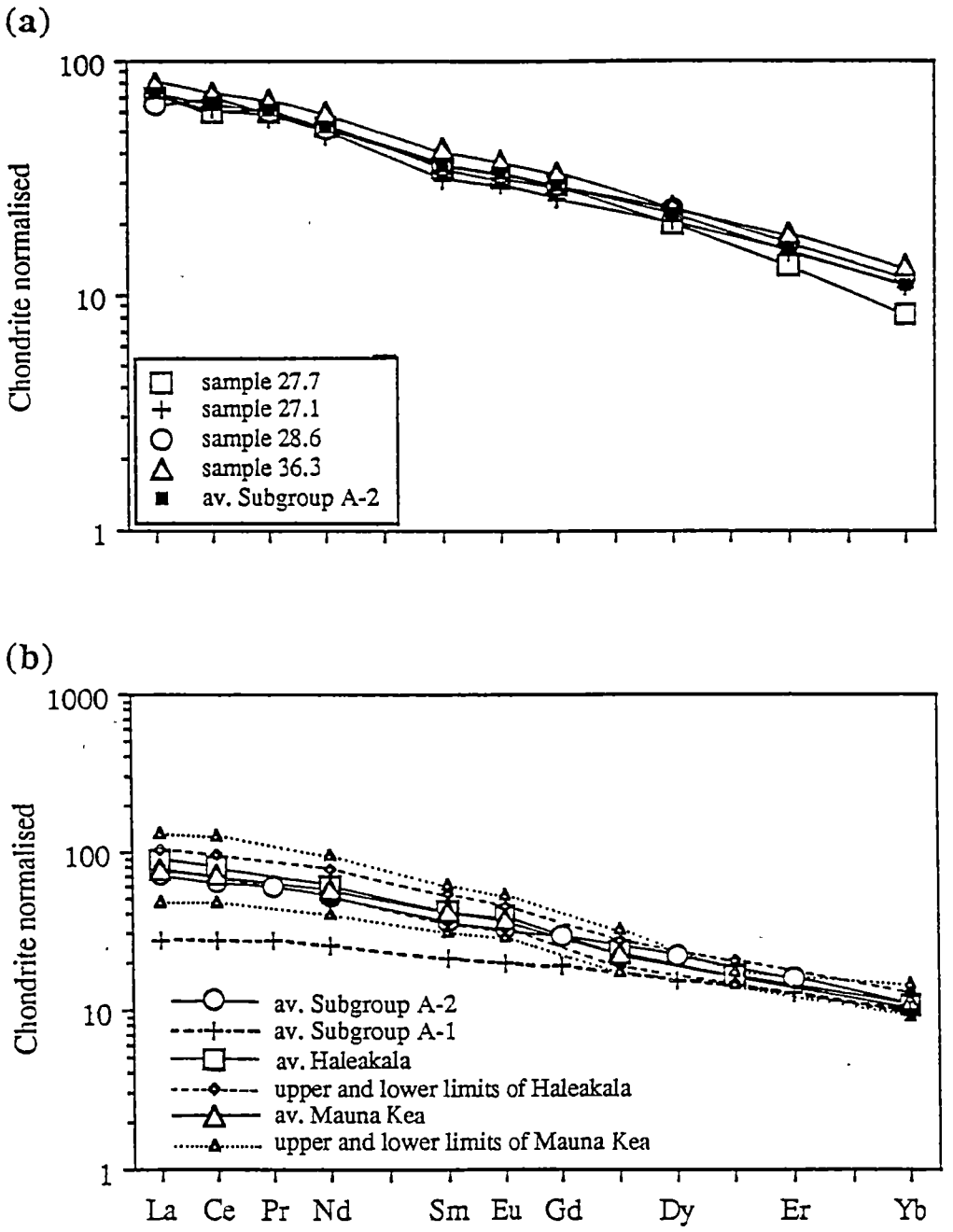

Figure 3.25. Chondrite-normalised REE plots for (a) the studied ocean-island transitional tholeiitic and alkalic dolerites (Subgroup A-2) and their average, and (b) averaged modern analogues (alkalic basalts of Kula series, Haleakala Volcano, Maui (Chen and Frey, 1985), and Hamakua transitional tholeiites and alkalic basalts, Mauna Kea Volcano, Hawaii (Frey *et al.*, 1990)) and their ranges. Also shown in (b) are the averaged Subgroup A-1 tholeiites and Subgroup A-2 dolerites.

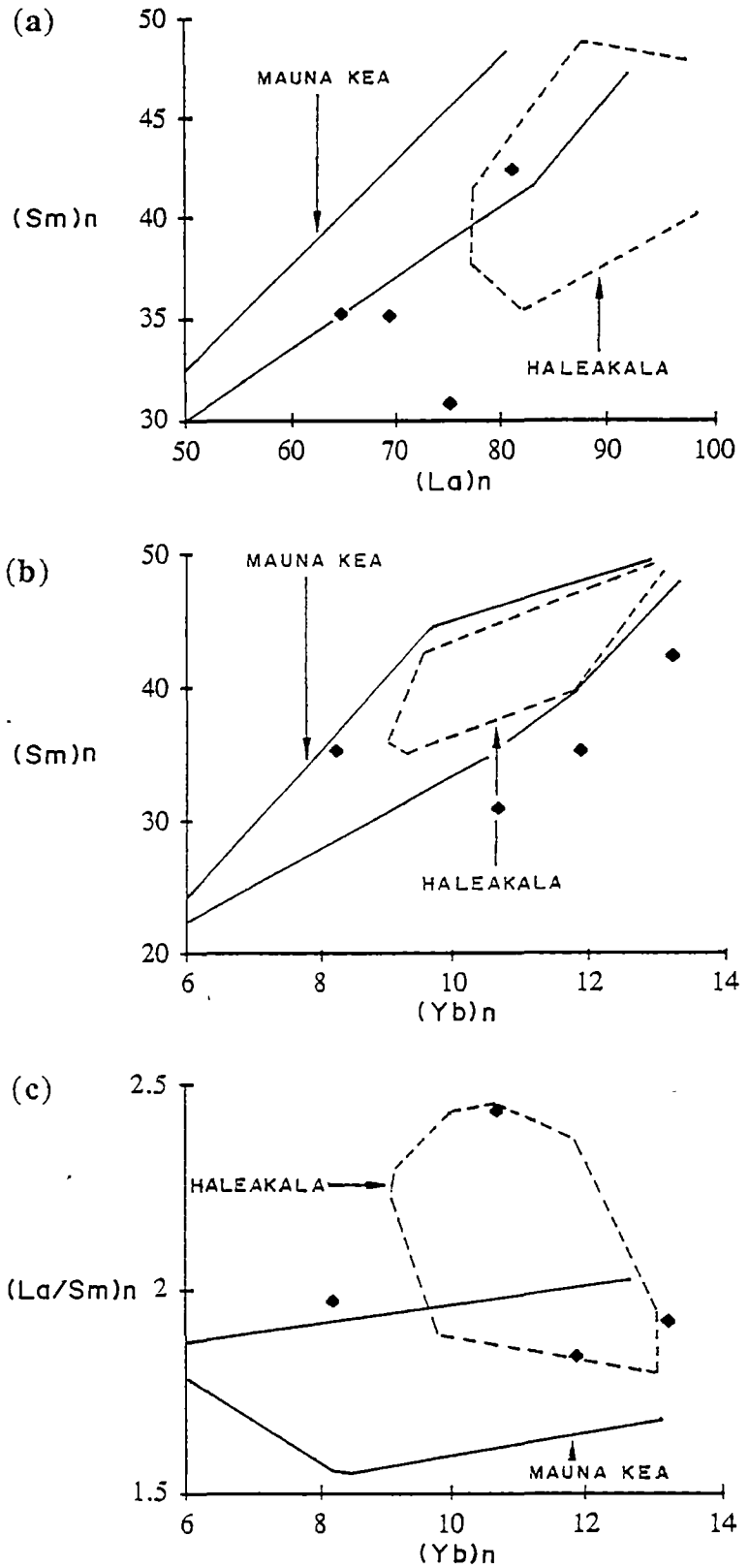

Figure 3.26. Diagrams showing variations in chondrite-normalised La and Sm (a), Yb and Sm (b), and Yb and La/Sm (c) for the studied ocean-island transitional tholeiitic and alkalic dolerites (Subgroup A-2) and modern analogues (data sources as in Fig. 3.25).

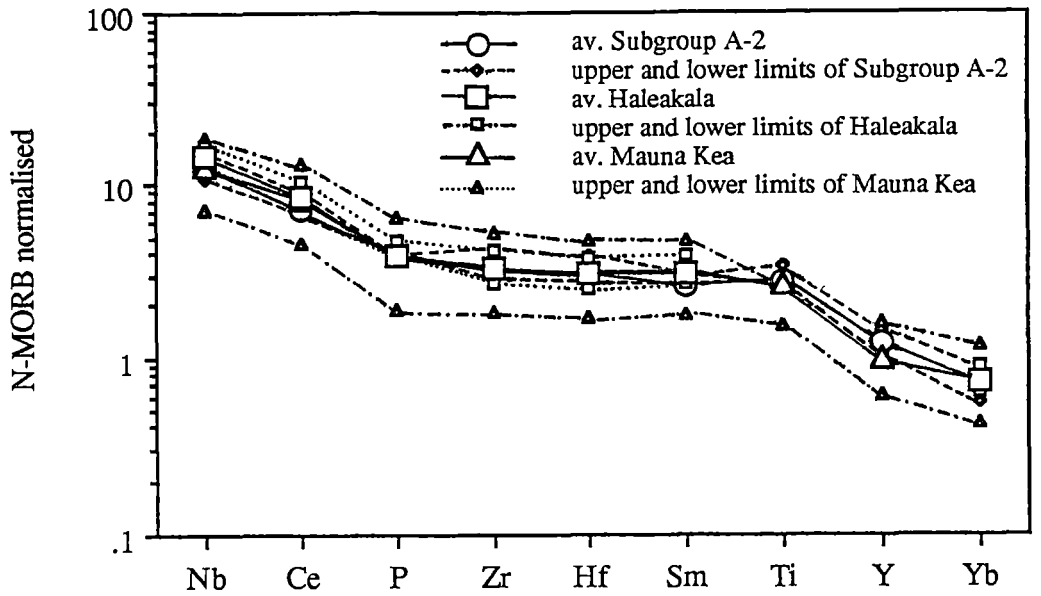

Figure 3.27. A subset of N-MORB normalised multi-element patterns for the averaged studied ocean-island transitional tholeiitic and alkalic dolerites (Subgroup A-2) and modern analogues (data sources as in Fig. 3.26). Also shown are the ranges for individual suites.

3.4.1 Summary of Ocean-island Tholeiites (Subgroup A-1)

The basaltic rocks in this subgroup include lavas and dolerites which are present in all key areas, except the Sirikit Reservoir area. They are made up mainly of albitised plagioclase and colourless clinopyroxene (calcian augite); altered olivine phenocrysts and microphenocrysts, chromian spinel microphenocrysts and devitrified glass may be present in some lava samples.

Chemically, they are tholeiitic basalts as indicated by their broad enrichment of FeO*, TiO_2 and V with increasing FeO*/MgO, Nb/Y values from 0.3 to 0.5, clinopyroxene and chromian spinel compositions, and relatively flat REE patterns with (La/Sm)n from 1.0 to 1.6, and slight HREE depletion with (Sm/Yb)n from 1.4 to 2.6. The values for Ti/Zr (90-119) and Zr/Nb (11-13) are only slightly less than the chondritic values, whereas Zr/Y (3.7-5.7) and Ti/V (37-48) are higher than the chondritic values.

The Subgroup A-1 tholeiites are chemically analogous to several Hawaiian and Tasmantid tholeiites, e.g. those from Kilauea, Mauna Loa, and Kohala Volcanoes, and Loihi Seamount (Hawaii), and Derwent Hunter and Britannia Seamounts (Tasmantids). Their clinopyroxene and chromian spinel compositions are also

comparable with those of Hawaiian tholeiitic basalts. Accordingly, they are considered to be ocean-island tholeiites.

3.4.2 Summary of Ocean-island Transitional Tholeiites and Alkalic Basalts (Subgroup A-2)

The Subgroup B-2 basaltic rocks, both lava and dolerite, are locally present in the Mae Charim, Doi Phuk Sung and Nan River areas. They consist predominantly of albitised plagioclase and pink clinopyroxene (titanian augite to diopside) with subordinate ilmenite and magnetite.

The basaltic rocks in this subgroup also exhibit broad FeO*, TiO_2 and V enrichment trends relative to FeO*/MgO, but they have notably higher Nb/Y (almost close to unity), characteristic of transitional tholeiites and alkalic basalts. This is well supported by their clinopyroxene compositions and REE patterns that show markedly greater LREE enrichment relative to HREE than those of Subgroup A-1 tholeiites. They are higher in FeO*, TiO_2, P_2O_5, Zr, Y and Nb, but lower in MgO than the Subgroup A-1 tholeiites. In terms of element ratios, they have lower values for Ti/Zr (<87) and Zr/Nb (<10), and higher levels of Ti/V (>50) and Zr/Y (>5.7).

The Subgroup A-2 transitional tholeiites and alkalic basalts are compositionally comparable with those erupted in the postshield stages of Haleakala (Maui) and Mauna Kea (Hawaii) Volcanoes. Consequently, they are considered to be postshield ocean-island transitional tholeiites and alkalic basalts.

CHAPTER 4

BACKARC BASIN SUITES (GROUP B)

4.1 General Chemical Characteristics

Rocks categorised as Group B have similar Y (20-55 ppm), but lower TiO_2 (1.0-2.5 wt%) and Nb (<2-8 ppm) contents relative to the Group A basalts, resulting in significantly lower Ti/Y (Fig. 3.2) and Nb/Y (Figs. 3.1 and 3.2), and higher Zr/Nb (Fig. 3.3) ratios. In addition, they have lower Ti/V (mostly 18-37) , Zr/Y (2.0-4.5), and Ni contents at similar values for MgO (Fig. 3.4).

These rocks have a fairly wide range of FeO*/MgO values (1.2-3.4) and are all basaltic to andesitic as suggested by their compositional field on the immobile element plot in Figure 4.1. They may be chemically separated into compositional Subgroups B-1, B-2, B-3 and B-4. Their whole-rock compositions are presented in Table 4.1.

4.2 Subgroup B-1 Basalts and Andesites

4.2.1 Occurrence and Petrography

The analysed samples (1 lava, 1 microgabbro and 10 dolerites) in Subgroup B-1 have been collected from float and outcrops in the Mae Charim and Doi Phuk - Sung areas. Dolerite and microgabbro crop out only in the northern part of the Doi Phuk Sung area, and are evidently faulted against Upper Triassic - Lower Jurassic molasse. Textures and grainsizes vary greatly, even in a single exposure, and show complex relationships, suggestive of sheeted dikes. Exact field relation of lavas in the Mae Charim area remains unknown due to extremely poor outcrop. Sample locations and detailed petrographic features of the analysed Subgroup B-1 samples are given in Table I-2 (Appendix I) and Table II-3 (Appendix II), respectively.

Petrography of lava sample

The analysed lava is slightly porphyritic, with subhedral albitised plagioclase phenocrysts and microphenocrysts, and subhedral altered clinopyroxene microphenocrysts. Its groundmass constituents are made up chiefly of albitised plagioclase laths, possibly altered intergranular clinopyroxenes (?) and subhedral titanomagnetite.

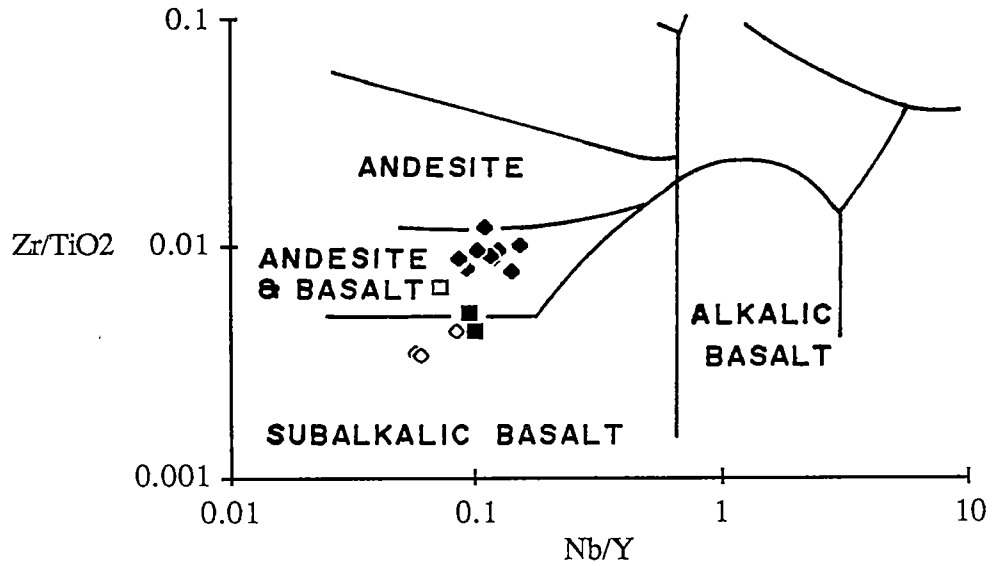

Figure 4.1. Zr/TiO_2 - Nb/Y diagram for Group B samples (solid diamond, Subgroup B-1; open diamond, Subgroup B-2; solid square, Subgroup B-3; open square, Subgroup B-4) compared to the fields of various rock types (after Winchester and Floyd, 1977). Data points for Subgroup B-3 samples with Nb content less than 2 ppm (close to the detection limit determined by XRF) are omitted.

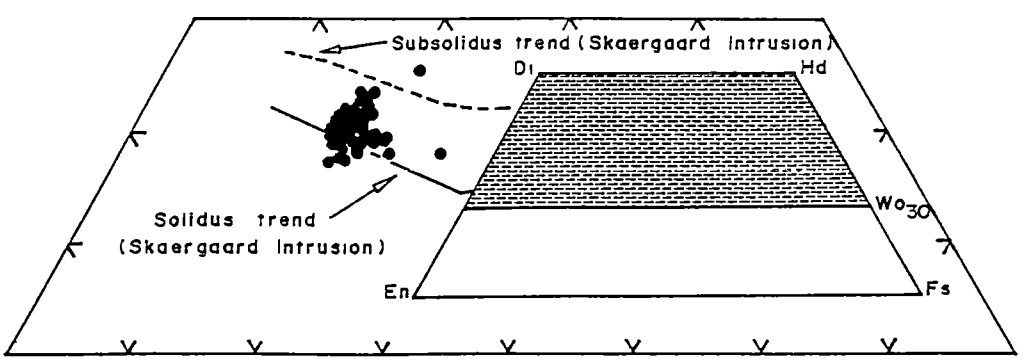

Figure 4.2. Analyses of colourless clinopyroxenes in Subgroup B-1 dolerites in the conventional pyroxene quadrilateral. The solidus and subsolidus compositional trends of Skaergaard clinopyroxenes shown are those of Brown (1967) and Nwe (1976), respectively.

TABLE 4.1. WHOLEROCK XRF ANALYSES AND SOME SELECTED RATIOS OF GROUP B BASALTS AND ANDESITES; MAJOR ELEMENTS ARE NORMALISED TO 100% ON THE BASIS OF LOSS ON IGNITION FREE

Subgroup	B-1												B-2			B-3					B-4
Sample no.	23.3	23.1	22.4	22.2	22.3	22.5	22.1	55.1A	23.7	55.1	1.29[1]	23.11[2]	19.8[2]	19.7[2]	18.1[2]	YP-9	45.4	45.2	45.1	26.7	27.2[1]
SiO2	51.96	51.29	51.40	52.15	51.97	50 40	52.16	52.25	52.59	50.69	57.39	56.29	50.87	51.47	53.1	50.47	48.75	49.28	48.91	50.72	50.16
TiO2	1.63	1.37	1.55	1.52	1.57	1.61	1.69	1.70	1.75	1.85	1.81	1.94	2.17	2.12	1.81	0.96	1.05	1.05	1.05	1.11	2.49
Al2O3	18.63	18.27	18.12	17.30	18.04	18.19	17.41	16.75	16.66	18.31	15.81	15.97	15.34	14.96	14.82	16.51	16.23	16.61	16.45	16.38	13.12
FeO*	11.01	10.51	10.23	10.63	10.51	10.41	10.61	11.39	11.16	11.33	8.46	10.32	12.60	12.99	12.62	10.15	9.98	10.01	9.94	10.26	14.01
MnO	0.21	0.17	0.17	0.19	0.18	0.18	0.18	0.20	0.20	0.18	0.20	0.22	0.19	0.19	0.26	0.20	0.18	0.18	0.18	0.20	0.23
MgO	5.77	5.43	5.10	5.27	5.15	4.77	4.83	4.98	4.80	4.18	2.97	3.06	6 62	5.92	4.72	8.80	8.22	8.15	8.04	7.23	6.55
CaO	5.34	8.68	7.94	7.30	7.82	9.24	8.04	9.24	8.19	8.99	5.50	5.96	8.27	8.77	7.69	8.49	12.15	10.70	11.68	10.81	9.15
Na2O	3.90	2.49	4.30	4.65	2.61	4.32	3.44	2.94	4.07	3.37	5.52	4.84	3.49	3.18	4.28	3 83	3.16	3.56	3.29	3.02	3.51
K2O	1.20	1.43	0.83	0.67	1.81	0.45	1.30	0.11	0.16	0.72	1.37	0.70	0.03	0.02	0.28	0.42	0.15	0.34	0.34	0.13	0.53
P2O5	0.34	0.37	0.35	0.33	0.34	0.44	0.33	0.44	0.42	0.37	0.96	0.70	0.42	0.40	0.41	0.17	0.15	0.12	0.14	0.14	0 26
LOI	3.67	2.88	3 04	2.91	2.97	3.28	2.51	3.66	3.06	2.57	1.52	2.60	2.95	2.95	1.82	2.41	2.72	2.08	2.28	1.97	2.69
FeO*/MgO	1.91	1.94	2.01	2.02	2.04	2.18	2.20	2.29	2.33	2.71	2.85	3.37	1.90	2.19	2.67	1.15	1.21	1.23	1.24	1.42	2.14
Nb	4	4	3	3	4	3	3	6	4	5	8	6	2	2	3	2	2	<1	1	1	4
Zr	142	129	138	119	143	137	148	172	167	141	180	234	75	71	77	49	44	46	47	51	165
Y	33	32	34	32	34	35	35	38	39	35	52	54	35	33	36	21	20	20	22	22	55
Sr	336	376	532	487	406	473	444	413	308	411	303	205	364	378	278	192	548	587	451	217	117
Rb	28	32	22	16	70	8	29	<2	5	14	24	13	1	2	2	8	1	4	3	2	11
Ni	35	38	30	30	31	27	28	26	27	28	8	4	14	13	18	84	131	107	110	59	48
Cr	60	45	43	40	41	43	36	34	31	27	6	2	9	11	16	299	275	287	280	195	95
V	309	248	280	310	275	261	360	314	302	347	146	107	463	462	396	312	328	339	331	343	472
Ba	206	220	167	125	295	135	217	77	135	257	448	192	28	43	128	58	109	164	106	38	86
Sc	34	28	27	30	28	28	37	30	30	33	24	28	47	48	46	44	49	48	49	50	44
Ti/Zr	69	64	67	77	66	70	68	59	63	79	60	50	173	179	141	117	143	136	133	130	90
Zr/Nb	36	32	46	40	36	46	49	29	42	28	23	39	38	36	26	24	22	>46	47	51	41
Zr/Y	4.3	4.0	4.1	3.7	4.2	3.9	4.2	4.5	4.3	4.0	3.5	4.3	2.1	2.2	2.1	2.3	2.2	2.3	2.1	2.0	3.0
Y/Nb	8	8	11	11	8	12	12	6	10	7	6	9	17	16	12	10	10	>20	22	22	14

[1] = LAVA, [2] = MICROGABBRO, FeO* = TOTAL IRON AS FeO, LOI = LOSS ON IGNITION.

Plagioclase is partially replaced by sericite and amphibole (pleochroic from yellowish to blue-green), whereas clinopyroxene is completely pseudomorphed by yellowish - blue-green amphibole. Fe-Ti oxides are partly altered to leucoxene. Other secondary minerals, sporadically occurring in groundmass, are epidote, chlorite, quartz and Fe sulphides. Veinlets of epidote, quartz and yellowish - blue-green amphibole are rarely present. The metamorphic assemblage is amphibole-epidote-chlorite-albite-sericite-leucoxene-quartz, typical of the greenschist facies of regional metamorphism of basic rocks.

Petrography of dolerites

The dolerites of Subgroup B-1 show pronounced textural variation, from porphyritic through seriate to equigranular. In porphyritic rocks, plagioclase is the sole phenocryst phase; groundmass constituents are mineralogically similar to the other textural types, and are made up mainly of plagioclase laths and colourless, subhedral to anhedral clinopyroxenes, with euhedral to subhedral Fe-Ti oxide, apatite, and rare zircon accessories. Clinopyroxenes are present either as intergranular or as subophitic crystals; Fe-Ti oxides often exhibit ilmenite exsolution lamellae.

All plagioclases have suffered albitisation and are partly to totally replaced by sericite, chlorite and epidote. Prehnite, pumpellyite and quartz may be present as additional secondary products. Clinopyroxenes are partly altered to yellowish brown to dark brown minerals (Fe oxide and ?incipient amphibole), chlorite and leucoxene. Magnetite is largely transformed to haematite whereas ilmenite is partially replaced by leucoxene. Other secondary minerals present in between the inferred primary phases in many samples are prehnite, calcite, quartz, epidote and Fe sulphides. Veinlets of calcite, epidote and quartz are rarely present. The secondary mineral assemblage suggests that they have undergone prehnite-pumpellyite facies of regional metamorphism.

Petrography of microgabbro sample

The microgabbro sample is equigranular, and consists principally of subhedral plagioclase and colourless intergranular clinopyroxene, with accessory anhedral to subhedral Fe-Ti oxides (magnetite and ilmenite), euhedral to subhedral apatite, and interstitial quartz.

Plagioclase is albitised and partly replaced by epidote and prehnite, whereas clinopyroxene is slightly pseudomorphed by dark brown minerals (Fe oxide and ?incipient amphibole) and chlorite. Fe-Ti oxides are largely altered to leucoxene, and

magnetite is transformed to haematite. Prehnite, quartz and calcite have also been observed in sporadic amounts. Again, it is a very low- to low-grade regional metamorphic rock.

4.2.2 Mineral Chemistry

Relict primary mineral analyses of Subgroup B-1 samples have been performed only on colourless clinopyroxenes in dolerites (Table 4.2). They are all broadly augitic and cluster on the conventional pyroxene quadrilateral (Fig. 4.2) mainly along a line of nearly constant Mg#, with variable wollastonite contents (37-45%). Their compositional field lying between the solidus and subsolidus trends of the Skaergaard Intrusion (Brown, 1967; and Nwe, 1976), may reflect variable subsolidus re-equilibration, but probably reflects cocrystallisation with plagioclase.

In terms of non-quadrilateral components, the Subgroup B-1 clinopyroxenes have Al_2O_3 (1.2-4.0 wt%), Al^{vi}/Al^{iv} (0.11-0.66), and Na (0-0.02), comparable to pyroxenes of Group A intraplate tholeiites. They differ from the Group A tholeiitic clinopyroxenes, however, in that Ti and total Al^{vi} display a strong positive correlation, with $Ti/Al^{iv} = 0.34 \pm 0.06$; Al^{vi} and Al^{iv} are broadly positively correlated (Fig. 4.3). These are evidence for multiple coupled substitutions mainly involving $(Ti^{4+}/2)$-Al^{iv}, and Al^{vi}-Al^{iv}; the former is the most important substitutional couple. Although they are broadly compositionally similar to the Subgroup A-2 pyroxenes (i.e. in terms of quadrilateral components and a clearly defined positive linear trend for Ti and Al^{iv}), their Ti contents are notably lower, and accordingly, they fall well within the field of subalkalic pyroxenes, straddling the field boundary between orogenic and non-orogenic pyroxenes (Fig. 4.4).

4.2.3 Whole-rock Chemistry

Major elements

The Subgroup B-1 samples have basaltic to andesitic compositions (Table 4.1 and Fig. 4.1). Their FeO*, TiO_2 and V behaviour during fractionation is typically tholeiitic (Fig. 4.5).

Subgroup B-1 basalts have FeO*, TiO_2 and MgO values typical of MORB and backarc basin tholeiites (Fig. 4.6). They have more TiO_2 at given FeO*/MgO and MgO than island-arc tholeiites (herein IAT), and lower FeO* and TiO_2 than most intraplate ocean-island tholeiites (Figs. 4.5 and 4.6). The trends toward high SiO_2 at FeO*/MgO and MgO greater than 2.5 and 5, respectively, and the relatively early

TABLE 4.2. ELECTRON MICROPROBE ANALYSES OF COLOURLESS CLINOPYROXENES IN BACKARC BASIN DOLERITES OF SUBGROUP B-1. FeO AND Fe_2O_3 ARE CALCULATED ASSUMING STOICHIOMETRY ON THE BASIS OF 4 CATIONS AND 6 OXYGENS. END-MEMBERS IN TERMS OF WOLLASTONITE, ENSTATITE AND FERROSILITE ARE CALCULATED ACCORDING TO THE METHOD RECOMMENDED BY THE SUBCOMMITTEE ON PYROXENES, IMA (1988).

Sample no.	22 1							22.2						22.3	
Analysis no.	1	2	3	4	5	6	7	1	2	3	4	5	6	1	2
SiO2	51.98	51.76	51.89	52.53	51.53	52.18	51.49	52.05	52.61	52.22	52.79	52.05	52.73	51.47	49.74
TiO2	0.75	0.92	0.91	0.65	0.98	0.60	0.80	0.48	0.75	0.67	0.83	0.86	0.68	0.92	1.15
Al2O3	1.71	2.24	2.36	1.63	2.33	1.57	2.01	1.23	1.55	1.37	1.84	1.83	1.39	1.78	3.34
Fe2O3	0.36	1.36	-	-	-	-	0.83	-	-	-	-	0.39	0.68	-	1.17
FeO	9.97	9.71	10.01	10.11	10.16	9.72	9.04	12.62	11.93	11.16	1.00	11.13	10.37	11.07	9.99
MnO	0 31	0.25	-	0.25	-	-	0.28	-	0 43	0.28	0.28	0.24	0.22	0.27	0.26
MgO	15.31	14.62	15.03	15.34	14.92	15.46	15.29	12.13	14.49	15.02	15.44	14.89	14.85	14.31	14.78
CaO	19.72	19.96	20.16	19.78	19.88	19.66	20.07	22.17	19.11	19.06	20.02	19 59	19.79	19.51	18.73
Na2O	-	0.24	-	-	-	-	-	-	-	-	-	-	0.27	-	-
Total	100.11	101.06	100.36	100.29	99.80	99.19	99.81	100.68	100.87	99.78	101.20	100.98	100.98	99.33	99.11
Si	1.937	1.915	1.926	1.950	1.924	1.953	1.922	1.960	1.955	1.955	1.942	1.931	1.951	1.940	1.877
ivAl	0.064	0.085	0.074	0.050	0.076	0.047	0.078	0.040	0.045	0.045	0.058	0.069	0.049	0.060	0.124
Total tetra.	2.000	2.000	2.000	2.000	2.000	2.000	2.000	2.000	2.000	2.000	2.000	2.000	2.000	2.000	2.000
viAl	0.012	0.013	0.029	0.021	0.027	0.023	0.010	0.014	0.022	0.016	0.021	0.011	0.012	0.019	0.025
Ti	0.021	0.026	0.025	0.018	0.027	0.017	0.022	0.014	0.021	0.019	0.023	0.024	0.019	0.026	0.033
Fe3+	0.010	0.038	-	-	-	-	0.023	-	-	-	-	0.011	0.019	-	0.033
Fe2+	0.311	0.301	0.311	0.314	0.317	0.304	0.282	0.397	0.371	0.349	0.308	0.345	0.321	0.349	0.315
Mn	0.010	0.008	-	0.008	-	-	0.009	-	0.014	0.009	0.009	0.008	0.007	0.009	0.008
Mg	0 850	0.806	0.831	0.849	0.830	0.863	0.851	0.680	0.803	0.838	0.846	0.823	0.819	0.804	0.828
Total octa.	1.213	1.192	1.196	1.210	1.202	1.207	1.197	1.105	1.230	1.231	1.207	1.221	1.196	1.207	1.243
Ca	0.787	0.791	0 802	0.787	0.796	0.789	0.803	0.894	0.761	0.765	0.789	0.779	0.785	0.788	0.757
Na	-	0 018	-	-	-	-	-	-	-	-	-	-	0.019	-	-
Total cats.	4.000	4.000	3.997	3 997	3.997	3.995	4.000	4.000	3.991	3.996	3.996	4.000	4.000	3.994	4.000
Mg#	0.732	0.728	0.728	0.730	0.723	0.739	0.751	0.631	0.684	0.706	0.733	0.705	0.718	0.697	0.724
Wo	40.01	40.70	41.24	40 19	40 94	40.32	40.80	45.35	39.07	38.99	40.42	39.62	40.23	40.41	38 98
En	43.20	41.49	42.77	43.36	42.73	44.12	43 24	34 50	41.21	42.74	43.37	41.88	41.99	41.24	42 65
Fs	16.79	17 82	15.99	16 45	16 33	15 56	15 96	20.14	19 72	18.27	16 21	18 50	17.79	18.35	18.37

Sample no.	22.3			22 4						22.5					
Analysis no	3	4	5	1	2	3	4	5	6	1	2	3	4	5	6
SiO2	50.80	51.27	50.90	52.71	51.45	51.65	50.38	50.99	52.26	49.90	51.82	49.75	51.48	49.62	50 45
TiO2	0.97	0.97	0.82	0.77	1.09	0.93	1.19	1.12	0.73	1.36	0.80	1.18	1.05	1.28	1.14
Al2O3	2.49	2.54	2.19	1.47	2.66	2.05	3.11	2.49	1.70	3.72	1.33	3.92	2.16	3.58	3.49
Fe2O3	-	0.09	-	0 15	0.53	0.07	-	-	-	1.05	-	1.98	0 26	0.89	0.09
FeO	9.88	10 09	11.63	10.77	11.04	11.94	10 31	10 41	10.31	9.50	15.38	10.73	11.07	10.11	10 51
MnO	-	0.30	0.23	0.28	0.35	0.33	-	-	-	0.25	0.49	0.28	0.29	-	-
MgO	14.52	14.70	14.24	15.74	15 18	14.42	14 22	14.04	15.46	13.78	12.71	13.98	14.05	13.94	13.91
CaO	20.12	19.96	19.02	19 21	18.78	19 21	19.91	20.41	18.88	20 76	18.48	19.22	20.38	19.93	20 34
Na2O	-	-	-	-	-	-	-	-	-	-	-	-	-	-	-
Total	98.78	99.92	99 03	101.10	101.08	100.60	99.12	99.46	99.34	100.32	101.01	101.04	100.74	99.35	99.93
Si	1.918	1.916	1.928	1.944	1.904	1.928	1.899	1.918	1.954	1.865	1.953	1.853	1.920	1.872	1.889
ivAl	0.082	0.084	0.072	0.056	0.096	0.072	0.101	0.083	0.046	0 135	0 047	0.147	0 081	0 129	0.111
Total tetra.	2.000	2.000	2.000	2.000	2.000	2.000	2.000	2.000	2.000	2.000	2.000	2.000	2 000	2.000	2.000
viAl	0.028	0.027	0.026	0.008	0.020	0.018	0.037	0.028	0.028	0.029	0.012	0.025	0.014	0 031	0.044
Ti	0.028	0 027	0.023	0.022	0.030	0.026	0.034	0.032	0.021	0.038	0 023	0.033	0.030	0.036	0 032
Fe3+	-	0.003	-	0.004	0.015	0.002	-	-	-	0 030	-	0.056	0.007	0.025	0.003
Fe2+	0.312	0.315	0 368	0.332	0.342	0.373	0.325	0.327	0 322	0 297	0.485	0.334	0.345	0.319	0 329
Mn	-	0.010	0 007	0.009	0.011	0.010	-	-	-	0.008	0.016	0.009	0.009	-	-
Mg	0.817	0.819	0.804	0.866	0.837	0.803	0.799	0.787	0.861	0.767	0.714	0.776	0.781	0.783	0.776
Total octa.	1.185	1.201	1.228	1.241	1.255	1.232	1.194	1.174	1.232	1.169	1.249	1.233	1.186	1 195	1.184
Ca	0.814	0.799	0.772	0 759	0.745	0.768	0 804	0 822	0.756	0.831	0.746	0.767	0.814	0.805	0.816
Na	-	-	-	-	-	-	-	-	-	-	-	-	-	-	-
Total cats.	3.999	4.000	4.000	4 000	4 000	4.000	3 999	3.996	3.988	4 000	3.995	4.000	4.000	4.000	4.000
Mg#	0.724	0 722	0.686	0.723	0.710	0.683	0.711	0.706	0.728	0.721	0.596	0.699	0 693	0.711	0.702
Wo	41.89	41.08	39.55	38.54	38.20	39.28	41.71	42.46	38.98	43.00	38.05	39.51	41.61	41.66	42.42
En	42.06	42.08	41.20	43.94	42.95	41.03	41.44	40.64	44.41	39.70	36.43	39.96	39.89	40.53	40.34
Fs	16 06	16 84	19 25	17.52	18 85	19 69	16.85	16.90	16.61	17.30	25.52	20.53	18.49	17 82	17.24

Table 4.2, CONTINUED

Sample no.	23.1						23.3						23.7		
Analysis no.	1	2	3	4	5	6	1	2	3	4	5	6	1	2	3
SiO2	52.59	51.62	51.26	51.49	52.25	51.58	52.69	51.12	51.43	51.63	51.60	52.42	50.94	52.44	52.46
TiO2	0.75	0.89	1.10	1.09	0.65	1.08	0.79	0.88	0.89	0.97	0.90	0.76	0.95	0.62	0.72
Al2O3	1.36	2.20	2.93	2.70	1.82	2.74	1 66	2.25	2.72	2.08	1.85	1.47	2.73	1.72	1.75
Fe2O3	-	0.23	0.14	-	0.25	0.28	-	1.56	0.33	1.24	-	-	1.56	0.11	1.41
FeO	10.81	9.96	10.13	10.52	9.75	10.20	11.55	8.48	9.80	9.47	11.29	13.33	9.18	9.93	9 09
MnO	-	0.29	-	-	0.27	0.25	0.25	-	-	0.24	0.24	0.37	0.26	0.23	0.27
MgO	15.22	14.88	14.65	14.97	15.69	15.22	15.22	14.98	15.47	15.12	14.73	14.32	14.73	15.37	15.34
CaO	19.29	20.11	20.32	19.36	19.58	19.57	18.72	19.83	19.46	19 23	18.90	18.74	20.35	20.06	19.82
Na2O	-	-	-	-	-	-	-	0.29	-	0.28	-	-	-	-	0.28
Total	100.02	100.18	100.53	100.13	100.26	100.92	100.88	99 39	100.38	100.26	99.51	101.41	100.70	100.48	101.14
Si	1.959	1.923	1.903	1.916	1.939	1.906	1.950	1.914	1.907	1.920	1.939	1.948	1.892	1.944	1.932
ivAl	0.041	0 077	0.097	0.084	0.062	0.094	0.050	0.086	0.093	0.080	0.061	0 052	0.108	0.056	0.068
Total tetra.	2.000	2.000	2.000	2.000	2.000	2.000	2.000	2.000	2.000	2.000	2.000	2.000	2.000	2.000	2.000
viAl	0.018	0.020	0.032	0.034	0.018	0.026	0.023	0.013	0.026	0.012	0.021	0.012	0.012	0.019	0.009
Ti	0.021	0.025	0.031	0.030	0.018	0.030	0.022	0.025	0.025	0.027	0.026	0.021	0.027	0.017	0.020
Fe3+	-	0.007	0.004	-	0.007	0.008	-	0.044	0.009	0.035	-	-	0.044	0.003	0.039
Fe2+	0.337	0.310	0.315	0.327	0.302	0.315	0.358	0.266	0.304	0.295	0.355	0.414	0 285	0.308	0.280
Mn	-	0.009	-	-	0.009	0.008	0.008	-	-	0.008	0.008	0.012	0.008	0.007	0.008
Mg	0.845	0.826	0.811	0.830	0.868	0.838	0.839	0.836	0.855	0.838	0.825	0.793	0.815	0.849	0.842
Total octa.	1.221	1.197	1.191	1.222	1.222	1.225	1.250	1.184	1.227	1.213	1.234	1.253	1.190	1.203	1.198
Ca	0.770	0.803	0.809	0.772	0.778	0.775	0.742	0.795	0.773	0.766	0.761	0.746	0.810	0.797	0.782
Na	-	-	-	-	-	-	-	0.021	-	0.020	-	-	-	-	0.020
Total cats.	3.991	4.000	4.000	3.994	4.000	4.000	3.992	4.000	4.000	4.000	3.995	3.999	4.000	4.000	4.000
Mg#	0.715	0.727	0.721	0.717	0.742	0.727	0.701	0.759	0.738	0.740	0.699	0.657	0.741	0.734	0.750
Wo	39.45	41.06	41.72	40.01	39.63	39.86	38.12	40.97	39.83	39 48	39.06	37.96	41.28	40.57	40.09
En	43.30	42.25	41.84	43.03	44.18	43.12	43.11	43.08	44 05	43.16	42.35	40.37	41.55	43.24	43.14
Fs	17 25	16.68	16.43	16.96	16.19	17 02	18 77	15.95	16.12	17 36	18.59	21.67	17.17	16.19	16.77

Sample no.	23.7			1	55.1					55.1A					
Analysis no.	4	5	6	1	2	3	4	5	6	1	2	3	4	5	6
SiO2	51.62	51.78	52.46	52.43	52.61	49 59	52 42	50.84	52.87	51.77	52.36	52.23	51.20	52.57	49.29
TiO2	0.75	0.82	0.65	0.60	0.65	1.21	0.57	1.10	0.58	0.73	0.56	0.64	0.99	0.64	1.29
Al2O3	2.14	2.43	1.73	1.90	1.70	3.48	1.71	3.49	1.84	1.90	1.48	1.72	2.76	1.82	3.96
Fe2O3	0.63	0.53	-	-	-	0 74	-	-	0.41	0 31	-	-	-	-	0.71
FeO	10.58	9.51	10.27	11.00	10.41	10.08	11.17	10.34	9.85	12.33	11.87	10.37	10.84	9 97	10.40
MnO	0.30	-	0.30	-	0.24	-	0.26	-	-	0.32	0.39	-	0.32	0.22	-
MgO	14.46	15.14	15.03	15.74	16.02	13.35	15.57	13.94	16.03	14.15	14.53	14.67	14.39	15.00	13.59
CaO	20.10	20.42	19.96	18.48	18.24	20.69	18.29	20.61	19.78	19.27	19.42	20.14	19.40	19.96	19.89
Na2O	-	-	-	-	-	-	-	-	-	-	-	-	-	-	-
Total	100.58	100.63	100.40	100.15	99.87	99.14	99.99	100.32	101.36	100.78	100.61	99.77	99.90	100.18	99.13
Si	1.923	1.917	1.948	1.947	1.954	1.878	1.953	1.895	1.939	1.933	1.953	1.952	1.916	1.952	1 865
ivAl	0.077	0.083	0.052	0.053	0.046	0.123	0.048	0.106	0.062	0.067	0 047	0.048	0.084	0 048	0.135
Total tetra.	2.000	2.000	2.000	2.000	2.000	2.000	2.000	2.000	2.000	2.000	2.000	2.000	2.000	2.000	2.000
viAl	0.017	0.023	0.024	0.030	0.029	0.033	0.028	0.048	0.018	0.017	0.018	0.028	0.038	0.032	0.042
Ti	0.021	0.023	0.018	0.017	0.018	0.034	0 016	0.031	0.016	0 021	0 016	0.018	0.028	0.018	0.037
Fe3+	0.018	0.015	-	-	-	0.021	-	-	0.011	0.009	-	-	-	-	0.020
Fe2+	0.330	0.294	0.319	0.342	0.323	0.319	0.348	0.322	0.302	0.385	0.370	0.324	0.339	0.310	0.329
Mn	0.009	-	0.010	-	0 007	-	0.008	-	-	0.010	0.012	-	0.010	0 007	-
Mg	0.803	0 835	0.832	0.871	0.887	0.753	0.864	0.774	0.876	0.788	0.808	0.817	0.802	0.830	0.766
Total octa.	1.198	1.190	1.202	1.260	1.265	1.161	1.264	1.175	1.223	1.229	1.223	1.186	1.217	1.196	1.194
Ca	0.802	0.810	0.794	0.735	0.726	0 839	0 730	0 823	0.777	0.771	0.776	0.806	0.778	0.794	0.806
Na	-	-	-	-	-	-	-	-	-	-	-	-	-	-	-
Total cats.	4.000	4.000	3.996	3.995	3.990	4.000	3.994	3.998	4.000	4.000	3.999	3.993	3.995	3 990	4.000
Mg#	0.709	0 739	0.723	0.718	0.733	0.702	0.713	0.706	0.744	0 672	0.686	0.716	0.703	0.728	0.700
Wo	40.90	41 44	40.64	37.74	37.34	43.42	37.43	42.87	39.52	39.28	39.47	41.41	40.32	40.91	41.95
En	40.91	42.73	42.56	44.72	45.64	38.98	44.31	40.34	44.55	40.14	41.08	41.95	41.59	42 78	39.88
Fs	18.19	15.83	16 81	17.54	17.01	17.60	18 26	16.79	15.93	20.58	19.45	16.64	18.09	16 31	18.17

- = BELOW DETECTION LIMIT

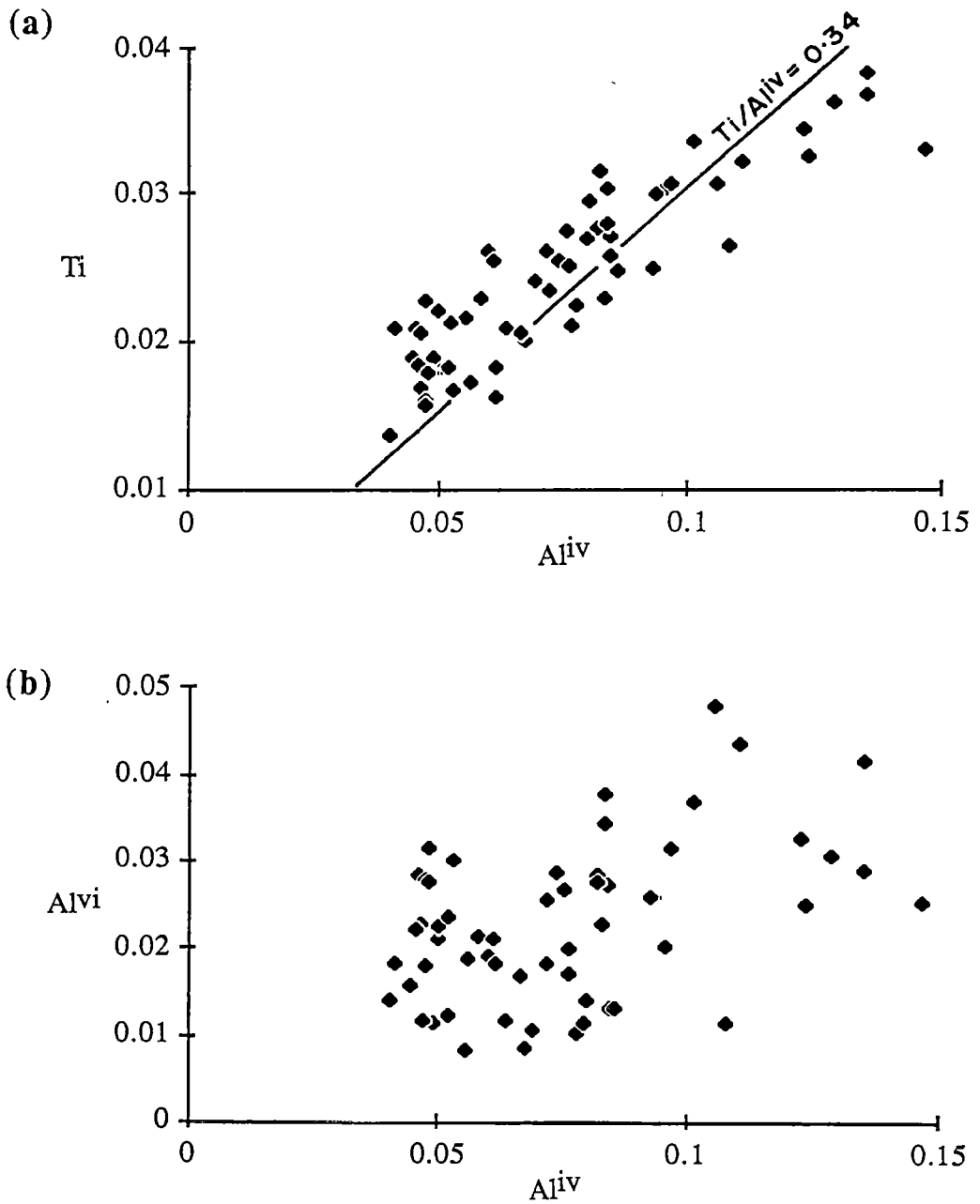

Figure 4.3. (a) Ti - Al^{iv} and (b) Al^{vi} - Al^{iv} plots (based on 6 oxygens) for clinopyroxenes in Subgroup B-1 dolerites displaying $(Ti^{4+}/2)$-Al^{iv} and Al^{vi}-Al^{iv} substitutions.

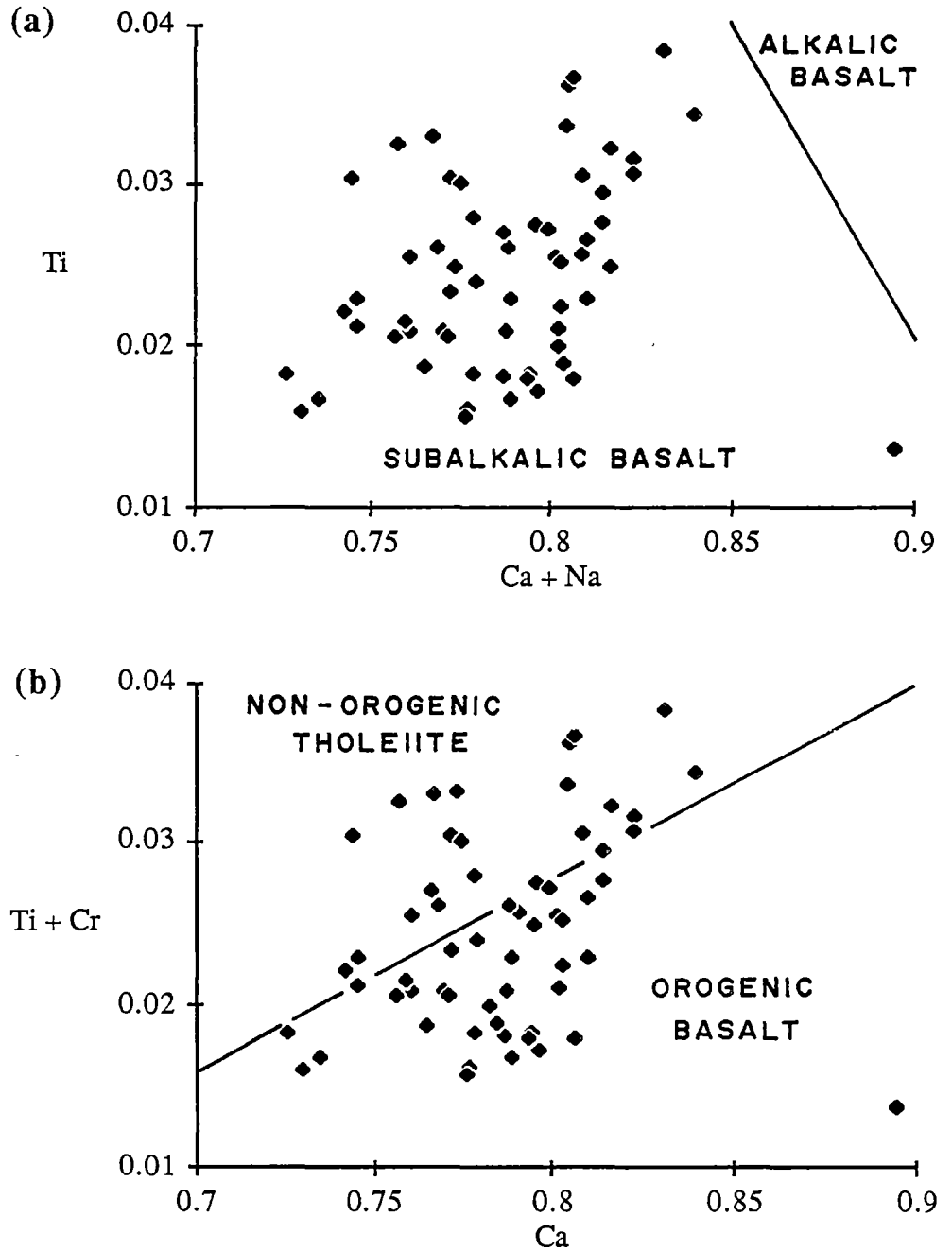

Figure 4.4. Tectonomagmatic discrimination diagrams (a) Ti against Ca+Na, and (b) Ti+Cr against Ca (based on 6 oxygens) in terms of clinopyroxene compositions (Leterrier *et al.*, 1982). Data plotted are for clinopyroxenes in Subgroup B-1 dolerites.

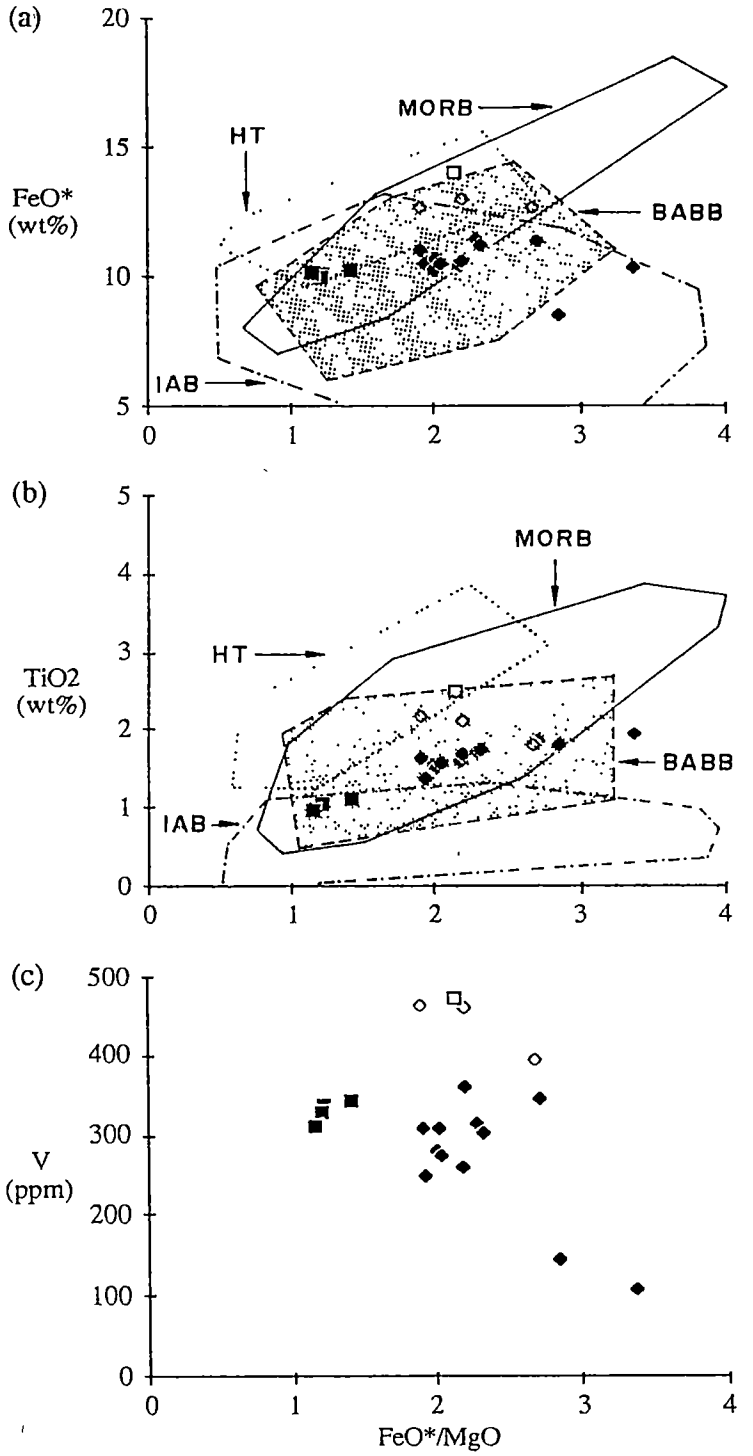

Figure 4.5. Variations of (a) FeO*, (b) TiO_2 and (c) V with FeO*/MgO for Group B rock samples (solid diamond, Subgroup B-1; open diamond; Subgroup B-2; solid square, Subgroup B-3; open square, Subgroup B-4). Data sources for the fields of mid-ocean ridge basalts (MORB), backarc basin basalts (BABB) and Hawaiian tholeiites (HT) are as in Figure 3.12. Compositional field boundary for island-arc subalkalic basalts (IAB) is based on the data from Vanuatu Arc (A.J. Crawford, pers. comm., 1990).

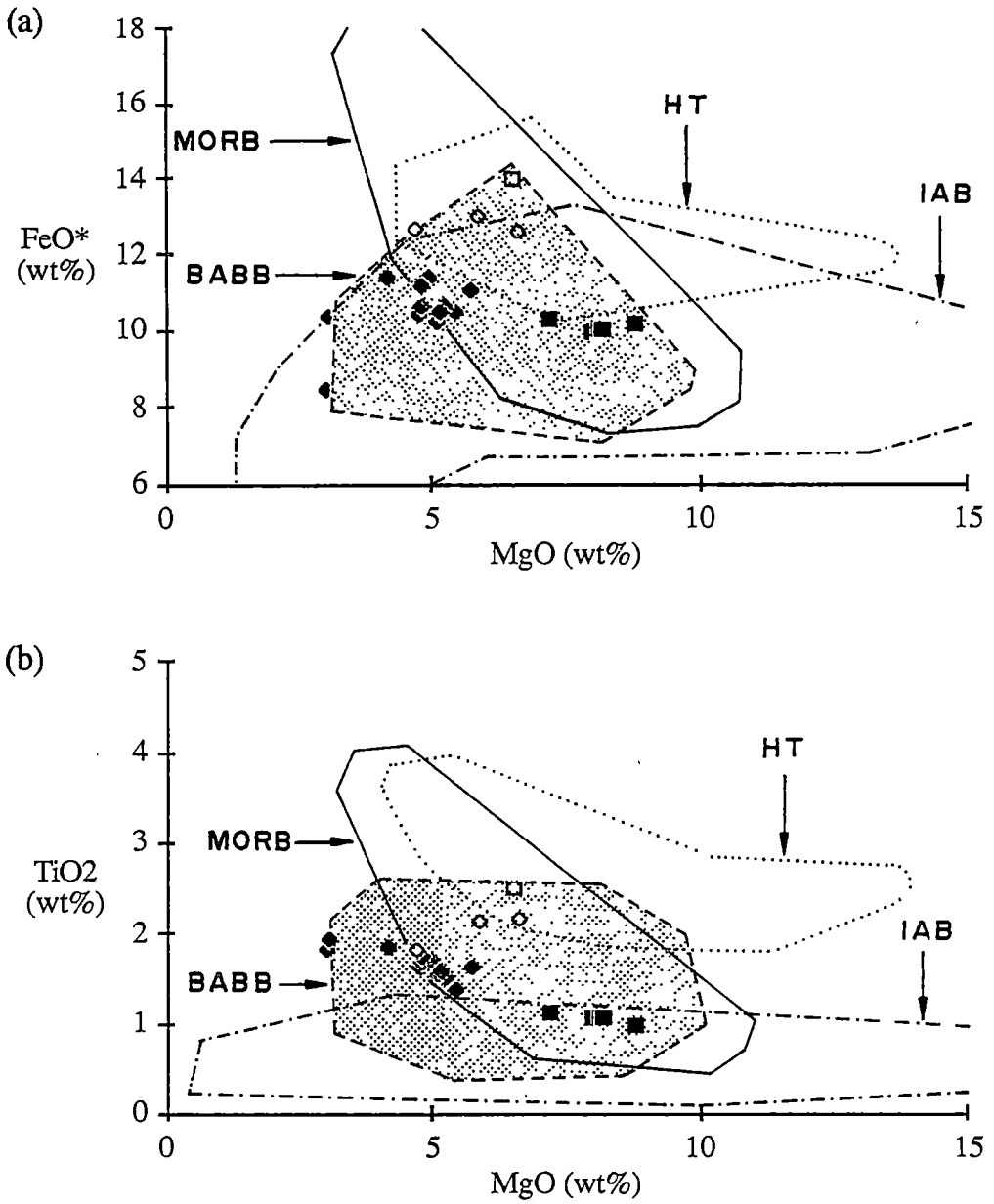

Figure 4.6. Plots of (a) FeO* and (b) TiO_2 against MgO for Group B samples (solid diamond, Subgroup B-1; open diamond, Subgroup B-2; solid square, Subgroup B-3; open square, Subgroup B-4), compared to the fields of mid-ocean ridge basalts (MORB), backarc basin basalts (BABB), Hawaiian tholeiites (HT) and island-arc subalkalic basalts (IAB)(data sources as in Fig. 4.5).

appearance of magnetite as a fractionating phase suggest that these may represent basalts transitional between backarc basin and arc basalts. This is examined further in the following sections.

Minor and trace elements

For the Subgroup B-1 suite, variation diagrams for P_2O_5, Zr, Nb, Y, Cr, Ni and Sc relative to FeO*/MgO are shown in Figure 4.7. Clearly, P_2O_5, Zr, Nb and Y are positively correlated with FeO*/MgO, and in contrast, Cr and Ni are markedly depleted with increasing fractionation as expected. Sc abundances are variable at lower FeO*/MgO values but generally decrease with advancing fractionation. These generally good correlations are evidence for the immobile nature of these elements during low-grade metamorphic alteration. The fractionation of clinopyroxene and plagioclase and later, Fe-Ti oxide, can adequately explain the variation of these elements against FeO*/MgO.

The least mobile minor- and trace-element concentrations in the Subgroup B-1 rocks are comparable to those in the Subgroup A-1 lavas at similar levels of FeO*/MgO, except that they have much lower Nb contents (3-8 ppm) compared with 7-13 ppm in the Subgroup A-1 rocks, giving rise to higher Zr/Nb (23-49) and Y/Nb (6-12). Although their Ti, Zr and Y contents are similar to those of the Subgroup A-1 rocks at similar FeO*/MgO, they have lower Ti/Zr (50-79) and Ti/Y (215-317).

The relationship between Ti and Zr for the Subgroup B-1 samples is illustrated in Figure 4.8. They are broadly positively correlated and comparable to those of backarc basin basalts (herein BABB). The discriminant Ti-V (Fig. 4.9) and Nb-Zr-Y (Fig. 4.10) plots also support BABB affinities.

Rare-earth elements

REE data for the representative Subgroup B-1 rocks (1 lava, 3 dolerites and 1 microgabbro) are given in Table 4.3, and REE patterns are shown in Figure 4.11. They are characterised by a slight LREE enrichment with convex-upwards LREE; (La/Sm)n and (Sm/Yb)n vary from 1.2 to 1.6, and 1.6 to 2.1, respectively. The patterns for dolerites and microgabbro show negative Eu anomalies, indicating that plagioclase fractionation may have played an important role during fractionation of this suite. However, Eu mobility during hydrothermal alteration is well-documented (Whitford *et al.*, 1988) and may explain the peculiar negative Eu anomaly in the more recrystallised samples.

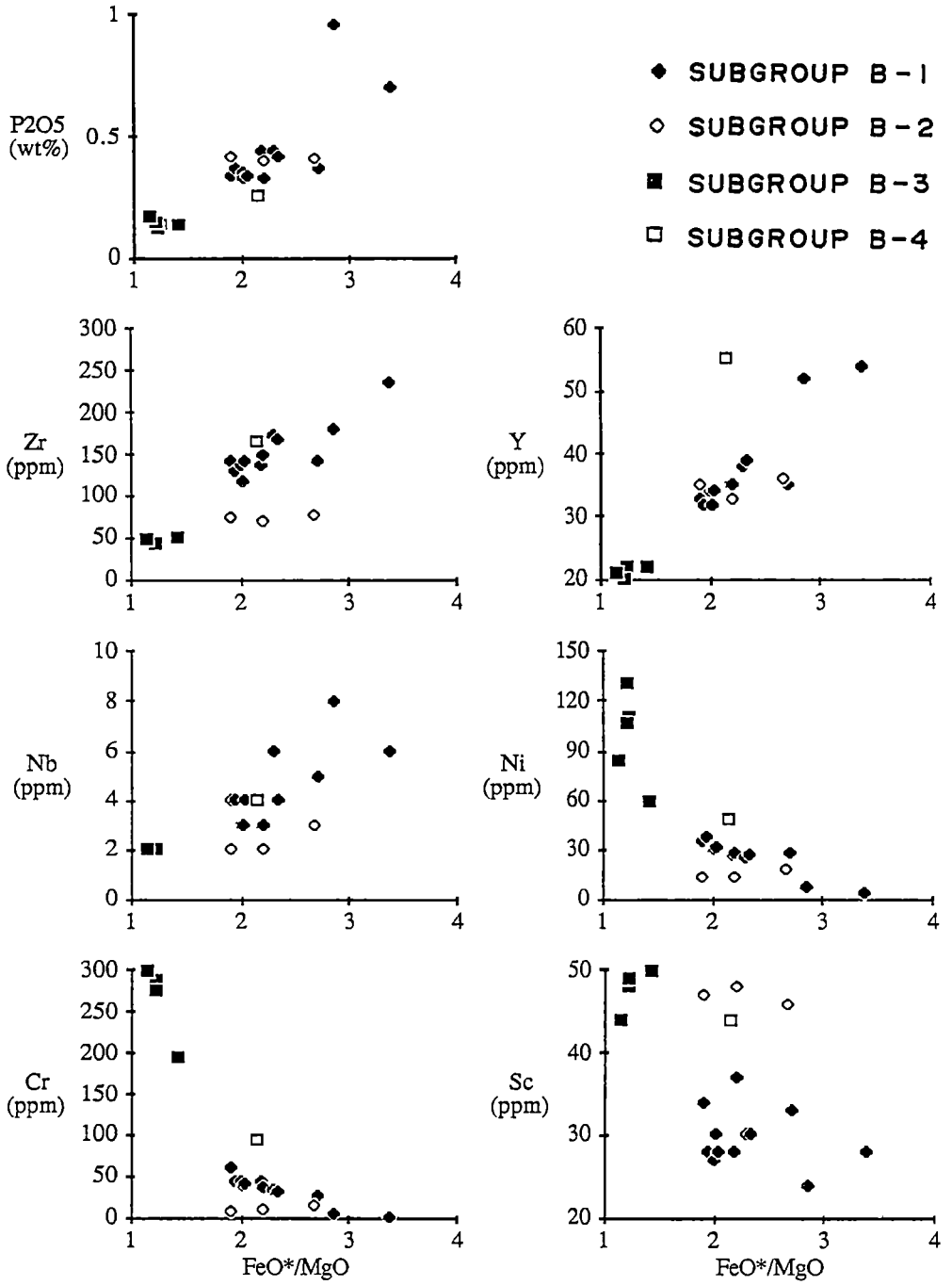

Figure 4.7. Minor- and trace-element variations in relation to FeO*/MgO for Group B samples. On Nb - FeO*/MgO diagram, Subgroup B-3 data with Nb content less than 2 ppm (below the detection limit determined by XRF) are omitted.

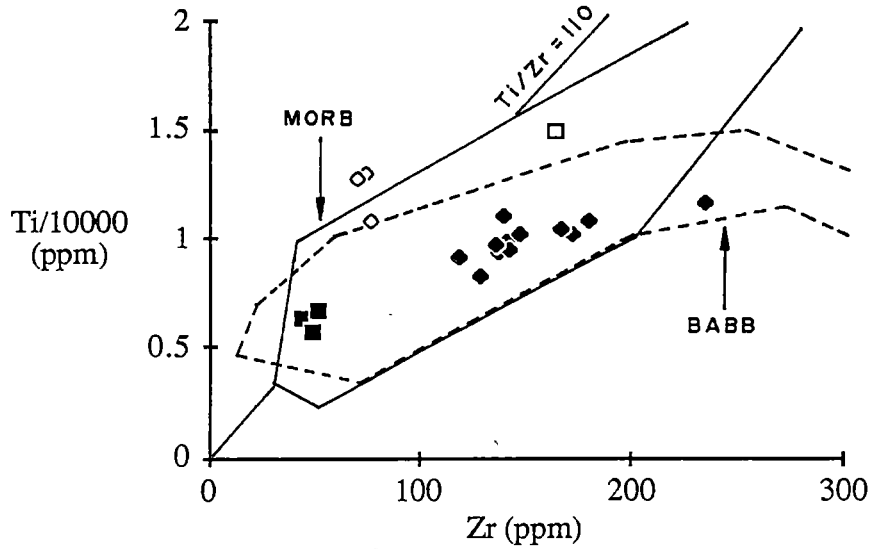

Figure 4.8. Ti-Zr relationship for Group B rock samples (solid diamond, Subgroup B-1; open diamond, Subgroup B-2; solid square, Subgroup B-3; open square, Subgroup B-4). Also shown are the compositional fields for modern mid-ocean ridge basalts (MORB)(data from Frey *et al.*, 1980; le Roex *et al.*, 1982, 1983, 1985, 1989; and Weaver *et al.*, 1985), and back-arc basin tholeiites (BABB)(data sources as in Fig. 3.12). Chondritic Ti/Zr = 110 is taken from Nesbitt and Sun (1976).

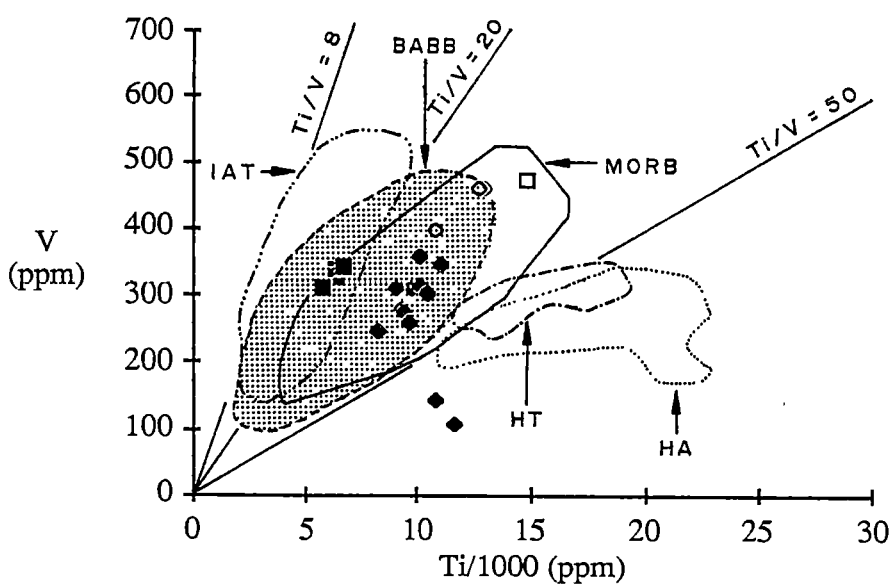

Figure 4.9. Ti-V plot of Shervais (1982) displaying the positions of Group B rock samples (solid diamond, Subgroup B-1; open diamond, Subgroup B-2; solid square, Subgroup B-3; open square, Subgroup B-4) relative to the fields of island-arc tholeiites (IAT), back-arc basin basalts (BABB), mid-ocean ridge basalts (MORB), Hawaiian tholeiites (HT), and Hawaiian alkalic basalts (HA). A chondritic Ti/V value = 8 is taken from Nesbitt and Sun (1976).

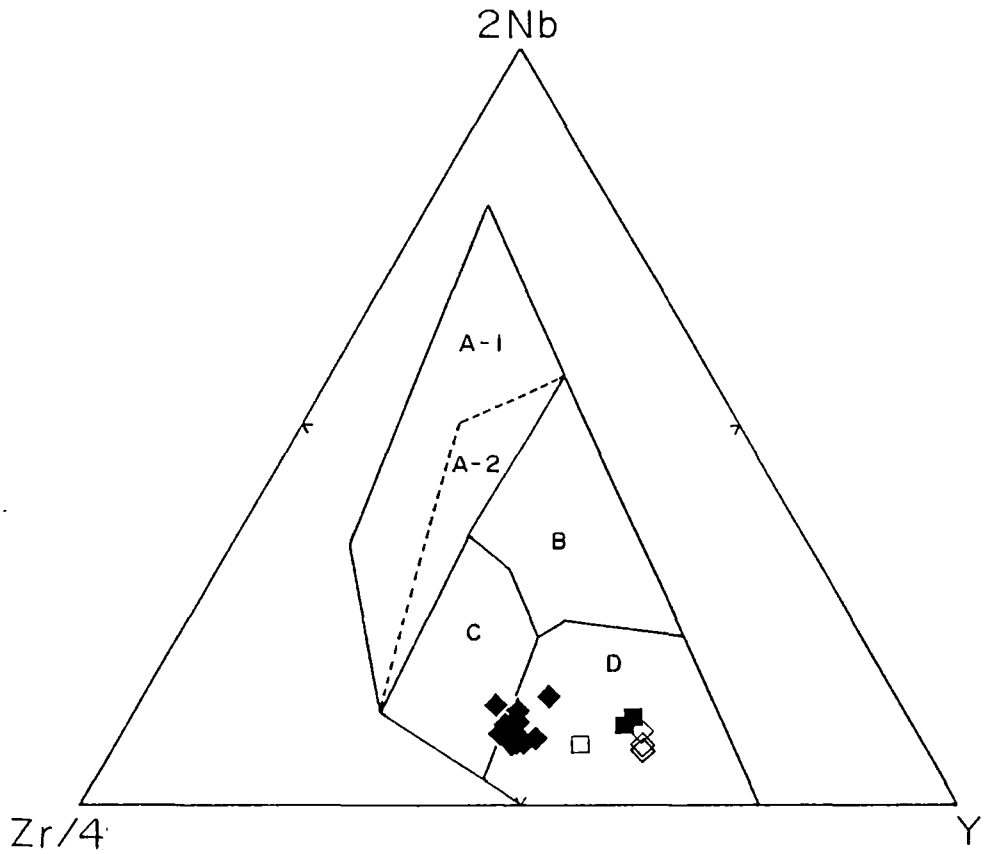

Figure. 4.10. Ternary discrimination Nb-Zr-Y plot (after Meschede, 1986) for Group B rock samples (solid diamond, Subgroup B-1; open diamond, Subgroup B-2; solid square, Subgroup B-3; open square, Subgroup B-4). A-1 and A-2 = alkalic within-plate basalts, A-2 and C = tholeiitic within-plate basalts, B = E-MORB, D = N-MORB and backarc basin basalts, and C and D = volcanic arc basalts.

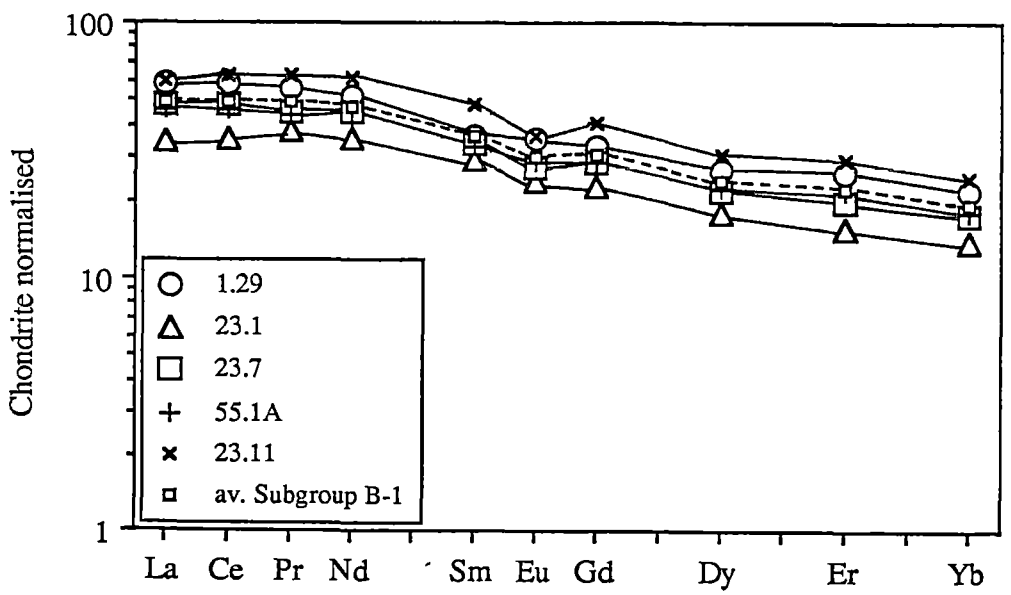

Figure 4.11. Chondrite-normalised REE patterns for Subgroup B-1 samples and their averages.

TABLE 4.3. REE ANALYSES AND SELECTED CHONDRITE-NORMALISED RATIOS FOR GROUP B BASALTIC AND ANDESITIC LAVAS, DOLERITES, AND MICROGABBROS.

Subgroup	B-1					B-2		B-3	B-4
Sample no.	23.1	23.7	1.29[1]	23.11[2]	55.1A	19.7[2]	18.1[2]	45.2	27.2[1]
La	10.80	15.10	18.10	18.70	14.50	8.81	8.14	2.96	6.67
Ce	28.90	38.50	46.70	50.40	37.00	22.30	22.10	8.48	20.70
Pr	4.08	5.34	6.38	7.30	5.02	3.20	3.36	1.38	3.41
Nd	20.80	26.70	31.00	36.50	24.50	15.80	17.40	7.03	18.60
Sm	5.60	6.46	6.93	9.24	6.30	4.20	4.70	2.30	6.12
Eu	1.73	1.95	2.52	2.59	2.03	1.57	1.85	0.89	2.27
Gd	5.98	7.38	8.39	10.40	7.34	5.04	6.29	2.82	8.35
Dy	5.89	7.09	8.55	9.92	7.33	5.94	6.50	3.64	9.82
Er	3.41	4.19	5.15	6.17	4.32	3.65	3.90	2.54	6.23
Yb	2.89	3.64	4.58	5.18	3.74	3.33	3.58	2.08	6.01
[La/Sm]n	1.18	1.42	1.59	1.23	1.23	1.28	1.06	0.78	0.66
[Sm/Yb]n	2.10	1.92	1.64	1.93	1.93	2.25	1.42	1.20	1.10

[1] = LAVA, [2] = MICROGABBRO.

TABLE 4.4. SELECTED MAJOR AND MINOR OXIDES (WT%), TRACE ELEMENTS AND REE (PPM), AND ELEMENT RATIOS FOR THE AVERAGED SUBGROUP B-2 THOLEIITES, COMPARED WITH THOSE FOR EASTERN EPI THOLEIITE (SAMPLE 670), VANUATU (GORTON, 1977); AND SUBGROUP B-4 THOLEIITE, COMPARED WITH THOSE FOR THE AVERAGED UNIT 3, HOLE 474A, LEG 64, GULF OF CALIFORNIA (SAUNDERS *ET AL.*, 1982)

	B-2 tholeiite	E Epi tholeiite	B-4 tholeiite	Unit 3 tholeiite
SiO2	51.81	48.08	50.16	49.80
TiO2	2.03	0.54	2.49	2.02
FeO*	12.74	10.45	14.01	9.78
MgO	5.75	8.99	6.55	8.11
P2O5	0.41	0.09	0.26	0.20
Zr	74	19	165	10
Y	35	14	55	42
Nb	2	-	4	3
Ni	15	-	48	70
Cr	12	-	95	235
Sc	47	-	44	40
La	8.48	2.78	6.67	4.39
Yb	3.46	1.07	6.01	4.80
FeO*/MgO	2.6	1.2	2.1	1.2
Ti/Zr	164	170	90	110
Zr/Nb	33	-	41	37
Zr/Y	2.1	1.3	3.0	2.6
Y/Nb	15	-	14	10
La/Nb	4.24	-	1.67	1.46
[La/Sm]n	1.17	1.29	0.66	0.57
[Sm/Yb]n	1.84	1.33	1.10	1.46

- = NO DATA AVAILABLE.

Comparisons with modern suites

The best-studied modern backarc basins show a temporal change in magma composition from earliest IAT-like BABB, through typical depleted N-MORB as the backarc basin matures and steady-state spreading is established (Crawford *et al.*, 1981). This holds for the Lau (Hawkins and Melchior, 1985) and Mariana (Volpe *et al.*, 1988) backarc basins . It has also been documented for the uplifted backarc basin in the Patagonian Andes, where the less than 50 km wide Sarmiento ophiolite shows some island-arc tholeiitic features (high large-ion-lithophile elements (herein LILE) and LREE enrichment) whereas further north, the Tortuga ophiolite of the same basin, here over 100 km wide, shows N-MORB characteristics (Stern, 1980).

Sinton and Fryer (1987) defined a backarc basin magma type that resembles MORB in many respects but has higher Al_2O_3 and LILE abundances and lower FeO* at any stage of fractionation. However, Price *et al.* (1990) argue that the BABB are best interpreted as part of a spectrum of magmas possibly due to mixing of a MORB end-member magma with an alkalic end-member, and that any MORB-type basalt could have been generated by such a process.

When compared with modern suites, the Subgroup B-1 samples are compositionally most similar to Quaternary backarc-side remnant-arc medium-K basalts from Site D-621 (FeO*/MgO = 1.6), behind the Shichito Ridge in the Izu-Ogasawara Arc (Ikeda and Yuasa, 1989), and samples from Lau Ridge (FeO*/MgO = 2.2)(Lau Volcanic Group)(Cole *et al.*, 1990)(Fig. 4.12). However, the Subgroup B-1 rocks have somewhat higher TiO_2 contents relative to the cited modern suites at similar values for FeO*/MgO. This could be interpreted to imply that they are transitional between arc lavas and BABB. Acknowledging that an increasingly large spectrum of BABB compositions is being recorded, with lavas with compositions transitional to arc basalt/andesite being common (Jenner *et al.*, 1987), it is concluded that Subgroup B-1 samples are most likely to be BABB which generated just prior to backarc (interarc) opening.

4.3 Subgroup B-2 Tholeiites

4.3.1 Occurrence and Petrography

The three studied Subgroup B-2 samples are all microgabbros which are present as float in the Nan River and Uttaradit areas. Sample locations for these rocks are given in Table I-2 (Appendix I).

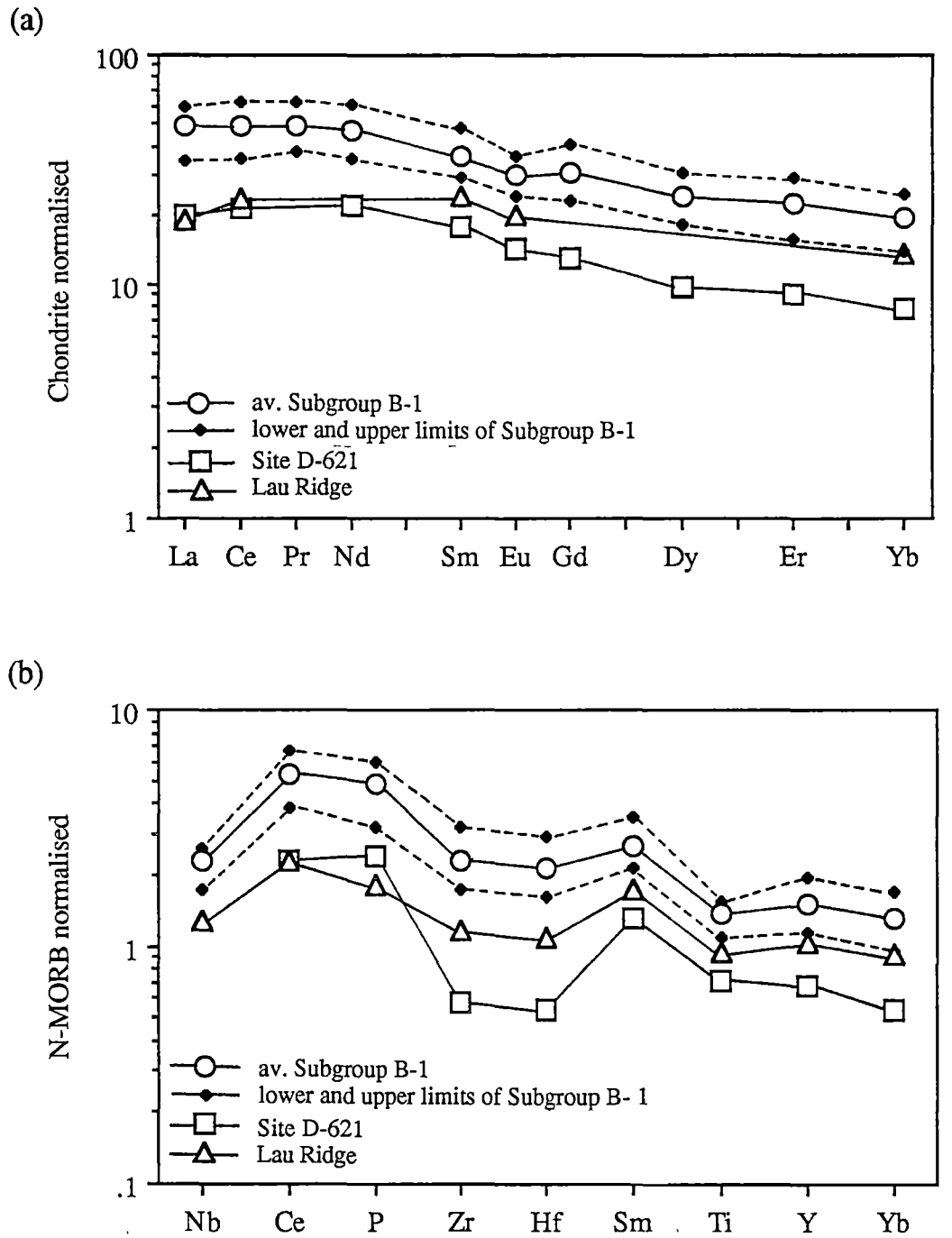

Figure 4.12. Comparative diagrams in terms of (a) chondrite-normalised REE and (b) N-MORB normalised immobile-element patterns for the averages and ranges of Subgroup B-1 samples, a Quaternary remnant arc tholeiite behind the Shichito Ridge (Site D-621) in the Izu-Ogasawara Arc, northwest Pacific (Ikeda and Yuasa, 1989), and a representative of Lau Volcanic Group (sample 29458) from Lau Ridge (Cole *et al.*, 1990). Note that Nb datum for Site D-621 is not available.

Petrographically, they are equigranular, made up principally of altered plagioclase and metamorphic amphibole. Their accessory minerals are Fe-Ti oxides (pseudomorphed by leucoxene), Fe sulphides, quartz, chlorite and epidote, and may include clinopyroxene, sphene, rutile and apatite. Epidote veinlets are occasionally present.

Plagioclases are largely subhedral and partially replaced by epidote, zoisite, clinozoisite and chlorite. Amphiboles are commonly subhedral to anhedral, and are partially replaced by chlorite and epidote. They occur either as prismatic or as fibrous crystals, and have blue-green or reddish brown colours. Their compositions range from actinolitic hornblende via magnesio-hornblende and tschermakitic hornblende to tschermakite when Fe^{3+} values are calculated by the method of Laird and Albee (1981), and the amphibole nomenclature of Leake (1978) is applied. Relict clinopyroxenes have been sporadically detected as inclusions in brown amphiboles.

The metamorphic mineral assemblage, as mentioned above, suggests that they have been metamorphosed at conditions transitional between greenschist and amphibolite facies (Moody *et al.*, 1983).

4.3.2 Whole-rock Chemistry

Major, trace and rare-earth elements

The Subgroup B-2 microgabbros are basaltic (Table 4.1 and Fig. 4.1) and rather evolved (FeO* = 12.6-13.0 wt% and TiO_2 = 1.8-2.2 wt%). The lack of positive correlations for incompatible immobile elements, and negative correlations for compatible elements on FeO*/MgO variation diagrams (Fig. 4.7) indicate a generally non-comagmatic origin for the Subgroup B-2 microgabbros.

They have low Nb (2-3 ppm), Zr (71-77 ppm), Ni (13-18 ppm) and Cr (9-16 ppm), but high TiO_2, Ti/Zr (141-179) and Zr/Nb (26-38) contents. Their high Zr/Nb values preclude the possibility of their being ocean-island basalts or E-MORB (Basaltic Volcanism Study Project, 1981). Their Ni and Cr contents are low compared to even evolved N-MORB, and their Zr contents are less than one-third the Zr contents of N-MORB at a similar level of fractionation (le Roex *et al.*, 1982). Their high TiO_2 contents suggest that they are unlikely to be arc basalts (Perfit *et al.*, 1980; Basaltic Volcanism Study Project, 1981).

REE analyses have been carried out on two Subgroup B-2 microgabbros (Table 4.3). Their chondrite-normalised REE patterns (Fig. 4.13a) are flat to slightly

LREE enriched ((La/Sm)n=1.1-1.3 and (Sm/Yb)n=1.4-2.3). These patterns are more typical of tholeiitic than calc-alkalic lavas, although this is not diagnostic.

Comparisons with modern suites

The Subgroup B-2 tholeiites have abnormal compositional features. Their high FeO and Ti/Zr values, and low Zr, Nb, Ni and Cr contents, and flat to slightly LREE-enriched REE patterns are all features typical of island-arc tholeiitic basalts. However, arc tholeiites rarely have TiO_2 contents more than 1.3 wt%. Therefore the high TiO_2 contents of the Subgroup B-2 microgabbros (1.8-2.2 wt%) are anomalous and appear to rule out any direct analogy with arc tholeiites. A careful re-examination of thin sections showed no accumulation of Fe-Ti oxides which might account for the high TiO_2 contents. Their Ti-V and Nb-Y-Zr relationships (Figs. 4.9 and 4.10) suggest that they are BABB or MORB.

Despite an extensive literature search, no convincingly comparable analogues to these compositionally unusual rocks could be found. In terms of REE patterns and MORB-normalised multi-element variation diagram (Fig. 4.13), the Subgroup B-2 rocks show remarkable parallelism with a typical low-K arc basalt (Gorton, 1977) from eastern Epi (Vanuatu); however, the Epi basalt pattern is at four-times lower normalised abundance levels. This may be partly due to the more primitive nature of the Epi basalt compared to the notably more evolved Subgroup B-2 tholeiites (Table 4.4), but probably reflects the more depleted source of the former.

If the eastern Epi source partially melted under lower fO_2 conditions, forcing delayed fractionation of Fe-Ti oxide during subsequent fractionation relative to the actual case, the opportunity would exist to drive TiO_2 and FeO* to higher values, perhaps similar to those of the Subgroup B-2 rocks. Arc-like trace-element signatures characterise many lavas erupted during the earliest stages of backarc basin opening and arc rifting (Saunders and Tarney, 1979; Muenow *et al.*, 1980). Therefore, although this assignment is far from conclusive, it seems that the unusual Subgroup B-2 tholeiites might reflect products of magmatism associated with the earliest phase of splitting of an arc and opening of a backarc basin. Melting conditions in this transitional settings would vary with time from more oxidised (producing more arc-like magmas) to more reducing (generating more MORB-like lavas).

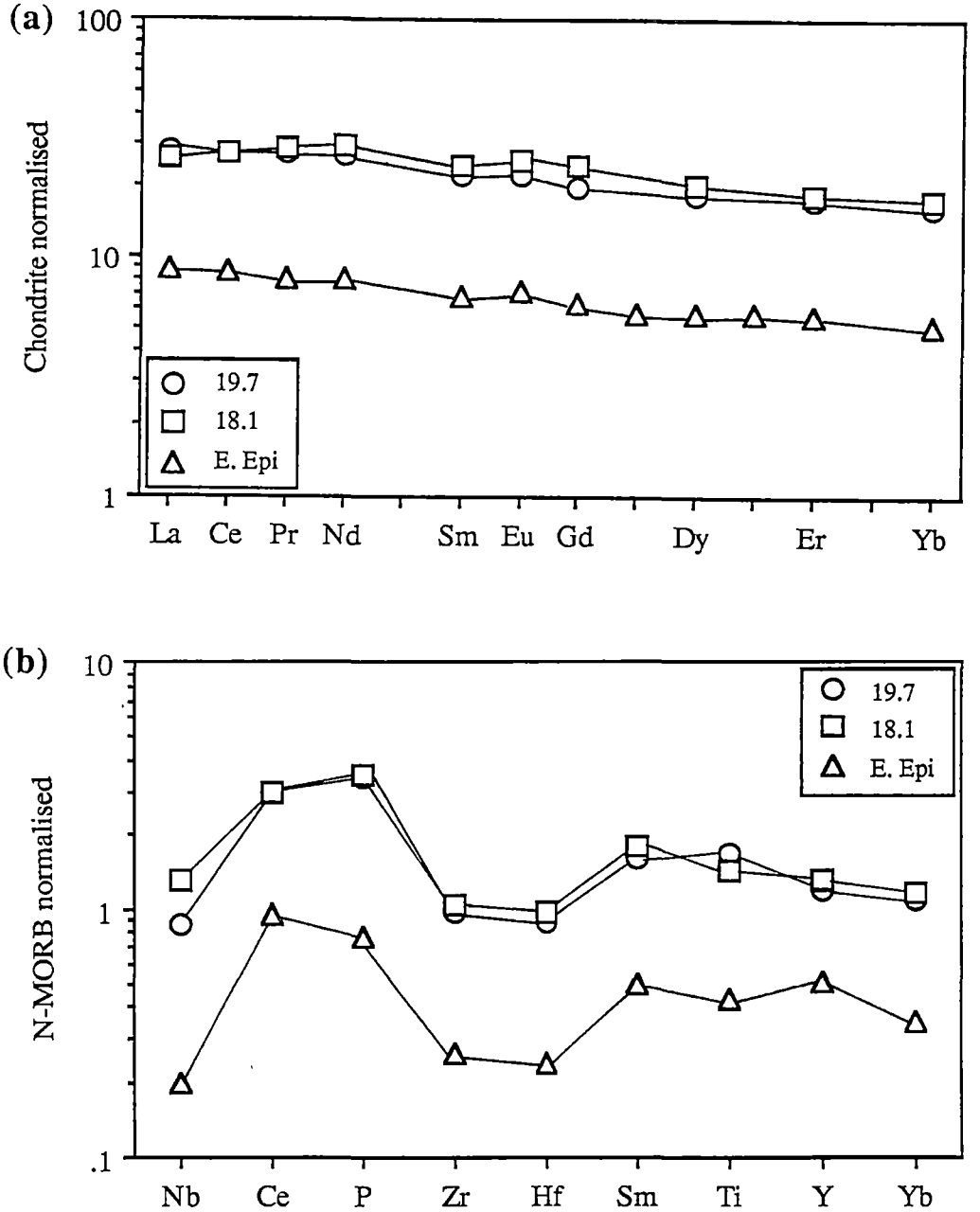

Figure 4.13. Chondrite-normalised REE (a) and N-MORB normalised multi-element (b) patterns for Subgroup B-2 microgabbros compared with those for eastern Epi tholeiite (sample 670), Vanuatu (Gorton, 1977).

4.4 Subgroup B-3 Tholeiites

4.4.1 Occurrence and Petrography

The five least altered Subgroup B-3 samples are all dolerites, collected from an outcrop in the Doi Phuk Sung area and float in the Nan River and Sirikit Reservoir areas. In the Doi Phuk Sung area, the Subgroup B-3 sample crops out between gabbro/amphibolite exposures, and probably occurs as a dike cutting through gabbro (amphibolite). In the Sirikit Reservoir area, the Subgroup B-3 rocks are associated with float serpentinite and serpentinised peridotite, and are possibly blocks in serpentinite matrix. Sample locations and petrographic features of individual samples are given in Table I-2 (Appendix I) and Table II-4 (Appendix II), respectively.

The Subgroup B-3 dolerites are porphyritic to aphyric, fine-grained rocks (<1 mm across), composed mainly of altered plagioclase, and amphibole. Accessories may include clinopyroxene, altered orthopyroxene, Fe oxide (totally pseudomorphed by leucoxene), Fe sulphides, quartz, apatite, epidote and calcite. Phenocryst and microphenocryst assemblages are: plagioclase+orthopyroxene, and plagioclase+ orthopyroxene+clinopyroxene; plagioclase is the most abundant phenocryst/ microphenocryst phase. Vein minerals include albite, epidote and amphibole (actinolite).

All plagioclases are subhedral to euhedral, and heavily specked with dark brown cryptocrystalline aggregates (mainly Ca hydrosilicates) and sericite. Other alteration products may be epidote, clinozoisite, prehnite, pumpellyite and clear plagioclase (andesine).

Amphiboles vary compositionally from actinolite through actinolitic hornblende, magnesio-hornblende and tschermakitic hornblende to tschermakite (largely tschermakitic hornblende and tschermakite) when the calculation method for Fe^{3+} of Laird and Albee (1981), and the classification scheme of Leake (1978) are followed. They are predominantly reddish brown and yellowish brown-green, and show subophitic textures intergrown with plagioclase (Fig. 4.14). Many contain colourless clinopyroxene inclusions, suggesting that they pseudomorph clinopyroxene. They are slightly replaced by chlorite, pale green amphibole and opaque minerals.

Orthopyroxenes are present in some samples as distinctive orthorhombic phenocrysts and microphenocrysts. They are euhedral to anhedral, and totally altered to chlorite with small amounts of pale green amphibole and brown amphibole.

(a)

(b)

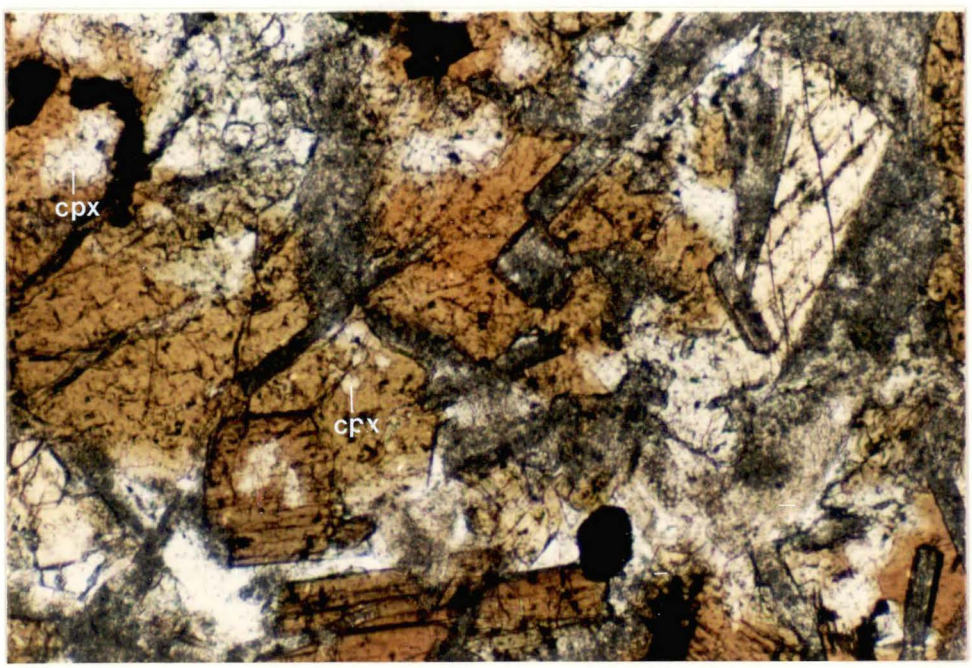

Figure 4.14. Photomicrographs of representative Subgroup B-3 tholeiites showing subophitic green - yellowish green amphiboles in sample YP-9 (a) and subophitic brown - pale brown amphiboles with colourless clinopyroxene (cpx) inclusions in sample 45.4 (b). Ordinary light, X 130.

Clinopyroxene phenocrysts and microphenocrysts occur in a few samples; many form glomerocrysts and subophitically enclose plagioclase laths. Relict groundmass clinopyroxenes have been detected as anhedral inclusions in amphiboles in almost all samples.

According to the mineral assemblages above, these are likely to be medium-grade regional metamorphic rocks (transitional between greenschist and amphibolite facies).

4.4.2 Mineral Chemistry

Analyses of colourless clinopyroxene in four Subgroup B-3 dolerites (Table 4.5) show that they are all calcian augites (Subcommittee on Pyroxenes, I.M.A.,1988). In terms of quadrilateral components, they have a limited range of Mg# (0.79-0.84) but variable wollastonite contents (37-44%), giving rise to an unusual compositional field with fairly constant Mg# (Fig. 4.15) that extends between the solidus and subsolidus trends of the Skaergaard Intrusion (Brown, 1967; Nwe, 1976). This trend probably reflects the subsolidus re-equilibration in these dolerites of augites of near-constant Mg#, due to the near-constant FeO*/MgO of the analysed Subgroup B-3 rocks (1.15-1.42).

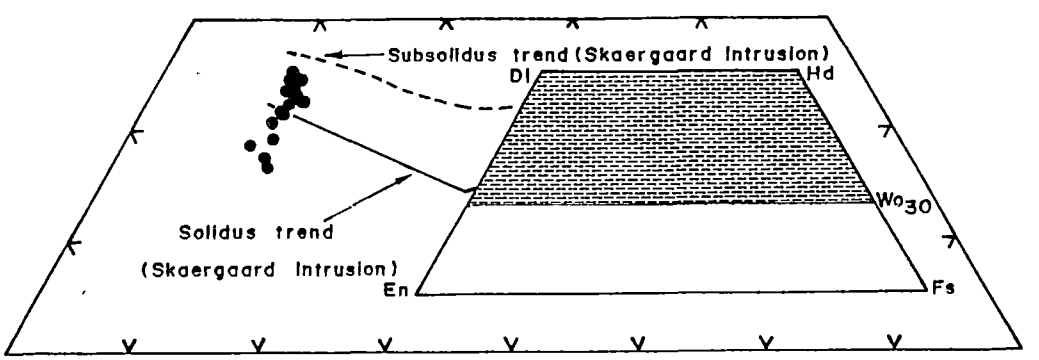

Figure 4.15. Pyroxene ternary diagram for colourless clinopyroxenes in Subgroup B-3 dolerites. The solidus and subsolidus trends for Skaergaard clinopyroxenes are after Brown (1967) and Nwe (1976), respectively.

TABLE 4.5. ELECTRON MICROPROBE ANALYSES OF COLOURLESS CLINOPYROXENES IN DOLERITES OF SUBGROUP B-3. FeO AND Fe_2O_3 ARE CALCULATED ASSUMING STOICHIOMETRY ON THE BASIS OF 4 CATIONS AND 6 OXYGENS. END-MEMBERS IN TERMS OF WOLLASTONITE, ENSTATITE AND FERROSILITE ARE CALCULATED ACCORDING TO THE METHOD RECOMMENDED BY THE SUBCOMMITTEE ON PYROXENES, IMA (1988).

Sample no.	26.7						45.1					45.2					45.4					
Anal. no.	1	2	3	4	5	6	1	2	3	4	5	1	2	3	4	5	1	2	3	4	5	6
SiO2	51.12	51.67	52.67	52.38	49.88	50.29	50.01	51.99	50.56	51.94	53.78	53.47	52.23	51.56	50.96	51.13	50.69	50.83	50.10	49.92	51.66	52.97
TiO2	0.45	0.57	0.30	0.33	0.66	0.59	0.66	0.40	0.73	0.50	0.67	0.24	0.47	0.51	0.58	0.57	0.71	0.64	0.89	0.68	0.52	0.28
Al2O3	5.37	4.77	2.72	2.50	5.05	5.25	5.79	3.17	5.61	3.83	2.70	2.49	2.95	3.54	5.68	5.34	5.53	5.32	6.51	6.39	4.59	2.29
Cr2O3	0.74	0 65	-	0.41	1.18	0.88	0.75	-	0.78	0 40	-	0.36	0.38	0.86	0.34	0.52	0.77	0.61	0.30	0.47	0.19	-
Fe2O3	0.13	-	-	-	-	-	0.34	-	-	-	-	-	0.24	-	-	-	-	-	-	-	-	-
FeO	6.49	6.89	7.62	7.32	6.63	6.25	6.72	6.89	6.30	6.44	6.52	6.46	6.67	6.08	6.86	6.44	6 03	6.24	7.41	6.64	6.82	7.27
MgO	15.83	16.10	17.78	17.83	15.26	15.44	15.50	16.59	15.36	15.95	17.35	18.33	16.74	15.86	16.00	15.49	15.37	15.48	15.32	14.94	16.02	17.48
CaO	20.94	20.58	17.79	18.31	20.53	20.46	20.33	20.00	20 94	20.96	20.17	19 23	20 59	21.54	20.20	21.47	21.64	21.18	20.10	21.00	20.87	19 30
Total	101.07	101.23	98.88	99.08	99.19	99.16	100.10	99.04	100.28	100.02	100.81	100.58	100.27	99.95	100.62	100.96	100.74	100.30	100.63	100.04	100.67	99.59
Si	1.860	1.877	1.944	1.934	1.855	1.863	1.841	1.924	1.854	1.906	1.948	1.939	1.914	1.898	1.859	1.863	1.851	1.863	1.833	1.837	1.886	1.947
ivAl	0.140	0.124	0.056	0.066	0.145	0.137	0.159	0.076	0.147	0.094	0.052	0.061	0.086	0.102	0.141	0.137	0.149	0.137	0.167	0.163	0.114	0.053
Total tetra.	2.000	2.000	2.000	2.000	2.000	2.000	2.000	2.000	2.000	2.000	2.000	2.000	2.000	2.000	2.000	2.000	2.000	2.000	2.000	2.000	2.000	2.000
viAl	0.091	0.081	0.063	0.043	0.076	0.092	0.092	0.063	0 096	0.072	0.063	0.045	0.042	0.052	0.104	0.093	0 090	0.093	0.114	0.114	0.083	0.047
Ti	0.012	0.016	0.008	0.009	0.018	0.017	0.018	0.011	0.020	0.014	0.008	0.007	0.013	0.014	0.016	0.016	0.020	0.018	0.024	0.019	0.014	0.008
Cr	0.021	0.019	-	0.012	0.035	0.026	0.022	-	0 023	0.012	-	0.010	0.011	0.025	0.010	0.015	0.022	0.018	0 009	0.014	0 006	-
Fe3+	0.004	-	-	-	-	-	0.009	-	-	-	-	-	0.007	-	-	-	-	-	-	-	-	-
Fe2+	0.198	0 209	0.235	0.226	0.206	0.194	0.207	0.213	0.193	0.198	0.198	0.196	0.204	0.187	0.209	0.196	0.184	0.191	0.227	0.204	0.208	0.223
Mg	0.859	0.872	0.978	0.981	0.846	0.853	0.850	0.915	0.839	0.873	0.936	0.991	0.914	0.870	0.870	0.841	0.837	0.845	0.836	0.819	0.871	0.958
Total octa.	1.184	1.196	1.285	1.272	1.181	1.181	1.198	1.202	1.171	1.167	1.204	1.249	1.191	1.149	1.208	1.161	1.152	1.164	1.209	1.170	1.183	1.235
Ca	0.816	0.801	0.704	0.724	0.818	0.812	0.802	0.793	0.823	0.824	0.783	0.747	0.809	0.850	0.790	0.838	0.847	0.832	0.788	0.828	0.816	0.760
Total cats.	4.000	3.997	3.988	3.996	3.999	3.993	4.000	3.995	3.994	3.992	3.987	3.996	4.000	3.998	3.998	3.999	3.999	3.996	3.998	3.999	3.999	3.995
Mg#	0.813	0.806	0.806	0.813	0.804	0.815	0.804	0.811	0.813	0.815	0.826	0.835	0.817	0.823	0.806	0.811	0.820	0.816	0.787	0.800	0.807	0.811
Wo	43.51	42.55	36.70	37.50	43.74	43.70	42.92	41.28	44.35	43.51	40.84	38.63	41.81	44.55	42.25	44.69	45.33	44.51	42.59	44.72	43.05	39.16
En	45.77	46.33	51.03	50.80	45.24	45.89	45.51	47.62	45.24	46.06	48.85	51.23	47.28	45.64	46.55	44.85	44.81	45.25	45.16	44.24	45.96	49.34
Fs	10.72	11.11	12.27	11.70	11.02	10.42	11.57	11.10	10.41	10.43	10.31	10.13	10.92	9.81	11.19	10.47	9.86	10.23	12.25	11.03	10.99	11.51

- = BELOW DETECTION LIMIT.

The Subgroup B-3 clinopyroxenes show obviously positive correlations between Ti and Al^{iv}, and Al^{vi} and Al^{iv}, with average Ti/Al^{iv} and Al^{vi}/Al^{iv} values of 0.13±0.02 and 0.72±0.16 (Fig. 4.16), respectively, suggesting that 'Others' multiple coupled substitutions are governed significantly by $(Ti^{4+}/2)$ - Al^{iv}, and Al^{vi} and Al^{iv} pairs. On grounds of discriminant plots of Leterrier *et al.* (1982), they appear to be subalkalic clinopyroxenes; however, the orogenic versus non-orogenic nature of these pyroxenes cannot be diagnosed (Fig. 4.17).

4.4.3 Whole-rock Chemistry

Major, trace and rare-earth elements

The Subgroup B-3 dolerites are all basaltic with 49-51 wt% SiO_2 and FeO*/MgO = 1.2-1.4 (Table 4.1 and Fig. 4.1). Despite a narrow range of FeO*/MgO, TiO_2 and V seem to increase with increasing FeO*/MgO (Fig.4.5), suggesting that they may have broad tholeiitic affinities. They have a restricted range of least mobile elements (9.9-10.3 wt% FeO*, 1.0-1.1 wt% TiO_2, 0.12-0.17 wt% P_2O_5, ≤ 2 ppm Nb, 44-51 ppm Zr, 20-22 ppm Y, 59-131 ppm Ni, 195-299 ppm Cr, 312-343 ppm V, and 44-50 ppm Sc). They have uniformly low K_2O contents (0.13-0.42), suggesting low-K tholeiitic affinities, a hypothesis supported by the regularly high Ti/Zr (117-143) values.

REE analyses have been conducted on one representative sample (Table 4.3), which shows a rather flat chondrite-normalised REE pattern ((La/Yb)n=0.9) with slight LREE depletion ((La/Sm)n=0.8)(Fig. 4.18a), emphasizing compositional similarity with low-K arc tholeiites.

Comparisons with modern suites

An extensive search for modern analogues have been made. The closest matches were made with subalkaline basalts from the Witu Islands, on the western margin of the actively spreading Manus Basin, and Kimbe Island on the southern side of the same backarc basin. Basalts from Mundua Island in the Witu Group (Johnson and Arculus, 1978) and from Wambu Island, also in the Witu Islands, (A.J. Crawford, unpubl. data, 1989) have flat REE patterns around 10 times chondrite, whereas that from Kimbe is flat to very slightly LREE-depleted but at 5-7 times chondrite (Fig. 4.18a). MORB-normalised multi-element patterns (ignoring Nb data which are all below detection limit for XRF) show strong similarities with these Witu

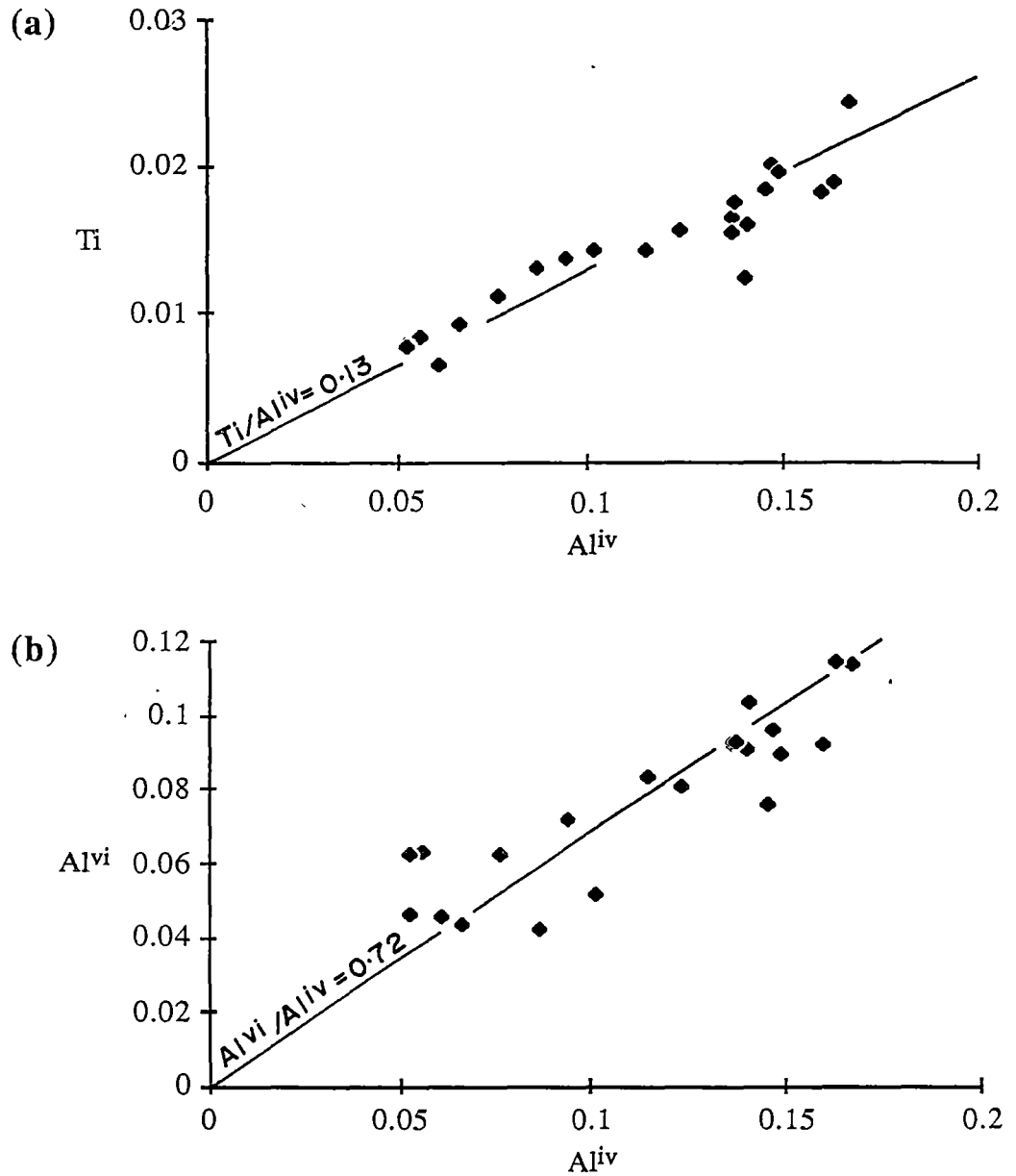

Figure 4.16. Ti -Al^{iv} (a) and Al^{vi} - Al^{iv} (b) covariations for Subgroup B-3 clinopyroxenes (based on 6 oxygens), showing the significance of (Ti^{4+}/2) - Al^{iv} and Al^{vi} - Al^{iv} substitutional couples.

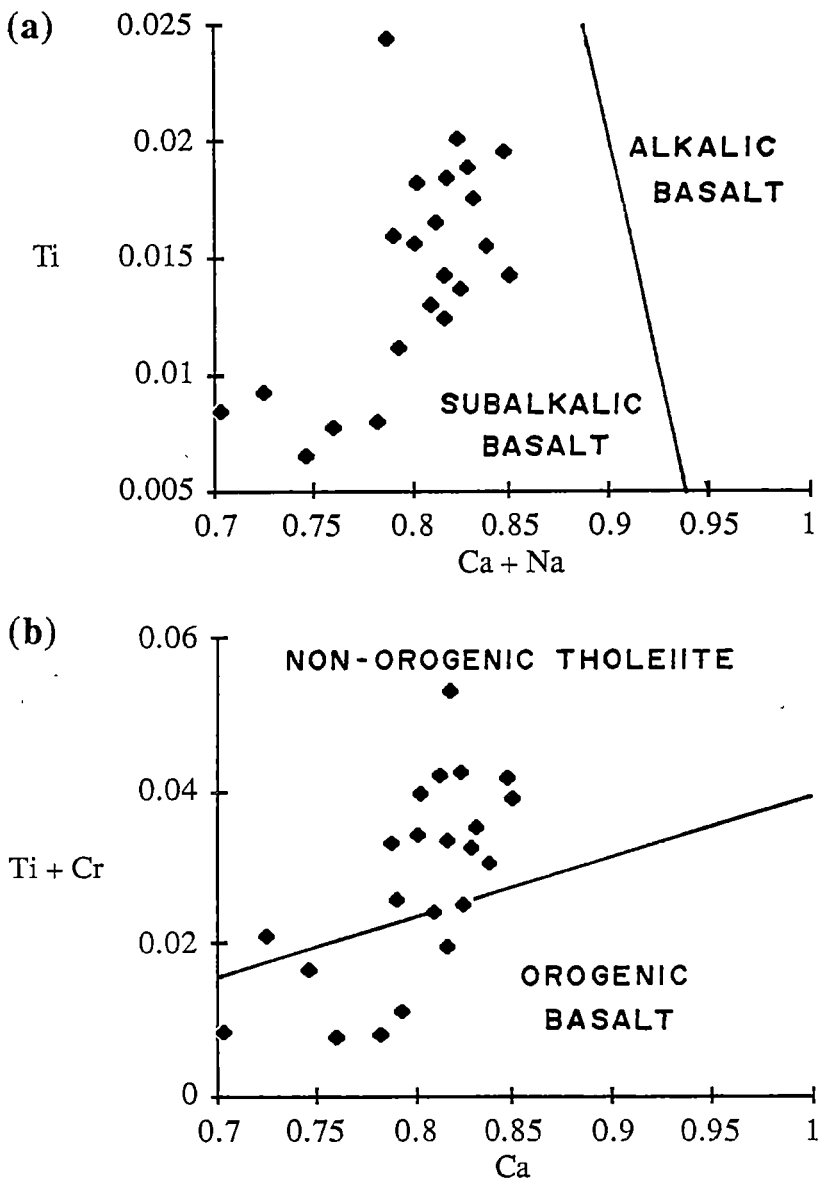

Figure 4.17. Clinopyroxene data for Subgroup B-3 dolerites (based on 6 oxygens) compared with the compositional fields for clinopyroxenes in basalts erupted in various tectonic settings (Leterrier *et al.*,1982).

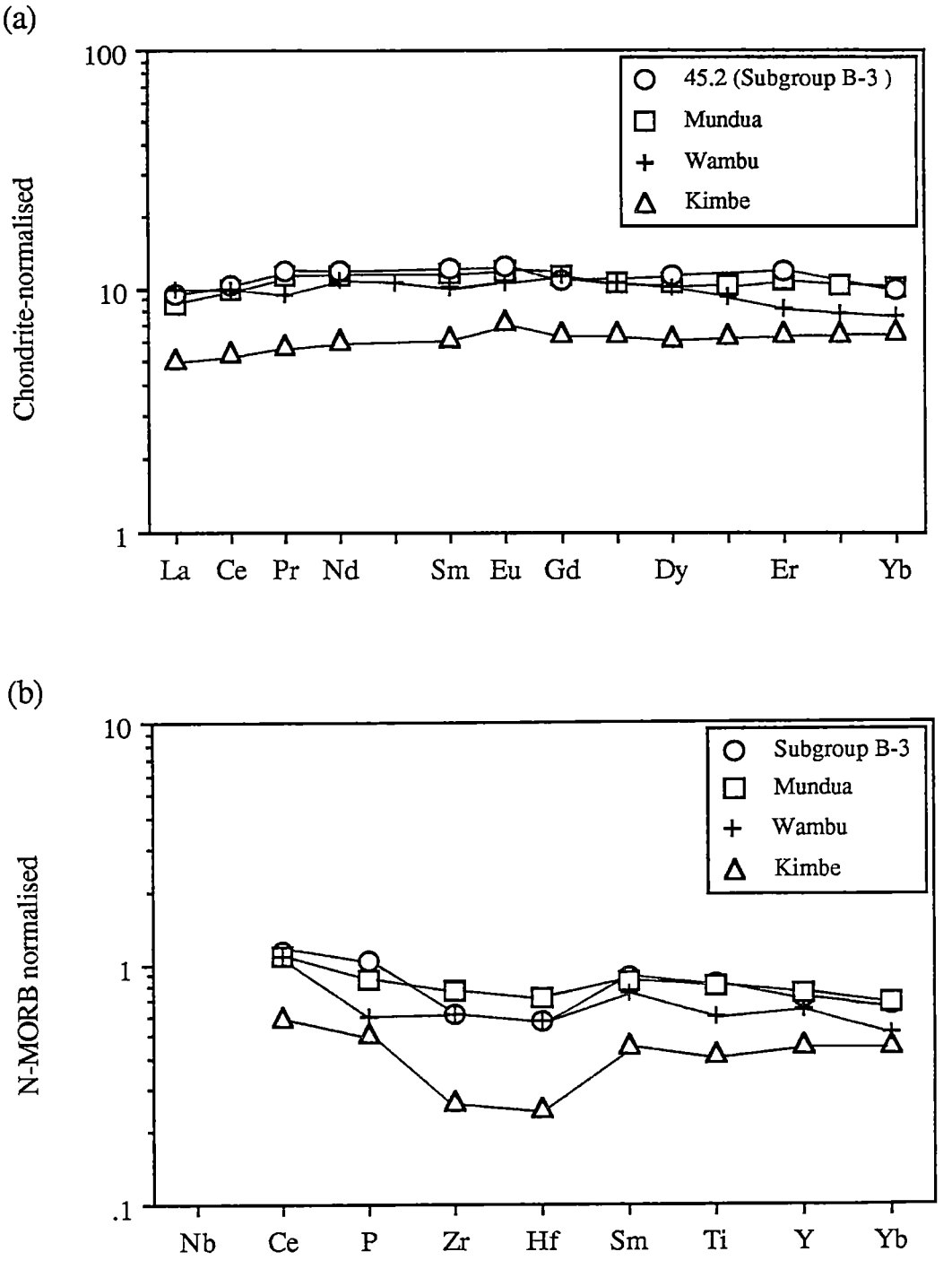

Figure 4.18. Chondrite-normalised REE (a) and N-MORB normalised multi-element (b) patterns for Subgroup B-3 dolerites, Quaternary supra-subduction zone basalts from the Witu Islands (Mundua (sample 6; Johnson and Arculus, 1978) and Wambu Island (sample 68892; A.J. Crawford, unpubl. data, 1989)) and Kimbe Island (sample IA-5; Basaltic Volcanism Study Project, 1981). Data points for Nb are omitted since their absolute abundances are less than 2 ppm (close to the detection limit determined by XRF). See discussion in the text.

Island and particularly with the Kimbe Island basalt (though at a higher level, due to fractionation)(Fig. 4.18b).

The Witu/Kimbe Island rocks were unambiguously erupted in a supra-subduction zone setting. They show unusual compositional features reflecting a transition between arc tholeiites and backarc basin tholeiites. Rather than being erupted at a spreading ridge, however, these rocks were erupted in central volcanoes, possibly contemporaneous with establishment of the backarc spreading centre. In this context,, therefore, it can be confidently concluded that the Subgroup B-3 dolerites represent supra-subduction zone magmatism transitional between arc tholeiitic and backarc basin tholeiitic magmas.

4.5 Subgroup B-4 Tholeiitic sample

4.5.1 Occurrence and Petrography

Only one Subgroup B-4 basaltic lava has been identified from float in the northernmost part of the Nan River area (sample location in Table I-2, Appendix I). The outcrop where the lava has been collected is cumulus gabbro/amphibolite.

Petrographically, this basaltic lava is aphyric, and has undergone severe alteration; colourless clinopyroxene is the only igneous phase surviving. Other primary igneous minerals are totally replaced by low-grade metamorphic minerals, including chlorite, sericite, clay minerals and leucoxene. A few clinopyroxene crystals are sparsely fringed with blue amphibole.

Although igneous clinopyroxenes are well preserved in the studied sample, they are considered to be uninformative with regard to tectonic setting of eruption, as they occur as groundmass constituents and are likely to have strong cooling rate-control on compositional features (Grove and Bence, 1979).

4.5.2 Whole-rock Chemistry

Immobile elements

The Subgroup B-4 sample is characterised by low Nb/Y, intermediate Zr/TiO_2, and high FeO*, TiO_2 and V (Table 4.1 and Fig. 4.1), indicating that it is a tholeiitic basaltic andesite. It differs from the Subgroup B-1,B-2 and B-3 samples in having higher FeO*, TiO_2 and Y at similar values for FeO*/MgO (Figs. 4.5 and 4.7).

Its FeO* and TiO_2 contents are comparable to those of MORB, BABB and intraplate oceanic tholeiites at similar FeO*/MgO and MgO values (Figs. 4.5 and 4.6). The possibility of it being E-MORB and intraplate basalts is, however, precluded by its high Zr/Nb (41) and low Nb (4 ppm) values, more characteristic of N-MORB or BABB. It also lies within the fields of MORB and BABB on the Ti-V and Nb-Zr-Y plots (Figs. 4.9 and 4.10).

The chondrite-normalised REE pattern for the Subgroup B-4 sample analysed (Fig. 4.19) emphasizes the N-MORB character since it shows a fairly flat HREE (Yb to Nd) pattern and LREE (Nd to Ce) depletion. Its evolved nature is also accentuated by higher REE abundances (Table 4.3) relative to those of typical N-MORB (Basaltic Volcanism Study Project, 1981).

Comparisons with modern suites

From the foregoing discussion, the Subgroup B-4 basaltic andesite has affinities with N-MORB generated in major oceans or backarc basins. On the basis of a single sample, it is not possible to confidently discriminate between major ocean basin MORB and BABB.

The Subgroup B-4 sample is very similar to the Quaternary (?) unit 3 tholeiitic rocks (possibly off-axis postdating axis lavas), penetrated in Hole 474A, Leg 64, Gulf of California (Saunders *et al.*, 1982), on the basis of REE and N-MORB normalised element variation patterns (Fig. 4.19), chondrite-normalised REE and immobile-element ratios (Table 4.4). The differences in their absolute abundances (Table 4.4) are attributed to different degrees of fractionation. This sample is a N-MORB-type tholeiite generated at a spreading centre, probably in a backarc basin, based on the petrochemistry of other suites of non-intraplate lavas in the Nan Suture.

4.6 Summary

Rocks constituing Group B are significantly different from the Group A tholeiites in having higher Zr/Nb (>22), but lower Nb (<2-8 ppm), Ti/Y (209-385) and Nb/Y contents. They may be chemically subdivided into four subgroups, B-1, B-2, B-3 and B-4.

4.6.1 Modern Embryonic Backarc Basin Basalts

In this chapter, four compositionally quite distinctive suites have been recognised. Three of these suites have been assigned to eruption settings in an

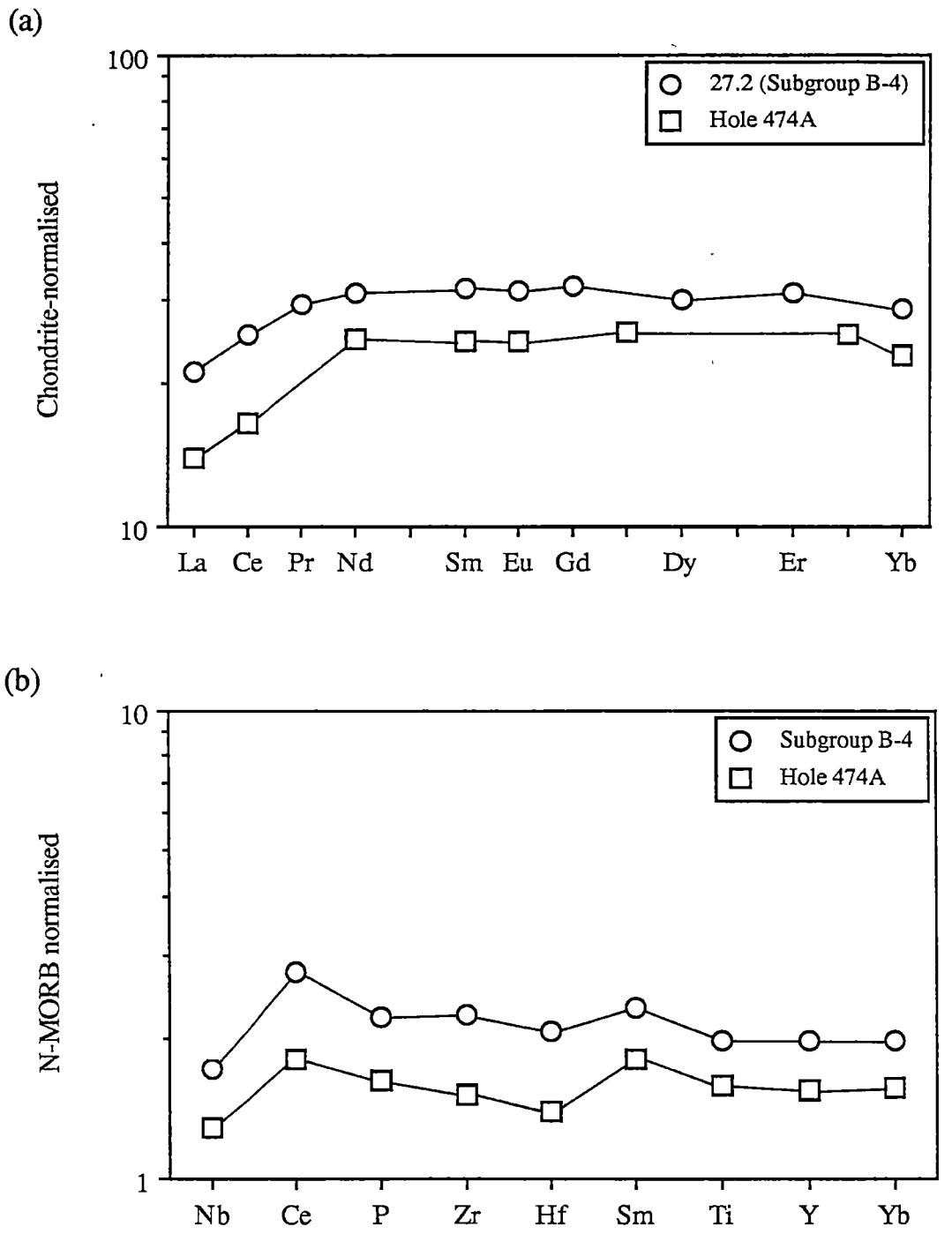

Figure 4.19. Chondrite-normalised REE (a) and N-MORB normalised multi-element (b) patterns for Subgroup B-4 basaltic andesite and Quaternary(?) tholeiite from unit 3, Hole 474A, Leg 64, Gulf of California (Saunders *et al.*, 1982).

embryonic backarc basin in an oceanic arc characterised by arc tholeiitic magmatism. These assignments have been based mainly on immobile element/REE characteristics that are transitional between arc (tholeiitic) lavas, with typical depletion of HFSE, and MORB (N- to E-MORB). That three compositionally distinct magmatic suites might form in a single tectonomagmatic setting, such as an embryonic/immature backarc basin, might at first glance, seem anomalous or surprising. However, data emerging from intensive studies of backarc basin crust show that this need not be the case.

Early models for BABB generation (e.g. Crawford *et al.*, 1981; Saunders and Tarney, 1979, 1984) predicted that those basalts produced during the earliest stages of backarc basin opening would inherit an LILE-enriched 'slab' component due to proximity of ascending source diapirs to the subducted slab. As backarc opening progressed, the diapirs necessarily move further from the slab, the enriched 'slab' component diminishes, and the basalts approach N-MORB compositions. Subsequent studies (Hawkins and Melchior, 1985; Sinton and Fryer,1987; Volpe *et al.*, 1988) have shown this to be substantially correct, for both the Lau and Mariana backarc basins, where the most recently-erupted basalts in the widest parts of the basins (e.g. spreading ridge in N Lau Basin) are more N-MORB-like than basalts on the older flanks of the basins.

However, recent studies of backarc (Lau, Manus, Woodlark, N Fiji, Cariolis Trough and Mariana Trough-Sumisu Rift) basins have shown a considerable diversity and complexity among dredged and drilled backarc basin crust samples. For instance, lavas erupted at the Valu Fa Ridge in the southern Lau Basin (only 40 km W of active Tongan Arc) are basaltic andesites with pronounced arc affinities (Jenner *et al.*, 1987). Similarly, arc-type basaltic andesites erupted in those ridge segments in the Manus Basin closest to the active New Britain Arc (Liu *et al.*, 1988). Basalts with strong arc signatures, and dacites-rhyolites, occur in the immature Sumisu Rift in the Izu Arc (Hochstaedter *et al.*, 1988, 1990). In the Bransfield Straits, rifting of the Antarctic Peninsula - South Shetland Island Arc has generated a diverse suite of basaltic (from tholeiitic to slightly alkalic) and andesitic lavas (Weaver *et al.*, 1979; Keller *et al.*, 1988). Finally, recent studies of seamounts between the active southern Lau Basin Spreading Centre and the active Tongan Arc show the presence of strongly depleted tholeiitic basalts that range through to high-Ca boninite compositions (Sunkel, 1991).

Clearly, the sources and processes of generation of magmas produced during early backarc basin opening are complex and poorly understood. However, ophiolitic basalts that compositionally show some characteristics of backarc basin MORB-type basalts, and some features typical of arc lavas might reasonably be assumed to have

formed in an immature spreading centre in an oceanic island arc. This hypothesis in the case of the Nan Suture rocks, is strengthened by the occurrence of typical arc volcanics as blocks in the serpentinite melange (see Chapter 5) at each locality where the BABBs have been recorded and described.

4.6.2 Summary of Subgroup B-1 Basalts and Andesites

The Subgroup B-1 covers lava, dolerite and microgabbro that occur locally in the Mae Charim and Doi Phuk Sung areas; they are best classified as basalts and andesites. In the Doi Phuk Sung area, dolerites are evidently faulted against Upper Triassic - Lower Cretaceous molasse, and show complicated internal structures, suggestive of a sheeted dike complex.

Petrographically, they consist mainly of albitised plagioclase and colourless clinopyroxene, and vary texturally from equigranular through seriate to strongly porphyritic. Plagioclase occurs as the sole phenocryst phase in the dolerites, but in the lava, plagioclase and ?clinopyroxene (completely pseudomorphed by yellowish - blue-green amphibole) are common phenocrysts and microphenocrysts.

Chemically, the Subgroup B-1 samples are basalts and andesites. They show FeO*, TiO_2 and V enrichment with increasing FeO*/MgO in the earlier stages of fractionation and slightly LREE enriched patterns, typical of medium-K tholeiitic basalts. They are compositionally intermediate between IAT and E-MORB in terms of both whole-rock and clinopyroxene chemistries.

These basaltic and andesitic rocks are closely analogous to the Quaternary remnant arc tholeiite (Site D-261), behind the Shichito ridge in the Izu-Ogasawara arc, northwest Pacific (Ikeda and Yuasa, 1989), and basalts from Lau Ridge (Lau Volcanic Group)(Cole *et al.*, 1990), particularly in terms of REE and MORB multi-element patterns. However, the Subgroup B-1 rocks are somewhat enriched in TiO_2 relative to the modern suites, suggesting that they are transitional between BABB and arc lavas. Consequently, Subgroup B-1 rocks are most akin to BABB generated possibly in the earliest stages of backarc (interarc) spreading.

4.6.3 Summary of Subgroup B-2 Tholeiites

The Subgroup B-2 tholeiites are all microgabbros from melange blocks in the Nan River and Uttaradit areas. They are equigranular rocks, consisting principally of altered plagioclases and blue-green or reddish brown amphiboles (altered from clinopyroxene).

They have unusual chemical compositions. Their TiO_2 (1.8-2.2 wt%) contents are comparable to those of oceanic intraplate basalts and MORB but their Ni (13-18 ppm) and Cr (9-16 ppm) contents and very high Ti/Zr (141-179) resemble those of IAT. They have flat to slightly LREE enriched patterns also similar to arc tholeiites. Arc basalts from eastern Epi, Vanuatu Arc (Gorton, 1977) have similar REE and multi-element variation patterns but are much lower normalised abundance levels. In terms of MORB-normalised variation diagram, the significant difference between Subgroup B-2 and Epi basalts is the Ti depletion relative to Sm and Y for the Epi tholeiite but not for the Subgroup B-2 basalt. No directly comparable modern analogues of the Subgroup B-2 samples are known. Their transitional characteristics between arc basalts and evolved BABB may suggest formation in an embryonic backarc basin.

4.6.4 Summary of Subgroup B-3 Tholeiites

The Subgroup B-3 dolerites have been collected from an outcrop in the Doi Phuk Sung area, and float in the Nan River and Sirikit Reservoir areas. In the Doi Phuk Sung area, they occur as dikes in gabbro/amphibolite, whereas in the Nan River and Sirikit Reservoir areas, they are probably blocks in serpentinite matrix.

Petrographically, they are made up mainly of altered plagioclase and metamorphic amphibole. Generally, these rocks are fine-grained, and exhibit porphyritic to non-porphyritic textures. Their phenocryst and microphenocryst assemblages are: plagioclase+orthopyroxene, and plagioclase+orthopyroxene+ clinopyroxene; plagioclase is the most predominant phenocryst/ microphenocryst phase.

Chemically, Subgroup B-3 samples are basalts with a narrow compositional range, particularly for least mobile elements (9.9-10.3 wt% FeO*, 1.0-1.1 wt% TiO_2, 0.12-0.17 wt% P_2O_5, $\leq$ 2 ppm Nb, 44-51 ppm Zr, 20-22 ppm Y, 59-131 for Ni, 195-299 ppm Cr, 312-343 ppm V, and 44-50 ppm Sc). A rather flat REE pattern ((La/Yb)n=0.9) with slight LREE depletion ((La/Sm)n=0.8), high Ti/Zr (117-143) and low K_2O values, and clinopyroxene compositions indicate low-K tholeiitic affinities. They are most similar to Quaternary low-K tholeiites from the Witu Islands and Kimbe Island in Manus backarc basin (SW Pacific). These rocks, and by analogy Subgroup B-3 samples are considered to have been erupted during transitional magmatic stage between arc tholeiite and backarc tholeiite magmatism, possibly in the embryonic stages of backarc opening.

4.6.5 Summary of Subgroup B-4 tholeiitic samples

Only one sample of Subgroup B-4 has been chemically identified from float samples in the northernmost part of the Nan River area. It is an altered aphyric basaltic andesite, made up mainly of altered plagioclase and colourless clinopyroxene.

Chemically, it is an evolved N-MORB which has REE and MORB normalised patterns comparable to the Quaternary(?), possibly off-axis tholeiites of unit 3 from Hole 474A, Leg 64, Gulf of California. It could have formed in a major or minor ocean basin; the association of other supra-subduction zone basalts in the Nan Suture might suggest that this sample also formed at a backarc basin spreading centre.

CHAPTER 5

ARC BASALT SUITES (GROUP C)

5.1 General Chemical Characteristics

The rocks belonging to Group C are all characterised by their relatively low values of TiO_2 (0.3-1.0 wt%), Zr (10-115 ppm), Nb (≤2 ppm), Y (9-33 ppm), Nb/Y (<0.3), Ti/Y (<400) and Ti/V (largely between 10-20), and high Zr/Nb ratios (>10). They are subalkalic, and range from basalt to andesite (Fig. 5.1), with 47.3-59.7 wt% SiO_2 and FeO*/MgO = 0.98-3.07. The Group C samples may be subdivided, on geochemical grounds (Table 5.1), into Subgroups C-1 and C-2.

5.2 Subgroup C-1 Arc Basalts and Andesites

5.2.1 Occurrence and Petrography

The analysed Subgroup C-1 samples include lavas (2 samples), dolerite (1 sample) and microgabbros (4 samples) that are present in every key area. Only three of them are outcrop samples, collected from the Nan River and Uttaradit areas, whereas the others are float samples almost certainly of blocks weathered from serpentinite melange. The microgabbro cropping out at Khao Sam Sen clearly cross-cuts the foliation of massive amphibolite (originally gabbro). Sample locations and detailed petrographic features of individual analysed Subgroup C-1 samples are given in Table I-3 (Appendix I) and Table II-5 (Appendix II), respectively.

Petrography of lavas

The analysed lavas are strongly porphyritic to porphyritic. Their phenocryst and microphenocryst assemblage is albitised plagioclase and an unknown mafic mineral (totally pseudomorphed by chlorite and epidote). Plagioclase phenocrysts and microphenocrysts are notably more abundant than mafic phenocrysts and microphenocrysts, subhedral to anhedral, and often show rounded edges and occasional embayment. They are all completely replaced by albite, epidote, clinozoisite and pumpellyite. Groundmass constituents are largely albitised plagioclase, and sparse leucoxene and epidote. Quartz, epidote and calcite veinlets may be locally present. The alteration products are an indicative of low-grade regional metamorphic rocks.

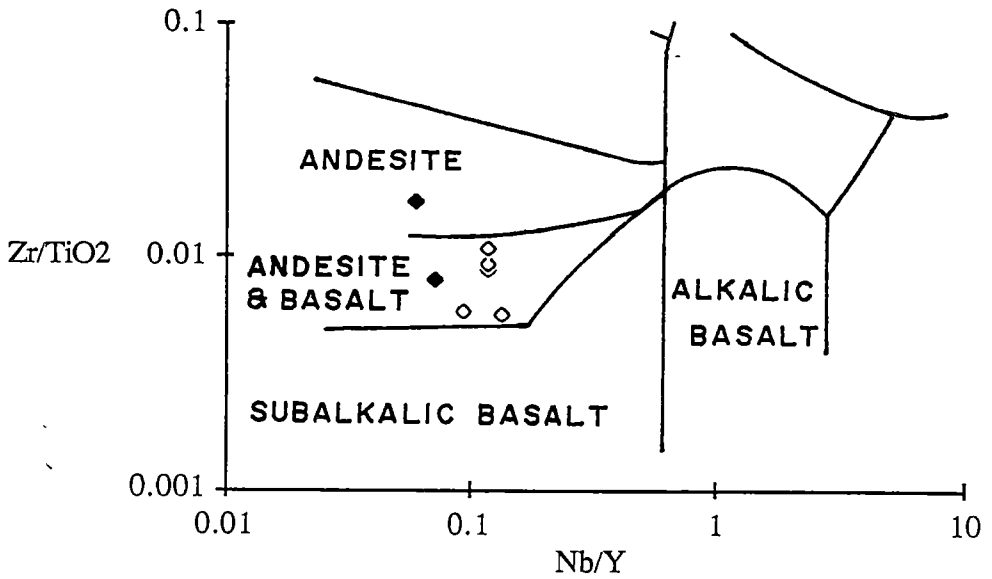

Figure 5.1. Minor- and trace-element data for Group C samples (solid diamond, Subgroup C-1; open diamond, Subgroup C-2) projected in the Zr/TiO_2 versus Nb/Y diagram of Winchester and Floyd, 1977. The data points for rocks with Nb content less than 2 (close to the detection limit determined by XRF) are omitted.

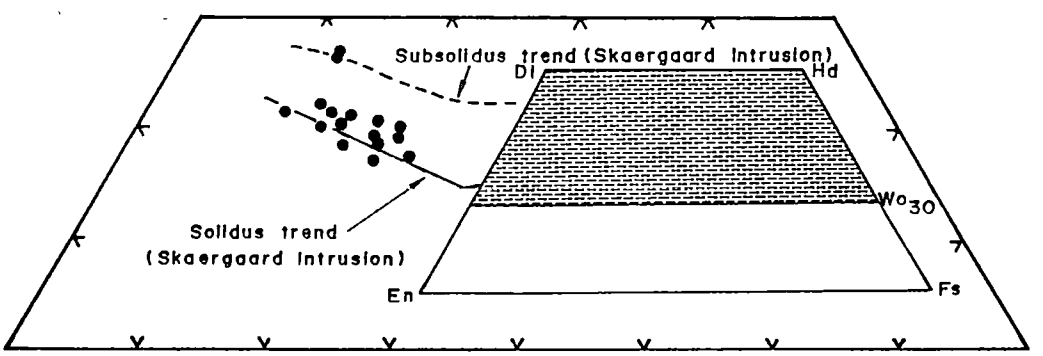

Figure 5.2. Wo-En-Fs diagram for colourless clinopyroxenes in Subgroup C-1 dolerite and microgabbro. Note that they almost follow the equilibrium crystallisation trend of Skaergaard clinopyroxenes (Brown, 1967), except those of sample S-9.2 which are on the subsolidus clinopyroxene trend of the Skaergaard Intrusion (Nwe, 1976).

TABLE 5.1. WHOLEROCK XRF ANALYSES AND SOME SELECTED RATIOS OF GROUP C LAVAS, DOLERITES AND MICROGABBROS; MAJOR ELEMENTS ARE NORMALISED TO 100% ON THE BASIS OF LOSS ON IGNITION FREE

Subgroup	C-1							C-2					
Sample no.	S9-2[2]	32.1	18.6[2]	47.1[1]	38.4[2]	42.1[1]	1.20[2]	11[1]	24.2[1]	24.1[1]	18A	18.3	18.2
SiO2	47.32	54.95	52.86	59.66	54.61	55.13	53.15	52.29	54.48	55.13	49.15	49.56	50.78
TiO2	0.29	0.75	0.94	0.68	0.97	0.78	0.86	0.74	0.65	0.62	0.79	0.77	0.94
Al2O3	16.90	17.21	16.22	19.18	19.23	20.74	14.77	17.67	15.48	15.90	18.99	19.03	16.50
FeO*	9.81	9.05	12.04	6.05	10.05	7.51	12.32	10.12	10.20	9.87	11.04	10.89	12.66
MnO	0.19	0.11	0.21	0.12	0.21	0.14	0.20	0.18	0.19	0.18	0.18	0.18	0.21
MgO	10.01	5.62	5.44	2.30	3.37	2.46	4.01	5.74	5.75	5.53	4.47	4.38	4.60
CaO	13.03	6.44	9.97	6.98	6.31	10.15	8.75	8.16	10.14	10.09	11.62	10.86	10.50
Na2O	1.86	3.64	1.92	3.76	4.73	2.70	4.30	4.68	2.42	2.24	1.76	2.69	2.54
K2O	0.57	2.05	0.30	1.12	0.37	0.27	1.56	0.17	0.50	0.25	1.72	1.34	0.85
P2O5	0.03	0.18	0.08	0.16	0.15	0.11	0.10	0.26	0.19	0.20	0.29	0.30	0.42
LOI	2.94	2.85	1.53	3.36	3.65	2.57	1.55	2.33	1.98	2.27	2.26	2.19	1.75
FeO*/MgO	0.98	1.61	2.21	2.63	2.98	3.05	3.07	1.76	1.77	1.78	2.47	2.49	2.75
Nb	<1	<1	1	2	2	<1	1	2	2	2	1	2	2
Zr	10	47	25	115	76	63	33	65	59	66	39	43	54
Y	9	19	15	33	28	20	22	17	17	17	14	15	21
Sr	466	355	284	320	466	513	1234	417	475	518	717	746	752
Rb	5	28	4	19	7	4	13	7	6	4	34	27	15
Ni	84	25	13	14	5	10	29	35	37	35	23	24	21
Cr	143	49	15	8	3	12	10	92	92	102	35	32	18
V	281	311	598	133	184	247	509	315	337	318	427	435	512
Ba	155	320	83	260	120	92	602	49	176	107	554	413	226
Sc	63	35	62	20	23	28	47	42	43	41	38	37	41
Ti/Zr	174	96	225	35	77	74	156	68	66	56	121	107	104
Zr/Nb	>10	>47	25	58	38	>63	33	33	30	33	39	22	27
Zr/Y	1.1	2.5	1.7	3.5	2.7	3.2	1.5	3.8	3.5	3.9	2.8	2.9	2.6
Y/Nb	>9	>19	15	16	14	>20	22	8	8	8	14	7	10

[1] = LAVA, [2] = MICROGABBRO, FeO* = TOTAL IRON AS FeO, LOI = LOSS ON IGNITION.

Petrography of dolerite sample

A Subgroup C-1 dolerite is fine-grained, and contains fairly abundant plagioclase phenocrysts, embedded in a matrix composed mainly of plagioclase and colourless clinopyroxene. Fe-Ti oxides occur as accessory minerals. Plagioclases, both as phenocryst and groundmass phases, are largely subhedral, and partially replaced by albite, sericite, chlorite and epidote. Clinopyroxenes are subhedral to anhedral, and slightly altered to chlorite; some display subophitic textures with plagioclase. Fe-Ti oxides are irregular-shaped, altered to leucoxene, and commonly show exsolution lamellae. Other secondary minerals present are prehnite, green amphibole (actinolite), pumpellyite and quartz. Pumpellyite occurs only in tiny fractures along with prehnite. The secondary minerals suggest that this rock has suffered low-grade regional metamorphism.

Petrography of microgabbros

Subgroup C-1 microgabbros have textures ranging from porphyritic, with plagioclase as the sole phenocryst phase, to equigranular. In general, their principal constituents are altered plagioclase and one or more mafic minerals, including colourless clinopyroxene, amphibole and chlorite. Other minerals present may be epidote, clinozoisite, quartz, calcite, prehnite, pumpellyite, apatite, Fe oxide, leucoxene and Fe sulphides. Quartz and epidote veinlets rarely occur.

Plagioclase is subhedral to anhedral, and thoroughly altered. Common alteration products are indeterminate dark brown cryptocrystalline aggregates (mainly Ca hydrosilicates), and may include epidote, clinozoisite, quartz, calcite, chlorite, amphibole, prehnite, pumpellyite, albite and intermediate plagioclase. The plagioclases in sample 18.6 often show brownish clouded cores and clear rims (An_{55-64}); the outer clear rims are partially fringed with granophyric-like quartz-feldspar intergrowths.

Almost anhedral clinopyroxene is fresh in some samples, but commonly altered to chlorite and amphiboles. Amphiboles, present in variable amounts in almost all samples, are mainly green to blue-green, and evidently pseudomorph clinopyroxene. According to the calculation method for Fe^{3+} of Laird and Albee (1981) and the classification scheme of Leake (1978), they range compositionally from actinolite to magnesio-hornblende, except those in sample 1.20 which are ferro-hornblende. Many contain numerous plagiolcase and clinopyroxene inclusions, and occur as rims on clinopyroxenes which are partly replaced by chlorite. They are also present as clots associated with chlorite and carbonate.

Most microgabbros are greenschist facies metamorphic rocks. However, the presence of amphibole and intermediate plagioclase in sample 18.6, and the absence of chlorite, sphene (leucoxene) and epidote suggest that it has been metamorphosed under amphibolite facies of regional metamorphism (Maruyama *et al.*, 1983; Moody *et al.*, 1983).

5.2.2 Mineral Chemistry

Relict igneous clinopyroxenes have been analysed in one dolerite and two microgabbro samples (Table 5.2). According to the nomenclature proposed by the Subcommittee on Pyroxenes, I.M.A. (1988), they are augites and diopsides (largely augites) with Mg# values ranging from 0.64 to 0.82. On the conventional pyroxene quadrilateral (Fig. 5.2), they form a typically tholeiitic Fe-enrichment, Ca-depletion trend almost coincident with the solidus trend of the Skaergaard Intrusion (Brown, 1967); two analyses plot away from the trend, but fall on the subsolidus trend of the Skaergaard Intrusion (Nwe, 1976).

The Subgroup C-1 clinopyroxenes have TiO_2 and Cr typical of clinopyroxenes in orogenic tholeiitic basalts according to the discrimination diagrams of Leterrier *et al.* (1982)(Fig. 5.3). Na_2O abundances are low and typical of of low-pressure clinopyroxenes in orogenic arc basalts.

5.2.3 Whole-rock Chemistry

Major, minor and trace elements

The Subgroup C-1 subalkalic rocks span the compositional range of all the Group C samples (i.e. basalt to andesite)(Table 5.1 and Fig. 5.1). On FeO*/MgO variation diagrams, FeO*, TiO_2 and V are poorly correlated with FeO*/MgO (Fig. 5.4), whereas P_2O_5, Zr and Y are broadly enriched, and Ni, Cr and Sc are depleted with progressive fractionation (Fig. 5.5). They have low concentrations of HFSE (0.3-1.0 wt% TiO_2, 10-115 ppm Zr, 9-33 ppm Y, and $\leq$2 ppm Nb), Ni (mainly between 5 and 29 ppm), and Cr (largely between 3 and 49 ppm), characteristic of arc basalts and andesites (Perfit *et al.*, 1980; Bailey, 1981; Basaltic Volcanism Study Project, 1981).

REE have been analysed in five Subgroup C-1 samples which include the most primitive and the most evolved samples (Table 5.3). Their chondrite-normalised patterns (Fig. 5.6) vary from relatively flat to slightly LREE enriched ((La/Yb)n=1.1-

TABLE 5.2. ELECTRON MICROPROBE ANALYSES OF COLOURLESS CLINOPYROXENES IN SUBGROUP C-1 SAMPLES. FeO AND Fe_2O_3 ARE CALCULATED ASSUMING STOICHIOMETRY ON THE BASIS OF 4 CATIONS AND 6 OXYGENS. END-MEMBERS IN TERMS OF WOLLASTONITE, ENSTATITE AND FERROSILITE ARE CALCULATED ACCORDING TO THE METHOD RECOMMENDED BY THE SUBCOMMITTEE ON PYROXENES, IMA (1988).

Sample no.	1.20							S9-2		32.1						
Anal. no.	1	2	3	4	5	6	7	1	2	1	2	3	4	5	6	7
SiO2	50.08	51.08	51.92	50.32	51.96	51.72	52 26	52.21	53.45	50.92	52.14	50 99	50 88	51.84	51.96	51 02
TiO2	0.39	0.25	0.43	0.35	0 34	0 27	0 28	-	-	0.42	0 38	0.41	0 49	0.26	0.45	0.39
Al2O3	3.44	2.58	2.72	3.41	2.55	2.23	2.18	2.94	1.57	3.81	3.43	3 54	3.68	2.56	3.28	4.40
Cr2O3	-	-	-	-	-	-	-	0.37	0.43	0.21	-	0.21	0.21	0.47	-	-
Fe2O3	1.76	0.15	0.70	0.57	0.94	-	-	-	-	1.12	-	0.99	0.76	0.46	0.92	1.36
FeO	11.22	13.68	11.32	12.14	11.94	12.07	11.62	7.78	7.88	8.08	9.95	7.59	9.27	6.51	9.94	8.04
MnO	0 22	0.37	0.35	0.28	0 24	0.27	0.25	0.28	0 23	-	0 22	-	-	-	-	-
MgO	13.54	13.62	14.57	13.64	15 10	14.32	14.07	14.24	14.41	15.81	14.59	15.44	15.10	16.71	15.71	15.35
CaO	19 25	17.94	19.37	18 54	18 20	18.75	19 69	22 62	23 33	19 52	19 82	20 49	19.59	20.25	19.20	20 27
Total	99.90	99.67	101.38	99.25	101.27	99.63	100.35	100 44	101 30	99 89	100 53	99 66	99 98	99.06	101.46	100.83
Si	1.888	1.933	1.919	1.906	1 922	1 945	1.950	1 931	1.962	1.886	1.926	1 894	1.892	1.923	1.904	1.875
IVAl	0 113	0.067	0.081	0.094	0.078	0 055	0 050	0.069	0.038	0.114	0 074	0 106	0 108	0.077	0.096	0.125
Total tetra	2 000	2.000	2.000	2.000	2.000	2 000	2 000	2 000	2 000	2.000	2 000	2.000	2.000	2.000	2.000	2.000
VIAl	0.040	0.048	0.038	0.058	0 033	0 044	0.046	0.059	0.030	0 053	0 076	0 049	0.053	0 036	0.046	0.066
Ti	0.011	0.007	0.012	0.010	0.010	0 008	0 008	-	-	0 012	0.010	0.012	0.014	0 007	0.012	0.011
Cr	-	-	-	-	-	-	-	0.010	0.012	0.006	-	0.005	0.007	0.013	-	-
Fe3+	0.050	0 004	0.019	0 016	0.026	-	-	-	-	0 031	-	0.028	0 021	0.013	0.026	0.038
Fe2+	0.354	0.433	0.350	0.385	0 369	0.380	0.363	0.241	0 242	0.250	0 307	0.236	0.288	0.202	0.305	0.247
Mn	0.007	0.012	0.011	0.009	0 008	0.009	0.008	0 009	0 007	-	0 007	-	-	-	-	-
Mg	0.761	0.768	0 803	0.770	0.832	0 803	0.783	0 785	0.789	0.873	0.803	0 855	0.837	0.924	0.858	0.841
Total octa.	1 223	1.273	1.233	1.248	1.278	1 242	1.207	1.104	1 080	1 225	1 204	1.185	1.220	1.195	1.246	1.202
Ca	0 777	0 728	0 767	0 752	0 722	0 756	0 787	0 896	0 918	0 775	0 785	0 815	0 781	0 805	0.754	0 798
Total cats.	4.000	4.000	4.000	4.000	4 000	3.998	3 994	4 000	3.998	4 000	3 988	4.000	4 000	4.000	4.000	4 000
Mg#	0.683	0.640	0.696	0 667	0 693	0 679	0 683	0 765	0 765	0.777	0.723	0.784	0.744	0 821	0.738	0.773
Wo	39 89	37.42	39.33	38.94	36 89	38 82	40 57	46 43	46 93	40.15	41.25	42.17	40.51	41.41	38.81	41.48
En	39 05	39.50	41.16	39.86	42 52	41.24	40 33	40.67	40 32	45 26	42.23	44.21	43.43	47.54	44.20	43.71
Fs	21 06	23.08	19 51	21.21	20 59	19 94	19 10	12 91	12.75	14.59	16.52	13.62	16 06	11.05	16.99	14.81

- = BELOW DETECTION LIMIT.

TABLE 5.3. REE ANALYSES AND SOME SELECTED RATIOS OF GROUP C SAMPLES

Subgroup	C-1					C-2		
Sample no.	S9-2[3]	1.20[3]	42 1[1]	38 43	47.1[1]	11[1]	24.1[1]	18.2[2]
La	2.02	4.16	5.64	7.80	8 97	14.90	13.90	17.10
Ce	5.07	10 50	13.60	18.60	22 20	31.30	29.80	37.10
Pr	0.87	1.54	1 97	2 67	3 15	3 71	3.50	4.79
Nd	3.87	8.46	9.06	13 50	15 40	15.20	14.70	21.50
Sm	1.22	2.61	2 16	3.75	4 04	2.91	3 00	4.81
Eu	0.45	0.93	0 87	1.47	1.27	0.75	0.82	1.46
Gd	1.39	3.20	2.80	4 64	4 93	2.95	2.93	4.60
Dy	1.54	3.85	3.30	4 96	5 24	2.95	2.79	3.85
Er	1.10	2.64	2.37	3 08	3 53	1.87	1.78	2.28
Yb	0.88	2.42	2.08	2.66	2.92	1.66	1.77	1.89
[La/Sm]n	1.01	0.97	1.59	1 27	1.24	3 12	2 82	2.17
[Sm/Yb]n	1 50	1.17	1 13	1 53	1 36	1.90	1.84	2.76

[1] = LAVA, [2] = DOLERITE, [3] = MICROGABBRO

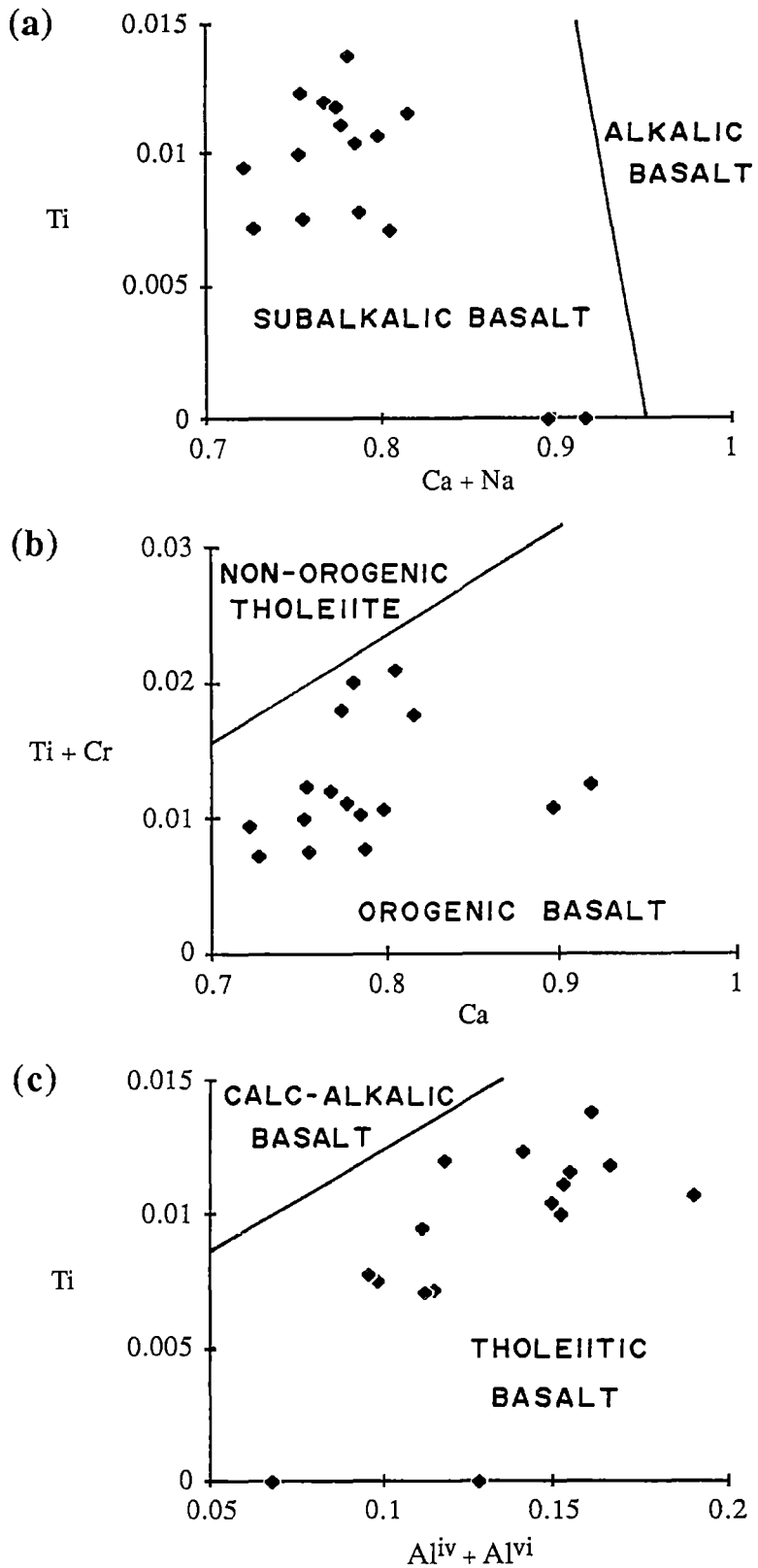

Figure 5.3. Tectonomagmatic discrimination diagrams in terms of clinopyroxene compositions (based on 6 oxygens)(Leterrier *et al.*, 1982) showing the distribution of data points for Subgroup C-1 colourless clinopyroxenes relative to the compositional fields of basaltic clinopyroxenes from various tectonic settings.

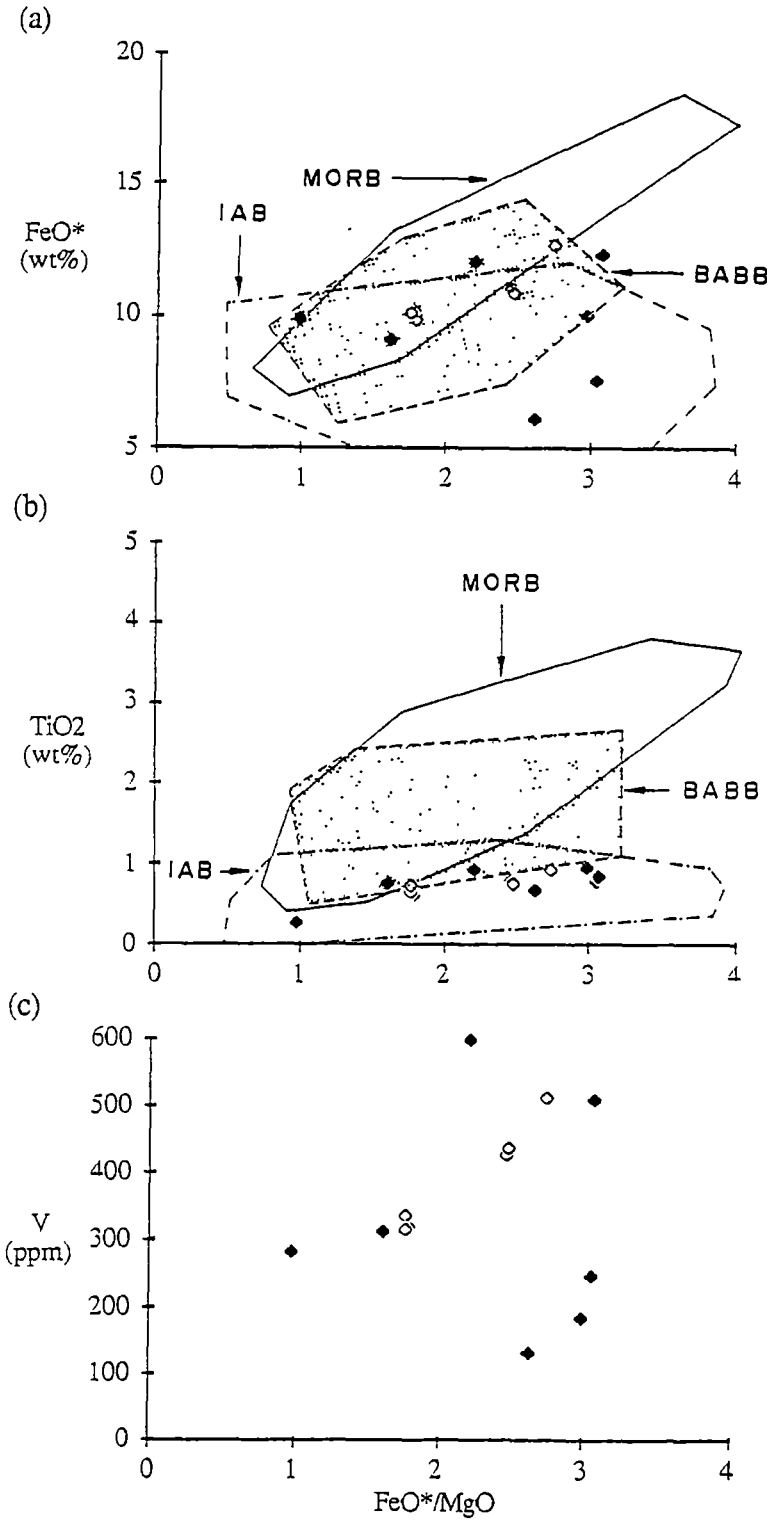

Figure 5.4. Plots of (a) FeO*, (b) TiO_2 and (c) V versus FeO*/MgO for Group C samples (solid diamond, Subgroup C-1; open diamond, Subgroup C-2). Data sources for the fields of mid-ocean ridge basalts (MORB), backarc basin basalts (BABB) and island-arc subalkalic basalts (IAB) are as in Figure 4.5.

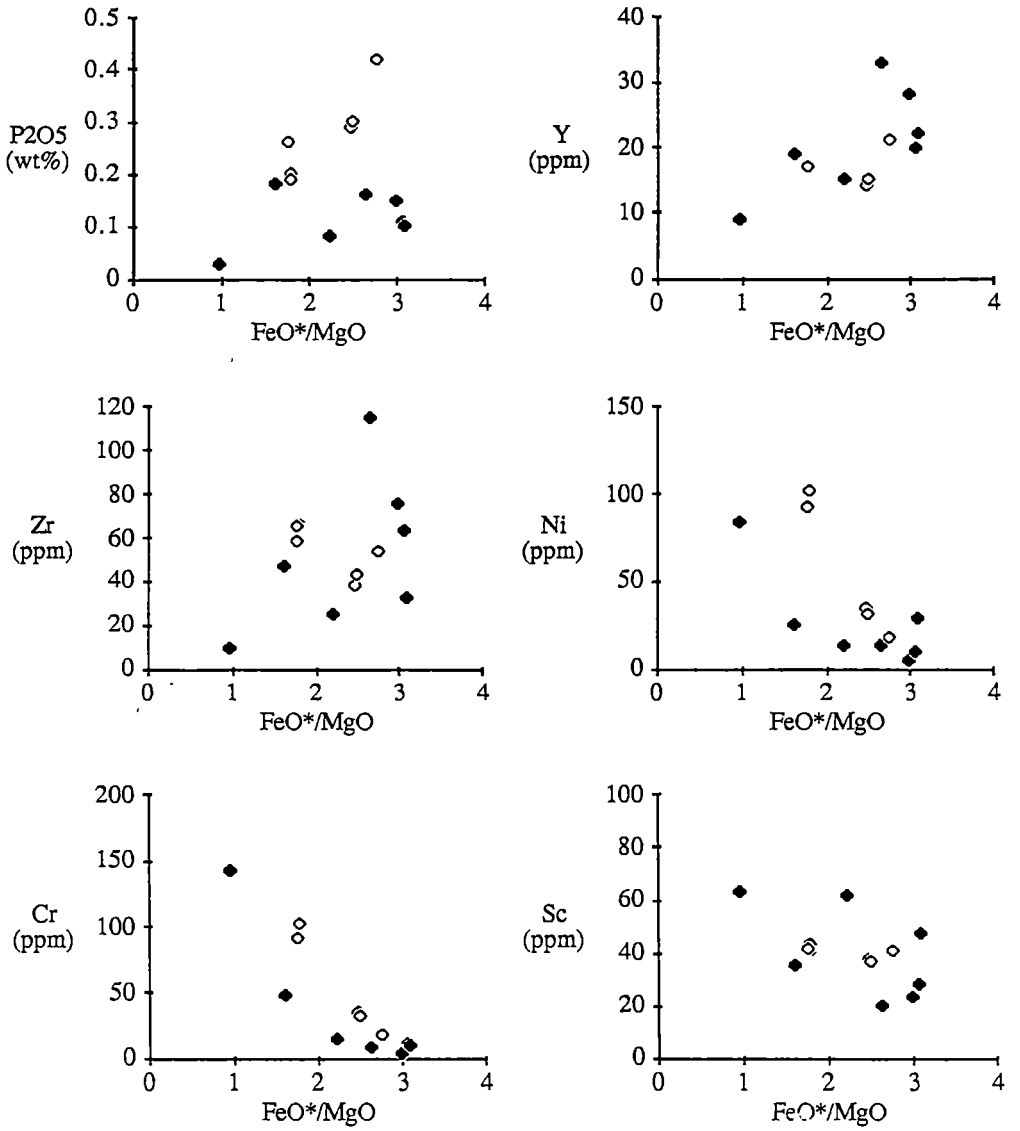

Figure 5.5. Least-mobile minor oxides and trace elements plotted against FeO*/MgO for Group C samples (solid diamond, Subgroup C-1; open diamond, Subgroup C-2).

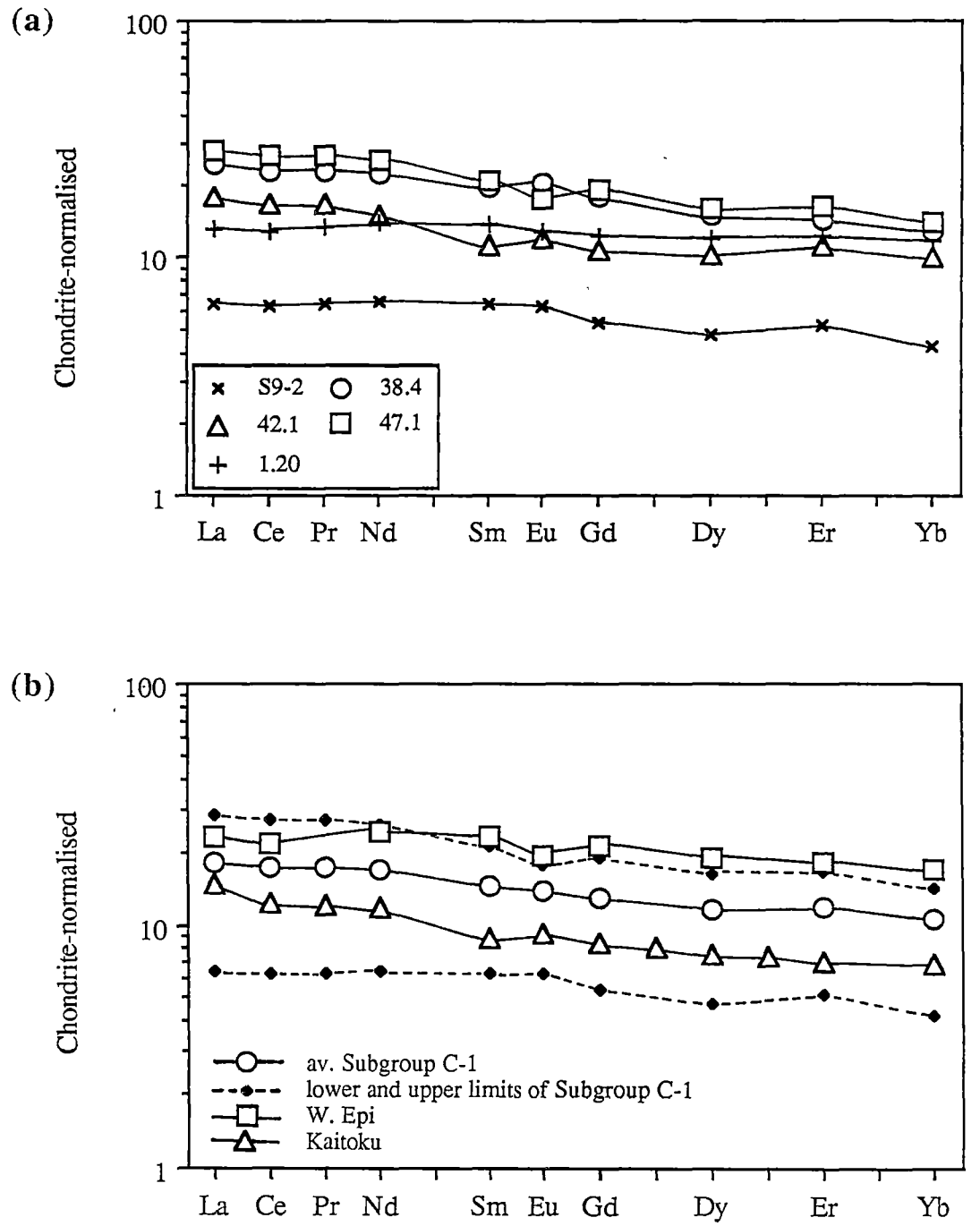

Figure 5.6. Chondrite-normalised REE patterns for (a) Subgroup C-1 samples, and (b) a western Epi tholeiite (sample 71047), Vanuatu (Barsdell and Berry, 1990) and the averaged tholeiitic rocks of Kaitoku Seamount (samples D75-4 and D77-1), northern Mariana Arc (Lin *et al.*, 1989). Also shown in (b) are a range and an average for Subgroup C-1 patterns.

2.0), typical of many low- to medium-K arc lavas (Wheller *et al.*, 1987; Lin *et al.*, 1989; Barsdell and Berry, 1990).

Although they range compositionally from basalt to andesite, they largely lie in the fields of arc basalts in discrimination diagrams (Figs. 5.4, 5.7, 5.8 and 5.9), but they have La/Yb (2.7-3.1) and Sc/Ni (2.5-4.7) values comparable with oceanic island-arc andesites on the discrimination diagram suggested by Bailey (1981).

On grounds of pyroxene and whole-rock chemistries discussed above, it is concluded that the Subgroup C-1 samples are low-K to medium-K arc basalts and andesites.

Comparisons with modern suites

It is well documented that island-arc lavas have extremely variable chemical characteristics, particularly in terms of LILE and REE. The variations may occur either across arc (Jakes and Gill, 1970; Jakes and White, 1972; Whitford *et al.*, 1979; Gill, 1981; Basaltic Volcanism Study Project, 1981) or along arc (Wheller *et al.*, 1987; Stern *et al.*, 1988; Bloomer *et al.*, 1989; Lin *et al.*, 1989), or even within a single suite (Barsdell and Berry, 1990). The highly mobile behaviour of LILE during metamorphism makes comparisons with modern suites rather dubious, and therefore, REE patterns are used as a prime clue to find out their modern analogues. The approach taken here was to find, from the recent literature, modern lavas most compositionally akin to the Subgroup C-1 samples. Numerous examples of oceanic arc basalts and andesites, such as the Marianas (Bloomer *et al.*, 1989; Lin *et al.*, 1989), New Britain (Basaltic Volcanism Study Project, 1981), Vanuatu (Barsdell and Berry, 1990) and the Sunda arcs (Wheller *et al.*, 1987), were found to have strong compositional affinities to the Subgroup C-1 rocks. Three thoroughly-analysed examples of these comparable arc basalts have been selected to highlight the compositional similarities with the Subgroup C-1 rocks. These are a typical low- to medium-K arc basalt (sample 71047) from western Epi in the Vanuatu Arc, and medium-K arc andesites (samples D75-4 and D77-1) from the submarine Kaitoku Seamount in the northern Mariana Arc (Fig. 5.6).

The similarity between Subgroup C-1 rocks and the selected modern analogues is also supported by N-MORB normalised spider patterns (Fig. 5.10). The averaged Subgroup C-1 pattern falling between those for the reference samples is in agreement with the fact that the averaged Subgroup C-1 sample has lower FeO*/MgO than the lavas from Kaitoku Seamount (Bloomer *et al.*, 1989) but higher than the western Epi tholeiite.

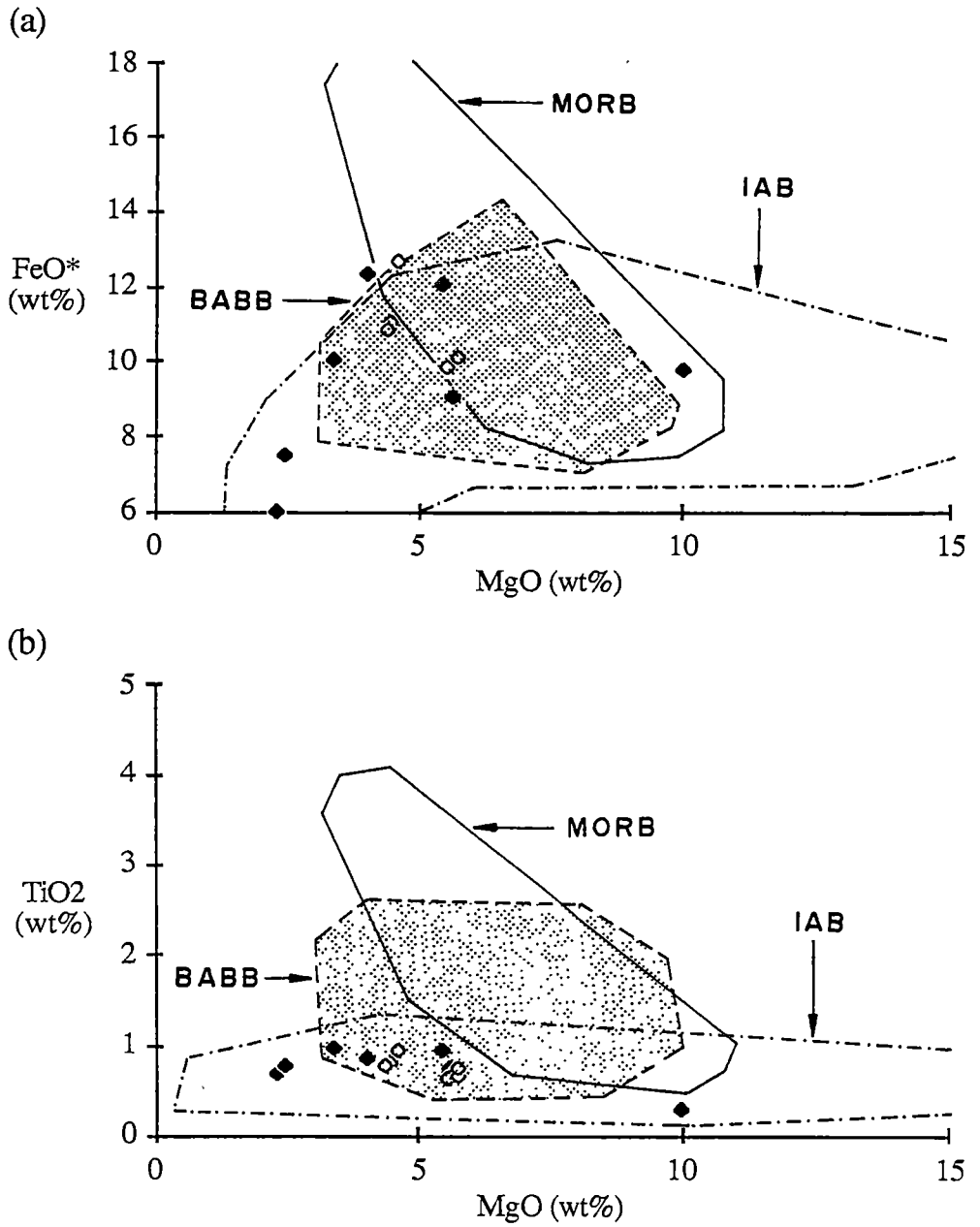

Figure 5.7. Plots of (a) FeO* and (b) TiO_2 versus MgO for Group C samples (solid diamond, Subgroup C-1; open diamond, Subgroup C-2). Data sources for the fields of mid-ocean ridge basalts (MORB), backarc basin basalts (BABB) and island-arc subalkalic basalts (IAB) are as in Figure 4.5.

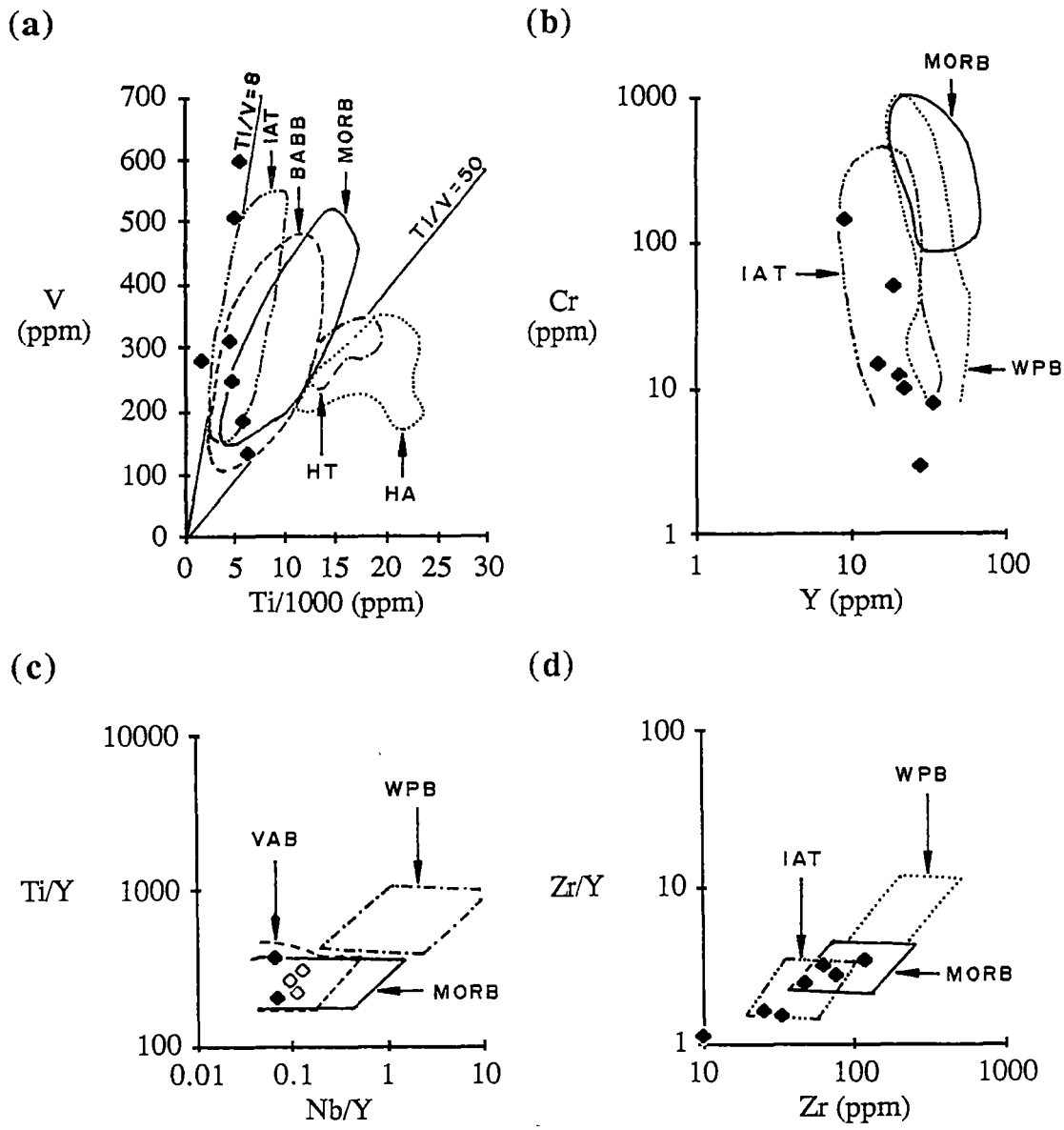

Figure 5.8. Plots of (a) V against Ti, (b) Cr against Y, (c) Ti/Y against Nb/Y and (d) Zr/Y against Zr for Group C samples (solid diamond, Subgroup C-1; open diamond, Subgroup C-2). Field boundaries of basalts from different tectonic settings in (a), (b), (c), and (d) are after Shervais (1982), Pearce (1980), Pearce (1982), and Pearce and Norry (1979), respectively. Samples with Nb content less than 2 ppm (close to the detection limit determined by XRF) are excluded from (c). Data for Subgroup C-2 samples are not plotted in (a), (b) and (d) since they are transitional between arc tholeiitic and arc calc-alkalic rocks. HA = Hawaiian alkalic basalts, HT = Hawaiian tholeiites, MORB = mid-ocean ridge basalts, BABB = backarc basin basalts, IAT = island-arc tholeiites; WPB = within-plate basalts; VAB = volcanic arc basalts. A chondritic Ti/V ratio of 8 is taken from Nesbitt and Sun (1976).

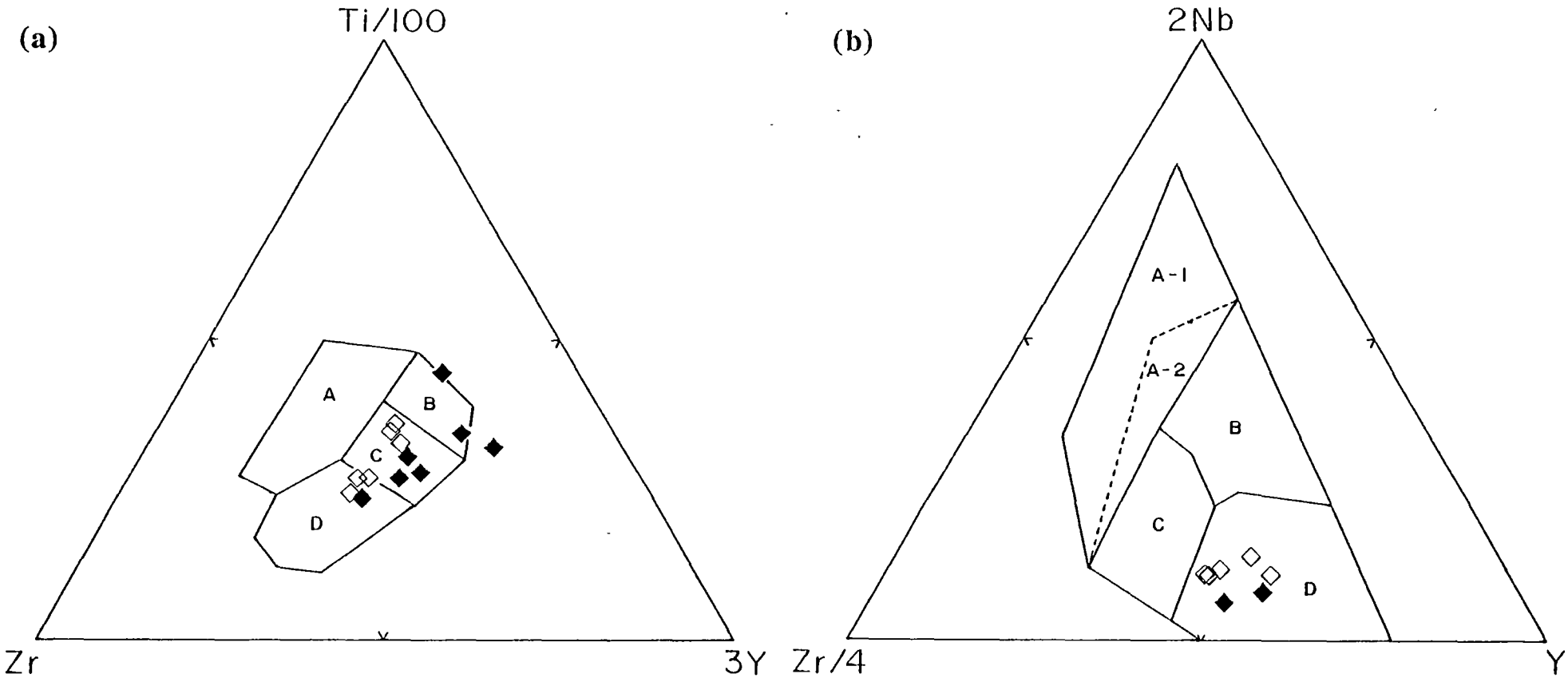

Figure 5.9. Ternary immobile-element discrimination diagrams in terms of (a) Ti-Zr-Y (Pearce and Cann, 1973) and (b) Nb-Zr-Y (Meschede, 1986) for Group C basalts and andesites (solid diamond, Subgroup C-1; open diamond, Subgroup C-2). Samples with Nb content less than 2 ppm (close to the detection limit determined by XRF) are excluded from the Nb-Y-Zr diagram. The reported fields are as follows: (a) A = within-plate basalts, B + C = low-K tholeiites, C = MORB, and C + D = calc-alkalic basalts; and (b) A-1 = alkalic within-plate basalts, A-2 and C = tholeiitic within-plate basalts, B + D = MORB, and C + D = volcanic arc basalts.

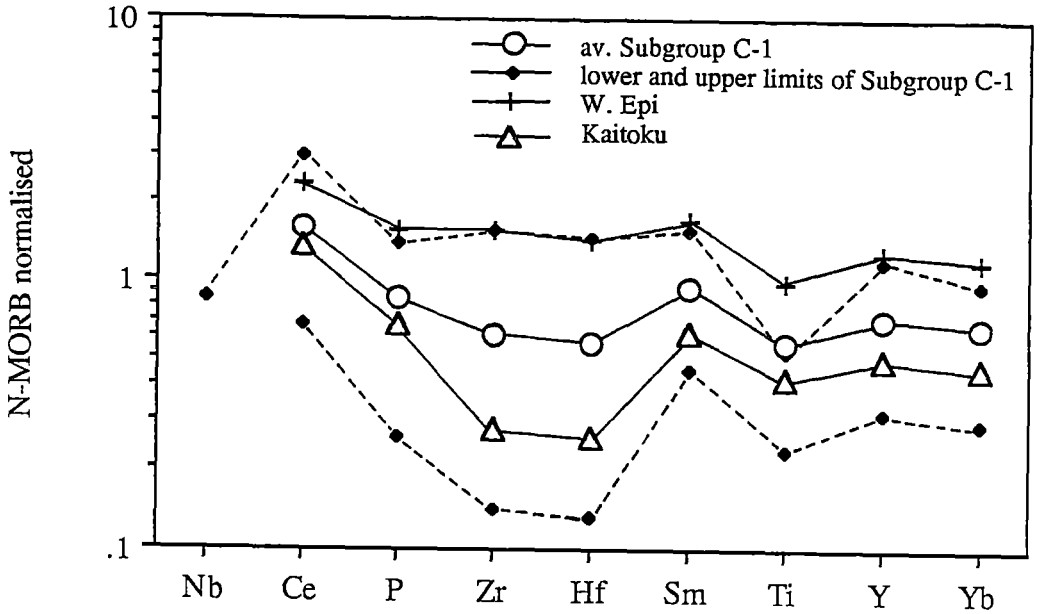

Figure 5.10. A subset of N-MORB normalised multi-element plot for an average and a range of Subgroup C-1 samples, compared with those of western Epi (sample 71047), Vanuatu (Barsdell and Berry, 1990), and Kaitoku Seamount (samples D75-4 and D77-1), northern Mariana Arc (Bloomer *et al.*, 1989; Lin *et al.*, 1989). Data points for Nb in the Subgroup C-1 samples and the western Epi tholeiite (close to the detection limit determined by XRF), and the Kaitoku tholeiites (no data available) are omitted.

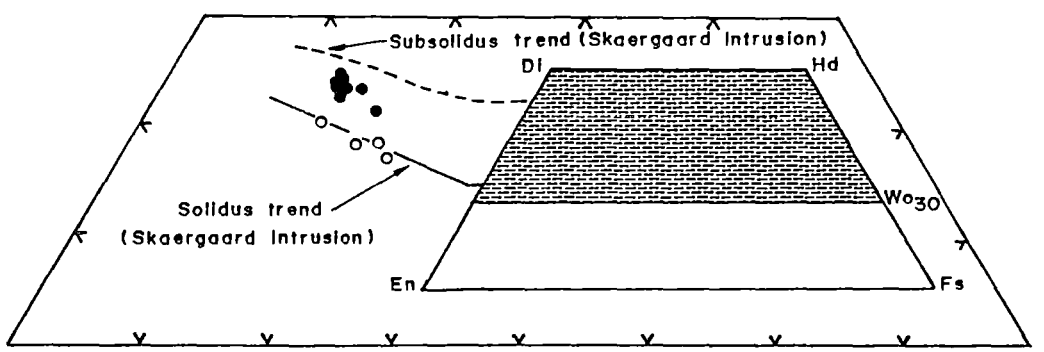

Figure 5.11. Ca-Mg-Fe (molecular %) for Ca-pyroxenes of Subgroup C-2 lava and dolerite. The solidus and subsolidus trends for clinopyroxenes from the Skaergaard Intrusion are after Brown (1967) and Nwe (1976), respectively. Symbols: open circles, phenocrysts in lava; solid circles, clinopyroxenes in dolerites.

5.3 Subgroup C-2 Arc Basalts and Andesites

5.3.1 Occurrence and Petrography

The least altered Subgroup C-2 samples comprise three basaltic lavas and three dolerites, collected from float and outcrops in the Nan River area. Sample locations and petrographic features of individual samples are presented in Table I-3 (Appendix I) and Table II-6 (Appendix II), respectively.

Petrography of lavas

The Subgroup C-2 lavas are highly phyric with abundant plagioclase and subordinate colourless clinopyroxene phenocrysts and microphenocrysts. Principal groundmass constituents are altered plagioclase, actinolite and chlorite. Fe oxide, Fe sulphides, quartz and epidote may occur as accessories. A few veinlets of prehnite and calcite are present in sample 11.

All plagioclases are euhedral to anhedral, and partly or totally replaced by sericite, epidote, clinozoisite, and rare quartz and chlorite.

Clinopyroxene phenocrysts and microphenocrysts are euhedral to subhedral, and largely pseudomorphed by fibrous blue-green amphibole (actinolite). Other minor alteration products may be epidote, chlorite, quartz and Fe oxide. Many clinopyroxene phenocrysts display corroded outlines and rounded edges. Groundmass clinopyroxenes are also extensively altered to blue-green amphibole (actinolite) and chlorite.

Fe-Ti oxide occurs either as irregular patches or as evenly distributed, subhedral to anhedral grains, and are partially replaced by leucoxene. Quartz is commonly present as an interstitial mineral.

The metamorphic minerals present in the Subgroup C-2 lavas indicate that they have been regionally metamorphosed under greenschist facies.

Petrography of dolerites

Subgroup C-2 dolerites vary texturally from porphyritic to equigranular. The porphyritic type is composed of plagioclase phenocrysts and microphenocrysts, and colourless clinopyroxene microphenocrysts, sitting in fine-grained groundmass (<1 mm across) made up principally of plagioclase and blue-green amphibole with accessory clinopyroxene, quartz, apatite, haematite, and Fe sulphides. The

equigranular rocks are medium-grained (ca. 2 mm across), and have similar minerals to the porphyritic rocks but contain clinopyroxene and chlorite as additional major and minor phases, respectively.

Plagioclases are largely subhedral and heavily charged with epidote, clinozoisite, sericite and rare chlorite, and often have clear albite to oligoclase rims.

Clinopyroxenes are variably altered to blue-green amphiboles. In the porphyritic type, they are extensively replaced by amphiboles, whereas in the equigranular rocks, they are thinly rimmed by amphiboles or occur as inclusions in amphiboles.

Blue-green amphiboles show subophitic texture where they totally or almost completely pseudomorph clinopyroxenes. They are slightly altered to chlorite and Fe oxide. According to the method for estimating Fe^{3+} of Laird and Albee (1981) and the amphibole nomenclature of Leake (1978), all are tschermakitic hornblende and tschermakite.

Fe oxides are subhedral to anhedral, and often associated with mafic phases. They are partly altered to leucoxene and haematite, and show exsolution texture. Apatite occurs as tiny discrete euhedral to subhedral crystals, and is common inclusions in other phases. Quartz is present as an interstitial mineral.

The secondary minerals present suggest that the Subgroup C-2 dolerites are probably medium-grade metamorphic rocks, restricted to the transitional facies between greenschist and amphibolite facies of regional metamorphism.

5.3.2 Mineral Chemistry

Clinopyroxene phenocrysts in one lava sample and clinopyroxenes in three dolerites of Subgroup C-2 have been chemically analysed; their compositions are listed in Table 5.4. They are all calcian augites according to the nomenclature of the Subcommittee on Pyroxenes, I.M.A. (1988), and have a limited Mg# range (0.69-0.78). Despite the narrow range of Mg#, clinopyroxene phenocrysts in the lava form a notably linear trend overlapping the equilibrium crystallisation trend of the Skaergaard Intrusion (Brown, 1967), whereas those in dolerites exhibit a broad trend subparallel to the former at higher levels of $CaSiO_3$ (Fig. 5.11), suggesting that dolerites have undergone re-equilibration at lower temperatures.

These clinopyroxenes show broad correlations between Ti and Al^{iv} (average $Ti/Al^{iv} = 0.12\pm0.02$), and Al^{vi} and Al^{iv} (average $Al^{vi}/Al^{iv} = 0.47\pm0.14$)(Fig. 5.12),

TABLE 5.4. ELECTRON MICROPROBE ANALYSES OF COLOURLESS CLINOPYROXENES IN SUBGROUP C-2 LAVA AND DOLERITE SAMPLES. FeO AND Fe_2O_3 ARE CALCULATED ASSUMING STOICHIOMETRY ON THE BASIS OF 4 CATIONS AND 6 OXYGENS. END-MEMBERS IN TERMS OF WOLLASTONITE, ENSTATITE AND FERROSILITE ARE CALCULATED ACCORDING TO THE METHOD RECOMMENDED BY THE SUBCOMMITTEE ON PYROXENES, IMA (1988).

Sample no.	24.2[1]				18A						18.2		18.3					
Anal. no.	1	2	3	4	1	2	3	4	5	6	1	2	1	2	3	4	5	6
SiO2	52.15	52.08	51.96	50.99	51.66	51.45	51.87	51.41	52.06	51.99	50.61	51.26	51.00	51.73	51.54	50.94	51.93	50.93
TiO2	0.32	0.28	0.29	0.43	0.41	0.34	0.39	0.56	0.34	0.39	0.46	0.40	0.49	0.45	0.50	0.37	0.39	0.43
Al2O3	1.83	2.11	2.68	2.58	2.83	3.12	3.25	3.66	2.31	3.03	3.76	3.61	3.49	2.81	3.66	3.88	3.02	3.83
Cr2O3	-	-	0.23	-	-	-	-	-	-	-	-	0.25	-	0.22	-	0.22	0.19	-
Fe2O3	0.81	1.16	1.26	1.61	0.55	1.43	1.35	1.32	-	0.53	1.60	-	0.73	1.03	0.28	1.32	0.33	1.27
FeO	11.57	10.11	8.12	11.65	8.33	7.76	7.55	8.11	9.90	8.73	7.38	8.41	8.14	7.74	8.83	9.59	9.07	7.53
MnO	0.28	0.29	-	0.22	-	-	-	-	0.23	-	-	-	-	-	-	0.33	-	-
MgO	14.82	15.42	16.13	14.69	14.94	15.10	15.04	14.78	14.23	15.00	14.59	14.34	14.58	14.97	14.74	13.80	15.03	14.65
CaO	19.04	19.24	19.92	18.19	21.22	21.20	21.87	21.50	21.02	21.13	21.50	21.57	21.31	21.73	21.06	19.62	20.76	21.59
Na2O	-	-	-	-	-	-	-	-	-	-	-	-	-	-	-	0.34	-	-
Total	100.82	100.69	100.59	100.36	99.94	100.40	101.32	101.34	100.09	100.80	99.90	99.84	99.74	100.68	100.61	100.41	100.72	100.23
Si	1.939	1.930	1.913	1.908	1.919	1.903	1.900	1.887	1.941	1.916	1.882	1.907	1.899	1.909	1.903	1.895	1.916	1.887
ivAl	0.061	0.070	0.087	0.092	0.081	0.097	0.100	0.113	0.059	0.084	0.118	0.094	0.101	0.091	0.097	0.105	0.084	0.113
Total tetra.	2.000	2.000	2.000	2.000	2.000	2.000	2.000	2.000	2.000	2.000	2.000	2.000	2.000	2.000	2.000	2.000	2.000	2.000
viAl	0.020	0.022	0.029	0.022	0.043	0.039	0.041	0.045	0.043	0.048	0.047	0.065	0.053	0.031	0.062	0.065	0.047	0.054
Ti	0.009	0.008	0.008	0.012	0.012	0.010	0.011	0.016	0.010	0.011	0.013	0.011	0.014	0.013	0.014	0.010	0.011	0.012
Cr	-	-	0.007	-	-	-	-	-	-	-	-	0.007	-	0.007	-	0.006	0.006	-
Fe3+	0.023	0.032	0.035	0.045	0.015	0.040	0.037	0.036	-	0.015	0.045	-	0.021	0.029	0.008	0.037	0.009	0.035
Fe2+	0.360	0.313	0.250	0.365	0.259	0.240	0.232	0.249	0.309	0.269	0.230	0.262	0.254	0.239	0.273	0.298	0.280	0.233
Mn	0.009	0.009	-	0.007	-	-	-	-	0.007	-	-	-	-	-	-	0.011	-	-
Mg	0.821	0.851	0.885	0.819	0.827	0.832	0.821	0.808	0.791	0.824	0.809	0.795	0.809	0.824	0.811	0.765	0.827	0.809
Total octa.	1.241	1.236	1.214	1.271	1.155	1.160	1.141	1.155	1.159	1.166	1.143	1.140	1.150	1.141	1.167	1.193	1.180	1.143
Ca	0.759	0.764	0.786	0.729	0.845	0.840	0.859	0.845	0.840	0.834	0.857	0.859	0.850	0.859	0.833	0.782	0.821	0.857
Na	-	-	-	-	-	-	-	-	-	-	-	-	-	-	-	0.025	-	-
Total cats.	4.000	4.000	4.000	4.000	4.000	4.000	4.000	4.000	3.999	4.000	4.000	3.999	4.000	4.000	4.000	4.000	4.000	4.000
Mg#	0.695	0.731	0.780	0.692	0.762	0.776	0.780	0.765	0.719	0.754	0.779	0.752	0.761	0.775	0.748	0.720	0.747	0.776
Wo	38.49	38.77	40.18	37.11	43.41	43.03	44.07	43.60	43.14	42.96	44.16	44.85	43.98	44.06	43.29	41.31	42.38	44.30
En	41.65	43.22	45.25	41.68	42.51	42.63	42.14	41.69	40.62	42.43	41.70	41.50	41.85	42.23	42.14	40.43	42.69	41.82
Fs	19.86	18.01	14.57	21.21	14.08	14.34	13.79	14.71	16.23	14.61	14.14	13.65	14.17	13.71	14.58	18.27	14.94	13.88

[1] = LAVA, - = BELOW DETECTION LIMIT.

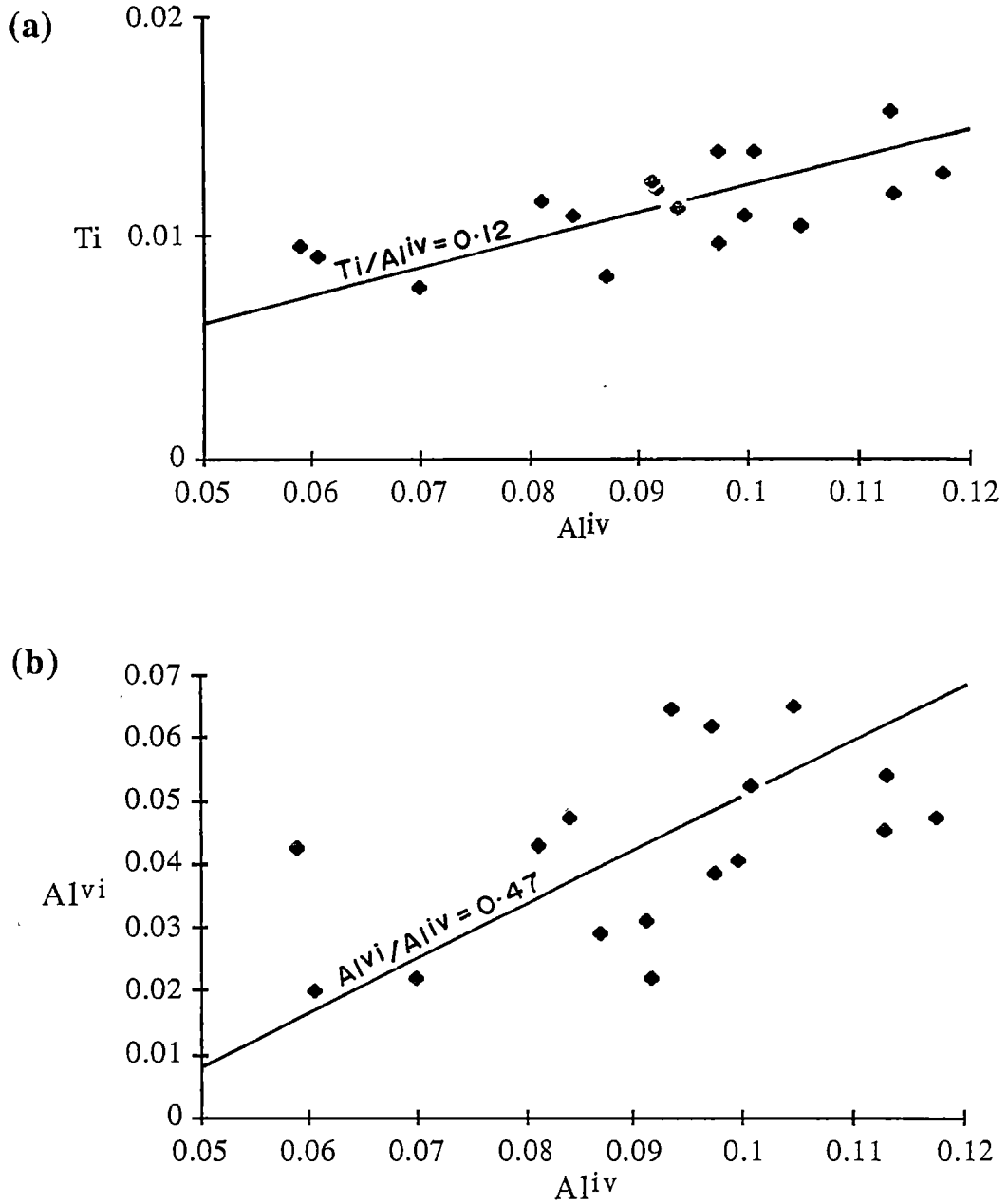

Figure 5.12. Ti - Al^{iv} (a) and Al^{vi} - Al^{iv} (b) relationships for Subgroup C-2 clinopyroxenes (based on 6 oxygens). See text for discussion.

reflecting significant ($Ti^{4+}/2$) - Al^{iv}, and Al^{vi} - Al^{iv} substitutions. Their compositional fields on discrimination diagrams of Leterrier *et al.* (1982) suggest that Subgroup C-2 samples are probably subalkalic rocks which formed in an orogenic environment (Fig. 5.13).

5.3.3 Whole-rock Chemistry

Major, trace and rare-earth elements

The Subgroup C-2 samples range compositionally from subalkalic basalts to andesites (Table 5.1 and Fig. 5.1). They show FeO* and V enrichment, and fairly constant TiO_2 with increasing FeO*/MgO (Fig. 5.4). These samples have very similar immobile major, minor and trace-element concentrations (0.6-0.9 wt% TiO_2, 9.9-12.7 wt% FeO*, 4.4-5.7 wt% MgO, ≤2 ppm Nb, 39-66 ppm Zr, 14-21 ppm Y, 21-37 ppm Ni, 18-102 ppm Cr, 315-512 ppm V, and 37-43 ppm Sc) to the Subgroup C-1 samples except for P_2O_5. The Subgroup C-2 samples contain notably higher P_2O_5 contents (0.2-0.4 wt%) at similar values for FeO*/MgO (Fig. 5.5).

Minor and trace-element variations (Fig. 5.5) demonstrate that P_2O_5 is enriched, whereas Cr and Ni are depleted with fractionation. The slight decrease in Zr with increasing FeO*/MgO suggests that these rocks are not co-magmatic. They appear to be volcanic arc rocks when discriminant Ti/Y - Nb/Y, Ti-Zr-Y and Nb-Zr-Y plots are applied (Figs. 5.8c, 5.9).

REE contents and chondrite-normalised REE patterns for two lavas and one dolerite samples are shown in Table 5.3 and Figure 5.14, respectively. Although the Subgroups C-1 and C-2 have similar values for least-mobile major and trace elements, their REE patterns are significantly different. The patterns for Subgroup C-2 samples show relatively flat HREE from Yb to Dy, and LREE enrichment ((La/Sm)n = 2.2-3.1), typical of calc-alkalic andesites. According to the discrimination diagram of Bailey (1981) based on La/Yb and Sc/Ni values, these rocks probably formed in a continental margin arc.

It can be inferred from the foregoing discussion that Subgroup C-2 samples have transitional arc tholeiitic to arc calc-alkalic affinities, and certainly formed in an island arc or active continental margin above a subduction zone.

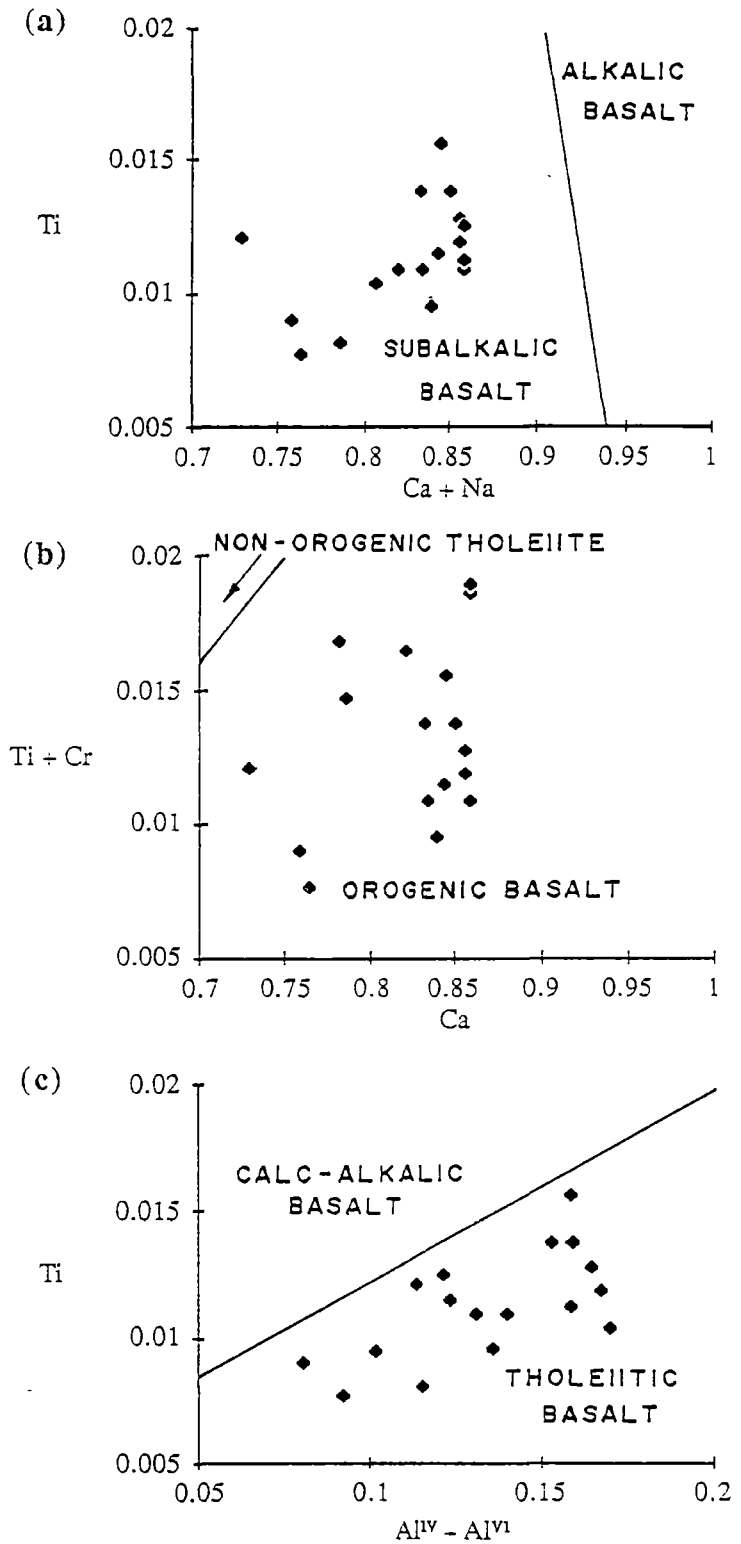

Figure 5.13. Plots of (a) Ti against Ca+Na, (b) Ti+Cr against Ca, and (c) Ti against total Al for Subgroup C-2 clinopyroxenes (based on 6 oxygens). Also shown are compositional fields for clinopyroxenes in basalts formed in various tectonic settings (after Leterrier *et al.*, 1982).

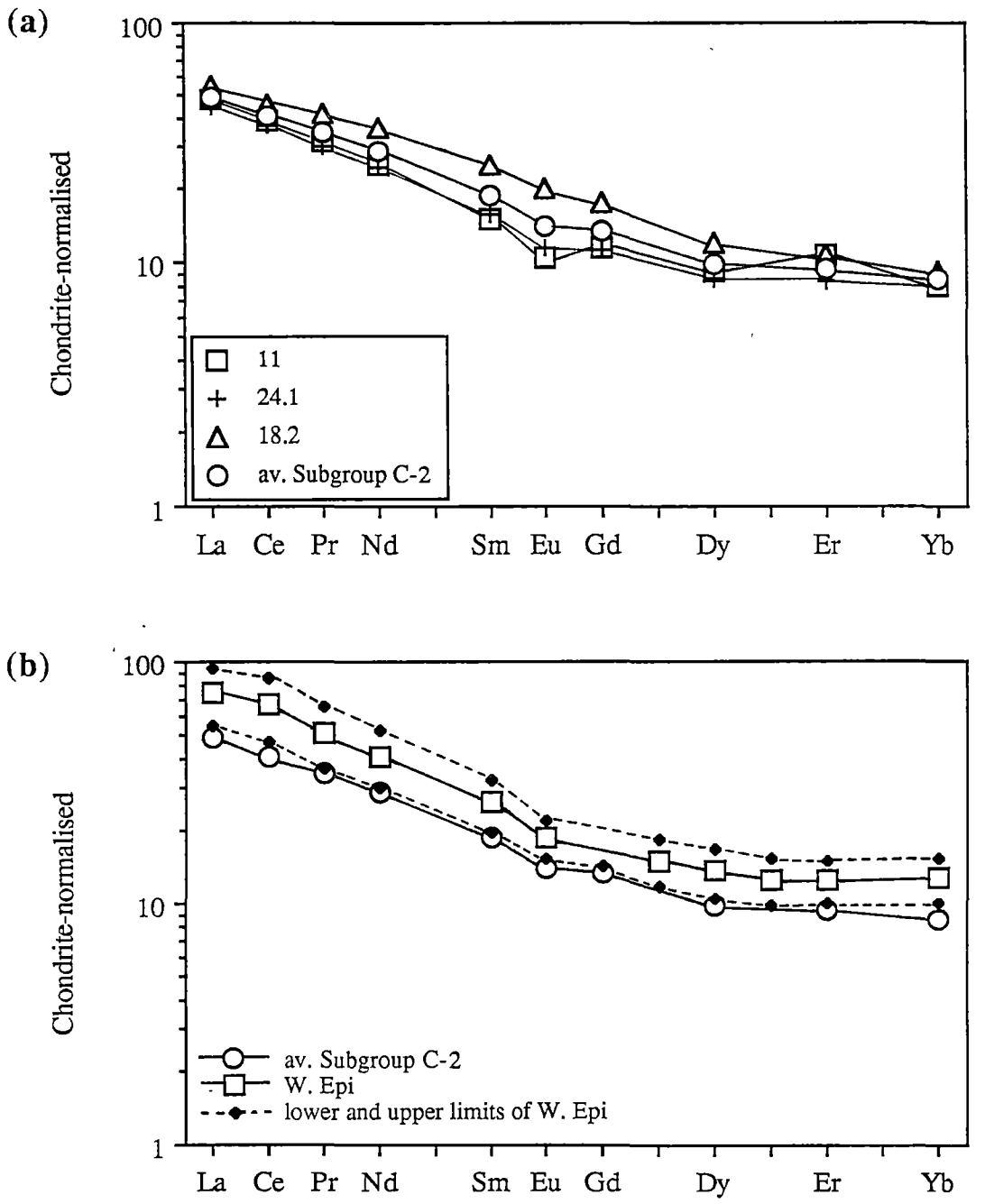

Figure 5.14. Chondrite-normalised REE patterns for (a) Subgroup C-2 samples and (b) the averaged Subgroup C-2 samples and Quaternary basaltic andesites and andesites of western Epi (samples 666 and 667), Vanuatu (Gorton, 1977). Also shown is a range of the Epi samples.

Comparisons with modern suites

The Subgroup C-2 transitional tholeiitic to calc-alkalic rocks are similar to the Quaternary calc-alkalic basaltic andesites and andesites of Western Epi (samples 666 and 667), Vanuatu Arc (Gorton, 1977), especially in terms of chondrite-normalised REE and N-MORB normalised spider patterns (Figs. 5.14 and 5.15). Therefore, a conclusion can be drawn that they are transitional island-arc tholeiites to island-arc calc-alkalic rocks.

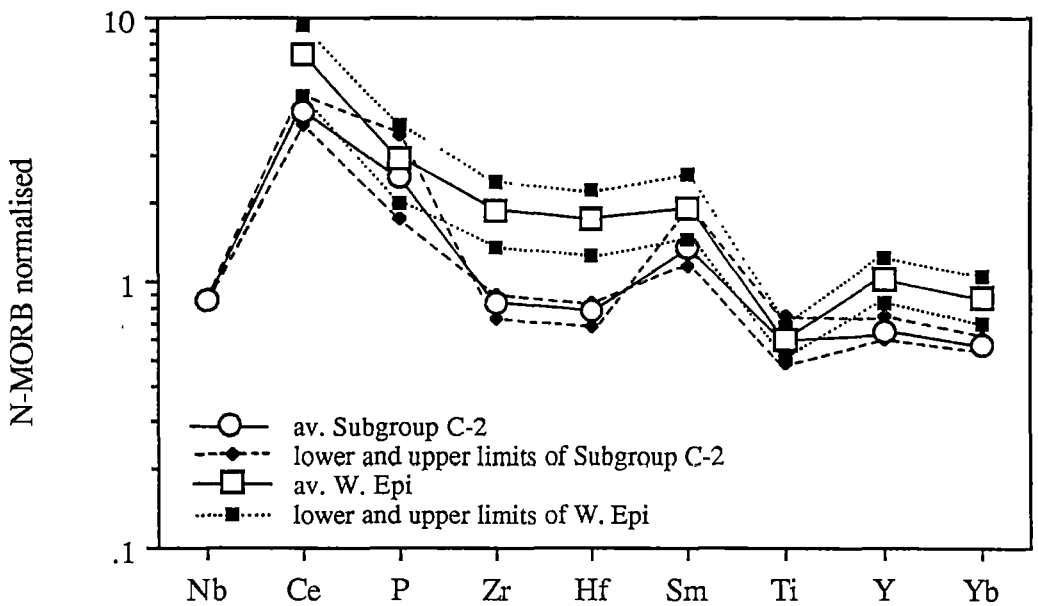

Figure 5.15. N-MORB normalised multi-element patterns of the averaged Subgroup C-2 samples compared with the pattern for the averaged Quaternary basaltic andesites and andesites of western Epi (samples 666 and 667), Vanuatu (Gorton, 1977). Nb data for the western Epi samples are not available.

5.4 Summary

The rocks assigned to Group C have diverse chemical compositions, and are characterised by relatively low contents of TiO_2 (0.3-1.0 wt%), Zr (10-115 ppm), Nb ($\leq$2 ppm), Y (9-33 ppm), Nb/Y (<0.3 ppm), Ti/Y (<400) and Ti/V (largely between 10 and 20), and high Zr/Nb (>10). They may be subdivided into 2 subgroups, C-1 and C-2.

5.4.1 Summary of Subgroup C-1 Arc Basalts and Andesites

Subgroup C-1 samples include lava, dolerite and microgabbro, collected from float and outcrops in all key areas. In the Uttaradit area, this rock type forms dikes cutting across foliation of massive amphibolite (derived from isotropic gabbro).

These samples have textures varying from porphyritic, with plagioclase as the dominant phenocryst/microphenocryst, to non-porphyritic. They contain altered plagioclase, colourless clinopyroxene (largely calcian augite), green to blue-green metamorphic amphiboles (actinolite to magnesio-hornblende, and ferro-hornblende), and accessory minerals. Plagioclase is the most abundant phase; clinopyroxene, amphibole and chlorite may be additionally principal constituents.

Chemically, the Subgroup C-1 samples are basalts and andesites with low HFSE (0.3-1.0 wt% TiO_2, 10-115 ppm Zr, 9-33 ppm Y, and ≤2 ppm Nb), Ni (largely between 5 and 29 ppm), Cr (largely between 3 and 49 ppm), and Ti/V (largely between 10-20) contents, and.relatively flat to slightly LREE enriched chondrite-normalised REE patterns ((La/Yb)n=1.1-2.0). These characteristics and clinopyroxene compositions are most similar to those of many island-arc low- to medium- K basalts and andesites. They are chemically most comparable to a typical low- to medium-K lava from western Epi (sample 71047), Vanuatu (Barsdell and Berry, 1990), and basalts from Kaitoku Seamount (samples D75-4 and D77-1), northern Mariana arc (Bloomer *et al.*, 1989; Lin *et al.*, 1989). Consequently, they are inferred to be arc rocks of island-arc tholeiitic affinities.

5.4.2 Summary of Subgroup C-2 Arc Basalts and Andesites

The analysed Subgroup C-2 samples include lavas and dolerites, collected from float and outcrops in the Nan River area. They vary texturally from porphyritic, with plagioclase and colourless clinopyroxene phenocrysts and microphenocrysts, to non-porphyritic. Their principal mineral assemblages are altered plagioclase+blue-green amphibole±colourless clinopyroxene (calcian augite)±chlorite.

Chemically, they are transitional island-arc tholeiitic to calc-alkalic basalts and andesites, and have very similar immobile major, minor and trace-element concentrations (0.6-0.9 wt% TiO_2, 9.9-12.7 wt% FeO*, 4.4-5.7 wt% MgO, ≤2 ppm Nb, 39-66 ppm Zr, 14-21 ppm Y, 21-37 ppm Ni, 18-102 ppm Cr, 315-512 ppm V, and 37-43 ppm Sc) to the Subgroup C-1 samples except for P_2O_5 and REE. The Subgroup C-2 samples have higher P_2O_5 (0.2-0.4 wt%) at similar levels of FeO*/MgO, and show relatively flat HREE (Yb to Dy) and LREE-enriched patterns,

with (La/Sm)n ranging from 2.2 to 3.1, typical of calc-alkalic andesites. They closely resemble the Quaternary calc-alkalic basaltic andesites and andesites of western Epi (samples 666 and 667), Vanuatu Arc (Gorton, 1977) in terms of chondrite-normalised REE and N-MORB normalised spider patterns. As a consequence, they are most likely to be transitional island-arc tholeiitic to calc-alkalic rocks, formed in island arc or active continental margin above a subduction zone.

CHAPTER 6

PETROLOGY AND MINERAL CHEMISTRY OF PLUTONIC AND SIGNIFICANT METAMORPHIC ROCKS

6.1 Gabbros and Amphibolites

Gabbros occurring along the Nan Suture comprise isotropic and layered gabbros which have experienced variable degrees of deformation and metamorphism. They show weak to pronounced foliation, and some are best classified as massive and banded amphibolites (Ishizuka, 1987). Following the terminology suggested by Jackson (1967), the layered gabbros differ from the isotropic gabbros in having mineral- and size-graded layers which vary in thickness from millimetre to metre scales. Grainsizes of the layered gabbros vary greatly from fine (<1 mm) to coarse (4 mm) whereas those of the isotropic gabbros are medium to coarse (1-5 mm).

6.1.1 Occurrence and Petrography

Gabbros and amphibolites have been observed in all key areas. They occur as tectonic blocks in serpentinite matrix. They have been intruded by basic dikes at some localities. Unfortunately, almost all the samples collected from these dikes are too altered for meaningful analysis. A microgabbro with affinities to Subgroup C-1 island-arc basalts and andesites (sample S9-2) has invaded isotropic gabbro (massive amphibolite) represented by sample S9-1 (Uttaradit area). A second analysed dolerite with affinities to Subgroup B-3 BABB (sample YP-9) might also represent a dike, as it crops out between exposures of layered gabbros (Doi Phuk Sung area).

The studied gabbros and amphibolites have been collected from outcrops and float; sample locations are listed in Table I-4 (Appendix I). Some float samples are classified as layered gabbros, since they show layering and/or cumulus features. Many of them, however, lack such features, and are difficult to assign to any particular type because the samples might be too small to identify layering, and their cumulus signatures might have been obliterated by subsequent recrystallisation. Accordingly, the isotropic and cumulus gabbros and equivalent amphibolites are grouped together.

The gabbros and amphibolites generally exhibit granoblastic to grano-nematoblastic textures, except for a few least altered samples in which cumulus

textures predominate (Fig. 6.1). The pronounced foliation developed in many samples is shown by the preferred orientations of prismatic crystals, particularly amphiboles (Fig. 6.2), and elongated clusters of different proportions and/or sizes of minerals. The primary constituents of these rocks may have consisted largely of plagioclase and clinopyroxene, and in some cases, orthopyroxene, as revealed by their relict textures and mineralogies. These primary minerals have been partially or totally obliterated by variable degrees of recrystallisation during deformation and metamorphism, and in turn, their alteration products, such as secondary plagioclases, amphiboles, epidote minerals, garnet and less commonly, chlorite, may become major phases. Rarely, quartz present as sheared veins is an additional principal mineral. Other accessory minerals present may include indeterminate dark cryptocrystalline Ca-hydrosilicate aggregates (after plagioclase), apatite, carbonates, sphene, Fe oxides (haematite, magnetite and ilmenite), Fe sulphides, white mica, stilpnomelane, rutile and green aluminous spinel. Veinlets of fibrous amphibole, chlorite, calcite, epidote, white mica, quartz and stilpnomelane occur in some samples. Petrographic features of individual samples are given in Table II-7 (Appendix II).

Plagioclases are present in almost all samples and have suffered variable degrees of transformation. Their common alteration products are zoisite, clinozoisite and epidote, and may include secondary plagioclase, scapolite, amphibole, chlorite, calcite, pumpellyite and dark cryptocrystalline mineral aggregates. The transformation to epidote minerals is conspicuous in highly foliated samples; in many samples, epidote minerals form atolls around, or completely replace plagioclases. In most cases, plagioclases are anhedral, but in rocks displaying relict cumulus features, they are subhedral to anhedral, and much less altered. Polygonal plagioclases with triple-junction grain boundaries and kink banding have been observed in a few samples.

Pyroxenes, especially clinopyroxenes, are well preserved in many samples; only two gabbronorite samples (samples 24.3 and 32.6) contain fresh orthopyroxenes. Clinopyroxenes are colourless to pale green, whereas orthopyroxenes are pale pink. They are variably altered to amphiboles; many are rimmed by amphiboles (Fig. 6.3) or poikiloblastically enclosed in amphiboles.

Amphiboles vary greatly in colour and composition from sample to sample, and even within individual samples. According to the calculation method of Laird and Albee (1981) and the amphibole nomenclature of Leake (1978), their compositions range from actinolite via actinolitic hornblende, magnesio-hornblende and tschermakitic hornblende to tschermakite; however, the majority are magnesio-hornblende, tschermakitic hornblende and tschermakite. In general, they are

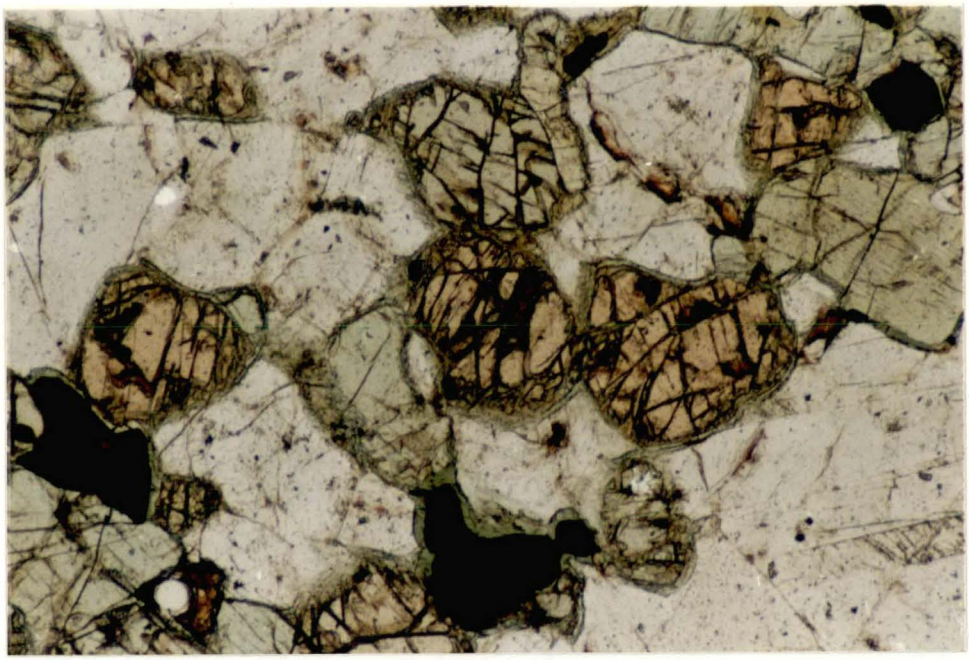

Figure 6.1. Photomicrograph of gabbronorite (sample 32.6) showing relict cumulus texture, principal constituents (plagioclase, white; clinopyroxene, pale green; orthopyroxene, pink) and accessory minerals (amphibole, green; haematite, black). Pyroxenes and haematite are often rimmed with amphibole. Ordinary light, x65.

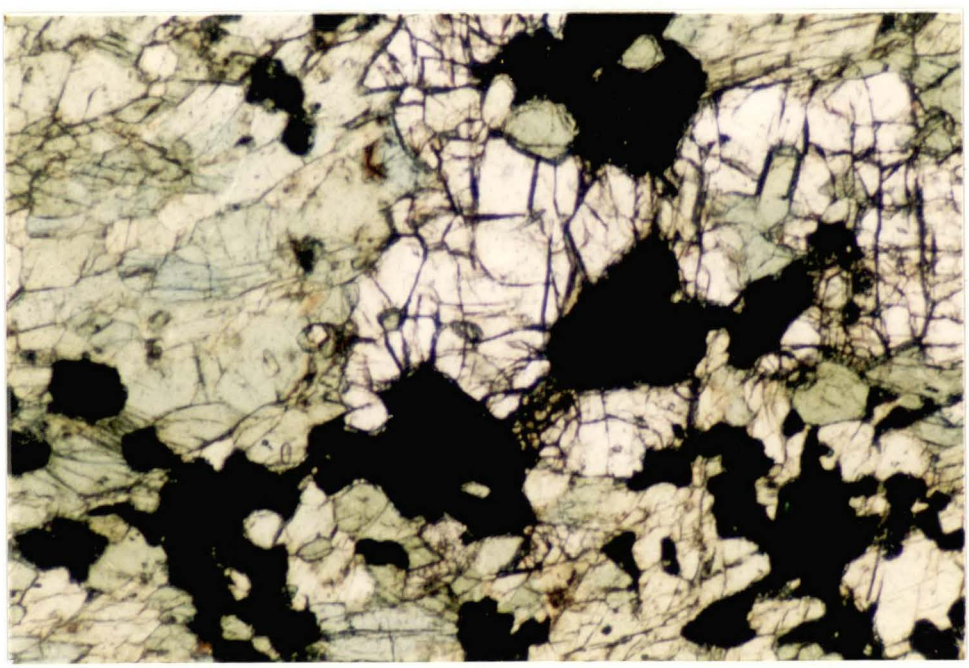

Figure 6.2. Photomicrograph of garnet amphibolite (sample 32.2) where garnet (white) coexists with amphibole (pale green), magnetite (black) and aluminous spinel (dark green, enclosed in magnetite). Ordinary light, x65.

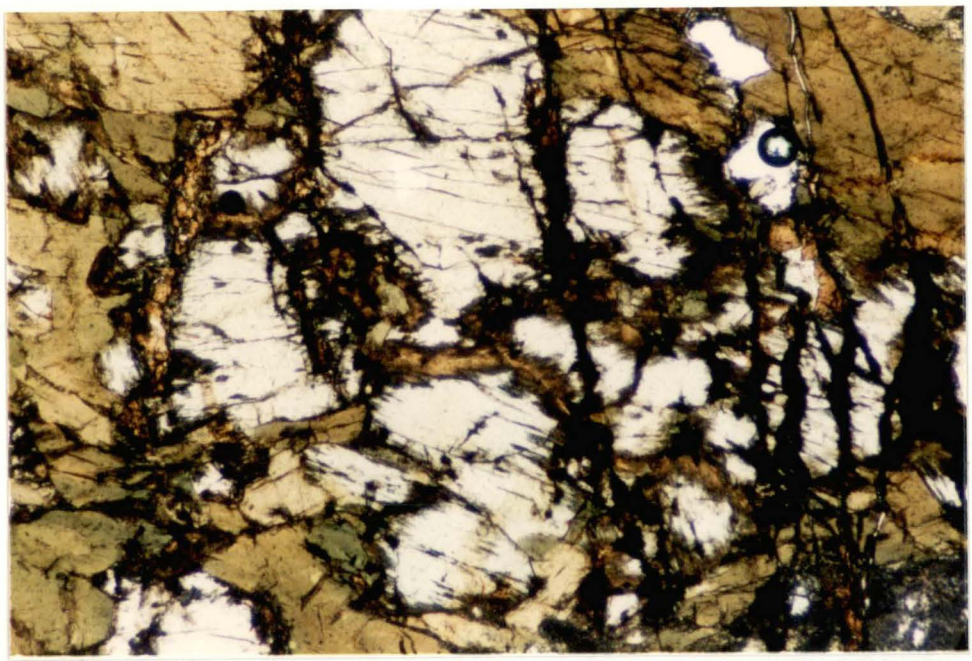

Figure 6.3. Photomicrograph of amphibolite (sample 9.3) illustrating pervasive replacement of colourless clinopyroxene (white) by amphibole (brown) and haematite (black). Ordinary light, x65.

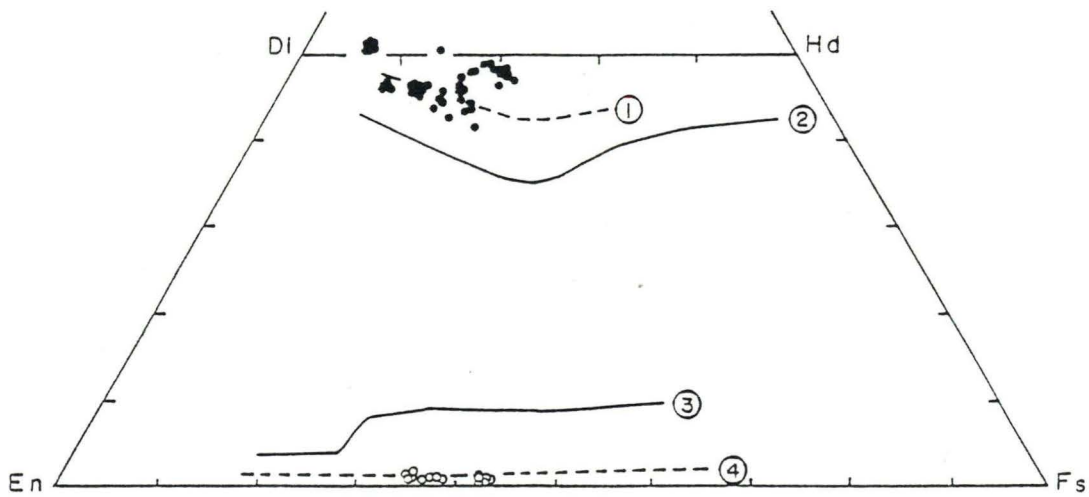

Figure 6.4. Pyroxene quadrilateral showing analyses of clinopyroxenes and orthopyroxenes in gabbros and amphibolites compared with the solidus trends (2 and 3) and the subsolidus trends (1 and 4) of Skaergaard pyroxenes (Brown, 1967; Nwe, 1976).

prismatic, except for very few samples in which the fibrous variety is dominant. They may be intergrown and roughly orientated in two directions like fish bones, or show a mosaic texture with triple-junction grain boundaries at 120°. Some amphiboles in a few garnet-free gabbros/amphibolites contain clinopyroxene inclusions, whereas those in garnet-bearing amphibolites may poikiloblastically enclose garnet, clinopyroxene, quartz, plagioclase, rutile and haematite. Amphiboles are slightly replaced by chlorite, zoisite/clinozoisite and epidote along fractures. On the basis of their colours and relict igneous pyroxene inclusions and cores, all the amphiboles are likely to be metamorphic amphiboles.

Garnets occur as allotriomorphic crystals of variable size (Fig. 6.2), and many show poikiloblastic texture. They may be replaced by pinite, quartz, epidote and white mica along cracks. Inclusions in these garnets may be plagioclase, amphibole, aluminous spinel, rutile, sphene, epidote and quartz.

On grounds of mutual grain contacts, the dominant equilibrium metamorphic assemblages may be summarised as follows:

1. garnet + epidote minerals + hornblende + clinopyroxene
2. garnet + epidote minerals + hornblende + magnetite
3. garnet + epidote minerals + hornblende + rutile + quartz + white mica ± plagioclase
4. plagioclase + epidote minerals + hornblende ± chlorite ± sphene ± haematite ± quartz ± sulphides
5. plagioclase + epidote minerals + hornblende + clinopyroxene + chlorite ± haematite
6. epidote minerals + hornblende + haematite + sphene
7. hornblende + clinopyroxene + chlorite + haematite
8. plagioclase + hornblende + haematite + sphene ± clinopyroxene ± apatite ± sulphides
9. garnet + hornblende + clinopyroxene + plagioclase + haematite
10. plagioclase + hornblende + clinopyroxene
11. plagioclase + hornblende + haematite ± apatite ± sulphides

Assemblages 1 to 6 contain epidote minerals and hornblende, signifying that they represent metamorphism at conditions transitional between greenschist and amphibolite facies of regional metamorphism (epidote-amphibolite facies). Assemblages 7 and 8, although they lack epidote minerals, also belong to epidote-amphibolite facies. Assemblages 9 to 11 are indicators of amphibolite facies of regional metamorphism. Haematite has been detected in many samples, suggesting

that these gabbros and amphibolites have been metamorphosed under high fO_2 condition (HM buffer)(Moody *et al.*, 1983).

6.1.2 Mineral Chemistry

Although gabbros and amphibolites have undergone variable degrees of metamorphism, clinopyroxenes and orthopyroxenes seem to be the only informative relict igneous minerals present. Accordingly, their chemical compositions are reported in Tables 6.1 and 6.2, and plotted in terms of quadrilateral components in Figure 6.4. Following the terminology of the Subcommittee on Pyroxenes, I.M.A.(1988), clinopyroxenes are almost diopsidic whereas orthopyroxenes are enstatites. Calcian augites and clinopyroxenes extremely enriched in wollastonite molecule are present in a few samples. Clinopyroxenes form a broad trend with Mg# values varying from 0.59 to 0.89, superimposing on the subsolidus clinopyroxene trend of the Skaergaard Intrusion. Similarly, orthopyroxenes form a notably linear trend with a limited range of Mg# (0.57-0.66), following the subsolidus orthopyroxene trend of the Skaergaard Intrusion. This suggests that the pyroxenes have undergone variable subsolidus re-equilibration during cooling and subsequent metamorphism as expected from mineral assemblages noted above.

In terms of 'Others' components, both clinopyroxenes and orthopyroxenes show positively collinear relationship between Al^{vi} and Al^{iv} with Al^{vi}/Al^{iv} values of 0.96±0.34 (Figs. 6.5a), implying that the significant 'Others' coupled substitution involved is Al^{vi}-Al^{iv}. Almost all clinopyroxenes have lower Al^{iv} than clinopyroxenes in mid-ocean ridge gabbroic cumulates, and are in the compositional clinopyroxene envelope of arc cumulates (Fig. 6.6a).

6.1.3 Whole-rock Chemistry

Whole-rock analyses of gabbros and amphibolites have been carried out on sixteen least altered samples, and REE analyses have been done on five samples (Tables 6.3 and 6.4).

Gabbros and amphibolites are characterised by low contents of incompatible elements, such as HFSE (0.1-1.4 wt% TiO_2, <1-4 ppm Nb, <1-41 ppm Zr and 5-24 ppm Y), P_2O_5 (trace-0.4 wt%) and REE (0.59-3.11 ppm La and 0.69-1.75 ppm Yb), reflecting their relatively primitive cumulus nature as expected. When the Serri (1981) TiO_2 - FeO*/(FeO*+MgO) discrimination diagram (Fig. 6.7), established on the basis of well studied ophiolites, is applied, the Nan Suture gabbros clearly fall in the field of

TABLE 6.1. ELECTRON MICROPROBE ANALYSES OF CLINOPYROXENES IN GABBROS AND AMPHIBOLITES. FeO AND Fe_2O_3 ARE CALCULATED ASSUMING STOICHIOMETRY ON THE BASIS OF 4 CATIONS AND 6 OXYGENS. END-MEMBERS IN TERMS OF WOLLASTONITE, ENSTATITE AND FERROSILITE ARE CALCULATED ACCORDING TO THE METHOD RECOMMENDED BY THE SUBCOMMITTEE ON PYROXENES, IMA (1988).

Sample no.	9.1	9.2										9.3		
Analysis no.	1	1	2	3	4	5	6	7	8	9	10	1	2	3
SiO2	48.86	50.35	50.69	50.30	49.96	50.23	50.96	51.16	51.80	51.07	51.53	51.52	51.09	50.63
TiO2	0.83	0.44	0.38	0.41	0.33	0.23	0.36	-	0.26	0.27	0.28	0.34	0.45	0.31
Al2O3	6.30	3.48	3.37	3.36	3.44	3.31	3.43	3.27	2.52	3.28	3.04	3.11	3.79	3.72
Cr2O3	-	-	-	0.20	-	-	-	-	-	-	0.21	-	-	-
Fe2O3	0.59	1.53	1.15	1.56	1.57	1.97	1.40	1.64	0.66	1.25	0.64	0.89	1.12	0.41
FeO	7 96	11.12	11.25	11.64	11.92	11.18	11.14	11.42	10.72	11.14	11.23	9.45	9.51	10.51
MnO	-	-	-	-	-	-	-	-	-	-	-	0.31	0.28	-
MgO	11.86	9.89	10.11	10.02	9.82	9.90	10.22	10.64	10.70	10.47	10.48	11.83	11.29	11.08
CaO	23.48	22.23	22.06	21.74	21.39	21.74	22.07	21.68	22.82	22.46	22.78	22.38	22.23	22.06
Na2O	-	0.73	0.74	0.68	0.69	0.78	0.78	0.65	0.68	0.59	0.59	0.52	0.67	0.50
Total	99.88	99.77	99.75	99.91	99.12	99 34	100.36	100.46	100.16	100.53	100.78	100.35	100.43	99.22
Si	1.830	1.914	1.924	1.913	1.916	1.920	1.922	1.928	1.952	1.923	1.935	1.928	1.912	1.920
ivAl	0.171	0.086	0.076	0.087	0.084	0.081	0.078	0.072	0.048	0.077	0.066	0.072	0.088	0.080
Total tetra.	2 000	2.000	2.000	2.000	2.000	2.000	2.000	2.000	2.000	2.000	2.000	2.000	2.000	2.000
viAl	0.107	0.070	0 075	0.064	0.071	0.069	0.075	0.073	0.064	0.069	0.069	0.065	0.080	0 087
Ti	0 023	0.013	0.011	0.012	0.010	0.007	0.010	-	0.007	0.008	0.008	0.010	0.013	0 009
Cr	-	-	-	0.006	-	-	-	-	-	-	0.006	-	-	-
Fe3+	0.017	0.044	0.033	0.045	0.045	0.057	0.040	0.047	0 019	0.036	0.018	0.025	0.032	0.012
Fe2+	0.249	0.354	0.357	0 370	0.382	0.357	0.352	0.360	0.338	0.351	0.353	0.296	0.298	0.333
Mn	-	-	-	-	-	-	-	-	-	-	-	0.010	0.009	-
Mg	0.662	0.561	0.572	0.568	0.562	0.564	0.574	0.598	0.601	0.588	0.587	0.660	0.630	0.627
Total octa.	1.058	1.041	1.048	1.064	1.070	1.052	1.051	1.077	1.029	1.051	1.040	1.065	1.060	1.067
Ca	0.942	0.906	0.897	0.886	0.879	0.890	0.892	0.875	0.921	0.906	0.917	0.898	0.892	0.896
Na	-	0.054	0 054	0.051	0.052	0.058	0 057	0.048	0.050	0.043	0.043	0.037	0.049	0.036
Total cat.	4 000	4.000	4.000	4.000	4.000	4.000	4.000	4.000	4.000	4.000	4.000	4.000	4.000	4.000
Mg/(Mg+Fe^{2+})	0.727	0.613	0.616	0.605	0.595	0.612	0.620	0 624	0 640	0 626	0 625	0.690	0.679	0.653
Wo	50.39	48.59	48.26	47.41	47.05	47.66	48.02	46.58	49.03	48.19	48.91	47.54	47.96	47.98
En	35.39	30 08	30.76	30.39	30.06	30.19	30.92	31.80	31.99	31.26	31.31	34.94	33.86	33 55
Fs	14.22	21.33	20.98	22.20	22.89	22.15	21.05	21.63	18.98	20.55	19.78	17 52	18.18	18.47

Sample no.	9.3	20.1							24 3				32.6		
Anal. no	4	1	2	3	4	5	6	7	1	2	3	4	1	2	3
SiO2	50.49	50.94	51.94	50.94	50.98	51 30	51 62	52.04	52.08	52.41	52 18	52.73	51.24	50.65	50.85
TiO2	0.46	-	-	0.18	0.21	-	-	-	0.29	0.27	0.29	-	0.30	0.28	0 29
Al2O3	4.03	5.44	4.70	5.23	5.30	5.79	5.62	4.80	2.43	2.26	2.41	1.66	3.66	3.59	3.72
Cr2O3	-	-	-	0 19	0 22	-	0.25	0.21	-	-	-	-	-	-	-
Fe2O3	0.58	0 68	0.03	0 37	0 23	0.71	0.12	0.16	-	-	-	-	0.50	1.58	1 05
FeO	10.38	3.33	3.68	3.77	3.71	3.97	3.99	4 10	8.16	8.56	8.45	8.10	10.14	9 22	9.56
MnO	-	-	-	-	-	-	-	-	0.22	-	0.27	-	-	0.32	0.30
MgO	11.07	14.46	14.71	14.41	14.52	14.58	14.91	14.99	13.70	13.74	13.86	14 17	12.03	11.74	12.07
CaO	21.86	24 83	25.14	24.68	24.62	24.50	24.32	24 53	22.15	22.38	22.26	22.60	21.77	21.29	21.32
Na2O	0.58	-	-	-	-	-	-	-	0.25	-	-	-	0.45	0 66	0.51
Total	99.45	99 68	100.20	99.77	99.79	100.85	100.83	100.83	99.28	99.62	99.72	99 26	100.09	99.33	99.67
Si	1.910	1 873	1.898	1.874	1.873	1.866	1.875	1.892	1.949	1.955	1.947	1.971	1.920	1.914	1.913
ivAl	0.090	0.127	0.102	0.126	0.127	0.134	0.125	0.108	0.051	0.045	0.053	0.029	0.080	0.086	0.087
Total tetra.	2.000	2.000	2.000	2.000	2.000	2.000	2.000	2.000	2.000	2.000	2.000	2.000	2.000	2.000	2.000
viAl	0.090	0.109	0.101	0 101	0.103	0.114	0.115	0.098	0.057	0 055	0.053	0.044	0.082	0.074	0.078
Ti	0.013	-	-	0.005	0.006	-	-	-	0.008	0.007	0.008	-	0.008	0.008	0.008
Cr	-	-	-	0 006	0.007	-	0.007	0.006	-	-	-	-	-	-	-
Fe3+	0.017	0.019	0.001	0.010	0.006	0.019	0.003	0.005	-	-	-	-	0.014	0.045	0.030
Fe2+	0.328	0 102	0.112	0.116	0.114	0.121	0.121	0.125	0.256	0.267	0.264	0.253	0.318	0.291	0.301
Mn	-	-	-	-	-	-	-	-	0.007	-	0.008	-	-	0.010	0.009
Mg	0.624	0.792	0.801	0.790	0.795	0.790	0.807	0.812	0.764	0.764	0.770	0.790	0.672	0.662	0.677
Total octa.	1.072	1.022	1.015	1.027	1.031	1.045	1.054	1.045	1.091	1.093	1.103	1.087	1.094	1.090	1.103
Ca	0 886	0.978	0.985	0.973	0 969	0.955	0 947	0.955	0.889	0.895	0.890	0.905	0.874	0.862	0.860
Na	0.043	-	-	-	-	-	-	-	0.018	-	-	-	0.032	0.049	0 037
Total cat.	4.000	4.000	4 000	4.000	4.000	4.000	4.000	4.000	3.998	3.988	3.992	3.992	4.000	4.000	4.000
Mg/(Mg+Fe^{2+})	0.655	0.886	0.877	0.872	0.875	0.867	0.870	0.867	0.749	0.741	0.745	0.757	0.679	0.694	0.692
Wo	47.76	51.71	51.85	51 50	51.42	50.65	50.40	50.38	46.39	46.46	46.05	46.47	46.55	46.10	45.80
En	33.65	41.89	42.19	41.83	42.19	41.92	42.97	42.82	39.90	39.67	39 87	40.53	35.78	35.38	36.07
Fs	18.59	06.40	05.96	06.68	06.39	07.44	06.62	06 80	13.71	13.88	14.08	12.99	17 67	18.53	18.12

TABLE 6.1. CONTINUED

Sample no	32.6						S-2						S-9.1	
Anal. no.	4	5	6	7	8	9	1	2	3	4	5	6	1	2
SiO2	51 02	51.09	50.89	51.25	50.92	50.77	53.54	53.17	53.56	53.30	53.70	53.30	53.48	53.87
TiO2	0.38	0.33	0.41	0 29	0.26	0.39	-	-	0.18	-	-	-	-	-
Al2O3	3.58	3.51	3.87	3.93	3.73	3.62	1.23	1.24	1.33	1.00	0.90	1.15	0.96	0 80
Cr2O3	-	-	-	-	-	-	0.19	-	0.25	-	0.20	-	-	-
Fe2O3	1.98	0.21	1.83	0 89	1.05	0.95	-	-	-	-	-	-	-	-
FeO	8.87	11.32	9.28	11.11	10.60	11.93	6.57	6.71	6.67	6.89	6.72	6.64	8 21	8.37
MnO	0.26	0 42	0.40	0.28	0.29	0.34	-	-	-	0.25	-	-	-	0.25
MgO	12.10	12.28	12.26	12.14	12.01	12.34	15.55	15.10	15.25	15.11	15.07	15.23	14.46	14.24
CaO	21.59	20.21	20.97	20.58	20.62	19.39	22.83	22.87	22.88	22.55	23.14	22.91	23.05	22.72
Na2O	0 65	0.41	0.61	0.46	0.52	0.42	-	-	-	-	-	-	-	-
Total	100.43	99.78	100.52	100.93	100.00	100.15	99.91	99.09	100.12	99.10	99.73	99.23	100.16	100.25
Si	1.906	1.925	1.900	1.910	1.914	1.911	1.976	1.980	1.973	1.986	1.988	1.981	1.984	1.996
ivAl	0.094	0.076	0.100	0.090	0 086	0.090	0.025	0.020	0.027	0.014	0.012	0.019	0.017	0.004
Total tetra.	2.000	2.000	2.000	2.000	2.000	2.000	2.000	2.000	2.000	2.000	2.000	2.000	2.000	2.000
viAl	0.064	0.081	0.070	0.083	0.079	0.071	0.029	0.034	0.031	0.030	0.027	0.032	0.026	0.031
Ti	0.011	0.009	0.011	0.008	0 007	0.011	-	-	0.005	-	-	-	-	-
Cr	-	-	-	-	-	-	0 006	-	0 007	-	0.006	-	-	-
Fe3+	0.056	0.006	0.051	0.025	0.030	0.027	-	-	-	-	-	-	-	-
Fe2+	0.277	0.356	0.290	0.346	0.333	0.376	0 203	0.209	0.206	0.215	0.208	0.206	0.255	0.259
Mn	0.008	0.013	0.013	0.009	0.009	0 011	-	-	-	0.008	-	-	-	0 008
Mg	0 674	0.689	0 682	0.674	0.673	0 692	0.855	0 838	0.837	0 839	0.832	0.844	0.799	0.786
Total octa.	1.089	1.155	1.117	1.145	1.132	1.188	1.093	1.081	1.086	1.092	1 072	1.081	1.079	1.085
Ca	0 864	0.816	0 839	0.822	0.830	0.782	0.902	0 912	0.903	0 900	0 918	0.912	0.916	0.902
Na	0 047	0.030	0 044	0 034	0 038	0.031	-	-	-	-	-	-	-	-
Total cat.	4.000	4.000	4.000	4.000	4.000	4.000	3.995	3.993	3.989	3.992	3 990	3.994	3.996	3.986
Mg/(Mg+Fe^{2+})	0.708	0 659	0.702	0.661	0 669	0.648	0 808	0.800	0 803	0.796	0.800	0.803	0 759	0.752
Wo	45 99	43.37	44.74	43.79	44.28	41.42	46.03	46.56	46 42	45.89	46.88	46.50	46.50	46.12
En	35.85	36.66	36.39	35.94	35.88	36.67	43 63	42.77	43.02	42.77	42.49	42.99	40.58	40.22
Fs	18 16	19.98	18 87	20.27	19 84	21 92	10 34	10.66	10.56	11.34	10 63	10 52	12.92	13 66

Sample no.	S-9.1					S-12B					H			
Anal no.	3	4	5	6	7	1	2	3	4	5	1	2	3	4
SiO2	53 34	52.97	53.57	53.83	53.45	52.93	53.01	52.22	51.87	53.07	53 04	51.61	52.48	53 16
TiO2	-	0.24	-	-	-	-	-	-	-	-	0.22	0.21	0.31	0.19
Al2O3	0.96	2.02	1.54	1.21	0.92	1.09	1.03	1 54	2.15	1 24	1.95	3.22	2.35	1.66
Cr2O3	-	-	-	-	0 23	-	-	-	-	-	-	-	-	-
Fe2O3	-	-	-	-	-	0.21	-	-	1.33	1.47	-	0.17	0 86	0.86
FeO	8.46	8 66	8.50	9.25	8.48	10.22	10.43	10 05	9.89	8.68	8 45	9.89	8.08	7 16
MnO	-	-	0.22	-	-	0.34	-	0.30	0.40	0.30	0.30	0.36	0.32	0.34
MgO	14.54	14.36	13.86	14 24	14.18	13.36	13.38	13.41	13 45	13.34	14.02	13.79	13.48	14.28
CaO	22.86	22.35	22.72	22.15	23.01	21.56	21.63	21.59	20.72	22.56	22.76	21.13	22.58	22.85
Na2O	-	-	-	-	-	0 28	-	-	0.26	0.39	-	-	0.36	0.32
Total	100 16	100.60	100.41	100.68	100.27	99 99	99.48	99.11	100 07	101.05	100.74	100.38	100.82	100.82
Si	1.980	1.956	1.982	1.988	1.984	1.983	1.992	1.971	1.943	1.966	1 959	1.921	1.941	1.959
ivAl	0.020	0.044	0 018	0.012	0.017	0.017	0.008	0.029	0.057	0 034	0 041	0.079	0 059	0.042
Total tetra.	2.000	2 000	2.000	2.000	2.000	2.000	2.000	2.000	2.000	2 000	2.000	2.000	2.000	2.000
viAl	0 022	0.044	0 049	0.041	0.024	0.031	0.038	0 040	0.038	0.021	0 044	0.063	0.043	0.031
Ti	-	0 007	-	-	-	-	-	-	-	-	0.006	0.006	0.009	0 005
Cr	-	-	-	-	0.007	-	-	-	-	-	-	-	-	-
Fe3+	-	-	-	-	-	0.006	-	-	0.037	0 041	-	0.005	0.024	0 024
Fe2+	0.263	0.267	0.263	0 286	0.263	0.320	0.328	0.317	0.310	0.269	0.261	0.308	0.250	0.221
Mn	-	-	0 007	-	-	0 011	-	0.010	0 013	0.010	0.009	0 012	0.010	0.011
Mg	0 804	0.790	0.764	0.784	0.784	0.746	0.749	0.755	0.751	0.737	0.772	0.765	0.743	0.784
Total octa.	1 090	1.109	1.084	1.110	1.078	1.114	1.115	1.121	1.150	1.077	1.092	1.158	1.079	1.075
Ca	0.909	0.885	0.901	0 876	0.915	0.866	0.871	0 873	0.832	0.895	0.901	0.843	0.895	0.902
Na	-	-	-	-	-	0.020	-	-	0.019	0 028	-	-	0.026	0.023
Total cat.	3.999	3.993	3.985	3.986	3.993	4.000	3 985	3.995	4.000	4.000	3 992	4.000	4.000	4 000
Mg/(Mg+Fe^{2+})	0.754	0.747	0.744	0.733	0.749	0.700	0.696	0.704	0.708	0.733	0.747	0.713	0.748	0 780
Wo	46.01	45.54	46.55	45 04	46.63	44.42	44.71	44.67	42.80	45.88	46.36	43.62	46.56	46.47
En	40.70	40.69	39.50	40 28	39.97	38.29	38.47	38.61	38 67	37.76	39.73	39.61	38.65	40.40
Fs	13.30	13.77	13 95	14 68	13.41	17.30	16.82	16.72	18.52	16 36	13.91	16.78	14.79	13.14

low-Ti ophiolitic gabbros associated with the early stages of backarc spreading in an intra-oceanic environment. Therefore, it is likely that these gabbros and amphibolites have originated in a supra-subduction zone setting.

Chondrite-normalised REE patterns for representative samples are flat to slightly depleted from Sm to Yb ((Sm/Yb)n=0.9-2.1)), and flat to depleted from Sm to La ((La/Sm)n=0.6-1.0); three of them exhibit positive Eu anomalies with Eu/Eu* ranging from 1.2 to 1.4 (Fig. 6.8).

Gabbros have similar TiO_2 to Subgroup C-1 and C-2 arc lava-dolerite-microgabbro samples at similar levels of Mg#. Their REE patterns show strong similarities to those for Subgroups B-1 and B-2 backarc rocks, and Subgroup C-1 lava-dolerite-microgabbro arc samples (Fig. 6.9). Accordingly, these gabbros are most similar to and probably comagmatic with the Subgroup C-1 arc samples. However, a problem exists with this correlation. Typical foliated Nan Suture gabbroic rocks are clearly cross-cut by non-foliated Subgroup C-1 microgabbros at one locality, indicating that more than one episode of Subgroup C-1 - type arc magmatism may be represented among the Nan Suture rocks. Without more detailed field and geochronological data (not readily available due to the melange/block nature of the Nan Suture), this scenario cannot be clarified further.

TABLE 6 2. ELECTRON MICROPROBE ANALYSES OF ORTHOPYROXENES IN GABBROS AND AMPHIBOLITES. FeO AND Fe_2O_3 ARE CALCULATED ASSUMING STOICHIOMETRY ON THE BASIS OF 4 CATIONS AND 6 OXYGENS. END-MEMBERS IN TERMS OF WOLLASTONITE, ENSTATITE AND FERROSILITE ARE CALCULATED ACCORDING TO THE METHOD RECOMMENDED BY THE SUBCOMMITTEE ON PYROXENES, IMA (1988).

Sample no	24 3								32 6								
Anal. no.	1	2	3	4	5	6	7	8	1	2	3	4	5	6	7	8	9
SiO2	51.09	52.69	52.73	52.60	53.23	52.87	52.93	52.77	51.81	51.00	51.14	51.96	51 64	51.79	50.76	51.45	51.42
TiO2	-	-	-	0.17	-	-	-	-	-	0.16	-	-	-	-	-	-	-
Al2O3	2.88	1.36	1.41	1.44	1 59	1.31	1.54	1.56	2.44	2.31	2.20	2.28	2.20	2.30	2.37	2.48	2.22
Fe2O3	1.19	0.41	0.12	0.52	0.16	0.37	0.33	1.05	0.80	1.01	0.88	0 81	1.00	0.41	0 89	1.55	1 18
FeO	22.27	21.59	23.81	21.29	22.09	22.56	21.15	22.51	25.09	24.53	25.14	25.13	25.04	25.79	25.35	25.07	25.36
MnO	0.55	0.53	0.72	0.51	0.46	0.52	0.60	0.57	0.74	0.82	0.76	0.85	0 68	0.72	0 81	0.81	0 77
MgO	21.06	22.57	21.25	22.58	22.37	22.15	22.84	22.01	19.86	19.55	19.48	19 93	19.91	19.41	19.06	19.64	19.50
CaO	0.57	0.51	0 51	0.77	0.96	0 52	0 65	0.61	0.57	0.73	0.41	0 48	0.42	0.64	0 43	0.48	0 46
Total	99.61	99.66	100.55	99.88	100.86	100.30	100 04	101.08	101.31	100.11	100.01	101.44	100.89	101.06	99.67	101 48	100 91
Si	1.919	1.965	1.967	1.957	1.963	1.966	1.962	1.951	1.935	1 929	1.938	1.938	1.937	1.943	1.934	1.924	1.934
ivAl	0.081	0.036	0.033	0.044	0.037	0.034	0.038	0.049	0.065	0 071	0.062	0.062	0.063	0.057	0.066	0.076	0.066
Total tetra.	2.000	2.000	2.000	2.000	2.000	2.000	2.000	2.000	2.000	2.000	2.000	2.000	2.000	2.000	2.000	2.000	2.000
viAl	0.047	0.024	0.029	0.020	0 033	0.023	0.029	0 019	0 042	0.033	0.037	0.039	0.035	0 045	0.041	0.033	0.033
Ti	-	-	-	0.005	-	-	-	-	-	0.005	-	-	-	-	-	-	-
Fe3+	0.034	0.011	0.003	0.014	0.004	0.011	0.009	0.029	0 023	0.029	0.025	0.023	0.028	0.012	0.025	0.044	0.033
Fe2+	0.700	0.673	0.743	0.662	0.681	0.702	0.656	0.696	0.784	0.776	0.797	0.784	0.786	0.809	0.808	0.784	0.798
Mn	0.017	0.017	0.023	0.016	0.014	0 016	0.019	0.018	0.023	0 026	0.025	0.027	0.022	0.023	0.026	0.026	0.024
Mg	1.179	1.254	1.182	1.252	1.230	1.228	1.262	1.213	1.105	1.102	1.100	1.108	1.113	1.086	1.082	1.095	1.094
Total octa.	1.977	1.980	1.980	1.969	1.962	1.979	1.975	1.976	1.977	1.970	1.983	1.981	1.983	1.974	1.982	1.981	1.982
Ca	0.023	0 020	0.020	0 031	0 038	0.021	0.026	0.024	0.023	0 030	0 017	0.019	0.017	0.026	0.018	0.019	0 019
Total cat.	4.000	4.000	4.000	4.000	4.000	4.000	4.000	4.000	4.000	4.000	4.000	4 000	4.000	4.000	4.000	4 000	4 000
$Mg/(Mg+Fe^{2+})$	0.628	0.651	0 614	0 654	0 644	0.636	0.658	0.635	0.585	0.587	0.580	0.586	0.586	0 573	0.573	0.583	0.578
Wo	1.18	1.02	1.02	1.56	1.93	1.04	1.30	1.22	1.16	1.51	0.85	0 98	0.86	1.32	0.90	0.98	0.94
En	60.38	63.47	59.95	63.37	62.50	62.11	64.02	61.26	56.47	56.15	56.03	56.51	56.63	55.53	55.23	55.65	55.58
Fs	38.44	35.51	39 02	35 07	35 57	36 84	34.68	37.52	42.37	42.34	43.12	42.51	42.51	43.15	43 86	43.37	43 48

- = BELOW DETECTION LIMIT.

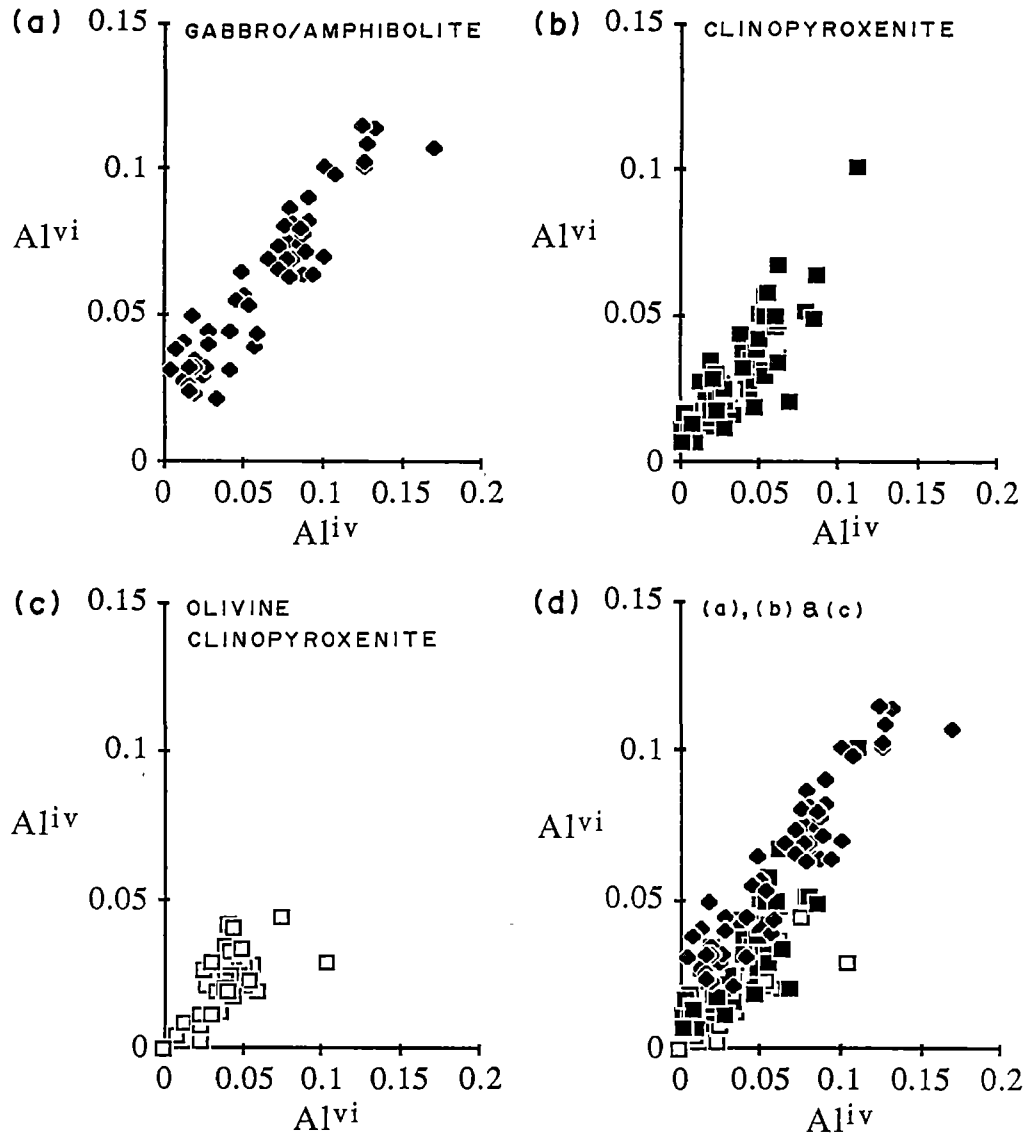

Figure 6.5. Relationship between Al^{vi} and Al^{iv} for clinopyroxenes in (a) gabbros and amphibolites, (b) clinopyroxenites and (c) olivine clinopyroxenites,showing important Al^{vi}-Al^{iv} coupled substitution. Note that these clinopyroxenes have similar Al^{vi}/Al^{iv} ratios (d).

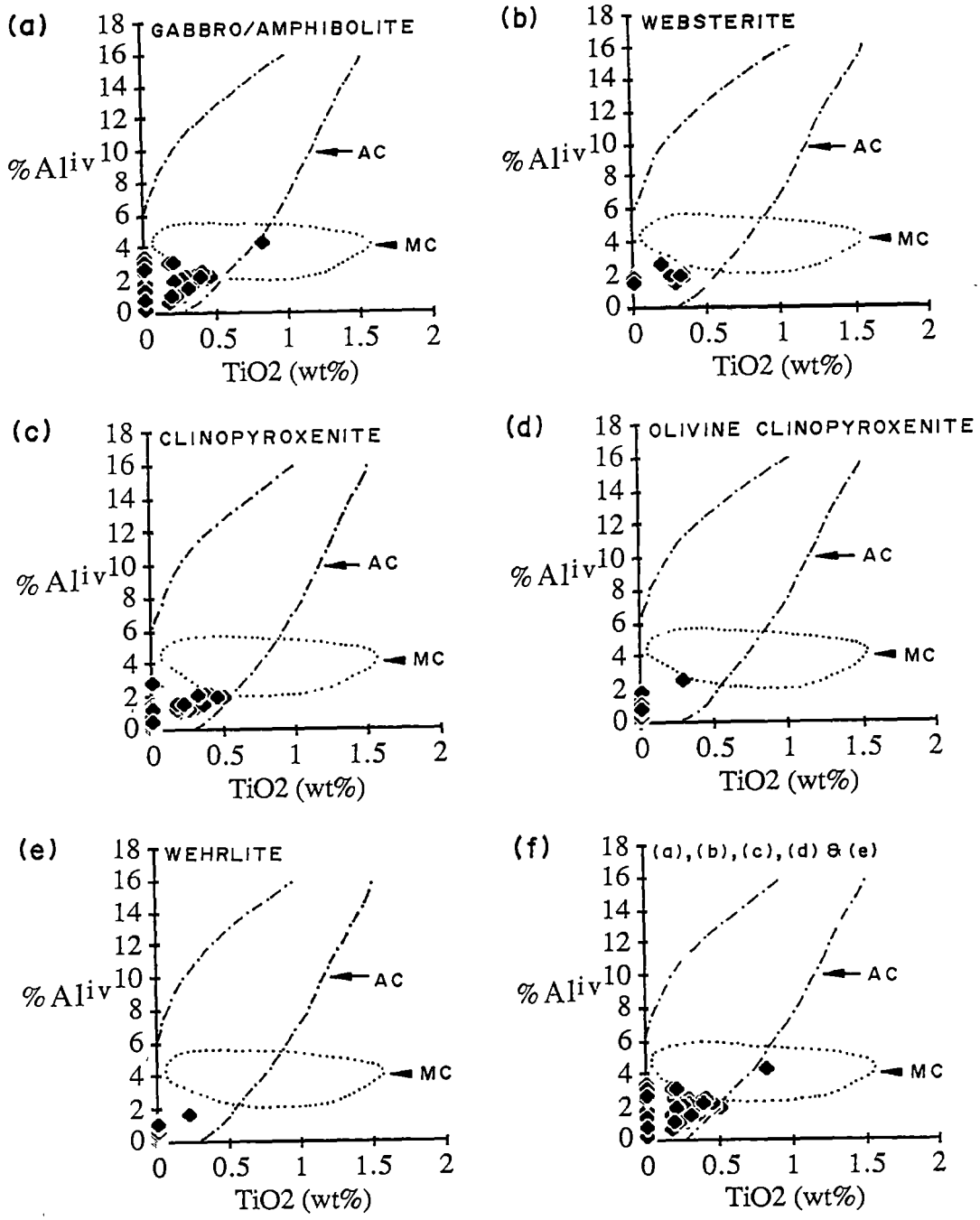

Figure 6.6. Tectonomagmatic discrimination diagram for mafic-ultramafic cumulates in terms of clinopyroxene compositions (Loucks, 1990). Data plotted are Nan Suture clinopyroxenes in gabbros/amphibolites (a), websterites (b), clinopyroxenites (c), olivine clinopyroxenites (d), wehrlites (e) and all cumulates (f). AC = arc cumulates; MC = mid-ocean ridge cumulates.

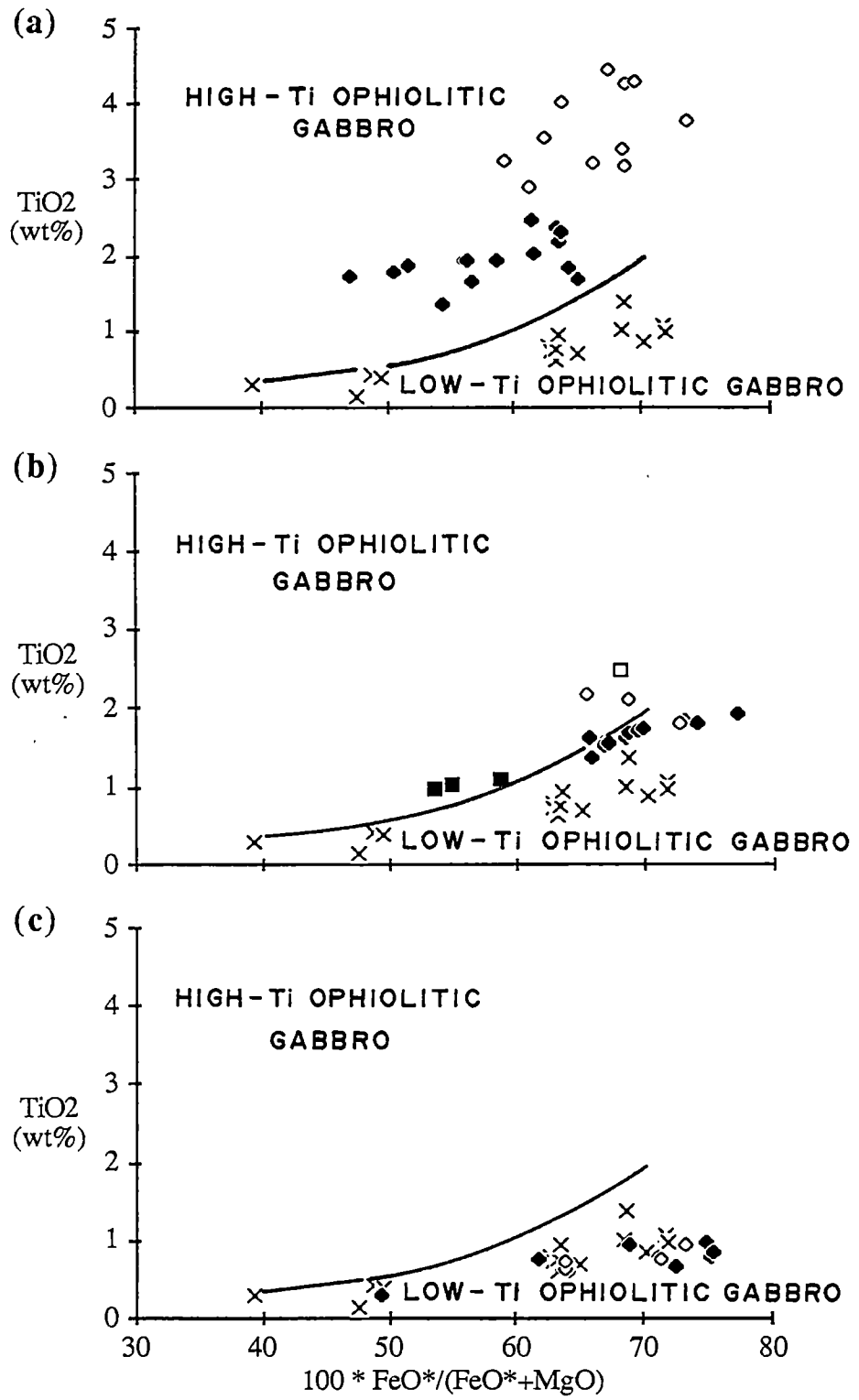

Figure 6.7. Tectonomagmatic discrimination diagram in terms of TiO_2 against mafic index (after Serri, 1981) showing Nan Suture gabbroic rocks (cross) falling exclusively in the field of low-Ti ophiolitic gabbros. Also plotted are (a) Group A ocean-island basalts (solid diamond, Subgroup A-1 tholeiites; open diamond, Subgroup A-2 transitional tholeiites and alkalic basalts), (b) Group B backarc basin basalts and andesites (solid diamond, Subgroup B-1, open diamond, Subgroup B-2, solid square Subgroup B-3; open square, Subgroup B-4), and (c) Group C arc basalts and andesites (solid diamond, Subgroup C-1; open diamond, Subgroup C-2).

TABLE 6.3. WHOLEROCK XRF ANALYSES OF GABBROIC ROCKS;
MAJOR ELEMENTS ARE NORMALIZED TO 100% ON THE BASIS OF LOSS ON IGNITION FREE.

Sample no.	S-2	S9-1	F	G	YP-7	24.3	27.5	YP-12	S-12B	YP-15	32.6	17.7	45.3	H	17.6	17.5
SiO2	51.28	49.89	57.45	49.58	42.93	46.16	55.40	42.60	49.78	44.84	50.20	48.20	46.40	45.84	48.02	49.49
TiO2	0.30	0.13	0.43	0.38	0.78	0.74	0.62	0.77	0.95	0.71	0.70	1.02	1.39	0.87	1.08	0.98
Al2O3	14.36	19.05	13.82	16.54	20.53	16.96	15.70	21.89	16.92	22.41	18.06	19.41	19.70	19.78	19.21	19.74
FeO	7.33	6.45	7.45	9.10	14.01	13.41	9.55	11.93	12.90	12.11	11.00	12.00	12.17	14.28	12.72	11.80
MnO	0.14	0.15	0.17	0.18	0.17	0.19	0.17	0.13	0.19	0.24	0.22	0.27	0.22	0.18	0.29	0.25
MgO	11.29	7.10	7.81	9.25	8.32	7.93	5.55	6.91	7.43	6.51	5.91	5.53	5.53	6.07	5.00	4.62
CaO	13.14	14.14	8.13	12.57	10.62	13.32	9.58	13.80	7.24	9.64	11.07	9.66	10.24	8.99	10.01	8.76
Na2O	1.76	2.27	4.31	2.26	1.71	1.26	2.82	1.50	4.29	2.42	2.62	3.53	3.56	2.95	3.26	3.83
K2O	0.35	0.79	0.34	0.12	0.89	0.03	0.39	0.45	0.08	1.10	0.12	0.20	0.58	0.68	0.13	0.28
P2O5	0.05	0.04	0.08	0.02	0.04	-	0.22	0.03	0.22	0.02	0.11	0.20	0.22	0.36	0.28	0.26
LOI	2.54	3.26	1.89	2.75	4.06	0.24	2.52	3.86	3.21	3.83	0.45	1.62	1.60	3.15	1.52	2.06
FeO*/MgO	0.65	0.91	0.95	0.98	1.68	1.69	1.72	1.73	1.74	1.86	1.86	2.17	2.20	2.35	2.54	2.55
Nb	2	<1	2	<1	<1	<1	1	<1	2	<1	1	<1	4	<1	<1	1
Zr	25	4	41	5	1	<1	4	<1	12	<1	6	7	25	<1	4	6
Y	10	5	16	10	6	6	12	6	12	8	13	23	19	10	21	24
Sr	191	458	175	213	347	298	261	216	262	397	368	469	397	421	500	570
Rb	2	8	3	1	18	<2	2	8	<2	19	<2	<2	<2	10	<2	<2
Ni	99	46	71	78	9	27	19	15	36	7	24	6	10	14	7	5
Cr	437	209	382	328	13	45	46	7	56	9	63	3	18	21	7	5
V	188	206	216	309	440	627	372	773	778	356	374	318	364	614	282	285
Ba	76	210	85	23	72	24	55	22	29	20	63	82	63	54	57	114
Sc	64	58	42	68	72	59	53	97	43	68	47	53	49	57	60	40

FEO* = TOTAL IRON AS FEO, - = BELOW DETECTION LIMIT.

TABLE 6.4. REE ANALYSES AND SELECTED CHONDRITE-NORMALISED RATIOS FOR GABBROIC ROCKS

Sample no.	YP-7	S-12B	32.6	H	17.6
La	0.59	3.20	2.45	1.44	3.11
Ce	1.73	8.53	7.16	3.76	10.7
Pr	<0.31	1.44	1.05	0.63	2.20
Nd	1.43	7.05	5.88	3.65	12.5
Sm	0.59	1.96	1.82	1.20	3.63
Eu	0.31	0.73	0.64	0.67	1.81
Gd	1.05	2.33	2.14	1.88	4.34
Dy	1.28	2.51	2.44	1.85	4.00
Er	0.87	1.76	1.47	1.10	2.21
Yb	0.69	1.72	1.35	0.87	1.75
[La/Sm]n	0.61	1.00	0.82	0.73	0.59
[Sm/Yb]n	0.93	1.23	1.46	1.49	2.09

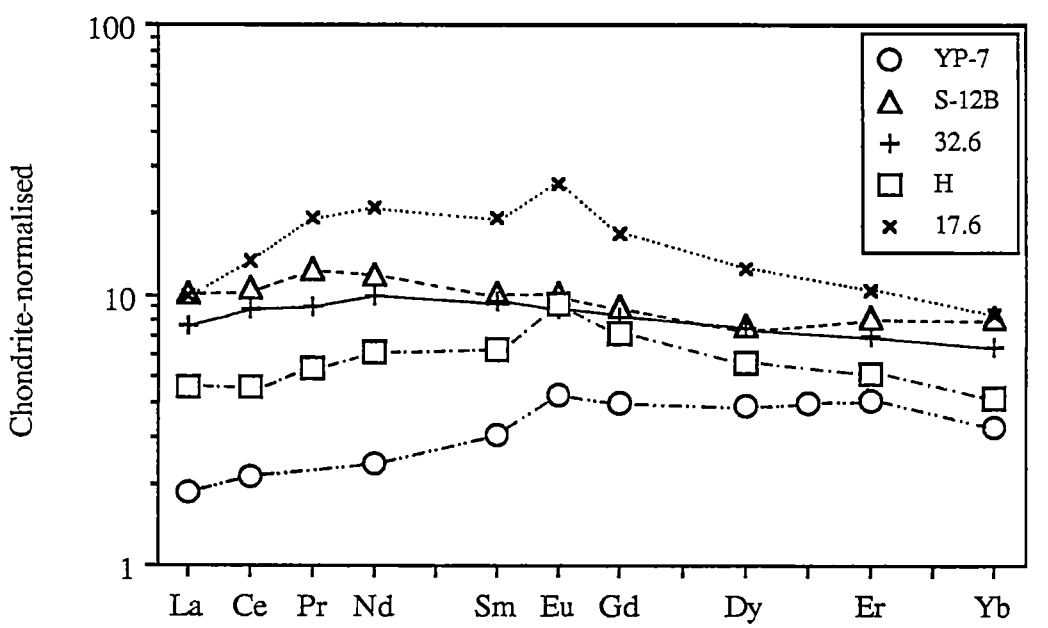

Figure 6.8. Chondrite-normalised REE patterns for Nan Suture gabbroic rocks.

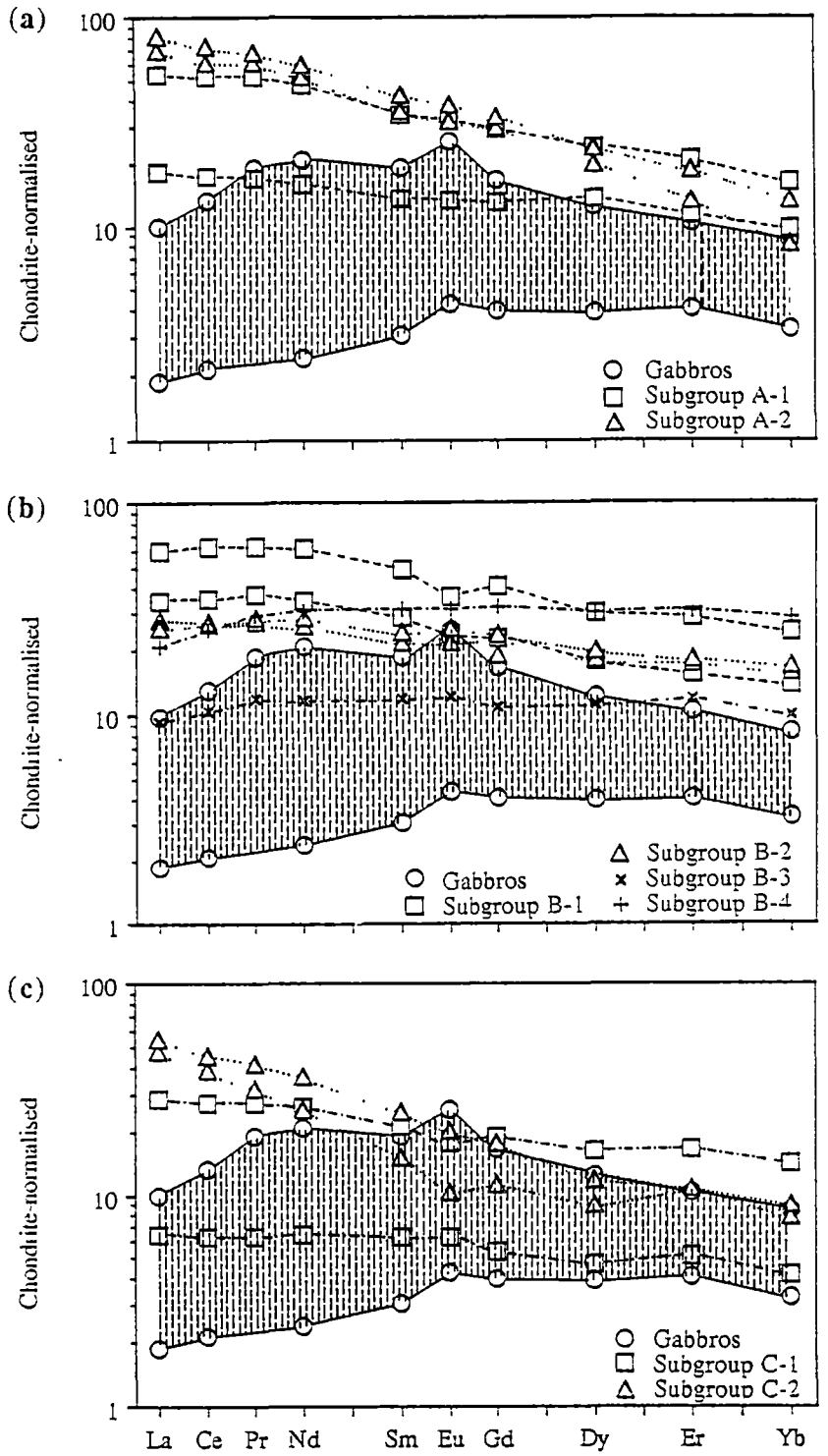

Figure 6.9. Ranges of chondrite-normalised patterns for Nan Suture gabbroic rocks compared with those for (a) Group A ocean-island basalts, (b) backarc basin basalts and andesites, and (c) Group C arc basalts and andesites.

6.2 Ultramafic Rocks

The studied ultramafic rocks were collected from outcrops and float in every key area, and include clinopyroxenite, websterite, olivine clinopyroxenite, wehrlite, harzburgite and dunite. They most commonly occur as blocks in serpentinite matrix; however, at a few localities in the Doi Phuk Sung area, pyroxenites are interlayered with gabbros/amphibolites and peridotites. Sample locations are given in Table I-5 (Appendix I).

6.2.1 Petrography

Clinopyroxenites

Clinopyroxenites are almost equigranular rocks in which grainsize ranges from fine (<1 mm) to coarse (4 mm); they may show diffuse foliation or relict cumulus textures. They have been variably amphibolitised and/or chloritised, and as a consequence, amphibole and chlorite may become major phases along with clinopyroxene. Altered orthopyroxene, magnetite, Fe sulphides and calcite may be present in small amounts. Petrographic features of individual samples are given in Table II-8 (Appendix II).

Clinopyroxenes are colourless, have anhedral outlines and are generally replaced by amphiboles along grain boundaries and fractures. In some samples, they are also partially altered to chlorite and magnetite. They may contain chromite lamellae and inclusions that are totally transformed to ferritchromite.

Amphiboles are pale green to green, and are actinolite, tremolitic hornblende and magnesio-hornblende according to the calculation method of Laird and Albee (1981) and the amphibole nomenclature of Leake (1978). They show euhedral to anhedral outlines and may be partly altered to chlorite and magnetite. They may occur as poikiloblastic crystals enclosing clinopyroxenes and show 120° triple points.

Websterite sample

The single websterite sample is a fine-grained cumulate (<1 mm) made up mainly of colourless clinopyroxene and orthopyroxene (Fig. 6.10). These pyroxenes are largely anhedral, and may contain haematite inclusions and exhibit kink banding. Clinopyroxenes are slightly altered to chlorite whereas orthopyroxenes are totally or partly pseudomorphed by chlorite/serpentine. Rare Fe sulphides are present.

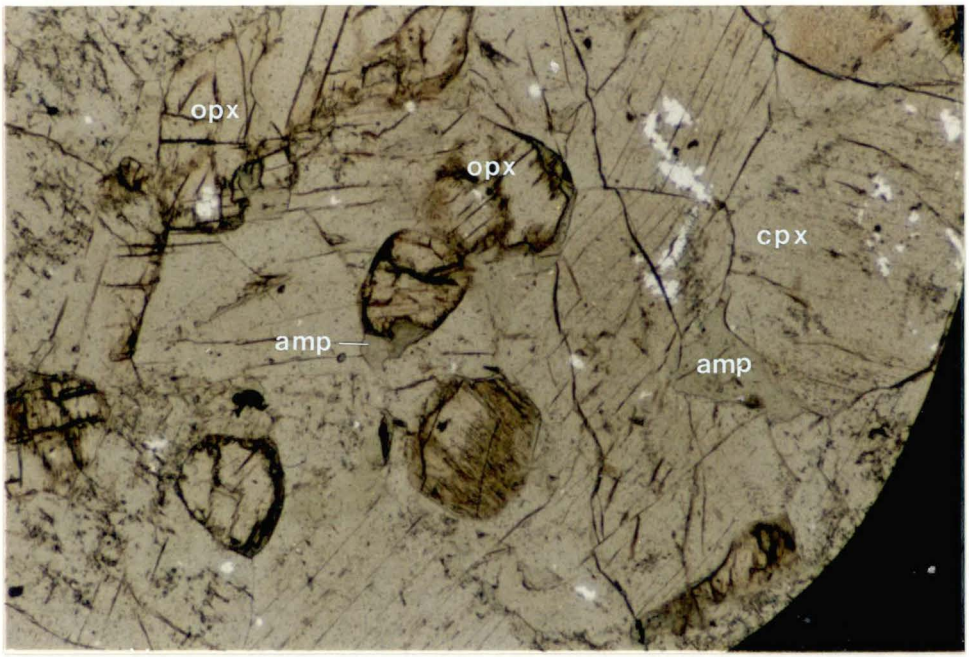

Figure 6.10. Photomicrograph of websterite (sample 47.3A) showing relict cumulus texture and major constituents (cpx, clinopyroxene; opx, orthopyroxene). Both pyroxenes are slightly replaced by amphibole (amp). Ordinary light, x65.

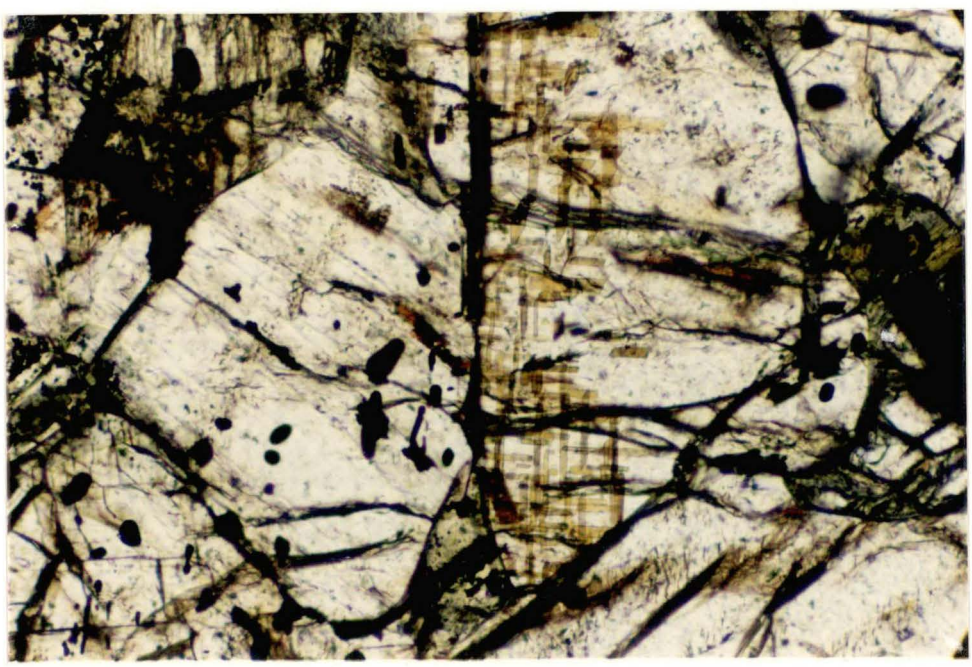

Figure 6.11. Photomicrograph of olivine clinopyroxenite (sample 8.1A) illustrating spinel lamellae and inclusions in clinopyroxene crystals. Ordinary light, x130.

Olivine clinopyroxenites and wehrlites

Olivine clinopyroxenites and wehrlites show variable textures from equigranular to inequigranular with grainsizes ranging from fine (<1 mm) to coarse (5 mm). Foliation defined by olivine-rich and clinopyroxene-rich lenticular aggregates has also been observed in very few samples. They are made up principally of clinopyroxene and olivine in different proportions. Other minerals present include chlorite/serpentine, magnetite, chromite, amphiboles, orthopyroxene, talc, Fe sulphides and epidote. Epidote is associated with chlorite in lenticular shaped (possibly sheared) veinlets. Petrographic features of individual samples are given in Table II-8 (Appendix II).

Clinopyroxenes are colourless and largely anhedral. In general, they are slightly altered to chlorite and pale green amphibole (magnesio-hornblende). They may contain chromite lamellae and inclusions that are not uniformly distributed even in a single crystal (Fig. 6.11), and orthopyroxene lamellae. Kink banding has been observed in some crystals. In inequigranular rocks, the smaller clinopyroxene grains locally show triple-junction grain boundaries at 120°.

Olivines are highly fractured and variably altered. Their common alteration products are serpentinite/chlorite and magnetite, and in a few cases, carbonate, talc and colourless amphibole (tremolite ?). They may contain chromite inclusions.

Orthopyroxenes have been observed as lamellae in some clinopyroxene crystals in olivine clinopyroxenite and wehrlite, and as discrete grains in very few wehrlite samples. They are partly replaced by pale green amphibole, particularly at contacts between clinopyroxene and orthopyroxene.

Harzburgites

Harzburgites are variably altered; original constituents were olivine, colourless orthopyroxene and chromite. Their alteration products include chlorite/serpentine, colourless amphibole (tremolite) and magnetite. Talc may occur as an additional secondary product. Petrographic descriptions of individual samples are given in Table II-8 (Appendix II).

Dunites

The studied dunites are largely serpentinised and in very rare cases, amphibolitised. In serpentinised dunites, the major constituent is serpentine with minor or no relict olivine. Other minerals which may occur in small amounts are

magnetite, carbonate and colourless orthoamphibole (tremolite). An amphibolitised dunite consists largely of olivine and colourless amphibole (anthophyllite)(Fig. 6.12), signifying that it has been metamorphosed at temperatures around 700°C. These minerals are slightly replaced by serpentine and magnetite along grain boundaries and fractures.

6.2.2 Mineral Chemistry

Clinopyroxenes

Clinopyroxenes are present in clinopyroxenites, olivine clinopyroxenites, wehrlites and a websterite sample. Their chemical compositions are reported in Tables 6.5, 6.6, 6.7 and 6.8, respectively.

They are almost diopsidic according to the Subcommittee on Pyroxenes, I.M.A. (1988). Their Mg# values are relatively high and have a limited range (0.79-0.94). The Mg# values for clinopyroxenes in clinopyroxenites, olivine clinopyroxenites and werhlites attain higher values than those for a websterite sample but also span the range recorded in the websterite clinopyroxenes. Clinopyroxenes fall between the trends extrapolated from the solidus and subsolidus trends of the Skaergaard Intrusion (Fig. 6.13), i.e. they have undergone variable degrees of subsolidus re-equilibration, as expected.

In terms of 'Others' components, clinopyroxenes in clinopyroxenites and olivine clinopyroxenites show broadly positive relationships between Al^{vi} and Al^{iv} with similar Al^{vi}/Al^{iv} (Fig. 6.5b,c), suggesting that Al^{vi}-Al^{iv} pair is the most important 'Others' coupled substitution and that clinopyroxenites and olivine clinopyroxenites are probably comagmatic. Moreover, these Al^{vi}/Al^{iv} are comparable to those of gabbros and amphibolites (Fig. 6.5d). This also suggests that the clinopyroxenites, olivine clinopyroxenites, and gabbros (and amphibolites) are probably broadly comagmatic. Although Al^{vi} and Al^{iv} in clinopyroxenes in wehrlites do not define a collinear relationship, wehrlites are interpreted to be co-magmatic with the foregoing discussed mafic-ultramafic rocks since they are interlayered with olivine clinopyroxenites in the Doi Phuk Sung area. As for the clinopyroxenes in gabbros and amphibolites, clinopyroxenes in all ultramafic rocks fall well within the field of arc cumulates of Loucks (1990)(Fig. 6.6)

(a)

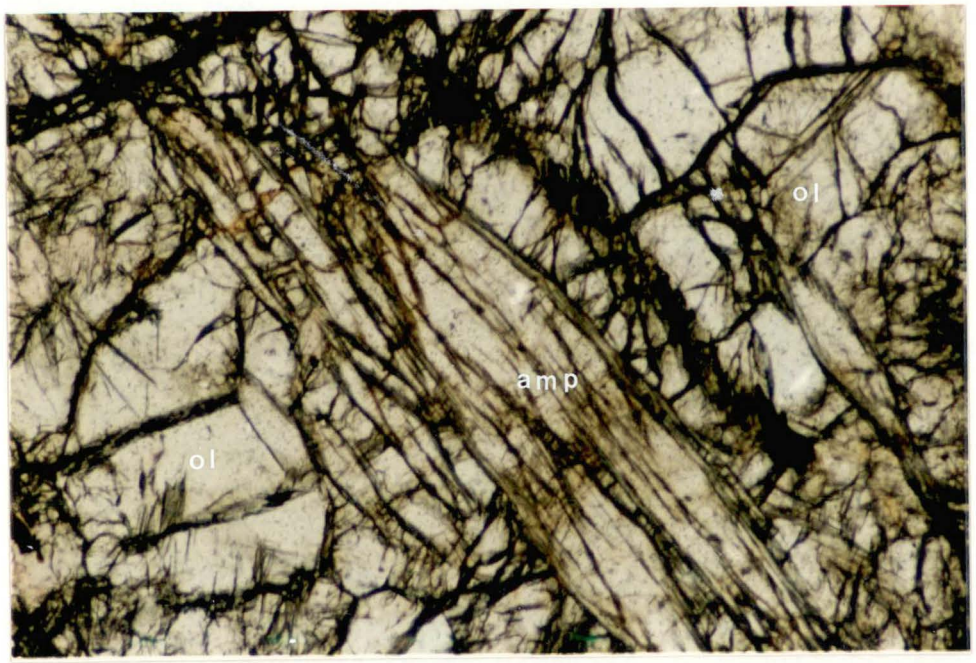

(b)

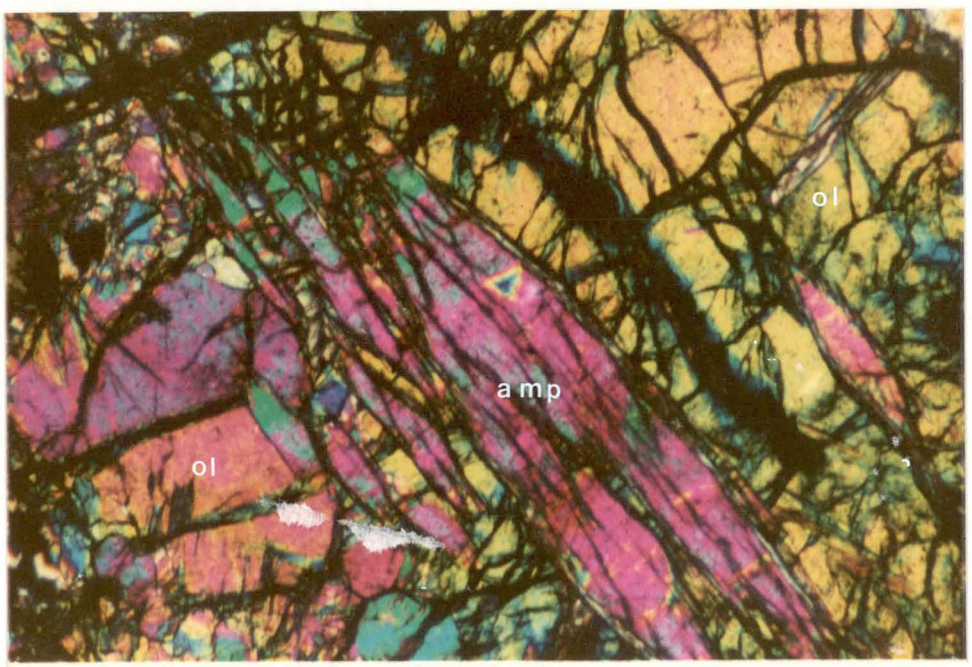

Figure 6.12. Photomicrograph of amphibolitised dunite displaying pervasive replacement of olivine (ol) by amphibole (amp). Sample 64.1, (a) ordinary light, (b) crossed polars, x65.

TABLE 6.5. ELECTRON MICROPROBE ANALYSES OF CLINOPYROXENES IN CLINOPYROXENITES. FeO AND Fe_2O_3 ARE CALCULATED ASSUMING STOICHIOMETRY ON THE BASIS OF 4 CATIONS AND 6 OXYGENS. END-MEMBERS IN TERMS OF WOLLASTONITE, ENSTATITE AND FERROSILITE ARE CALCULATED ACCORDING TO THE METHOD RECOMMENDED BY THE SUBCOMMITTEE ON PYROXENES, IMA (1988).

Sample no.	9 6									10.3						
Anal. no	1	2	3	4	5	6	7	8	9	1	2	3	4	5	6	7
SiO2	51.75	51.47	52.49	52.73	52.76	52.14	52.20	52.31	52.57	54.70	53.81	53.14	53.44	52.78	52.63	53.66
TiO2	0.40	0.37	0.30	0.26	0.19	0.50	0.35	0.46	0.33	-	-	-	0.21	-	0.22	-
Al2O3	3.01	3.41	2.41	2.31	1.79	3.00	2.96	3.02	3.10	0.93	1.58	1.83	2.09	2.02	2.17	1.65
Cr2O3	0.20	0.25	0.31	0.23	0.23	0.33	-	0.36	0.29	-	-	-	0.26	-	0.25	-
Fe2O3	0.89	0.72	-	-	-	-	-	0.79	1.36	-	0.73	0.41	1.11	0.38	0.36	0.61
FeO	5.59	5.81	6.19	6.26	6.13	6.71	6.39	5.91	5.44	4.20	4.34	4.34	3.82	4.29	4.42	4.30
MgO	13.97	14.08	14.27	14.28	14.29	14.01	13.96	13.97	14.27	16.63	16.54	16.11	16.56	15.94	15.92	16.46
CaO	23.68	22.86	23.62	23.86	24.15	23.91	23.40	23.66	23.82	24.41	23.82	23.80	24.00	23.74	23.68	23.83
Na2O	0 30	0 37	-	-	-	-	0.25	0 40	0.38	-	-	-	-	-	-	-
Total	99.79	99.34	99.59	99 93	99.54	100.60	99.51	100.88	101.56	100.87	100.82	99.63	101.49	99.15	99.65	100.51
Si	1.919	1.914	1.946	1.950	1.960	1.921	1.938	1.920	1.915	1.983	1.956	1.955	1.931	1.951	1.938	1.956
ivAl	0.081	0.086	0.054	0.050	0.040	0.079	0.062	0.080	0.085	0.017	0.044	0.045	0.069	0.049	0.062	0.044
Total tetra	2.000	2.000	2.000	2.000	2.000	2.000	2.000	2.000	2.000	2.000	2.000	2.000	2.000	2.000	2.000	2.000
viAl	0 050	0.064	0 052	0.050	0.038	0.051	0.067	0 051	0 048	0.023	0.024	0 034	0.020	0.039	0.033	0 027
Ti	0 011	0.010	0.008	0.007	0 005	0.014	0.010	0.013	0.009	-	-	-	0.006	-	0.006	-
Cr	0.006	0 007	0 009	0.007	0.007	0 010	-	0.010	0.008	-	-	-	0.007	-	0.007	-
Fe3+	0.025	0.020	-	-	-	-	-	0 022	0.037	-	0.020	0.011	0.030	0.011	0.010	0.017
Fe2+	0.173	0.181	0.192	0.194	0.190	0.207	0.198	0.182	0.166	0.127	0 132	0.134	0.116	0.133	0.136	0.131
Mg	0.772	0.781	0.789	0.787	0.791	0.769	0.773	0 764	0.775	0.899	0.896	0.883	0.892	0.878	0.874	0.894
Total octa.	1.037	1.063	1.049	1.045	1.032	1 051	1 048	1.041	1.043	1.049	1.072	1.062	1.071	1.060	1.066	1.069
Ca	0 941	0.911	0.939	0.945	0.961	0.944	0.931	0.930	0.930	0.948	0.928	0.938	0.929	0.940	0.934	0.931
Na	0 022	0.026	-	-	-	-	0 018	0.028	0 027	-	-	-	-	-	-	-
Total cat.	4.000	4.000	3.988	3.990	3 993	3.995	3.997	4.000	4.000	3.997	4.000	4 000	4.000	4.000	4.000	4.000
$Mg/(Mg+Fe^{2+})$	0 817	0 812	0.804	0.803	0.806	0.788	0.796	0.808	0.824	0.876	0.872	0.869	0.885	0.869	0.865	0.872
Wo	49.23	48.13	48.91	49.08	49.47	49.16	48.95	49.02	48.74	48.04	46.96	47.70	47.24	47.93	47.81	47.17
En	40 40	41.25	41.09	40.87	40.73	40.07	40.63	40.27	40 61	45.51	45.36	44 93	45.35	44.76	44.71	45 33
Fs	10.37	10.62	10.00	10.05	9.80	10 77	10.43	10.71	10.65	6.44	7.69	7.37	7.41	7.30	7 48	7 49

Sample no.	10 3			19.2						19.3		40.1A		44.1		
Anal. no	8	9	10	1	2	3	4	5	6	1	2	1	2	1	2	3
SiO2	54.28	53.19	53.69	54.09	51.77	53.30	54.22	52.98	54.34	52.83	53.38	55.17	54.77	55.27	54.40	54.39
TiO2	-	-	0.18	-	-	0.18	-	0.21	-	-	0.17	-	-	-	-	-
Al2O3	1.45	2.27	2.19	1 92	4 93	2.12	1.05	1 98	1 24	1.93	2.02	0 29	0.58	0.50	0.99	1.14
Cr2O3	0.22	0.22	-	0.26	0 27	0.48	0.22	0.23	-	0.24	0.33	-	-	-	0.30	0.34
Fe2O3	0.14	0.72	0.50	-	1.03	-	-	0.19	-	0.67	-	-	-	-	0.39	0 28
FeO	4.60	4.30	4.48	4.23	4 73	4.72	4.65	4.85	4 75	3.82	4.94	3 23	3.37	2.18	2.37	2.45
MgO	16.58	16.25	16.48	16 26	16.30	16.27	16.57	15.97	16.59	16.01	15.96	16.97	16.74	17.34	17.20	17 08
CaO	24.01	23.69	23.81	24.11	20 62	23.52	23.75	23.59	23.37	24.05	23.58	25.00	25.19	25.40	25.00	25.09
Na2O	-	-	-	-	0 37	-	-	-	-	-	-	-	-	-	-	-
Total	101.28	100.64	101.33	100.87	100.02	100 59	100 46	100.00	100.29	99.55	100.38	100.66	100.65	100.69	100.65	100 65
Si	1.964	1.938	1.942	1.961	1.889	1.943	1.977	1.946	1.981	1.945	1.951	1.998	1.998	1.994	1.969	1.967
ivAl	0 036	0 062	0.058	0.039	0.111	0.057	0.024	0.055	0.019	0.055	0.049	0.002	0.012	0.006	0.031	0.033
Total tetra	2.000	2.000	2.000	2.000	2.000	2.000	2 000	2 000	2.000	2 000	2.000	2.000	2.000	2.000	2.000	2.000
viAl	0 026	0 036	0.035	0.043	0.101	0.034	0.022	0.031	0 034	0 029	0.038	0 011	0 013	0.015	0.011	0.016
Ti	-	-	0 005	-	-	0.005	-	0.006	-	-	0.005	-	-	-	-	-
Cr	0.006	0 006	-	0.007	0.008	0.014	0.006	0.007	-	0.007	0.010	-	-	-	0.009	0.010
Fe3+	0.004	0.020	0.014	-	0.028	-	-	0 005	-	0.019	-	-	-	-	0.009	0.010
Fe2+	0.139	0.131	0.135	0.128	0.144	0.144	0.141	0.149	0.145	0.118	0.151	0.098	0.102	0.066	0.072	0.074
Mg	0 894	0.883	0.888	0.879	0.887	0.884	0.900	0.874	0.901	0.879	0.870	0.916	0.906	0.932	0.928	0.921
Total octa.	1.069	1.075	1.077	1.058	1.168	1 081	1.070	1.072	1.080	1.051	1.073	1.025	1.020	1.014	1.030	1.028
Ca	0.931	0.925	0.923	0.937	0.806	0.919	0.928	0.928	0.913	0.949	0.923	0.970	0.980	0.982	0.970	0.972
Na	-	-	-	-	0.026	-	-	-	-	-	-	-	-	-	-	-
Total cat.	4.000	4.000	4.000	3.994	4.000	4.000	3.998	4 000	3.993	4.000	3.996	3.995	4.000	3.995	4.000	4.000
$Mg/(Mg+Fe^{2+})$	0 865	0.871	0.868	0.873	0 860	0.860	0.864	0.854	0.862	0.882	0 852	0.903	0.898	0.934	0.928	0.926
Wo	47.31	47.24	47.08	48.18	43.21	47.20	47.11	47.44	46.59	48.32	47.49	48.90	49.29	49.58	48.97	49.24
En	45.43	45.07	45 32	45.21	47.53	45.41	45.71	44.69	46.02	44.75	44.74	46 16	45.56	47 09	46.88	46.63
Fs	7.26	7.69	7.60	6 61	9 26	7.39	7.18	7 88	7.39	6.94	7.77	4 94	5.15	3.33	4 15	4.13

TABLE 6.5. CONTINUED

Sample no.	44.1				57.2								R			
Anal. no.	4	5	6	7	1	2	3	4	5	6	7	8	1	2	3	4
SiO2	54.26	54.28	55.01	53.99	53.96	53.49	53.82	53.08	53.86	54.01	53.02	53.27	55.58	55.21	55.48	55.63
TiO2	-	-	-	-	-	0.19	-	-	0.22	0.18	0.23	-	-	-	-	-
Al2O3	0.90	0.70	0.75	0.92	1.39	2.25	2.58	2.12	2.43	2.50	2.56	2.56	0.42	0.58	0.40	0.46
Cr2O3	0.28	0 21	-	0.27	0.30	0.38	0.41	0.37	0.32	0.52	0.47	0.46	0.23	-	-	-
Fe2O3	0.36	-	0.11	0 31	0.07	0.30	-	-	-	-	-	-	-	-	-	-
FeO	2.19	2.44	2.71	2.35	2.64	2.56	2.75	2.60	2.68	2.65	2.81	2.91	2.25	2.33	2.07	2.29
MgO	17.13	17.01	17.08	16.91	16.77	16.68	16.48	16.45	16.79	16 67	16.38	16.56	17.72	17.54	17.69	17.52
CaO	25.10	25.07	25.47	25 04	24.97	24.86	24.56	24.58	24.32	24.90	24.24	24.32	24.99	24.47	25.27	24.82
Na2O	-	-	-	-	-	-	-	-	-	-	-	-	-	-	-	-
Total	100.22	99.71	101.13	99.79	100.10	100.71	100.60	99.20	100.62	101.43	99.71	100.08	101.19	100.50	101.29	101.07
Si	1.972	1.982	1.983	1.972	1.965	1.937	1.947	1.950	1.946	1.940	1.937	1.940	1.937	1.940	1.994	1.993
ivAl	0.028	0.018	0 018	0.028	0.035	0.063	0.053	0.051	0.054	0.060	0.063	0.061	0.006	0.007	0.010	0.003
Total tetra.	2.000	2.000	2.000	2.000	2.000	2.000	2.000	2.000	2.000	2.000	2.000	2.000	2.000	2.000	2.000	2.000
viAl	0.010	0.013	0.015	0.012	0 025	0.033	0 057	0.041	0.050	0.046	0.048	0.049	0.012	0 018	0.007	0 017
Ti	-	-	-	-	-	0.005	-	-	0.006	0.005	0.006	-	-	-	-	-
Cr	0.008	0.006	-	0.008	0.009	0 011	0.012	0.011	0.009	0.015	0.014	0 013	0.007	0.011	0.011	0.010
Fe3+	0.010	-	0.003	0.009	0 002	0.008	-	-	-	-	-	-	-	-	-	-
Fe2+	0.066	0.075	0 082	0 072	0.080	0 077	0.083	0.080	0.081	0 080	0.086	0.089	0.067	0.070	0.062	0.069
Mg	0.928	0.926	0.918	0.920	0.910	0.900	0.889	0.900	0.904	0.892	0 899	0.948	0.944	0.946	0.938	0.944
Total octa.	1.023	1.019	1.017	1.020	1.026	1 035	1.041	1.032	1.050	1.037	1.046	1.050	1.033	1.042	1.025	1.033
Ca	0.977	0 981	0.983	0.980	0 974	0.965	0.952	0 967	0.942	0.958	0.949	0 949	0.961	0.947	0.971	0.955
Na	-	-	-	-	-	-	-	-	-	-	-	-	-	-	-	-
Total cat.	4.000	4.000	4 000	4.000	4.000	4.000	3.992	3.999	3.992	3.995	3.994	3.999	3.994	3.989	3.996	3.988
Mg/(Mg+Fe^{2+})	0.933	0.925	0.918	0.928	0.919	0 921	0.914	0.919	0.918	0.918	0.912	0.910	0.934	0.931	0.938	0.932
Wo	49.31	49.50	49.52	49 47	49.53	49.46	49.48	49 66	48.86	49.64	49 25	49.00	48.63	48.29	49.07	48.68
En	46.83	46.73	46.21	46.47	46 29	46.15	46.19	46.24	46.93	46.23	46.30	46.43	47.96	48.13	47.80	47 81
Fs	3.86	3.77	4.27	4 06	4 18	4 39	4 33	4 10	4.21	4 13	4 45	4 58	3.41	3 58	3.13	3 51

Sample no.	R		SC-4												
Anal. no.	5	6	1	2	3	4	5	6	7	8	9	10	11	12	13
SiO2	55.30	55.22	55.00	54.48	54 67	54.46	54 19	54.29	54 08	54 01	53.25	54 74	54.20	53 67	54.79
TiO2	-	-	-	-	-	-	-	-	-	-	-	-	-	-	-
Al2O3	0.50	0.50	0.92	1.30	1.23	0.90	1.29	1.15	1.18	1.25	2.62	1.20	1.24	1 54	1.17
Cr2O3	0.22	-	-	0.35	0 27	0.28	0.25	0.34	0.24	0.34	0.38	0.41	0.39	0.37	0.26
Fe2O3	-	-	-	-	-	-	-	-	-	-	-	-	-	0 66	-
FeO	2.25	2.21	3.21	3.50	3.46	3.10	3.32	3.51	3.37	3.25	3.38	3.50	3.33	3.09	3.41
MgO	17.58	17.81	17.31	17.05	17 02	16.98	17.17	17 16	17.06	16 82	16.56	17 13	16.95	17.38	17.10
CaO	24.90	24.87	24.19	24.38	24.34	24 58	24.08	24 04	23.96	23.86	23.56	24.23	24.17	23.49	24.16
Na2O	-	-	-	-	-	-	-	-	-	-	-	-	-	-	-
Total	100.75	100.61	100 63	101.06	100.99	100 30	100.30	100 49	99 89	99.53	99 75	101.21	100.28	100.20	100.89
Si	1.993	1.992	1.988	1.968	1.974	1.979	1.969	1.971	1.973	1.976	1.944	1.973	1.971	1.953	1.978
ivAl	0 007	0.008	0 013	0 032	0.026	0.021	0.031	0.029	0 027	0.024	0.056	0.027	0.029	0.047	0.022
Total tetra.	2.000	2 000	2.000	2.000	2.000	2.000	2.000	2.000	2.000	2.000	2.000	2.000	2 000	2.000	2.000
viAl	0 014	0 013	0.027	0.023	0.026	0.018	0.024	0 020	0.024	0 030	0 057	0.024	0 024	0.019	0.028
Ti	-	-	-	-	-	-	-	-	-	-	-	-	-	-	-
Cr	0.006	-	-	0.010	0 008	0.008	0.007	0.010	0.007	0.010	0.011	0 012	0.011	0 011	0.008
Fe3+	-	-	-	-	-	-	-	-	-	-	-	-	-	0.018	-
Fe2+	0 068	0.067	0.097	0.106	0.104	0.094	0.101	0.107	0.103	0.099	0.103	0.105	0.101	0.094	0.103
Mg	0.944	0.957	0.932	0.918	0.916	0.920	0.930	0 929	0 928	0 917	0.901	0.920	0.919	0.943	0.920
Total octa.	1.032	1.037	1.056	1.056	1.055	1.040	1.062	1 065	1.062	1.057	1.072	1.061	1.055	1.084	1.059
Ca	0.961	0.961	0.937	0.944	0.942	0.957	0.937	0.935	0.936	0.935	0.922	0.935	0.942	0.916	0.934
Na	-	-	-	-	-	-	-	-	-	-	-	-	-	-	-
Total cat.	3.993	3.998	3.993	4.000	3.996	3 997	4.000	4.000	3.998	3.992	3.994	3.996	3.997	4.000	3.993
Mg/(Mg+Fe^{2+})	0.933	0.935	0.906	0 897	0.898	0.907	0.902	0.897	0 900	0 902	0.897	0.897	0.901	0.909	0.899
Wo	48.71	48.41	47.64	47.97	47 98	48.55	47.63	47 46	47.60	47 92	47.85	47.70	48.01	46.47	47.72
En	47.85	48.23	47.42	46.66	46.69	46.67	47 24	47.13	47.17	46.98	46.79	46 93	46.83	47.83	47.01
Fs	3.44	3.36	4.94	5 37	5.32	4.78	5.13	5.42	5.23	5 09	5.36	5.37	5.16	5.69	5.27

- = BELOW DETECTION LIMITS.

TABLE 6 6. ELECTRON MICROPROBE ANALYSES OF CLINOPYROXENES IN OLIVINE CLINOPYROXENITES. FeO AND Fe_2O_3 ARE CALCULATED ASSUMING STOICHIOMETRY ON THE BASIS OF 4 CATIONS AND 6 OXYGENS. END-MEMBERS IN TERMS OF WOLLASTONITE, ENSTATITE AND FERROSILITE ARE CALCULATED ACCORDING TO THE METHOD RECOMMENDED BY THE SUBCOMMITTEE ON PYROXENES, IMA (1988).

Sample no.	8.1A											
Anal. no.	1	2	3	4	5	6	7	8	9	10	11	12
SiO2	53.95	53.08	53.80	53 65	53.61	53.74	53.79	53.72	53.80	54.05	53.97	53.54
TiO2	-	-	-	-	-	-	-	-	-	-	-	-
Al2O3	1.69	1.95	1.89	1.84	1.74	1.76	1.92	1.98	1.77	1.73	1.54	1.74
Cr2O3	0 50	0.54	0.50	0.50	0.38	0.44	0.53	0.57	0 50	0.32	0.35	0.46
Fe2O3	0.24	0.41	0.28	0.90	0.04	-	-	-	-	-	0.02	-
FeO	3.68	3.20	3.16	2.43	3.37	3.51	3.37	3.51	3 29	3.22	3.15	3.01
MgO	16.87	16.55	16.97	17.05	16.61	17.02	16.56	16 62	16.75	16.86	16.90	16.77
CaO	24.00	24.02	24.14	24 46	24 30	23.66	23 87	23 81	24.12	24.31	24.40	24 14
Total	100.93	99.75	100.74	100 83	100.05	100.13	100.04	100.21	100.23	100.49	100.33	99.66
Si	1.954	1.944	1.949	1.941	1.957	1.957	1.960	1.955	1.958	1.961	1.962	1.958
ivAl	0.047	0.056	0.051	0.059	0.044	0.043	0.040	0.045	0.042	0.039	0.038	0.042
Total tetra.	2.000	2.000	2.000	2.000	2.000	2.000	2.000	2.000	2.000	2.000	2.000	2.000
viAl	0.026	0.029	0.029	0.020	0.031	0.033	0.042	0.040	0 034	0.035	0.028	0.033
Ti	-	-	-	-	-	-	-	-	-	-	-	-
Cr	0.014	0.016	0.014	0.014	0 011	0.013	0.015	0.016	0.014	0.009	0.010	0.013
Fe3+	0.007	0.011	0 008	0.025	0.001	-	-	-	-	-	0.001	-
Fe2+	0.112	0.098	0.096	0 074	0.103	0.107	0.103	0.107	0.100	0.098	0.096	0.092
Mg	0.911	0.904	0.916	0.920	0 903	0.924	0 899	0 902	0.908	0.911	0.916	0.914
Total octa	1.069	1.057	1.063	1.052	1.050	1.076	1.059	1.065	1 057	1.053	1.050	1.052
Ca	0.931	0.943	0.937	0 948	0.950	0 923	0 932	0.929	0 941	0 945	0.950	0.946
Total cat.	4.000	4.000	4 000	4 000	4.000	3.999	3.991	3.994	3 997	3.998	4.000	3.998
Mg/(Mg+Fe^{2+})	0.891	0.902	0 906	0.926	0 898	0 896	0.898	0.894	0.901	0.903	0 905	0.908
Wo	47.51	48.21	47.89	48.24	48.54	47.25	48 19	47.95	48.25	48.36	48.43	48.46
En	46.46	46.20	46.83	46.77	46.15	47.28	46.50	46.53	46.61	46.63	46.66	46.82
Fs	6 03	5.59	5.29	4 99	5.31	5.47	5.31	5 52	5.14	5.00	4 91	4.72

Sample no.	8 1A			52.2					S-11A			
Anal. no.	14	15	16	1	2	3	4	5	1	2	3	4
SiO2	53.67	53.48	53.81	54.98	54 83	54.86	54.82	54.45	53.13	51.95	54.03	54.17
TiO2	-	-	-	-	-	-	-	-	-	0.29	-	-
Al2O3	1.93	1.66	1.79	0.31	0.52	0.60	0.75	0 83	2.79	3.09	1.57	1.47
Cr2O3	0.42	0.50	0.41	0.20	-	0 23	0.21	0.22	0.35	0.62	0.27	-
Fe2O3	0.12	0.27	0.72	-	0.16	0.53	0.37	0.21	0.76	1.49	0.38	0 58
FeO	3.23	3.05	2.95	2.46	2.59	2.32	2.57	2.78	4.13	4 34	4 04	3.30
MgO	16.76	16.98	16.96	17.04	17.04	17.16	17.21	16.89	15 65	15.48	16.53	16.56
CaO	24.25	23.91	24 33	25 63	25 44	25.51	25.22	25.15	24 59	23 77	24 27	24.95
Total	100 38	99.85	100.97	100.62	100.58	101.21	101.15	100.53	101.40	101.03	101.09	101.03
Si	1.951	1.953	1.946	1.991	1.987	1.977	1.976	1.976	1.925	1.896	1.958	1.961
ivAl	0.049	0.047	0 054	0.009	0.013	0.023	0.024	0.024	0.075	0.104	0 043	0.039
Total tetra.	2.000	2.000	2.000	2.000	2.000	2.000	2.000	2.000	2 000	2.000	2.000	2.000
viAl	0.034	0.025	0 023	0 004	0 009	0 002	0.008	0.012	0.044	0.029	0.024	0 023
Ti	-	-	-	-	-	-	-	-	-	0.008	-	-
Cr	0.012	0.014	0.012	0 006	-	0 007	0.006	0 006	0.010	0.018	0.008	-
Fe3+	0.003	0.007	0.020	-	0.005	0.014	0 010	0.006	0.021	0 041	0.010	0.016
Fe2+	0.098	0.093	0.089	0.075	0 079	0 070	0.077	0 084	0.125	0.132	0.123	0.100
Mg	0.908	0.924	0 914	0.920	0 921	0.922	0.925	0 914	0.845	0.842	0.893	0 893
Total octa.	1.056	1.064	1.057	1.005	1 013	1 015	1.026	1.022	1.046	1.070	1.058	1.032
Ca	0 945	0.936	0 943	0.995	0 988	0 985	0 974	0 978	0 954	0 930	0 942	0 968
Total cat.	4.000	4 000	4.000	3.999	4 000	4.000	4.000	4.000	4.000	4 000	4.000	4.000
Mg/(Mg+Fe^{2+})	0.902	0 908	0.911	0 925	0.921	0.929	0.923	0.915	0.871	0.864	0.879	0.900
Wo	48.33	47.73	47 97	50.00	49 60	49.46	49.03	49.34	49.05	47.79	47 88	48.95
En	46.47	47.14	46.51	46.25	46.23	46.30	46.57	46 11	43.44	43.30	45 37	45.19
Fs	5.19	5.13	5 52	3.75	4.17	4 24	4 40	4 55	7 50	8.91	6 75	5.85

Sample no.	S										
Anal. no.	1	2	3	4	5	6	7	8	9	10	11
SiO2	53.45	53.70	53.82	53.83	53 66	53.94	53.94	53.47	54.02	53.46	53.98
TiO2	-	-	-	-	-	-	-	-	-	-	-
Al2O3	1.18	1.23	1.10	1.13	1.20	1.23	1.38	1.41	1.38	1.39	0.96
Cr2O3	0.21	0.24	0.33	0.23	-	0.29	0.31	0.21	0.19	0.25	0.28
Fe2O3	0.07	-	0.49	-	-	0.22	0.34	0.72	-	0.52	0.35
FeO	3.57	3.54	2.76	3.63	3 41	3.28	3.26	2.98	3 54	3 05	2.81
MgO	16.86	16.74	17.27	16.88	16 87	17.16	17 06	17.13	17.26	16.97	17 09
CaO	23.65	24.02	24.05	23 91	23.90	23.91	24 07	23 75	23 43	23.90	24 42
Total	98.99	99.47	99 82	99.61	99 04	100.03	100.36	99.67	99.82	99.54	99.89
Si	1.971	1.971	1.965	1.973	1.975	1.967	1.962	1.957	1.971	1.959	1.971
ivAl	0.030	0.029	0.035	0.027	0.025	0.033	0.039	0.043	0.030	0.041	0.030
Total tetra.	2.000	2.000	2.000	2.000	2.000	2.000	2.000	2.000	2.000	2.000	2.000
viAl	0.022	0 024	0 012	0.021	0 027	0.019	0.020	0.018	0.030	0.019	0.012
Ti	-	-	-	-	-	-	-	-	-	-	-
Cr	0.006	0.007	0.010	0 007	-	0.008	0.009	0.006	0.006	0.007	0.008
Fe3+	0.002	-	0.014	-	-	0.006	0.009	0.020	-	0.014	0.010
Fe2+	0.110	0.109	0 084	0.111	0.105	0.100	0 099	0.091	0 108	0 093	0.086
Mg	0.926	0.916	0.940	0 922	0.925	0.933	0.925	0 934	0.938	0 927	0 930
Total octa.	1.066	1 055	1.060	1.061	1.057	1.066	1.063	1.069	1.082	1.061	1.045
Ca	0.934	0.944	0 941	0.939	0 942	0.934	0 938	0.931	0 916	0 939	0.955
Total cat.	4.000	3.999	4.000	4.000	3 999	4 000	4 000	4.000	3.997	4 000	4.000
Mg/(Mg+Fe^{2+})	0.894	0.894	0.918	0.892	0.898	0.903	0 903	0.911	0.897	0.908	0 916
Wo	47.37	47.98	47.54	47.60	47.77	47 35	47.57	47.11	46.66	47.56	48.22
En	46.96	46.51	47 51	46.75	46.92	47.28	46.93	47 27	47.83	46.98	46.96
Fs	5 67	5 52	4 95	5 64	5.32	5.37	5.50	5 62	5.51	5.45	4 81

- = BELOW DETECTION LIMIT.

TABLE 6.7. ELECTRON MICROPROBE ANALYSES OF CLINOPYROXENES IN WEHRLITES
FeO AND Fe_2O_3 ARE CALCULATED ASSUMING STOICHIOMETRY ON THE BASIS OF 4 CATIONS AND 6 OXYGENS.
END-MEMBERS IN TERMS OF WOLLASTONITE, ENSTATITE AND FERROSILITE ARE CALCULATED ACCORDING TO
THE METHOD RECOMMENDED BY THE SUBCOMMITTEE ON PYROXENES, IMA (1988).

Sample no	8 1					8 3				8 4				8.5		
Anal. no.	1	2	3	4	5	1	2	3	4	1	2	3	4	1	2	3
SiO2	53 62	54.27	53.95	54.04	53.64	53.27	53.15	54.11	53.26	53.85	53.68	53.35	52.98	54.06	53.58	54.14
TiO2	-	-	-	-	-	-	-	-	-	-	-	-	-	-	-	-
Al2O3	1.74	1.48	1.49	1.62	1.53	1.79	1.89	1.58	1.57	1.58	1.81	1.62	1.67	1.66	1.62	1.19
Cr2O3	0.47	0.31	0.36	0.48	0.41	0.51	0.48	0.29	0.37	0.42	0.64	0.37	0.32	0.44	0.34	0.29
Fe2O3	0.04	0.18	0 06	-	0.64	0.13	0.15	-	0.51	-	0.09	0.44	0.77	0.44	0.43	0.43
FeO	3.27	3.10	3.09	3.22	2.45	2.96	2.99	3.41	2.60	3.07	3.35	2.67	2.81	3.46	2.75	2.62
MgO	16.98	17.21	17.25	17.06	17.33	17 02	16.96	17.35	17.11	16.47	16.76	17.78	16.97	17.65	16.89	17.12
CaO	23.88	24.29	23.94	24.19	24.05	23.73	23.68	23.60	23.88	24.38	24.18	22.98	23.65	23.20	24.37	24.67
Na2O	-	-	-	-	-	-	-	-	-	-	-	-	-	-	-	-
Total	100.00	100.84	100.14	100.61	100.05	99.41	99.30	100.34	99.30	99.77	100.51	99.21	99.17	100.91	99.98	100.46
Si	1.955	1.962	1.962	1.959	1.953	1.952	1.950	1.964	1.954	1.967	1.951	1.954	1.949	1.952	1.954	1.965
ivAl	0.045	0.038	0.038	0.042	0.047	0.048	0.050	0 037	0.046	0.033	0.049	0.046	0 052	0.048	0.046	0.036
Total tetra.	2.000	2.000	2.000	2.000	2.000	2.000	2.000	2.000	2.000	2.000	2.000	2.000	2.000	2.000	2.000	2.000
viAl	0.030	0 025	0.026	0.028	0.018	0.029	0.032	0.031	0.021	0.035	0.028	0.024	0.021	0.023	0.024	0.015
Ti	-	-	-	-	-	-	-	-	-	-	-	-	-	-	-	-
Cr	0.014	0.009	0.010	0 014	0.012	0.015	0.014	0.008	0.011	0.012	0.019	0.011	0.009	0 012	0.010	0.008
Fe3+	0 001	0.005	0.002	-	0 018	0.004	0.004	-	0.014	-	0 002	0.012	0.021	0.012	0.012	0 012
Fe2+	0.100	0 094	0 094	0.098	0.075	0 091	0.092	0.103	0.080	0 094	0.102	0.082	0 087	0.105	0.084	0.080
Mg	0 923	0.927	0.935	0.922	0 940	0.930	0.928	0.938	0.935	0.897	0.908	0.970	0.930	0.950	0.918	0.926
Total octa	1.067	1.059	1.067	1.061	1 062	1.068	1.069	1 081	1.062	1 038	1.058	1.099	1.068	1.102	1.048	1.041
Ca	0.933	0.941	0.933	0.939	0.938	0.932	0.931	0.917	0.939	0.955	0.942	0.902	0.932	0.898	0.952	0.959
Na	-	-	-	-	-	-	-	-	-	-	-	-	-	-	-	-
Total cat.	4.000	4.000	4.000	4.000	4.000	4.000	4.000	3.999	4.000	3.993	4.000	4.000	4.000	4 000	4.000	4.000
Mg/(Mg+Fe^{2+})	0.903	0.908	0.909	0.904	0.926	0.911	0.910	0.901	0.921	0.905	0 899	0 922	0.915	0.901	0.916	0.921
Wo	47.71	47.96	47.55	47.95	48.03	47.73	47.74	46 83	48.04	49.08	48.26	46.14	47.83	45.98	48.73	48.83
En	47.19	47.26	47 66	47.06	48.15	47 62	47.56	47.89	47.88	46.09	46.52	49.67	47.73	48.67	46.98	47.13
Fs	5.09	4 78	4 80	4.98	3.82	4.65	4 70	5.28	4.08	4.82	5.21	4.19	4.44	5.35	4.30	4 05

Sample no	8.5		8.7A							YP-5						
Anal. no	4	5	1	2	3	4	5	6	7	1	2	3	4	5	6	7
SiO2	53.87	53.19	54.08	54.45	54.89	55.03	55.66	55.33	54.38	54.50	54.81	54.79	55.02	54 63	53.89	53.58
TiO2	-	0.22	-	-	-	-	-	-	-	-	-	-	-	-	-	-
Al2O3	1.66	1.97	1.12	0.78	0.92	1.19	0.46	0.31	0 81	0.95	1.08	1.38	1.40	1.10	1.05	1.23
Cr2O3	0.43	0 53	0.33	0.38	0.39	0.27	0.30	0.21	0 30	0.24	0.33	0.43	0.43	0.42	0 41	0.36
Fe2O3	-	0.77	-	-	-	-	-	-	-	-	-	-	-	-	-	-
FeO	3.42	2.79	2.10	2.13	2.27	2.25	2.13	2.15	2.32	2.58	2.37	2.79	2.76	2.49	2.48	2.62
MgO	16.75	17.17	17.64	17.17	17.51	17.65	17.87	17 71	17.34	16.70	17.02	17.27	17.55	17.35	17.00	17.04
CaO	24.18	23.73	23.73	24.63	24.29	24.56	24.82	24 68	24 68	23 88	24 63	24.33	23.94	24.56	24.24	24.26
Na2O	-	-	-	-	-	-	-	-	-	0.36	-	-	-	-	-	-
Total	100.31	100 37	99 00	99.54	100.27	100 95	101 24	100 39	99.83	99 21	100 24	100 99	101.10	100.55	99.07	99.09
Si	1.960	1.934	1.978	1.986	1.985	1.977	1.994	1.999	1.980	1.995	1.985	1.973	1.975	1.975	1.978	1 968
ivAl	0.040	0.066	0.022	0.014	0.015	0.023	0 006	0.001	0.020	0 005	0.015	0.028	0 025	0.025	0.022	0 032
Total tetra.	2.000	2 000	2.000	2.000	2.000	2.000	2.000	2.000	2 000	2.000	2.000	2.000	2.000	2.000	2.000	2.000
viAl	0.031	0.018	0.027	0.020	0 025	0 028	0.013	0.012	0.015	0.036	0.031	0.031	0 034	0.022	0.023	0 022
Ti	-	0.006	-	-	-	-	-	-	-	-	-	-	-	-	-	-
Cr	0.012	0 015	0.010	0.011	0 011	0.008	0 009	0.006	0.009	0.007	0.010	0.012	0 012	0.012	0 012	0 010
Fe3+	-	0.021	-	-	-	-	-	-	-	-	-	-	-	-	-	-
Fe2+	0.104	0.085	0.064	0.065	0.069	0.068	0.064	0.065	0.071	0.079	0.072	0.084	0 083	0.075	0.076	0.081
Mg	0.908	0 930	0.962	0.934	0 944	0.946	0.954	0.954	0.941	0.911	0.919	0.926	0.939	0.935	0.930	0 933
Total octa	1.056	1 076	1.063	1.029	1.048	1 048	1.040	1.037	1.035	1.032	1 031	1.054	1.069	1.044	1.041	1 046
Ca	0.943	0.925	0.930	0.963	0.941	0.945	0.953	0 955	0.963	0.936	0.956	0.938	0.921	0 951	0.953	0 955
Na	-	-	-	-	-	-	-	-	-	0 025	-	-	-	-	-	-
Total cat.	3 998	4.000	3.993	3.992	3.990	3.994	3.993	3.992	3.998	3 994	3.987	3 992	3.989	3.995	3.994	4.000
Mg/(Mg+Fe^{2+})	0.897	0.916	0.937	0.935	0.932	0.933	0.937	0.936	0.930	0.920	0.928	0.917	0.919	0.925	0.924	0.921
Wo	48.22	47.66	47.54	49.08	48.17	48.27	48.33	48.39	48.76	48.62	49.11	48.16	47 39	48.50	48.64	48.50
En	46.46	47.96	49.17	47.60	48 31	48.28	48.42	48.32	47.67	47.29	47.22	47 54	48 34	47.66	47.47	47.41
Fs	5.33	4.38	3.29	3 32	3.52	3.46	3.25	3.29	3.57	4 10	3.67	4 31	4.27	3.84	3.88	4 09

Sample no	YP-5	Y-7				SC-6			Q				
Anal. no	8	1	2	3	4	5	1	2	3	4	5	1	2	3	4
SiO2	54.99	54.48	54.64	54.84	54.25	54.66	54.21	54 47	54 59	54.38	53.63	53.79	53.68	53.27	53.86
TiO2	-	-	-	-	-	-	-	-	-	-	-	-	-	-	-
Al2O3	1.00	0.81	0.89	1.12	1.12	1 02	1.88	1.15	1.26	1.19	1.29	1.78	1.76	1.81	1.82
Cr2O3	0.22	0.36	0.33	0.58	0.53	0.43	0.22	0.23	-	0 24	0.36	0 47	0.46	0 48	0.43
Fe2O3	-	-	-	-	-	-	0.01	-	-	-	0.23	-	-	-	-
FeO	2.55	2.56	2.33	2.64	2.65	2 62	2.68	2.55	2.75	2.54	2.43	3.25	3.46	3.27	3.41
MgO	17.36	17.34	17.35	17.45	17.19	17.44	17.16	17.07	17.45	17.04	17.13	16.69	17 20	16.69	16.75
CaO	24 42	24.55	24.65	24.53	24.30	24.53	24.64	24 91	24.41	24 64	24.33	24 01	23.18	23 83	24.32
Na2O	-	-	-	-	-	-	-	-	-	-	-	-	-	-	-
Total	100.54	100.10	100.19	101.16	100.04	100.70	100.80	100.38	100 46	100.03	99.40	99.99	99.74	99.35	100.59
Si	1.986	1.980	1.981	1.972	1.973	1.975	1.957	1.975	1.975	1.977	1.964	1.961	1 960	1.955	1.955
ivAl	0.015	0.020	0.019	0 028	0.027	0.025	0.043	0.025	0.025	0.023	0.036	0.039	0.041	0.045	0.045
Total tetra.	2.000	2.000	2.000	2.000	2.000	2.000	2.000	2.000	2.000	2.000	2 000	2.000	2.000	2.000	2.000
viAl	0.028	0 014	0 019	0.019	0.021	0.018	0.037	0.024	0 029	0.028	0 019	0.037	0.035	0.034	0 033
Ti	-	-	-	-	-	-	-	-	-	-	-	-	-	-	-
Cr	0.006	0.010	0.010	0.017	0.015	0.012	0.006	0.007	-	0.007	0.011	0.013	0 013	0.014	0.012
Fe3+	-	-	-	-	-	-	0.001	-	-	-	0.007	-	-	-	-
Fe2+	0 077	0.078	0.071	0 080	0.081	0.079	0.081	0 077	0.083	0.077	0.074	0.099	0.106	0.101	0.103
Mg	0.934	0.939	0.938	0.936	0.932	0.939	0.923	0 923	0.941	0.923	0.935	0.907	0.936	0.913	0.906
Total octa.	1.045	1.042	1 037	1.051	1.049	1.048	1.047	1.030	1.052	1.035	1.046	1.057	1.090	1.061	1.054
Ca	0.945	0.956	0.958	0.945	0.947	0.949	0.953	0.968	0.946	0.960	0.954	0.938	0.906	0.937	0.946
Na	-	-	-	-	-	-	-	-	-	-	-	-	-	-	-
Total cat.	3.990	3.998	3.995	3.996	3.995	3.998	4 000	3.998	3 998	3.994	4 000	3.994	3.996	3.999	4.000
Mg/(Mg+Fe^{2+})	0.924	0.924	0.930	0.922	0 920	0.922	0.920	0 923	0.919	0.923	0.926	0.901	0.899	0.901	0.898
Wo	48.30	48.44	48.72	48.22	48 33	48.25	48.66	49.18	48.03	48.96	48.44	48.25	46.54	48.05	48.37
En	47.76	47.62	47.69	47.73	47.56	47.72	47.16	46 89	47.76	47.10	47.46	46.64	48.05	46 80	46.34
Fs	3.94	3.94	3.60	4.06	4 11	4 03	4.18	3.92	4 21	3.93	4 10	5.10	5.42	5.15	5 29

- = BELOW DETECTION LIMIT.

TABLE 6.8. ELECTRON MICROPROBE ANALYSES OF CLINOPYROXENES IN A WEBSTERITE SAMPLE. FeO AND Fe_2O_3 ARE CALCULATED ASSUMING STOICHIOMETRY ON THE BASIS OF 4 CATIONS AND 6 OXYGENS. END-MEMBERS IN TERMS OF WOLLASTONITE, ENSTATITE AND FERROSILITE ARE CALCULATED ACCORDING TO THE METHOD RECOMMENDED BY THE SUBCOMMITTEE ON PYROXENES, IMA (1988).

Sample no.	47 3A								
Analysis no.	1	2	3	4	5	6	7	8	9
SiO2	52.72	51.39	52.76	52.73	52.65	52.40	52.73	52.36	52.59
TiO2	-	0.19	0.33	0.28	0.34	-	0.25	-	0.32
Al2O3	3 23	3.74	3 02	2.94	3.19	3.17	3 37	3	3.13
Cr2O3	0.21	-	-	-	0.21	-	-	-	0.20
Fe2O3	0.20	1.24	-	-	0 12	0 41	-	-	-
FeO	4.59	3.93	4 67	4.06	4.76	4.38	4.91	4 81	4.67
MgO	15.44	15.59	15 47	15.79	15.74	15.46	15.43	15.59	15.40
CaO	24.14	23.34	23.97	23.28	23 77	23 98	23 92	23 22	23.94
Total	100.53	99.42	100.22	99.08	100.78	99 80	100.61	98.98	100 25
Si	1.925	1.896	1.930	1.941	1 917	1.926	1.923	1.937	1.925
ivAl	0.075	0.104	0.070	0.059	0 083	0 074	0.077	0 063	0.075
Total tetra.	2.000	2.000	2.000	2.000	2.000	2.000	2.000	2.000	2.000
viAl	0.064	0.059	0.061	0.069	0.054	0 063	0.068	0.068	0.060
Ti	-	0.005	0.009	0 008	0 009	-	0.007	-	0 009
Cr	0.006	-	-	-	0.006	-	-	-	0 006
Fe3+	0 006	0.034	-	-	0.150	0.149	-	-	-
Fe2+	0.140	0.121	0.143	0.125	0.145	0.135	0.150	0.149	0.143
Mg	0 840	0.857	0 843	0 866	0.855	0.847	0.839	0 860	0 840
Total octa.	1.056	1.077	1.056	1.068	1.073	1.056	1.063	1.077	1 058
Ca	0 944	0.923	0.940	0.919	0.928	0.944	0 935	0 921	0 939
Total cat.	4.000	4 000	4.000	4.000	4.000	4.000	4.000	4.000	4.000
$Mg/(Mg+Fe^{2+})$	0.857	0.876	0 855	0.874	0.855	0 862	0.848	0.852	0.855
Wo	48.92	47.67	48.79	48.09	48 06	48.74	48.59	47.71	48.85
En	43.52	44.29	43.79	45.37	44.28	43 72	43.62	44.57	43.71
Fs	7.56	8.05	7.42	6.55	7.65	7.54	7.79	7.71	7.44

- = BELOW DETECTION LIMIT.

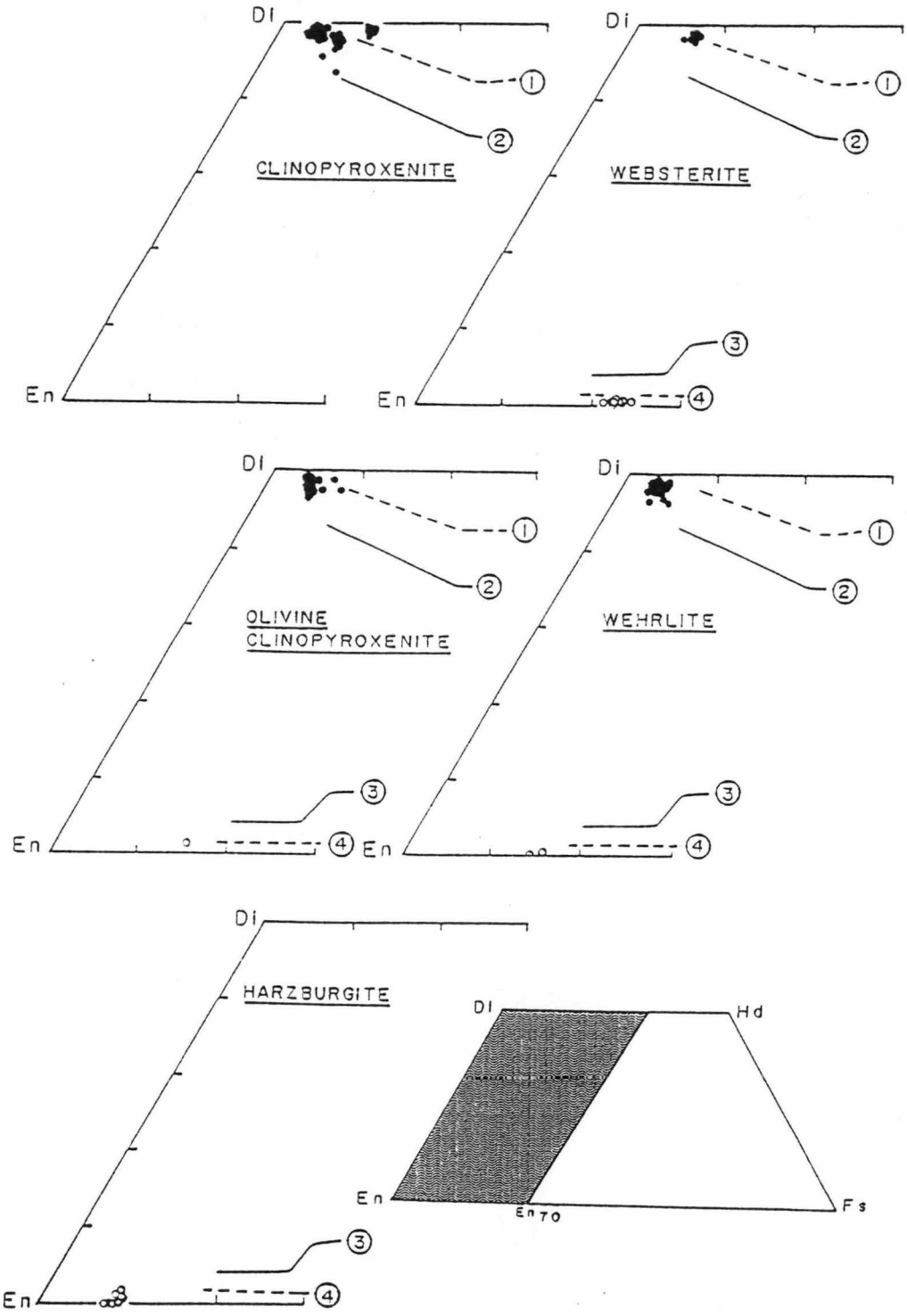

Figure 6.13. Pyroxene compositional variations in the Nan Suture clinopyroxenites, olivine clinopyroxenites, wehrlites, harzburgites and a websterite in terms of their wollastonite, enstatite and ferrosilite contents. Also shown are the solidus pyroxene trends (2 and 3; Brown, 1967) and subsolidus pyroxene trends (1 and 4; Nwe, 1976) of the Skaergaard Intrusion.

Orthopyroxenes

Orthopyroxenes occur as exsolution lamellae in clinopyroxenes in olivine clinopyroxenite and wehrlite samples, and as discrete grains in wehrlites, harzburgites and a websterite sample. Their chemical compositions are given in Tables 6.9 and 6.10, and plotted in the conventional pyroxene quadrilateral in Figure 6.13.

They are classified as enstatites following the pyroxene nomenclature of the Subcommittee on Pyroxenes, I.M.A. (1988), and have a narrow range of Mg#. Their Mg# numbers increase from websterite (0.77-0.79) to olivine clinopyroxenite and wehrlite (0.85-0.87), and harzburgite (0.91-0.92). These enstatites have extremely low wollastonite contents, suggesting that they have experienced subsolidus re-equilibration.

Averaged clinopyroxene-orthopyroxene pairs in individual cumulus gabbros, wehrlites and a websterite sample are plotted in the pyroxene quadrilateral in Figure 6.14. They form continuous trends very close to the subsolidus and extrapolated subsolidus trends of pyroxenes from the tholeiitic Skaergaard Intrusion. This suggests that most pyroxenes are likely to be broadly comagmatic, and crystallised prior to plagioclase, since pyroxenes in gabbros have lowest Mg#. Similarly, orthopyroxenes in harzburgites also lie close to the extrapolated subsolidus orthopyroxene trend of the Skaergaard Intrusion and have higher Mg# than orthopyroxenes in the other rock types (Fig 6.13), suggesting that all are possibly comagmatic and that orthopyroxene crystallised before clinopyroxene in these rocks.

Olivines

Relict olivines with rather high Mg# are present in olivine clinopyroxenites, wehrlites, harzburgites and dunites (Tables 6.11 to 6.14). Their Mg# values decrease in descending order from harzburgites (average 0.91) to dunites (average 0.90), wehrlites (average 0.86) and olivine clinopyroxenites (average 0.82)(Fig. 6.15), signifying that if they are comagmatic, orthopyroxene and olivine crystallised before clinopyroxene.

Chromites

Relict chromites exist in some harzburgite, olivine clinopyroxenite and wehrlite samples, and range from magnesio-chromite in harzburgite (Table 6.15) to chromian hercynite in olivine clinopyroxenite (Table 6.16) and wehrlite (Table 6.17). Their compositions on Cr# and Fe^{3+}# versus Mg# (Fig. 6.16) show that at similar Mg#,

TABLE 6 9. ELECTRON MICROPROBE ANALYSES OF ORTHOPYROXENES IN OLIVINE CLINOPYROXENITES, WEHRLITES AND A WEBSTERITE SAMPLE. FeO AND Fe_2O_3 ARE CALCULATED ASSUMING STOICHIOMETRY ON THE BASIS OF 4 CATIONS AND 6 OXYGENS. END-MEMBERS IN TERMS OF WOLLASTONITE, ENSTATITE AND FERROSILITE ARE CALCULATED ACCORDING TO THE METHOD RECOMMENDED BY THE SUBCOMMITTEE ON PYROXENES, IMA (1988).

Sample no.	8.1A [1]	8.5 [2]		YP-5 [2]	47.3A [3]										
Anal. no.	1[4]	1[4]	2[4]	1	1	2	3	4	5	6	7	8	9	10	11
SiO2	55.91	56.54	55.46	56.86	54.99	54.64	54.64	53.83	54.24	54.11	54 18	54.46	54 05	54.50	54.64
Al2O3	1.61	1.39	1.60	1.46	3.02	3.21	3 11	3.20	3.22	3.12	3.18	2.82	3.30	3.00	2.92
Cr2O3	0 23	-	0.22	-	-	-	-	-	-	-	-	-	-	-	-
Fe2O3	0.76	0.16	0.51	-	0.04	0.81	0.22	0.60	0.98	1.02	1.06	0 52	0.56	0.68	-
FeO	9.39	9.76	9.82	8.91	13.70	13.57	14 00	14 25	13.43	13.36	13.57	14.18	14.96	14.90	14.24
MnO	0.22	0.27	0.22	-	0 29	-	-	0.21	0.26	0.34	-	0.29	0.22	0.38	0.23
MgO	31 69	32.17	31.29	32.22	28.86	28 82	28.59	27 80	28.28	28.43	28.44	28.13	27.51	27.71	28.17
CaO	0 60	0.19	0.40	0.29	0 24	0 32	0 30	0.28	0.60	0.26	0 42	0 40	0.33	0.39	0.48
Total	100.41	100 48	99.52	99.74	101.14	101.37	100.86	100.17	101.01	100.64	100.85	100 80	100.93	101.56	100.68
Si	1 954	1.970	1.957	1.983	1.937	1.923	1.932	1.924	1.920	1.921	1.920	1.934	1.923	1.928	1.939
ivAl	0 046	0 031	0.043	0.018	0.063	0.077	0.068	0.076	0.080	0.079	0.081	0.066	0 077	0 072	0.061
Total tetra.	2.000	2.000	2.000	2.000	2.000	2.000	2.000	2.000	2.000	2.000	2.000	2.000	2.000	2.000	2.000
viAl	0.020	0.026	0.024	0.043	0 062	0.056	0.062	0.059	0.054	0.052	0.052	0 052	0.062	0.054	0.062
Cr	0.006	-	0.006	-	-	-	-	-	-	-	-	-	-	-	-
Fe3+	0.020	0 004	0.014	-	0.001	0.022	0.006	0.016	0.026	0.027	0.028	0.014	0.015	0 018	-
Fe2+	0.275	0.284	0.290	0.260	0.404	0.399	0.414	0.426	0.397	0.397	0.402	0.421	0.445	0.441	0.423
Mn	0.006	0.008	0.007	-	0.009	-	-	0.006	0.008	0.010	-	0.009	0 007	0 011	0.007
Mg	1.650	1.670	1.645	1.674	1.515	1.511	1.507	1.481	1.492	1.505	1.502	1.489	1.459	1.461	1.491
Total octa.	1.977	1.993	1.985	1.977	1.991	1.988	1.989	1 989	1.977	1.990	1.984	1.985	1.988	1.985	1.981
Ca	0 023	0 007	0.015	0 011	0 009	0 012	0 012	0 011	0 023	0 010	0 016	0.015	0 013	0 015	0 018
Total cat.	4.000	4.000	4.000	3.988	4.000	4.000	4.000	4 000	4 000	4.000	4 000	4.000	4.000	4 000	4.000
$Mg/(Mg+Fe^{2+})$	0.857	0.855	0.850	0.866	0.790	0.791	0.784	0.777	0.790	0.791	0.789	0.779	0.766	0.768	0.779
Wo	1.15	0.36	0.76	0.56	0 47	0.61	0.59	0 56	1.16	0 50	0.81	0.78	0.64	0 76	0.94
En	83.61	84.62	83.51	86.08	78.19	77.74	77.75	76 33	76.67	77.23	77.09	76 43	75.27	75.08	76.91
Fs	15.25	15 02	15.73	13.36	21.33	21 65	21 66	23 11	22.17	22 27	22.10	22.79	24.09	24 16	22.15

[1] = OLIVINE CLINOPYROXENITE, [2] = WEHRLITE, [3] = WEBSTERITE, [4] = LAMELLAE IN CLINOPYROXENES.
- = BELOW DETECTION LIMIT.

TABLE 6 10 ELECTRON MICROPROBE ANALYSES OF ORTHOPYROXENES IN HARZBURGITES. FeO AND Fe_2O_3 ARE CALCULATED ASSUMING STOICHIOMETRY ON THE BASIS OF 4 CATIONS AND 6 OXYGENS. END-MEMBERS IN TERMS OF WOLLASTONITE, ENSTATITE AND FERROSILITE ARE CALCULATED ACCORDING TO THE METHOD RECOMMENDED BY THE SUBCOMMITTEE ON PYROXENES, IMA (1988).

Sample no.	1.2						1 7					41.2				
Anal. no.	1	2	3	4	5	6	1	2	3	4	5	1	2	3	4	5
SiO2	56.81	56.33	56.46	56.99	56 60	56.69	59.44	59.10	58.75	59 01	58.99	58 24	58.07	58.78	58.51	58.81
Al2O3	2.72	2.58	2.77	2.84	2.76	2.81	-	-	-	-	-	-	-	-	-	0 20
Cr2O3	0 52	0 45	0.44	0.56	0.55	0.56	-	-	-	-	-	-	-	-	-	-
FeO	5.69	5.71	5.60	5.69	5 80	5.63	5.76	5 78	5 42	5 63	5.71	5.91	5.99	6.12	5.95	6 02
MgO	33 82	33.75	33.23	34 03	33 77	33 85	35 85	35.52	35.99	36.10	35.76	35.14	34.90	35.41	35 64	35 03
CaO	0 41	0 39	0.94	0 54	0 45	0 50	-	-	-	-	-	-	-	-	-	-
Total	99 97	99 21	99.44	100.65	99.93	100.04	101.05	100 40	100.16	100.74	100.46	99 29	98.96	100.31	100.10	100 06
Si	1.952	1.951	1.952	1.946	1.947	1.947	2.014	2.015	2.007	2.006	2.010	2.011	2.012	2.010	2.005	2.014
ivAl	0.048	0.049	0.048	0.054	0.053	0.053	-	-	-	-	-	-	-	-	-	-
Total tetra.	2.000	2.000	2.000	2.000	2.000	2.000	2.000	2.000	2.000	2.000	2.000	2.000	2.000	2.000	2.000	2.000
viAl	0.062	0.056	0.065	0.060	0.059	0.061	-	-	-	-	-	-	-	-	-	0 008
Cr	0.014	0.012	0.012	0.015	0.015	0 015	-	-	-	-	-	-	-	-	-	-
Fe2+	0.163	0.165	0.162	0 162	0.167	0.162	0 163	0 165	0 155	0.160	0.163	0 171	0.174	0.175	0.171	0.172
Mg	1.732	1.742	1.712	1.732	1.732	1.733	1.810	1.805	1.832	1.829	1.817	1.808	1.802	1.805	1.820	1.788
Total octa.	1.971	1.976	1.951	1.970	1.973	1.970	1.973	1.970	1.987	1.989	1.979	1.979	1.976	1.980	1.990	1.968
Ca	0.015	0.015	0.035	0 020	0 017	0 018	-	-	-	-	-	-	-	-	-	-
Total cat.	3.986	3.990	3.986	3 989	3.989	3 989	3.987	3.985	3.994	3.994	3.990	3 989	3 988	3.990	3 995	3.982
$Mg/(Mg+Fe^{2+})$	0.914	0.913	0.914	0.914	0.912	0.915	0.917	0 916	0.922	0.920	0 918	0.914	0.912	0 912	0 914	0.912
Wo	0.80	0.76	1.82	1.03	0.87	0.96	-	-	-	-	-	-	-	-	-	-
En	90.65	90.63	89.70	90.49	90.41	90.58	91.73	91.63	92.21	91 96	91.78	91.38	91.21	91.16	91.43	91.20
Fs	8.55	8.61	8.48	8.48	8.72	8.46	8 27	8 37	7.79	8 04	8 22	8 62	8.79	8.84	8.57	8.80

- = BELOW DETECTION LIMIT.

TABLE 6.11. ELECTRON MICROPROBE ANALYSES OF OLIVINES IN OLIVINE CLINOPYROXENITES. NUMBERS OF CATIONS ARE CALCULATED ON THE BASIS OF 4 OXYGENS.

Sample no.	8.1A							52 2				
Anal no.	1	2	3	4	5	6	7	1	2	3	4	5
SiO2	39.77	39 41	39.90	39.91	40.06	40.03	40 02	39 49	39.11	38.94	38.60	39.53
FeO	14.84	15.65	15.32	14.54	15.17	15 06	14.90	18.58	18.39	18 49	19.08	18.77
MnO	-	-	-	-	-	-	-	0.28	0.33	0.29	0.28	0.22
MgO	45.35	44 94	44 62	45.34	45 50	45 46	45 31	42.33	41 02	41 13	41 39	42 16
Total	99 96	100 00	99.84	99.79	100 73	100.55	100 23	100 68	98.85	98.85	99.35	100.68
Si	0 997	0.992	1.003	1.001	0.998	0 998	1.000	1.001	1.009	1 006	0 996	1.002
Fe2+	0.311	0.330	0.322	0 305	0.316	0.314	0 312	0.394	0.397	0 399	0.412	0.398
Mn	-	-	-	-	-	-	-	0.006	0.007	0.006	0.006	0 005
Mg	1 695	1 686	1 672	1.694	1.689	1 690	1 688	1.599	1.578	1 583	1 591	1.593
Total cat.	3.003	3.008	2.997	3.000	3.002	3.002	3.000	2.999	2.991	2.994	3.004	2.998
Mg/(Mg+Fe^{2+})	0 845	0 837	0 838	0.847	0.842	0 843	0 844	0.802	0.799	0 799	0.794	0.800

- = BELOW DETECTION LIMIT.

TABLE 6 12. ELECTRON MICROPROBE ANALYSES OF OLIVINES IN WEHRLITES. NUMBERS OF CATIONS ARE CALCULATED ON THE BASIS OF 4 OXYGENS.

Sample no	8.1						8.3			8 4					8.5
Anal. no	1	2	3	4	5	6	1	2	3	1	2	3	4	5	1
SiO2	40.52	40.29	40.33	39 80	40.19	40 44	40.48	40 27	40.26	40.45	40.45	40.46	40.45	40.22	39 78
FeO	14.72	14.54	14.54	14.49	14.78	14.74	14 78	14 74	14.95	14.36	14.54	14.56	14.38	14.49	14.97
MnO	-	-	-	-	-	-	-	-	-	-	-	-	0.23	-	-
MgO	46.13	45.93	46 06	45 69	46 06	45.70	46 12	46.02	46.24	45.72	45.58	45.35	45.53	45 38	45.37
Total	101.37	100.76	100.93	99.98	101.03	100 88	101 38	101 03	101.45	100.53	100.57	100.37	100 59	100.09	100.12
Si	1.000	1.000	0.999	0 996	0.996	1.003	0 999	0.998	0.995	1.005	1.005	1.007	1.005	1.004	0.996
Fe2+	0.304	0.302	0.301	0.303	0.306	0.306	0.305	0.305	0.309	0 298	0.302	0.303	0.299	0.303	0.314
Mn	-	-	-	-	-	-	-	-	-	-	-	-	0 005	-	-
Mg	1.697	1 699	1.701	1.704	1.701	1 689	1 697	1 699	1.702	1.692	1.688	1.683	1 686	1 689	1 694
Total cat.	3.000	3.000	3.001	3.004	3.004	2.997	3 001	3.002	3.006	2.995	2.995	2.993	2.995	2.996	3.004
Mg/(Mg+Fe^{2+})	0 848	0 849	0.850	0 849	0 847	0.847	0 848	0 848	0.846	0 850	0.848	0 847	0 849	0 848	0 844

Sample no.	8.5							YP-5					Q		
Anal. no.	2	3	4	5	6	7	8	1	2	3	4	5	1	2	3
SiO2	39.55	40.27	39.69	39.83	39.51	39.56	39 66	40.51	39 92	40.46	40.43	40.58	40 40	40.57	39.95
FeO	15.42	15.05	15.26	15.39	15.26	15.17	15.40	13.50	14.15	13.89	13.75	14.03	14 84	14.56	14 00
MnO	-	-	-	-	-	-	-	0 23	0.21	0.22	-	-	-	-	-
MgO	44.35	45 39	45.07	45 29	44.96	45 21	44 85	46.72	45 90	45.92	46.28	46.11	45 77	45.55	44.77
Total	99.32	100.71	100.02	100.51	99 73	99.94	99 91	100.96	100.18	100.50	100 46	100 73	101.01	100.68	98.72
Si	1.001	1.002	0.995	0 996	0.994	0 994	0 998	0 997	0.995	1 004	1.002	1.004	1.001	1.007	1.009
Fe2+	0.326	0.313	0.320	0.322	0 321	0.319	0 324	0.278	0.286	0 288	0 285	0 290	0.308	0.302	0.296
Mn	-	-	-	-	-	-	-	0 005	0.009	0 005	-	-	-	-	-
Mg	1.672	1 683	1.685	1 687	1.686	1 693	1 681	1 715	1 705	1.699	1.710	1 701	1 690	1.685	1 686
Total cat.	2.999	2.998	3.000	3 004	3 001	3 006	3.003	2.995	2.996	2.996	2.998	2.996	2.999	2.993	2.991
Mg/(Mg+Fe^{2+})	0 837	0 843	0 840	0 840	0 840	0 842	0 838	0 860	0 856	0.855	0 857	0 854	0 846	0 848	0 851

Sample no.	Q			Y-7					SC-6							
Anal. no.	4	5	6	1	2	3	4	5	1	2	3	4	5	6	7	8
SiO2	40 69	40 47	40.11	40.63	40 74	40.73	40 99	40.87	41 12	40.89	41.17	41.19	41 01	41.06	41.11	40.96
FeO	14.63	14 46	14.38	12.53	12.33	12 69	12 67	12.44	11.55	11.58	11.78	11.83	12 13	11.97	12.18	11.44
MnO	-	-	0.25	-	-	-	-	-	0.21	-	-	-	-	-	-	-
MgO	45.79	44 93	45 35	47 05	46.66	47.33	47.42	47 07	47 89	47 78	47 63	47 46	47 65	47 95	47 47	47 66
Total	101.11	99 86	100.09	100.21	99.73	100.75	101.08	100.38	100 77	100.25	100.58	100.48	100.79	100.98	100.76	100 06
Si	1.006	1.012	1.003	1.004	1.010	1.002	1.004	1 007	1.006	1.005	1.009	1.011	1.005	1.004	1 008	1.008
Fe2+	0.302	0 302	0.300	0 259	0.256	0.261	0.260	0.256	0.236	0.238	0.241	0.243	0 249	0 245	0.250	0.235
Mn	-	-	0.005	-	-	-	-	-	0 004	-	-	-	-	-	-	-
Mg	1.686	1.674	1.689	1.733	1.724	1.735	1.732	1.729	1 747	1.751	1.740	1.736	1.741	1.747	1.734	1.748
Total cat.	2.994	2.988	2.998	2.996	2.990	2.998	2.996	2.993	2.994	2.995	2.991	2.989	2.995	2.996	2.992	2.992
Mg/(Mg+Fe^{2+})	0 848	0 847	0 849	0 870	0 871	0 869	0 870	0 871	0 881	0 880	0 878	0 877	0 875	0 877	0.874	0.881

- = BELOW DETECTION LIMIT.

TABLE 6.13. ELECTRON MICROPROBE ANALYSES OF OLIVINES IN HARZBURGITES.
NUMBERS OF CATIONS ARE CALCULATED ON THE BASIS OF 4 OXYGENS

Sample no	1.2						1.9			
Anal no.	1	2	3	4	5	6	1	2	3	4
SiO2	42.12	41.88	41.43	41 86	41.44	41 56	42.13	41.83	41.61	41.92
FeO	8.29	9.19	8.56	8.43	8.54	8.56	8.22	7.97	9.05	8.16
NiO	0.37	-	0.41	0.44	-	0.37	0.43	0.40	0.42	0 35
MgO	50.19	49.47	49.93	49.71	49.21	49.68	50.53	50 45	49.73	50 31
Total	100.97	100.54	100.33	100 44	99.19	100.17	101.31	100.65	100.81	100.74
Si	1.013	1.014	1.006	1.014	1.015	1.010	1.010	1.009	1.007	1.011
Fe	0.167	0.186	0.174	0.171	0.175	0.174	0.165	0 161	0.183	0.164
Ni	0.007	-	0.008	0.009	-	0.007	0.008	0.008	0.008	0.007
Mg	1.800	1.786	1.807	1.794	1.796	1.799	1 806	1.814	1.794	1 807
Total cat.	2.987	2.986	2.994	2.987	2.985	2.990	2.990	2.991	2.993	2.989
Mg/(Mg+Fe^{2+})	0.915	0.906	0.912	0.913	0 911	0 912	0.916	0.919	0 907	0 917
Sample no.	1.9		41.2							
Anal. no.	5	6	1	2	3	4	5	6	7	8
SiO2	41.28	41.66	40.82	41.29	41.14	41.32	41.53	41.02	41.13	41.49
FeO	8.48	8.28	8.99	8.70	8 92	9.17	8.61	8.75	8.69	9.15
NiO	0.39	0.38	0.47	0 32	0.44	-	-	0.37	0.34	0.46
MgO	50 13	50 44	49.04	49.75	49.15	49.11	49.54	49.04	49.48	49 51
Total	100.28	100 75	99 32	100 06	99.65	99.60	99.68	99.18	99.64	100.61
Si	1.003	1.006	1.004	1.005	1.007	1.011	1 012	1.008	1.006	1 007
Fe	0.172	0.167	0.185	0.177	0.183	0.188	0.176	0.180	0.178	0 186
Ni	0 008	0 007	0.009	0.006	0.009	-	-	0.007	0.007	0.009
Mg	1 815	1 815	1.798	1.806	1 794	1.791	1 800	1.796	1.804	1 791
Total cat.	2.997	2.994	2.996	2.995	2.993	2.989	2.988	2.992	2.994	2.993
Mg/(Mg+Fe^{2+})	0 913	0.916	0 907	0.911	0 908	0.905	0 911	0 909	0 910	0.906

- = BELOW DETECTION LIMIT.

TABLE 6.14. ELECTRON MICROPROBE ANALYSES OF OLIVINES IN DUNITES.
NUMBERS OF CATIONS ARE CALCULATED ON THE BASIS OF 4 OXYGENS.

Sample no.	1.10						1.8						1.1B		
Anal. no.	1	2	3	4	5	6	1	2	3	4	5	6	1	2	3
SiO2	41.70	41.92	41.85	41.12	41.66	42.06	41.05	41.51	41 83	41.24	41 29	41.25	41.70	41.92	41.85
FeO	8.94	8 83	9 60	9.78	10.39	9.12	8.29	8.45	8 59	8.21	8 67	8.26	8.94	8 83	9 60
NiO	-	-	0.35	0.37	-	-	0.33	0.42	0 41	0.40	0.40	0.41	-	-	0.35
MgO	49.74	49.77	49 45	49 01	49 04	49 86	49.45	49 26	50.31	49.43	49 74	49 68	49 74	49.77	49 45
Total	100 38	100.53	101.25	100.28	101.09	101.04	99 12	99 64	101.14	99.28	100.10	99.60	100.38	100.52	101.25
Si	1.011	1 014	1.010	1.004	1.009	1.013	1.007	1.014	1.007	1.010	1.005	1.007	1.011	1 014	1.010
Fe	0 181	0.179	0.194	0.200	0.211	0.184	0 170	0.173	0.173	0.168	0.176	0.169	0.181	0 179	0 194
Ni	-	-	0.007	0.007	-	-	0 007	0.008	0.008	0.008	0.008	0.008	-	-	0 007
Mg	1 797	1.794	1.779	1 784	1 771	1.790	1 809	1.792	1.805	1.804	1 805	1 808	1.797	1.794	1.779
Total	2 989	2.986	2.990	2.996	2.991	2.987	2 993	2.987	2.993	2.990	2.995	2.993	2.989	2.986	2 990
Mg/(Mg+Fe^{2+})	0.908	0 909	0.902	0 899	0 894	0.907	0 914	0.912	0.913	0.915	0.911	0.915	0 908	0.909	0 902
Sample no	1 1B			28.1											
Anal. no.	4	5	6	1	2	3	4	5	6	7	8	9	10	11	12
SiO2	41.12	41.66	42.06	41.23	41.51	41.38	41 30	41.30	41.55	41.63	41.31	41.26	41.46	41.71	41.87
FeO	9.78	10.39	9.12	9.51	9.71	9.72	9.73	9 41	9.24	9.58	9.74	9 58	9.22	9.48	9 56
NiO	0.37	-	-	0 38	-	-	0.37	0.38	0.34	-	0.44	0.43	0 40	-	-
MgO	49.01	49 04	49 86	49 12	48 86	49.32	49.15	49 15	48.88	49.12	48 97	49 32	49.12	49 06	49 38
Total	100.28	101.09	101.04	100 24	100.08	100 42	100.55	100.24	100.01	100.33	100.46	100.59	100 20	100.25	100.81
Si	1.004	1.009	1.013	1.006	1.013	1.007	1.006	1.007	1.014	1.012	1.007	1.004	1.010	1.014	1.013
Fe	0.200	0.211	0.184	0.194	0.198	0.198	0.198	0.192	0.189	0.195	0.199	0.195	0.188	0.193	0 193
Ni	0 007	-	-	0.008	-	-	0.007	0.008	0.007	-	0.009	0 008	0.008	-	-
Mg	1.784	1.771	1.790	1.786	1.777	1.789	1.784	1.786	1.777	1.780	1.779	1.789	1.784	1.778	1.781
Total	2.996	2.991	2.987	2.994	2.987	2.993	2.994	2.993	2.986	2.988	2.993	2.996	2.990	2.986	2.987
Mg/(Mg+Fe^{2+})	0.899	0 894	0.907	0.902	0 900	0.900	0 900	0 903	0 904	0 901	0 900	0 902	0 905	0 902	0 902
Sample no.	28.1					65 1									
Anal. no.	13	14	15	16	17	1	2	3	4	5	6	7			
SiO2	41.47	41.64	41.64	41.40	41.75	41.29	41.67	41.35	41.22	41.55	41.63	41.40			
FeO	9.67	9.51	9.54	9.49	9.50	9.47	9.56	9 75	9.74	9.86	9.86	9.83			
NiO	-	0.35	-	0.40	0 31	-	0.31	-	-	0.35	-	0.41			
MgO	49 02	49.27	49.29	48.93	49.29	48.85	48 90	49.45	48.88	49.32	49 11	49 27			
Total	100.16	100.77	100.47	100.22	100 85	99.61	100.44	100.55	99.84	101.08	100.60	100.91			
Si	1 011	1.010	1.011	1.010	1.011	1.011	1.013	1.005	1.009	1.006	1.011	1.005			
Fe	0.197	0.193	0.194	0.194	0.192	0.194	0.194	0 198	0.199	0.200	0.200	0.200			
Ni	-	0.007	-	0.008	0.006	-	0.006	-	-	0.007	-	0 008			
Mg	1.781	1.781	1.784	1.779	1.779	1.783	1.773	1.791	1.783	1.781	1.778	1.783			
Total	2.989	2.990	2.989	2.990	2.989	2.989	2 987	2.995	2.991	2.994	2.989	2.995			
Mg/(Mg+Fe^{2+})	0.900	0 902	0.902	0 902	0 902	0.902	0 901	0.900	0.899	0 899	0.899	0.899			

- = BELOW DETECTION LIMIT.

TABLE 6.15. ELECTRON MICROPROBE ANALYSES OF CHROME-SPINELS IN A HARZBURGITE SAMPLE.
FeO AND Fe_2O_3 ARE CALCULATED ASSUMING STOICHIOMETRY ON THE BASIS OF 3 CATIONS AND 4 OXYGENS.

Sample no.	41 2												
Anal. no.	1	2	3	4	5	6	7	8	9	10	11	12	13
TiO2	0.31	0.42	0.29	0.29	0.42	0.32	0.30	0.36	0 39	0.22	0.30	0.31	0.24
Al2O3	12.25	11 88	12.97	12.59	12.49	12.93	12.99	12.54	12.38	11.97	10.89	13.10	11.84
Cr2O3	50.94	50.35	49 59	49.72	49.92	49.39	49.55	48.83	50 67	50.21	51.48	48.88	50.55
Fe2O3	6 31	6 88	6.44	6.41	6.42	6.76	6 50	8.03	6.55	7.18	5.96	6.72	6.07
FeO	23 02	22.79	23.43	24.48	23.27	23.40	23.41	24.22	24.03	24.06	25.19	22.67	23.72
MgO	7 48	7 46	7 11	6.39	7.05	7.24	6 94	6.82	7.01	6.76	5.80	7.32	6 44
Total	100.31	99.78	99.83	99 88	99.57	100 04	99 69	100.80	101.03	100.40	99.62	99 00	98.86
Ti	0.008	0.011	0.007	0 007	0.011	0.008	0.008	0.009	0.010	0.006	0.008	0.008	0.006
Al	0 482	0 470	0.512	0.500	0 493	0.510	0.511	0.494	0.485	0.475	0.440	0.518	0.474
Cr	1.345	1.336	1.312	1.324	1.322	1.306	1.308	1.289	1.333	1.335	1.394	1.295	1.357
Fe3+	0.157	0 173	0.162	0 162	0.164	0.168	0.166	0.200	0.163	0.179	0.151	0.171	0.157
Fe2+	0 635	0 637	0.653	0.687	0.659	0.647	0.662	0.670	0.662	0 666	0.712	0.642	0.681
Mg	0.373	0.373	0 354	0.321	0.352	0 361	0.345	0.339	0.348	0.339	0.296	0.366	0.326
Total cat.	3.000	3.000	3.000	3.000	3.000	3.000	3.000	3 000	3.000	3 000	3.000	3.000	3 000
$Fe^{2+}/(Fe^{2+}+Mg)$	63.03	63.07	64.82	68.15	65.17	64.21	65.72	66.36	65.57	66 27	70.64	63.70	67.63
Cr/(Cr+Al)	73 61	73 97	71.94	72.59	72.83	71.92	71.90	72.30	73.30	73.77	76.02	71.44	74.11
$Fe^{3+}/(Fe^{3+}+Al+Cr)$	7.90	8 74	8.14	8 15	8 26	8 48	8.34	10 08	8.20	9 00	7.63	8.63	7 88

- = BELOW DETECTION LIMIT.

TABLE 6.16. ELECTRON MICROPROBE ANALYSES OF CHROME-SPINELS IN AN OLIVINE CLINOPYROXENITE.
FeO AND Fe_2O_3 ARE CALCULATED ASSUMING STOICHIOMETRY ON THE BASIS OF 3 CATIONS AND 4 OXYGENS.

Sample no.	8 1A								
Anal. no.	1	2	3	4	5	6	7	8	9
TiO2	0 40	0 37	0.37	0.42	0.56	0.43	0 44	0 45	0.43
Al2O3	20.40	26.01	26.94	23.54	24.38	22 58	25 64	24 65	23.43
Cr2O3	33.28	28.25	27.22	27 98	25.77	28 34	26.50	26.11	27.30
Fe2O3	14.94	14.32	13.42	16 06	16.96	16 67	14.74	17.11	16 93
FeO	25.18	23 61	26.16	26.98	26 84	27.37	26.97	26.74	26 10
MgO	6 94	8 64	6 99	6 03	6 21	5 80	6 25	6 42	6 54
Total	101.14	101.20	101.10	101.01	100.72	101.19	100.54	101.48	100.73
Ti	0.010	0 009	0.009	0 010	0.014	0.010	0 011	0.011	0.010
Al	0.773	0.956	0.994	0 886	0.916	0 857	0 962	0.918	0 882
Cr	0.846	0 696	0 674	0.706	0.649	0.721	0.666	0.652	0.689
Fe3+	0.361	0.332	0.315	0.387	0.409	0 401	0.351	0.408	0.408
Fe2+	0.677	0.607	0 683	0.723	0.719	0 732	0.714	0.708	0.699
Mg	0 333	0.401	0.326	0 287	0.295	0 279	0.297	0 303	0.311
Total cat.	3.000	3 000	3.000	3.000	3.000	3.000	3 000	3.000	3 000
$Fe^{2+}/(Fe^{2+}+Mg)$	67.06	60.21	67.68	71.60	70.90	72.44	70 66	70.07	69.20
Cr/Cr+Al	52.24	42.14	40.39	44.35	41.48	45.71	40.93	41.53	43.86
$Fe^{3+}/(Fe^{3+}+Al+Cr)$	18.25	16.72	15.90	19.57	20 71	20.27	17.74	20 62	20 61

- = BELOW DETECTION LIMIT

TABLE 6 17. ELECTRON MICROPROBE ANALYSES OF CHROME-SPINELS IN WEHRLITES
FeO AND Fe_2O_3 ARE CALCULATED ASSUMING STOICHIOMETRY ON THE BASIS OF 3 CATIONS AND 4 OXYGENS.

Sample no.	8.1			8.3	8.4					8.5				
Anal. no.	1	2	3	1	1	2	3	4	5	1[1]	2	3	4	5
TiO2	0.47	0.36	0 37	0.39	0.33	0.36	0 25	0.32	0.41	0.45	0.22	0.48	0 45	0.53
Al2O3	25.59	26.39	26.99	27.24	28 54	30 19	27 15	26.94	26.87	21.73	31.50	25.72	24.88	23.22
Cr2O3	28.07	26 87	28.53	26.95	27.36	26.42	28.98	27.51	27 87	26 45	22.02	26.41	24.86	26.23
Fe2O3	13.44	12.88	12.52	12.38	11.60	10.53	11 68	13.29	12.01	17.97	13.44	16.14	16.56	17.75
FeO	25.93	25 62	25 08	25.17	24.42	24 47	25 26	25.47	25 81	27 92	25 06	21.75	26.93	27.31
MnO	-	-	-	0.43	0.52	-	-	-	-	-	-	-	-	-
MgO	6.89	6 82	7.70	7 09	7 82	8.25	7 46	7 35	6 99	4 93	7 85	9.53	5.96	5.83
Total	100.39	98 94	101.19	99.65	100.59	100.22	100.78	100.88	99.96	99.45	100.09	100.03	99.64	100.87
Ti	0.011	0 009	0.009	0.009	0 008	0.008	0 006	0 008	0.010	0.011	0 005	0.011	0.011	0.013
Al	0.955	0.994	0.989	1.014	1.043	1.096	0.999	0.992	1.000	0 844	1.143	0.947	0 944	0 879
Cr	0.703	0.679	0.701	0 673	0.671	0.643	0 715	0.680	0 695	0.689	0.536	0.652	0.633	0.666
Fe3+	0.320	0.310	0.293	0.294	0.271	0.244	0.274	0.312	0 285	0.445	0.311	0.379	0.401	0.429
Fe2+	0.687	0.685	0 652	0.665	0.633	0 630	0 659	0.666	0.681	0.769	0.645	0.568	0.725	0.734
Mn	-	-	-	0.012	0.014	-	-	-	-	-	-	-	-	-
Mg	0.325	0.325	0 357	0.334	0.361	0 379	0.347	0 342	0 329	0.242	0 360	0 443	0 286	0.279
Total cat.	3.000	3.000	3.000	3.000	3.000	3.000	3.000	3.000	3.000	3 000	3 000	3.000	3 000	3.000
Cr/Cr+Al	67.87	67 83	64 62	66.58	63.68	62.48	65.51	66.03	67.44	76.07	64.18	56.16	71.72	72.44
$Fe^{2+}/(Fe^{2+}+Mg)$	42.40	40.58	41.49	39.89	39.14	36.99	41.72	40.65	41.03	44.94	31.92	40.78	40.12	43.10
$Fe^{3+}/(Fe^{3+}+Al+Cr)$	16 19	15 62	14.77	14.86	13.64	12.30	13 80	15.74	14 40	22.52	15.64	19.18	20 29	21.73

Sample no.	8 5	8 7A		Q						YP-5				
Anal. no.	6	1	2	1	2	3	4	5	6	1	2	3	4	5
TiO2	0.41	0.48	0.41	0.39	0.32	0 25	0 29	0.60	0.38	0.43	0.49	0 54	0.70	0 66
Al2O3	24.53	13.13	17.90	27 45	29.48	28 45	27 18	23.06	29.69	25.28	24.58	24.94	24 76	24.41
Cr2O3	27 86	38.19	37.56	26.10	25.55	26.94	26.44	27.42	23 84	36.72	35.65	36.37	35.84	35.03
Fe2O3	14.87	16.89	13 07	13.52	11.60	12.67	13 61	16.38	13.60	5.73	7.77	5.99	6.75	8.71
FeO	25.92	24.65	21.91	23.77	24 22	24 03	25.75	27.68	24.55	24.49	23.92	25.17	25.01	22.08
MnO	0.45	0.49	-	-	-	-	-	-	0 37	-	0.52	0.47	-	-
MgO	6.41	5.97	8 47	8.26	8 10	8 38	7.05	5.61	7.91	7.89	7.92	7 19	7 69	9 43
Total	100.45	99 80	99.32	99 49	99 27	100 72	100.32	100.75	100.34	100.54	100.85	100.67	100.75	100.32
Ti	0.010	0 012	0.010	0.009	0.007	0.006	0.007	0.015	0 009	0.010	0.012	0 013	0 017	0.016
Al	0.921	0.524	0.689	1.015	1 083	1 036	1.007	0.875	1.082	0.934	0.909	0.926	0.917	0.899
Cr	0.702	1.022	0.970	0 647	0 630	0 658	0 657	0.698	0.583	0.910	0.884	0.906	0.890	0.865
Fe3+	0.358	0.430	0.321	0.319	0.272	0.294	0 322	0.397	0.317	0.135	0.183	0.142	0.160	0.205
Fe2+	0.693	0.698	0.598	0.623	0.631	0.621	0.677	0.746	0 635	0.642	0.628	0.663	0 657	0 577
Mn	0.012	0.014	-	-	-	-	-	-	0.010	-	0.014	0.013	-	-
Mg	0 304	0 301	0 412	0 386	0.376	0.386	0 331	0 269	0.365	0 369	0 370	0.338	0 360	0 439
Total cat.	3.000	3.000	3.000	3.000	3.000	3.000	3 000	3.000	3.000	3.000	3.000	3.000	3.000	3.000
Cr/Cr+Al	69.50	69.85	59.21	61.75	62.65	61 67	67.19	73.46	63.52	49.36	49.31	49.45	49.27	49.05
$Fe^{2+}/(Fe^{2+}+Mg)$	43.24	66.12	58.48	38 94	36.76	38 85	39.49	44.37	35.01	63.53	62.90	66.26	64.61	56.78
$Fe^{3+}/(Fe^{3+}+Al+Cr)$	18 07	21 77	16.23	16 11	13 71	14 81	16.21	20 15	15 97	6 83	9.28	7.19	8.12	10 40

[1] = LAMELLA IN CLINOPYROXENE.
- = BELOW DETECTION LIMIT.

chromites in olivine clinopyroxenite and wehrlites have lower Cr#(average 0.65±0.07) but are higher in Fe^{3+}#(average 0.16±0.04) than those in a harzburgite (average 0.73±0.01 for Cr# and 0.08±0.01 for Fe^{3+}#).

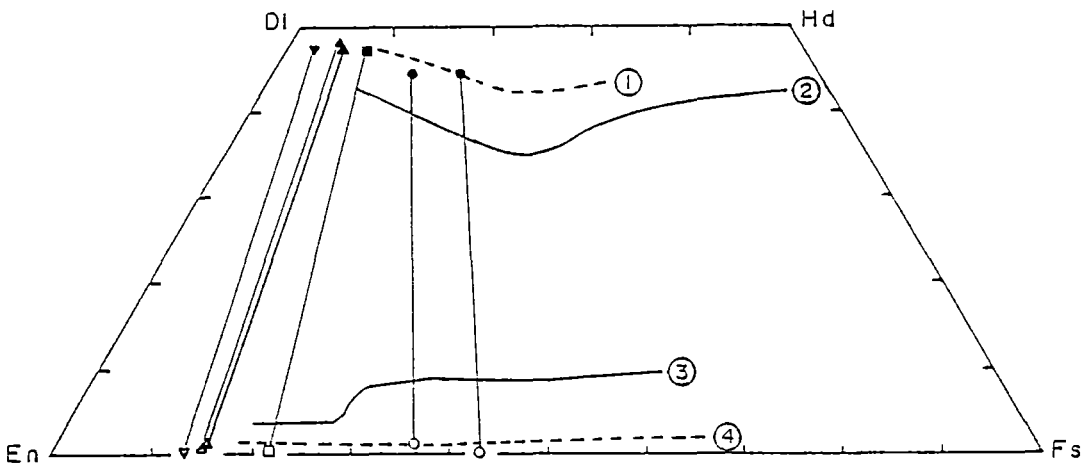

Figure 6.14. Pyroxene quadrilateral displaying the average compositions for coexisting clinopyroxenes (solid symbols) and orthopyroxenes (open symbols) in gabbros and amphibolites (circle), websterite (square), and olivine clinopyroxenite and wehrlite (triangles and an inverted triangle; triangles represent orthopyroxene lamellae and clinopyroxene hosts). Also shown are the solidus trends (2 and 3) and the subsolidus trends (1 and 4) of Skaergaard tholeiitic pyroxenes (Brown, 1967; Nwe, 1976).

It has been well documented that Fe^{2+}-Mg exchange between mafic silicates and chromites continues to subsolidus temperatures (e.g. Irvine, 1967; Roedder *et al.*, 1979; Ozawa, 1983), resulting in lowering of Mg# and increasing Fe^{3+}#, and little change in Cr# with decreasing temperatures (Dick and Bullen, 1984). However, it is the Cr# values of chromites that are most diagnostic in assigning magmatic affinities to chromite-bearing cumulates and related rocks.

Generally, these spinels have Cr#, Fe^{3+}# and Mg# comparable to spinels in Oshima-Oshima arc lavas and cumulates (Fig. 6.16). Their TiO_2 contents (0.22 -0.70 wt%) are lower than those of Oshima-Oshima spinels with lower Fe^{3+}# values (Yamamoto, 1984). Consequently, these ultramafics are most likely to have crystallised from an arc-related magma.

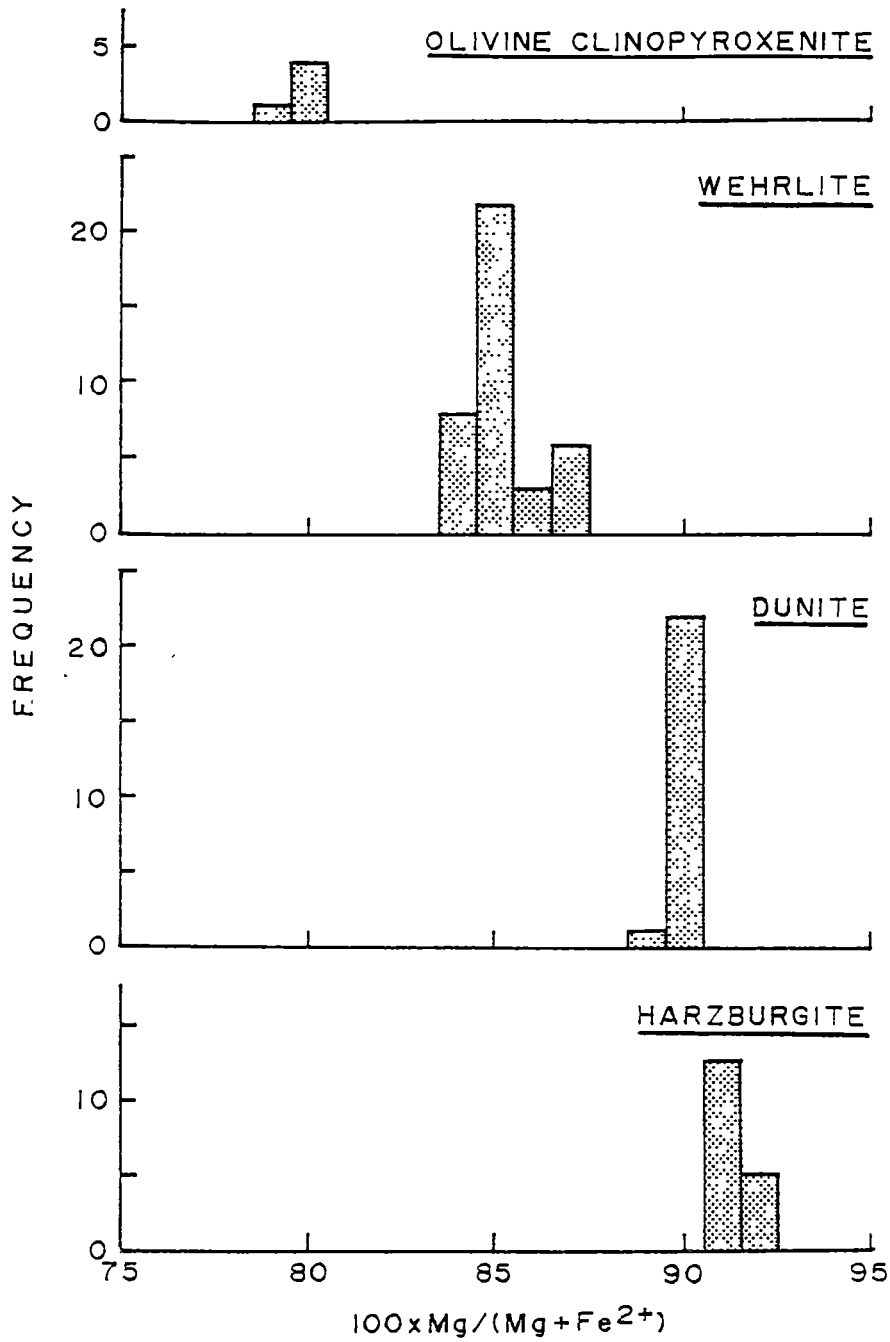

Figure 6.15. Frequency diagrams showing the variation in Mg# of relict olivines in olivine clinopyroxenites, wehrlites, dunites and harzburgites (see text for discussion).

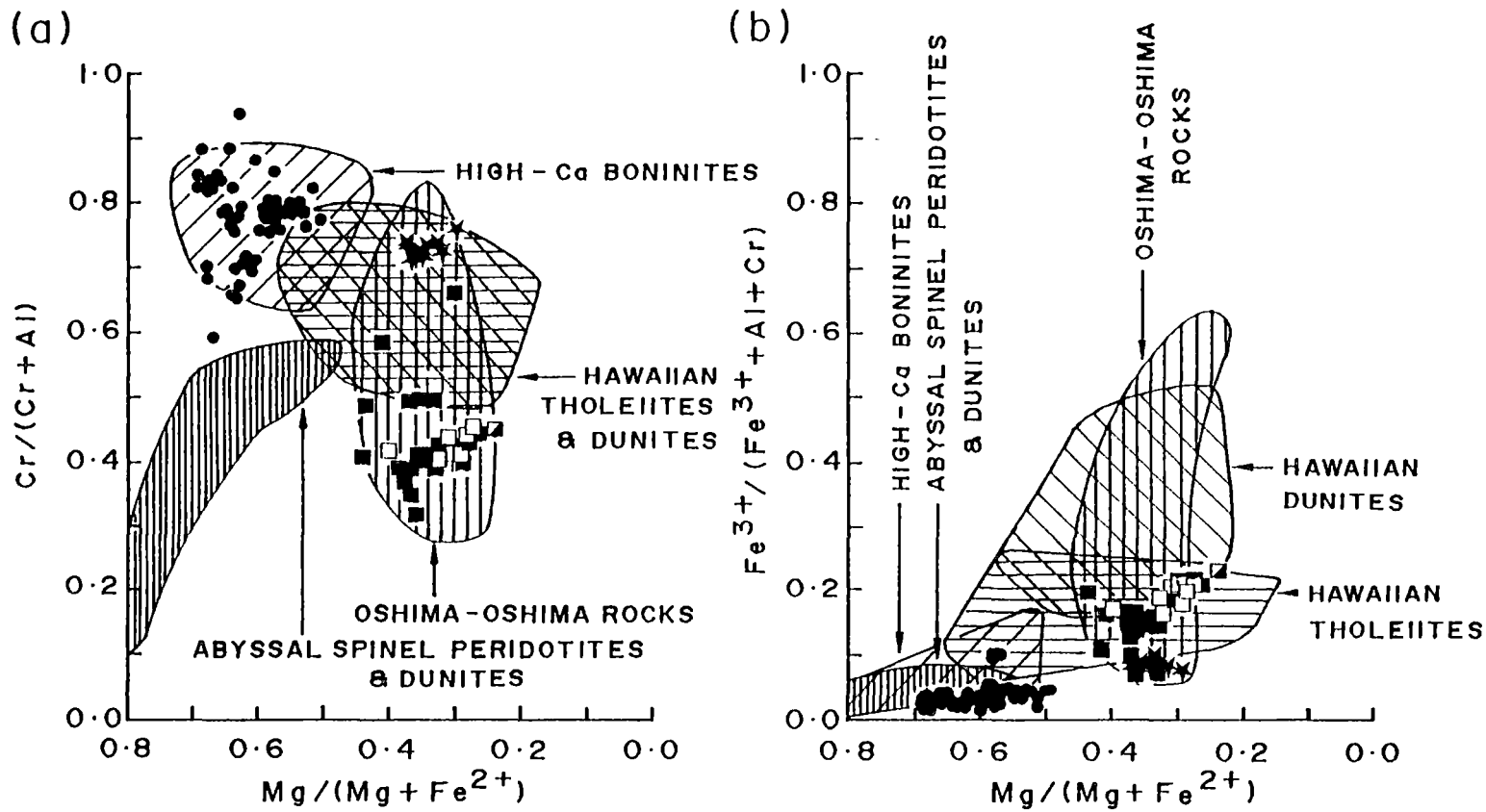

Figure 6.16. Compositions of chromites in harzburgite (solid star), olivine clinopyroxenite (open square), wehrlite (solid square and half- solid square), and chromitite and associated dunite (solid circle) in terms of (a) Cr/(Cr+Al) and (b) $Fe^{3+}/(Fe^{3+}+Al+Cr)$ against $Mg/(Mg+Fe^{2+})$. The half-solid square represents spinel lamella in a clinopyroxene crystal. Also shown are compositional fields for chromites in abyssal peridotites and dunites (Dick and Bullen, 1984), Hawaiian tholeiites (compiled from Evans and Wright, 1972; Clague *et al.*, 1980; Basaltic Volcanism Study Project, 1981; Hawkins and Melchior, 1983; and Sen and Presnall, 1986), Hawaiian dunites (data from Sen and Presnall, 1986), Oshima-Oshima lavas and associated ultramafics (Yamamoto, 1984) and high-Ca boninites (compiled from Cameron, 1985; Duncan and Green, 1987; Falloon and Green, 1986; and Falloon *et al.*, 1989).

6.3 Chromitites and Associated dunites

6.3.1 Occurrence and Petrography

Chromitites are present in the Mae Charim, Doi Phuk Sung and Nan River areas. In the Doi Phuk Sung and Nan River areas, chromitites occur as sheared layers, schlieren, pods and blocks in serpentinite (derived from dunite). They also occur as angular blocks in dolomite matrix (transformed from serpentinite) in the Doi Phuk Sung area. The ore concentrations vary from disseminated to massive. Nodular ores have also been recognised. In some cases, primary internal structure such as size-graded layering (Fig. 6.17) has been observed, indicating a cumulus origin.

Most of the chromitites studied were collected from mining faces in the Doi Phuk Sung and Nan River areas; one float sample from the Mae Charim area was donated by the CIG (Chromite Investment Group) Company. Sample locations are given in Table I-6 (Appendix I).

Microscopically, the studied samples are fine- to medium-grained (<1 - 4 mm), inequigranular rocks and made up mainly of chromites. Other minerals such as serpentine, amphiboles (tremolitic hornblende and magnesio-hornblende), quartz, dolomite and uvarovite may be present in variable amounts. From relict textures, serpentine has been transformed from olivine, and in turn, serpentine has been altered to carbonate. Petrographic features of individual chromitite samples are presented in Table II-9 (Appendix II).

6.3.2 Chromite Chemistry

Chromites in chromitites and associated dunites have Mg#, Cr# and Fe^{3+}# ranging from 0.50 to 0.69, 0.59 to 0.94, and 0.01 to 0.10, respectively (Table 6.18), and therefore, are classified as magnesiochromites. Although their TiO_2 contents (trace-0.71 wt%) are comparable to those of chromites in harzburgite, olivine clinopyroxenite and wehrlite, they generally have higher Mg# and Cr#, and lower Fe^{3+}# (Fig. 6.16), overlapping with those of chromites in high-Ca boninites. This implies that chromitites and associated dunites might have crystallised from a highly refractory melt (Duncan and Green, 1980, 1987), probably generated in a supra-subduction zone environment.

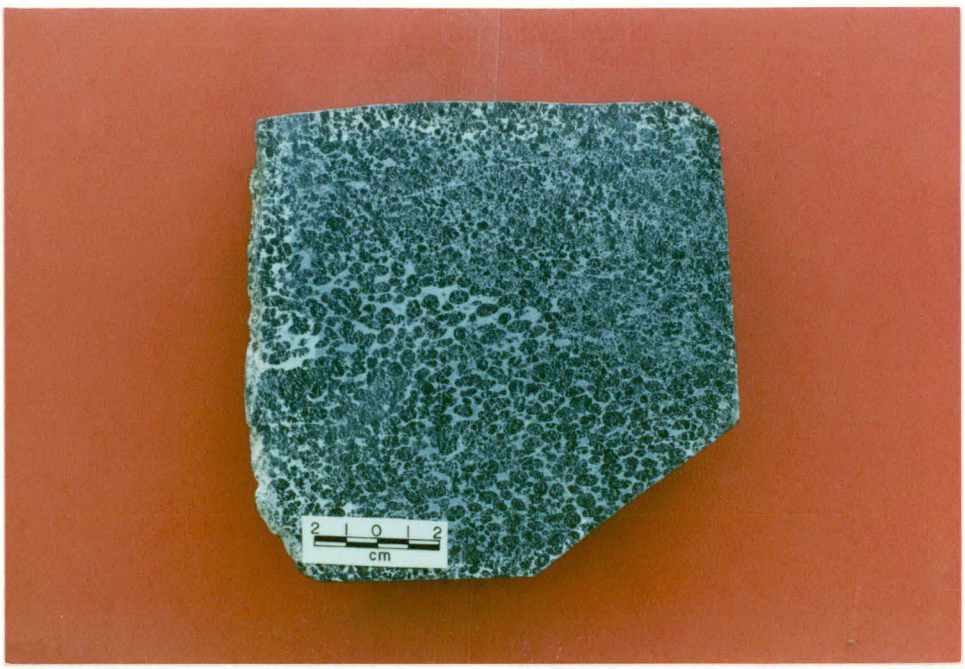

Figure 6.17. A chromitite with cumulus texture and size-graded layering from the southern mining face in the Doi Phuk Sung area. Chromite is black, serpentine is white (etched by HF).

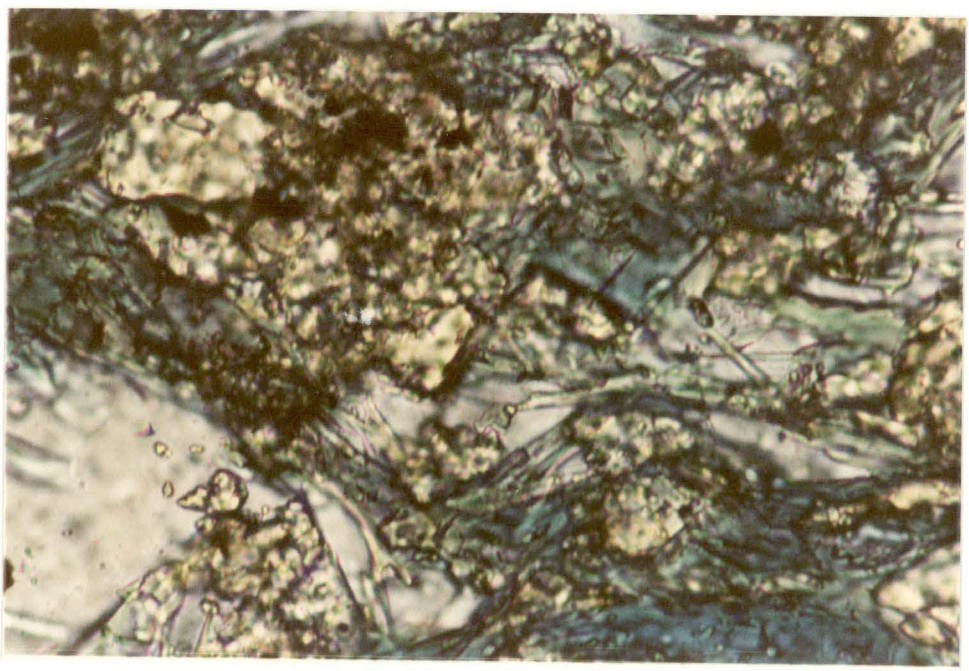

Figure 6.18. Photomicrograph of blueschist showing nematoblastic blue amphibole (blue and bluish green), anhedral epidote (light brown), anhedral albite (white) and magnetite (black). Ordinary light, x130.

TABLE 6.18. ELECTRON MICROPROBE ANALYSES OF CHROME-SPINELS IN CHROMITITES. FeO AND Fe_2O_3 ARE CALCULATED ASSUMING STOICHIOMETRY ON THE BASIS OF 3 CATIONS AND 4 OXYGENS.

Sample no.	5.1								5.2									
Anal. no.	1	2	3	4	5	6	7	8	1	2	3	4	5	6	7	8	9	10
TiO2	0.32	0 33	0 40	0.31	0 33	0.28	0 31	0.34	-	0 18	0 26	0.21	0.21	-	0 28	0.19	0.26	-
Al2O3	11.03	10 67	10 69	10 89	10.30	10.64	11.76	11.05	14 68	10 86	15.67	11.40	14 67	11 26	12.78	15.10	11.23	12.28
Cr2O3	60.00	59.96	60.37	59.71	58.83	58.10	56.75	56.34	55 07	59 23	54.56	58.53	55 79	59.38	57.99	54.49	58.61	58.65
Fe2O3	2.65	2.31	2.31	2.70	3 26	3.73	3.54	3.75	2.94	2.58	2.22	2.48	2.28	2.59	1.55	1.95	2.33	2.32
FeO	13.22	13.41	13.49	13.29	14.12	16.49	17.66	18.35	14 51	15.77	14 21	15.40	14.70	15.69	15.82	14.26	15.20	15.23
MgO	13 87	13 53	13 67	13.69	12.92	11.61	11.02	10 31	13 03	12.01	13.53	12.25	13 15	12.06	12.24	13.11	12.32	12.47
Total	101.09	100.21	100.93	100.59	99.76	100.85	101.04	100.14	100.23	100 63	100.45	100.27	100 80	100.98	100.66	99.10	99.95	100.95
Ti	0.008	0.008	0.010	0.007	0.008	0 007	0.008	0 008	-	0.004	0.006	0.005	0.005	-	0.007	0.005	0 006	-
Al	0.414	0.580	0.434	0.545	0.427	0.482	0.568	0 429	0.462	0.413	0.404	0.402	0 410	0.394	0.406	0 448	0.428	0.549
Cr	1.507	1.524	1.523	1.510	1.510	1.489	1.450	1.463	1.381	1.514	1.355	1.495	1.391	1.510	1.467	1.376	1.501	1.482
Fe3+	0.063	0.056	0.055	0.065	0.080	0.091	0.086	0.093	0.070	0.063	0.053	0 060	0 054	0.063	0.037	0.047	0.057	0.056
Fe2+	0.351	0.360	0.360	0.355	0.383	0.447	0.477	0 504	0.385	0.426	0.373	0 416	0.388	0.422	0.423	0.381	0.412	0.407
Mg	0 657	0 648	0.650	0.653	0 625	0 561	0.531	0 505	0.616	0.579	0.634	0.590	0 618	0 578	0.584	0.624	0 595	0 594
Total cat.	3.000	3.000	3.000	3.000	3.000	3.000	3 000	3 000	3.000	3.000	3.000	3.000	3 000	3.000	3.000	3.000	3.000	3.000
$Fe^{2+}/(Fe^{2+}+Mg)$	0.348	0.357	0.356	0.353	0.380	0.444	0.474	0.500	0.385	0 424	0.371	0.414	0 385	0 422	0.420	0.379	0.409	0.407
Cr/(Cr+Al)	0.785	0.790	0.791	0.786	0.793	0.786	0.764	0.774	0.716	0.785	0.700	0.775	0.718	0.780	0.753	0.708	0.778	0.762
$Fe^{3+}/(Fe^{3+}+Al+Cr)$	0 032	0.028	0 028	0 033	0.040	0.046	0.043	0.047	0.035	0 032	0.026	0 030	0 027	0 031	0.019	0 024	0 029	0 028

Sample no	5 3								5.4									
Anal. no	1	2	3	4	5	6	7	8	1	2	3	4	5	6	7	8	9	10
TiO2	0.27	0.19	0.36	0.39	0.26	0.35	0.32	0.21	0 26	0.32	-	0 24	0.32	0.22	0.26	0.18	0 23	0.26
Al2O3	11.95	11.24	12.70	15.45	11.26	15.59	16.77	11.61	8.65	12.64	15.72	18.35	17.97	22.04	11.38	15.03	11.51	19 06
Cr2O3	59.49	60 07	58.68	55.11	59.76	55.44	53.88	60.06	61.49	57 84	53.95	51 89	51.89	47.87	58.72	55.77	59.36	51.37
Fe2O3	1.94	2.32	1.79	2.08	2.17	2.34	2.41	1.65	1.41	2.26	2.75	2.49	2.56	2.80	2.49	2.17	2.02	2.27
FeO	13 93	13.97	13.92	12.59	13.84	12.63	12.69	14.22	17.57	15 88	14.86	14 39	14.05	13.41	15 81	15.32	16.08	14.51
MgO	13 47	13 33	13 61	14 60	13.36	14.74	14 75	13 19	10.50	12.34	12.89	13.83	13.96	14 83	12.11	12.89	12.03	13 86
Total	101.05	101.12	101.06	100.22	100 65	101.09	100 82	100.94	99.88	101 28	100.17	101.19	100.75	101.17	100.77	101.36	101.23	101.33
Ti	0.007	0.005	0.009	0.009	0.006	0.008	0.008	0 005	0.006	0 008	-	0 006	0 007	0.005	0.006	0.004	0.006	0 006
Al	0.447	0.422	0.473	0 570	0.424	0.570	0 611	0 436	0.338	0.474	0.586	0.666	0.655	0.784	0.432	0.556	0.435	0 689
Cr	1.493	1.513	1.467	1 363	1.511	1.359	1.317	1.514	1.613	1.456	1.349	1.264	1.270	1.142	1.495	1.384	1.505	1.246
Fe3+	0 046	0.056	0 043	0.049	0 052	0.055	0.056	0 040	0.035	0.054	0.065	0.058	0.060	0.064	0 060	0.051	0.049	0.052
Fe2+	0 370	0 372	0.368	0.329	0.370	0.328	0 328	0 379	0.488	0.423	0.393	0.371	0.364	0.339	0 426	0 402	0 431	0.372
Mg	0 637	0.633	0.641	0 681	0.637	0.681	0 680	0.627	0.519	0 585	0 608	0 635	0.644	0.667	0 581	0.603	0.575	0 634
Total cat.	3.000	3.000	3.000	3.000	3.000	3.000	3 000	3.000	3.000	3 000	3.000	3 000	3.000	3.000	3.000	3.000	3.000	3.000
$Fe^{2+}/(Fe^{2+}+Mg)$	0.367	0.370	0.365	0 326	0 368	0.325	0 326	0.377	0.484	0 419	0 393	0 369	0.361	0.337	0.423	0.400	0.428	0.370
Cr/(Cr+Al)	0.770	0.782	0.756	0.705	0.781	0.705	0 683	0.776	0 827	0 754	0 697	0.655	0 660	0.593	0 776	0.713	0.776	0.644
$Fe^{3+}/(Fe^{3+}+Al+Cr)$	0 023	0 028	0 022	0 025	0 026	0 028	0 028	0 020	0 018	0 027	0 033	0 029	0 030	0 032	0.030	0 026	0 025	0 026

Sample no	5.4	5.5													5.6			
Anal. no.	11	1	2	3	4	5	6	7	8	9	10	11	12	13	1	2	3	4
TiO2	0.28	0.35	0.37	0.36	0.42	0.36	0.31	0.42	0.33	0 31	0.35	0.35	0.24	0.37	0.34	0.36	0.40	0.33
Al2O3	17.89	10.39	10.34	10.50	10.43	10.36	10.18	10.54	10.13	9.87	10.37	10.52	10.79	10.71	9 82	9.74	10 65	10.37
Cr2O3	52.07	58 02	57 93	58 46	58 67	58.07	57.94	57.36	58.23	58.17	57.81	58.24	56.22	57.57	58 35	58 87	57.73	58.26
Fe2O3	2.25	3.61	3.93	3 41	3 36	3.79	3.18	3.52	3.23	4.10	3 26	3.58	3.61	3.60	3.59	3.19	3.59	3.71
FeO	14.93	17.06	16.43	16.76	16.93	16.45	16.92	16.66	16.46	16.86	17.10	16.93	18 30	17.38	16.99	17.15	17.34	16.51
MgO	13.37	11 20	11 62	11 49	11 47	11.60	11 03	11.36	11 38	11.24	11 03	11.38	10 08	11 05	11.09	11 02	10 81	11.58
Total	100.79	100 63	100.62	100.98	101.28	100.63	99.56	99.86	99.76	100.55	99.92	101.00	99.24	100.68	100.18	100.33	100.52	100.76
Ti	0.007	0 009	0.009	0 009	0 010	0.009	0.008	0.010	0 008	0 008	0 009	0.009	0 006	0.009	0 008	0.009	0.010	0.008
Al	0.474	0.399	0.396	0.401	0.397	0.397	0.396	0.407	0.392	0.380	0 401	0.402	0.422	0.411	0 380	0.376	0.408	0.397
Cr	1.456	1.495	1.489	1.498	1.500	1.492	1.510	1.485	1.511	1.503	1.500	1.493	1.475	1.482	1.514	1.527	1.484	1.496
Fe3+	0.053	0.089	0.096	0.083	0.082	0.093	0.079	0.087	0.080	0.101	0.081	0.087	0 090	0 088	0 089	0.079	0.088	0.091
Fe2+	0 388	0.465	0.447	0.454	0.458	0.447	0.466	0.456	0.452	0 461	0.469	0.459	0.508	0.473	0.466	0.470	0.472	0.448
Mg	0 619	0 544	0.563	0.555	0 553	0.562	0 542	0 555	0 557	0 548	0 540	0.550	0.499	0.536	0.543	0 539	0 524	0.561
Total cat.	3 000	3.000	3.000	3.000	3 000	3.000	3 000	3.000	3.000	3 000	3.000	3.000	3.000	3.000	3.000	3.000	3.000	3.000
$Fe^{2+}/(Fe^{2+}+Mg)$	0.385	0.461	0.442	0.450	0.453	0.443	0.462	0.451	0.448	0 457	0.465	0 455	0.505	0.469	0.462	0.466	0 474	0.444
Cr/(Cr+Al)	0.661	0 789	0.790	0.789	0.791	0.790	0.792	0.785	0.794	0.798	0.789	0.788	0.777	0.783	0.799	0.802	0.784	0.790
$Fe^{3+}/(Fe^{3+}+Al+Cr)$	0 026	0 045	0 049	0 042	0 041	0.047	0 040	0 044	0.040	0 051	0 041	0 044	0.045	0.044	0 045	0.040	0.044	0.046

TABLE 6.18. CONTINUED

Sample no.	5 6		5.7							25.2								
Anal. no.	5	6	1	2	3	4	5	6	7	1	2	3	4	5	6	7	8	9
TiO2	0.33	0.29	0.41	0.38	0.37	0.32	0.43	0.47	0.39	0.28	0.26	0.32	0.32	0.29	0.26	0.45	0.40	0.23
Al2O3	9.95	10.26	10.11	10.40	10.78	10.23	11.94	10.87	9 98	9.13	5.69	9 08	8.43	8.90	7.83	5.63	7.55	8.39
Cr2O3	59.12	58.20	58.58	58.41	57.12	58.34	56.17	57.79	59.32	63.14	66.44	63.32	62.82	62.25	62.78	65.97	63.11	63.14
Fe2O3	3.37	3.10	3.74	3.93	4.02	3.96	3.34	3.17	3.36	1.99	1.47	1.98	2.03	2.56	2.89	1.16	2.43	1 86
FeO	16.65	16.26	16.00	15.54	15.23	15.57	16.15	16.07	15.73	11 88	13.11	11.80	11.99	11.63	11.65	15.66	12.70	12.16
MgO	11.47	11.47	11 93	12.28	12.26	12.12	11.86	11 89	12.11	14 49	13.17	14 60	14.12	14 46	14.21	11.70	13.63	13.96
Total	100.89	99.58	100.77	100.94	99.78	100.54	99.89	100.26	100.89	100.91	100.14	101.10	99.71	100.09	99.62	100.57	99 82	99 74
Ti	0 008	0.007	0.010	0.009	0.009	0.008	0.011	0.011	0.010	0 007	0.007	0.008	0.008	0.007	0.006	0.011	0.010	0 006
Al	0.381	0.397	0.387	0.396	0.413	0.391	0.456	0.416	0.381	0.344	0.221	0 341	0.323	0.338	0.300	0.220	0.291	0.321
Cr	1.520	1.511	1.502	1.490	1.470	1.496	1.441	1.483	1.518	1.595	1.729	1 596	1.612	1.585	1.616	1.728	1.630	1.622
Fe3+	0.082	0.077	0.091	0.095	0.098	0.097	0.081	0.078	0 082	0 048	0.036	0 048	0.050	0.062	0 071	0.029	0.060	0.046
Fe2+	0.453	0.446	0.434	0.419	0.415	0.422	0 438	0.436	0.426	0 317	0.361	0.315	0.326	0.313	0 317	0.434	0.347	0.330
Mg	0 556	0.561	0 577	0.591	0.595	0.586	0.573	0.576	0 584	0.690	0.646	0 694	0 683	0.694	0.690	0 578	0 664	0 676
Total cat.	3 000	3.000	3.000	3.000	3.000	3.000	3.000	3.000	3.000	3.000	3.000	3.000	3.000	3.000	3 000	3.000	3.000	3.000
$Fe^{2+}/(Fe^{2+}+Mg)$	0.449	0 443	0.429	0.415	0.411	0.419	0.433	0.431	0.422	0.315	0 358	0.312	0.323	0.311	0.315	0 429	0.343	0.328
Cr/(Cr+Al)	0.799	0.792	0.795	0.790	0 780	0.793	0.759	0.781	0 800	0 823	0.887	0 824	0.833	0 824	0 843	0.887	0.849	0.835
$Fe^{3+}/(Fe^{3+}+Al+Cr)$	0 042	0.039	0 046	0.048	0 050	0 049	0 041	0.039	0 041	0 024	0.018	0 024	0.025	0 031	0 036	0.015	0.030	0 023

Sample no	25 2			25 5						DSP-1							
Anal no.	10	11	12	1	2	3	4	5	6	7	8	1	2	3	4	5	6	7
TiO2	0 26	0 38	0.40	0.19	0.27	0.34	0.22	0.25	0 35	0.31	0.30	0.53	0.56	0.62	0.71	0.66	0 55	0.58
Al2O3	7 74	9 29	2.97	9.23	7 95	8.20	8.91	8.93	6.93	8 85	8.27	10.40	10.26	10.25	10.57	10.76	10 66	10.60
Cr2O3	63.32	62.10	68.17	61.97	62.94	62.35	61.86	62.34	64.86	62.19	62.19	57.56	57.20	57.60	57.15	57.35	57.70	57.05
Fe2O3	2.21	1.20	1.89	3.06	3.13	3.26	2.45	2.79	0.85	2.77	3.03	3 93	4.13	4.15	3.83	3.16	3 54	3.42
FeO	12.46	12.17	13.43	11.99	12.92	12.42	12.23	11.65	14.59	12.30	12.62	15.86	15.23	15.36	15.63	16.57	16.11	16.15
MgO	13 69	14 02	12.62	14.34	13.67	13 99	13.92	14.50	12.34	14 12	13.77	12.02	12.31	12.40	12.27	11 65	11 94	11.72
Total	99.68	99 16	99.48	100.78	100 88	100 56	99.59	100.46	99.92	100.54	100.18	100.30	99.69	100.38	100.16	100.15	100.50	99.52
Ti	0 006	0 009	0.010	0.005	0.007	0.008	0.006	0.006	0.009	0.008	0.007	0.013	0.014	0 015	0.017	0.016	0.013	0.014
Al	0.298	0.356	0.118	0 348	0.303	0.312	0.341	0.338	0.269	0.336	0.316	0.398	0.395	0.392	0.404	0.413	0.407	0.409
Cr	1.635	1.596	1.814	1.568	1.607	1.592	1.588	1.582	1.692	1.582	1.595	1.479	1.476	1.476	1.467	1.477	1.479	1.478
Fe3+	0.054	0.029	0.048	0.074	0.076	0.079	0.060	0.067	0 021	0.067	0.074	0.096	0.101	0.101	0.094	0.078	0.086	0.084
Fe2+	0.340	0.331	0.378	0.321	0.349	0.335	0.332	0.313	0.403	0.331	0.342	0 431	0.416	0.416	0.424	0.451	0.437	0.443
Mg	0 667	0 679	0 633	0 684	0.658	0.673	0.674	0.694	0 607	0 677	0 666	0.583	0 599	0.599	0.594	0.565	0.577	0.572
Total cat.	3.000	3.000	3.000	3.000	3 000	3.000	3.000	3.000	3.000	3.000	3.000	3.000	3.000	3.000	3.000	3.000	3.000	3.000
$Fe^{2+}/(Fe^{2+}+Mg)$	0.338	0.327	0.374	0.319	0 347	0.333	0.330	0.311	0.399	0.328	0.340	0.425	0.410	0.410	0.417	0.444	0.431	0.436
Cr/(Cr+Al)	0.846	0.818	0.939	0 818	0.841	0.836	0.823	0.824	0.863	0.825	0.835	0.788	0.789	0.790	0.784	0.782	0.784	0.783
$Fe^{3+}/(Fe^{3+}+Al+Cr)$	0 027	0 015	0 024	0 037	0 038	0 040	0 030	0 034	0 011	0 034	0 037	0 049	0 051	0 051	0 048	0 039	0 044	0.043

Sample no.	DSP-1			MC-1					
Anal. no	8	9	10	1	2	3	4	5	6
TiO2	0.58	0.48	0.58	0.39	0.44	0.50	0.45	0.51	0.44
Al2O3	10 68	10.40	10 44	8.93	8.91	8.91	8.80	9.09	9.11
Cr2O3	58.00	58.10	57.49	55.42	55.87	56.12	55.80	55 88	55.76
Fe2O3	3 66	3.92	3.04	8 00	7.59	7.91	8.04	7.98	8.07
FeO	16 55	16 07	16.39	15 83	15.53	15.60	15.77	15 80	15.58
MgO	11 84	11.99	11 55	11 78	12.01	12.17	11.93	12.10	12.14
Total	101 31	100.96	99 49	100 35	100.35	101.21	100.79	101.36	101.10
Ti	0 014	0 012	0 014	0 010	0.011	0.012	0.011	0.013	0 011
Al	0 406	0 396	0 404	0.345	0.344	0.341	0.339	0.347	0.349
Cr	1.477	1.485	1.492	1.437	1.447	1.441	1.441	1.432	1.432
Fe3+	0 089	0 095	0 075	0.198	0.187	0.193	0.198	0.195	0 197
Fe2+	0.446	0 434	0.450	0.434	0.425	0.424	0.431	0.428	0 423
Mg	0 569	0 578	0 565	0.576	0.586	0.589	0.581	0.585	0 588
Total cat.	3.000	3.000	3.000	3.000	3.000	3.000	3.000	3.000	3.000
$Fe^{2+}/(Fe^{2+}+Mg)$	0.439	0 429	0.443	0.430	0 420	0.418	0 426	0.423	0 419
Cr/(Cr+Al)	0.785	0.789	0.787	0.806	0.808	0.809	0.810	0.805	0.804
$Fe^{3+}/(Fe^{3+}+Al+Cr)$	0 045	0 048	0 038	0 100	0 095	0 098	0.100	0 099	0 100

- = BELOW DETECTION LIMIT.

6.4 Mineral Equilibria in Cumulates

Many cumulate samples contain clinopyroxene-orthopyroxene, clinopyroxene-garnet and hornblende-garnet pairs that may yield subsolidus or metamorphic equilibration temperatures. The majority of minerals in individual pairs are, however, not contiguous, suggesting that they may not be in equilibrium. To avoid this problem, equilibrium temperatures have been calculated only from mineral pairs in very close contact. The analyses used in thermometry calculations are given in Tables 6.19, 6.20 and 6.21.

Several geothermometers have been applied: these include two-pyroxene solvus (Wells,1977), and Fe-Mg exchange equilibria between clinopyroxene and garnet (Ellis and Green, 1979), and amphibole and garnet (Graham and Powell, 1984). The results (Table 6.22) show that the two-pyroxene thermometer yields equilibration temperatures ranging from 839 to 897°C for cumulus gabbro, websterite, olivine clinopyroxenite and wehrlite. This range of temperatures corresponds to subsolidus cooling. The temperatures derived from the Fe-Mg exchange equilibria between garnet and clinopyroxene in a garnet amphibolite (771-782°C at 5 kb) are also comparable to the upper amphibolite facies of regional metamorphism as suggested by its mineral assemblage. The temperatures obtained from hornblende-garnet equilibria in two garnet amphibolites have a restricted range (601-617°C); these are in agreement with epidote-amphibolite facies of regional metamorphism, as revealed by their mineral assemblages.

6.5 Blueschists

6.5.1 Occurrence and Petrography

Blueschists with quartzite intercalations have only been recognised in a small creek just south of Doi Phuk Sung (grid reference: 04293032, sheet 5145 I, Ban Nam Muap, 1:50,000 Royal Thai Army Survey map), Doi Phuk Sung area. They occur as block(s) in serpentinite matrix.

Petrographically, they are fine-grained rocks with two sets of pronounced foliation produced by subparallel alignment of nematoblastic and lepidoblastic minerals, and elongated lenticular layers. They are made up of subhedral to anhedral albite, euhedral to subhedral blue amphibole, euhedral to subhedral green amphibole (actinolite), subhedral to anhedral epidote, white mica, chlorite, hexagonal carbonate, quartz and fibrous stilpnomelane in different proportions. Their colours vary from

TABLE 6.19 AVERAGE ELECTRON MICROPROBE ANALYSES CLOSE TO THE CONTACTS OF CLINOPYROXENE-ORTHOPYROXENE PAIRS IN MAFIC AND ULTRAMAFIC PLUTONIC ROCKS. FeO AND Fe_2O_3 ARE CALCULATED ASSUMING STOICHIOMETRY ON THE BASIS OF 4 CATIONS AND 6 OXYGENS.

Sample no.	32.6				8.1A		8.5		YP-5		47.3A			
Pair no	1		2		1		1		1		1		2	
Mineral	Cpx	Opx	Cpx	Opx	Cpx	Opx[1]	Cpx	Opx	Cpx	Opx	Cpx	Opx	Cpx	Opx
n[2]	4	3	3	2	1	1	1	2	4	4	4	4	4	4
SiO2	51.26	50.79	51.68	50.91	53.95	55.91	53 50	56.00	57.78	55.29	53.18	54.45	53.03	54.44
TiO2	0.33	-	0.28	-	-	-	-	-	-	-	0.22	-	0.21	-
Al2O3	3 66	2.30	3.53	2.27	1.69	1.61	1.57	1.50	0 57	0.43	2.46	2.75	2.54	2.89
Cr2O3	-	-	-	-	0.50	0.23	0.32	0.11	0.25	-	-	-	-	-
Fe2O3	0.99	1.19	1.17	1.33	0.24	0.76	0.98	0 34	0.07	0.07	-	-	-	-
FeO	9.10	25.24	9.08	25.12	3.68	9.39	2.60	9.79	2.28	8.34	4.43	14.22	4.46	14.26
MnO	0.12	0.73	0.29	0.78	-	0.22	-	0.25	-	0.13	-	0.28	-	0.26
MgO	12.18	19.22	12 27	19.32	16 87	31.69	17.17	31.73	18.14	32.87	15.84	28.11	15.75	27.97
CaO	21.97	0.04	22.10	0.41	24.00	0.60	24.02	0.30	24.30	1.16	23.92	0.26	23.99	0.34
Na2O	0 55	-	0.54	-	-	-	-	-	-	-	-	-	-	-
Total	100 13	101.42	100.93	100.13	100.93	100.41	100.16	100.00	100.90	100.07	100.05	100.06	99.97	100.15
Si	1.916	1.932	1.918	1.930	1.953	1.954	1.948	1.963	1.987	1.996	1.946	1.943	1.943	1.942
Ti	0.009	-	0.008	-	0.008	-	-	-	-	-	0 006	-	0 006	-
Al	0 161	0.103	0.154	0.101	0 142	0.066	0.067	0.062	0.024	0.017	0.106	0.116	0.110	0.121
Cr	-	-	-	-	-	-	0.009	0.003	0.071	-	-	-	-	-
Fe3+	0 028	0 034	0 033	0 038	0.007	0.020	0.027	0 009	-	-	-	-	-	-
Fe2+	0 284	0 803	0 282	0.797	0.112	0 274	0.079	0 287	0.068	0.243	0.136	0.426	0.137	0.426
Mn	0 004	0.023	0.009	0.025	-	0.006	-	0 007	-	0.004	-	0.008	-	0.008
Mg	0 678	1 089	0.679	1.092	0.911	1.650	0.932	1 658	0.972	1.692	0.863	1.495	0.860	1.487
Ca	0.880	0.016	0.879	0 017	0.931	0.023	0.937	0.011	0.936	0.043	0.938	0.010	0.942	0.013
Na	0 040	-	0 039	-	-	-	-	-	-	-	-	-	-	-
Total cat.	4 000	4 000	4 000	4 000	4.000	4.000	4.000	4 000	3 995	3 995	3 995	3.998	3.996	3 990
Mg/(Mg+Fe^{2+})	0.705	0.576	0.707	0.578	0 891	0.857	0.922	0.852	0.934	0.876	0 864	0.778	0.864	0.777
[X_{Mg}]M1 [3]	0.624	0.536	0.627	0.538	0.849	0 818	0.874	0.821	0.917	0.863	0.814	0.733	0.813	0.728
[X_{Mg}]M2 [3]	0.054	0.553	0.052	0.554	0.061	0.833	0.058	0.837	0.055	0.825	0.050	0.759	0.047	0.756
a $Mg_2Si_2O_6$ [3]	0 034	0 297	0 033	0 298	0.052	0 681	0 051	0 687	0 050	0.712	0.040	0.556	0.038	0 550

[1] = EXSOLUTION LAMELLA, [2] = NUMBERS OF ANALYSES, [3] = CALCULATED BY THE METHOD OF WOOD AND BANNO (1973).
- = BELOW DETECTION LIMIT.

TABLE 6.20. AVERAGE ELECTRON MICROPROBE ANALYSES CLOSE TO THE CONTACTS OF CLINOPYROXENE-GARNET PAIRS IN A GARNET AMPHIBOLITE. FeO AND Fe_2O_3 ARE CALCULATED ASSUMING STOICHIOMETRY ON THE BASIS OF 4 CATIONS AND 6 OXYGENS FOR CLINOPYROXENES, AND 8 CATIONS AND 12 OXYGENS FOR GARNETS.

Sample no.	9.2					
Pair no	1		2		3	
Mineral	Cpx	Gt	Cpx	Gt	Cpx	Gt
n[1]	2	4	2	3	2	3
SiO2	51.47	38.16	51.48	38 31	51.30	38 37
TiO2	0.27	-	0 13	-	-	-
Al2O3	3.00	21.33	2.90	21.35	3.16	21.48
Cr2O3	0 10	0.70	-	-	0.11	-
Fe2O3	0 68	25.92	1.15	0 87	0.95	1.00
FeO	11.94	1.11	11 07	25.56	11.19	25 85
MnO	-	-	-	1.09	-	1.09
MgO	10 26	3.59	10 67	3 76	10.48	4.40
CaO	22.28	9 53	22.25	9.73	22.62	8.66
Na2O	0 66	-	0 67	-	0.59	-
Total	100.53	100 34	100.31	100.67	100.66	100.85
Si	1.939	2.993	1.940	2.995	1.929	2 985
Ti	0.007	-	0 004	-	0.008	-
Al	0.133	1.972	0 128	1.971	0.140	1.970
Cr	0.003	-	-	-	0.003	-
Fe3+	0.034	0.042	0 040	0.039	0.042	0.059
Fe2+	0.361	1.700	0.342	1.692	0.336	1 682
Mn	-	0.074	-	0.073	-	0 072
Mg	0.576	0.420	0 599	0.461	0.687	0.511
Ca	0 899	0 800	0.898	0.769	0.911	0.721
Na	0 048	-	0 049	-	0 043	-
Total cat.	4.000	8 000	4.000	8.000	4.000	8.000
X_{Ca} [2]	-	0 274	-	0 279	-	0.248
Fe2+/Mg	0 627	4 051	0 570	3 818	0.573	3 293

[1] = NUMBERS OF ANALYSES, [2] = Ca/(Ca+Fe^{2+}+Mn+Mg), - = BELOW DETECTION LIMIT.

TABLE 6.21. AVERAGE ELECTRON MICROPROBE ANALYSES CLOSE TO THE CONTACTS OF GARNET-AMPHIBOLE PAIRS IN GARNET AMPHIBOLITES. FeO AND Fe_2O_3 ARE CALCULATED ASSUMING STOICHIOMETRY ON THE BASIS OF 8 CATIONS AND 12 OXYGENS FOR GARNETS, AND 12 CATIONS AND 23 OXYGENS FOR AMPHIBOLES.

Sample no.	9.2				64.1	
Pair no	1		2		3	
Mineral	Gt	Hb	Gt	Hb	Gt	Hb
n [1]	3	3	3	3	1	3
SiO2	38.00	49.51	38.60	46.27	38.64	54.21
TiO2	-	0.20	-	0.82	-	-
Al2O3	21.54	10.17	21.99	12.53	20.63	2.24
FeO	23.74	11.04	25.24	12.68	23.54	15.11
MnO	0.68	-	0.71	-	1.06	0.36
MgO	4.50	14.30	4.74	12.56	4.99	13.79
CaO	10.87	10.74	9.07	11.14	10.19	11.63
Na2O	-	2.38	-	2.14	-	0.62
K2O	-	0.18	-	0.49	-	0.19
Total	99.33	98.51	100.35	98.63	100.42	98.17
Si	2.983	7.039	2.997	6.669	3.002	7.839
Ti	-	0.021	-	0.089	-	-
Al	1.993	1.705	2.012	2.130	2.004	0.381
Fe2+	1.558	1.312	1.639	1.528	1.635	1.831
Mn	0.045	-	0.047	-	0.047	0.045
Mg	0.527	0.030	0.548	2.697	0.530	2.969
Ca	0.914	1.636	0.754	1.721	0.777	1.803
Na	-	0.656	-	0.598	-	0.173
K	-	0.032	-	0.090	-	0.036
Total cat.	4.000	8.000	4.000	8.000	4.000	8.000
X_{Ca} [2]	0.300	-	0.252	-	0.260	-
Fe2+/Mg	0.253	0.697	0.251	0.671	0.245	0.671

[1] = NUMBERS OF ANALYSES, [2] = Ca/(Ca+Fe^{2+}+Mn+Mg).
- = BELOW DETECTION LIMIT.

TABLE 6.22. TEMPERATURES ESTIMATES (°C) OBTAINED FROM THE DATA GIVEN IN TABLES 6.19, 6.20 AND 6.21.

Sample no.	Cpx-Opx [1]	Cpx-Gt [2]	Hb-Gt [3]
32.6 [4]	839 - 846		
47.3A [5]	845 - 853		
8.1A [6]	897		
YP-5 [7]	889		
8.5 [7]	859		
9.2 [8]		759 - 770 at 1 kb 771 - 782 at 5 kb	
63.2 [8]			603 - 617
64.1 [8]			601

[1] = clinopyroxene-orthopyroxene geothermometer of Wells (1977).
[2] = clinopyroxene-garnet geothermometer of Ellis and Green (1979).
[3] = hornblende-garnet geothermometer of Graham and Powell (1984).
[4] = cumulus gabbro, [5] = websterite, [6] = olivine clinopyroxenite, [7] = wehrlite.
[8] = garnet amphibolite.

bluish to greenish depending on the amounts of blue amphibole relative to chlorite, i.e. bluish when blue amphibole is dominant (Fig. 6.18), and greenish when chlorite is dominant. Furthermore, they may be characterised by alternate light-coloured (quartz-rich) and dark-coloured (amphibole and epidote- or chlorite and epidote-rich) layers.

6.5.2 Chemistry of Blue Amphiboles

Analyses and site occupancy of blue amphiboles are given in Table 6.23. Two modes of normalisation have been used for estimating Fe^{3+}, including total cations - K = 15 and total cations - (Ca + Na + K) = 13 (Laird and Albee, 1981). Assuming that Ca occurs only in M4, the former has been chosen for the analyses with Ca + Na^{M4} less than or equal to 2, otherwise the latter has been applied.

These amphiboles are mainly crossitic (Fig. 6.19a) according to the amphibole nomenclature compiled by Leake (1978). The chemical variations are explicable in terms of glaucophane substitution, Na^{M4}, (Al^{vi}, Fe^{3+}, Ti, Cr) = Ca, (Fe^{2+}, Mg, Mn) as their Na^{M4} contents are highly negatively and positively correlated with Ca and (Al^{vi} + Fe^{3+} + Ti + Cr), respectively (Fig. 6.19b,c). This implies that they result from high-pressure metamorphism.

6.5.3 Pressure-Temperature Conditions of Formation

Two approaches have been taken in assessing the pressure-temperature conditions of formation of these blueschists, including mineral stability relations and a suitable geobarometer. From the petrogenetic grid in Figure 6.20, a minimum pressure of 4.5 kb and a maximum temperature of 550°C may be inferred from the maximum stability curve of glaucophane (Maresch, 1977). The lack of aragonite suggests that they have not reached extremely high-pressure conditions, i.e. a maximum pressure of 13 kb. The absence of lawsonite marks a minimum temperature of 350 to 450°C. The empirical geobarometer of Brown (1977) on the basis of Na^{M4} and Al^{iv} contents of crossite, which is associated with epidote, quartz, actinolite, albite, chlorite and magnetite, yields a pressure of 7 kb (Fig. 6.21). Therefore, it may be concluded that these blueschists have been formed at a pressure of approximately 7 kb and temperatures in a range of 390 to 450°C (geothermal gradients = 15 - 18°C/km).

TABLE 6.23. ANALYSES OF BLUE AMPHIBOLES WITH SITE DISTRIBUTION FOR CATIONS PER 23 OXYGENS

Sample no.	Bsc N				Bsc O	Bsc P			
Anal. no.	1	2	3	4	1	1	2	3	4
SiO2	55.65	55.72	56.07	54.55	55.65	56.07	51.07	55.82	55.42
TiO2	-	-	0.22	0.18	-	-	0.25	-	0.20
Al2O3	3.95	3.31	4.22	4.61	3.08	3.35	4.66	3.87	3.70
FeO	23.21	23.78	21.45	22.68	23.13	22.50	21.85	22.38	23.54
MgO	7.57	7.72	8.30	7.48	8.36	7.39	4.57	8.14	7.82
MnO	-	-	-	-	-	-	-	0.27	0.23
CaO	0.72	0.38	0.80	2.25	1.03	1.34	5.27	1.24	1.00
Na2O	6.98	7.14	6.83	6.32	6.92	7.16	10.03	6.76	6.67
Total	98.09	98.04	97.88	98.07	98.17	97.80	97.69	98.48	98.58
Si	7.950	7.959	7.965	7.859	7.942	7.900	7.917	7.935	7.881
ivAl	0.050	0.041	0.035	0.141	0.058	0.100	0.083	0.065	0.119
Total tetra.	8.000	8.000	8.000	8.000	8.000	8.000	8.000	8.000	8.000
viAl	0.615	0.516	0.672	0.642	0.461	0.797	0.739	0.583	0.502
Ti	-	-	0.023	0.020	-	0.057	0.043	-	0.021
Fe3+	1.282 [1]	1.433 [1]	1.191 [1]	0.998 [1]	1.365 [1]	0.910 [1]	1.006 [1]	1.240 [1]	1.414 [2]
Mg	1.612	1.644	1.756	1.606	1.779	1.721	1.848	1.724	1.658
Fe2+	1.492	1.407	1.358	1.735	1.396	1.489	1.364	1.420	1.385
Mn	-	-	-	-	-	0.027	-	0.032	0.020
Total M1-3	5.000	5.000	5.000	5.000	5.000	5.000	5.000	5.000	5.000
Mn	-	-	-	-	-	-	-	-	0.008
Ca	0.111	0.058	0.122	0.348	0.158	0.238	0.209	0.189	0.153
Na	1.889	1.942	1.878	1.652	1.842	1.762	1.791	1.811	1.839
Total M4	2.000	2.000	2.000	2.000	2.000	2.000	2.000	2.000	2.000
Na[A]	0.044	0.034	0.004	0.115	0.074	0.041	0.042	0.053	-
Mg#	0.519	0.539	0.564	0.481	0.560	0.536	0.575	0.548	0.545
Na[M4] [2]	1.927	1.972	1.881	1.753	1.907	1.799	1.828	1.858	1.839
Al^{iv} [2]	0.073	0.059	0.037	0.201	0.097	0.122	0.106	0.093	0.119

[1] = DETERMINED BY NORMALISING CATIONS OTHER THAN Ca, Na AND K TO 13.

[2] = DETERMINED BY NORMALISING CATIONS OTHER THAN K TO 15.

- = BELOW DETECTION LIMIT.

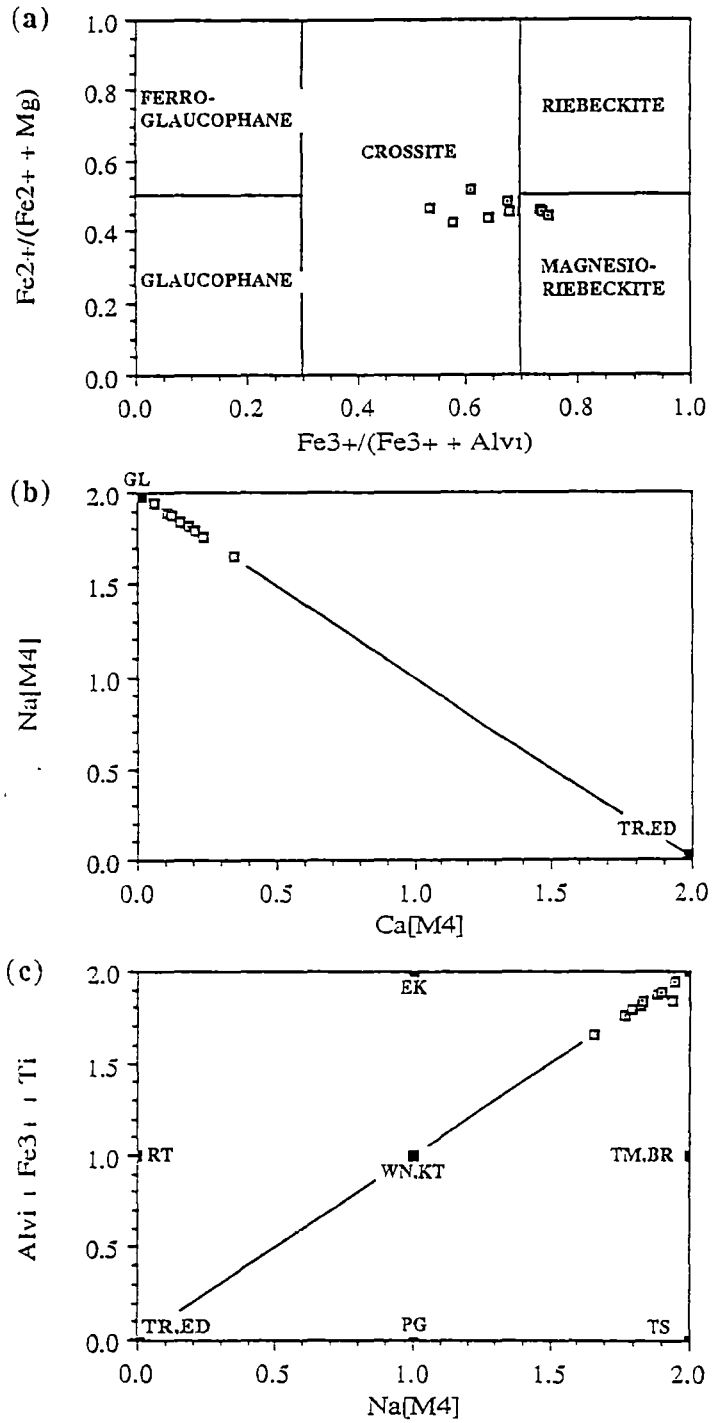

Figure 6.19. Variation diagrams for blue amphiboles in blueschists in terms of (a) $Fe^{2+}/(Fe^{2+}+Mg)$ against $Fe^{3+}/(Fe^{3+}+Al^{vi})$, showing the positions of data points relative to the compositional fields for alkali amphiboles with $(Na+K)_A < 0.5$ (Leake, 1978), and (b) Na^{M4} against Ca and (c) Na^{M4} against $Al^{vi}+Fe^{3+}+Ti+Cr$ for blue amphiboles in blueschists, illustrating glaucophane substitution, Na^{M4}, (Al^{vi}, Fe^{3+}, Ti, Cr) = Ca, (Fe^{2+}, Mg, Mn). TR=tremolite, ED=edenite, PG=pargasite, TS=tschermakite, RT=richterite, WN=winchite, KT=kataphorite, BR=barroisite, TM=taramite, EK=eckermanite, GL=glaucophane.

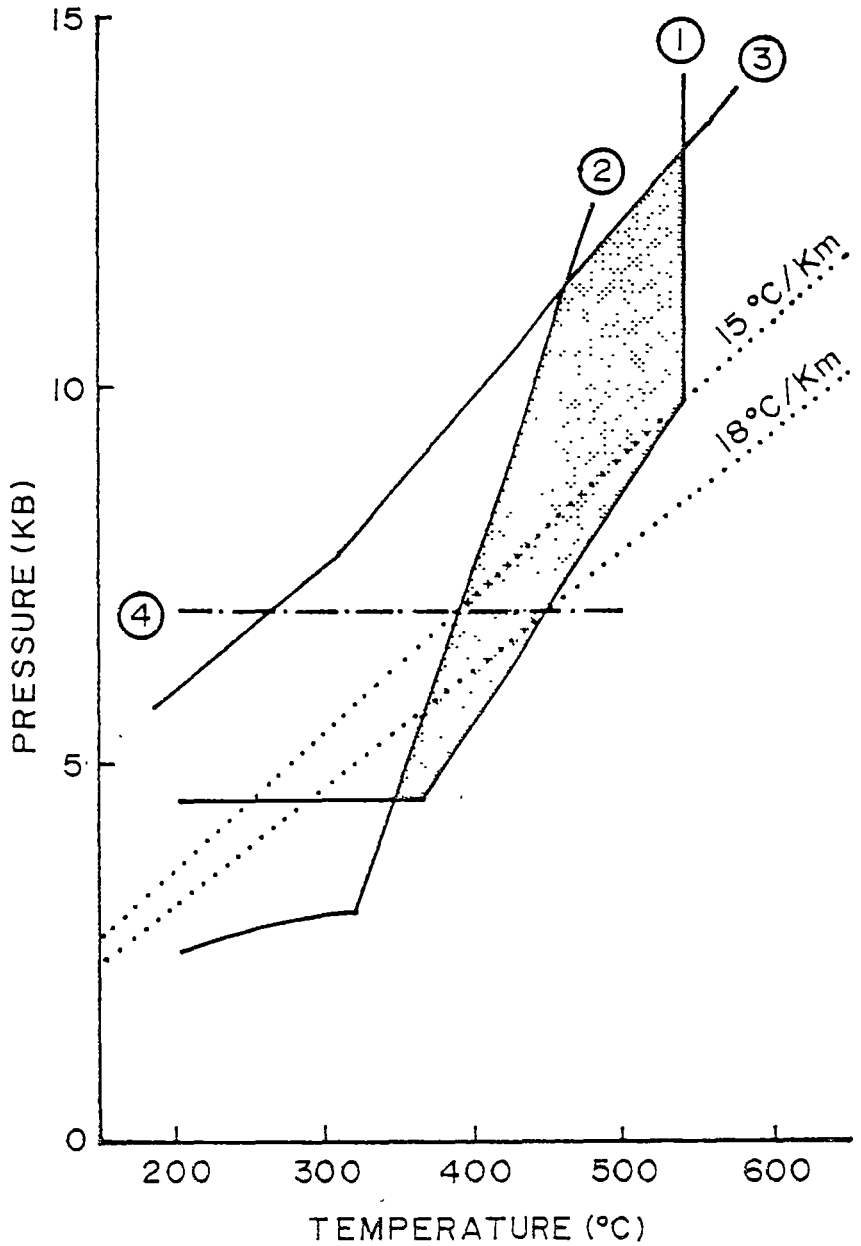

Figure 6.20. Selected equilibria that constrain pressure-temperature conditions of formation of blueschists. (1) maximum stability limit of glaucophane (Maresch, 1977). (2) stability curve for lawsonite (Droop, 1985). (3) curve for aragonite-calcite transformation (Johannes and Puhan, 1971). (4) estimated pressure from Figure 6.21. Shaded region indicates possible pressure-temperature conditions for blueschists based on mineral stability relations. Dotted lines are geothermal gradients proposed for the the formation of blueschist based on (1), (2) and (4).

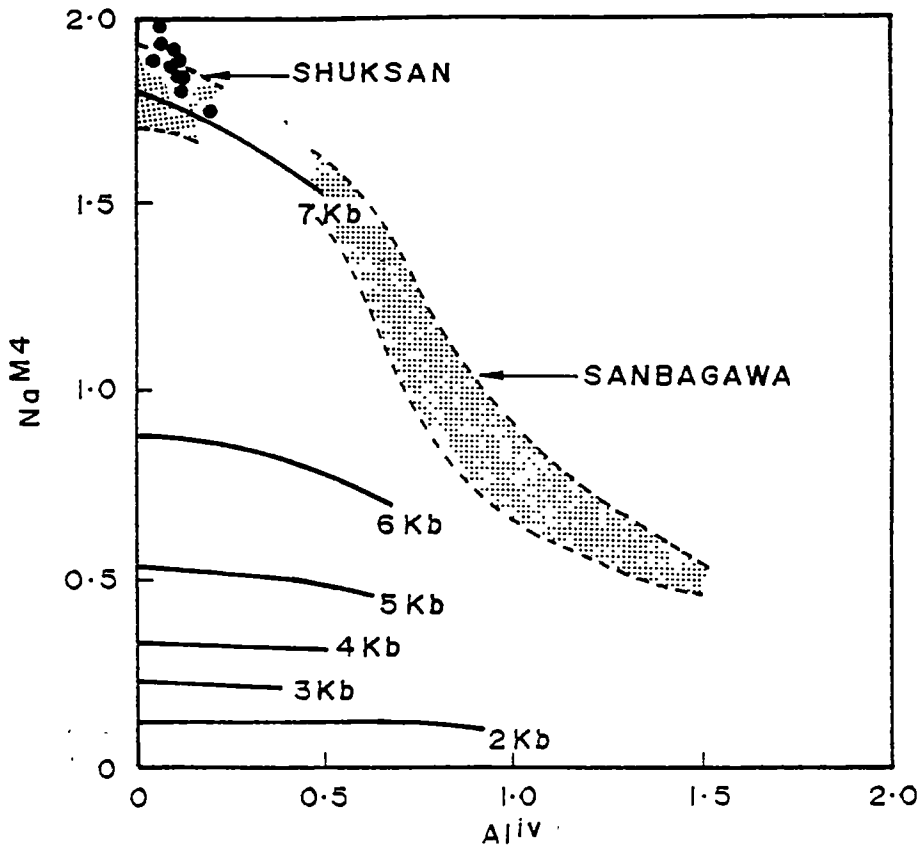

Figure 6.21. The empirical geobarometer for buffer reaction: crossite+epidote+quartz = actinolite+magnetite+albite+chlorite+H_2O of Brown (1977), showing the pressure of formation for blueschists presented in this study.

6.6 Summary

6.6.1 Summary of Mafic and Ultramafic Plutonic Rocks

On the basis of their occurrences and mineral chemistries, mafic and ultramafic plutonic rocks may be separated into two groups: (1) cumulus gabbros/amphibolites, clinopyroxenites, olivine clinopyroxenites, wehrlites, dunites and harzburgites, and (2) cumulus chromitites and associated dunites. These rocks have suffered variable degrees of chloritisation, saussuritisation, amphibolitisation and serpentinisation. Cumulus textures are preserved in many samples.

Gabbros/amphibolites and associated ultramafics

The rocks constituing this group are much more abundant relative to other igneous types, and occur in every key area, most commonly as blocks in serpentinite matrix. Gabbros/ amphibolites with pronounced foliation are evidently intruded by non-foliated Subgroup C-1 arc microgabbros.

Gabbros are characterised by low contents of incompatible elements (0.1-1.4 wt% TiO_2, trace-0.4 wt% P_2O_5, <1-4 ppm Nb, <1-41 ppm Zr and 5-24 ppm Y, 0.59-3.11 ppm La, and 0.69-1.75 ppm Yb) and have chondrite-normalised REE patterns that are flat to slightly enriched from Yb to Sm, and flat to depleted from Sm to La; most exhibit positive Eu anomalies. They cannot have formed by crystal accumulation from liquids giving rise to ocean-island basalts (Group A) and backarc basin basalts and andesites (Group B) as their TiO_2 contents are comparable to those in low-Ti ophiolitic gabbros at similar Mg#. Although their TiO_2 contents and REE patterns are similar to those of Subgroup C-1 arc samples, field relationships (i.e. foliated gabbroic rocks are intruded by non-foliated Subgroup C-1 microgabbro) do not support direct affinities with Group C arc lavas, dolerites and microgabbros. They might represent another magmatic suite which formed in a supra-subduction zone environment prior to the generation of Subgroup C-1 arc lavas and related rocks.

Analyses of relict clinopyroxenes, orthopyroxenes, olivines and chromites in gabbros/amphibolites and associated ultramafic rocks, and field relationships show that these rocks are likely to be comagmatic. Crystallisation sequence may be inferred as follows: olivine+chromite+orthopyroxene - clinopyroxene - plagioclase. This inference together with spinel compositions (in harzburgite, wehrlite and olivine clinopyroxenite), which are comparable to those in Oshima-Oshima arc lavas and cumulates, and affinities with the low-Ti ophiolitic association (Serri, 1981) and implies supra-subduction zone arc-related magmatism (Pearce *et al.*, 1984).

Chromitites and associated dunites

The occurrences of rocks in this association are restricted in the Mae Charim, Doi Phuk Sung and Nan River areas. Chromitites occur as sheared layers, schlieren, pods or blocks in serpentinite (derived from dunites). They also occur as angular blocks in dolomite matrix (transformed from serpentine). They are highly refractory rocks as indicated by their chromite compositions comparable to those in high Ca-boninites, and are probably generated in a supra-subduction environment.

6.6.2 Summary of Blueschists

Blueschists with quartzite intercalations have been recognised only in the Doi Phuk Sung area. They are made up of albite, blue amphiboles (crossitic), green amphiboles (actinolite), epidote, white mica, chlorite, magnetite, carbonate, quartz and stilpnomelane in different proportions. Pressure-temperature conditions of formation have been determined by using mineral stability curves and Na^{M4} and Al^{iv} contents of blue amphiboles. It appears that they have formed at a pressure of about 7 kb and temperatures in a range of 390 to 450°C, i.e. geothermal gradients 15-18°C/km.

CHAPTER 7

IMPLICATIONS FOR PLATE TECTONIC MODELS

7.1 Significance of Meta-igneous Rocks and Blueschists

Prior to this study, the Nan Suture has been widely referred to as an ophiolitic suture marking the collision zone between the Shan-Thai and Indochina cratons. This study has shown that the Nan Suture is not a series of discontinuous ophiolitic massifs, but rather, is an extensive serpentinite melange zone, with blocks up to a few kilometres across. These blocks are constituted by three major volcanic suites, namely ocean-island basalts (Chapter 3), immature back-arc basin basalts and andesites (Chapter 4), and island-arc basalts and andesites (Chapter 5). In addition, mafic plutonic blocks are inferred to have formed in a 'supra-subduction zone' environment (Chapter 6).

Occan-island basalts in the Nan Suture might have formed as a chain of islands in either a major ocean basin (e.g. Hawaiian-Emperor Chain) or in a mature backarc basin (e.g. Tasmantid Seamounts in Tasman Sea). The presence of immature backarc basin basalts and andesites might preclude the latter possibility. The absence of MORB in the Nan Suture blocks is not a problem for either scenario above, as at most subduction zones on the modern Earth, oceanic crust is very efficiently subducted, whereas positive features (e.g. seamounts and ridges) on the subducting oceanic crust are often scraped off and incorporated into the forearc (Bloomer, 1983).

The presence of 'supra-subduction zone' rocks (backarc basin basalts and andesites) indicate that subduction was occurring at one (or both) margins of the ocean which was consumed leading up to the collision of the Shan-Thai and Indochina cratons in the Middle Permian to Late Triassic. The intraplate basalts may well have been a seamount chain in that ocean basin; this implies that they should be older than Middle Permian. Although no direct evidence for the age of these rocks is available, the volcanic breccia with a calcareous matrix containing Permo-Carboniferous fossils from the area between Doi Phuk Sung and Nan River (Hahn, 1985), is likely to have ocean-island basalt affinities, since where best exposed in the Mae Charim area, the ocean-island basalt blocks are frequently volcanic breccia and tuff, with marble common.

Blueschists also occur as blocks in serpentinite matrix. Their protoliths appear to have been tuffs or tuffaceous sediments with ocean-island affinities, as suggested by

a chemical analysis given by Busse *et al.* (1989); this shows a high TiO_2 content, comparable to those in the studied ocean-island transitional tholeiitic and alkalic basalts. These blueschists were formed at relatively moderate pressures (about 7 kb)(Chapter 6).

7.2 Plate Tectonic Model

It is emphasised that the model discussed below is suggested on the basis of available data, constrained by comparisons with better preserved ophiolites and modern tectonic settings. Further structural studies (S. Singharajwarapan: Ph.D. programme, Univ. of Tasmania, in progress) and Ar-Ar dating on Subgroup A-2 ocean-island basalt, Subgroup B-1 BABB, and gabbros/amphibolites (R.A. Duncan; work in progress) should provide tighter constraints on this model. In addition, little is known of the Lower Carboniferous volcanic rocks in the Loei Foldbelt, to the east of the Nan Suture (Hahn *et al.*, 1986), or the belts of Permo-Carboniferous to Permo-Triassic arc-type lavas west of the Nan Suture (Hahn *et al.*, 1986; Barr *et al.*, 1990).

The ocean-island basalts in the Nan Suture were probably scraped off at the trench of a major ocean basin into the forearc of an island arc. However, the polarity of the subduction zone associated with this arc-trench system remains unknown. It might have dipped westward towards and under the Shan-Thai craton, or eastward beneath the Indochina craton, or there may have been contemporaneous subduction beneath both cratons.

Normal arc-continent collisions occur when thinned passive margin crust underthrusts an island arc, colliding initially with the forearc region. In such a case, forearc may be sliced up and emplaced as one or more massive slabs of ophiolite onto the passive margin (e.g. Oman; Lippard *et al.*, 1986). Such ophiolite 'massifs' bear little resemblance to the Nan Suture ophiolitic melange, which is considerably more tectonically disrupted and disorganised.

With the meagre constraints available on the timing and polarity of arcs, collisions and subduction reversals, any tectonic model for the evolution of this foldbelt and suture is necessarily preliminary. A preferred model is described below, and stages in the development of the foldbelt are shown schematically in Figure 7.1.

During Late Carboniferous, it is likely that the once-contiguous continental blocks of the Shan-Thai and Indochina cratons were separated by a major ocean basin. An east-dipping subduction zone formed at the leading edge of the Indochina craton (Fig. 7.1a), and this arc may have been rifted, to form a backarc basin by Early

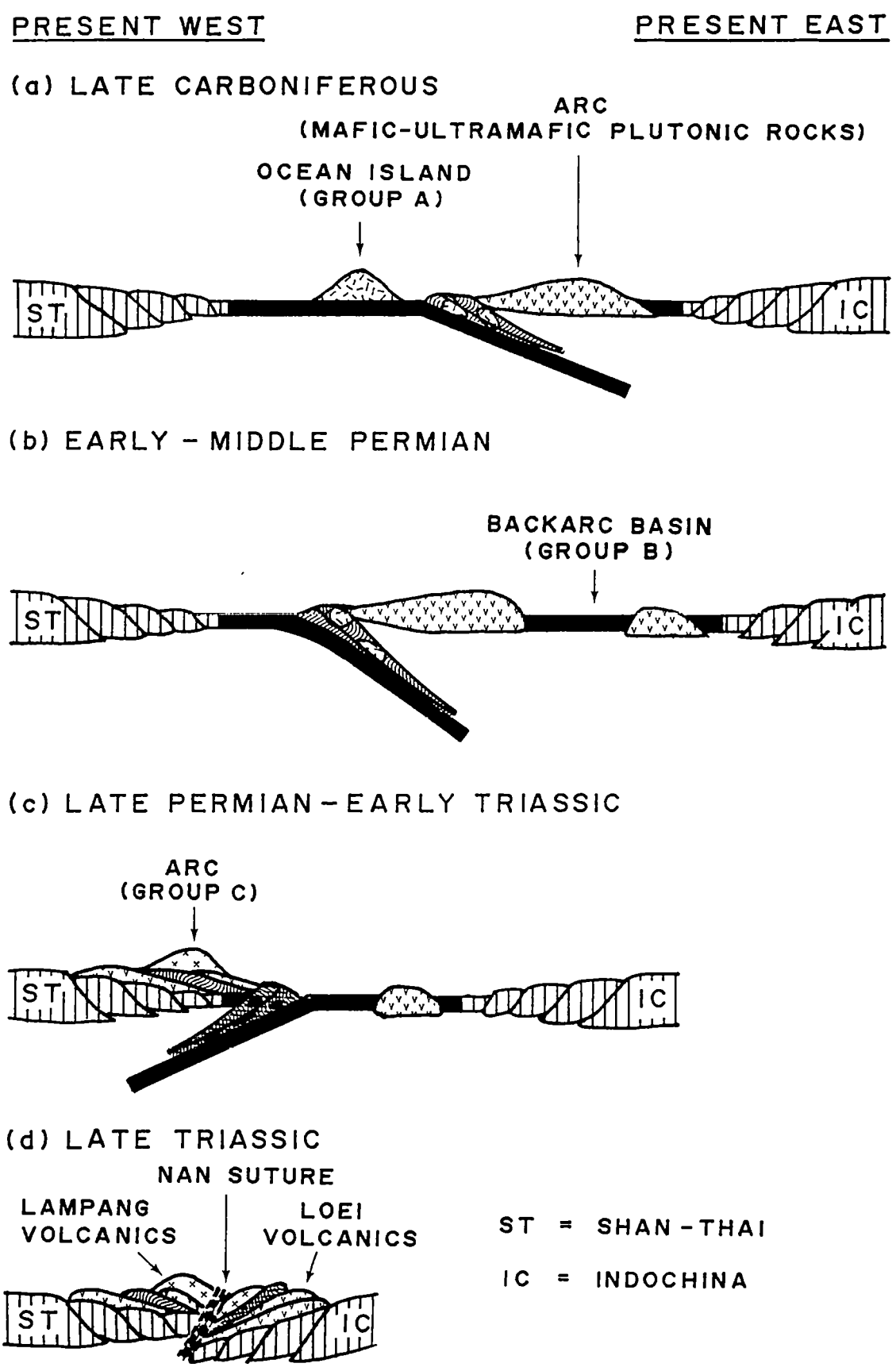

Figure 7.1. Schematic diagrams showing one hypothetical model for the Nan Suture from Late Carboniferous to Late Triassic times (see explanation in text).

Permian time (Fig. 7.1b). Fragments of the basement of this arc are represented by the huge blocks of arc mafic/ultramafic plutonics, while the Group B lavas are representative of those produced in the early stages of arc splitting and backarc basin formation. Ocean-island basalts (group A) formed seamounts on the subducting oceanic plate, and were eventually plastered onto the trench-forearc slope of this arc. Some of the volcaniclastic apron of one or more of these seamounts was subducted to depths of at least 25 km beneath the forearc, to form blueschists.

It is hypothesised that the leading edge of the Shan-Thai craton began colliding with this arc in the Middle Permian, causing allochthonous sheets of forearc, arc and closest-to-arc backarc basin crust to be emplaced on the Shan-Thai thinned passive margin crust.

Continued subduction of backarc crust dragged the Carboniferous remnant arc and the Indochina craton into the trench, where another more complex arc-continent collision occurred, probably during Late Permian. During both this second collision event on the arc suture, and later post-collisional extensional collapse and strike-slip movement, the first collision complex was considerably disrupted, eventually to form a massive mélange. The remnant arc rocks of the first Carboniferous arc may be represented by the volcanics in the little-known Loei Foldbelt, east of the Nan Suture (fig. 7.1d). Extensive molasse deposition (Khorat Group) occurred in pull-apart basins formed after the final Late Triassic collision.

PART II

AN EMPIRICAL STUDY OF THE EFFECTS OF Ca/Na, Al/Si and H_2O ON PLAGIOCLASE - MELT EQUILIBRIA AT 5 - 10 KB PRESSURE

CHAPTER 8

AN EMPIRICAL STUDY OF THE EFFECTS OF Ca/Na, Al/Si AND H_2O ON PLAGIOCLASE - MELT EQUILIBRIA AT 5 - 10 KB PRESSURE

8.1 Introduction

The study described below was carried out to provide the author with an opportunity to become experienced with modern methods of experimental petrology. This study is concerned with a method of petrological characterisation of magmas and an experimental evaluation of the petrological significance of such a characterisation.

Extremely calcic plagioclase compositions (An_{80-100}) have been commonly recorded from high-Al basalts and gabbroic nodules in island-arcs (Arculus and Wills, 1980; Brophy, 1986; Crawford *et al.*, 1987; Stolz *et al.*, 1988; Beard and Borgia, 1989), and from mid-ocean ridge basalts (herein MORB)(Donaldson and Brown, 1977; Stakes *et al.*, 1984; Autio and Rhodes, 1984; Price *et al.* 1986; Koyaguchi, 1986; see summary by Wilkinson 1982). However, the physico-chemical conditions required for their formation remain poorly understood. Three controls on the presence of highly calcic plagioclase in basalts have been proposed:

1. Numerous workers have appealed to the effect of high-water pressure in a magma, which significantly modifies the shape of the solidus loop in simple systems (Johannes 1978, 1989), stabilising more calcic plagioclase compositions than would crystallise from the same composition under anhydrous conditions,
2. Plagioclase equilibria in a range of compositions under anhydrous conditions show that strongly anorthitic plagioclase crystallisation requires high Ca/Na bulkrock compositions (Drake, 1976; Falloon and Green, 1986), and
3. Reactions for plagioclase-melt equilibria demonstrate that in addition to high bulk Ca/Na, high bulk Al/Si could stabilise calcic plagioclase (Drake, 1976). Beard and Borgia (1989) have also argued that high Al_2O_3 in the bulkrock compositions could stabilise more calcic plagioclase under anhydrous compositions than in similar compositions with lower Al_2O_3 contents.

This study reports an experimental investigation of some factors thought to affect the composition of plagioclase crystallising in complex basaltic systems, including composition (with particular emphasis on Ca/(Ca+Na) and Al/(Al+Si) ratios), at controlled temperatures, pressures and water contents.

8.2 Experiments

8.2.1 Starting materials

Eight starting compositions (Table 8.1) were prepared by mixing AR GRADE oxides (SiO_2, TiO_2, Al_2O_3, Fe_2O_3, MnO and MgO), carbonates ($CaCO_3$, Na_2CO_3 and K_2CO_3) and $Ca_2P_2O_7$ as required under acetone in an agate mortar and firing at 1000°C for 12 hours. Pure fayalite, synthesised from a stoichiometric mixture of specpure Fe sponge, Fe_2O_3 and SiO_2 heated for three days in an evacuated silica tube at 1,000°C, was then added to the mixes and recrushed under acetone before igniting in a 1-atmosphere furnace at 450°C in an argon atmosphere. The prepared starting mixes were not melted to obtain further homogenisation before use in experiments in order to avoid possible Na_2O losses by volatilisation from the melt. The synthetic mixes were checked by microprobe analysis of above-liquidus glasses (Table 8.2). As expected, iron gain occurred in anhydrous glasses using specpure Fe containers and in contrast, iron loss occurred in hydrous glasses using $Ag_{50}Pd_{50}$ and Pt containers. However, in all the above-liquidus runs, bulk molecular 100*Ca/(Ca+Na) (herein Ca#) and 100*Al/(Al+Si)(herein Al#) values, remain comparable to those for theoretical starting compositions. The small iron additions produce liquids with slightly lower normative quartz contents and thus lower polymerisation, while iron loss in hydrous runs increases melt polymerisation. The effects are small in most experiments and do not appear to be significant.

Mix A with bulk Ca# of 79.4 is chemically equivalent to an arc tholeiite (sample 71047)(Table 8.1) from western Epi, Vanuatu Arc (Barsdell and Berry, 1990) + 10% plagioclase (An_{80}). Compositions for Mixes E, F, B and C were calculated from the composition of Mix A by fixing molecular proportions of normative minerals other than albite and anorthite, and varying CaO, Na_2O, Al_2O_3 and SiO_2 to obtain normative plagioclase values (i.e. An values) of 87.0, 61.4, 50.0 and 30.0. Compositions for mixes H, I and G were calculated by adding 20% plagioclase ($An_{79.4}$), 20% plagioclase ($An_{61.8}$) and 30% plagioclase ($An_{46.3}$) to mixes A, B and C, respectively. The purpose of these additions was to obtain plagioclase as a liquidus phase for these compositions under hydrous conditions without changing bulk Ca#. These starting compositions (Table 8.1) almost cover the compositional range of high-Al basalts in terms of Ca# and Al# (Al# =27 at Ca# = 35 - 69 to Al# = 34 at Ca# = 91)(Crawford *et al.*, 1987).

TABLE 8.1. STARTING COMPOSITIONS USED IN PARTIAL MELTING EXPERIMENTS

	71047	Mix E	Mix A	Mix H	Mix F	Mix B	Mix I	Mix C	Mix G
SiO2	48.27	46.15	48.25	48.24	50.02	51.78	51.95	54.93	55.41
TiO2	0.55	0.50	0.50	0.40	0.50	0.50	0.40	0.50	0.35
Al2O3	18.58	21.48	20.06	22.70	18.87	17.68	20.21	15.56	19.19
Fe2O3	1.16	1.04	1.04	0.83	1.04	1.04	0.83	1.04	0.73
FeO	9.40	8.46	8.46	6.77	8.46	8.46	6.77	8.46	5.92
MnO	0.19	0.17	0.17	0.14	0.17	0.17	0.14	0.17	0.12
MgO	6.87	6.18	6.18	4.94	6.18	6.18	4.94	6.18	4.33
CaO	12.62	14.65	12.99	13.63	11.60	10.21	10.71	7.72	8.29
Na2O	1.82	0.89	1.86	1.95	2.68	3.49	3.66	4.95	5.32
K2O	0.45	0.41	0.41	0.33	0.41	0.41	0.33	0.41	0.29
P2O5	0.08	0.07	0.07	0.06	0.07	0.07	0.06	0.07	0.05
Total	99.99	100.00	99.99	99.99	99.99	99.99	99.99	99.99	99.99
CIPW NORMS (WT%)									
Or	2.66	2.42	2.42	1.94	2.42	2.42	1.95	2.42	1.70
Ab	15.40	7.53	15.74	16.52	22.64	29.53	30.97	41.89	44.99
An	41.20	53.40	45.18	52.21	38.27	31.37	37.74	19.03	27.65
Di	17.24	15.53	15.52	12.42	15.53	15.54	12.38	15.52	10.87
Hy	10.17	9.09	9.15	7.32	9.16	9.18	7.44	9.15	6.40
Ol	10.42	9.41	9.37	7.49	9.36	9.34	7.42	9.37	6.56
Mt	1.68	1.51	1.51	1.21	1.51	1.51	1.20	1.51	1.06
Il	1.04	0.95	0.95	0.76	0.95	0.95	0.76	0.95	0.66
Ap	0.19	0.16	0.16	0.13	0.16	0.16	0.14	0.16	0.11
Molecular									
Al#	31.20	35.42	32.88	35.67	30.78	28.69	31.44	25.02	28.98
Ca#	79.30	90.10	79.42	79.42	70.56	61.78	61.79	46.29	46.29
Norm Ca#	71.60	86.99	73.01	74.87	61.44	50.03	53.46	29.98	36.68

71047 = HIGH ALUMINA BASALT FROM W. EPI.
MIX A = W. EPI THOLEIITES (71047) + 10% PLAGIOCLASE (An_{80}).
MIXES B, C, E AND F WERE DESIGNED TO RETAIN THE SAME NORMATIVE COMPOSITIONS EXCEPT FOR THE COMPOSITION OF NORMATIVE PLAGIOCLASE (An_{73} = A, An_{50} = B, An_{30} = C, An_{87} = E, $An_{61.4}$ = F).
MIX F = 50% MIX A + 50% MIX B.
MIX H = MIX A + 20% PLAGIOCLASE ($An_{79.42}$).
MIX I = MIX B + 20% PLAGIOCLASE ($An_{61.78}$).
MIX G = MIX C + 30% PLAGIOCLASE ($An_{46.29}$).
Ca# = 100*(CaO/56.08)/((CaO/56.08)+(2*Na_2O/61.98)).
Al# = 100*(2*Al_2O_3/101.96)/((2*Al_2O_3/101.96)+(SiO_2/60.08)).
Norm Ca# = 100*(MOLECULAR CaO FOR NORMATIVE ANORTHITE)/
(MOLECULAR CaO FOR NORMATIVE ANORTHITE)+
(2*MOLECULAR Na_2O FOR NORMATIVE ALBITE).

TABLE 8.2. SYNTHETIC STARTING COMPOSITIONS (ABOVE LIQUIDUS) COMPARED WITH THEORETICAL VALUES. ALL ANALYSES ARE NORMALISED TO 100% ON VOLATILE- AND P_2O_5-FREE BASIS.

	MIX E		MIX A			MIX F		MIX B			MIX C		MIX G	
	TC	T-3094[1]	TC	T-2986[1]	T-3017[2]	TC	T-3092[1]	TC	T-2945[1]	T-2946[1]	TC	T-3052[1]	TC	T-3073[1]
n		3		4	5		3		4	3		9		3
SiO2	46.23	45.15	48.34	47.15	51.00	50.11	50.37	51.88	51.19	51.30	55.03	54.83	55.48	53.75
TiO2	0.50	0.56	0.50	0.54	0.63	0.50	0.59	0.50	0.57	0.61	0.50	0.60	0.35	0.35
Al2O3	21.52	20.79	20.10	19.33	20.05	18.90	18.56	17.71	17.07	17.18	15.59	15.05	19.21	18.39
FeO	9.41	10.93	9.41	11.03	4.92	9.41	9.02	9.41	10.50	10.29	9.41	9.85	6.59	9.13
MnO	0.17	0.19	0.06	0.17	0.11	0.17	0.18	0.17	0.25	0.29	0.17	0.25	0.12	0.06
MgO	6.19	6.17	6.19	6.17	6.82	6.19	6.21	6.19	6.17	6.15	6.19	6.17	4.33	4.45
CaO	14.68	14.91	13.01	13.37	14.00	11.62	11.97	10.23	10.45	10.33	7.73	8.00	8.30	8.55
Na2O	0.89	0.96	1.86	1.87	2.03	2.68	2.66	3.50	3.43	3.45	4.96	4.84	5.32	5.06
K2O	0.41	0.35	0.41	0.37	0.43	0.41	0.44	0.41	0.37	0.39	0.41	0.42	0.29	0.25
P2O5[3]	0.07	0.07	0.07	0.07	0.07	0.07	0.07	0.07	0.07	0.07	0.07	0.07	0.07	0.07
Mg#	53.97	50.15	53.97	49.93	71.19	53.97	55.10	53.97	51.13	51.58	53.97	52.75	53.97	46.49
Ca#	90.10	89.56	79.42	79.80	79.21	70.56	71.32	61.78	62.74	62.33	46.29	47.74	46.29	48.29
		(1.00)		(0.78)	(0.82)		(0.25)		(0.43)	(1.23)		(1.63)		(0.46)
Al#	35.42	35.18	32.88	32.58	31.66	30.78	30.28	28.69	28.21	28.30	25.02	24.44	28.98	28.74
		(0.53)		(0.46)	(1.87)		(0.49)		(0.92)	(0.45)		(0.48)		(0.26)

[1] = DRY EXPERIMENT, Fe CAPSULE; [2] = HYDROUS EXPERIMENT, $Ag_{50}Pd_{50}$ CAPSULE.

[3] = NOT ANALYSED (CLOSE TO DETECTION LIMIT).

TC = THEORETICAL COMPOSITION, Mg# = 100*(MgO/40.31)/((MgO/40.31)+(FeO/71.85)).

Ca# = 100*(CaO/56.08)/((CaO/56.08)+(2*Na_2O/61.98)), Al# = 100*(2*Al_2O_3/101.96)/((2*Al_2O_3/101.96)+(SiO_2/60.08)).

n = NUMBER OF ANALYSES, NUMBER IN PARENTHESIS IS 2 STANDARD DEVIATIONS.

8.2.2 Experimental techniques

All anhydrous and hydrous experiments were carried out at the University of Tasmania by melting synthetic powder (melting experiments) in a high pressure, solid media 0.5 inch piston cylinder apparatus using the 'piston in' technique, very similar to that of Boyd and England (1960, 1963), and Green and Ringwood (1967a, 1967b). Temperature was measured using a Eurotherm 818P programmable temperature controller with $Pt/Pt_{90}Rh_{10}$ thermocouple and was controlled to ±2°C of the set point. Accuracy in the pressure determination which includes a minus 10% pressure correction is considered to be ±0.5 kb. Runs were quenched at run pressure by cutting power to the furnace.

Sample containers, designed for 11-18 mg of sample powder, were specpure Fe for anhydrous experiments, and $Ag_{75}Pd_{25}$, $Ag_{50}Pd_{50}$ and Pt for hydrous experiments. Specpure Fe capsules were covered by snug-fitting lids and sealed by pressure, whereas the noble metal containers were welded shut. Anhydrous experiments were carried out at pressures of 5 and 10 kb using a talc-pyrex assembly. Hydrous experiments were performed using a NaCl-pyrex assembly; oxygen fugacity in a few hydrous runs was controlled by the haematite-magnetite (H-M) buffer. In anhydrous runs, fO_2 is required to be at or below the iron-wustite buffer.

At the end of each run, the capsule was opened, and run products were crushed and examined by microscope and electron microprobe coupled with backscattered electron imaging. A fully automated Cameca SX50 fitted with a WDS system at operating conditions of 15 kV and 10 nA at the University of Tasmania was used to determine phase compositions. To minimise Na loss, Na was counted first (20 and 10 seconds for peak and background, respectively), and area mode (Broad beam) was used to analyse glass. Mineral analyses were done by spot mode (1-2 μm) or area mode depending on sizes of crystals. Various mineral standards were used; X-ray intensities were corrected for deadtime, background, and matrix effects using the Cameca ZAF routine. All quoted analyses were made on adjacent plagioclase-glass pairs. However, in many hydrous runs, glass compositions immediately adjacent to plagioclases were altered by quench crystallisation overgrowths onto primary crystals. In such cases, the melt composition was obtained as the average of large area scans on pools of glass.

Details of experimental conditions and products are listed in Tables 8.3 (anhydrous) and 8.4 (hydrous). Only analyses of glasses and plagioclases are reported. Compositions of equilibrium partial melts produced in anhydrous experiments at 5 and 10 kb, and hydrous experiments are given in Tables 8.5, 8.6 and

TABLE 8.3. SUMMARY OF ANHYDROUS RUN CONDITIONS AND PRODUCTS

RUN NO.	T(°C)	P(KB)	DURATION (HRS)	CAPSULE	PRODUCTS
MIX E					
T-3094	1340	5	9.5	Fe	L
T-3076	1320	5	48	Fe	L+PL
MIX A					
T-2986	1300	5	20.5	Fe	L
T-2990	1275	5	20.7	Fe	L+Pl
T-3037	1300	10	24	Fe	L+Pl
T-3040	1292	10	48	Fe	L+Pl
T-3008	1285	10	24	Fe	L+Pl
T-2997	1275	10	20.5	Fe	L+Pl
T-3000	1265	10	23.1	Fe	L+Pl
MIX H					
T-3139	1305	5	48	Fe	L+Pl
MIX F					
T-3092	1270	5	20.5	Fe	L
T-3060	1250	5	24	Fe	L+Pl
MIX B					
T-2945	1260	5	17	Fe	L
T-2946	1235	5	17.7	Fe	L
T-2951	1220	5	18	Fe	L+Pl
T-2956	1205	5	17	Fe	L+Pl
T-2953	1190	5	17.3	Fe	L+Pl+Ol
T-3038	1230	10	24	Fe	L+Pl+Cpx
T-3003	1220	10	24	Fe	L+Pl+Cpx
MIX I					
T-3147	1245	5	24	Fe	L+Pl
T-3159	1275	10	48	Fe	L+Pl
MIX C					
T-3052	1225	5	24	Fe	L
T-3048	1210	5	23.8	Fe	L+Ol
T-2957	1190	5	17	Fe	L+Ol
T-2962	1182	5	18	Fe	L+Ol+Pl
T-2959	1175	5	21.5	Fe	L+Ol+Pl
T-3042	1225	10	24	Fe	L+Pl+Cpx
T-3010	1213	10	24	Fe	L+Pl+Cpx
T-3005	1200	10	24	Fe	L+Pl+Cpx+Ol
MIX G					
T-3073	1245	5	24	Fe	L
T-3069	1220	5	23.5	Fe	L+Pl
T-3066	1180	5	24	Fe	L+Pl+Ol
T-3079	1255	10	24	Fe	L+Pl
T-3085	1280	10	24.5	Fe	L+Pl

L = LIQUID, Pl = PLAGIOCLASE, Cpx = CLINOPYROXENE, Ol = OLIVINE.

TABLE 8.4. SUMMARY OF HYDROUS RUN CONDITIONS AND PRODUCTS

RUN NO.	T(°C)	P(KB)	H2O (WT%)	DURATION (HRS)	CAPSULE	PRODUCTS	REMARKS
MIX E							
T-3127	1200	5	2	24	Pt	L+V^1	
T-3083	1180	5	2	24	Pt	L+Pl+Cpx+V^1	
T-3086	1095	5	5	24	Ag50Pd50	L+Pl+V^2	
T-3123	1095	5	5	13	Ag50Pd50	L+Mt+V^2	H-M Buffer
MIX A							
T-3017	1160	5	2	12	Ag50Pd50	L+V^1	
T-3035	1135	5	2	23	Ag50Pd50	L+Pl+V^2	
T-3026	1060	5	5	16	Ag50Pd50	L+Pl+Cpx+Ol+V^2	
T-3112	1050	5	5	10	Ag50Pd50	L+Mt+V^2	H-M Buffer
T-3118	1035	5	5	13.5	Ag75Pd25	L+Mt+Cpx+V^2	H-M Buffer
T-3116	1020	5	5	15	Ag75Pd25	L+Mt+Cpx+V^2	H-M Buffer
T-3125	1000	10	5	41	Ag75Pd25	L+Amp+Cpx+V^2	
T-3030	950	10	5	41	Ag75Pd25	L+Amp+Pl+V^2	
MIX H							
T-3157	1000	10	5	48	Ag75Pd25	L+Pl+Cpx+V^2	
T-3128	960	10	10	48	Ag75Pd25	L+Amp+V^2	
MIX F							
T-3064	1120	5	2	24	Ag50Pd50	L+Pl+Ol+V^1	
T-3080	1020	5	5	49	Ag75Pd75	L+Ol+V^2	
T-3107	1000	5	5	47	Ag75Pd25	L+Ol+Pl+V^2	
T-3103	980	5	5	33.5	Ag75Pd25	L+Ol+Pl+V^2	
MIX B							
T-2984*	1100	5	2	6	Ag50Pd50	L+Cpx+Ol+Plag+V^1	
T-2988	1080	5	2	10	Ag50Pd50	L+Cpx+V^1	
T-2999	1050	5	2	15.5	Ag50Pd50	L+Cpx+Ol+V^2	
T-2998	1050	5	2	11.3	Ag50Pd50	L+Cpx+Ol+V^2	
T-2972	1040	5	5	6.5	Ag50Pd50	L+Cpx+V^1	
T-2978	990	5	5	24	Ag75Pd25	L+Ol+Cpx+V^2	
T-2981	940	5	5	24	Ag75Pd25	L+Ol+Amp+V^2	
MIX I							
T-3250	1135	5	2	24	Ag50Pd50	L+Pl+V^2	
T-3156	1030	5	5	48	Ag75Pd25	L+Pl+Cpx+V^2	
T-3162	1020	5	5	48	Ag75Pd25	L+Pl+Cpx+V^2	
MIX C							
T-3019	1070	5	2	23	Ag50Pd50	L+Pl+Ol+Cpx+V^2	
MIX G							
T-3137	1140	5	2	24	Ag50Pd50	L+Cpx+Pl+V^2	
T-3078	1125	5	2	24	Ag50Pd50	L+Cpx+Pl+V^2	
T-3104	1020	5	5	30	Ag75Pd25	L+Cpx+V^2	
T-3091	995	5	5	38.5	Ag75Pd25	L+Cpx+Pl+Amp(Tr)	

L = LIQUID, Pl = PLAGIOCLASE, Cpx = CLINOPYROXENE, Ol = OLIVINE, Amp = AMPHIBOLE.
Mt = MAGNETITE, H-M BUFFER = HAEMATITE-MAGNETITE BUFFER, Tr =TRACE.
THE PRESENCE OF 'VAPOUR (V)' IS RECORDED WHEN VESICLES ARE OBSERVED IN GLASS. COMMONLY, VESICLES ARE RARE IN 2% H_2O-RUNS AND MAY REFLECT TRAPPED AIR (NITROGEN) IN CHARGE RATHER THAN WATER SATURATION. HOWEVER, IN RUNS WITH 5% H_2O AT 5 KB OR WITH A HIGH DEGREE OF CRYSTALLISATION (FIG. 8.1C), THE ABUNDANCE OF VESICLES CLEARLY INDICATES WATER-RICH VAPOUR SATURATION.
^{1} = TRAPPED AIR (NITROGEN), ^{2} = WATER-RICH VAPOUR.
* THIS RUN HAS HIGHER %CRYSTALS THAN RUNS AT LOWER TEMPERATURES AND MAY HAVE SUFFERED LOSS OF WATER IN THE WELDING PROCESS.

8.7, respectively. Plagioclase compositions from anhydrous experiments at 5 and 10 kb, and hydrous experiments are given in Tables 8.8, 8.9 and 8.10, respectively.

8.2.3 Assessment of equilibrium

Proof of equilibrium in the distribution of Ab and An components between plagioclase and melt is important, since reaction rates are sluggish; this is particularly so for hydrous experiments at low temperatures (Johannes, 1978). A number of procedures for assessing equilibrium compositional exchange have been applied in recent literature. The most effective method is to perform both melting and crystallisation experiments (i.e. reversal) on the same starting composition at similar experimental conditions, as demonstrated by Gust and Perfit (1987), and Johnson and Rutherford (1989). Since crystallisation experiments were not carried out in this study, other criteria were used to demonstrate that plagioclases and coexisting melts have achieved equilibrium.

In this study, equilibrium between plagioclase and melt is based on phase homogeneities, as determined by backscattered electron imaging and microprobe analyses. If the experimental products are unzoned, equilibrium has been attained. Representative backscattered electron photomicrographs of equilibrium run products are shown in Figure 8.1. The attainment of equilibrium is also supported by compositional homogeneity of glass and plagioclase in terms of Ca#. Almost all glasses have Ca# dispersed about the mean compositions (2σ) less than 1.5; a few show variation (2σ) in Ca# values from 2 to 3. Similarly, Ca# values for plagioclases lie within ± 3 about mean compositions (2σ). This limited compositional variability is attributed to analytical uncertainty. Furthermore, it has been demonstrated that in hydrous systems, the reaction rate between plagioclase and melt decreases exponentially with decreasing temperature, and that plagioclase-melt equilibria can be achieved within one hour at 1000°C (Johannes, 1978). As all plagioclase-melt pairs reported herein are from experiments at temperatures above 1000°C, and run durations at least 6 hours, disequilibrium is considered unlikely to occur. Finally, using extremely fine-grained synthethic mixes as starting compositions favours attaining equilibrium in relatively short run times.

8.3 Experimental Results

Analyses of glass-plagioclase pairs are plotted in terms of Ca# and Al# in Figure 8.2. All analysed plagioclase compositions fall within error or slightly below a line defining ideal plagioclase compositions. Glasses from near-liquidus experiments

TABLE 8.5. COMPOSITIONS OF GLASSES COEXISTING WITH PLAGIOCLASES FROM ANHYDROUS RUNS AT 5 KB.

Mix	E	E	A	H	F	F	B	B	B	I	C	C	G	G
Run no.	T-3076[1]	T-3076[2]	T-2990	T-3139	T-3060[1]	T-3060[2]	T-2953	T-2956	T-2951	T-3147	T-2959	T-2962	T-3066	T-3069
T(°C)	1320	1320	1275	1305	1250	1250	1190	1205	1220	1245	1175	1182	1180	1220
Other phases	-	-	-	-	-	-	Ol	-	-	-	Ol	Ol	Ol	-
n	3	3	4	4	3	3	3	3	3	8	9	8	3	3
SiO2	44.44	44.65	46.27	46.49	48.61	47.99	50.60	50.48	50.83	51.63	54.83	55.61	54.77	53.66
TiO2	0.62	0.61	0.60	0.46	0.59	0.56	0.69	0.56	0.60	0.51	0.59	0.71	0.56	0.38
Al2O3	20.21	20.06	18.38	22.42	17.10	17.24	14.50	16.02	16.43	18.76	15.45	14.37	14.58	17.81
FeO	11.42	11.06	11.51	9.43	10.86	10.82	12.61	11.74	10.19	8.83	10.60	10.05	9.88	10.00
MnO	0.11	0.15	0.21	0.11	0.23	0.19	0.21	0.22	0.21	0.11	0.15	0.14	0.10	0.18
MgO	6.73	6.90	6.17	4.91	6.57	6.49	5.58	6.04	6.49	5.33	4.71	4.89	5.03	4.59
CaO	14.75	15.13	12.85	14.07	11.92	11.76	10.18	9.94	10.40	10.55	7.82	8.36	7.92	8.15
Na2O	0.97	0.92	1.81	1.82	2.66	2.54	3.60	3.48	3.50	3.66	5.03	4.92	4.96	4.95
K2O	0.40	0.33	0.40	0.28	0.41	0.41	0.60	0.50	0.49	0.40	0.45	0.39	0.43	0.27
P2O5[3]	-	-	-	-	-	-	-	-	-	-	-	-	-	-
Total	99.66	99.81	98.19	99.99	98.95	98.00	98.57	98.98	99.13	99.79	99.63	99.45	98.23	99.98
Mg#	51.23	52.65	48.86	48.13	51.88	51.67	44.09	47.84	53.17	51.83	44.20	46.45	47.57	45.00
Ca#	89.37	90.10	79.68	81.02	71.26	71.89	60.96	61.19	62.17	61.43	46.21	48.42	46.88	47.61
	(1.03)	(0.42)	(0.93)	(1.05)	(1.12)	(0.84)	(1.38)	(0.75)	(1.24)	(1.19)	(0.90)	(1.83)	(0.36)	(0.53)
Al#	34.90	34.62	31.89	36.24	29.31	29.74	25.25	27.22	27.59	29.99	24.93	23.35	23.88	28.11
	(0.73)	(0.41)	(0.45)	(0.34)	(0.61)	(0.34)	(0.39)	(0.16)	(0.82)	(0.35)	(0.32)	(1.09)	(0.90)	(0.39)

[1] = AREA 1, [2] = AREA 2, [3] = NOT ANALYSED (CLOSE TO DETECTION LIMIT).

Mg# = 100*(MgO/40.31)/((MgO/40.31)+(FeO/71.85)), Ca# = 100*(CaO/56.08)/((CaO/56.08)+(2*Na_2O/61.98)).

Al# = 100*(2*Al_2O_3/101.96)/((2*Al_2O_3/101.96)+(SiO_2/60.08)).

n = NUMBER OF ANALYSES, NUMBER IN PARENTHESIS IS 2 STANDARD DEVIATIONS.

TABLE 8.6. COMPOSITIONS OF GLASSES COEXISTING WITH PLAGIOCLASES FROM ANHYDROUS RUNS AT 10 KB.

Mix	A	A	A	A	A	B	B	I	C	C	C	G	G
Run no.	T-3000[1]	T-2997[1]	T-3008[1]	T-3040	T-3037[1]	T-3003	T-3038	T-3159	T-3005	T-3010	T-3042	T-3079	T-3085
T(°C)	1265	1275	1285	1292	1300	1220	1230	1275	1200	1213	1225	1255	1280
Other phases	-	-	-	-	-	Cpx	Cpx	-	Cpx+Ol	Cpx	Cpx	-	-
n	5	3	3	2	2	5	4	6	6	4	3	7	3
SiO2	46.34	46.69	46.70	47.45	46.79	49.40	50.09	50.54	53.51	53.05	53.59	55.74	54.12
TiO2	0.63	0.59	0.55	0.57	0.61	0.61	0.59	0.50	0.68	0.58	0.62	0.47	0.38
Al2O3	16.98	18.25	18.66	18.31	18.40	15.90	16.75	18.99	15.12	15.12	15.30	16.70	18.13
FeO	13.58	12.41	11.84	10.66	10.52	13.58	11.25	9.48	11.89	11.83	10.54	8.39	8.28
MnO	0.22	0.20	0.15	0.12	0.18	0.21	0.16	0.13	0.20	0.17	0.14	0.13	0.15
MgO	7.30	6.50	6.18	6.51	6.58	5.83	5.73	5.00	4.78	5.14	5.09	5.25	4.28
CaO	12.66	12.96	13.14	13.37	13.52	9.26	9.70	10.82	7.01	7.20	7.40	8.11	8.52
Na2O	1.78	1.84	1.90	1.89	1.88	3.55	3.69	3.52	5.18	5.25	5.06	5.13	5.16
K2O	0.46	0.42	0.39	0.42	0.39	0.58	0.52	0.32	0.59	0.50	0.50	0.33	0.26
P2O5[2]	-	-	-	-	-	-	-	-	-	-	-	-	-
Total	99.95	99.87	99.51	99.30	98.87	98.93	98.47	99.29	98.96	98.86	98.24	100.25	99.27
Mg#	48.93	48.28	48.20	52.12	52.72	43.35	47.59	48.46	41.74	43.64	46.26	52.73	47.95
Ca#	79.72	79.53	79.26	79.62	79.89	59.02	59.23	62.98	42.77	43.13	44.69	46.66	47.72
	(1.32)	(0.57)	(0.17)	(1.26)	(0.26)	(2.06)	(0.73)	(1.47)	(2.68)	(0.52)	(1.24)	(1.26)	(0.78)
Al#	30.16	31.54	32.02	31.26	31.67	27.50	28.27	30.69	24.99	25.15	25.18	26.10	28.31
	(1.84)	(0.32)	(0.23)	(0.14)	(0.45)	(0.40)	(0.43)	(0.65)	(0.34)	(0.42)	(0.20)	(0.88)	(0.34)

[1] = PLAGIOCLASES ARE TOO SMALL TO ANALYSE, [2] = NOT ANALYSED (CLOSE TO DETECTION LIMIT).
Mg# = 100*(MgO/40.31)/((MgO/40.31)+(FeO/71.85)), Ca# =100*(CaO/56.08)/((CaO/56.08)+(2*Na_2O/61.98)).
Al# = 100*(2*Al_2O_3/101.96)/((2*Al_2O_3/101.96)+(SiO_2/60.08)).
n = NUMBER OF ANALYSES, NUMBER IN PARENTHESIS IS 2 STANDARD DEVIATIONS.

TABLE 8.7. COMPOSITIONS OF GLASSES COEXISTING WITH PLAGIOCLASES FROM HYDROUS EXPERIMENTS

Mix	E	E	A	A	H	F	F	B	I	I	I	C	G	G
Run no.	T-3083	T-3086	T-3035	T-3026	T-3157	T-3064	T-3107[1]	T-2984	T-3250	T-3162[1]	T-3156	T-3019	T-3078	T-3137
%H2O	2	5	2	5	5	2	5	2	2	5	5	2	2	2
P(kb)	5	5	5	5	10	5	5	5	5	5	5	5	5	5
T(°C)	1180	1095	1135	1060	1000	1120	1000	1100	1135	1020	1030	1070	1125	1140
Other phases	Cpx	-	-	Ol+Cpx	Cpx	Ol	Ol	Ol+Cpx	-	Cpx	Cpx	Ol+Cpx	Cpx	Cpx
n	5	3	3	9	6	3	3	6	6	6	8	4	5	4
SiO2	46.27	43.91	46.61	46.44	46.36	49.85	49.24	51.41	52.36	49.74	49.50	55.06	55.52	55.23
TiO2	0.60	0.60	0.62	0.53	0.44	0.58	0.73	0.79	0.51	0.44	0.47	0.60	0.47	0.46
Al2O3	19.55	18.30	16.83	18.75	19.91	17.89	17.68	16.74	18.66	18.94	19.17	16.61	18.81	17.76
FeO	6.69	8.60	8.54	6.50	7.35	7.26	9.08	9.68	4.52	6.70	6.69	7.65	5.13	5.25
MnO	0.19	0.09	0.18	0.17	0.08	0.18	0.17	0.23	0.19	0.11	0.13	0.16	0.07	0.08
MgO	6.77	6.47	6.90	5.57	4.01	6.68	4.02	5.02	5.59	4.46	4.39	4.26	4.09	4.40
CaO	13.48	13.81	12.20	11.72	10.51	11.46	8.80	9.07	10.69	9.34	9.45	6.96	7.81	7.87
Na2O	1.06	0.89	1.95	2.04	2.05	2.63	2.62	3.63	3.62	3.53	3.48	4.55	5.20	4.92
K2O	0.48	0.40	0.45	0.42	0.37	0.39	0.58	0.61	0.36	0.35	0.36	0.45	0.28	0.29
P2O5[2]	-	-	-	-	-	-	-	-	-	-	-	-	-	-
Total	95.09	93.08	94.29	92.14	91.09	96.92	92.94	97.19	96.51	93.64	93.65	96.29	97.39	96.26
Mg#	64.33	57.28	59.02	60.43	49.30	62.12	44.11	48.03	68.79	54.27	53.91	49.81	58.70	59.90
Ca#	87.53	89.51	77.52	76.04	73.95	70.68	65.03	58.00	61.98	59.38	60.02	45.86	45.36	46.92
	(0.64)	(0.27)	(1.17)	(0.88)	(1.83)	(0.69)	(3.09)	(1.19)	(0.80)	(1.35)	(1.90)	(2.63)	(2.63)	(0.64)
Al#	33.24	32.94	29.86	32.24	33.60	29.72	29.73	27.73	29.58	30.97	31.34	26.23	28.54	27.48
	(0.41)	(0.66)	(0.62)	(0.69)	(0.43)	(0.23)	(0.66)	(0.59)	(0.48)	(0.36)	(0.38)	(2.41)	(1.02)	(0.70)

[1] = PLAGIOCLASES ARE TOO SMALL TO ANALYSE, [2] = NOT ANALYSED (CLOSE TO DETECTION LIMIT).
Mg# = 100*(MgO/40.31)/((MgO/40.31)+(FeO/71.85)), Ca# = 100*(Ca/56.08)/((CaO/56.08)+(2*Na_2O/61.98)).
Al# = 100*(2*Al_2O_3/101.96)/((2*Al_2O_3/101.96)+(SiO_2/60.08)), Ca/Na = (Ca/56.08)/(2*Na_2O/61.98).
n = NUMBER OF ANALYSES, NUMBER IN PARENTHESIS IS 2 STANDARD DEVIATIONS.

TABLE 8.8. PLAGIOCLASE COMPOSITIONS FROM ANHYDROUS EXPERIMENTS AT 5 KB.

Mix	E	E	A	H	F	F	B	B	B	I	C	C	G	G
Run no.	T-3076[1]	T-3076[2]	T-2990	T-3139	T-3060[1]	T-3060[2]	T-2953	T-2956	T-2951	T-3147	T-2959	T-2962	T-3066	T-3069
T(°C)	1320	1320	1275	1305	1250	1250	1190	1205	1220	1245	1175	1182	1180	1220
n	5	4	3	4	4	3	4	4	4	11	4	8	4	6
SiO2	44.81	44.72	47.06	45.99	48.64	48.57	53.03	52.00	51.80	51.32	55.84	55.76	56.22	53.82
Al2O3	34.96	35.02	33.29	33.56	31.00	30.92	28.58	29.13	29.58	29.95	26.84	26.65	26.64	29.15
FeO	0.52	0.40	0.50	0.47	0.54	0.53	0.65	0.83	0.61	0.54	0.83	0.57	0.49	0.53
MnO	0.02	0.02	-	-	0.03	-	0.03	0.02	-	0.03	-	0.02	0.01	-
MgO	0.20	0.16	0.19	0.23	0.19	0.18	0.27	0.36	0.19	0.22	0.14	0.13	0.18	0.13
CaO	19.69	19.74	17.81	18.06	15.93	15.83	12.85	13.60	13.99	14.20	10.19	10.10	10.23	12.33
Na2O	0.61	0.57	1.45	1.23	2.46	2.49	4.20	3.66	3.65	3.36	5.66	5.79	5.64	4.52
K2O	0 04	0.04	0.09	0 05	0 07	0.09	0.14	0.12	0.10	0.08	0 08	0.09	0.10	0.05
Total	100.84	100.67	100.40	99.60	98.87	98.61	99.74	99.71	99.93	99.70	99.57	99.11	99.51	100.54
CATIONS (BASED ON 8 OXYGENS)														
Si	2.062	2.060	2.161	2.131	2.258	2.260	2.417	2.378	2.364	2.347	2.531	2.537	2.545	2.427
Al	1.896	1.901	1.801	1.833	1.696	1 695	1.536	1.570	1.591	1.614	1.434	1.429	1.421	1.549
Fe	0.020	0.015	0.019	0.018	0.021	0.021	0.025	0.032	0.023	0.021	0.031	0.022	0.019	0.020
Mn	0.001	0.001	-	-	0.001	-	0.001	0.001	-	0.001	-	0.001	0.001	-
Mg	0.013	0.011	0.013	0.016	0.013	0.012	0.018	0.024	0.013	0.015	0.009	0.009	0.012	0.009
Ca	0.971	0.974	0.876	0.897	0.792	0.789	0.628	0.666	0.684	0.696	0.495	0.492	0.496	0.596
Na	0.054	0.051	0.129	0.110	0.221	0.225	0.371	0.325	0.323	0.298	0 497	0.511	0.495	0.395
K	0.002	0.003	0.005	0.003	0.004	0.005	0 008	0.007	0.006	0.004	0 004	0.005	0.006	0.003
Total	5.019	5.016	5.005	5.009	5.007	5.007	5.004	5.003	5.005	4.997	5.002	5.006	4.995	4.998
Ca#	94.69	95.01	87.17	89.06	78.16	77.82	62.83	67.24	67.92	69.99	49.89	49.07	50.05	60.10
	(0.73)	(1.27)	(1.05)	(1.08)	(1.45)	(1.67)	(1.99)	(2.39)	(0.91)	(1.96)	(1.61)	(1.44)	(2.47)	(3.04)
Al#	47.90	48.00	45.46	46.23	42.89	42.86	38.85	39.76	40.23	40.75	36.16	36.03	35.83	38.96
	(0.68)	(0.22)	(0.47)	(0.77)	(0.50)	(0.57)	(0.84)	(1.01)	(0.36)	(0.72)	(0.91)	(0.47)	(0.53)	(1.07)
K_DCa#	1.06	1.05	1.09	1.10	1.10	1.08	1.03	1.10	1.09	1.14	1.08	1.01	1.07	1.26

[1] = AREA 1, [2] = AREA 2, - = BELOW DETECTION LIMIT, Ca# = 100*Ca/(Ca+Na), Al# = 100*Al/(Al+Si).
n = NUMBER OF ANALYSES, NUMBER IN PARENTHESIS IS 2 STANDARD DEVIATIONS

TABLE 8.9. PLAGIOCLASE COMPOSITIONS FROM ANHYDROUS EXPERIMENTS AT 10 KB.

Mix	A	B	B	I	C	C	C	G	G
Run no.	T-3040	T-3003	T-3038	T-3159	T-3005	T-3010	T-3042	T-3079	T-3085
T(°C)	1292	1220	1230	1275	1200	1213	1225	1255	1280
n	1	6	7	3	7	7	3	5	5
SiO2	48.79	53.44	53.66	51.34	57.82	57.70	58.57	56.01	56.21
Al2O3	30.41	28.76	27.88	30.35	26.04	25.50	25.30	26.97	26.31
FeO	0.57	0.55	0.56	n.d.	0.58	0.65	0.48	0.39	0.57
MnO	-	-	0.05	n.d.	0.02	0.03	0.03	-	0.02
MgO	0.34	0.13	0.26	0.13	0.15	0.14	0.13	0.15	0.11
CaO	15.60	11.61	11.68	13.27	8.19	8.38	8.49	9.97	10.39
Na2O	2.61	4.66	4.68	3.92	6.64	6.59	6.52	5.83	5.67
K2O	0.16	0.21	0.19	0.10	0.21	0.18	0.18	0.09	0.08
Total	98.48	99.36	98.95	99.11	99.65	99.17	99.69	99.41	99.36
CATIONS (BASED ON 8 OXYGENS)									
Si	2.274	2.436	2.458	2.350	2.602	2.612	2.632	2.537	2.551
Al	1.670	1.545	1.505	1.638	1.381	1.361	1.340	1.440	1.407
Fe	0.022	0.021	0.021	n.d.	0.022	0.024	0.018	0.015	0.022
Mn	-	-	0.002	n.d.	0.001	0.001	0.001	-	0.001
Mg	0.023	0.009	0.017	0.009	0.010	0.009	0.009	0.010	0.007
Ca	0.779	0.567	0.573	0.651	0.395	0.406	0.409	0.484	0.505
Na	0.236	0.412	0.415	0.349	0.580	0.579	0.568	0.512	0.499
K	0.009	0.012	0.011	0.006	0.012	0.010	0.010	0.005	0.005
TOTAL	5.014	5.002	5.003	5.003	5.003	5.002	4.987	5.002	4.997
Ca#	76.75	57.96	57.99	65.14	40.53	41.24	41.87	48.56	50.31
	(-)	(1.27)	(3.46)	(0.57)	(2.48)	(2.34)	(1.07)	(2.99)	(2.68)
Al#	42.35	38.81	37.98	41.08	34.67	34.25	33.73	36.21	35.55
	(-)	(0.72)	(1.55)	(0.08)	(0.80)	(1.36)	(0.24)	(0.74)	(0.56)
K_DCa#	0.96	0.98	0.98	1.03	0.95	0.96	0.94	1.04	1.05

Ca# = 100*Ca/(Ca+Na), Al# = 100*Al/(Al+Si).
n = NUMBER OF ANALYSES, NUMBER IN PARENTHESIS IS 2 STANDARD DEVIATIONS.
- = BELOW DETECTION LIMIT, n.d. = NOT DETERMINED.

TABLE 8.10. PLAGIOCLASE COMPOSITIONS FROM HYDROUS EXPERIMENTS

Mix	E	E	A	A	A	H	F	B	I	I	C	G	G
Run no.	T-3083	T-3086	T-3035	T-3026	T-3030[1]	T-3157	T-3064	T-2984	T-3250	T-3156	T-3019	T-3078	T-3137
%H2O	2	5	2	5	5	5	2	2	2	5	2	2	2
P(kb)	5	5	5	5	10	10	5	5	5	5	5	5	5
T(°C)	1180	1095	1135	1060	950	1000	1120	1100	1135	1030	1070	1125	1140
n	2	3	5	3	1	6	2	4	1	6	7	5	5
SiO2	44.56	43.57	44.93	44.99	46.24	44.63	46.37	51.98	50.30	48.57	55.31	53.81	53.94
Al2O3	34.16	34.63	32.71	33.74	33.86	35.55	31.86	30.23	31.21	31.17	26.79	28.95	28.25
FeO	0.84	0.84	0.92	0.62	0.51	n.d.	0.59	0.77	n.d.	0.62	0.83	0.50	0.62
MnO	0.03	0.02	0.02	0.04	0.01	n.d.	0.02	-	n.d.	0.02	0.03	0.03	-
MgO	0.16	0.11	0.45	0.05	0.19	0.03	0.33	0.17	0.16	0.22	0.11	0.19	0.34
CaO	19.26	19.93	18.62	18.68	18.48	19.62	17.49	13.94	14.76	16.36	10.51	12.35	11.88
Na2O	0.67	0.32	0.93	0.79	1.21	0.72	1.61	3.53	3.31	2.21	5.48	4.54	4.69
K2O	0.03	0.02	0.05	0.03	0.06	0.01	0.05	0.08	0.06	0.03	0.07	0.04	0.05
Total	99.71	99.45	98.63	98.94	100.56	100.56	98.31	100.70	99.81	99.20	99.13	100.40	99.76
CATIONS (BASED ON 8 OXYGENS)													
Si	2.075	2.039	2.114	2.103	2.126	2.053	2.177	2.353	2.298	2.249	2.521	2.430	2.450
Al	1.875	1.910	1.814	1.858	1.835	1.928	1.763	1.613	1.681	1.701	1.440	1.540	1.512
Fe	0.033	0.033	0.036	0.020	0.024	n.d.	0.023	0.029	n.d.	0.024	0.032	0.019	0.023
Mn	0.001	0.001	0.001	0.001	0.002	n.d.	0.001	-	n.d.	0.001	0.001	0.001	-
Mg	0.011	0.008	0.032	0.013	0.003	0.002	0.023	0.011	0.011	0.015	0.007	0.013	0.023
Ca	0.961	1.000	0.939	0.935	0.910	0.967	0.880	0.676	0.723	0.812	0.513	0.597	0.578
Na	0.060	0.029	0.085	0.072	0.108	0.064	0.146	0.310	0.293	0.198	0.484	0.397	0.413
K	0.002	0.001	0.003	0.002	0.003	0.001	0.003	0.005	0.003	0.002	0.004	0.002	0.003
Total cat.	5.018	5.021	5.023	5.004	5.012	5.015	5.016	4.997	5.009	5.001	5.003	5.000	5.001
Ca#	94.12	97.18	91.67	92.77	89.44	93.78	87.75	68.57	71.17	80.37	51.45	60.06	58.29
	(0.40)	(0.68)	(1.92)	(2.06)	(-)	(3.05)	(1.49)	(1.96)	(-)	(3.82)	(1.27)	(2.59)	(2.71)
Al#	47.46	48.36	46.18	46.75	46.33	48.42	44.74	40.67	42.24	43.06	36.34	38.80	38.16
	(0.59)	(0.09)	(1.19)	(1.70)	(-)	(0.89)	(1.47)	(0.31)	(-)	(0.88)	(0.45)	(0.69)	(1.56)
KDCa#	1.08	1.09	1.18	1.22		1.27	1.24	1.18	1.15	1.34	1.12	1.32	1.24

[1] = GLASS ANALYSES CANNOT BE REPRODUCED AND ARE NOT REPORTED.

n = NUMBER OF ANALYSES, NUMBER IN PARENTHESIS IS 2 STANDARD DEVIATIONS.

- = BELOW DETECTION LIMIT, n.d. = NOT DETERMINED.

Figure 8.1. (a) Backscattered electron image photograph of run no. T-2990 (Mix A, anhydrous experiment, T=1275°C, P=5 kb). Dark grey is plagioclase and bright white is iron globule from specpure Fe capsule. (b) Backscattered electron image photograph of run no. T-3085 (Mix G, anhydrous experiment, T=1280°C, P=10 kb).showing large crystals of plagioclase (dark grey) with well-developed plagioclase quench evident as projections from the crystal corners into the surrounding glass. Bright white is iron globule from specpure Fe capsule. (c) Backscattered electron image photograph of run no. T-3137 (Mix G, hydrous experiment with 2%H_2O, T=1140°C, P=5 kb). Dark grey is plagioclase, light grey is clinopyroxene and bright white is vesicle infilled with polishing powder.


a
10µm20.0kV 1.25E3 0003/00 T-2990

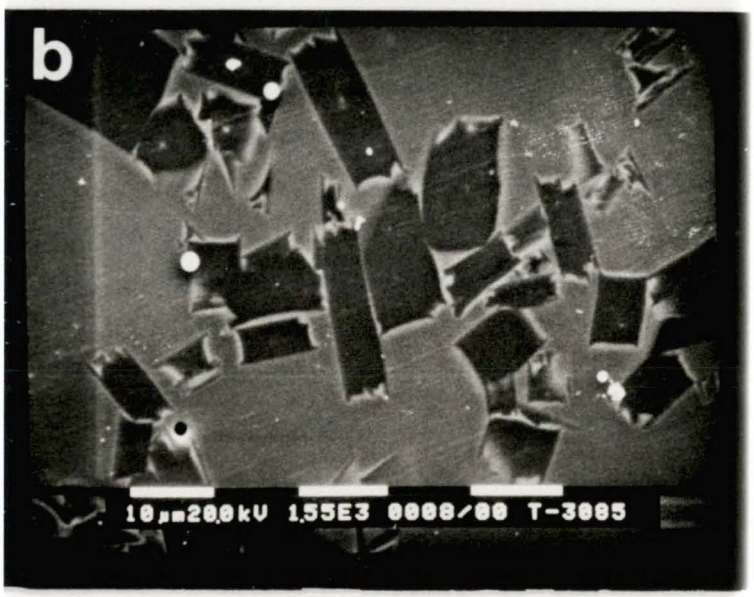
b
10µm20.0kV 1.55E3 0008/00 T-3085

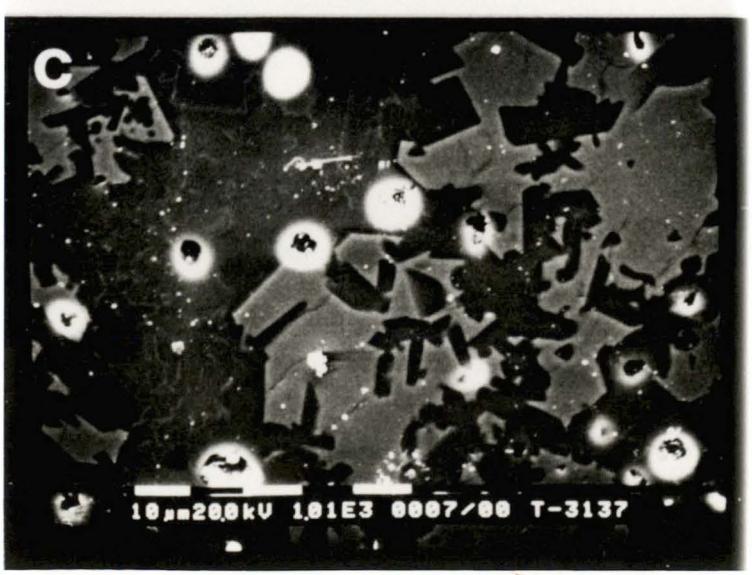
c
10µm20.0kV 1.01E3 0007/00 T-3137

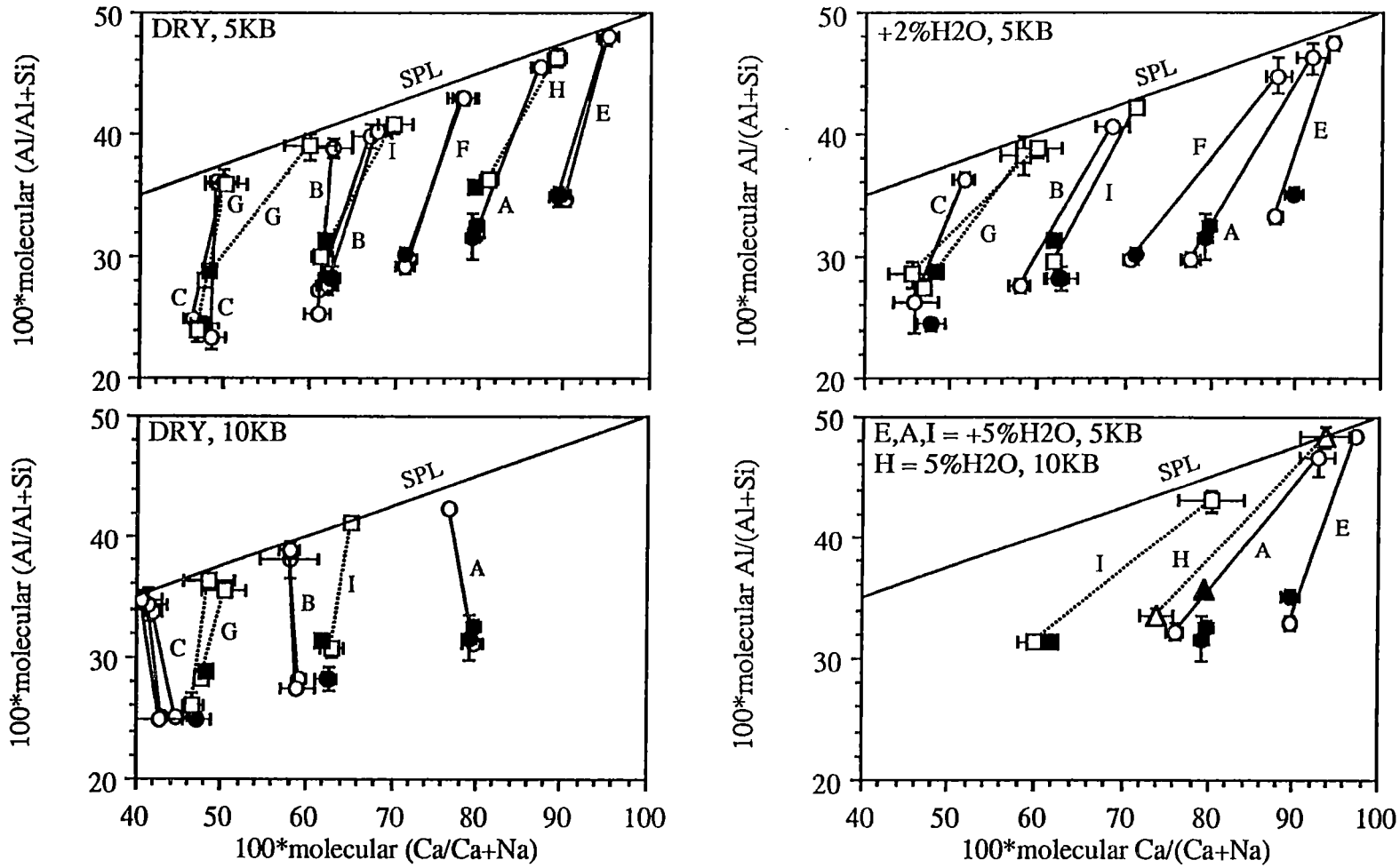

Figure 8.2. Plots of Al# against Ca# for plagioclase-glass pairs (open symbols) from anhydrous experiments at 5 and 10 kb, and hydrous experiments with 2%H2O and 5%H2O at 5 and 10 kb. Plagioclases lie close to the stoichiometric plagioclase line (SPL) whereas glasses lie at the other ends of tie lines. Starting compositions for individual plagioclase-glass pairs are shown by similar solid symbols. Starting compositions for Mixes E, A, F, B, C and G are those from above-liquidus runs whereas for Mixes H and I are those from theoretical values. Bar indicates 2 standard deviations.

have compositions very similar to bulk compositions. Starting materials form a linear trend subparallel to the stoichiometric plagioclase line.

8.3.1 Mix E

Mix E has highest Ca# (90) and crystallised the most calcic plagioclase observed in this study (Fig. 8.3a). There is no significant difference in Ca# of plagioclases between anhydrous and hydrous runs with 2% H_2O at 5 Kb (Ca# = 94-95) although they contain different mineral assemblages (i.e. plagioclase in anhydrous run, and plagioclase+clinopyroxene in hydrous run). Liquidus plagioclase in an experiment with 5% H_2O shows slightly higher Ca# (97). K_DCa# values for plagioclase-glass pairs from the anhydrous run vary from 1.05 to 1.06, whereas those for the hydrous experiments with 2% H_2O and 5% H_2O are 1.08 and 1.09, respectively.

8.3.2 Mixes A and H

Mixes A and H have similar Ca# values (79) but different Al# (33 and 36, respectively) values. For Mix A, plagioclase from anhydrous experiment at 10 kb (T-3040) has much lower Ca# value (77) relative to plagioclase from anhydrous experiment (87) at 5 kb (T-2990) despite the higher temperature of the former (Fig. 8.3b). Plagioclases from hydrous runs with 2% and 5% H_2O at 5 kb have even higher Ca# values (92-93). K_DCa# values for plagioclase-glass pairs from anhydrous runs at 5 and 10 kb are 1.09 and 0.96, respectively, whereas those from hydrous runs range from 1.18 to 1.22.

In a run on Mix A with 5% H_2O at 950°C and 10 kb (T-3030), amphibole occurs instead of clinopyroxene, and plagioclase has a Ca# value of 89, slightly higher than the value for plagioclase obtained from the anhydrous experiment (87) on the same mix. K_DCa# cannot be reliably determined, since there is not much glass present in the assemblage and glass analyses are not reproducible.

The liquidus temperature for Mix H is higher than for Mix A at a given pressure. Plagioclase, the only crystalline phase present in anhydrous run at 5 kb (T-3139), has slightly higher Ca# (89 vs 87) than plagioclase from the anhydrous run on Mix A at 5 kb (T-2990) but similar K_DCa# (1.09 for Mix A, 1.10 for Mix H)(Fig. 8.3b). This difference reflects the difference in normative plagioclase compositions (Table 8.1) from Ca# = 73 to Ca# = 75. The experiment on Mix H with 5% H_2O at 10 kb (T-3157) produced plagioclase and clinopyroxene; Ca# (94) and K_DCa# (1.27)

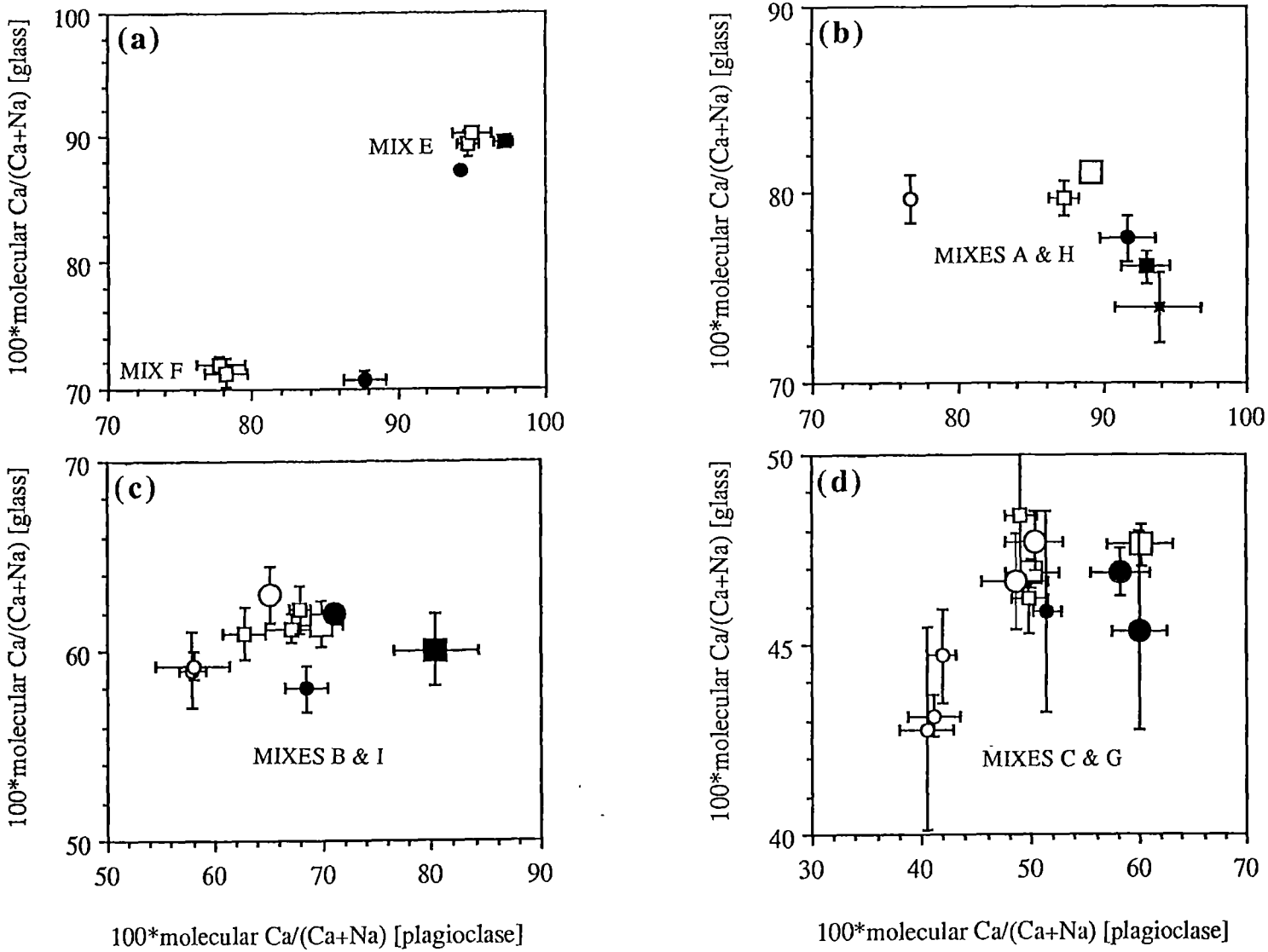
(a)
MIX E
MIX F
100*molecular Ca/(Ca+Na) [glass]
(b)
MIXES A & H
(c)
MIXES B & I
(d)
MIXES C & G
100*molecular Ca/(Ca+Na) [plagioclase]

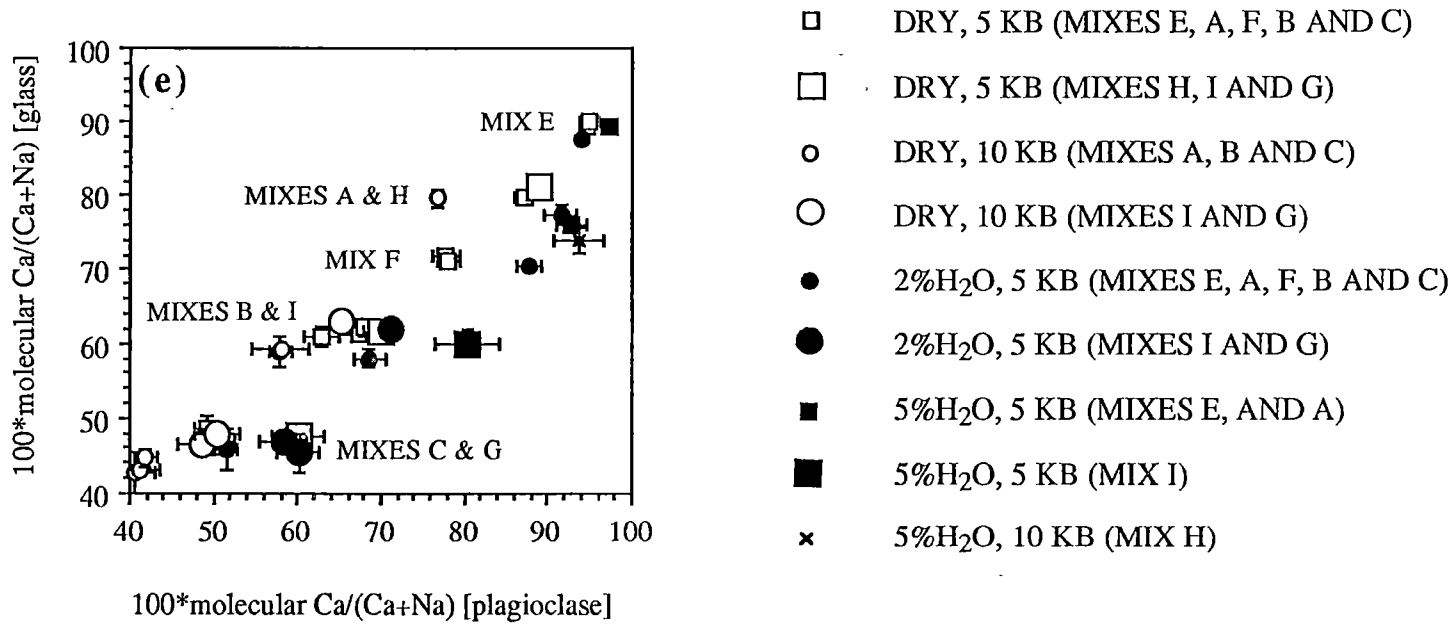

Figure 8.3. Ca# of glass versus Ca# of plagioclase for plagioclase-glass pairs from melting experiments on (a) Mixes E and F, (b) Mixes A and H, (c) Mixes B and I, (d) Mixes C and G, and (d) all mixes. Bar indicates 2 standard deviations.

values of plagioclase are not significantly different from those in the hydrous run on Mix A with 5% H_2O at 5 kb (Ca# = 93, $K_DCa\#$ = 1.22).

In a run with 10% H_2O at 960°C and 10 kb, amphibole occurs instead of clinopyroxene, and plagioclase has Ca# = 89, comparable to the value for plagioclase obtained from the anhydrous experiment at 5 kb, but very different from that at 10 kb.

8.3.3 Mix F

Anhydrous and hydrous experiments on Mix F (Ca# = 71) with 2% H_2O at 5 kb crystallised plagioclase, and plagioclase and olivine, respectively. Plagioclase from the hydrous run has higher Ca# (88) than plagioclase from the anhydrous run (78)(Fig. 8.3a). $K_DCa\#$ is also greater, i.e. 1.24 for hydrous experiment and 1.08-1.10 for anhydrous experiments.

8.3.4 Mixes B and I

Both mixes have similar values for Ca# (62), however, Mix I has higher Al# (31) relative to Mix B (29). Anhydrous experiments on Mix B at 5 kb show highest Ca# (67-68) on near-liquidus plagioclases (T-2951, T-2956), ranging to 63 in lower temperature run (T-2953)(Fig. 8.3c). $K_DCa\#$ values show a parallel variation from 1.10 to 1.03. Plagioclase from anhydrous experiments on Mix B at 10 kb has lower Ca# (58) and $K_DCa\#$ (0.98) compared to anhydrous experiments at 5 kb. Ca# for plagioclase (69) from the hydrous experiment with 2% H_2O at 5 kb is similar to that from the near-liquidus anhydrous experiment at 5 kb, however, $K_DCa\#$ from the hydrous run (1.18) is higher than for the latter (1.09-1.10). In the hydrous run, clinopyroxene and olivine coexist with plagioclase, giving a lower Ca# for the liquid and thus increasing $K_DCa\#$.

The liquidus temperature for Mix I is also higher than for Mix B. Plagioclase is the sole crystalline phase in an anhydrous experiments at 5 and 10 kb, and in a hydrous experiment with 2% H_2O on Mix I at 5 kb. Plagioclases in the anhydrous experiment at 5 kb and hydrous experiment have similar Ca# (70-71) and $K_DCa\#$ (1.14-1.15) values that are slightly higher than the near-liquidus plagioclase from the anhydrous experiment at 5 kb on Mix B (Fig. 8.3c). Under anhydrous condition at 10 kb, the liquidus temperature for Mix I is higher than for Mix B, giving rise to plagioclase with notably higher Ca# (63) and $K_DCa\#$ (1.03). Similar to the results obtained from Mixes A and H, Mix I plagioclase (coexisting with clinopyroxene) from an experiment with 5% H_2O at 5 kb has markedly higher Ca# (80) and $K_DCa\#$ (1.34) than that from an anhydrous experiment on the same composition at 5 kb.

8.3.5 Mixes C and G

Ca# values for Mixes C and G are similar (46); however, Al# for Mix C (25) is lower than for Mix G (29). In anhydrous experiments on Mix C, plagioclases (coexisting with clinopyroxene ± olivine) from runs at temperatures = 1220, 1213 and 1225°C, and pressure = 10 kb have similar Ca# (41-42) and K_DCa# (0.94-0.96); these values are notably different from those (coexisting with olivine) at 5 kb (Ca# = 49-50 and K_DCa# = 1.01-1.08)(Fig. 8.3d). A hydrous experiment with 2% H_2O at 5 kb formed plagioclase (coexisting with olivine and clinopyroxene) with only very slightly higher Ca# (51) and K_DCa# (1.12) values.

As for Mixes A and H, and B and I, the liquidus temperature for higher Al# Mix G is higher than for Mix C. Plagioclase, the only solid phase in anhydrous runs of Mix G at 10 kb has Ca# (49-50) and K_DCa# (1.04-1.05) values comparable to those from anhydrous runs of Mix C at 5 kb (Fig. 8.3d). Similarly, plagioclase from a near-liquidus anhydrous experiment on Mix G at 5 kb has notably higher Ca# (60) and K_DCa# (1.26) than those from an anhydrous experiment on Mix C at 5 kb. This compares with a difference of Ca# = 30 and Ca# = 37 for normative plagioclase contents of the two compositions. At similar temperatures (1175°-1182°C), plagioclases obtained from Mixes C (T-2959, T-2962) and G (T-3066) coexist with olivine, and are not compositionally different. Moreover, near-liquidus plagioclase-glass pairs from anhydrous and hydrous experiments at 5 kb on Mix G are not compositionally significantly different (Ca# = 60 and K_DCa# = 1.26 for anhydrous run and Ca# = 58 and K_DCa# =1.24 for hydrous run).

8.4 Summary of P-T-X-H_2O Effects on Plagioclase Crystallisation

8.4.1 Bulk composition

This study shows that the values of Ca# of plagioclase and K_DCa# for plagioclase-glass pairs are dependent on many variables including bulk composition (Ca# and Al#), temperature, pressure, water content and presence or absence coexisting phases (Figure 8.3).

Clearly, bulk compositions with higher Ca# values crystallised plagioclase with higher Ca# (Fig. 8.3e). This appears to be the dominant influence on plagioclase-melt equilibria.

Recently, Beard and Borgia (1989) suggested that the cause of the highly calcic plagioclase phenocrysts in high-Al basalts may be unusually high Al_2O_3 in these

magmas. This possibility was investigated in the present study by running at similar conditions, melt pairs with similar bulk Ca# (Table 8.1) but different normative plagioclase contents (e.g. Mixes A (20.1% Al_2O_3) and H (22.7%), Mixes B (17.7%) and I (20.2%), and Mixes C (15.6%) and G (19.2%)). The most important effect of increased Al# in any bulk composition is to increase the liquidus temperature over that for its lower Al# pair. For example, at 5 kb, the liquidus temperature for Mix A is around 1275°C, whereas for higher Al# Mix H, it is closer to 1305°C. This results in a slightly more calcic liquidus plagioclase in the higher Al# run (An_{89} vs An_{87}), but no significant difference in the $K_DCa\#$ (1.10 vs 1.09), and simply reflects the difference in normative plagioclase compositions of the two runs. The same is generally true at 10 kb, where for example, for Mixes B and I, liquidus plagioclase and $K_DCa\#$ for higher Al# Mix I are An_{65} and 1.03, respectively, compared with An_{58} and 0.98 for Mix B; note however, that clinopyroxene precedes plagioclase for a short interval in the runs with Mix B. More sodic Mixes C and G show a similar feature, with the difference in An content between liquidus or near-liquidus plagioclase in the higher Al# and lower Al# compositions being 8 mol% at 10 kb and 11 mol% at 5 kb

The effect of phases co-crystallising with plagioclase is well shown in the 5 kb sequence of experiments on Mix B, in which plagioclase becomes more sodic (Ca# = 68 to Ca# = 63), and $K_DCa\#$ decreases with decreasing temperature.

In summary, whereas increasing Al# in a given melt composition does lead to an increase in the An content of crystallising plagioclase (up to 10 mol% An change in the more sodic compositions and only a few mol% change for typical basalt compositions), this probably reflects the increasing liquidus temperature for the higher Al# composition. It is unlikely therefore, that the highly anorthitic plagioclases in arc high-Al basalts are due to abnormally high Al# values of these magmas.

8.4.2 Effect of pressure

Ca# and $K_DCa\#$ of near-liquidus plagioclases for any bulk composition anhydrous at 5 kb are significantly higher than from anhydrous experiments at 10 kb, even though liquidus temperatures for experiments at 10 kb are higher. $K_DCa\#$ values at 10 kb are consistently significantly lower than those at 5 kb, and notably, are less than 1 (i.e. plagioclases are more sodic than the coexisting liquid). Although limited 10 kb $K_DCa\#$ data of Drake (1976) were claimed to show no significant difference to data for 1-atmosphere runs, the results of the present study are in agreement with experimental results of Green *et al.* (1979) and Duncan and Green (1987). This pressure effect occurs in the absence of any other crystalline phase, and implies a significant change in melt structure and melt-plagioclase partitioning due to pressure

alone.

The independent effects of the factors discussed above on plagioclase-melt equilibria are highlighted in Figure 8.4a. The pairs from anhydrous experiments at 5 and 10 kb form different subparallel compositional trends, the 10 kb runs showing lower Ca# plagioclase for any chosen bulk composition. The pairs from experiments with 2% H_2O at 5 kb form a loop with higher K_DCa# compared to anhydrous experiments at 5 kb, particularly Ca# values for plagioclases of about 70 and 95, whereas those pairs from experiments with 5% H_2O at 5 kb form a trend with highest K_DCa#, overlapping the 2% H_2O, 5 kb loop over a range of Ca# for plagioclase of 88-97.

Also shown on Figure 8.4b are data for plagioclase-glass pairs from 1-atmosphere near-liquidus experiments on different starting compositions (calc-alkalic basalts and andesites, mildly alkalic basalts, low-K - medium-K tholeiites and MORB) with Al# values of glasses greater than 27 (Walker *et al.*, 1979; Mahood and Baker, 1986; Tormey *et al.*, 1987; Ussler and Glazner, 1989; Meen, 1990). Tormey *et al.* (1987) have demonstrated that Na loss, due to volatilisation, is a problem in 1-atmosphere Pt wire loop experiments and that this can be compensated for by increasing the partial pressure of Na in 1-atmosphere furnace (using a Na_2O-SiO_2 liquid), reducing Na loss about 7% of the bulkrock Na_2O. All previous 1-atmosphere experiments have suffered Na loss to variable amounts, depending on run time, temperature, fO_2, gas-flow rate and surface area to volume ratio of sample charge. Accordingly, continuous re-equilibration of plagioclase-glass interfaces, until quenching, is expected, eventually producing plagioclase-glass pairs more calcic than those expected from the starting compositions. The data derived therefrom should be interpreted with caution. However, it is clear that these data define a narrow compositional field, displaced at around Ca# > 60, towards more calcic plagioclase compositions in a similar manner and extent to the displacement of the 10 kb vs 5 kb trends.

Therefore, for a given composition, decreasing pressures from 10 to 5 kb produces a significant increase in Ca# of near-liquidus plagioclase. A continuation of this trend to atmospheric pressure may be responsible for the broad compositional overlap between 2% H_2O, 5 kb and natural atmospheric pressure examples. The effect of pressure on plagioclase-melt equilibria is most pronounced for compositions with bulk Ca# from 70 to 80. In this interval, a model basalt similar to that studied here, with Ca# = 75, would crystallise An_{73} plagioclase at 10 kb, An_{80} at 5 kb and

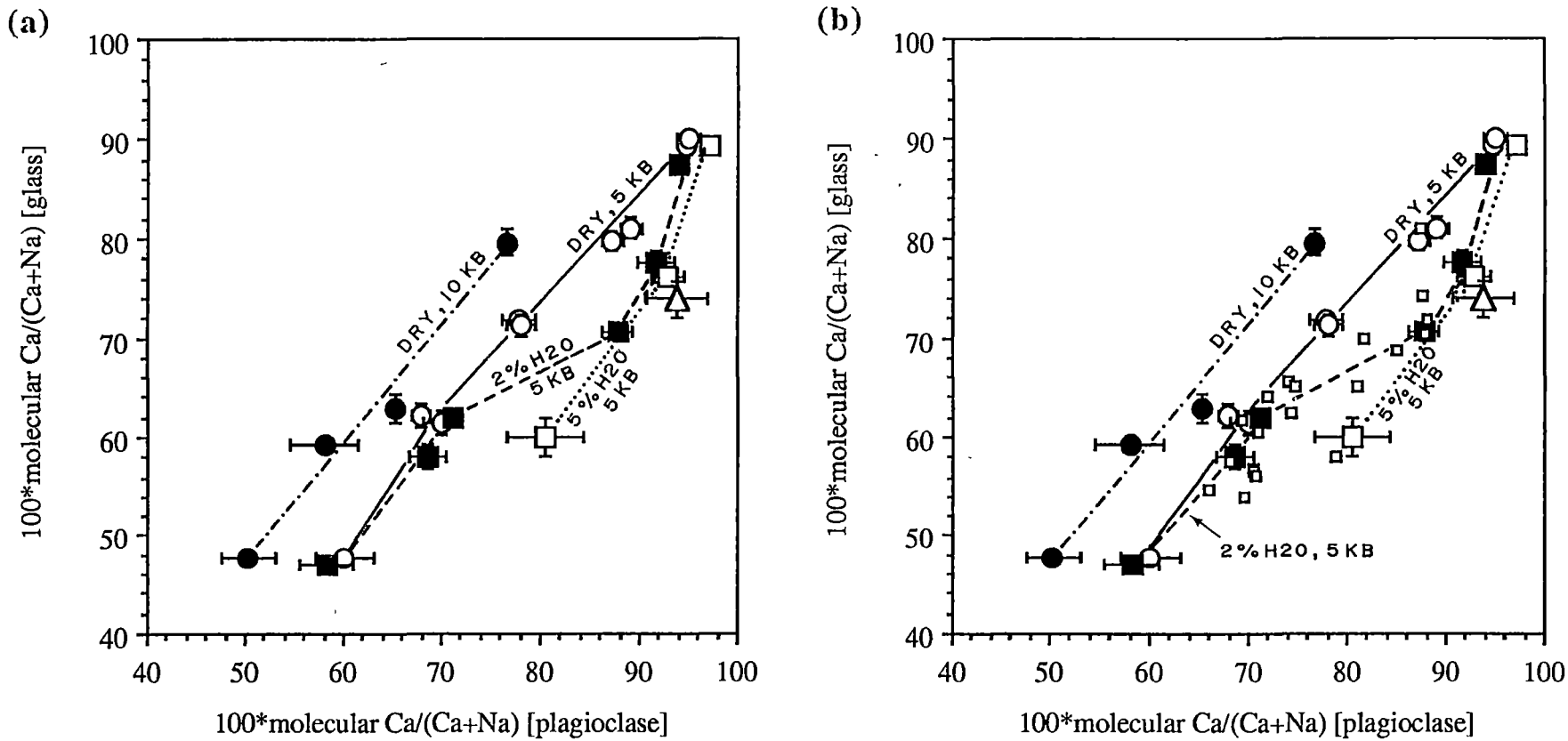

Figure 8.4. Plots of (a) Ca# of glass against Ca# of plagioclase for plagioclase-glass pairs of which Al# values for glasses are higher than 27 (open circles = anhydrous experiments at 5 kb, solid circles = anhydrous experiments at 10 kb, solid squares = hydrous experiments with 2%H_2O at 5 kb, open squares =hydrous experiments with 5%H_2O at 5 kb, open triangle = hydrous experiment with 5%H_2O at 10 kb), and (b) Ca# of glass against Ca# of plagioclase as shown in (a) with additional plagioclase-glass pairs (Al# for glasses >27)(small open squares) from calc-alkalic basalts and andesites (Ussler and Glazner, 1989), mildly alkalic basalts (Mahood and Baker, 1986), low-medium K tholeiites (Meen, 1990) and MORBs (Walker *et al.*, 1979; Tormey *et al.*, 1987).

An_{90} at 1 atmosphere. The pressure effect is less marked for more sodic bulk compositions, particularly in the range Ca# = 70 to 50.

8.4.3 Effect of water

The effect of increasing water pressures in crystallising significantly more calcic plagioclase (higher Ca# and K_DCa#) relative to anhydrous experiments on the same composition is most pronounced between bulk Ca# from 60 to 80, and water pressures show little effect at runs outside this bulk compositional range. The effect of even small amounts of water is shown well on 5 kb experiments on Mix F (Ca# = 71), for which anhydrous liquidus plagioclase has Ca# = 78, whereas with only 2% H_2O, liquidus plagioclase has Ca# = 88. For compositions B and I (Ca# = 62), at 5 kb, runs with 5% H_2O crystallised significantly more calcic plagioclase (Ca# = 80) than runs with 2% H_2O (Ca# = 68-71), which in turn, showed increased Ca# over plagioclase crystallised in anhydrous experiments on these compositions (Ca# = 63-70).

8.5 Application to Natural Samples

The main aim of this experimental investigation of factors affecting plagioclase-melt equilibria was to explain the presence, and assess the petrogenetic significance of highly calcic plagioclases in many natural lavas and cumulates, particularly in some MORB and arc basalts. Many workers have claimed that the presence of water in arc basalts forces crystallisation of highly calcic plagioclase. However, the same argument cannot hold for the highly calcic ($An_{>85}$) plagioclase megacrysts in some MORB (albeit much less common than in arc lavas and cumulates), since MORB are essentially anhydrous. More than one factor, therefore, can significantly influence the composition of plagioclase crystallising from any magma, a point demonstrated clearly by this experimental study. In the following section, the plagioclase-melt K_D values obtained in this study are applied empirically to MORB and arc basalts, in an effort to clarify the petrogenetic significance of plagioclase in these suites.

8.5.1 MORB

A histogram showing the Ca# distribution for 1,000 Pacific MORB glasses is shown in Figure 8.5a. A peak concentration of melts with Ca# = 66-72 is evident, although glasses having Ca# = 72-78 are also common. A diagram of Ca# versus Mg# from a compilation of primitive MORB glasses (T.J. Falloon, pers. comm. 1990) shows that MORB with Ca# values from 78-84 are also present in the ocean

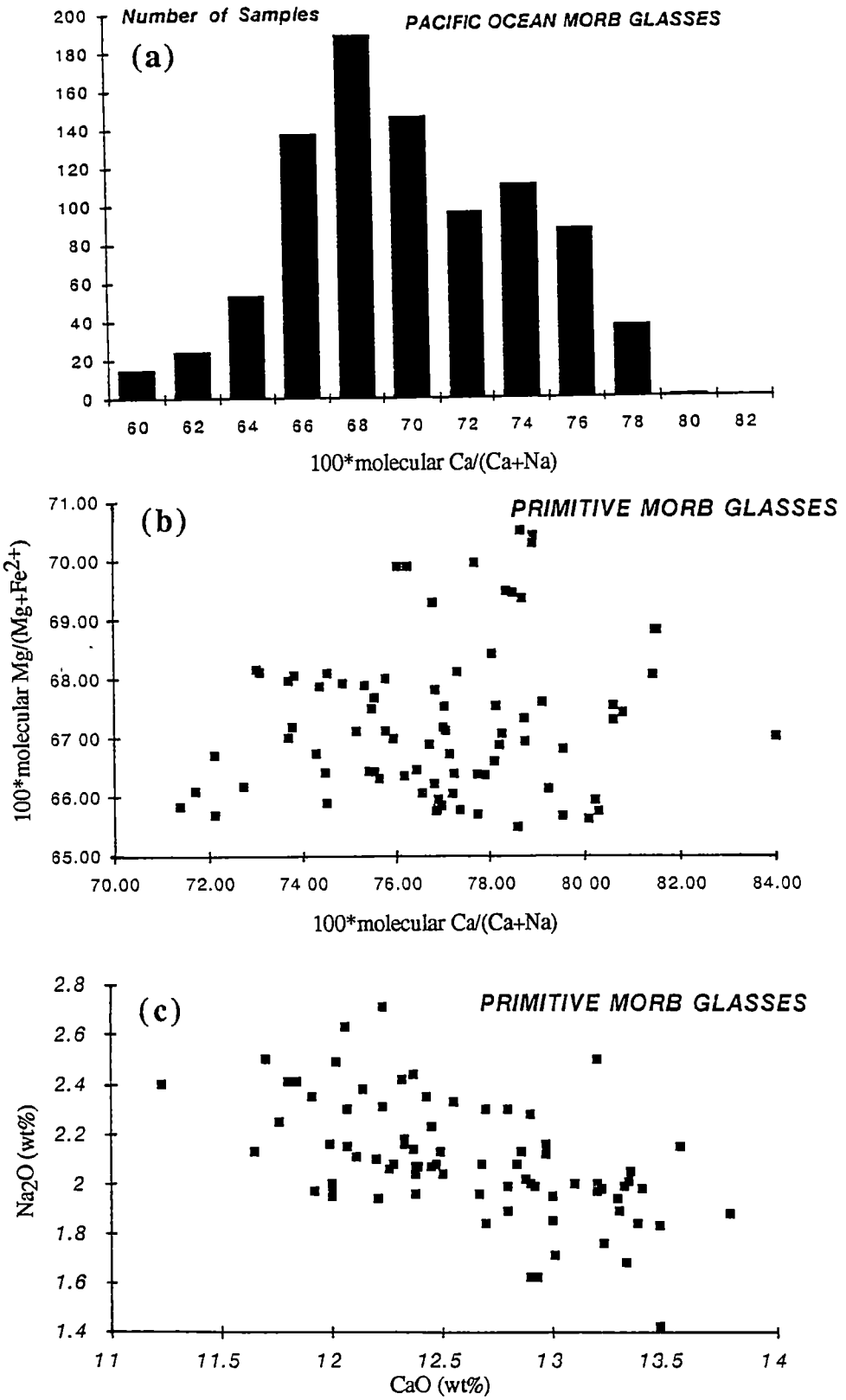

Figure 8.5. (a) Frequency histogram for Ca# of 1,000 Pacific MORB glasses (data compiled by A.J. Crawford, pers. comm., 1990). (b) Mg# versus Ca# and (c) Na_2O versus CaO diagrams for primitive MORB glasses (data compiled by T.J. Falloon, pers. comm., 1990).

crust (Fig. 8.5b), but are volumetrically insignificant relative to typical MORB with Ca# < 78. Only anhydrous equilibria need be considered for MORB. For runs at 10 kb (Tables 8.6 and 8.9), melts coexisting with plagioclase (or plagioclase plus minor clinopyroxene for runs on Mix B) define a K_DCa# = 0.96-1.03 (average 0.99). Thus liquidus plagioclase in typical MORB, if crystallised at 10 kb, is predicted to be An_{65-77}.

For 5 kb anhydrous runs (Tables 8.5 and 8.7), glasses with broadly MORB compositions in terms of Ca# (64-80) coexisting with plagioclase define K_DCa# = 1.08-1.10, predicting maximum compositions for plagioclases in typical MORB of An_{72-85}. A continuation of this trend of increasing K_DCa# with decreasing pressure is indicated by available 1-atmosphere data for mixes with broadly basaltic - andesitic compositions (Fig. 8.4), particularly for those with Al# > 27. This could generate, for example, plagioclase compositions as calcic as An_{90} in magmas with Ca# = 74.

Typical plagioclase phenocrysts and microphenocrysts in MORB are An_{66-80} (Green *et al.* 1979; Natland, 1989). More anorthitic plagioclase compositions (An_{85-91}) in some MORB, particularly in megacrystic plagioclases, were noted by Donaldson and Brown (1977), and are now known to be widespread in MORB (see summary of occurrences in Wilkinson, 1982), with compositions as calcic as $An_{94.5}$ being recorded in a Hole 504 B East Pacific Rise tholeiite (Natland, 1989). At 10 kb, using the anhydrous K_DCa# determined in this study (0.99), melts with Ca# = 91-95 would be required to produce the more calcic megacrystic plagioclase compositions ($An_{90-94.5}$). This translates as CaO/Na_2O >18. For 5 kb anhydrous runs, the K_DCa# determined herein (1.08-1.10) demands melts with Ca# = 83-87 to crystallise plagioclase $An_{90-94.5}$. This requires CaO/Na_2O values of 8.8-11.5.

MORB glasses with >8% MgO have CaO/Na_2O values from 3 to 10, although CaO/Na_2O values in excess of 8 and Na_2O abundances less than 1.4 % are rare (Fig. 8.5c). Therefore, the megacrystic plagioclases $An_{90-94.5}$ in MORB, if they crystallise at pressures between 5 and 10 kb, require parent magmas significantly more refractory than any known MORB glasses.

Duncan and Green (1980) used the presence of these highly anorthitic plagioclase megacrysts to infer the existence within the oceanic crust of low volume, refractory (high Ca/Na) 'second-stage' melts. Building on the work of Duncan and Green (1980, 1987), Natland (1989) proposed a model for MORB petrogenesis involving high-temperature polybaric crystallisation and mixing of a range of low-Ti, low-Na refractory melts, which later coalesced with cooler, less refractory magmas derived from more fertile sources, to produce 'typical MORB'. Crystallisation of

olivine, spinel and plagioclase from the more refractory melts occurs probably mainly from 10-5 kb in the Natland (1989) model. Although, as noted above, no MORB glasses have suitable compositions to match the 'second stage' melts of Duncan and Green (1980) and Natland (1989), glass inclusions in some MORB olivines (Danjushevsky *et al.*, 1987), spinels (Donaldson and Brown, 1977) and plagioclases (Natland, 1989) show emphatically that highly depleted second stage melts do contribute to the ocean crust, but are rarely preserved due to effective mixing and homogenisation of magmas in transit to, or within, sub-ridge magma chambers.

Lavas with compositions similar to the proposed 'second-stage melts' of Duncan and Green (1980) are known from several ophiolites, perhaps the best studied of which is the Troodos Complex, in Cyprus. Gabbros in the cumulate section of this ophiolite contain plagioclases as anorthitic as An_{95} (Duncan and Green 1987). The latter authors studied the phase relationships of a model parent magma to the Troodos Upper Pillow Lavas (Mg# = 76.5, Ca# = 18.2). At 5 kb anhydrous, this composition crystallises An_{85} at 1200°C, whereas at 2 kb, 1200°C, (after limited Ca-clinopyroxene crystallisation), it crystallises An_{89}.

Recent geochemical and isotopic studies have shown that the Troodos Complex formed in a supra-subduction zone setting. The presence of some small amount of water (0.5-1% according to Duncan and Green, 1987) in the Troodos parent magmas is indicated both by the presence of quench amphibole (Cameron 1985), and the low-pressure pyroxene stability relationships in these rocks (Duncan and Green 1987). Results of the present experimental study indicate that at 5 kb pressure, Mix A, with Ca# = 80 (close to the Ca# value for the Troodos model liquid, Ca# = 83, in equilibrium with An_{85}), crystallises An_{87} dry, An_{92} with 2% H_2O and An_{93} with 5% H_2O. The effect of water is even more pronounced at 10 kb, where the same Mix A crystallises An_{77} dry, but An_{89} with 5% H_2O (even after some amphibole crystallisation for the latter case). Even small amounts of water can clearly exert a strong control on plagioclase composition, forcing crystallisation of more anorthitic plagioclase than would crystallise at the same pressure under anhydrous conditions. This may well be part of the explanation of the existence of extremely calcic plagioclase in many arc-related magmas (An_{85-100}) and ophiolites. Water is not involved in the petrogenesis of MORB, and no glasses are known from the ocean ridge systems that have CaO/Na_2O values sufficiently high to crystallise the more calcic plagioclase megacryst compositions ($An_{90-94.5}$) in MORB. It is likely, therefore, that the refractory melts parental to the megacrysts are coalesced with less depleted magmas, either in sub-ridge magma chambers or during pooling of melt

fractions in ascending diapirs, to erupt as typical 'hybrid MORB' (Duncan and Green, 1980, 1987; Natland 1989).

8.5.2 Arc magmas

Typical arc high-Al basalts have abundant plagioclase phenocrysts, probably accumulative in the lavas due to selective floatation (Crawford *et al.* 1987). For oceanic arcs, these plagioclase phenocrysts generally have relatively wide, unzoned and inclusion-free, anorthitic cores (An_{85-95}) surrounded by sieved and inclusion-rich rims with more sodic compositions, usually from An_{50-80} (Vanuatu arc: Barsdell, 1988; Tongan arc: Ewart, 1976; New Britain arc: Heming, 1977; Kurile arc: Bailey *et al.*, 1989; dredged and subaerial Mariana arc: Crawford *et al.*, 1986; Meijer and Reagan, 1981; Lesser Antilles: Arculus, 1978). Plagioclase phenocrysts in continental margin arc high-Al basalts (e.g. Central America: Rose *et al.*, 1978; Walker and Carr, 1986; Japan: Fujimaki, 1986) and gabbroic plutons (Smith *et al.*, 1983) and inclusions (Beard and Borgia, 1989) can also be highly anorthitic, with values of core compositions from An_{90-95} not uncommon. However, in general, continental margin high-Al basalts have slightly less anorthitic plagioclase (An_{80-85}) phenocrysts (Southern Andes: Lopez-Escobar *et al.*, 1981; western USA: Gerlach and Grove, 1982; New Zealand: Cole, 1978).

Plagioclase phenocrysts in some oceanic forearc lavas compositionally transitional from arc tholeiites to high-Ca boninites are frequently more calcic than An_{95}; pure anorthite phenocrysts are recorded from such lavas from the northern Tongan forearc (Falloon and Crawford 1991), and *groundmass* plagioclase laths in similar basalts from the Mariana forearc are commonly An_{85-91} (Crawford *et al.*, 1986).

In summary, plagioclase crystallising in arc basalts and gabbros is usually much more anorthitic than that crystallising in MORB, intraplate basalts or large layered intrusions. This has been clearly shown by Beard and Borgia (1989) using a plot of coexisting plagioclase and olivine from numerous magma suites. Three separate causes for the crystallisation of such anorthitic plagioclase in arc magmas have been proposed (see Section 8.1); these are: effect of water, high Ca/Na, and high Al contents of arc magmas.

It has been claimed that water present in arc magmas can modify the shape of the plagioclase loop, to force crystallisation of more calcic plagioclase than would crystallise from the same composition under anhydrous conditions (e.g. Arculus and Wills, 1980). In basaltic magmas, water is well known to markedly suppress

plagioclase appearance temperatures, leading to the crystallisation of olivine and/or pyroxene as liquidus and near-liquidus phases at low pressures (Yoder and Tilley, 1962; Sekine *et al.*, 1979; Green, 1982). Extensive low- or moderate-pressure clinopyroxene crystallisation, well documented in many arc basalt suites (Barsdell, 1988; Barsdell and Berry, 1990; Foden, 1986), must lead to a rapid decrease in the Ca/Na value of residual magmas. Thus when it crystallises eventually, plagioclase would reasonably be expected to have lower An content than if it crystallised from the same composition in the absence of water. Accordingly, in comparing plagioclase compositions in basalts with similar Ca/Na or normative plagioclase compositions, the presence of water cannot by itself explain the highly anorthitic plagioclase in many arc basalts.

Moreover, this experimental study has shown that for a broadly basaltic bulk composition (Ca# = 80), addition of each 1% H_2O produces an anorthite increase of crystallising plagioclase of around 1-2.5 mol%. As the water contents of arc basalts are generally regarded to be in the range 1-3% (e.g. Baker and Eggler, 1983; Sekine *et al.*, 1979; Baker, 1987), it seems unlikely that the highly anorthitic plagioclases in arc basalts and gabbros can be attributed entirely to the effect of water on melt structure.

Figure 8.4 clearly shows that bulk Ca# of a magma exerts a pronounced control on the composition of crystallising plagioclase. Sub-arc magma chambers in oceanic arcs are believed to be mainly in the pressure range 2-5 kb (Baker, 1987). The present experimental study indicates that at 5 kb, An_{95} plagioclase crystallises from a bulk composition (Mix E) with Ca# = 90 under anhydrous conditions, and also with 2% H_2O. With 5% H_2O at 5 kb, this composition crystallises An_{97} (Table 8.10). Bulk compositions with Ca# = 80 (Mixes A and H) can crystallise plagioclase An_{87-89} anhydrous at 5 kb, but An_{92-93} with 2-5% H_2O. As already seen for the highly calcic plagioclase megacrysts in MORB, plagioclase with $An_{>90}$ in arc lavas and gabbros requires parental melts with Ca# > 80, and CaO/Na_2O values in excess of about 8, *whether or not any water is present in the melt.* Note that this CaO/Na_2O value >8 is for the liquid at the time that plagioclase crystallises. For most arc magmas, there is abundant evidence of extended clinopyroxene crystallisation prior to plagioclase appearance. Merelava volcano in the Vanuatu arc crystallised plagioclase An_{93} phenocrysts after extensive clinopyroxene fractionation (Barsdell, 1988). Thus the CaO/Na_2O values of parental arc magmas are likely to have been much greater than 8

Aphyric lavas in arcs are rare, and estimates of parental arc magma compositions are notoriously difficult to determine. However, glass inclusions in forsteritic olivine phenocrysts should preserve parental CaO/Na_2O values. For lavas

from the Tongan forearc, melt inclusions in Fo_{92-94} phenocrysts have CaO/Na_2O from 18-29; these rocks contain plagioclase phenocrysts from An_{81} to An_{100} (Falloon and Green , 1986), although the wholerock compositions of these lavas have CaO/Na_2O values from 7 to 8. Implied is a complex magma mixing history (see discussion in Falloon and Crawford, 1991) for these forearc lavas, involving at least one highly depleted, very high Ca# melt component. The thin, tensional Tongan forearc crust provides relatively easy access to eruption of these magmas, thus evidence of their existence is preserved.

Beneath arc axial chains, thicker crust forces extensive pooling, mixing and fractionation of parental arc magmas. Little evidence is preserved in the mafic phenocryst assemblages in erupted arc lavas of the existence beneath these volcanoes of highly depleted magmas, since olivine, chromite and pyroxenes will sink. However, plagioclase phenocrysts, which are more buoyant than the mafic phenocrysts, continually concentrate by floatation in the upper parts of arc magma chambers. These accumulate in fractionated residual liquids, to be erupted as arc high-Al basalts. Crawford *et al.* (1987) showed that arc high-Al basalts have groundmass (liquid) compositions ranging from basaltic andesite to rhyolite, and that the entrained plagioclase phenocrysts were unlikely to be in equilibrium with the host liquids. Experimental results from the present study reinforce that conclusion. Moreover, contrary to the suggestion of Beard and Borgia (1989), this study has shown that high melt Al_2O_3 and Al# contents in arc basalts at the stage at which plagioclase commences crystallising are not an important control on the highly calcic nature of plagioclase phenocrysts in arc magmas. Highly anorthitic plagioclase phenocryst cores are the best evidence that very depleted, high CaO/Na_2O magmas were involved in the petrogenesis of typical arc basalts, and that extensive mixing, selective floatation of plagioclase, and settling of mafic phenocrysts are major processes in the generation of arc basalts.

8.6 Conclusion

The presence of highly calcic plagioclase ($>An_{80}$) in arc lavas and cumulates and in some MORB is well known, but there is presently no adequate model explaining such occurrences. An experimental study has been carried out to test the effects of bulk composition, pressure, temperature and water pressure on the composition of liquidus or near-liquidus plagioclase formed in a variety of starting compositions covering the calcic basalt to andesite range.

Probably the strongest single control of the composition of crystallising plagioclase is the Ca# of the bulk composition. The K_DCa# values for plagioclase (coexisting with glass with broadly basaltic to andesitic compositions) crystallising from any bulk composition from anhydrous experiments at 5 kb are always significantly higher than those from anhydrous experiments at 10 kb, but lower than those for hydrous experiments at 5 or 10 kb, or anhydrous experiment at 1 atmosphere. The effect of water on the composition of plagioclase is most marked for bulk compositions with Ca# ranging from 60 to 80, in which plagioclase is up to 10 mol% An more calcic than plagioclase crystallising from the same bulk composition under anhydrous conditions at similar pressure.

These results form the basis of a discussion of the various models for the existence of highly calcic plagioclase in many arc lavas and cumulates, and provide a more thorough assessment of the petrogenetic significance of highly calcic plagioclases in MORB. Most importantly, the highly calcic plagioclase megacrysts in MORB, and phenocrysts in many arc basalts and cumulates, demand the presence in petrogenetic schemes for these magma suites, of melts significantly more refractory (especially in terms of higher CaO/Na_2O) than those presently believed to be involved in normal MORB and arc magma genesis. This has important implications for mechanisms of magma segregation and accumulation from source diapirs ascending beneath spreading centres and arc volcanoes.

REFERENCES

Aggrey, K.E., Muenow, D.W., and Sinton, J.M., 1988, Volatile abundances in submarine glasses from the North Fiji and Lau back-arc basins: Geochimica et Cosmochimica Acta, v. 52, p. 2501-2506.

Arculus, R.J., 1978, Mineralogy and petrology of Grenada, Lesser Antilles Island Arc: Contributions to Mineralogy and Petrology, v. 65, p. 413-424.

Arculus, R.J., and Wills, K.J.A., 1980, The petrology of plutonic blocks and inclusions from the Lesser Antilles island arc: Journal of Petrology, v. 21, p. 743-799.

Asanachinda, P., 1978, The mineralization in the Burmese-Malayan Peninsula - a plate-tectonic model, *in* Proceedings, 3rd Regional Conference on Geology and Mineral Resources of Southeast Asia, Bangkok: Bangkok, Thailand, Asian Institute of Technology, p. 313-318.

Autio, L.K., and Rhodes, J.M., 1984, Costa Rica rift zone basalts - geochemical and experimental data from a possible example of multistage melting, *in* Stout, L.N., and Bailey, M.G., eds., Initial Reports of the Deep Sea Drilling Project, v. 69, p. 729-745.

Bailey, J.C., 1981, Geochemical criteria for a refined tectonic discrimination of orogenic andesites: Chemical Geology, v. 32, p. 139-154.

Bailey, J.C., Frolova, T.I., and Burikova, I.A., 1989, Mineralogy, geochemistry and petrogenesis of Kurile island-arc basalts: Contributions to Mineralogy and Petrology, v. 102, p. 265-280.

Baker, D.R., 1987, Depths and water content of magma chambers in the Aleutian and Mariana island arcs: Geology, v. 15, p. 496-499.

Baker, D.R., and Eggler, D.H., 1983, Fractionation paths of Atka (Aleutians) high-alumina basalts - constraints from phase relations: Journal of Volcanology and Geothermal Reserch, v. 18, p. 387-404.

Barr, S.M., and MacDonald, A.S., 1987, Nan River suture zone, northern Thailand: Geology, v. 15, p. 907-910.

Barr, S.M., MacDonald, A.S., Yaowanoiyothin, W., and Panjasawatwong, Y., 1985, Occurrence of blueschists in the Nan River mafic-ultramafic belt, northern Thailand: Warta Geologi, v. 11, p. 47-50.

Barr, S.M., Tantisukrit, C., Yaowanoiyothin, W., and MacDonald, A.S., 1990, Petrology and tectonic implications of Late Paleozoic volcanic rocks of the Chiang Mai Belt, northern Thailand: Journal of Southeast Asian Earth Sciences, v. 4, p. 37-47.

Barsdell, M., 1988, Petrology and petrogenesis of clinopyroxene-rich tholeiitic lavas, Merelava Volcano, Vanuatu: Journal of Petrology, v. 29, p. 927-964.

Barsdell, M., and Berry, R.F., 1990, Origin and evolution of primitive ankaramitic lavas from western Epi, Vanuatu: Journal of Petrology, v. 31, p. 747-777.

Basaltic Volcanism Study Project, 1981, Basaltic volcanism on the terrestrial planets: New York, Pergamon Press Inc., 1286 p.

Beard, J.S., and Borgia, A., 1989, Temporal variation of mineralogy and petrology in cognate gabbroic enclaves at Arenal volcano, Costa Rica: Contributions to Mineralogy and Petrology, v. 103, p. 110-122.

Beccaluva, L., Piccardo, G.B., and Serri, G., 1979, Petrology of northern Apennine ophiolites and comparison with other Tethyan ophiolites: Ofioliti, v. 4, p. 43-66.

Beckinsale, R.D., Suensilpong, S., Nakapadungrat, S., and Walsh, J.N., 1979, Geochronology and geochemistry of granite magmatism in Thailand in relation to a plate tectonic model: Journal of Geological Society of London, v. 136, p. 529-540.

Bloomer, S.H., 1983, Distribution and origin of igneous rocks from the landward slopes of the Mariana Trench - Implications for its structure and evolution: Journal of Geophysical Research, v. 88, p. 7411-7428.

Bloomer, S.H., Stern, R.J., Fisk, E., and Geschwind, C.H., 1989, Shoshonitic volcanism in the northern Mariana Arc - 1. Mineralogic and major and trace element characteristics: Journal of Geophysical Research, v. 94, p. 4469-4496.

Boyd, F.R., and England, J.L., 1960, Apparatus for phase-equilibrium measurements at pressures up to 50 kb and temperatures up to 1750°C: Journal of Geophysical Research, v. 65, p. 741.

Boyd, F.R., and England, J.L., 1963, Effect of pressure on the melting of diopside, $CaMgSi_2O_6$, and albite, $NaAlSi_3O_8$, in the pressure range up to 50 kilobars: Journal of Geophysical Research, v. 68, p. 311-322.

Bristow, C.S., 1990, Evidence for the nature of the 'Indosinian Orogeny' in Thailand: International Interdisciplinary Meeting at the Geological Society of London 18-20th April, 1990, London, Abstracts, p. 11.

Brophy, J.G., 1986, The Cold Bay volcanic centre, Aleutian volcanic arc: Contributions to Mineralogy and Petrology, v. 93, p. 368-380.

Brouxel, M., and Lapierre, H., 1988, Geochemical study of an early Paleozoic island-arc - back arc basin system. Part 1 - The Trinity Ophiolite (northern California): Geological Society of America Bulletin, v. 100, p. 1111-1119.

Brown, E.H., 1977, The crossite content of Ca-amphibole as a guide to pressure of metamorphism: Journal of Petrology, v. 18, p. 53-72.

Brown, G.M., 1967, Mineralogy of Basaltic rocks, *in* Hess, H.H., and Poldervaart, A., eds., Basalts, The Poldervaart treatise of rocks of basaltic composition, v. 1, p. 103-162.

Bunopas, S., 1981, Paleogeographic history of western Thailand and adjacent parts of Southeast Asia - A plate tectonics interpretation [Ph.D. thesis]: Wellington, Victoria, University of Wellington, 810 p.

Bunopas, S., and Vella, P., 1978, Late Paleozoic and Mesozoic structural evolution of northern Thailand - A plate tectonic model, *in* Proceedings, 3rd Regional Conference on Geology and Mineral Resources of Southeast Asia, Bangkok: Bangkok, Thailand, Asian Institute of Technology, p. 133-172.

Bunopas, S., and Vella, P., 1983, Tectonic and geologic evolution of Thailand, *in* Proceedings, Workshop on Stratigraphic correlation of Thailand and Malaysia, Volume 1, Haad Yai: Bangkok, Thailand, Geological Society of Thailand, and Kuala Lumpur, Malaysia, Geological Society of Malaysia, p. 213-232.

Burton, C.K., 1984, The tectonic framework of mainland Southeast Asia, *in* Proceedings, Applications of Geology and the National Development, Bangkok, November 1984, Volume 1, Bangkok: Bangkok, Thailand, Chulalongkorn University, p. 255-268.

Busse, A.G., Orberger, B., Pitragool, S., Zenker, L., and Friedrich, G., 1989, Preliminary petrographic and geochemical investigations on mafics and ultramafics from the Rhae Nan Chromite Mining District in comparison to the Ban Pak Nai area, the Nan River Suture Zone, northern Thailand, *in* Proceedings, International Symposium on Intermontane Basins - Geology and Resources, Chiang Mai: Chiang Mai, Thailand, University of Chiang Mai, p. 493-501.

Cameron, W.E., 1985, Petrology and origin of primitive lavas from the Troodos ophiolite, Cyprus: Contributions to Mineralogy and Petrology, v.89, p. 239-255.

Cann, J.R., 1970, Rb, Sr, Y, Zr and Nb in some ocean floor basaltic rocks: Earth and Planetary Science Letters, v. 10, p. 7-11.

Chantaramee, S., 1978, Tectonic synthesis of the Lansang area and discussion on regional tectonic evolution, *in* Proceedings, 3rd Regional Conference on Geology and Mineral Resources of Southeast Asia, Bangkok: Bangkok, Thailand, Asian Institute of Technology, p. 177-186.

Chaturongkawanich, S., and Leewongcharoen, S., 1987, Geology of map sheets Ban Na Num and Ban Na Thanung, scale 1:50,000: Summarized Annual Report of Geological Survey Division, Department of Mineral Resources, Bangkok, Thailand, p. 121-123.

Chen, C.-Y., and Frey, F.A., 1985, Trace element and isotopic geochemistry of lavas from Haleakala volcano, East Maui, Hawaii - Implications for the origin of Hawaiian basalts: Journal of Geophysical Research, v. 90, p. 8743-8768.

Clague, D.A., Fisk, M.R., and Bence, A.E., 1980, Mineral chemistry of basalts from Ojin, Nintoku, and Suiko Seamounts, Leg 55, DSDP, *in* Shambach, J., ed., Initial Reports of the Deep Sea Drilling Project, v. 55, p. 607-637.

Coish, R.A., 1977. Ocean floor metamorphism in the Betts Cove ophiolite, Newfoundland: Contributions to Mineralogy and Petrology, v. 60, p. 255-270.

Cole, J.W., 1978, Andesites of the Tongariro volcanic centre, North Island, New Zealand: Journal of Volcanology and Geothermal Research, v. 3, p. 121-153.

Cole, J.W., Graham, I.J., and Gibson, I.L., 1990, Magmatic evolution of Late Cenozoic volcanic rocks of the Lau Ridge, Fiji: Contributions to Mineralogy and Petrology, v. 104, 540-554.

Cooper, M.A., Herbert, R., and Hill, G.S., 1989, The structural evolution of Triassic intermontane basins in northern Thailand, *in* Proceedings, International Symposium on Intermontane Basins - Geology and Resources, Chiang Mai: Chiang Mai, Thailand, University of Chiang Mai, p. 231-242.

Cowan, D.S., 1985, Structural styles in Mesozoic and Cenozoic melanges in the western Cordillera of North America: Geological Society of America Bulletin, v. 56, p. 451-462.

Crawford, A.J., and Keays, R., 1987, Petrogenesis of Victorian Cambrian tholeiites and implications for the origin of associated boninites: Journal of Petrology, v. 28, p. 1075-1109.

Crawford, A.J., Beccaluva, L., and Serri, G.,1981, Tectono-magmatic evolution of the West Philippine - Mariana region and the origin of boninites: Earth and Planetary Science Letters, v. 54, p. 346-356.

Crawford, A.J., Beccaluva, L., Serri, G., and Dostal, J., 1986, Petrology, geochemistry and tectonic implications of volcanics dredged from the intersection of the Yap and Mariana trenches: Earth and Planetary Science Letters, v. 80, p. 265-280.

Crawford, A.J., Falloon, T.J., and Eggins, S., 1987, The origin of island arc high-alumina basalts: Contributions to Mineralogy and Petrology, v. 97, p. 417-430.

Danjushevsky, L.V., Solobev, A.V., and Dmitriev, L.V., 1987, Orthopyroxene-bearing low-Ti tholeiites - the new type of ocean ridge tholeiite: Doklady of the Academy of Sciences of the U.S.S.R: Earth Sciences Sections, v. 292, p. 1449-1452.

Dick, H.J.B., and Bullen, T., 1984, Chromian spinel as a petrogenetic indicator in abyssal basalt and alpine-type peridotites and spatially associated lavas. Contributions to Mineralogy and Petrology, v. 86, p. 54-76.

Donaldson, C.H., and Brown, R.W., 1977, Refractory megacrysts and magnesium-rich melt inclusions within spinel in oceanic tholeiites - Indicators of magma mixing and parental magma composition: Earth and Planetary Science Letters, v. 37, p. 81-89.

Drake, M.J., 1976, Plagioclase-melt equilibria: Geochimica et Cosmochimica Acta, v. 40, p. 457-465.

Droop, G.T.R., 1985, Alpine metamorphism in the southeast Tauern window, Austria - 1. P-T variations in space and time : Journal of metamorphic Petrology, v. 3, p.371-402.

Duncan, R.A., 1987, The Karoo igneous province - a problem area for inferring tectonic setting from basalt geochemistry: Journal of Volcanology and Geothermal Research, v. 32, p. 13-34.

Duncan, R.A., and Green, D.H., 1980, Role of multistage melting in the formation of oceanic crust: Geology, v. 8, p. 22-26.

Duncan, R.A., and Green, D.H., 1987, The genesis of refractory melts in the formation of oceanic crust: Contributions to Mineralogy and Petrology, v. 96, p. 326-342.

Eggins, S., Green, D.H., and Falloon, T.J., 1990, The Tasmantid Seamounts - Shallow melting and contamination of deeply-derived EM1 mantle: Earth and Planetary Science Letters (in press).

Ellis, D.J., and Green, D.H., 1979, An experimental study of the effect of Ca upon garnet-clinopyroxene Fe-Mg exchange equilibria: Contributions to Mineralogy and Petrology, v. 71, p. 13-22.

Evans, B.W., and Wright, T.L., 1972, Composition of liquidus chromite from the 1959 (Kilauea Iki) and 1965 (Makaopuhi) eruptions of Kilauea volcano, Hawaii: American Mineralogist, v. 57, p. 217-230.

Ewart, A., 1976, A petrological study of the younger Tongan andesites and dacites, and the olivine tholeiites of Niua Fo'ou Island, S.W. Pacific: Contributions to Mineralogy and Petrology, v. 58, p. 1-21.

Falloon, T.J., and Crawford, A.J., 1991, The petrogenesis of high-calcium boninite lavas dredged from the north Tonga ridge: Earth and Planetary Science Letters (in press).

Falloon, T.J., and Green, D.H., 1986, Glass inclusions in magnesian olivine phenocrysts from Tonga - evidence for highly refractory parental magmas in the Tongan arc: Earth and Planetary Science Letters, v. 81, p. 95-103.

Falloon, T.J., Green, D.H., and McCulloch, M.T., 1989, Petrogenesis of high-Mg and associated lavas from the north Tonga Trench: *in* Crawford, A.J., ed., Boninites and related rocks: London, Unwin Hyman Ltd., p. 357-395.

Feigenson, M.D., Hofmann, A.W., and Spera, F.J., 1983, Case study on the origin of basalt - II. The transition from tholeiitic to alkalic volcanism on Kohala volcano, Hawaii: Contributions to Mineralogy and Petrology, v. 84, p. 390-405.

Fisk, M.R., and Bence, A.E., 1980, Experimental crystallization of chrome spinel in FAMOUS basalt 527-1-1: Earth and Planetary Science Letters, v. 48, p. 111-123.

Floyd, P.A., 1977, Rare earth element mobility and geochemical characteristics of spilitic rocks: Nature, v. 269, p. 38-48.

Floyd, P.A., and Winchester, J. A., 1975, Magma type and tectonic setting discrimination using immobile elments: Earth and Planetary Science Letters, v. 27, p. 211-218.

Foden, J., 1986, The petrology of Tambora Volcano, Indonesia - A model for the 1815 eruption: Journal of Volcanology and Geothermal Research, v. 27, p. 1-41.

Frey, F.A., 1974, Atlantic ocean floor - Geochemistry and petrology of basalts from Legs 2 and 3 of the Deep Sea Drilling Project: Journal of Geophysical Research, v. 79, p. 5507-5527.

Frey, F.A., and Clague, D.A., 1983, Geochemistry of diverse basalt types from Loihi Seamount, Hawaii - petrogenetic implications: Earth and Planetary Science Letters, v. 66, p. 337-355.

Frey, F.A., Bryan, W.B., and Thompson, G., 1974, Atlantic ocean floor - Geochemistry and petrology of basalts from Legs 2 and 3 of the Deep Sea Drilling Project: Journal of Geophysical Research, v. 70, p. 5507-5527.

Frey, F.A., Dickey, J.S., Thompson, G.,, Bryan, W.B., and Davies, H.L., 1980, Evidence for heterogeneous primary MORB and mantle sources, NW Indian Ocean: Contributions to Mineralogy and Petrology, v. 74, p. 387-402.

Frey, F.A., Wise, W.S., Garcia, M.O., West, H., Kwon, S.T., and Kennedy, A.,1990, Evolution of Mauna Kea Volcano, Hawaii - Petrologic and geochemical constraints on postshield volcanism: Journal Geophysical Research, v. 95, p. 1271-1300.

Fujimaki, H., 1986, Fractional crystallization of the basaltic suite of Usu volcano, southwest Hokkaido, Japan, and its relationships with the associated felsic suite: Lithos, v. 19, p. 129-140.

Gatinsky, Y.G., Mischina, A.V., Vinogradov, I.V., and Kovalev, A.A., 1978, The main metallogenic belts of southeast Asia as the result of different geodynamic conditions interference, *in* Proceedings, 3rd Regional Conference on Geology and Mineral Resources of Southeast Asia, Bangkok: Bangkok, Thailand, Asian Institute of Technology, p. 313-318.

Gerlach, D.C., and Grove, T.L., 1982, Petrology of Medicine Lake Highland volcanics - Characterization of end members of magma mixing: Contributions to Mineralogy and Petrology, v. 80, p. 147-159.

Gill, J.B., 1981, Orogenic andesites and plate tectonics, Springer Verlag, Berlin, 390 p.

Gorton, M.P., 1977, The geochemistry and origin of Quaternary volcanism in the New Hebrides: Geochimica et Cosmochimica Acta, v. 41, p. 1257-1270.

Graham, C.M., and Powell, R., 1984, A garnet-hornblende geothermometer - Calibration, testing, and application to the Pelona schist, southern California: Journal of Metamorphic Petrology, v. 2, p. 13-31.

Green, D.H., and Ringwood, A.E., 1967a, An experimental investigation of the gabbro to eclogite transformation and its petrological applications: Geochimica et Cosmochimica Acta, v. 31, p. 767-833.

Green, D.H., and Ringwood, A.E., 1967b, The genesis of basaltic magmas: Contributions to Mineralogy and Petrology, v. 15, p. 103-190.

Green, D.H., Hibberson, W.O., and Jaques, A.L., 1979, Petrogenesis of mid-ocean ridge basalts, *in* McElhinny, M.W., ed., The earth - its origin, structure and evolution: Academic Press, p. 265-290.

Green, T.H., 1982, Anatexis of mafic crust and high pressure crystallization of andesite, *in* Thorpe, R.S., ed., Andesites: John Wiley & Sons, p. 465-487.

Grenne, T., and Roberts, R., 1980, Geochemistry and the volcanic setting of the Ordovician Forbordfjell and Jonsvatn greenstones, Trondheim region, central Norwegian Caledonides: Contributions to Mineralogy and Petrology, v. 74, p. 375-386.

Griffin, B.J., 1979, Energy dispersive analysis system calibration and operation with TAS-SUEDS, and advanced interactive data-reduction package: Department of Geology Publication 343, University of Tasmania.

Grove, T.L., and Bence, A.E., 1979, Crystallization kinetics of multiply saturated basaltic magma - An experimental study of Lunar 24 ferrobasalt, *in* Proceedings, 10th Lunar and Planetary Science Conference, Volume 1, Houston, Texas, Lunar and Planetary Institute, p. 439-478.

Gust, D.A., and Perfit, M.R., 1987, Phase relations of a high-Mg basalt from the Aleutian Island Arc - Implications for primary island arc basalts and high Al-basalts: Contributions to Mineralogy and Petrology, v. 97, p. 7-18.

Hahn, L., 1985, The Indosinian orogeny in Thailand and adjacent ares: Me'moires de la Socie'te' ge'ologique de France 147, p. 71-82.

Hahn, L., Koch, K.E., and Wittekindt, H., 1986, Outline of the geology and the mineral potential in Thailand: Geologisches Jarbuch, Reihe B, v. 59, p. 3-49.

Hawkins, J. , and Melchoir, J., 1983, Petrology of basalts from Loihi seamount, Hawaii: Earth and Planetary Science Letters, v. 66, p. 356-368.

Hawkins, J.W., and Evans, C.A., 1983, Geology of the Zambles Range, Luzon, Philippine islands - Ophiolite derived from an island arc-back arc basin pair, *in* Hayes, D.E., ed., The tectonic and geologic evolution southeast Asian Seas and islands, part 2: Geophysical Monograph 27, p. 95-123.

Hawkins, J.W., and Melchoir, J.T., 1985, Petrology of basalts of Mariana Trough and Lau Basin basalts: Journal of Geophysical Research, v. 90, p. 11431-11468.

Hayashi, M., 1989, The hydrocarbon potential and tectonics of Indochina: Geological Society of Malaysia Bulletin, v. 25, p. 65-78.

Hellman, P.J., and Henderson, P., 1979, Are rare earth elements mobile during spilitization?: Nature, v. 267, p. 38-48.

Helmcke, D., 1985, The Permo-Triassic Paleotethys in mainland southeast Asia and adjacent parts of China: Geologische Rundschau, v. 74, p. 215-228.

Helmcke, D., 1986, On the geology of Petchabun fold-belt (central Thailand) - Implications for the geodynamic evolution of mainland southeast Asia, *in* Proceedings, 5th Regional Conference on Geology and Mineral Resources of Southeast Asia, Kuala Lumpur, April 1984, Volume 1: Kuala Lumpur, Malaysia, Geological Society of Malaysia, p. 79-85.

Helmcke, D., and Kraikhong, C., 1982, On the geosynclinal and orogenic evolution of central and northeastern Thailand: Journal of Geological Society of Thailand, v. 5, p. 52-74.

Helmcke, D., and Lindenberg, H.-G., 1983, New data on the Indosinian orogeny from central Thailand: Geologische Rundschau, v. 72, p. 317-328.

Heming, R.F., 1977, Mineralogy and proposed P-T paths of basaltic lavas from Rabaul Caldera, Papua New Guinea: Contributions to Mineralogy and Petrology, v. 61, p. 15-33.

Hess, A., and Koch, K.E., compilers, 1975, Geologic map of northern Thailand, sheet 1 (Nan): Federal Institute for Geosciences and Natural Resources, Germany, scale 1:250,000.

Hochstaedter, A., Morris, J., and Langmuir, C., 1988, Arc rifting produces BABB-Composition basalts at the Sumisu Rift, Izu Arc: EOS, v. 69, p. 1471.

Hochstaedter, A.G., Gill, J.B., Kusakabe, M., Newman, S., Pringle, M., Taylor, B., and Fryer, P., 1990, Volcanism in the Sumisu Rift, I. Major element, volatile, and stable isotope geochemistry: Earth and Planetary Science Letters, v. 100, p. 179-194.

Holm, P.E., 1982, Non-recognition of continental tholeiites using the Ti-Zr-Y diagram: Contributions to Mineralogy and Petrology, v. 79, p. 308-310.

Holm, P.E., 1985, The geochemical fingerprints of different tectonomagmatic environments using hygromagmatophile element abundances of tholeiitic basalts and basaltic andesites: Chemical Geology, v. 51, p. 303-323.

Humphris, S.E., Morrison, M.A., and Thompson, R.N., 1978, Influence of rock crystallization history upon subsequent lanthanide mobility during hydrothermal alteration of basalts, Chemical Geology, v. 23, p. 125-137.

Hutchison, C.S., 1983, Multiple Mesozoic Sn-W-Sn granitoids of Southeast Asia: Geological Society of America Memoir 159, p. 35-60.

Hutchison, C.S., 1989, Geological evolution of southeast Asia, Clarendon Press, Oxford, 368 p.

Ikeda, Y., and Yuasa, M., 1989, Volcanism in nascent back-arc basins behind the Shichito Ridge and adjacent areas in the Izu-Ogasawara arc, northwest Pacific - Evidence for mixing between E-type MORB and island arc magmas at the initiation of back-arc rifting: Contributions to Mineralogy and Petrology, v. 101, p. 377-393.

Imjai, S., Junkrueng, T., and Pramapan, S., 1986, Geology of the Kaeng Luang area, Amphoe Na Noi, Nan [B.S. thesis]: Chiang Mai, University of Chiang Mai, 98 p.

Irvine, T.N., 1967, Chromian spinel as a petrogenetic indicator. Part 2. Petrologic applications: Canadian Journal of Earth Sciences, v. 4, p. 71-103.

Ishizuka, H., 1987, Igneous and metamorphic petrology of the Horokanai ophiolite in the Kamuikotan zone, Hokkaido, Japan - a synthetic thesis: Memoirs of the Faculty of Science, Kochi University, Series E, Geology 8, p. 1-70.

Ivanov, T., Misar, Z., Bowes, D.R., Dudek, A., Dumurdzanov, N., Jaros, J., Jenlinek, E., and Pacesova, M., 1987, The Demir Kapija-Gevgelija ophiolite massif, Macedonia, Yugoslavia: Ofioliti, v. 12, p. 457-478.

Jackson, E.D., 1967, Ultramafic cumulates in the Stillwater, Great Dike, and Bushveld Intrusions, *in* Wyllie, P.J., ed., Ultramafic and related rocks: New York, John Wiley and Sons, Inc., p. 20-38.

Jakes, P., and Gill, J.B., 1970, Rare earth elements and the island arc tholeiite series: Earth and Planetary Science Letters, v. 9, p. 17-28.

Jakes, P., and White, A.J.R., 1972, Major and trace element abundances in volcanic rocks of orogenic areas: Geological Society of America Bulletin, v. 83, p. 29-39.

Jenner, G.A., Cawood, P.A., Rautenschlein, M., and White, W.M., 1987, Composition of back-arc basin volcanics, Valu Fa Ridge, Lau Basin - Evidence for a slab-derived component in their mantle source: Journal of Volcanology and Geothermal Research, v. 32, p. 209-222.

Johannes, W., 1978, Melting of plagioclase in the system Ab-An-H_2O and Qz-Ab-An-H_2O at PH_2O=5 kbars, an equlilbrium problem: Contributions to MIneralogy and Petrology, v. 66, p. 295-303.

Johannes, W., 1989, Melting of plagioclase-quartz assemblages at 2 kbar water pressure: Contributions to Mineralogy and Petrology, v. 103, p. 270-276.

Johannes, W., and Puhan, D., 1971, The calcite-aragonite transition, reinvestigated: Contributions to Mineralogy and Petrology, v. 31, p. 28-38.

Johnson, M.C., and Rutherford, M.J., 1989, Experimentally determined conditions in the Fish Canyon tuff, Colorado, magma chamber: Journal of Petrology, v. 30, p. 711-737.

Johnson, R.W., and Arculus, R.J., 1978, Volcanic rocks of the Witu Islands, Papua New Guinea - The origin of magmas above the deepest part of the New Britain Benioff zone: Bulletin of Volcanologique, v. 41, p. 609-655.

Keller, R.A., Fisk, M.R., and Birkenmajer, K., 1988, Late Tertiary - Quaternary transition from arc to back-arc volcanism, South Shetland Islands and Bransfield Strait, Antarctica: EOS, v. 69, p. 1471.

Kleebai, A., Hongjaisee, U., and Sonthichai, W., 1986, Geology of the Ban Huai Lao area, Amphoe Na Noi, Nan [B.S. thesis]: Chiang Mai, University of Chiang Mai, 95 p.

Koyaguchi, T., 1986, Evidence for two-stage mixing in magmatic inclusions and rhyolitic lava domes on Niijima Island, Japan: Journal of Volcanology and Geothermal Research, v. 29, p. 71-98.

Laird, J., and Albee, A.L., 1981, High-pressure metamorphism in mafic schist from northern vermont: American Journal of Science, v. 281, p. 97-126.

le Roex, A.P., Dick, H.J.B., and Fisher, R.L., 1989, Petrology and geochemistry of MORB from 25°E to 46°E along the Southwest Indian Ridge - evidence for contrasing styles of mantle enrichment: Journal of Petrology, v. 30, p. 947-986.

le Roex, A.P., Dick, H.J.B., Erlank, A.J., Reid, A.M., Frey, F.A., and Hart, S.R., 1983, Geochemistry, mineralogy and petrogenesis of lavas erupted along the Southwest Indian Ridge between the Bouvet Triple Junction and 11 degrees east: Journal of Petrology, v. 24, p. 267-318.

le Roex, A.P., Dick, H.J.B., Reid, A.M., and Erlank, A.J., 1982, Ferrobasalts from the Spiess Ridge Segment of the Southwest Indian Ridge: Earth and Planetary Science Letters, v. 60, p. 437-451.

le Roex, A.P., Dick, H.J.B., Reid, A.M., Frey, F.A., Erlank, A.J., and Hart, S.R., 1985, Petrology and geochemistry of basalts from the American-Antarctic Ridge, Southern Ocean - implications for the westward influence of the Bouvet mantle plume: Contributions to Mineralogy and Petrology, v. 90, p. 367-380.

Leake, B.E., 1978, Nomenclature of amphiboles: Canadian Mineralogist, v. 16, p. 501-520.

Leterrier, J., Maury, R.C., Thonon, P., Girard, D., and Marchal, M., 1982, Clinopyroxene composition as a method of identification of the magmatic affinities of paleo-volcanic series: Earth and Planetary Science Letters, v. 59, p. 139-154.

Lin, P.-N., Stern, R.J., and Bloomer, S.H., 1989, Shoshonitic volcanism in the northern Mariana Arc - 2. Large-ion-lithophile and rare earth element abundances - evidence for the source of incompatible element enrichments in intraoceanic arcs: Journal of Geophysical Research, v. 94, p. 4497-4514.

Lippard, S.J., Shelton, A.W., and Gass, I.G., 1986, The ophiolite of Northern Oman: Geological Society of London Memoirs 11, 178 p.

Liu, L., Sinton, J.M., and Chappel, B., 1988, Contrasting magma types in the Manus Back-Arc Basin - Implications for source compositions and metasomatic processes behind island arcs: EOS, v. 69, p. 1470.

Lopez-Escobar, L., Vergara, M., and Frey, F.A., 1981, Petrology and geochemistry of lavas from Antuco Volcano, a basaltic volcano of the southern Andes (37° 25'S): Journal of Volcanology and Geothermal Research, v. 11, p. 329-352.

Loucks, R.R., 1990, Discrimination of ophiolitic from nonophiolitic ultramafic-mafic allochthons in orogenic belts by the Al/Ti ratio in clinopyroxene: Geology, v. 18, p. 346-349.

Lumjuan, A., and Sinpoonanunt, S., 1987, Geology of map sheets Tha Pla and Khuan Sirikit, scale 1:50,000: Summarized Annual Report of Geological Survey Division, Department of mineral Resources, Bangkok, Thailand, p. 118-120.

MacDonald, A.S., and Barr, S.M., 1984, The Nan River mafic-ultramafic belt, northern Thailand - Geochemistry and tectonic significance: Geological Society of Malaysia Bulletin, v. 17, p. 209-224.

Mahood, G.A., and Baker, D.R., 1986, Experimental constraints on depths of fractionation of mildly alkalic basalts and associated felsic rocks - Pantelleria, Strait of Sicily: Contributions to Mineralogy and Petrology, v. 93, p. 251-264.

Maresch, W.V., 1977, Experimental studies on glaucophane - an analysis of present knowledge: Tectonophysics, v. 43, p. 109-125.

Marsh, N.G., Saunders, A.D., Tarney, J. and Dick, H.J.B., 1980, Geochemistry of basalts from the Shikoku and Daito basins, Deep Sea Drilling Project Leg 58, *in* Stout, L.N., ed., Initial Reports of the Deep Sea Drilling Project, v. 58, p. 805-842.

Maruyama, S., Suzuki, K., and Liou, J.G., 1983, Greenschist-amphibolite transitional equilibria at low pressures: Journal of Petrology, v. 24, p. 583-604.

Meen, J.K., 1990, Elevation of potassium content of basaltic magma by fractional crystallization - the effect of pressure: Contributions to Mineralogy and Petrology, v. 104, p. 309-331.

Meijer, A., and Reagan, M., 1981, Petrology and geochemistry of the island of Sarigan in the Mariana Arc; calc-alkaline volcanism in an oceanic setting: Contributions to Mineralogy and Petrology, v. 77, p. 337-354.

Meschede, M., 1986, A method of discriminating between different types of mid-ocean ridge basalts and continental tholeiites with the Nb-Zr-Y diagram: Chemical Geology, v. 56, p. 207-218.

Miyashiro, A., 1973, The Troodos ophiolite complex was probably formed in an island arc: Earth and Planetary Science Letters, v. 19, p. 218-224.

Miyashiro, A., 1975a, Reply to comment on 'Origin of the Troodos and other ophiolites': Earth and Planetary Science Letters, v. 25, p. 217-222.

Miyashiro, A., 1975b, Volcanic rock series and tectonic setting: Annual Review of Earth and Planetary Sciences, v. 3, p. 251-269.

Miyashiro, A., 1975c, Classification, characteristics, and origin of ophiolites: Journal of Geology, v. 83, p. 249-281.

Moody, J.B., Meyer, D., and Jenkins, J.E., 1983, Experimental characterization of the greenschist/amphibolite boundary in mafic systems: American Journal of Science, v. 283, p. 48-92.

Muenow, D.W., Liu, N.W.K., Garcia, M.O., and Saunders, A.D., 1980, Volatiles in submarine volcanic rocks from the spreading axis of the East Scotia Sea Back-arc basin: Earth and Planetary Science Letters, v. 47, p. 272-278.

Myers, R., and Breitkopf, J.H., 1989, Basalt geochemistry and tectonic settings - A new approach to relate tectonic and magmatic processes: Lithos, v. 23, p. 53-62.

Natland, J.H., 1989, Partial melting of a lithologically heterogeneous mantle - inferences from crystallization histories of magnesian abyssal tholeiites from the Siqueiros Fracture Zone. *in*: Saunders, A.D., and Norry M.J., eds., Magmatism in the Ocean Basins: Blackwell Scientific Publications, p. 41-70.

Nesbitt, R.W., and Sun, S.S., 1976, Geochemistry of Archean spinifex-textured peridotites and magnesian and low-magnesian tholeiites: Earth and Planetary Science Letters, v. 31, p. 433-453.

Norrish, K., and Chappel, B.W., 1967, X-ray fluorescence spectrography, *in* Zussman, J., ed., Physical methods in determinative mineralogy: London, Academic Press, p. 161-214.

Norrish, K., and Hutton, J.T., 1969, An accurate X-ray spectrographic method for the analysis of a wide range of geological samples: Geochimica et Cosmochimica Acta, v. 33, p. 431-455.

Nwe, Y.Y., 1976, Electron-probe studies of the earlier pyroxenes and olivines from the Skaergaard Intrusion, East Greenland: Contributions to Mineralogy and Petrology, v. 55, p. 105-126.

Orberger, B., Friedrich, G., and Pitragool, S., 1989, Platinum-group-element distribution in ultramafics, chromite, magnetite and pyrrhotite, Nan-Uttaradit mafic-ultramafic belt, northern Thailand - preliminary results, *in* Proceedings, International Symposium on Intermontane Basins - Geology and Resources, Chiang Mai: Chiang Mai, Thailand, University of Chiang Mai, p. 483-492.

Ozawa, K., 1983, Evaluation of olivine-spinel geothermometry as an indicator of thermal histories for peridotites: Contributions to Mineralogy and Petrology, v. 82, p. 52-65.

Pearce, J.A., 1980, Geochemical evidence for the genesis and eruptive setting of lavas from Tethyan ophiolites, *in* Proceedings, International Ophiolite Symposium, Cyprus, 1979: Cyprus, Geological Survey Department, p. 261-272.

Pearce, J.A., 1982, Trace element characteristics of lavas from destructive plate boundaries, *in* Thrope, R.S., ed., Andesites - orogenic andesites and related rocks: Page Bros. (Norwich) Limited, p. 525-548.

Pearce, J.A., 1983, Role of Subcontinental lthosphere in magma genesis at active continental margins, *in* Hawkesworth, C.J., and Norry, M.J., eds., Continental basalts and mantle xenoliths: Nantwich, Shiva Publishing, p. 230-249.

Pearce, J.A., and Cann, J.R., 1973, Tectonic setting of basic volcanic rocks determined using trace element analyses: Earth and Planetary Science Letters, v. 19, p. 290-300.

Pearce, J.A., and Norry, M.J., 1979, Petrogenetic implications of Ti, Zr, Y and Nb variations in volcanic rocks: Contributions to Mineralogy and Petrology, v. 69, p. 33-47.

Pearce, J.A., Lippard, S.J., and Roberts, S., 1984, Characteristics and tectonic significance of supra-subduction zone ophiolites, *in* Kokelaar, B.P., and Howells, M.F., eds., Marginal Basin Geology : Geological Society Special Publication 16, p. 77-94.

Pearce, T.H., Gorman, B.E.and Birkett, T.C., 1975, The TiO_2-K_2O-P_2O_5 diagram - A method of discriminating between oceanic and non-oceanic basalts: Earth and Planetary Science Letters, v. 24, p. 419-426.

Perfit, M.R., Gust, D.A., Bence, A.E., Arculus, R.J., and Taylor, S.R., 1980, Chemical characteristics of island-arc basalts - implications for mantle sources: Chemical Geology, v. 30, p. 227-256.

Plang, P., Munyoo, C., and Khonsombat, C., 1986, Geology of the Doi Puk Cham Peng - Doi Pu Lon area, Amphoe Na Noi, Nan [B.S. thesis]: Chiang Mai, University of Chiang Mai, 87 p.

Polachan, S., and Sattayarak, N., 1989, Strike-slip tectonics and the development of Tertiary basins in Thailand, *in* Proceedings, International Symposium on Intermontane Basins - Geology and Resources, Chiang Mai: Chiang Mai, Thailand, University of Chiang Mai, p. 243-253.

Prestvik, T., 1982, Basic volcanic rocks and tectonic setting. A discussion of the Zr-Ti-Y discrimination diagram and its suitability for classification purposes: Lithos, v. 15, p. 241-247.

Price, R.C., Johnson, L.E., and Crawford, A.J., 1990, Basalts of the North Fiji Basin - The generation of back arc basin magmas by mixing of depleted and enriched mantle sources: Contributions to Mineralogy and Petrology, v. 105, p. 106-121.

Price, R.C., Kennedy, A.K., Riggs-Sneeringer, M., and Frey, F.A., 1986, Geochemistry of basalts from the Indian Ocean triple junction - Implications for the generation and evolution of Indian Ocean ridge basalts: Earth and Planetary Science Letters, v. 78, p. 379-396.

Robinson, P., Higgins, N.C., and Jenner, G.A., 1986, Determination of rare-earth elements, yttrium and scandium in rocks by an ion exchange - X-ray fluorescence technique: Chemical Geology, v. 55, p. 121-137.

Roeder, P.L., Campbell, I.H., and Jamieson, H.E., 1979, A re-evaluation of the olivine-spinel geothermometer: Contributions to Mineralogy and Petrology, v. 68, p. 325-334.

Rose, W.I., Jr., Anderson, A.T., Jr., Woodruff, L.G., and Bonis, S.B., 1978, The October 1974 basaltic tephra from Fuego Volcano - description and history of the magma body: Journal of Volcanology and Geothermal Research, v. 4, p. 3-53.

Sattayarak, N., Srikulwong, S., and Pum-Im, S., 1989, Petroleum potential of the Triassic pre-Khorat intermontane basin in northeastern Thailand, *in* Proceedings, International Symposium on Intermontane Basins - Geology and Resources, Chiang Mai: Chiang Mai, Thailand, University of Chiang Mai, p. 43-58.

Saunders, A.D., and Tarney, J., 1979, The geochemistry of basalts from a back-arc spreading centre in the East Scotia Sea: Geochimica et Cosmochimica Acta, v. 43, p. 555-572.

Saunders, A.D., and Tarney, J., 1984, Geochemical characteristics of basaltic volcanism within back-arc basins, *in* Kokelaar, B.P., and Howells, M.F., eds., Marginal basin geology: Geological Society Special Publication 16, p. 59-76.

Saunders, A.D., Fornari, D.J., Joron, J.-L., Tarney, J., and Trueil, M., 1982, Geochemistry of basic igneous rocks, Gulf of California , Deep Sea Drilling Project Leg 64, *in* Blakeslee, J, Platt, L.W., and Stout, L.N. eds., Initial Reports of the Deep Sea Drilling Project, v. 64, p. 595-642.

Saunders, A.D., Tarney, J., Stern, C.R., and Dalziel, I.W.D., 1979, Geochemistry of Mesozoic marginal basin floor igneous rocks from Southern Chile: Geological Society of America Bulletin, v. 90, p. 237-258.

Sekine, T., Katsura, T., and Aramaki, S., 1979, Water saturated phase relations of some andesites with application to the estimation of the initial temperature and water pressure at the time of eruption: Geochimica et Cosmochimica Acta, v. 43, p. 1367-1376.

Sen, G., and Presnall, D.C., 1986, Petrogenesis of dunite xenoliths from Koolau volcano, Oahu, Hawaii - implications for Hawaiian Volcanism: Journal of Petrology, v. 27, p. 197-217.

Sengor, A.M.C., 1984, The Cimmeride orogenic system and the tectonics of Eurasia: Geological Society of America Special Paper 195, 82 p.

Serri, G., 1981, The petrochemistry of ophiolite gabrroic complexes - A key for the classification of ophiolites into low-Ti and high-Ti types: Earth and Planetary Science Letters, v. 52, p. 203-212.

Shervais, J.W., 1982, Ti-V plots and the petrogenesis of modern and ophiolitic lavas: Earth and Planetary Science Letters, v. 59, p. 101-118.

Sinton, J.M., and Fryer, 1987, Mariana Trough lavas from 18°N - implications for the origin of back arc basin basalts: Journal of Geophysical Research, v. 92, p. 12782-12802.

Smith, T.E., Huang, C.H., Walawender, M.J., Cheung, P., and Wheeler, C., 1983, The gabbroic rocks of the peninsular ranges batholith, southern California - Cumulate rocks associated with calc-alkalic basalts and andesites: v. 18, p. 249-278.

Stakes, D.S., Shervais, J.W., and Hopson, C.A., 1984, The volcanic-tectonic cycle of the FAMOUS and AMAR Valleys, mid-Atlantic Ridge (36°47') - Evidence from basalt glass and phenocryst compositional variations for a steady state magma chamber beneath the valley midsections, AMAR 3: Journal of Geophysical Research, v. 89, p. 6995-7028.

Stern, C.R., 1980, Geochemistry of Chilean ophiolites - Evidence for the compositional evolution of the mantle source of back-arc basin basalts: Journal of Geophysical Research, v. 85, p. 955-966.

Stern, R.J., Bloomer, S.H., Lin, P.-N., Ito, E., and Morris, J., 1988, Shoshonitic magmas in nascent arcs - New evidence from submarine volcanoes in northern Marianas: Geology, v. 16, p. 426-430.

Stolz, A.J., Varne, R., Wheller, G.E., Foden, J.D., and Abbott, M.J., 1988, The geochemistry and petrogenesis of K-rich alkaline volcanics from the Batu Tara volcano, eastern Sunda arc: Contributions to Mineralogy and Petrology, v. 98, p. 374-389.

Streckeisen, A., 1976, To each plutonic rocks its proper name: Earth and Planetary Science Letters, v. 12, p. 1-33.

Subcommittee on Pyroxenes, I.M.A., 1988, Nomenclature of pyroxenes: American Mineralogist, v. 73, p. 1123-1133.

Sukvattananunt, P., and Assavapatchara, S., 1987, Geology of map sheets Amphoe Sa and Ban Nam Muap, scale 1:50,000: Summarized Annual Report of Geological Survey Division, Department of mineral Resources, Bangkok, Thailand, p. 124-138.

Sun, S.S-. and McDonough, W.F., 1989, Chemical and isotopic systematics of oceanic basalts - Implications for mantle composition and processes, *in* Saunders, A.D., and Norry, M.J., eds., Magmatism in ocean basins : Geological Society Special Publication 42, p. 313-345.

Sunkel, G., 1991, Origin of petrological and geochemical variations of Lau Basin lavas (SW Pacific): Marine Mining (in press).

Taylor, S.R., and Gorton, M.K., 1977, Geochemical application of spark-source mass spectrometry. III. element sensitivity, precision and accuracy: Geochimica et Cosmochimica Acta, v. 41, p. 1375-1380.

Thanasuthipitak, T., 1978, Geology of Uttaradit area and its implications on tectonic history of Thailand, *in* Proceedings, 3rd Regional Conference on Geology and Mineral Resources of Southeast Asia, Bangkok: Bangkok, Thailand, Asian Institute of Technology, p. 187-197.

Tormey, D.R., Grove, T.L., and Bryan, W.B., 1987, Experimental petrology of normal MORB near the Kane Fracture Zone - 22°-25° N, mid-Atlantic ridge: Contributions to Mineralogy and Petrology, v. 96, p.121-139.

Ussler III, W., and Glazner, A.F., 1989, Phase equilibria along a basalt-rhyolite mixing line - implications for the origin of calc-alkaline intermediate magmas: Contributions to Mineralogy and Petrology, v. 101, p. 232-244.

Volpe, A.M., Douglas, J., Macdougall, J.D., and Hawkins, J.W., 1988, Mariana Trough basalts (MTB) - Trace element and Sr-Nd isotopic evidence for mixing between MORB-like and Arc-like melts: Earth and Planetary Science Letters, v. 82, p. 241-254.

Walker, D., Shibata, T., and DeLong, S.E., 1979, Abyssal tholeiites from the Oceanographer Fracture Zone. II. Phase equilibria and mixing: Contributions to Mineralogy and Petrology, v. 70, p. 111-125.

Walker, J.A., and Carr, M.J., 1986, Compositional variations caused by phenocryst sorting at Cerro Negro volcano, Nicaragua: Geological Society of America Bulletin, v. 97, p. 1156-1162.

Wannapeera, A., and Kosuwan, S., 1987, Geology of map sheets Ban Huai Pu and King Amphoe Mae Charim, scale 1:50,000: Summarized Annual Report of Geological Survey Division, Department of mineral Resources, Bangkok, Thailand, p. 124-138.

Weaver, A.D., Tarney, J., and Saunders, A.D., 1985, Geochemistry and mineralogy of basalts recovered from the central North Atlantic, *in* Whalen, E., ed., Initial Reports of the Deep Sea Drilling Project, v. 82, p. 395-419.

Weaver, S.D., Saunders, A.D., Pankhurst, R.J., and Tarney, J., 1979, A geochemical study of magmatism associated with the initial stages of back-arc spreading - the Quaternary volcanics of Bransfield Strait, from south Shetland Islands: Contributions to Mineralogy and Petrology, v. 68, p. 151-169.

Wells, P.R.A., 1977, Pyroxene thermometry in simple and complex systems: Contributions to Mineralogy and Petrology, v. 62, p. 129-139.

Wheller, G.E., Varne, R., Foden, J.D. and Abbott, M.J., 1987, Geochemistry of Quaternary volcanism in the Sunda-Banda arc, Indonesia, and three-component genesis of island-arc basaltic magmas: Journal of Volcanology and Geothermal Research, v. 32, p. 137-160.

Whitford, D.J., Korsch, M.J., Porritt, P.M., and Craven, S.J., 1988, Rare-earth mobility around the volcanogenic polymetallic massive sulphide deposit at Que River, Tasmania, Australia: Chemical Geology, v. 68, p. 105-119.

Whitford, D.J., Nicholls, I.A., and Taylor, S.R., 1979, Spatial variations in the geochemistry of Quaternary lavas across the Sunda Arc in Java and Bali: Contributions to Mineralogy and Petrology, v. 70, p. 341-356.

Wilkinson, J.F.G., 1982, The genesis of mid-ocean ridge basalts: Earth-Science Reviews, v. 18, p. 1-57.

Winchester, J.A., and Floyd, P.A., 1977, Geochemical discrimination of different magma series and their differentiation products using immobile elements: Chemical Geology, v. 20, p. 325-343.

Wolfart, R., 1987, Geology of Amphoe Sop Prap (sheet 1:50,000) no.,4944-4), Thailand: Geologisches Jahrbuch, Reihe B, v. 65, p. 48-52.

Wood, B.J., and Banno, S., 1973, Garnet-orthopyroxene and orthopyroxene-clinopyroxene relatioships in simple and complex systems: Contributions to Mineralogy and Petrology, v. 42, p. 109-124.

Wood, D.A., Joron, J.L., and Treuil, M., 1979, A reappraisal of the use of trace elements to classify and discriminate between magma series erupted in different tectonic settings: Earth and Planetary Science Letters, v. 45, p. 326-336.

Yamamoto, M., 1984, Origin of calc-alkaline andesite from Oshima-Oshima volcano, north Japan: Journal of Faculty of Science, Hokkaido University, series IV, v. 21, p. 77-131.

Yoder, H.S., and Tilley, C.E., 1962, Origin of basalt magmas - an experimental study of natural and synthetic rock systems: Journal of Petrology, v. 3, p. 342-532.

APPENDIX I

TABLE I-1. SAMPLE LOCATIONS AND FIELD RELATIONSHIPS OF THE STUDIED OCEAN-ISLAND LAVAS, AND DOLERITES (GROUP A) THE LETTERS 'M', 'D', 'N', AND 'U' IN BRACKETS INDICATE MAE CHARIM, DOI PHUK SUNG, NAN RIVER AND UTTARADIT AREAS, RESPECTIVELY. MAP SHEETS REFERRED TO ARE 1:50,000 ROYAL THAI ARMY SURVEY MAPS

Sample numbers and self-contained areas	Locations and field relations
OCEAN-ISLAND THOLEIITIC SAMPLES (SUBGROUP A-1)	
1.3 (M) 1.4 (M) 1.6 (M) 1.7 (M) 1.15 (M) 1.17[1] (M) 1.18 (M) 1.26 (M) 1.30 (M) 1.31 (M)	Float in the Wa River near bridge on Mae Charim - Nam Phang road (grid reference:12606190, sheet 5246 III King Amphoe Mae Charim).
68 (M)	Outcrop just east of the Wa River, approximately 6 km SSE of Mae Charim (grid reference: 14556400, sheet 5246 III King Amphoe Mae Charim). Occurring as a block in serpentinite matrix.
A (D)	Lensoid mass in metasedimentary rock in a small creek at grid reference: 06592740, sheet 5145 I Ban Nam Muap).
B (D)	Outcrop in Huai Kha, approximately 5 km SSE of Doi Phuk Sung (grid reference: 06392655, sheet 5145 I Ban Nam Muap). Probably a block in serpentinite matrix.
C[1] (D)	Outcrop in creek about 6.5 km south of Doi Phuk Sung (grid reference: 04732431, sheet 5145 I Ban Nam Muap). Probably a block in serpentinite matrix.
56.1 (N) 56.3 (N)	Outcrop in Huai Luang, approximately 7 km NE of Pak Nai (grid reference: 83550155, sheet 5145 III Ban Na Num) Intercalated with volcanic breccia, tuff and marble.
50.2 (U)	Float on a small hill, approximately 3.5 km NEE of Khao Sam Sen (grid reference: 48405700, sheet 5044 II Ban Hat Ngiu). Occurring among float of tuff and agglomerate.
OCEAN-ISLAND TRANSITIONAL THOLEIITIC AND ALKALIC SAMPLES (SUBGROUP A-2)	
1.25 (M)	Float in the Wa River near bridge on Mae Charim - Nam Phang road (grid reference: 12606190, sheet 5246 III King Amphoe Mae Charim).
36.1 [1](D) 36.3 [1](D)	Float in Huai Kham near bridge on Na Noi - Pak Tha road (grid reference. 02952310, sheet 5145I Ban Nam Muap) Outcrop in this area is greywacke with slumped chert blocks.
27.1 [1](N) 27.3 [1](N) 27 4 [1](N) 27.6 [1](N) 27.7 [1](N)	Float in Huai Pang at grid reference: 93151150, sheet 5145 III Ban Na Nam. Outcrop at this location is cumulus gabbro/amphibolite.
28.2 [1](N) 28.4 [1](N) 28.6 [1](N) 28.8 [1](N)	Float in the Nan River at grid reference: 91801070, sheet 5145 III Ban Na Nam.

[1] = DOLERITE.

TABLE I-2. SAMPLE LOCATIONS AND FIELD RELATIONSHIPS OF GROUP B LAVAS, DOLERITES, AND MICROGABBROS. THE LETTERS 'M', 'D', 'N', 'S' AND 'U' IN BRACKETS INDICATE MAE CHARIM, DOI PHUK SUNG, NAN RIVER, SIRIKIT RESERVOIR AND UTTARADIT AREAS, RESPECTIVELY. MAP SHEETS REFERRED TO ARE 1.50,000 ROYAL THAI ARMY SURVEY MAPS.

Sample numbers and self-contained areas	Locations and field relations
SUBGROUP B-1	
1.29[1] (M)	Float in the Wa River near bridge on Mae Charim - Nam Phang road (grid reference: 12606190, sheet 5246 III King Amphoe Mae Charim).
22.1 (D) 22.2 (D) 22.3 (D) 22.4 (D) 22.5 (D)	Outcrop approximately 3 km NNE of Doi Phuk Sung (grid reference: 06003370, sheet 4145 I Ban Nam Muap).
23.1 (D) 23.3 (D) 23.7 (D) 23.11[2] (D)	Float in Huai Sali near Ban Sali, approximately 3 km NE of Doi Phuk Sung (grid reference: 06803275, sheet 4145 I Ban Nam Muap).
55.1 (D) 55.1A (D)	Outcrop at a road-cut approximately 8 km NNE of Ban Huai Lao (grid reference: 09203405, sheet 4145 I Ban Nam Muap). It shows complicated internal structures suggestive of a sheeted dike complex and is faulted against Upper Triassic - Lower Jurassic molasse.
SUBGROUP B-2	
18.1[2] (N)	Outcrop in the Nan River between grid references 91751100 (sheet 5145 II Ban Na Num) and 79009620 (sheet 5145 III Ban Na Thanung).
19.7[2] (U) 19.8[2] (U)	Float on Khao Sam Sen between grid references 45205610 and 45955555, sheet 5044 II Ban Hat Ngiu.
SUBGROUP B-3	
YP-9 (D)	Outcrop in a small creek, approximately 2 km W of Ban Huai Lao (grid reference: 04722794, sheet 4145 I Ban Nam Muap).
26.7 (N)	Float in Huai Pan, approximately 7 km E of Pak Nai (grid reference. 85259725, sheet 5145 I Ban Na Num).
45.1 (S) 45.2 (S) 45.4 (S)	Float on a N-S trending ridge, approximately 10 km NNE of Sirikit Dam (grid reference: 70407685, sheet 5144 IV Khuan Sirikit).
SUBGROUP B-4	
27.2[1] (N)	Float in Huai Pang, the northernmost part of the Nan River area (grid reference: 93151150, sheet 5145 III Ban Na Nam).

[1] = LAVA, [2] = MICROGABBRO.

TABLE I-3. SAMPLE LOCATIONS AND FIELD RELATIONSHIPS OF THE STUDIED ARC LAVAS, DOLERITES AND MICROGABBROS (GROUP C). THE LETTERS 'M', 'D', 'N', 'S', AND 'U', IN BRACKETS INDICATE MAE CHARIM, DOI PHUK SUNG, NAN RIVER, SIRIKIT RESERVOIR, AND UTTARADIT AREAS, RESPECTIVELY
MAP SHEETS REFERRED TO ARE 1:50,000 ROYAL THAI ARMY SURVEY MAPS.

Sample numbers and self-contained areas	Locations and field relations
SUBGROUP C-1	
1.20[2] (M)	Float in the Wa River near bridge on Mae Charim - Nam Phang road (grid reference:12606190, sheet 5246 III King Amphoe Mae Charim).
38.4[2] (D)	Float in Huai Khu near Ban Huai Khu, approximately 6 km NE of Doi Phuk Sung (grid reference. 08703490, sheet 4145 I Ban Nam Muap).
18.6[2] (N)	Outcrop in the Nan River between grid references 91751100 (sheet 5145 II Ban Na Num) and 79009620 (sheet 5145 III Ban Na Thanung).
32.1 (N)	Float in Huai Ngom Mot, approximately 4 km SSE of Pak Nai (grid reference: 79509315, sheet 5145 III Ban Na Thanung). Outcrop at this locality is sedimentary rocks.
42.1[1] (S)	Float in a small creek, approximately 14 km N of Sirikit Dam (grid reference: 69507790, sheet 5144 IV Khuan Sirikit). Outcrop at this locality is amphibolite.
47.1[1] (S)	Float on a N-S trending ridge, approximately 10 km NNE of Sirikit Dam (grid reference: 70307620, sheet 5144 IV Khuan Sirikit).
S9-2[2] (U)	Outcrop on Khao Sam Sen at grid reference 45655505, sheet 5044 II Ban Hat Ngiu. It evidently intrudes foliated amphibolite (isotropic gabbro).
SUBGROUP C-2	
11[1] (N) 18A (N) 18.2 (N) 18.3 (N)	Outcrops in the Nan River between grid references 91751100 (sheet 5145 II Ban Na Num) and 79009620 (sheet 5145 III Ban Na Thanung).
24.1[1] (N)	Float in Huai Pan, approximately 4 km E of Pak Nai (grid reference: 82559645, sheet 5145 III Ban Na Thanung).
24.2[1](N)	Outcrop at this locality is silicified serpentinite.

[1] = LAVA, [2] = MICROGABBRO.

TABLE I-4 SAMPLE LOCATIONS AND FIELD RELATIONSHIPS OF THE STUDIED GABBROS AND AMPHIBOLITES. THE LETTERS 'M', 'D', 'N', 'S', AND 'U' IN BRACKETS STAND FOR MAE CHARIM, DOI PHUK SUNG, NAN RIVER, SIRIKIT RESERVOIR, AND UTTARADIT AREAS, RESPECTIVELY MAP SHEETS REFERRED TO ARE 1:50,000 ROYAL THAI ARMY SURVEY MAPS.

Sample numbers and self-contained areas	Locations and field relations
63.2 (M)	Float in the Tuang River, approximately 5 km E of Mae Charim (grid reference:17507020, sheet 5246 III King Amphoe Mae Charim).
64.1 (M)	Float in the Tuang River, approximately 6 km E of Mae Charim (grid reference:18406940, sheet 5246 III King Amphoe Mae Charim).
9.1 (D) 9.2 (D) 9.3 (D)	Float in a creek, approximately 5 km SW of Ban Huai Lao (grid reference: 02652510, sheet 4145 I Ban Nam Muap).
20.1 (D)	Outcrop on a NE-SW trending ridge, approximately 2 km S of Doi Phuk Sung (grid reference: 04302930, sheet 4145 I Ban Nam Muap). A part of lenticular-shaped block in serpentinite matrix.
WC-3 (D)	Outcrop in a creek, approximately 5 km SW of Ban Huai Lao (grid reference: 02652510, sheet 4145 I Ban Nam Muap). A part of block in serpentinite matrix.
F (D)[1]	Outcrop near Huai Kham, approximately 5.5 km S of Ban Huai Lao (grid reference: 07002230, sheet 4145 I Ban Nam Muap).
G (D)[1]	Outcrop at a road-cut, approximately 6 km S of Ban Huai Lao (grid reference: 07002230, sheet 4145 I Ban Nam Muap).
H (D)[1]	Outcrop in Huai Nam Khang, approximately 2 km SW of Ban Huai Lao (grid reference: 05602670, sheet 4145 I Ban Nam Muap). A part of block in serpentinite matrix.
YP-7 (D)[1]	Outcrop in a small creek, approximately 2 km W of Ban Huai Lao (grid reference: 04792845, sheet 4145 I Ban Nam Muap). Probably a part of block in serpentinite matrix.
YP-12 (D)[1]	Outcrop in a small creek, approximately 2 km SSW of Ban Huai Lao (grid reference 04932703, sheet 4145 I Ban Nam Muap). Probably a part of block in serpentinite matrix.
YP-15 (D)[1]	Outcrop in a small creek, approximately 2.5 km SW of Ban Huai Lao (grid reference: 05062671, sheet 4145 I Ban Nam Muap). Probably a part of block in serpentinite matrix.
YP-31 (D)	Outcrop in a small creek, approximately 2.5 km SW of Ban Huai Lao (grid reference· 05632680, sheet 4145 I Ban Nam Muap). Probably a part of block in serpentinite matrix.
13 (N) 17.5 (N)[1] 17.6 (N)[1] 17.7 (N)[1]	Outcrops in the Nan River between grid references 91751100 (sheet 5145 II Ban Na Num) and 79009620 (sheet 5145 III Ban Na Thanung).
24.3 (N)[1]	Float in Huai Pan, approximately 4 km E of Pak Nai (grid reference: 82559645, sheet 5145 III Ban Na Thanung).
24.4 (N)[1]	Outcrop at this locality is silicified serpentinite.
25.3 (N)	Float in a small creek, approximately 7 km E of Pak Nai (grid reference: 85709730, sheet 5145 II Ban Na Num)
26.1 (N) 26.3 (N)	Float in Huai Pan, approximately 7 km E of Pak Nai (grid reference. 85259725, sheet 5145 II Ban Na Num).
27.5 (N)[1]	Outcrop in Huai Pang at grid reference: 93151150, sheet 5145 III Ban Na Nam.
28.10 (N)	Float in the Nan River, approximately 18 km NE of Pak Nai (grid reference: 91801065, sheet 5145 II Ban Na Num
32.2 (N) 32.3 (N)[1] 32.6 (N)	Float in Huai Ngom Mot, approximately 4 km SSE of Pak Nai (grid reference: 79509315, sheet 5145 III Ban Na Thanung).
34.1 (N)	Float in Huai Ngom Mot, approximately 4.5 km SSE of Pak Nai (grid reference: 79709280, sheet 5145 III Ban Na Thanung).
40.1 (S)	Outcrop in a small creek, approximately 14 km N of Sirikit Dam (grid reference· 68957785, sheet 5144 IV Khuan Sirikit).
42.2 (S)	Float in a small creek, approximately 14 km N of Sirikit Dam (grid reference: 69507790, sheet 5144 IV Khuan Sirikit).
45.3 (S)[1]	Float on a N-S trending ridge, approximately 10 km NNE of Sirikit Dam (grid reference: 70407685, sheet 5144 IV Khuan Sirikit).
S-2 (U)[1]	Float on Khao Sam Sen at grid reference 45255610, sheet 5044 II Ban Hat Ngiu.
S9-1 (U)[1]	Outcrop on Khao Sam Sen at grid reference 45655505, sheet 5044 II Ban Hat Ngiu.
S-12B (U)	Float on Khao Sam Sen at grid reference 45805460, sheet 5044 II Ban Hat Ngiu.

[1] = WHOLEROCK XRF ANALYSED SAMPLE.

TABLE I-5. SAMPLE LOCATIONS OF THE STUDIED ULTRAMAFIC ROCKS. THE LETTERS 'M', 'D', 'N', 'S', AND 'U' IN BRACKETS STAND FOR MAE CHARIM, DOI PHUK SUNG, NAN RIVER, SIRIKIT RESERVOIR, AND UTTARADIT AREAS, RESPECTIVELY. MAP SHEETS REFERRED TO ARE 1:50,000 ROYAL THAI ARMY SURVEY MAPS.

Sample numbers and self-contained areas	Locations
Clinopyroxenites	
9.6 (D)	Float in a creek, approximately 5 km SW of Ban Huai Lao (grid reference: 02652510, sheet 4145 I Ban Nam Muap).
10.2 (D) 10.3 (D)	Outcrop at the southern mining face of Nan Mine, approximately 5 km SW of Ban Huai Lao (grid reference: 02702525, sheet 4145 I Ban Nam Muap).
SC-4 (D)	Outcrop near a road, approximately 1 km SWW of Ban Huai Lao (grid reference: 06302750, sheet 4145 I Ban Nam Muap).
R (D)	Outcrop in Huai Kaeng Luang, approximately 5 km SWW of Ban Huai Lao (grid reference: 02852580, sheet 4145 I Ban Nam Muap).
57.2 (N)	Float in Huai Luang, approximately 7 km NE of Pak Nai (grid reference: 01708355, sheet 5145 III Ban Na Thanung).
40.1A (S)	Outcrop in a small creek, approximately 14 km N of Sirikit Dam (grid reference: 68957785, sheet 5144 IV Khuan Sirikit).
44.1 (S)	Float on a N-S trending ridge, approximately 10 km NNE of Sirikit Dam (grid reference: 70357720, sheet 5144 IV Khuan Sirikit).
19.2 (U) 19.3 (U)	Float on Khao Sam Sen between grid references 45205610 and 45955555, sheet 5044 II Ban Hat Ngiu.
Olivine clinopyroxenites	
8.1A (D)	Outcrop at grid reference 05602710, sheet 4145 I Ban Nam Muap (approximately 1.5 km SW of Ban Huai Lao).
S (D)	Outcrop near a road, approximately 1 km SWW of Ban Huai Lao (grid reference: 06402745, sheet 4145 I Ban Nam Muap).
S-11A (U)	Outcrop on Khao Sam Sen at grid reference 45355460, sheet 5044 II Ban Hat Ngiu.
52.2 (U)	Float in rice field near Ban Wang Daeng, approximately 2.5 km E of Khao Sam Sen (grid reference: 42905560, sheet 5044 II Ban Hat Ngiu).
Wehrlites	
8.1 (D) 8.3 (D) 8.4 (D) 8.5 (D) 8.7A (D)	Outcrop at grid reference 05602710, sheet 4145 I Ban Nam Muap (approximately 1.5 km SW of Ban Huai Lao).
YP-5 (D)	Outcrop in a small creek, approximately 2 km NWW of Ban Huai Lao (grid reference: 04902873, sheet 4145 I Ban Nam Muap).
Y-7 (D)	Outcrop in Huai Kha, approximately 1.5 km SSW of Ban Huai Lao (grid reference: 06342742, sheet 4145 I Ban Nam Muap).
Q (D)	Outcrop in a creek, approximately 2 km SW of Ban Huai Lao (grid reference: 05852685, sheet 4145 I Ban Nam Muap).
SC-6 (D)	Outcrop at the southern mining face of Nan Mine, approximately 5 km SW of Ban Huai Lao (grid reference: 02702525, sheet 4145 I Ban Nam Muap).
Websterites	
47.3A (S)	Float on a N-S trending ridge, approximately 10 km NNE of Sirikit Dam (grid reference: 70307620, sheet 5144 IV Khuan Sirikit).
Harzburgites	
1.2 (M) 1.9 (M)	Float in the Wa River near bridge on Mae Charim - Nam Phang road (grid reference.12606190, sheet 5246 III King Amphoe Mae Charim).
41.2 (S)	Float in a small creek, approximately 12 km N of Sirikit Dam (grid references: 69357780, sheet 5144 IV Khuan Sirikit).
Dunites	
1.10 (M) 1.8 (M) 1.1B (M)	Float in the Wa River near bridge on Mae Charim - Nam Phang road (grid reference:12606190, sheet 5246 III King Amphoe Mae Charim).
65.1 (M)	Float in the Tuang River, approximately 7 km E of Mae Charim (grid reference: 18406920, sheet 5246 III King Amphoe Mae Charim).
28.1 (N)	Float in the Nan River, approximately 18 km NE of Pak Nai (grid reference: 91801065, sheet 5145 II Ban Na Num).

TABLE I-6. SAMPLE LOCATIONS OF THE STUDIED CHROMITITES. THE LETTERS 'M', 'D', AND 'N', IN BRACKETS STAND FOR MAE CHARIM, DOI PHUK SUNG,AND NAN RIVER AREAS, RESPECTIVELY. MAP SHEETS REFERRED TO ARE 1:50,000 ROYAL THAI ARMY SURVEY MAPS.

Sample numbers and self-contained areas	Locations
MC-1 (M)	Unknown (donated by CIG company).
DSP-1 (D)	Outcrops at the northern mining face of Nan Mine, approximately 3.7 km NW of Ban Huai Lao (grid reference: 04503100, sheet 4145 I Ban Nam Muap).
5.1 (D) 5.2 (D) 5.3 (D) 5.4 (D) 5.5 (D) 5.6 (D) 5.7 (D)	Outcrop at the southern mining face of Nan Mine, approximately 5 km SW of Ban Huai Lao (grid reference: 02702525, sheet 4145 I Ban Nam Muap).
25.2 (N) 25.5 (N)	Outcrops on a hill at grid reference 85709730, sheet 5145 II Ban Na Num.

TABLE I-7. SAMPLE LOCATIONS OF THE STUDIED BLUESCHISTS. MAP SHEETS REFERRED TO ARE 1:50,000 ROYAL THAI ARMY SURVEY MAPS.

Sample numbers and self-contained areas	Locations
N O P	Outcrop in a small creek just south of Doi Phuk Sung (grid reference: 04293032, sheet 4145 I Ban Nam Muap).

APPENDIX II

TABLE II-1. PETROGRAPHIC FEATURES OF THE STUDIED OCEAN-ISLAND THOLEIITIC LAVAS AND DOLERITES (SUBGROUP A-1); THE AREAS FROM WHICH THE ROCKS COLLECTED ARE INDICATED AS FOLLOWS: M, MAE CHARIM AREA, D, DOI PHUK SUNG AREA; N, NAN RIVER AREA; AND U, UTTARADIT AREA

Sample numbers and self-contained areas	Phenocryst and/or microphenocryst assemblages	Groundmass minerals	Other secondary minerals
56.3 (N)	Porphyritic with chlorite pseudomorphs after olivine phenocrysts and microphenocrysts, and sporadic spinel microphenocrysts	Glassy with quenched feldspars in stellate aggregates.	Fe sulphides + indeterminate materials (altered from glass).
56.1 (N)		Felted albitised plagioclase laths, and intergranular colourless clinopyroxenes with occasionally interstitial glass.	
B (D) 50 2 (U)	Slightly microphyric with chlorite pseudomorphs after olivine microphenocrysts, and occasional spinel microphenocrysts	Felted albitised plagioclase laths and intergranular colourless clinopyroxenes. Amygdale are present in small amount	Leucoxene + calcite ± magnetite ± pumpellyite ± stilpnomelane ± quartz ± Fe sulphides
1.26 (M)	Slightly microphyric with chlorite pseudomorphs after olivine microphenocrysts.	Glassy with quenched feldspar laths in variolitic style.	Epidote + calcite + quartz + Fe sulphides + indeterminate reddish brown minerals
1.7 (M) 1.30 (M) 68 (M)	Porphyritic with albitised plagioclase, colourless clinopyroxene and chlorite pseudomorphs after olivine phenocrysts and microphenocrysts.	Felted albitised plagioclase laths and intergranular colourless clinopyroxenes are predominant phases. Irregular patches of Fe-Ti oxides are present in small amount.	Chlorite + epidote + sericite + pumpellyite + Fe sulphides ± ± leucoxene ± bluish amphibole ± quartz ± zoisite/clinozoisite
1.6 (M) 1 18 (M)	Porphyritic with albitised plagioclase and colourless clinopyroxene phenocrysts and microphenocrysts.		
1 4 (M)	Porphyritic with albitised plagioclase and colourless clinopyroxene phenocrysts and microphenocrysts.	Altered glass made up mainly of greenish minerals.	Leucoxene + epidote + Fe-Ti oxides + quartz + pumpellyite
1.3 (M)	Porphyritic with albitised plagioclase and colourless clinopyroxene phenocrysts and microphenocrysts, and Fe-Ti oxide microphenocrysts (ilmenite and magnetite).	Felted albitised plagioclase laths and intergranular colourless clinopyroxenes.	Chlorite + epidote + leucoxene+ quartz + Fe sulphides
1 31 (M)	Microporphyritic with albitised plagioclase, colourless clinopyroxene and Fe-Ti oxide (ilmenite and magnetite) microphenocrysts.	Felted albitised plagioclase and intergranular colourless clinopyroxene. calcite.	Quartz + chlorite + epidote + pumpellyite ± bluish amphibole ±
1.15 (M)		Hyalophitic groundmass, made up mainly of glass specked with Fe-Ti oxides, plagioclase and colourless clinopyroxene	
1 17[1] (M)	Slightly porphyritic with albitised plagioclase, colourless clinopyroxene and Fe-Ti oxide (ilmenite and magnetite) microphenocrysts.	Fine-grained with predominant felted albitised plagioclase and subophitic colourless clinopyroxene.	Quartz + chlorite + epidote + calcite + pumpellyite + Fe-Ti oxides. calcite + pumpellyite + Fe-Ti oxides
C[1] (D)	Non-porphyritic	Medium-grained made up of albitised plagioclase intergrown with colourless clinopyroxene in subparallel style Interstitial minerals include colourless clinopyroxene and leucoxene pseudomorphs after Fe-Ti oxides (ilmenite and magnetite)	Chlorite + quartz + calcite.

[1] = DOLERITE

TABLE II-2. PETROGRAPHIC FEATURES OF THE STUDIED OCEAN-ISLAND TRANSITIONAL THOLEIITIC AND ALKALIC BASALTS (SUBGROUP A-2); THE AREAS FROM WHICH THE ROCKS COLLECTED ARE INDICATED AS FOLLOWS: M, MAE CHARIM AREA; D, DOI PHUK SUNG AREA; AND N, NAN RIVER AREA.

Sample numbers and self-contained areas	Phenocryst and/or microphenocryst assemblages	Groundmass	Other secondary minerals
1.25[1](M)	Slightly porphyritic with albitised plagioclase and pink clinopyroxene microphenocrysts.	Felted albitised plagioclase laths, and intersertal green mixture of chlorite, actinolitic hornblende and leucoxene	Pumpellyite + epidote + Fe-Ti oxides + Fe sulphides + quartz.
36.1 (D) 36.3 (D) 27.4 (N) 27.6 (N) 28.2 (N) 28 4 (N)	Seriate textured, consisting largely of albitised plagioclase laths and pink clinopyroxene, and subordinate ilmenite and magnetite. Apatite occurs as inclusions in plagioclase in a few samples		Pumpellyite + chlorite + epidote + leucoxene ± bluish amphibole ± ± brown amphibole ± quartz ± sulphides ± prehnite ± calcite.
27.1 (N) 27.3 (N) 27.6 (N) 27.7 (N) 28 8 (N)	Non-porphyritic	Equigranular, made up chiefly of albitised plagioclase and pink clinopyroxene, and minor ilmenite and magnetite	Pumpellyite + chlorite + epidote + leucoxene ± bluish amphibole ± brown amphibole ± quartz.

[1] = LAVA.

TABLE II-3. PETROGRAPHIC FEATURES OF SUBGROUP B-1 ANDESITIC AND BASALTIC LAVA, DOLERITE, AND MICROGABBRO; THE AREAS FROM WHICH THE ROCKS COLLECTED ARE INDICATED AS FOLLOWS: M, MAE CHARIM AREA; AND D, DOI PHUK SUNG AREA.

Sample numbers and self-contained areas	Phenocryst and/or microphenocryst assemblages	Groundmass minerals	Other secondary minerals
1.29[1] (M)	Slightly porphyritic with albitised plagioclase phenocrysts and microphenocrysts and clinopyroxene microphenocrysts (pseudomorphed by yellowish - blue-green amphiboles.	Pilotaxitic, made up mainly of albitised plagioclase laths, and intersertal yellowish - blue-green amphiboles (pseudomorph after ?clinopyroxene), and accessory titanomagnetite, Fe sulphides, epidote, chlorite and quartz.	Sericite + leucoxene.
23 1 (D)	Slightly porphyritic with albitised plagioclase phenocrysts.	Medium-grained, consisting largely of albitised plagioclase laths, and-colourless subophitic clinopyroxenes Accessories include haematite, ilmenite and apatite.	Chlorite + sericite + epidote +quartz + prehnite + leucoxene + ? amphiboles.
23 7 (D)	Porphyritic with albitised plagioclase phenocrysts.	Fine-grained, made up mainly of albitised plagioclase laths, and intergranular colourless clinopyroxenes. A few are subophitic to plagioclases. Haematite, magnetite, apatite, prehnite, quartz and calcite are accessories.	Leucoxene + epidote + chlorite.
55.1 (D)	Strongly porphyritic with albitised plagioclase phenocrysts.	Fine-grained rock,made up mainly of albitised plagioclase, and subophitic colourless clinopyroxene, with accessory magnetite, ilmenite, apatite, chlorite, pumpellyite, calcite, quartz and epidote	Leucoxene
22.1 (D) 22.2 (D) 22.3 (D 22 4 (D) 22.5 (D)	Seriate textured, made up mainly of albitised plagioclase laths, and colourless subophitic clinopyroxenes Accessory minerals include haematite ilmenite, and apatite. Zircon, Fe sulphides, epidote, prehnite and chlorite are sparsely present.		Leucoxene + sericite + quartz + ?amphibole ± calcite
23.3 (D) 55.1A (D)	Non-porphyritic.	Fine- to medium-grained, consisting largely of albitised plagioclase and colourless subophitic clinopyroxene, with accessory haematite, ilmenite, apatite, chlorite, quartz and epidote	Leucoxene ± pumpellyite ± calcite.
23.11[2] (D)	Non-porphyritic.	Fine-grained, made up mainly of felted albitised plagioclase laths and colourless intergranular clinopyroxenes, with accessory haematite, ilmenite, apatite, quartz, prehnite and calcite	Epidote.

[1] = LAVA, [2] = MICROGABBRO.

TABLE II-4. PETROGRAPHIC FEATURES OF SUBGROUP B-3 DOLERITES. THE AREAS FROM WHICH THE ROCKS COLLECTED ARE INDICATED AS FOLLOWS: D, DOI PHUK SUNG AREA; N, NAN RIVER AREA, AND S, SIRIKIT RESERVOIR AREA.

Sample numbers and self-contained areas	Phenocryst and/or microphenocryst assemblages	Groundmass minerals	Other secondary minerals
YP-9 (D)	A non-porphyritic, fine-grained rock, made up mainly of albitised plagioclase laths, and fibrous and prismatic green amphiboles with accessory apatite, Fe oxides, Fe sulphides and calcite. Plagioclases are largely subophitically intergrown with amphiboles. Veinlets of plagioclase and epidote are sparsely present.		Brown cryptocrystalline aggregates (prehnite + pumpellyite + epidote + hydrogrossular) + leucoxene
26.7 (N)	Slightly microporphyritic with dominant albitised plagioclase microphenocrysts and subordinate (?) orthopyroxene microphenocrysts (totally pseudomorphed by chlorite and actinolite).	Fine-grained, consisting of albitised plagioclase laths, subophitic colourless clinopyroxene and brown-green amphibole, Fe oxide Fe sulphides and quartz.	Brown cryptocrystalline aggregates (prehnite + pumpellyite + epidote + hydrogrossular) + clinozoisite + pumpellyite + leucoxene
45 1 (S)	A microporphyritic rock with albitised plagioclase, clinopyroxene and altered orthopyroxene microphenocrysts in descending amounts. Clinopyroxene microphenocrysts show subophitic texture and tend to be glomerocrysts.	Fine-grained, made up largely of albitised plagioclase and brown amphibole. Clinopyroxene, Fe oxide, apatite and quartz are accessories. Amphiboles are subophitic to plagioclases	Chlorite + dark brown cryptocrystalline aggregates + actinolite + leucoxene.
45.4 (S)	Same as sample 45.1 but is slightly porphyritic Veinlets of pale green amphibole (actinolite) are sporadically present.		
45.2 (S)	A non-porphyritic, fine-grained rock, composed chiefly of albitised plagioclase and subophitic brown amphibole Clinopyroxene, quartz, and Fe oxide are accessories. Veinlets of pale green amphibole are scarcely present.		Chlorite + epidote + sericite + leucoxene

TABLE II-5. PETROGRAPHIC FEATURES OF SUBGROUP C-1 LAVA, DOLERITE, AND MICROGABBRO. THE AREAS FROM WHICH THE ROCKS COLLECTED ARE INDICATED AS FOLLOWS: M, MAE CHARIM AREA; D, DOI PHUK SUNG AREA; N, NAN RIVER AREA, S, SIRIKIT RESERVOIR AREA; AND U, UTTARADIT AREA

Sample numbers and self-contained areas	Phenocryst and/or microphenocryst assemblages	Groundmass minerals	Other secondary minerals
42.1[1] (S)	Highly porphyritic with abundant albitised plagioclase phenocrysts, and sporadic unknown altered mafic phenocrysts and microphenocrysts (pseudomorphed by chlorite).	Fine-grained, made up principally of albitised plagioclase laths, and sporadic leucoxene and epidote. Quartz, epidote and calcite veinlets may be locally present; some are sheared resulting in irregular patches.	Clinozoisite + pumpellyite + chlorite
47.1[1] (S)	Porphyritic with the same phenocryst and microphenocryst phases as above.		
32.1[2] (N)	Porphyritic with albitised plagioclase phenocrysts.	Fine-grained, consisting largely of albitised plagioclase laths, and colourless clinopyroxenes and accessory Fe oxides. Clinopyroxene bears either intergranular or subophitic relationships to plagioclase. Fe-Ti oxides are partly replaced by leucoxene and often exhibit exsolution texture	Sericite + chlorite + epidote + leucoxene + green amphibole (?actinolite) + quartz.
1.20 (M)	An equigranular, fine-grained rock, consisting mainly of highly altered plagioclase, anhedral colourless clinopyroxenes and euhedral to sub-blue-green amphiboles Quartz, apatite and altered Fe oxides (leucoxene) are accessories. Clinopyroxenes are altered partly to chlorite and and amphiboles,and almost rimmed with amphiboles. veinlets of quartz and epidote are scarcely present		Pumpellyite + indeterminate brown to dark brown minerals (pseudomorph after plagioclase)
S9-2 (U)	An equigranular, fine-grained rock, made up largely of severely altered plagioclase and green amphiboles with occasional colourless clinopyroxenes. Plagioclases and clinopyroxenes are almost anhedral; some contain numerous plagioclase and clinopyroxene inclusions Amphibole clots are locally present and often associated with chlorites and carbonates.		Indeterminate reddish brown minerals (pseudomorph after plagioclase) + Fe sulphides
18 6 (N)	Slightly porphyritic with plagioclase phenocrysts.	Fine-grained, made up mainly of plagioclase and blue-green amphiboles with accessory apatite, heamatite, quartz and Fe sulphides	Indeterminate brown to dark brown minerals (pseudomorph after plagioclase).
38.4 (D)	Porphyritic with subhedral to anhedral albitised plagioclase phenocrysts.	Fine-grained, made up mainly of albitised plagioclase laths and chlorite with sporadic quartz, epidote, calcite, leucoxene and apatite.	Clinozoisite + prehnite + pumpellyite.

[1] = LAVA, [2] = DOLERITE.

TABLE II-6. PETROGRAPHIC FEATURES OF SUBGROUP C-2 LAVAS AND DOLERITES FROM THE NAN RIVER AREA.

Sample numbers and self-contained areas	Phenocryst and/or microphenocryst assemblages	Groundmass minerals	Other secondary minerals
11[1] 24 1[1] 24 2[1]	Highly porphyritic with euhedral to anhedral plagioclase and colourless clinopyroxene phenocrysts and microphenocrysts (plagioclase>clinopyroxene). Some clinopyroxenes show corroded outlines and rounded edges.	Fine-grained, made up chiefly of altered plagioclase, actinolite and chlorite. Accessory minerals may be Fe oxides, Fe sulphides, quartz and epidote. Prehnite and calcite veinlets are rarely present in sample 11.	Sericite + clinozoisite + leucoxene ± calcite
18.2	Porphyritic with subhedral to anhedral, altered plagioclase phenocrysts and microphenocrysts, and anhedral colourless clinopyroxene microphenocrysts (almost completely replaced by blue-green amphibole)(Plagioclase>clinopyroxene).	Fine-grained, made up largely of altered plagioclase and blue-green amphibole Amphibole often shows subophitic relationship to plagioclases. Clinopyroxene, quartz, apatite and Fe sulphides are accessories	Epidote + sericite + Leucoxene ± clinozoisite.
18A 18 3	Medium-grained, equigranular rocks, composed mainly of subhedral to anhedral altered plagioclases, and colourless clinopyroxene (altered largely to amphiboles). Amphiboles show subophitic texture Quartz, chlorite, apatite, Fe oxides and Fe sulphides are sparsely present.		Epidote + clinozoisite + sericite + leucoxene.

[1] = LAVA.

TABLE II-7. PETROGRAPHIC FEATURES OF THE STUDIED GABBROS AND AMPHIBOLITES

Sample no.	Petrographic features
9.1	Medium-grained; diffuse foliation produced by 2 sets of preferred orientations of nematoblastic amphiboles. Made up mainly of yellow-green amphibole (tschermakite) with subordinate colourless clinopyroxene and haematite. Some amphibole crystals have ilmenite lamellae, and show kink banding. Clinopyroxene inclusions in amphiboles. Both amphibole and clinopyroxene are slightly altered along cracks to reddish brown minerals (?amphibole+chlorite). Haematite forms irregular patches between amphibole grains and fills cracks in amphiboles.
9.2	A strongly foliated, medium-grained amphibolite with banded structure, characterised by plagioclase-rich and plagioclase-poor layers. Foliation is defined by subparallel alignment of nematoblastic amphiboles and elongate mineral aggregates. Dominant mineralogy - anhedral plagioclase, anhedral pale green pyroxene, subhedral to anhedral amphiboles, and anhedral garnet.($Alm_{60}Py_{16}Gr_{24}$). Sporadic irregular-shaped haematite and Fe sulphides, and subhedral to anhedral apatite. Plagioclase severely altered to albite, zoisite, clinozoisite, epidote, calcite, chlorite and indeterminate dark cryptocrystalline material. Amphiboles are yellow-greenish brown at cores, and blue-green at rims, and are tschermakitic hornblende and tschermakite. They contain haematite, garnet, clinopyroxene, plagioclase and apatite inclusions, and have fractures infilled with chlorite and epidote. Garnet has inclusions of plagioclase and amphibole, and is replaced by pinite along cracks.
9 3 WC-3	Strongly foliated, medium-grained amphibolites with banded structure, characterised by alternate layers of plagioclase (and its alteration products)-rich and -poor. Foliation defined by preferred orientations of elongate crystals, and lenticular crystals and mineral aggregates. Principal constituents - subhedral to anhedral plagioclases and amphiboles. Plagioclases highly altered to quartz, chlorite, epidote, zoisite, clinozoisite and indeterminate dark material; in WC-3, atoll clinozoisites are well-developed. Amphiboles (tschermakitic hornblende) occur as the replacement of colourless clinopyroxenes of which relicts still exist in 9.3. Their colours vary from yellow-yellowish brown (9.3) to yellow - blue-green (WC-3). Accessories are anhedral to subhedral sphene, bladed ilmenite, irregular-shaped haematite, chlorite and euhedral to subhedral apatite. Many sphene crystals contain ilmenite blades as cores.
20 1	Banded with highly variable sizes of constituent minerals (<0 5 mm - 2 mm across) and prominent foliation. Banded structure characterised by alternate light-coloured (clinozoisite/zoisite - rich) and dark-coloured (enriched in other mafic minerals) layers. Foliation defined by preferred orientations of nematoblastic amphiboles and elongate lenticular mineral layers. Principal assemblage - anhedral colourless clinopyroxene, subhedral to anhedral, colourless to pale green amphibole, anhedral garnet ($Alm_{32}Py_{47}Gr_{21}$), epidote minerals and chlorite. Clinopyroxenes often occur as large crystals, extensively replaced by prismatic and fibrous amphiboles (tschermakitic hornblende and tschermakite). Garnet concentrates mainly in light-coloured layers. Predominant epidote minerals are zoisite and clinozoisite, rarely contain fibrous amphibole inclusions. Chlorite, commonly associated with fibrous amphibole, fills in cracks in other minerals.
F G	Medium-grained isotropic gabbros with slight foliation, and brecciated features. Consisting chiefly of deformed plagioclase and prismatic green amphibole (magnesio-hornblende), and may contain quartz, fibrous pale green amphibole (actinolite), haematite and Fe sulphides. Kink banding in many plagioclase and amphibole crystals. Plagioclases severely albitised and pseudomorphed by albite, zoisite, clinozoisite, epidote, pale green amphibole and indeterminate dark cryptocrystalline material. Tiny veined fibrous amphibole, calcite and epidote may be locally present.
H	A medium-grained cumulus gabbro with well-developed foliation, defined by preferred orientation of elongate lenticular amphibole+chlorite+clinopyroxene clusters. Consisting mainly of subhedral to anhedral, altered plagioclase (andesine), anhedral colourless clinopyroxene, euhedral to anhedral, yellow-brown amphibole, and chlorite, with accessory irregular-shaped haematite, bladed ilmenite, subhedral to anhedral apatite, and Fe sulphides. Plagioclases - partly clouded with pumpellyite, epidote, calcite and indeterminate minerals. Amphiboles (magnesio-hornblende and tschermakitic hornblende) occur as replacement products of clinopyroxene, and sometimes, show euhedral to subhedral outlines with triple-junction grain boundaries at 120°. They are partly replaced by chlorite. Epidote, pumpellyite, chlorite, actinolite and quartz veinlets are common.
YP-7 YP-12 YP-15	Weakly foliated, medium- to coarse-grained, layered gabbros; made up largely of anhedrally altered plagioclase, and anhedral, pale green amphibole (tschermakitic hornblende and tschermakite). Irregular-shaped Fe sulphides and chlorite are common accessories; chlorite pseudomorphs after olivine (?), irregular-shaped haematite, bladed ilmenite, and carbonate may be present. Plagioclases - highly albitised and saussuritised to an assemblage: albite+clinozoisite+zoisite+epidote+chlorite+pumpellyite. Tiny veined epidote, carbonate, quartz, pumpellyite may be present.
YP-31 S9-1	Foliated, medium-grained isotropic gabbros Foliation defined by preferred orientations of elongate mineral grains and mineral aggregates, such as plagioclase and amphibole±clinopyroxene. Consisting principally of anhedral altered plagioclase and yellow-green amphiboles . Anhedral colourless clinopyroxene, an additional major phase in S9-1, is extensively replaced by amphiboles producing poikiloblastic texture. Rutile, apatite, haematite and sulphides may be sporadically present. Plagioclases highly altered to zoisite, clinozoisite, epidote and indeterminate cryptocrystalline material. Carbonate mineral and scapolite may be present as alteration products of plagioclases. Amphiboles in YP-31 are magnesio-hornblende and tschermakitic hornblende whereas those in S9-1 are actinolitic hornblende and magnesio-hornblende.
13 17 5 17.6 17 7	Weakly foliated, fine to medium-grained cumulates made up mainly of anhedral to subhedral plagioclases (An_{47-54}) and anhedral blue-green amphiboles (magnesio-hornblende, tschermakitic hornblende and tschermakite) with sporadic irregular-shaped haematite, bladed ilmenite, and subhedral to anhedral apatite. Anhedral Fe sulphides, interstitial quartz, anhedral epidote, and chlorite are sporadically present. Common alteration products of plagioclases are zoisite, clinozoisite and epidote with or without quartz and pumpellyite. Some amphibole crystals contain ilmenite lamellae. Epidote veinlets present in some samples. Almost all these samples show both size-graded and mineral graded layering. Plagioclases show polygonal texture with triple junction in parts, especially in the coarser-grained layers.
24 3 32 6	Weakly foliated, cumulus and size-graded layered gabbronorites, consisting mainly of subhedral to anhedral plagioclase (labradorite to bytownite), anhedral pale green clinopyroxene and anhedral pink orthopyroxene with subordinate brown-green and/or blue- green fibrous amphiboles. Common accessories are haematite, Fe sulphides and bladed ilmenite. Subhedral apatite is sporadically present in 32.6. Plagioclases partly polygonised forming triple junction grain boundaries at 120°, and slightly altered to dark cryptocrystalline material Pyroxenes rarely show exsolution texture; frequently surrounded or replaced by brown-green amphibole. Fibrous amphibole occurs in 32.6 as veinlets cutting through other minerals, occasionally, it pseudomorphs other minerals. Amphiboles are magnesio-hornblende, tschermakitic hornblende and tschermakite. Haematite and Fe sulphides occur as irregular patches throughout the rocks.
24 4 32.3 34 1	Slightly foliated, fine- to medium-grained rocks, made up mainly of anhedral altered plagioclase and/or epidote minerals, and one or more varieties of amphiboles. Plagioclases severely altered to zoisite+clinozoisite+epidote+indeterminate cryptocrystalline minerals+albite±calcite± pumpellyite. Epidote minerals are euhedral to anhedral, and locally show triple-junction grain boundaries at 120°, and atoll feature. Amphiboles in 34.1 are prismatic, and have blue-green colour (magnesio-hornblende and tschermakitic hornblende), whereas those in the others, at least two varieties are present, i.e. prismatic blue-green amphiboles (tschermakitic hornblende and tschermakite) and fibrous blue-green or pale green amphiboles (actinolitic hornblende). The non-fibrous amphiboles locally show triple-junction grain boundaries. Other sporadic minerals are subhedral to anhedral sphene, anhedral sulphides, irregular-shaped haematite, chlorite, bladed ilmenite and quartz. Tiny veined epidote may be present.
25.3 26.1 26 3 28.10 42.2	Fine- to medium-grained, with well-pronounced foliation defined by subparallel alignment of nematoblastic amphiboles or elongate lenticular bands of altered plagioclase and epidote. Consisting mainly of anhedral altered plagioclase and/or epidote minerals, and one or two varieties of subhedral to anhedral amphiboles. Accessories are subhedral to anhedral sphene, anhedral haematite, anhedral Fe sulphides, bladed ilmenite, subhedral to anhedral apatite, and chlorite. Plagioclases severely altered to zoisite, clinozoisite, epidote and indeterminate dark cryptocrystalline material. Pumpellyite pseudomorphs plagioclase in 26.3. Epidote minerals - subhedral to anhedral and forms atoll surrounding plagioclase in many samples. Amphiboles are actinolite, tschermakitic hornblende and tschermakite. They occur either as prismatic or as fibrous crystals, and have colours varying from pale brown, pale green to blue-green.

TABLE II-7. CONTINUED

Sample no	Petrographic features
27.5	A weakly foliated, medium-grained layered gabbro, made up mainly of anhedral to subhedral plagioclases, prismatic blue-green ampohibole (magnesio-hornblende and tschermakite) and chlorite. Plagioclases slightly altered to albite, zoisite, clinozoisite, epidote and calcite. Amphiboles - intergrown and orientate roughly in two directions like fish bones. Subhedral sphene, anhedral haematite, bladed ilmenite and subhedral apatite are rarely present.
32.2	A highly foliated, fine-grained rock consisting largely of nematoblastic pale green amphiboles (tschermakitic hornblende and tschermakite) with subordinate anhedral garnet, zoisite/clinozoisite, aluminous green spinel, magnetite, sphene, and chlorite. Amphiboles - euhedral to subhedral, and often show triple-junction grain boundaries. Garnet ($Alm_{39}Py_{25}Gr_{36}$) is locally present and contains amphibole, spinel and magnetite inclusions. Zoisite/clinozoisite occurs in some places and contains amphibole inclusions. Spinel is green and often surrounded by magnetite.
40.1	A banded rock with pronounced foliation defined by subparallel alignment of nematoblastic amphibole, elongate lenticular epidote, and elongate lenticular quartz aggregates. Banded structure is characterised by alternate quartz-rich and quartz-poor layers. Grainsizes highly vary up to 1.5 mm. Mineral assemblage - subhedral to anhedral amphibole, anhedral garnet ($Alm_{57}Py_{19}Gr_{24}$), anhedral quartz, subhedral to anhedral epidote minerals, anhedral rutile, subhedral to anhedral apatite, muscovite flakes and subhedral to anhedral Fe sulphides. Amphiboles - mostly blue-green at cores (magnesio-hornblende and tschermakitic hornblende), and colourless-blue at rims (actinolitic hornblende); quartz and rutile inclusions; and replaced by chlorite, zoisite/clinozoisite and epidote along fractures. Garnet - partially replaced by chlorite, quartz, epidote and white mica, particularly along cracks, and contains rutile inclusions. White mica occurs inbetween mineral grains or as fracture-filling mineral. Tiny veined stilpnomelane is locally present.
45.3	A slightly foliated, medium-grained gabbro made up largely of irregular-shaped plagioclase (An_{85}) and anhedral blue-green amphibole (tschermakite). Plagioclase - mostly replaced by epidote, calcite and indeterminate dark brown cryptocrystalline material. Accessories - bladed ilmenite, anhedral magnetite and subhedral to anhedral apatite. Tiny veined epidote is common.
S-2	Medium-grained gabbro consisting mainly of altered plagioclase, anhedral colourless clinopyroxene and pale brown amphibole (actinolitic hornblende and magnesio-hornblende). Plagioclase totally altered to zoisite, clinozoisite, carbonate, quartz and indeterminate dark cryptocrystalline material. Pyroxene - pervasively replaced by pale brown amphibole producing poikiloblastic texture. Large amphibole grains are euhedral, but small amphibole grains are euhedral to subhedral, and show mosaic texture with triple-junction boundaries at 120°. Subordinate pale brown fibrous amphibole closely associated with carbonate minerals. Chlorite, haematite and Fe sulphides are accessories.
S-12B	A slightly foliated, fine-grained cumulate made up chiefly of anhedral altered plagioclase with subordinate colourless clinopyroxene, green-brown amphibole (magnesio-hornblende), fibrous pale green amphibole (actinolite), chlorite, chlorite pseudomorphs after olivine (?) and opaque minerals (Fe oxides, Fe sulphides and ilmenite). Plagioclase - largely altered to indeterminate cryptocrystalline aggregates with some epidotes and pumpellyites. Pyroxene - partly replaced by -brown amphiboles. Fibrous amphibole and associated chlorite often occur along grain boundaries or cracks; sometimes, they replace other minerals.
63.2 64.1	Well-pronounced foliated, medium-grained garnet amphibolites made up mainly of subhedral to anhedral pale brown amphibole (magnesio-hornblende and tschermakitic hornblende) and garnet ($Alm_{56}Py_{12}Gr_{32}$). Common accessories - anhedral zoisite, clinozoisite, epidote, quartz and sphene, and irregular-shaped Fe sulphides and chlorite. White mica flakes, subhedral to anhedral apatite and anhedral plagioclase (albite) may be present. Amphibole contains garnet, quartz and apatite inclusions whereas garnet has epidote, quartz and sphene inclusions. Plagioclase; if present, is clear and commonly occur as vein-like invading along mineral grain boundaries and mineral grains. Epidote minerals, white mica, quartz and chlorite are present as fracture-filling minerals.

TABLE II-8. PETROGRAPHIC FEATURES OF THE STUDIED ULTRAMAFIC ROCKS

Sample no.	Petrographic features
Clinopyroxenites	
9.6	Equigranular, medium-grained, and consisting mainly of colourless clinopyroxenes (largely anhedral and variably replaced by calcite, actinolite and chlorite, particularly along grain boundaries and fractures).
10.2	An equigranular, medium-grained, amphibolitised clinopyroxenite with diffuse foliation, made up principally of colourless clinopyroxene and pale green amphiboles (tremolitic hornblende to magnesio-hornblende). Sporadic chlorite, orthopyroxene (pseudomorphed by serpentine) and Fe oxides. Clinopyroxenes - anhedral, largely replaced by amphiboles and chlorite, and rare magnetite inclusions. Amphiboles - euhedral, and partly altered to chlorite.
10.3	An equigranular, medium-grained, amphibolitised clinopyroxenite, consisting mainly of colourless clinopyroxene and pale green amphibole (magnesio-hornblende) with subordinate chlorite and accessory magnetite Clinopyroxenes - irregular outlines due to growth of amphiboles; amphiboles - euhedral to subhedral. Both partially replaced by chlorite along grain boundaries and fractures. Magnetite - subhedral to anhedral inclusions in pyroxenes and amphiboles, and irregular patches associated with chlorite.
19.2 19.3	Inequigranular, coarse-grained, amphibolitised clinopyroxenites, consisting largely of colourless clinopyroxene and fibrous and prismatic amphiboles (tremolite and actinolite to magnesio-hornblende) with subordinate chlorite and accessory Fe sulphides and Fe oxides. Clinopyroxenes - anhedral and partly replaced by pale green to green amphiboles along fractures and grain boundaries,producing poikiloblastic texture; many contain spinel lamellae and inclusions (replaced by magnetite). Prismatic amphiboles - subhedral to anhedral, and may show triple-junction grain boundaries at 120°, particularly the smaller crystals. Subhedral to anhedral Fe sulphides and Fe oxides, often associated with chlorite, are distributed throughout the rocks.
Olivine Clinopyroxenites	
40.1A R	An equigranular, medium-grained, amphibolitised clinopyroxenites, made up mainly of colourless clinopyroxene and pale green amphiboles (tremolite and tremolitic hornblende) with accessory chlorite, magnetite and Fe sulphides. Clinopyroxenes - anhedral, replaced by chlorite and amphibole along grain boundaries, and locally severely amphibolitised. They exhibit cumulus texture and contain spinel lamellae and inclusions (totally transformed to magnetite) in parts. Magnetite and Fe sulphides occur as irregular patches inbetween mineral grains.
44.1	An equigranular, fine-grained, amphibolitised clinopyroxenite with poorly defined foliation. Made up of colourless clinopyroxenes and pale green amphiboles with subordinate chlorite and accessory magnetite. Clinopyroxenes - replaced by euhedral to subhedral amphiboles along grain boundaries, producing irregular outlines; spinel lamellae and inclusions (transformed to magnetite). Clinopyroxenes and amphiboles - partly pseudomorphed by chlorite along grain boundaries and fractures.
57.2	An equigranular, coarse-grained cumulate, made up mainly of colourless clinopyroxenes with subordinate chlorite and trace Fe oxides. Clinopyroxenes - anhedral and partly transformed to chlorite and Fe oxides along fractures and grain boundaries. Kink banding in many clinopyroxene grains.
SC-4	An equigranular, medium-grained clinopyroxenite, made up largely of colourless clinopyroxene and accessory magnetite. Clinopyroxenes - subhedral to anhedral, and slightly altered to pale green to brown amphiboles (magnesio-hornblende), particularly along grain boundaries and fractures.
8.1A	An inequigranular, coarse-grained rock, consisting largely of colourless clinopyroxene with subordinate olivine and rare amphibole (actinolite), chlorite, chromite and magnetite. Clinopyroxenes - variable grain sizes and largely anhedral. Bigger clinopyroxenes always contain orthopyroxene and spinel lamellae, and spinel inclusions; lamellae are not uniformly distributed even in a single crystal. Smaller clinopyroxenes may have spinel lamellae and inclusions, and locally exhibit triple-junction grain boundaries. Clinopyroxenes - replaced by chlorite along fractures and grain boundaries. Olivines - anhedral, locally show mesh texture, and contain numerous fractures infilled with chlorite/serpentine and magnetite. Chromite also occurs as independent grains among other phases.
52.2	A foliated, coarse-grained rock, made up mainly of colourless clinopyroxene with subordinate olivine, colourless to very pale green amphiboles (magnesio-hornblende) and chlorite/serpentine, and accessory magnetite. Foliation defined by lenticular aggregates of olivine-rich, and clinopyroxene and amphibole-rich. Clinopyroxenes - anhedral and have spinel lamellae and inclusions. They altered along grain boundaries and fractures to amphibole and chlorite. Amphiboles - largely subhedral and partially replaced by chlorite. Olivines contain abundant cracks where extensively transformed to amphibole, chlorite/serpentine and magnetite. Spinels are almost transformed to magnetite.
S	Equigranular, medium-grained cumulate; consisting largely of colourless clinopyroxene with subordinate olivine and accessory sulphides and Fe oxides. Chlorite and epidote lenses (originally veinlets) are common. Clinopyroxenes - anhedral and partly altered to chlorite along fractures and grain boundaries. Olivines - almost pseudomorphed by serpentine.
S-11A	Equigranualr, coarse-grained, made up mainly of colourless clinopyroxene with subordinate altered olivine and amphibole, and accessory spinel (transformed to magnetite) and talc. Clinopyroxenes - anhedral and commonly contain spinel inclusions. They may have spinel lamellae, and partially altered to chlorite. Olivines - totally pseudomorphed by serpentine/chlorite, talc and magnetite. Amphiboles occur as irregular patches in clinopyroxenes.
Wehrlites	
8.1 8.5 Y-7	Inequigranular, medium-grained, consisting mainly of colourless clinopyroxene and olivine with sporadic chromite and magnetite. Clinopyroxenes - largely anhedral with irregular contacts and altered to chlorite and pale green amphibole along fractures and grain boundaries. Chromite lamellae and inclusions (not uniformly distributed) are common; some show kink banding. Olivines - highly fractured, and altered along cracks to serpentine and magnetite. Chromite also occurs as discrete grains inbetween other minerals.
8.3 8.4 8.7A	Inequigranular, coarse-grained, similar mineralogies to 8.1, 8.5 and Y-7 but olivines are extensively replaced serpentine, producing mesh texture.
Q	Inequigranular, medium-grained, made up mainly of olivine and clinopyroxene with small amounts of chromite and magnetite. Clinopyroxenes - largely anhedral, irregular contacts, and rare spinel and orthopyroxene lamellae but common spinel inclusions. Smaller pyroxene grains locally show triple-junction grain boundaries. Clinopyroxenes - slightly altered along cracks to chlorite and pale green amphibole. Olivines - highly fractured, replaced by serpentine, magnetite and carbonate along fractures.
SC-6	Equigranular, fine-grained, made up largely of olivine and colourless clinopyroxene with sporadic chromite, Fe sulphides and magnetite. Clinopyroxenes - anhedral and partly altered to chlorite; some exhibit kink banding. Olivines - anhedral, highly fractured; largely replaced by serpentine/chlorite, amphibole (magnesio-hornblende) and carbonate.
YP-5	Equigranular, fine-grained, made up largely of anhedral olivine and colourless clinopyroxene with irregular contacts. Clinopyroxenes may contain spinel lamellae and inclusions. Olivines may have spinel inclusions and locally altered to serpentine and magnetite.

TABLE II-8. CONTINUED

Sample no	Petrographic features
Websterite	
47.3A	Equigranular, fine-grained rock, made up largely of anhedral colourless clinopyroxene and pink orthopyroxene with accessory Fe sulphides. Orthopyroxenes - partly pseudomorphed by chlorite/serpentine.
Harzburgites	
1.2 41 2	Medium-grained, consisting largely of colourless orthopyroxene and olivine with accessory Fe oxides and carbonate. Orthopyroxenes - anhedral, and replaced by chlorite/serpentine along fractures. Olivines - numerous cracks and partly replaced by serpentine/chlorite, colourless amphibole (tremolite) and magnetite.
1.9	Highly altered, made up largely of olivine and orthopyroxene which are almost altered to serpentine, talc and magnetite
Dunites	
1.8	Serpentinised, made up largely of serpentine, and subordinate relict olivine and magnetite.
1.10 1.1B	Serpentinised,made up mainly of serpentine with subordinate relict olivine. Colourless amphibole (tremolite), magnetite and carbonate may be present in small amounts.
28.1	Serpentinised, made up largely of serpentine and olivine with subordinate colourless amphibole and accessory magnetite.
65.1	Amphibolitised, made up largely of olivine and colourless amphibole (anthophyllite). Both of them are slightly replaced by chlorite/ serpentine and magnetite along grain boundaries and fractures.

TABLE II.9. PETROGRAPHIC FEATURES OF THE STUDIED CHROMITITES

Sample no.	Petrographic features
5.1 5.3 5.7	Medium-grained chromitite pods in serpentinised dunite, consisting mainly of chromites (largely anhedral) with subordinate serpentine.
5.6	Chromitite layers and schlieren in amphibolitised dunite. Major constituents - chromites (largely anhedral) and serpentine; their proportions are variable from chromite- to serpentine-dominated. Colourless amphibole is an additional minor components.
5 2 5.4	Medium-grained chromitites made up largely of chromite (largely anhedral) with subordinate colourless, subhedral to anhedral amphiboles (tremolitic hornblende and magnesio-hornblende) and chlorite/serpentine
5 5	Medium-grained chromitite pods and streaks in serpentinised dunite, made up of chromite (largely anhedral) and serpentine in equal proportions.
25 2 25.5	Medium-grained chromitites (largely anhedral) consisting mainly of chromites (largely anhedral) with sporadic serpentine and uvarovite.
DSP-1	Fine-grained chromitite blocks in carbonatised serpentine matrix, made up principally of chromites with subordinate carbonate (dolomite) which show relict mesh texture; sporadic serpentine, quartz and uvarovite.
MC-1	A fine-grained chromitite made up mainly of chromite (largely anhedral) with minor serpentine.

Recommended Corrections.

p5	para1	13	"remain" should be "remains"
p5	para4	11	"was" should be "were"
p7	para1	14	"correlates" should be "correlatives"
p9	para3	17	"radiolarians" should be "radiolaria"
p15	para1	11	"radiolarians" should be "radiolaria"
p15	para2	11	"into" should be "in"
p15	para4	11	"in calcareous" should be "in the calcareous"
p16	para3	13	"in Late Triassic" should be "in the Late Triassic"
p18	para4	19	"Chappel" should be "Chappell"
p19	para4	19	Hellman and Anderson (1979) in text, but Hellman and Henderson (1979) in reference list (p213).
p20	para5	11	"done by" should be "done using"
p22	para3	11	"whole rock analysed" should be "analysed whole rock"
p29	para2	11	"similar mineralogies" should be "mineralogy similar"
p32	para4	11	"restricted in" should be "restricted to"
p32	para4	15	"whole rock analysed" should be "analysed whole rock"
p48	para4	13	"it is quite altered" should be "The rock is quite altered"
p56	para3	11	"the modern" should be "modern"
p61	para3	16	"Exact field relation.....remains" should be "The exact field relations.....remain"
p64	para1	14	"in groundmass" should be "in the groundmass"
p65	para1	12	"it is" should be "the microgabbro"
p82	para1	16	"float serpentinite" should be "serpentinite float"
p86	para4	11	"have been made" should be "has been made"
p91	para1	13	"E-MORB and intraplate basalts" should be "an E-MORB or an intraplate basalt"
p91	para2	11	"Subgroup B-4 sample analysed" should be "analysed Subgroup B-4 sample"
p94	para4	15	"chemistries" should be "chemistry"
p95	para1	13	"resemble those" should be "and resemble those"
p112	para3	12	"and are" should be "and is"
p121	para1	15	"in island arc" should be "in an island arc"
p123	para1	16	"mineralogies" should be "mineralogy"
p168	para1	11	"chemistries" should be "chemistry"
p169	para1	11	"restricted in" should be "restricted to"
p171	para4	13	"forearc" should be "the forearc"
p175	para2	114	"bulkrock" should be "bulk rock"
p195	para4	11-2	"bulk composition anhydrous" should be "anhydrous bulk composition"
p196	para2	19	"reducing Na loss" should be "reducing Na loss to"
p203	para3	17-8	"Bulk compositions.....anhydrous at 5 Kb," should be "Anhydrous bulk compositions.....at 5 Kb,"
p204	para2	17-8	"arc high-Al basalts" should be "high-Al arc basalts"
p204	para2	18	"arc high-Al basalts" should be "high-Al arc basalts"
p216			In Laird and Albee reference, "vermont" should be "Vermont"
p216			In le Roex et al.,1989 reference, "contrasing" should be "contrasting"
p216			In Liu et. al. reference, "Chappel" should be "Chappell"
p218			"Chappel" should be "Chappell"
p219			In Pearce 1982 reference, "Thrope" should be "Thorpe"